Identification of novel regulators of COP1-controlled morphogenesis in *Arabidopsis thaliana*

Inaugural-Dissertation

zur

Erlangung des Doktorgrades

der Mathematisch-Naturwissenschaftlichen Fakultät

der Universität zu Köln

vorgelegt von

Andrea Schrader

aus Bielefeld

Köln, 2011

Berichterstatter/in:	PD Dr. Joachim F. Uhrig
	Prof. Dr. Ute Höcker
Prüfungsvorsitzender:	Prof. Dr. Martin Hülskamp
Tag der mündlichen Prüfung:	09.06.2010

Zusammenfassung

COP1 ist ein essentielles Element, ein Regulator, in der Lichtsignaltransduktion in *Arabidopsis thaliana.* Dieser Regulator ist auf einer Ebene aktiv, die sich „unterhalb" der Photorezeptoren und „oberhalb" der Genexpression befindet. Das COP1 Protein ist Teil eines E3 Ligase Komplexes, der photomorphogenetische, lichtabhängige Genexpression durch Ubiquitin-abhängigen Abbau lichtregulierter Transkriptionsfaktoren unterdrückt. Bei im Dunkeln gewachsenen Keimlingen umfasst die Unterdrückung der Photomorphogenese die Hemmung des Hypokotylwachstums, Anthocyan-Ansammlung, Expression von Licht-regulierten Genen, Differenzierung von Etioplasten und Verhinderung der Bildung eines apikalen Hakens. Der Verlust der COP1-Funktion führt zu pleiotropischen Effekten, bestehend aus konstitutiver Photomorphogenese im Dunklen und resultiert in einem Wachstumsdefekt nach der Keimung. Beispiele für Aspekte der COP1 Funktion und Regulation sind der vegetative Wachstumsstopp von *cop1* Mutanten, eine mögliche Rolle von COP1 bzgl. des Zellzyklus und die molekularen Faktoren, die den Kern-Zytoplasma Transport von COP1 regulieren. Diese sind bisher schlecht verstanden.

Diese Arbeit zielte auf die Identifikation von Regulatoren COP1-kontrollierter Morphogenese, um ein besseres Verständnis dieser Effekte zu gewinnen. Über Hefe - Zwei - Hybrid Screenings wurden 32 neue Interaktionskandidaten für COP1 identifiziert und eine zweckorientierte Selektion durchgeführt. Alle Interaktionskandidaten für COP1 und zusätzlich für DET1 wurden in ein Netzwerk aus publizierten Interaktionen integriert, um neue putative Regulatoren von COP1 zu selektieren. Mit PAP2 (PRODUCTION OF ANTHOCYAN PIGMENT) wurde ein putatives Ziel und MID (MIDGET) ein putativer, neuer Regulator von COP1 erfolgreich identifiziert und selektiert.

MID ist Teil des Topoisomerase VI–Komplexes (TOPOVI), der benötigt wird, um mehr als zwei Endocyclen in Pflanzenzellen zu beenden. Diese Arbeit weist eine direkte Interaktion von MID und PAP2 mit COP1 nach.

Zusätzlich wurde eine neue Hefe-Zwei-Hybrid basierende Domänen-Kartierungs-Methode entwickelt und genutzt, um bisher unbekannte Domänen von PAP2 für die Interaktion mit COP1 und von COP1 für die Interaktion mit MID und TOPOVI-Bestandteilen zu identifizieren. Ähnlich wie *cop1* weisen *mid* und *topoVI* Mutanten im Dunklen alle Aspekte konstitutiver Photomorphogenese auf. Doppelmutantenanalysen weisen darauf hin, dass MID kein Ziel von COP1 ist. In infiltrierten Blättern von *Nicotiana benthamiana* war die Anwesenheit von MID nötig für COP1, um eine hohe Anzahl an subnukleären Foki zu bilden. Für MID und die TOPOVI wurde gezeigt, dass sie möglicherweise durch Stabilisation essentielle Regulatoren der COP1 Funktion sind. Die funktionale Relevanz der MID-COP1-Interaktion konnte durch Analyse von Einzelmutanten und genetische Interaktion bewiesen

werden. Erste Nachweise, die MID in einen SPA1 / phyA abhängigen Komplex oder pathway stellen, wurden durch Verifikation der SPA1-MID-Interaktion per BiFC, Ko-purifizierung von MID mit phyA und Analyse der Proteinstabilität von MID in Abhängigkeit von der Lichtqualität erbracht. Schließlich wurde festgestellt, dass *mid* und *topoVI* Mutanten eine Kopie des Phänotyps von *det1-1* Mutanten und Überexpressions-Linien der C-Termini von CRY1 und CRY2 sind. Damit ergeben sich neue Hinweise auf eine mögliche Verbindung zwischen Rotlicht- und Blaulicht-abhängige Regulations-mechanismen.

Abstract

In *Arabidopsis thaliana*, COP1 is an essential element of light signal transduction acting downstream of photoreceptors and upstream of light-regulated gene expression. The COP1 protein acts as part of an E3 ligase complex to suppress photomorphogenic gene expression by ubiquitin-dependent degradation of light-regulated transcription factors. In dark-grown seedlings, the repression of photomorphogenesis involves the inhibition of hypocotyl growth, anthocyanin accumulation, expression of light-responsive genes, differentiation of etioplasts and prevention of apical hook formation. Loss of COP1 function leads to a pleiotropic phenotype comprising of constitutive photomorphogenesis in the dark and resulting in a post-germination growth arrest. The vegetative growth arrest of *cop1* mutants, a possible role of COP1 concerning the cell cycle and the molecular factors regulating the nucleocytoplasmic partitioning of COP1 exemplify aspects of COP1 function and regulation that are poorly understood until now.

This work aimed at the identification of regulators of COP1-controlled morphogenesis to contribute to a better dissection of the latter. In yeast two hybrid screenings (YTH) 32 new interaction candidates for COP1 were identified and a purpose oriented selection was performed. In order to select a putative regulator of COP1, all COP1 and additional DET1 interaction candidates were integrated in a network of published interactors. Out of the network and the screening results PAP2 (PRODUCTION OF ANTHOCYAN PIGMENT) was identified and selected as a putative new target. MID (= MIDGET) was selected as a putative new regulator of COP1, respectively.

MID is a part of the topoisomerasis VI (TOPOVI) complex that is needed to complete more than two endocycles in plant cells. This work provides evidence for a physical interaction of MID and PAP2 with COP1.

In addition, a new YTH-based domain mapping method was developed and used to identify so far unknown domains of PAP2 for the interaction with COP1 and for COP1 for the interaction with MID

and TOPOVI components. Similar to *cop1*, *mid* and *topoisomerase VI* mutants exhibited all aspects of constitutive pohotomorphogenesis in the dark. Double mutant analysis indicated that MID is not a target of COP1. In infiltrated leaves of *Nicotiana benthamina*, the presence of MID is needed for COP1 to form a high number of subnuclear foci. MID and the TOPOVI were shown to be essential regulators of COP1 function probably by stabilising COP1 and thereby adding a new cell-cycle related factor to the regulation of COP1 activity. The functional relevance of the MID-COP1 interaction was proven by analysing phenotypes of the single mutants and genetic interaction. First evidence positioning MID in a SPA1 and phyA-dependent complex or pathway were obtained by the verification of the SPA1-MID interaction via BiFC, co-purification of MID with phyA and analysis of the protein stability of MID depending on light quality. Finally it was found that *mid* and *topoVI* mutants phenocopy *det1*-1 mutants and overexpressor lines of the C-termini of CRY1 and CRY2, possibly providing a new link to crosstalk between red and blue light mediated signaling.

Content

I. Introduction

II. Material and Methods

Abbreviations

AGI	*Arabidopsis* gene identification
2D-gel	two dimensional gel
3-AT	3-aminotriazole
5`FOA	5-Fluoroorotic acid
A. thaliana	*Arabidopsis thaliana*
A. tumefaciens	*Agrobacterium tumefaciens*
aa	amino acids
ACT7	ACTIN 7
AD	GAL4 activation domain
AGB1	GTP BINDING PROTEIN BETA 1
AGG1	ARABIDOPSIS GGAMMA-SUBUNIT 1
AGG2	G-PROTEIN GAMMA-SUBUNIT 2
AHK3	ARABIDOPSIS HISTIDINE KINASE 3
ANAC082	ARABIDOPSIS NAC DOMAIN CONTAINIG PROTEIN 82
ANAPC1	anaphase promoting complex subunit 1
ANAPC2	anaphase promoting complex subunit 2
APC	anaphase-promoting complex
ARP1	ARABIDOPSIS RIBOSOMAL PROTEIN 1
ARR14	ARABIDOPSIS RESPONSE REGULATOR 14
ARR4	INDUCED BY CYTOKININ 7, MATERNAL EFFECT EMBRYO ARREST 7
ASP2	ASPARTATE AMINOTRANSFERASE 2
ATB ALPHA	PROTEIN PHOSPHATASE 2A 55 Kda REGULATORY SUBUNIT B ALPHA ISOFORM
AtCID	*Arabidopsis thaliana* - COP1 Interacting Domain

Abbreviations

AtFAS1	FASCIATA1
AT-HSFB2B	HEAT SHOCK TRANSCRIPTION FACTOR B2B
ATKCO1	CA2+ ACTIVATED OUTWARD RECTIFYING K+ CHANNEL 1
ATM	ataxia-telangiectasia-mutated
AtMYC1	Arabidopsis thaliana myc-related transcription factor 1
ATP	Adenosin-triphosphate
ATR	ATM- and Rad3-related
AtS9	ARABIDOPSIS NON-ATPASE SUBUNIT 9
AtTOP6B	TOPOISOMERASE 6 SUBUNIT B
B	blue light
Bc	constant blue light
BD	GAL4 binding domain
BDP1	B double prime 1
bHLH	basic helix-loop-helix
BiFC	Bi-molecular fluorescence complementation
BIN3	BRASSINOSTEROID INSENSITIVE 3
BIN4	BRASSINOSTEROID INSENITIVE4 = MIDGET
BIT1	BLUE INSENSITIVE TRAIT 1
bp	base pairs
BRET	Bioluminescence Resonance Energy Transfer
BUN5	BRASSINOSTEROID INSENSITIVE 5
CAB	CHLOROPHYLL A/B BINDING PROTEIN
CAPS	Cleaved amplified polymorphism
CC	coiled coil domain
CCA1	CIRCADIAN CLOCK ASSOCIAETD 1
C-contents	nuclear DNA content

Abbreviations

ccs52	*cell-cycle switch 52*
CDD	CONSTITUTIVE PHOTOMORPHOGENIC 10, DDB1
CDF1	CYCLING DOF FACTOR 1
cDNA	complementary Desoxynucleotide Acid
CDS	coding sequence
CFP	Cyan Fluorescent Protein
CHS	CHALCONE SYNTHASE
CIB1	CRYPTOCHROME-INTERACTING BASIC-HELIX-LOOP-HELIX 1
CID	COP1 Interacting Domain
CIP1	COP1-INTERACTIVE PROTEIN 1, a cytoskeleton associated protein
CIP4	COP1-INTERACTING PROTEIN 4
CIP7	COP1-INTERACTING PROTEIN 7
CIP8	COP1-INTERACTING PROTEIN 8
CKB1	CASEIN KINASE II BETA CHAIN 1
CKB2	CASEIN KINASE II BETA CHAIN 2
CLS	cytoplasmic localisation signal
CLSM	Confocal Laser Scanning Microscopy
CO	CONSTANS
Co-IP	Co-immunoprecipitation
Col-0	Columbia-0
COL3	CONSTANS-LIKE3
COP1	CONSTITUTIVE PHOTOMORPHOGENIC 1
COP10	CONSTITUTIVE PHOTOMORPHOGENIC 10
COP9	CONSTITUTIVE PHOTOMORPHOGENIC 9; COP9 SIGNALOSOME SUBUNIT 8
COR27	COLD REGULATED GENE 27
cry	cryptochrome

Abbreviations

cry1	CRYPTOCHROME 1
cry2	CRYPTOCHROME 2
CSN	COP9-signalosom
CSN1	CONSTITUTIVE PHOTOMORPHOGENIC 11
CSN2	CONSTITUTIVE PHOTOMORGHOGENIC 12
CSN3	COP9 SIGNALOSOME SUBUNIT 3
CSN4	COP9 SIGNALOSOME SUBUNIT 4
CSN5A	COP9 SIGNALOSOME SUBUNIT 5A
CSN7	COP9 SIGNALOSOME SUBUNIT 7
CTT1	C-terminus of CRY1
CTT2	C-terminus of CRY2
CUL1	CULLIN 1
CUL4	CULLIN 4
Da	Dalton
dag	days after germination
dai	days after infiltration
DAPI	4',6-Diamidin-2'-phenylindol- dihydrochlorid
DDB1A	DAMAGED DNA BINDING PROTEIN 1A
DDB1B	DAMAGED DNA BINDING PROTEIN 1B
DDB2	damaged DNA-binding 2
DET1	DE-ETIOLATED 1
DFR	DIHYDROFLAVONOL 4-REDUCTASE
DNA	Desoxynucleotide Acid
dNTP	Desoxyribonukleosidtriphosphate
DOCK11	dedicator of cytokinesin 11
DR	direct repeats

DREB2A	DEHYDRATION-RESPONSE ELEMENT BINDING PROTEIN 2
DRIP2	DREBA2-INTERACTING PROTEIN 2, MIAP1
DSBs	double strand breaks
E. coli	*Eschericha coli*
EDTA	ethylenediaminetetraacetic acid
EF1αA4	ELONGATION FACTOR alpha A4
EGL3	ENHANCER OF GLABRA 3
eid	"empfindlicher im dunkelroten Licht"
EIF3C	EUCARYOTIC TRANSLATION INIATION FACTOR 3C
EIF4B1	EUCARYOTIC TRANSLATION INIATION FACTOR 4B1
ELF3	EARLY FLOWERING 3
EMS	ethane methyl sulfonate ;or methanesulfonic acid ethyl ester
EtBr	Ethidium bromide
EtOH	Ethanol
FACS	fluorescence activated cell sorting
FHL	FAR-RED ELONGATED HYPOKOTYL 1-LIKE
FHY1	FAR-RED ELONGATED HYPOKOTYL 1
FKBP15-1	FK 506-BINDING PROTEIN 15 KD-1
FKF1	FLAVIN BINDING; KELCH REPEAT; F-BOX 1
FMN	flavin mononucleotide
FR	far-red light
FRc	constant far-red light
FRET	Förster resonance energy transfer, fluorescence resonance energy transfer
FT	FLOWERING LOCUS T
fus	*fusca*

fw	foreward
FY	T6I14.10
FZR	FIZZY RELATED
G	gap
GA	gibberellic acid
GAPCP-1	GLYCERALDEHYD-3-PHOSPHATE DEHYDROGENASE OF PLASTID 1
GAPs	GTPase activating proteins
GARFILD	Gateway®-compatible random fragments YTH in frame library screening for domain mapping
GASA4	GAST2 PROTEIN HOMOLOG 4
GDP	Guanosin-diphosphate
GEFs	Guanine nucleotide exchange factors
gen.	genomic DNA
GFP	Green Fluorescent Protein
GHKL	gyrase–Hsp90–histidine kinase–MutL
GI	GIGANTEA
GL3	GLABRA 3
GRF1	GEGERAL REGULATORY FACTOR 1
GTP	Guanosin-triphosphate
GUS	beta-glucuronidase
H1.2	HISTONE H1.2
HA	hemagglutinin tag
hCID	human - COP1 Interacting Domain
hCOP1	human COP1
het	heterozygous
HFR1	LONG HYPOCOTYL IN FAR-RED1

HIR	high irradiance response
HKRD	His kinase-related domains
HY5	ELONGATED HYPOCOTYL 5
HYH	HY5-HOMOLOG
IgG	Immunglobulin G
IP	immunoprecipitation
KAK	KAKTUS
kb	kilo base pairs
KDR	KIDARI
LAF1	LONG AFTER FAR-RED LIGHT1
LD	long day (16h light, 8 h darkness)
L*er*	Landsberg *erecta*
LFR	low fluence response
LKP2	LOV KELCH PROTEIN 2
LNG2	LONGIFOLIA 2
LOV	LIGHT, OXYGEN, VOLTAGE REGULATED PROTEIN
LRE	light responsive elements
M	mitosis
mass spec	mass spectrometry
MIAP1	MIDGET ASSOCOIATED 1, DRIP2
MIAP2	MIDGET ASSOCOIATED 2
MID	MIDGET
MID-Col	MIDGET (Col-0 ecotype)
mRFP1 (Q66T)	optimised mono RFP form Jach et al. (2006)
mRNA	messenger RNA
MSI3	NUCLEOSOME/CHROMATIN ASSEMBLY FACTOR GROUP C 3

MTA1	METASTASIS ASSOCIATED PROTEIN 1
MTHF	methenyltetrahydropholat
MTP	microtiter plate
N. benthamiana	*Nicotiana benthamiana*
NaOCl	Sodium hypochlorite
NCBI	National Center for Biotechnology Information
NDL2	N-MYC DOWNREGULATED-LIKE 2
NDPK2	ARABIDOPSIS NUCLEOSIDE DIPHOSPHATE KINASE 2
NF-YB1	NUCLEAR FACTOR Y, SUBUNIT B1
NF-YB2	NUCLEAR FACTOR Y, SUBUNIT B2
NF-YB6	NUCLEAR FACTOR Y, SUBUNIT B6
NF-YB9	NUCLEAR FACTOR Y, SUBUNIT B9
NF-YC1	NUCLEAR FACTOR Y, SUBUNIT C1
NF-YC2	NUCLEAR FACTOR Y, SUBUNIT C2
NF-YC3	NUCLEAR FACTOR Y, SUBUNIT C3
NF-YC5	NUCLEAR FACTOR Y, SUBUNIT C5
NF-YC6	NUCLEAR FACTOR Y, SUBUNIT C6
NF-YC7	NUCLEAR FACTOR Y, SUBUNIT C7
NF-YC9	NUCLEAR FACTOR Y, SUBUNIT C9
NIA2	NITRATE REDUCTASE 2
NLS	nuclear localization signal
NPC	nuclear pore complex
nph1	*nonphototropic hypocotyl1*
nt	nucleotide
NUDT7	NUDIX HYDROLASE HOMOLOG 7
NuRD	nucleosome remodelling and histone deacetylation complex

o/n	over night
OD	optical density
PAP1	PRODUCTION OF ANTHOCYANIN PIGMENT 1
PAP2	PRODUCTION OF ANTHOCYANIN PIGMENT 2
PAS	PER/ARNT/SIM
PCR	polymerase chain reaction
PF1	PFIFFERLING
P_{fr}	far-red light absorbing form of phytochrome
Phot	Phototropin
phy	Phytochrome
phyA	PHYTOCHROME A
phyB	PHYTOCHROME B
PIF	PHYTOCHROME INTERACTING FACTOR
PIF1	PHY-INTERACTING FACTOR 1
PIF3	PHYTOCHROME INTERACTING FACTOR 3
PIF4	PHYTOCHROME INTERACTING FACTOR 4
PIF5	PHYTOCHROME INTERACTING FACTOR 3-LIKE
PIF6	PHYTOCHROME INTERACTING FACTOR 3-LIKE 2
PIF7	PHYTOCHROME INTERACTING FACTOR 7
PIMT1	PROTEIN-L-ISOASPARTATE METHYLTRANSFREASE 1
PKS1	PHYTOCHROME KINASE SUBSTRATE 1
p*Met25*	Methionin suppressable promotor
P_r	red light absorbing form of phytochrome
PRD	photolyase related domain
PRD3	PUTATIVE RECOMBINATION INITIATION DEFECTS 3
PRL	PROLIFERA

PRL1	PLEIOTROPIC REGULATORY LOCUS 1
Pro35S	Cauliflower mosaic virus promotor 35S
psi	pound-force per square inch
PSWII	PHOTOSYSTEM II REACTION CENTER W
PTAC	nuclear pore-targeting complex
PVDF	Polyvinylidenfluorid
PYM	POLYCHOME
R	red light
RACE	Rapid Amplification of cDNA Ends
Ran	Ras-related nuclear protein
RanBP1	Ran-binding protein 1
RBCS	*RIBULOSE BISPHOSPHATE CARBOXYLASE SMALL CHAIN*
Rc	constant red light
RCC1	Regulator of chromosome condensation 1
RCD1	RADICAL-INDUCED CELL DEATH 1
rDNA	ribosomal DANN
REGIA	REgulatory Gene Initiative in Arabidopsis
rev	reverse
RfA	reading frame A (Gateway cassette)
RFI	RASZAFARI
RFP	Red Fluorescent Protein
RHL1	ROOT HAIRLESS1
RHL2	ROOT HAIRLESS2
RING	REALLY INTERESTING NEW GENE
RNA	Ribonucleic acid
RNAi	RNA interference

RPP4	RECOGNITION OF PERONOSPORA PARASITICA 4
RT	reverse transcriptase
RUB	Related to Ubiquitin
S	synthesis
S. cerevisiae	*Saccharomyces cerevisiae*
SAM	shoot apical meristeme
SCF	SKIP/CULIN/F-BOX
SD	short day (8h darkness, 16h light)
SD	selective drop out media
SD-LW	selective drop out media lacking leucin and tryptophan
SD-LWH_3	selective drop out media lacking leucin, tryptophan and histidin, supplemented with 3mM 3-AT
SDS-PAGE	sodium dodecyl sulfate polyacrylamide gel electrophoresis
SNLS	subnuclear localization signal
SOPMA	Self Optimized Prediction Method from Alignment
SPA1	SUPPRESSOR OF PHYTOCHROME A-105
SPA2	SPA1-RELATED 2
SPA3	SPA1-RELATED 3
SPA4	SPA1-RELATED 4
SPL11	SQUAMOSA PROMOTOR-LIKE 11
SPY	SPINDLY
sqRT-PCR	semi-quantitative RT-PCR
STDEV	standard deviation
STH	SALT TOLERANCE HOMOLOGUE
STH3	SALT TOLERANCE HOMOLOGUE 3
STO	SALT TOLERANCE

STT3A	STAUROSPORIN AND TEMPERATUR SENSITIVE 3-LIKE A
SUMO	Small Ubiquitin-like Modifiers
sYFPN	N-terminal portion of YFP
SYT	SYNAPTOTAGMIN
TAIR	The Arabidopsis Information Resource
TDET1	Tomato DET1
t-DNA	transfer DNA
tH2B	tomato HISTONE 2B
TL	translational enhancer
TOC1	TIMING OF CAB EXPRESSION 1
TOC159	TRANSLOCON AT THE OUTER ENVELOPE OF CHLOROPLASTS 159
TOPOVI	*A. thaliana* topoismoerasis VI
trans.	transducer
TRIP-1	TGF-BETA RECEPTOR INTERACTING PROTEIN 1
TRY	TRIPTYCHON
TSA	TSK-ASSOCIATING PROTEIN 1
TSI	*TRANSCRIPTIONALLY SILENCING INFORMATION A*
TSK	TONSOKU
TT8	TRANSPARENT TESTA 8
Tub	Tubulin
UBC1	UBIQUITIN CARRIER PROTEIN 1
UBC4	UBIQUITIN CONJUGATING ENZYME 4
UBC8	UBIQUITIN CONJUGATING ENZYME 8
UBC9	UBIQUITIN CONJUGATING ENZYME 9
UBQ10	UBIQUITIN 10
UVR8	UVB-RESISTANCE 8

Abbreviations

VIP3	VERNALIZATION INDEPENDENCE 3
VLFR	very low fluence response
VOZ2	VASCULAR PLANT ONE ZINC FINGER PROTEIN 2
WOL	WOODEN LEG
wt	wildtype
XK2	XYLOSE KINASE 2
Y3H	Yeast Three Hybrid
YFP	Yellow Fluorescent Protein
YTH	Yeast Two Hybrid
ZTL	ZEITLUPE
αHA	anti hemagglutinin tag
αUb	anti Ubiquitin

Nomenclature for photoreceptors:

PHY: gene, wildtypish allele

phy: mutant allele of gene

PHY: apoprotein (without chromophore)

phy: holoprotein (with chromophore)

I. Introduction

1. The perception of light by plants

Plants are sessile and need to optimise their response to changing environmental conditions such as light, temperature, drought, salinity or pathogen attack. Light is not only the primary energy source for a plant (photosynthesis) but also influences the plant`s morphological developmental programme and growth throughout its live cycle.

One of the best studied stages in plant development - the seedling development - exemplifies the outstanding influence of light on plant development (Figure I - 1).

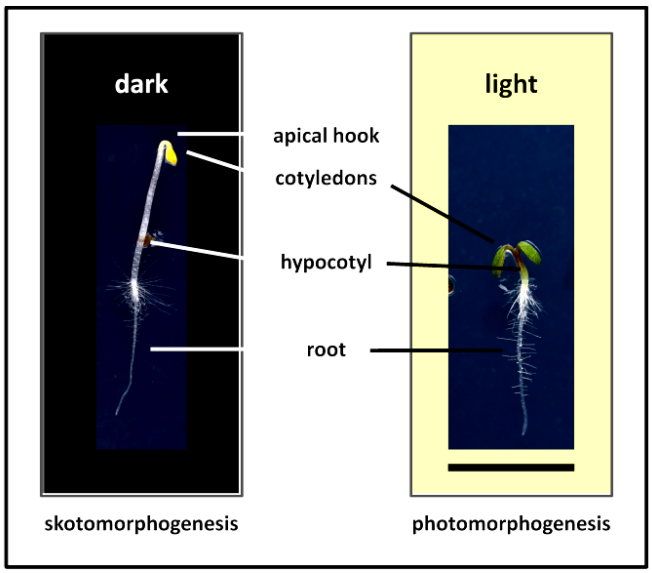

Figure I - 1: Seedling morphogenesis. Dark- and light-grown 3-day-old *Arabidopsis thaliana* (*A. thaliana)* seedlings. In the dark, seedlings exhibit an elongated hypocotyl, open cotyledons and an apical hook (left) whereas in the light the hypocotyl is short, the cotyledons are open and no apical hook is visible. Bar equals 5 mm.

In the dark, seedlings mobilise their energetic resources predominantly for hypocotyl elongation neglecting the root and cotyledon development. They exhibit an apical hook protecting the meristematic region and the unfolded cotyledons while allowing the seedling a facilitated pass through soil. Proplastide development results in etioplasts that lack chlorophyll. This developmental process is named skotomorphogenesis (*skotos* griech.: darkness) or etiolation. Light grown seedlings undergo photomorphogenesis or de-etiolation. The seedlings have a short hypocotyl, open cotyledons, a normal root development and proplastids develop to chloroplasts. In addition, the seedlings produce anthocyanin that protects the cells from high light damage (Takahashi et al.,

1991). Skotomorphogenesis allows plants to emerge through soil, whereas photomorphogenesis equips the plant with a morphology optimised for photosynthesis. (Fankhauser and Chory, 1997)

Plants do not only react to the presence or absence of light, but also to light quality, quantity, direction and duration. In order to detect the different light wavelength within the spectral range, plants have evolved several classes of photoreceptors. In *Arabidospis thaliana* (*A. thaliana*), red (R) and far-red light (FR) (600-750nm) is percieved by phytochromes (phy), blue (B) and UV-A light (320-500nm) by cryptochromes (cry), phototropins (phot) and zeitlupe (ztl)/flavin binding, kelch repeat, f-box (fkf1)/lov (light, oxygen, voltage-regulated proteins)-kelch protein2 (lkp2) proteins. A receptor for UV-B (282-320nm) has been shown to exist but has not been identified, yet. (Briggs and Christie, 2002; Briggs and Huala, 1999; Imaizumi et al., 2003; Kendrick and Kronemberg, 1994)

1.1. Phytochromes

Phytochromes are by far the most-studied photoreceptors in plants. The chromophore phytochromobilin - a linear tetrapyrrol - is covalently attached to the ~125 kDa apoprotein (Rudiger et al., 1983; Vierstra and Quail, 1983). The phy holoprotein can act as a Ser/Thr kinase in plants with two histidine kinase-related domains (HKRD) in its C-terminal half (McMichael and Lagarias, 1990; Schneider-Poetsch et al., 1991; Yeh and Lagarias, 1998). The first HKRD contains two PER/ARNT/SIM (PAS) domains that have been shown to mediate protein-protein interactions and ligand binding (Lagarias et al., 1995; Taylor and Zhulin, 1999).

The bilin chromophore is utilised for the light absorption and the reversible photoconversion between two forms, P_r and P_{fr}. The inactive, R absorbing P_r form accumulates in the dark. Absorption of R leads to a conformational change to the active, FR absorbing P_{fr} form that can be converted back to the P_r form by FR. The switch itself has been proposed as a short-lived signal. (Reed, 1999; Rockwell et al., 2006; Shinomura et al., 2000)

There are five different phytochromes in *A. thaliana*, phyA-phyE (Clack et al., 1994; Sharrock and Quail, 1989). These can be grouped in Type I (light labile, phyA) or Type II (light stable, phyB-D) phytochromes (Clack et al., 1994). PhyA dimerises only with itself whereas type II phytochromes can heterodimerise (Clack et al., 2009; Sharrock and Clack, 2004).

Four modes of phy response have been distinguished: very low fluence response (VLFR) after light pulses or constant irradiation (phyA), low fluence response (LFR) characterised by the reversible

response to R/FR at low light intensities (phyB), R (phyB) and FR (phyA) high irradiance response (HIR) that are dependent on duration and intensity of irradiation.

After perception of light, the signal needs to be transduced. Transcription factors are at the end of this signalling cascade. They bind to light-responsive elements (LRE, *cis*-regulative elements) of light regulated genes and activate or repress their expression. 10-30% of the *A. thaliana* genes are regulated by light (Ma et al., 2001; Tepperman et al., 2001). Light-activated phytochromes relocalise to the nucleus (Kircher et al., 2002; Kircher et al., 1999; Nagatani, 2004; Sakamoto and Nagatani, 1996). Phytochromes can physically interact with basic helix-loop-helix (bHLH) transcription factors, the PHYTOCHROME INTERACTING FACTORS (PIFs; Duek and Fankhauser, 2005: Monte et al. 2007). As a consequence of interaction with phytochromes e.g. PIF3 is phosphorylated and degraded via the 26S proteasome (Al-Sady et al., 2006; Bauer et al., 2004; Park et al., 2004). PIF3 can in turn lead to the turnover of the phytochrome photoreceptor (Al-Sady et al., 2008).

1.2. Cryptochromes

Most plant cryptochromes exhibit a sequence similarity to photolyases within their N-terminal photolyase related domain (PRD) and are characterised by a distinguishing C-terminal domain that is not present in photolyases (Cashmore et al., 1999). Photolyases mediate repair of UV-damaged DNA (Sancar, 1994). Similar to photolyases, cry1 contains a flavin and a pterin (methenyltetrahydropholat, MTHF) chromophore but does not show photolyase activity (Lin et al., 1995; Malhotra et al., 1995). Three cryptochromes have been identified whereas CRY1 and CRY2 share a high similarity, CRY3 lacks the C-terminal extension and has signal sequences directing it to chloroplasts and mitochondria. The function of CRY3 is presently unknown. Cry1 and cry2 localise to the nucleus (Cashmore et al., 1999; Kleiner et al., 1999) and regulate gene expression (Ma et al., 2001; Somers et al., 1998; Wang et al., 2001). Cry2 interacts with the transcription factor CRYPTOCHROME-INTERACTING BASIC-HELIX-LOOP-HELIX 1 (CIB1; Liu et al. 2008a). Cry1 has been shown to be activated by phosphorylation that, at least in part, is self-mediated (Bouly et al., 2003; Shalitin et al., 2003). Recently, new evidence for a synergism of R and B in gene expression and development via co-action of phyB and cryptochromes has been reported (Ahmad et al., 1998; Sellaro et al., 2009). Cry1 is known to be phosphorylated by phyA in vitro and phosphorylation is induced in R and suppressed in FR (Ahmad et al., 1998). CRY1 has not only been shown to interact with phyA but also with ZTL that itself interacts with phyB thereby probably integrating different light qualities (Jarillo et al., 2001).

1.3. Phototropins

Characterization of a mutant defective in phototropic response (*nonphototropic hypocotyl1* (*nph1*)) identified phototropin1 (phot1), a 996 amino acid (aa) protein with two LOV domains and a Ser/Thr kinase domain at its C-terminus (Huala et al., 1997). Each LOV domains binds one chromophore flavin mononucleotide (FMN; Christie et al., 1999). Phot1 can undergo autophosphorylation (Christie et al., 1998). A second phototropin has been identified by sequence similarity (phot2; Kagawa et al., 2001; Sakai et al., 2001). It binds the same chromophore and exhibits similar activities as phot1. Interestingly phot1 interacts with PHYTOCHROME KINASE SUBSTRATE 1 (PKS1) that also has been shown to interact with phyA and phyB (Fankhauser et al., 1999; Lariguet et al., 2006).

1.4. ZTL/FKF1/LKP2 family

The three proteins of the ZTL, FKF1, and LKP2 family share an N-terminal LOV domain binding FMN, an F-box motif and six Kelch repeats at the C-terminus (Imaizumi et al., 2003). The F-box is known to interact with an E2-E3 ubiquitin complex and the Kelch motif can form a β−propeller that is known to serve for protein-protein interaction (Adams et al., 2000; Xiao and Jang, 2000). The ZTL family proteins show very slow dark reversion of FMN (Imaizumi et al., 2003). Data in support of photoreceptor activity have been obtained for FKF1 (Imaizumi et al., 2003; Zikihara et al., 2006). FKF1 targets CYCLING DOF FACTOR 1 (CDF1), a repressor of CONSTANS (CO), and thereby is involved in the circadian clock regulation (Imaizumi et al., 2005).

2. CONSTITUTIVE PHOTOMORPHOGENIC 1 (COP1)

The *cop*/ *de-etiolated* (*det*) / *fusca* (*fus*) group of mutants have been isolated due to their phenotype in the dark showing all aspects of photomorphogenesis: short hypocotyls, open cotyledons, etioplasts that develop into chloroplasts, anthocyanin accumulation and up-regulation of light responsive genes (Chory et al., 1989; Deng et al., 1991).

Due to the recessive nature of the *cop*/*det*/*fus* mutants it can be concluded that *COP*/*DET*/*FUS* encode factors that suppress photomorphogenesis or promote skotomorphogenesis. As representatives of these three different loci *cop1*, *det1* and *cop9* have excessively been analysed and genetic interactions revealed that the activity of *HY5* and *HFR1* is down-regulated by *COP*/*DET*/*FUS* (Ang and Deng, 1994; Kim et al., 2002; Pepper and Chory, 1997). In the light, phytochromes and cryptochromes mediate the stabilisation of HY5, whereas it is destabilised in the dark. In contrast,

HY5 accumulates in *cop*/*det*/*fus* mutants. (Osterlund et al., 2000a; Osterlund et al., 2000b) Deng and coworkers (1992) cloned the *COP1* locus. COP1 has also been identified in other eukaryotes than plants e.g. in human (Wang et al., 1999). In *A. thaliana,* it is ubiquitously expressed at comparatively high levels in all tissues and developmental stages of the plant except pollen, sperm cell and the endosperm of the seed (genevestigator data, Hruz et al., 2008; Schmid et al., 2005). There is no significant difference of *COP1* mRNA and protein levels between light and dark grown seedlings (Deng et al., 1992; Zhu et al., 2008). The abundance of COP1 in the nucleus is regulated by nucleocytoplasmic partitioning with an accumulation of COP1 in the nucleus in darkness and a slow depletion from the nucleus in the light (von Arnim and Deng, 1994; von Arnim et al., 1997).

One of the most intense analysed transcription factors regulating light-dependent gene expression is ELONGATED HYPOCOTYL 5 (HY5). HY5 is involved in red, far-red, blue and UV-B signalling and can directly bind to the LREs in promoters of light responsive genes like *CHALCONE SYNTHASE* (*CHS*; Chattophadyay et al. 1998; Oyama et al., 1997; Ulm et al., 2004). There is no evidence for a physical interaction with one of the photoreceptors. The same holds true for LONG HYPOCOTYL IN FAR-RED1 (HFR1) and LONG AFTER FAR-RED LIGHT1 (LAF1). Therefore, there have to be factors regulating these transcription factors' activity acting downstream of the photoreceptors and upstream of the transcription factors.

2.1. COP1 domains

The COP1 protein harbours a RING (REALLY INTERESTING NEW GENE) motif at its N-terminus, followed by a coiled coil domain and a WD40 domain at its C-terminus. (Deng et al., 1992; McNellis et al., 1994; von Arnim and Deng, 1993; Figure I-2).

RING motifs are found in E3 ubiquitin ligases transferring ubiquitin to a target protein. The modification takes place in a three-step reaction starting with the activation of ubiquitin that is subsequently conjugated to an E2 enzyme and finally transferred to a substrate targeted by an E3 ligase (Hershko and Ciechanover, 1998). Poly-ubiquitylation has been identified as a signal for proteasomal dependent degradation (Hough et al., 1987; Waxman et al., 1987). COP1, as an E3 ubiquitin ligase, physically interacts with and poly-ubiquitylates a number of target proteins such as HY5, HFR1, LAF1, EARLY FLOWERING 3 (ELF3; Ang et al., 1998; Chen et al., 2010; Duek et al., 2004; Hardtke et al., 2002; Jang et al., 2005; Lau and Deng, 2009; Osterlund et al., 2000a; Saijo et al., 2003; Seo et al., 2003; Suzuki et al., 2002; Yanagawa et al., 2004; Yu et al., 2008). ELF3 is a clock-associated gene that is involved in the circadian gating pathway (Hicks et al., 1996; McWatters et al., 2000; see I.

3.5). Taken together, it can be concluded that COP1 labels its targets for proteasomal degradation by taking part in their poly-ubiquitylation.

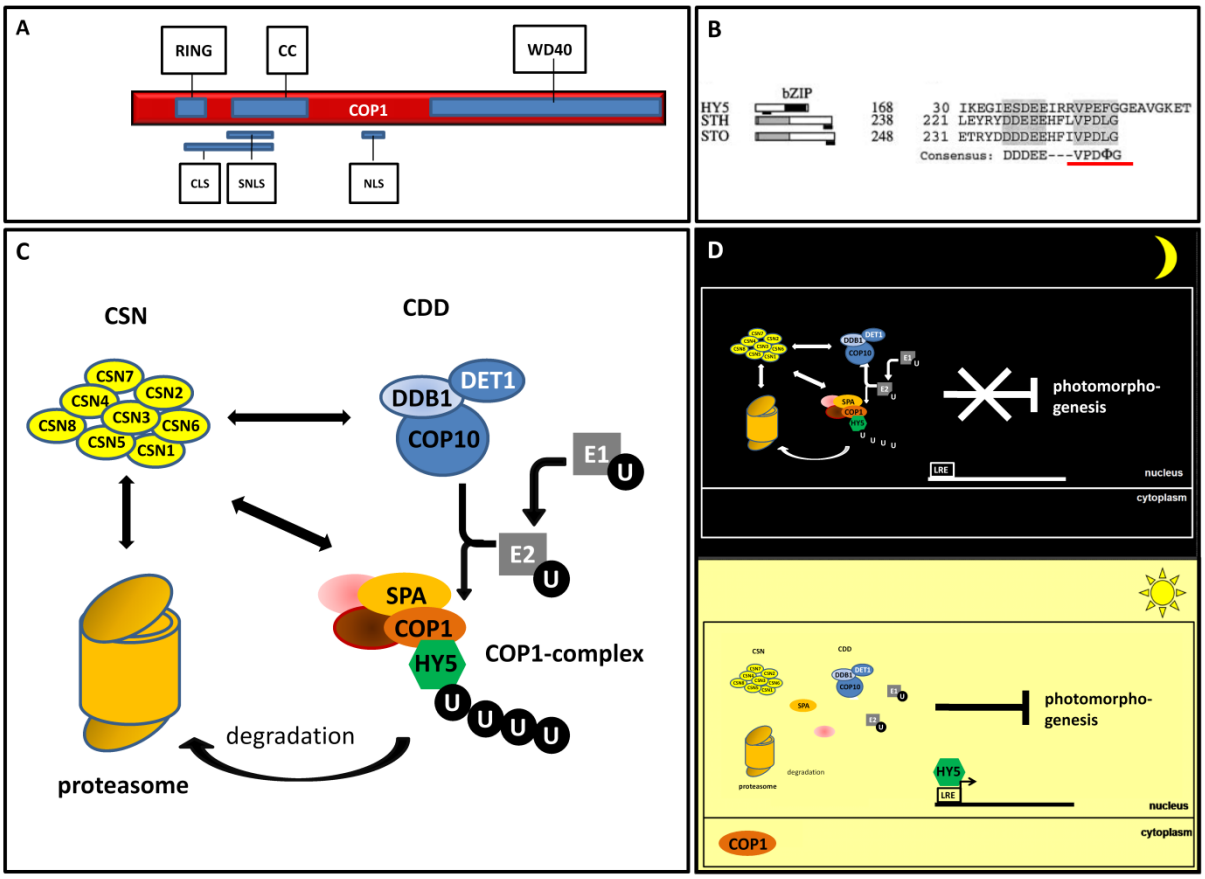

Figure I - 2: The COP1 protein: domains, conserved interaction motif, complexes and nucleocytoplasmic partitioning. **(A)** Schematic representation of the COP1 protein domains. RING: REALLY INTERESTING NEW GENE, CC: coiled coil domain, WD40: WD40 domain, CLS: cytoplasmic localisation signal, SNLS: subnuclear localisation signal, NLS: nuclear localisation signal. **(B)** Conserved motif in HY5, STO, STH, targets of COP1, that - when mutated - prevents the interaction with COP1 in yeast. Lys^{550} of COP1 is essential to constitute a salt bridge with the Asp or Glu of the core conserved motif (underlined with red). Modified from Holm et al., 2001. **(C)** COP1-dependent proteolytic degradation is mediated by four complexes in the nucleus. CDD enhances E2 activity. COP1 as an E3-ligases is part of larger complexes of different compositions containing SPA proteins. The complex polyubiquitylates HY5. HY5 is subsequently degraded by the proteasome. CSN1 has been shown to be essential for the nuclear localisation of COP1 (Wang et al., 2009). Components of all complexes have been shown to interact. CDD: CONSTITUTIVE PHOTOMORPHOGENIC 10, UV-DAMAGE DNA-BINDING PROTEIN (DDB1), DE-ETIOLATED1 (DET1); CSN: COP9-signalosom. Modified from Laubinger (2006). **(D)** Nucleoplasmatic partitioning regulates the COP1-dependent suppression in darkness (upper picture) and the absence or reduction of this suppression in the light due to the cytoplasmic localisation of COP1. Proteins are the same as in (C).

All three described domains of COP1 interact with other proteins but specifically WD40 domains often serve as an interaction platform for protein-protein interactions. The WD40 domain of COP1 (amino acids 374-670) consists of seven WD40 repeats with a total number of 28 predicted β-sheets which most likely fold as a seven bladed β-propeller (Holm et al., 2001; Sondek et al., 1996). HY5, STO, STH and homologues of HY5 from tomato, soybean and fava bean share a conserved interaction motif "with the core sequence V-P-E/D-Φ-G (Φ = hydrophobic residue) in conjugation with an

upstream stretch of 4-5 negatively charged residues" (Holm et al., 2001; Figure I-2). Holm and coworkers (2001) could show that a salt bridge between an aspartate or glutamate located in the conserved motif of SALT TOLERANCE (STO), STO HOMOLOG (STH) or HY5 and Lys^{550} of COP1 is necessary for the interaction with COP1.

2.2. COP1 acts in multi-subunit complexes

SPA1 (SUPPRESSOR OF PHYA-105 1) and COP1 interact *in vivo*. The interaction has been mapped to the coiled coil domain of both proteins that also mediates the self-association of COP1 (Hoecker et al., 1999; Torii et al., 1998). Seo and coworkers showed that COP1 ubiquitylates LAF1 more efficiently in the presence of SPA1. SPA1 fine-tunes the COP1-dependent degradation by co-acting with COP1 in high-molecular-weight complexes (Saijo et al., 2003; Saijo et al., 2008; Zhu et al., 2008). There are three SPA1-like proteins in *A. thaliana* SPA2, SPA3 and SPA4 (SPA1-RELATED 2-4) that also share complexes with COP1 and contribute to the degradation of HY5 (Zhu et al., 2008). Single mutants of the corresponding genes cause only weak or no phenotypical effect (e.g. spa1 mutants show only differences in R, FR and under short day (SD) conditions) whereas the quadruple mutant exhibits a strong *cop1*-mutant phenotype. SPA-family proteins respond partially redundant to light in seedling and adult stages (Ishikawa et al., 2006; Laubinger et al., 2004; Laubinger and Hoecker, 2003; Laubinger et al., 2006). It can be concluded that SPA-family proteins and COP1 act in concert to suppress photomorphogenesis (Baumgardt et al., 2002; Hoecker and Quail, 2001; Laubinger and Hoecker, 2003; Zhu et al., 2008).

The CDD (CONSTITUTIVE PHOTOMORPHOGENIC 10, UV-DAMAGE DNA-BINDING PROTEIN (DDB1), DE-ETIOLATED1 (DET1)) complex and COP9-signalosom (CSN) are involved in the modulation of COP1 activity (Chen et al., 2006; Nixdorf and Hoecker, 2010; Yanagawa et al., 2004). COP1 binds to COP10 via the RING domain. It has been shown that COP10 activates E2 ligase activity and binds itself to DET1 and UV-DAMAGE DNA-BINDING PROTEIN 1A (DDB1A) forming the small CDD complex (Suzuki et al., 2002; Yanagawa et al., 2004). Other proteins from the COP/DET/FUS group form the CSN that seem to directly interact with the proteasome and is also essential for the SCF (SKIP/CULIN/F-BOX) E3-ligases mediated degradation (Kwok et al., 1999; Peng et al., 2003; Serino and Deng, 2003; von Arnim, 2003).

According to genetic evidences and complex formation with other COP1 regulators, DET1 is thought to act upstream or in concert with COP1 (Ang and Deng, 1994; Chen et al., 2010; Chen et al., 2006; Nixdorf and Hoecker, 2010; Yanagawa et al., 2004). DET1 is not only a nuclear *A. thaliana* protein but

also a mammalian protein with conserved sequence. Mammalian DET1 modulates Cul4 (Cullin4) activity, to form a stable complex with E2 ubiquitin conjugating enzyme and associates with DDB1. The latter interacts with histone acetyltransferase complexes in mammalia. In plants, DET1 selectively binds to the nonacetylated N-terminus of histone H2B (Benvenuto et al., 2002) indicating an acetylation-dependent transcriptional regulation of light-activated genes. There is also evidence for COP1 to be involved in chromatin dependent processes. Brown and coworkers (2005) showed that UVB-RESISTANCE 8 (UVR8) associates with chromatin. COP1 interacts with UVR8 as was shown by BiFC (bimolecular fluorescence complementation) and Co-IP (Co-immunoprecipitation; Favory et al., 2009). UV-B induced *HY5* and *CHS* transcription requires UVR8 and COP1 and in contrast to the situation under other light conditions, the COP1-mediated HY5 degradation is reduced under UV-B light (Favory et al., 2009). COP1 is highly conserved throughout the plant kingdom and also human COP1 (hCOP1) shares all three domains of AtCOP1 and acts in an E3 ubiquitin ligase complex mediating the degradation of transcription factors and oncogenes like p53 and c-Jun (Dornan et al., 2004; Wertz et al., 2004). In humans, COP1 also regulates the stability and function of MTA1 (Metastasis-associated protein 1), a component of the nucleosome remodelling and histone deacetylation complex (NuRD; Li et al., 2009).

Taken together, all three types of complexes - COP1-SPA-complexes, CDD and CSN - are essential regulators of the light and proteasomal dependent degradation pathway in *A. thaliana*. (Figure I-2)

2.3. COP1 interacts with photoreceptors

COP1 physically interacts with the photoreceptors phyA, phyB, cry1 and cry2 (Seo et al., 2004; Wang et al., 2001; Yang et al., 2001). Degradation of photoreceptors by light provides the plant with a protection against hyperresponsiveness to light. PhyA is activated by light and localises FHY/FHL-dependend to the nucleus. In the nucleus it transduces the signal possibly by phosphorylating targets of COP1 in a COP1-SPA1-phyA complex (Al-Sady et al., 2006; Hiltbrunner et al., 2006). PhyA itself preferably associates in a phosphorylated form with the COP1/SPA complex whereas the unphosphorylated form predominantly associates with FHY3 and FHY1 (Saijo et al., 2008). Finally, phyA is degraded by COP1-dependent ubiquitylation via the proteasomal dependent degradation pathway (Seo et al., 2004). Cry1 and cry2 interact in darkness and light with COP1 (Wang et al., 2001). Light induces homodimerisation of the cryptochromes via their N-terminus, and plants expressing constitutive dimers of the cryptochromes or overexpressing the C-termini of CRY1 or CRY2 (CCT1 or CCT2), respectively, exhibit a constitutive photomorphogenic phenotype (Sang et al., 2005). Therefore, homodimers of cry1 and cry2 inhibit COP1-activity by physical interaction with COP1. B

and R mediated signalling overlaps. An involvement of *SPA1* and *SPA4* in the crosstalk of blue and red light responses in *A. thaliana* concerning hysteresis has been shown recently (Sellaro et al., 2009).

2.4. Nucleocytoplasmic partitioning of COP1

Similar to phyA, COP1 is regulated by nucleocytoplasmic partitioning of the protein (Figure I-2). GUS (beta-glucuronidase) fusions are depleted from the nucleus in the light but this process is slow. After 24h of light treatment, there is still GUS-signal visible in the nucleus that disappears after 36 h (von Arnim et al., 1997). Three amino acid motifs for subcellular COP-localisation have been identified: a NLS (nuclear localisation signal), a CLS (cytoplasmic localisation signal) and a subnuclear localisation signal (SNLS, residues 120-177) enabling COP1 to localise to subnuclear foci (Stacey et al., 1999; Stacey and von Arnim, 1999; Figure I-2). Localisation to subnuclear foci is also characteristic for SPA1 and for proteins interacting with COP1 e.g. tanscription factors that are degraded by COP1 and localise to subnuclear foci in the presence of COP1 (Zhu et al., 2008).

Stacey and coworkers (1999) identified a bipartide NLS located between the coiled coil and WD40 domain spanning the base pairs 290 and 317. This bipartite NLS is counteracted by a CLS (residues 67-177) in a light dependent manner (Von Arnim and Deng, 1996). Nuclear exclusion and dimerisation of COP1 correlates (Subramanian et al., 2004). Although the nuclear exclusion is comparably slow (von Arnim et al., 1997) Subramanian and coworkers (2004) conclude that COP1 is depleted from the nucleus by CLS-driven export and not by nuclear turnover. Other probably photoreceptor-dependent regulation is needed to quickly deactivate nuclear COP1 in response to light. CIP1 (COP1-INTERACTIVE PROTEIN 1, a cytoskeleton associated protein) and the CSN component CSN1 have been shown to physically interact with COP1 and to regulate the nucelocytoplasmic partitioning of COP1. The core CLS has been determined to residues 105-177 of COP1 (Matsui et al., 1995). The CLS and SNLS overlap, suggesting that masking by conformational change and interaction with different regulating proteins define the function of the region. In rice, Importin α 1b has been identified to preferentially mediate the nuclear import of COP1 (Jiang et al., 2001). In human, DNA damage triggers ATM phosphorylation of hCOP1 and stimulates a rapid autodegradation mechanism. ATM-dependent movement of hCOP1 from the nucleus to the cytoplasm is induced by ionising radiation (Dornan et al., 2006).

3. Photoreceptor-regulated morphogenesis

Light perception by the photoreceptors has specific but also overlapping influence on the morphogenesis of different developmental stages of *A. thaliana* (Figure I - 3).

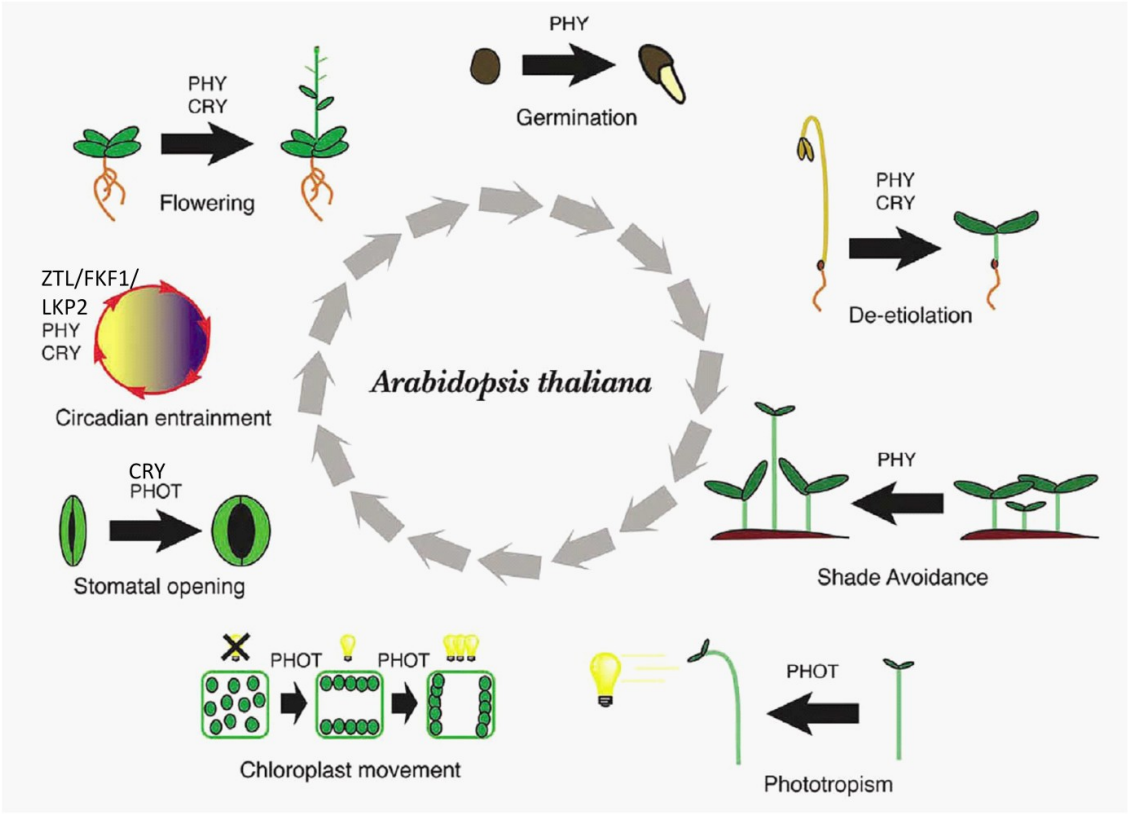

Figure I - 3: Photoreceptor-regulated development in *A. thaliana*. Light regulates the development of plants throughout their life-cycle. Light, perceived by photoreceptors, has specific and overlapping influence on the morphogenesis of *A. thaliana*. PHY: phytochrome; CRY: cryptochrome, PHOT: phototropin. Modified after Sullivan and Deng, 2003.

3.1. Germination

Seeds can stay dormant in a dry state when the environment is not optimal for germination (Koornneef et al., 2002). Experiments with Grand Rapids lettuce seeds showed that an alternating R/FR treatment of the seeds with a last FR pulse reduced the germination efficiency but with a last R pulse approximately 100 % of the seeds germinated (Borthwick et al., 1952). This was the first evidence for phytochromes acting in the LFR mode. Light induced germination is regulated by phytochromes (Franklin and Quail, 2010). Germination is mediated by phyB in R/FR LFR and by phyA in FR VFLR and FR HIR (Botto et al., 1996; Johnson et al., 1994; Reed et al., 1994; Shinomura et al., 1996). According to genetic analysis, phyE is also involved in germination (Hennig et al., 2002). At lower temperatures (16°C) phyE seems to be more active or abundant than phyB that predominantly

controls germination at higher temperatures (22°C, Heschel et al., 2007). Recently, Leivar and coworkers (2008) reported a pre-germination effect of light on seedling development due to photoactivated phytochromes in P_{fr} form in the embryo that can subsequently inhibit de-etiolation response during growth in darkness via PIF-regulation. *Pif* mutant have a mild constitutive phenotype that is not FR reversible or present in *phyB* mutant background. It is discussed that this might be a stored light-induced signal initiated in the seed during maturation while on the maternal plant (Magliano and Casal, 2004).

3.2. Photomorphogenesis

The periode that has been analysed most excessively comprises of the development between the germination and the formation of the first true leaves (Quail, 2002). Depending on the light conditions, the seedling follows skoto- or photomorphogenesis (see Figure I - 1). De-etiolation is complex regulated by phytochromes and cryptochromes (Franklin and Quail, 2010). In the dark skotomorphogenesis is maintained by the action of the COP1-SPA1 E3-ligases degrading photomorphogenesis-specific transcription factors. Additionally a regulation by PIF transcription factors has recently been reported essential for the switch between skoto- and photomorphogenesis. PIFs preferentially bind to the P_{fr} form of phytochromes, are phosphorylated and subsequently degraded in a rapid response (Al-Sady et al., 2006; Bauer et al., 2004; Nozue et al., 2007; Shen et al., 2008; Shen et al., 2007). In a feedback loop phyB is degraded (Al-Sady et al., 2008). Genetic analysis revealed that PIFs (PIF1, PIF3, PIF4, PIF5) sustain the skotomorphogenesis (Leivar et al., 2008). At low light intensities (VLFR) phyA regulates the de-etiolation. Increasing light intensities render phyA inactive and regulation by phyB and cryptochromes is dominant (Fankhauser and Chory, 1997).

The same holds true for another aspect of photomorphogenesis, the inhibition of hypocotyl elongation. The shorter hypocotyls in photomorphogenesis correlate with the inhibition of the third endocycle (that is the duplication of DNA without cell division) of hypocotyl epidermal cells mediated by phyA (Gendreau et al., 1998). Maximal suppression was achieved in FR and a lower extend was observed in R, pointing to a minor involvement of phyB. *Cry* mutants exhibited a longer hypocotyl than the wild type but had no increased C-contents (nuclear DNA content; Gendreau et al., 1997).

Other factors than light are also involved in de-etiolation as there are auxin, cytokinin, brassinosteroid, abscisic acid and ethylene (Nemhauser, 2008).

3.3. Shade avoidance, phototropism, chloroplast movement and stomatal opening

After emerging from soil, the seedling and adult plant show several responses to light. The phytochrome regulated shade avoidance response is necessary when plants compete for light because they grow in close proximity to each other. Leaves selectively absorb R reducing the R/FR ratio below them with a higher proportion of FR (Casal et al., 1997; Devlin et al., 1998; Devlin et al., 1999).

Plants exhibit phototropism. They position their organs by directional curvature in response to light. Phototropism is predominantly regulated by phototropins (Jarillo et al., 2001; Liscum and Stowe-Evans, 2000; Sakai et al., 2001).

Chloroplasts, the sites of photosynthesis, accumulate under low light conditions on the upper surface of the palisade mesophyll cells for optimal photosynthesis rates. At higher light intensities they move to the sides of these cells avoiding the light for protection against photodamage. Chloroplast movement is a blue light response mediated by phot1 and phot2 (Briggs and Christie, 2002; Jarillo et al., 2001; Kagawa and Wada, 2002; Kasahara et al., 2002; Sakai et al., 2001).

The two stomata guard cells control the opening of the pore that is surrounded by them by swelling and shrinking. Stomata opening is regulated by B. Phot1, phot2, cry1 and cry2 were identified as the involved photoreceptors (Briggs and Christie, 2002; Kinoshita et al., 2001; Mao et al., 2005).

3.4. Plant architecture

During vegetative development, phyB suppresses petiole elongation and apical dominance in light-grown plants. *PhyB* mutants have a reduced leaf area (Reed et al., 1993).

3.5. Circadian clock and flowering

A. thaliana flowers under long day conditions. Plants can perceive the daylength and thereby develop according to the annual season (Yanovsky and Kay, 2002). The underlying mechanism is the circadian clock. It includes three major components: (1) the input pathway synchronising the clock according to the daily light-dark cycle, (2) the central oscillator generating a 24h time-keeping mechanism, and (3) an output pathway. (McClung, 2001; Roenneberg and Merrow, 2000)

Clock resetting is mediated by ZTL/FKF1/LKP2 family proteins (Nelson et al., 2000; Schultz et al., 2001; Somers et al., 2000; and Figure I - 4-A). Blue light stabilises ZTL-GI (GIGANTEA) and FKF-GI

interactions that in turn stabilise the floral repressors CDF1 (CYCLING DOF FACTOR 1) and TOC1 (TIMING OF CAB EXPRESSION 1). GI is a clock-associated protein oscillating in expression and protein levels with the clock. (David et al., 2006; Fowler et al., 1999; Imaizumi et al., 2005; Kim et al., 2007; Mas et al., 2003; Sawa et al., 2007)

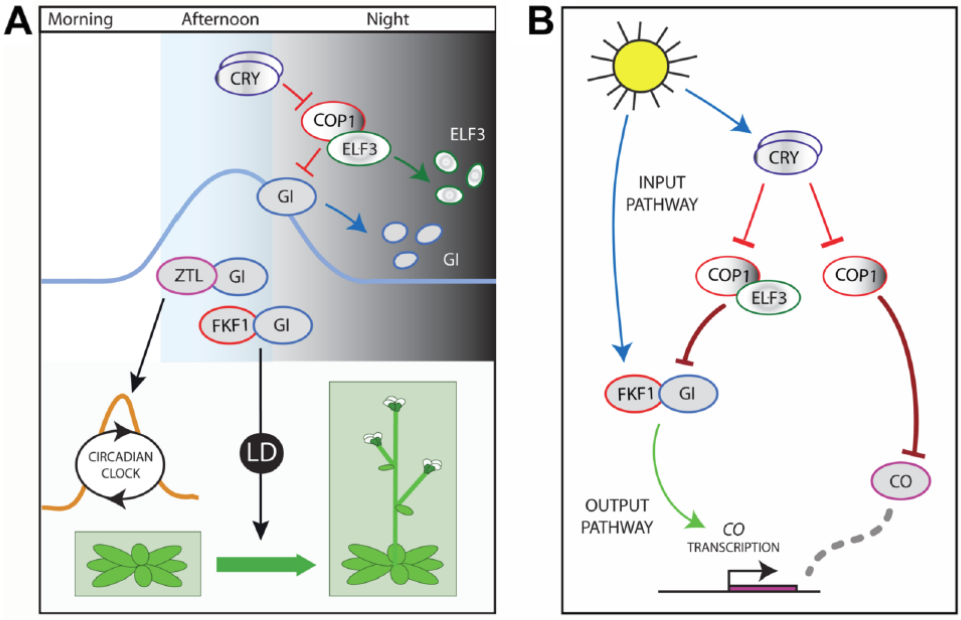

Figure I - 4: Control of flowering time and circadian function involving COP1 and ELF3. **(A)** Modulation of GI activity. ELF3 assisted degradation of GI by COP1 and degradation of ELF3. CRY dimers inhibit COP1 activity. **(B)** Regulation of CO on the transcriptional (FKF1/GI) and posttranslational (COP1) level. CRY dimers inhibit COP1 activity. See text for details. Figure 7 from Yu et al. 2008.

Phytochromes and cryptochromes act in the input pathway. *Cry1* mutants have a longer period length relative to wild-type in low and high intensity blue light whereas *cry2* only shows slight changes concerning period length under low intensity blue light (Somers et al., 1998). CRY1 and CRY2 act redundant in B input to the clock. Cryptochromes and phyB antagonise each other concerning the stability of CO (CONSTANS). CRY1 is required for phyA signalling to the clock in R and FR that includes the modulation of COP1 activity (Devlin and Kay, 2000; Liu et al., 2008b). CO mRNA abundance is regulated by the clock, accumulating late in the day under LD (long day) conditions (Suarez-Lopez and Coupland, 1998). In addition, CO is posttranslationally regulated probably by the COP1-SPA1 E3-ligase complex (Ishikawa et al., 2006; Jang et al., 2008; Laubinger et al., 2006; Liu et al., 2008b; see also Figure I - 4-B). Cryptochromes enhance CO stability whereas phyB promotes CO degradation (Valverde et al., 2004). CO as well as CRY2-CIB1 (CRYPTOCHROME-INTERACTING BASIC-HELIX-LOOP-HELIX 1) activate FT (FLOWERING LOCUS T) transcription. FT is a florigene that moves to the shoot

apex to promote flowering. (Kardailsky et al., 1999; Kobayashi et al., 1999; Liu et al., 2008a; Suarez-Lopez and Coupland, 1998; Yanovsky and Kay, 2002)

Gating (restricted clock responsiveness) is mediated by ELF3 (EARLY FLOWERING 3). ELF3 serves as an adaptor for COP1 - mediated ubiquitylation of GI. Flowering is repressed and the clock is desensitised to light signals after dusk by reducing the abundance of ZTL-GI and FKF1-GI. In a feed-back loop ELF3 is degraded by COP1. (Yu et al., 2008)

An effect of temperature on photoreceptor controlled flowering has been reported. At 22°C *phyB* mutants flower earlier than the wild type. This is not the case at 16°C and this seems to be due to the fact that phyE adopts a dominant role in cooler conditions. (Goto et al., 1991; Halliday et al., 2003; Halliday and Whitelam, 2003; Reed et al., 1993; Whitelam and Smith, 1991)

4. COP1-controlled morphogenesis

Light signals perceived by different photoreceptors regulate COP1 activity leading to crosstalk between the different photo-receptor-dependent signal-transductions pathways. On the molecular level the COP1-dependent signal-transduction is predominantly reduced to its E3-ligase-function in degradation of light-induced transcription factors that bind to LREs. The function of COP1 is mirrored in the *cop1* lack-of-function mutant morphogenic phenotype.

Strong *cop1* mutants - *cop1-1* and *cop1-8* - have been shown to exhibit a germination defect with a maximal effect by FR and R/FR treatment, indicating that the normal phytochrome mediated control of germination is present in *cop1* mutants seeds (Deng et al., 1991). Mutants carrying a strong allele are adult lethal (McNellis et al., 1994). The morphogenesis of dark grown *cop1* mutant seedling shows all aspects of photomorphogenesis: The mutants exhibit a short hypocotyl, open and enlarged cotyledons that also resemble light grown cotyledons on the cellular level, no apical hook, plastid morphology of light-grown seedlings, anthocyanin accumulation, constitutive expression of light regulated genes (Deng et al., 1991), differentiated cotyledon epidermal cells showing characteristic light-grown lobing, open developed stomata (Deng et al., 1992; Mao et al., 2005), reduced endoreduplication in hypocotyl cells that is controlled by phytochromes (Gendreau et al., 1998) and DNA-single or double strand breaks (Dohmann et al., 2008). They can develop their first true leaves and even flower when grown in the dark (Nakagawa and Komeda, 2004). The genome of light-grown *cop1* mutants shows an exaggerated light response correlating with an exaggerated photomorphogenic development of the mutants. *Cop1* mutants in the vegetative state have short

leaves and petioles, a changed leaf-index, a smaller leaf area, no trichome defect has been reported and they flower early under LD and SD conditions as they lack the COP1-mediated posttranslational down-regulation of CO (Jang et al., 2008; Liu et al., 2008b; Yu et al., 2008).

5. Aim of this work

Several aspects of photomorphogenesis are regulated not only by light alone. The hypocotyl elongation is promoted and inhibited by several factors. Beside light these are several plant hormones like cytokinin, auxin, brassinosteroid, absisic acid or ethylene (Nemhauser, 2008). In turn, *cop/det/fus* mutants do not only affect light-regulated genes but also diverse groups of different signal transduction pathways (Mayer et al., 1996). Due to the pleiotropic and specially plant organ size defective phenotype of *cop/det/fus* mutants it is surprising that only little is known about a probable involvement of COP1 in cell cycle regulation. This motivated the expectation that more factors need to exist that regulate the activity of COP1.

This work aimed at the identification of regulators of COP1-controlled morphogenesis in *A. thaliana* to achieve a more general understanding of the function of COP1. The vegetative growth arrest of *cop1* mutants, the role of COP1 concerning the cell cycle and the molecular factors regulating the nucleocytoplasmic partitioning of COP1 exemplify aspects of COP1 function and regulation that are poorly understood until now. Based on a Yeast-Two-Hybrid (YTH)-screening approach, intelligent strategies should be developed to select appropriate candidates according to their predicted COP1-related function *in planta* - being a target, co-factor or regulator of COP1. Subsequently the interaction with COP1 should be verified *in planta* and analysed in regard to its functional relevance. Finally, the question should be answered if, and in which extend, the identified regulators can contribute to dissecting or diversifying COP1-controlled morphogenesis and development in *A. thaliana*.

II. Material and Methods

1. Material

1.1. Water and sterilisation

Bi-distilled water was used for all solutions that were autoclaved or filter sterilised. DEPC-treated water was kept under a hood overnight and subsequently autoclaved to destroy the DEPC. Sterilisation took place at 121°C for 20 min in an autoclave. Yeast media and MS medium were autoclaved for 12 min only.

1.2. Chemicals, reagents and kits - sources

The chemicals (analytic purity grade), reagents and kits were obtained by Amersham (Germany), Analytic Jena (Germany), Applied Biosystems (Germany), Aventis (France), Bayer (Germany), Becton, Dickinson and Company (Germany), Biomol (Germany), Bioline (Germany), Bio-Rad (USA), Biozym (Germany), Boehringer (Mannheim), Clontech (France), Duchefa (Netherlands), Fermentas (Germany), Finnzymes (Finland), Fluka (Switzerland), Invitrogen (Paisly), Jackson ImmunoResearch (Germany), Loveland Industries (USA), Merck (Darmstadt), Milteny Biotec (Germany), Quiagen (Germany), ROCHE (Germany), Roth (Karlsruhe), Santa Cruz Biotechnology (Germany), Schleicher & Schuell (Germany), Serva (Heidelberg), Servoprax® (Germany), Sigma (Deisenhofen), Sigma-Aldrich (USA), USB Corporation (Germany), and VWR (Germany).

1.3. Kits

GeneJet Plasmid Miniprep Kit	Fermentas
ECL Western Blotting System	Amersham
MinElute™ Gel Extraction Kit (50)	Qiagen
QIAquick® Gel Extraction Kit (50)	Qiagen
QIAprep® Spin Miniprep Kit (250)	Qiagen
High Pure PCR purification Kit	ROCHE
innuPREP plant RNA Kit	Analytic Jena
µMACS GFP Tagged Protein Isolation Kit, human	Miltenyi Biotec

1.4. Enzymes

Restriction enzymes:

Restriction endonucleases were obtained by New England Biolabs GmbH and Fermentas.

Other enzymes and buffers:

Big Dye® Terminator Version 3.1.	Applied Biosystems
Bio*taq*™ DNA Polymerase	Bioline
BP Clonase™	Invitrogen
Complete, EDTA frei (Protease Inhibitor)	ROCHE
DNase I	Fermentas
ExoSAP-IT®	USB Corporation
LR Clonase™	Invitrogen
Phusion™ High-Fidelity DNA Polymerase	Finnzymes
Proteinase K	Invitrogen
Revert Aid H Minus FIrst Strand cDNA Synthesis Kit	Fermentas
RiboLock Rnase Inhibitor	Fermentas
RNase H	Fermentas
Taq DNA Polymerase	Fermentas
Shrimp Alkaline Phosphatase	Fementas
T4 DNA Ligase	Fermentas

1.5. Ladders

1 kb plus DNA ladder	Invitrogen
PageRuler™ Prestained Protein Ladder	Fermentas

1.6. Other material

Basic MicroBeads	Miltenyi Biotec
Biolistic® 1.0 Micron Gold	BioRad
Biolistic Macrocarrier	Bio Rad
Biolistic® Rupture Disks von	Bio Rad
Biolistic Stopping Shields	Bio Rad
Bradford Reagent (Biorad Protein Assay)	Bio Rad

BSA (Bovine Serum Albumine)	BioLabs
Gel-Blotting-Paper GB 002	Schleicher & Schuell
Goat anti-	
Hyperfilm™ ECL High Performance Chemiluminescence film	Amersham
Hypercassette™	Amersham
Milk powder	Sucofin von Real
Medical tape: mediware®	servoprax®
Mouse anti-GFP	Roche
Mouse anti-β-Tub	Sigma
Mouse anti-Ub	Santa Cruz Biotechnology
PVDF-membrane	Roth
Peroxidase-conjugated AffiniPure Goat anti-Mouse IgG (H + L)	Jackson ImmunoResearch
Peroxidase-conjugated AffiniPure Goat anti-Rat IgG (H + L)	Jackson ImmunoResearch
Proteingelsystem: Mighty small II for 8 x 7cm gels	Hoefer
Rat anti-HA High Affinity	Roche
Sterile filters	Millipore

1.7. Oligonucleotides (Primers)

All used primers were synthesised by Sigma (Deisenhofen) and Invitrogen (Paisly). Primers are listed in attachment A M-1.

1.8. Microorganisms and plants

Agrobacterium tumefaciens (A. tumefaciens):

GV3101: (pMP90) $Gent^R$, Rif^R (Koncz and Schell, 1986). Selection with Rif/Gent and plasmid specific antibioticum.

LBA4404: LBA4404pBBR1MCS-5.virGN54D (no $Spec^R$); LBA4404. pBBR1MCS.virGN54D ($Spec^R$) (van der Fits et al., 2000). Selection with Rif/Gent and plasmid specific antibioticum.

RK19: antisilencing strain harbouring the sequence for the P19 protein (Voinnet et al., 1999). Selection with Rif (150mg/ml) and Kan (50 mg/ml).

II. Material and Methods

***E. coli*:**

DH5α: F-, ϕ80*lac*Z ΔM15, Δ(*lac*ZYA-*arg*F), U169, *deo*R, *rec*A1, *end*A1, *hsd*R17, (r_k^-, m_k^+), *pho*A, *sup*E44, *thi*-1, *gyr*A96, *rel*A1, λ- (Hanahan, 1983)

DB3.1: F-, *gyr*A462, *end*A1, Δ(sr1-*rec*A), *mcr*B, *mrr*, *hsd*S20, (r_B^-, m_B^-), *sup*E44, *ara*14, *gal*K2, *lac*Y1, *pro*A2, *rps*L20 (Sm^R), *xyl*-5, λ-, *leu, mtl*1 (Invitrogen)

***Saccharomyces cerevisiae (S. cerevisiae)*:**

AH109: MATa, trp1-901, leu2-3, 112, ura3-52, his3-200, gal4Δ, gal80Δ, Lys2::$GAL1_{UAS}GAL1_{TATA}$-HIS3, MEL1, $GAL2_{UAS}$-$GAL2_{TATA}$-ADE2, URA3::$MEL1_{UAS}$-$MEL1_{TATA}$-lacZ (James et al., 1996)

Y187: MATα, ura3-52, his3-200, ade2-101, trp1-901, leu2-3, 112, gal4Δ, met-, gal80Δ, URA3::$GAL1_{UAS}$-$Gal1_{TATA}$-lacZ, MEL1 (Harper et al., 1993)

Nicotiana benthamina *(N. benthamiana)* for tobacco infiltration experiments.

Allium porrum (leek) and ***Allium cepa*** (onion) for biolistic transformation.

***A. thaliana**:*

wildtypes: Columbia (Col-0), Landsberg *erecta* (L*er*)

All used mutants, double mutants and over expression lines that were not generated in this work are listed in Table II - 1.

Table II - 1: Overview of all used mutants, double mutants and overexpression lines that were not generated in this work. Given are the name of the mutant/line, the background, the type of mutants, AGI code, the name of the corresponding protein and the cource in which the mutant was first generated or characzterized. All listed lines were homozygous.

mutante	background	type of mutant	AGI code	name of protein	source
mid-1	Col-0	lack-of-function, Weigel activation tagging line	At5g24630	MID	(Kirik et al., 2007; Weigel et al., 2000)
mid-2	Col-0	loss-of-function, SALK line	At5g24630	MID	SALK_110705, (Alonso et al., 2003; Kirik et al., 2007)
rhl2	Col-0	loss-of-function (probably a residual activity of misspliced *RHL2*) EMS (ethylmethane sulfonatemutants)	At5g02820	RHL2	(Santoni et al., 1997; Sugimoto-Shirasu et al., 2002)
hyp6	Col-0	loss-of-function EMS mutant, frame-shift	At3g20780	AtTOP6B	(Santoni et al., 1997; Sugimoto-Shirasu et al., 2002)
cop1-4	Col-0	$COP1^{1-282}$ is expressed, EMS mutant, weak mutant	At2g32950	COP1	(McNellis et al., 1994)
$cop1^{eid6}$	L*er*	aa exchange in RING finger, EMS mutant, weak mutant in the dark	At2g32950	COP1	(Dieterle et al., 2003)
spa1-100	Col-0	SAIL line, loss of function	At2g46340	SPA1	(Sessions et al., 2002; Yang et al., 2005)
hy5-215	Col-0	EMS mutant	At5g11260	HY5	(Oyama et al., 1997)
cop1-4 hy5-215	Col-0	double mutant	At2g32950 At5g11260	COP1, HY5	obtained from AG Höcker
Pro35S:*MID-*L*er-YFP*	*mid-1*	overexpression	At5g24630	MID-L*er*	(Kirik et al., 2007)

1.9. Vectors and constructs

All used DNA-vectors that were not generated in this work are listed in Table II - 2.

Table II - 2: DNA-vectors for cloning and expression in bacteria, yeasts and plants.

vector	source
Gateway® entry vectors	
pDONR207	Invitrogen
pENTR4-GFP	Joachim F. Uhrig
pDONR207-MID-L*er*	Viktor Kirik
pDONR207-RHL1	Viktor Kirik
pENTR4-PAP2	Ilona M. Zimmermann
yeast expression vectors	
pCD2-attR	(Durfee et al., 1993), modified J. F. Uhrig
pcACT2-attR	(Durfee et al., 1993), modified J. F. Uhrig
pAS2-1-attR	Invitrogen
pACT-attR	Invitrogen
pACT2	(www.clontech.com Protocol No. PT3022-5)
pAD-Gate1	(Maier et al., 2008)
pAD-Gate2	(Maier et al., 2008)
pAD-Gate3	(Maier et al., 2008)
pBRIDGE	Clonetech
pGBKT7-COP1	(Hoecker and Quail, 2001)
pGBKT7-DET1	Ute Höcker
pAS2-1-EGL3	Martina Pesch
pAS2-1-SNF1	(Celenza et al., 1989)
pACT-SNF4	(Celenza et al., 1989)
pCD2-RHL1	Viktor Kirik
pcACT2-RHL1	Viktor Kirik
pCD2-RHL2	Viktor Kirik
pCACT2-RHL2	Viktor Kirik
pCD2-AtTOP6B	my diploma thesis
pcACT2-AtTOP6B	my diploma thesis
pCD2-MID-L*er*	Viktor Kirik
pcACT2-MID-L*er*	Viktor Kirik
pCD2-MID$^{1\text{-}266}$	my diploma thesis
pcACT2-MID$^{220\text{-}330}$	my diploma thesis
pCD2-PAP2	Ilona Zimmermann
plant expression vectors	
pBatTL-B-p35S	this work, III.2
pBatTL-B-sYFPN	(Hackbusch et al., 2005)
pCL112	J. F. Uhrig, unpublished, S. Chapman, SCRI, Dundee, UK
pCL113	J. F. Uhrig, unpublished, S. Chapman, SCRI, Dundee, UK
pCL112-SPA1	AG Höcker
pCL113-SPA1	AG Höcker
pEarleyGate104	Earley u. a. 2006
pEarleyGate201	Earley u. a. 2006
pNmR	this work, III.2
pGJ2811	(Jach et al., 2006)
CFP-TALIN	transformation control for BiFC
CFP-GL3	transformation control for BiFC
pCL113-MIAP2	my diploma thesis
pCL112-MID-L*er*$^{260\text{-}450}$	my diploma thesis
pCL113-MID$^{1\text{-}260}$	my diploma thesis
pCL113-MID-L*er*$^{260\text{-}450}$	my diploma thesis
pCL113-MID$^{220\text{-}330}$	my diploma thesis

1.10. cDNA libraries from *A. thaliana* for YTH screening

"Clontech":

The Clontech Matchmaker cDNA library contains cDNA-transcripts of vegetative green leaf material of 3 week old *A. thaliana* plants. Insert size: 0.6-4.0 kb (average: 1.2), polyT and random-primed, 3*10 primary clones, vector: pGAD10, yeast strain: Y187 (Clontech).

"1699":

The 1699 cDNA library was based on an *A. thaliana* cell suspension culture. PolyT primed, 1*107 primary clones, vector pACT2, yeast strain Y187 (Nemeth et al., 1998).

"REGIA" (REgulatory Gene Initiative in *Arabidopsis*):

The REGIA library consists of different *A. thaliana* trabnscription factors and was constructed based on the cDNA collection of the REGIA project (Paz-Ares and The Regia, 2002). Vector: pACT2, yeast strain Y187 (J.F. Uhrig unpublished).

"HS":

The HS library contains cDNA from whole *A. thaliana* plant (Col-0). The library was generated by Hans Sommer (Max-Planck Institute for Plant Breeding Research, Cologne, Germany). Yeast strain: AH109.

1.11. Culture media, buffers, solutions and antibiotics

Culture media, buffers and solutions:

E.coli:

LB medium was prepared using the protocol by Bertani *et al*. (Bertani, 1951) and supplemented with the appropriate antibiotica for selection: 10 g/L tryptone/peptone from casein, 5 g/L yeast extract, 10 g/L NaCl, pH 7.0 (NaOH), (16 g/L microagar)

ψ-broth-medium: 20 g/L tryptone/peptone from casein, 5 g/L yeast extract, 4 g/L $MgSO_4$ x 7 H_2O, 0.7456 g/L KCl, pH 7.6 (KOH)

TfB1: 100 mM $RbCl_2$, 50 mM $MnCl_2$, 30 mM potassium acetate, 10 mM $CaCl_2$ x $2H_2O$, 15% (v/v) glycerol, pH 5,8 (0,2 M HAc).

TfB2: 10 mM $RbCl_2$, 75 mM $CaCl_2$ x $2H_2O$, 15% (v/v) glycerol, pH 7,0 (NaOH)

TfB1 and TfB2 were filter sterilised and kept at 4°C.

A. tumefaciens:

YEB medium contains per litre 5g beef extract (Roth), 1g yeast extract (BD, France), 5g peptone/tryptone (Roth), 5g glucose und 2 mM $MgSO_4$ (Merck). The pH was adjusted to 7. For plates, 15 g Agar (Roth) per litre Medium was used. Appropriate antibiotica were added for selection (see Table II - 3).

S. cerevisiae:

YPAD medium was prepared with 20 g peptone/tryptone (Roth), 10 g yeast extract (BD, France) and 100 mg adenine (Sigma) to 950 ml bi-distilled water. pH was adjusted to 5.8. After autoclaving, glucose was added to a final concentration of 2%. For plates, 18 g agar (Roth) per litre medium was used.

Single-Dropout-medium contains per litre 6.7 g yeast nitrogen base with (NH4)3SO4 w/o amino acids (Difco), 600 mg DO supplement^{-LWH} (Clontech), 100 mg adenine (Sigma) and 2 % glucose (final concentration). Depending on the auxotrophy 20 mg histidine (Duchefa), 50 mg tryptophan (Duchefa), and/or 100 mg leucine (Duchefa) was added, if necessary. The pH was adjusted to 5.8. For plates 18 g Agar (Roth) per litre Medium was used. The medium for Y2H-screenings contains additional 3 mM 3-AT (Sigma) and 0.5% Gelrite (Sigma).

N. benthamiana:

10x Agromix: 100mM MgCL2, 100 mM MES, pH5,6

A. thaliana:

Arabidopsis dark-grown white and light-grown green cell suspension culture (Columbia ecotype) was maintained by Irene Klinkhammer as well as the Pro35S:*MID*-L*er* (*mid-1*) cell suspension culture line was established and maintained by her. Used medium for maintenance: MS medium supplemented with 0.5 mg/L NAA and 0.1 mg/L KIN. The cultures were established and maintained as described previously (Mathur and Koncz, 1998a; Mathur and Koncz, 1998b; Mathur and Koncz, 1998d).

MS medium (Murashige und Skoog, 1962): MS medium contains 4.4g MS per litre and 1% or 3% of sucrosoe. The pH was adjusted to 5.8 with 2 N KOH. For plates 8 g Plant Agar per litre Medium was used. The medium was autoclaved for 12 min. Hygromycin or Kanamycin was added in a final concentration of 25 µg/ml for selection.

0,1% Agarose was prepared for plating of seeds and autoclaved.

BASTA: 0,1 g/L BASTA, 0,01% Tween80

Magic buffer: 50 mM Tris/HCl pH7.2, 300 mM NaCl, 10% sucrose.

Anthocyanin extraction buffer: 18% [v/v] 1-propanol and 1% [v/v] concentrated HCl

DNA and RNA work:

10xXLA: 50 mM EDTA pH 8, 50% glycerol, 0,1% xylene cyanol, 10 mM Tris

10x BFA: 50% glycerol, 75 mM EDTA, 0,2% Bromphenol blue

Running buffer (1xTAE-buffer): 2 mM Tris, pH 8,5 (acetic acid), 1 mM sodium acetate, 50 µM EDTA

DEPC (Diethyl pyrocarbonate)-water: 0.1% (v/v) DEPC

Protein work:

10x Western blotting buffer (WBB): 20 mM Tris, 150 mM glycin

Anode buffer: 1x WBB, 30% (v/v) methanol

Kathode buffer: 1x WBB, 0.1% (w/v) SDS

Running buffer (for SDS-PAGE): 75 mM Tris, 576 mM glycin, 0.25% (w/v) SDS

Cracking buffer: 60 mM Tris pH 6.8, 1% (v/v) β-mercaptoethanol, 1% SDS, 10% glycerol, 0.01% Bromphenol blue

PBS ("Phosphate buffered Saline"): 10.9 g/L Na_2HPO_4, 3.2 g/L NaH_2PO_4, 90 g/L NaCl, pH 7.2.

PBT: 1:10 10x PBS, 0.1% (v/v) Tween 20

Homogenisation buffer (for *A. thaliana* cell suspension culture):
50 mM Tris, 150 mM NaCl, 1% v/v Triton X-100, pH 8.0, 1 pill Complete per 50 ml buffer.

Denaturation buffer for ubiquitin western blot analysis:
6M guanidin hydrochlorid, 20 mM Tris, 1mM PMSF (Phenylmethylsulfonylfluorid), 5 mM β-mercaptoethanol.

Stripping solution: 0.1 M glycin, pH 2.4

Lysis buffer final (LF) for Co-immunoprecipitation (Co-IP) with Miltenyi beads:
950 µl Miltenyi Lysispuffer, 50 µl Complete without EDTA (1 pill in 2 ml Miltenyi lysis buffer), 10 µl 1 M DTT, 0.1% (w/v) SDS.

Antibiotics:

Table II - 3 depicts all antibiotics for selection of transgenic bacteria and their working concentrations. All antibiotics were obtained from Sigma Aldrich (USA) and Duchefa (Netherlands).

Table II - 3: Used antibiotics and their application.

antibiotic	organism	final concentration [mg/l]
Ampicillin	*E. coli*	100
Kanamycin	*E. coli*	50
Gentamicin	*E. coli*, *A. tumefaciens*	50
Spectinomycin	*E. coli, A. tumefaciens*	50
Rifampicin	*E. coli, A. tumefaciens*	100

Transformed yeast cells were selected by auxotrophy (W, L, H), bacteria by antibiotica resistance and transgenic plants via resistence to the herbizid BASTA (Bayer Crop Science).

2. Methods

2.1. Moleculare cloning

The standard molecular cloning methods (PCR, restriction digestion, ligation, DNA gel electrophoresis) were performed according to Sambrook et al., 1989.

Purification of Plasmid-DNA was done using the Fermentas or Quiagen Plasmid Kit. PCR products were in most cases recombined via Gateway® BP and LR reactions in the desired vectors according to the manufacturers instructions. Purification of PCR products was achieved by applying kits from Roche and Qiagen.

Inverse PCR was applied to generate pDONR207-COP1^{K550E}, pDONR201-GFP-CID and pDONR207-GFP-CID^{D246K} with pDONR207-COP1 and pDONR207-GFP-nostopp. The linear vector was phosphorylated and religated using T4-PNK and T4 DNA ligases from Fermentas. In order to obtain pBRIDGE-MID/RHL1 (*BD-MID*, ProMet25:*RHL1*), pBRIDGE-COP1/RHL1 (*BD-COP1*, Pro*Met25*:*RHL1*), pBRIDGE-*COP1/GFP-CID* (*BD-COP1*, *ProMet25:GFP-CID*) and pBRIDGE-*COP1/GFP-CID* (*BD-HY5*, *ProMet25:GFP-CID*) MID (*Xho*I, *Bam*HI), COP1 (*Hpa*I, *Sal*I) and HY5 (*Hpa*I, *Bam*HI) were cut form the corresponding pAS2-1 plasmids and ligated into pBRIDGE. Cloning of pNmR and of the controls for CoIP is described in the corresponding results part. All generated entry plasmids and plasmids after ligation were sequenced.

2.1.1. *E.coli* transformation

Chemically competent *E. coli* cells were generated according to the RbCl method. 10 ml of a starter culture was diluted 1:100 in 200 ml LB medium and grown at 37°C and 250 rpm to an OD_{600} of 0,5. The cells were incubated for 15 min on ice and then centrifuged at 2000 rpm for 10 min (Beckman Avanti™ J-25). The following steps were performed at 4°C: The cell pellets were gently resuspended in 15 ml TfB1. Another incubation on ice for 2 h was followed by centrifugation for 5 min. Pellets were resolved in 1 ml TfB2, pooled, portioned to aliquots of 100 µl, frozen in liquid N_2 and stored at -80 °C. 0,5 µg plasmid DNA was added to 100 µl competent *E. coli* cells, thawed on ice. After another 20 min of incubation on ice, the heat shock was performed for 45 s at 42 °C, followed by 1 min incubation on ice and addition of 900 µl LB medium. The transformed cells were shaken at 37 °C and 950 rpm, streaked out on selective LB agar plates and incubated at 37 °C o/n. Positive Transformants were verified by restriction analysis.

2.1.2. PCR protocols

20 or 50 µl PCR-reactions were carried out with a final concentration of 1x PCR reaction buffer (polymerase- and buffer-dependent $MgCl_2$ was added), 0.2 mM dNTPs, 0.2-0.4 µM of each primer, 50-100 ng template-DNA and 0.5-4 u DNA polymerase (depending on the reaction size and manufacturer, see Tabelle II-4).

Table II - 4: Used DNA polymerases. Given is the activity, velocity and $MgCl_2$ supplementation.

DNA polymerase	activity [u/µl]	speed	add $MgCl_2$
Bio*taq*® Polymerase	5	1 kb / 1 min	yes, 2.5 mM
Phusion™ High Fidelity DNA Polymerase	2	1 kb / 15-30 sec	10x Fermentas High Fidelity buffer with 25mM MgC_{l2}
Taq-Polymerase	5	1 kb / min	No

2.1.3. **Genotyping**

For genotyping, plant extracts were prepared by using the tissue-lyser. A small frozen (N_2 liq.) leaf or seedling was placed in a reaction tube and glass beads together with 300 µl of magic buffer were added. The plant material was homogenised in the tisssue-lyser applying two times 30 Hz for 1.5 min. After centrifugation at 13 000 pm in a table top centrifuge the supernatant was taken and 1 µl was used for PCR analysis in a 50 µl reaction.

In genotyping PCRs the optimal annealing temperature for the used primer combinations was determined with a temperature gradient in the annealing step. Table II - 5 shows the applied conditions. The template was obtained by homogenisation of plant material with the tissue-lyzer.

For the different anaylsed genotypes different primers were used. On the one hand, T-DNA insertion lines are analysed comparing the presence or absence of a PCR product with primers spanning the T-DNA insertion site and in the TDNA. Primer annealing temperature and size of the obtained fragment are listed in Table II - 5. In case of CAPS PCR, DNA gels of higher percentage were used to seperate the bands.

Table II - 5: Used primers (the number corresponds to the first number in the primer name given in A M-1 in the attachment), PCR conditions (annealing temperature and elongation time) for all aaplied genotyping PCRs. Depending on the type of PCR the size of tha band for a PCR on plants containing a TDNA insertion (TDNA) and those without this insertion (wildtype (wt)) is given or the Cleaved amplified polymorphism (CAPS) enzyme and corresponding band distinguishing between homozygous (hom), heterozygous (het) or wildtype (wt) allels. PCR for cop1^{eid6} and spa1 (with 208 and 228) was described before (Dieterle et al., 2003; Yang et al., 2005). Primer 176, 178, 179 and 180 were obtained from Viktor Kirik.

			annealing	elongation	TDNA	CAPS			size [bp]		
mutant	primer 1	primer 2	[°C]	[sec]	or wt	Size [bp]	primer	enzyme	hom	het	wt
mid-1	172	171	56	45	TDNA	~500	no	-	-	-	-
mid-1	172	186	56	45	wt	~600	no	-	-	-	-
mid-2	113	115	65	30	TDNA	880	no	-	-	-	-
mid-2	217	117	65	40	wt	509	no	-	-	-	-
spa1-100	228	208	64	40	TDNA	556	no	-	-	-	-
spa1-100	226	228	64	40	wt	473	no	-	-	-	-
rhl2	180	179	56	30	no	-	yes	*Ava*II	419	419/264/155	264/155
hyp6	178	176	52	30	no	-	yes	*Hae*III	321/ 179	321/294/ 179/28	294/ 179/28
cop1-4	183	184	56	30	no	-	yes	*Sna*BI	245/32	277/ 245/32	277
cop1^{eid6}	237	238	65	30	no	-	yes	*Ahd*I	440	440/403	37

2.1.4. **Sequencing**

Sequencing was done by the Cologne Centre of Genomics (University of Cologne, Germany) with an ABI 3730 sequencer. For the sequencing reaction, BigDye Terminator Version 3.1 (0.5µl and 0.25µl buffer), 0.25µl primer and up to 3 µl of sample were used.

Programme: 94°C 2min [94°C 20 sec, 54°C 30 sec, 60°C 3 min 30 sec] x 35 60°C 4 min

2.1.5. **RT-PCR analysis**

For RT-PCR analysis total RNA was isolated from 3-day-old dark-grown seedlings grown on MS-plates without sucrose using innuPREP Plant RNA Kit (Analytik Jena, Jena, Germany). Seedlings were harvested under green light. cDNA was prepared with the RevertAid™ H Minus First Strand cDNA Synthesis Kit and subsequently treated with RNase H to prevent false positive results due to reverse transcriptase activity of the Taq DNA polymerase (Martel et al., 2002). A reaction-mix lacking the reverse transcriptase was used as a negative control. The exponential phase of amplification was determined CHS, COP1 and UBQ10. All PCRs were done with one mastermix for all samples and performed at least twice. Used primers and expected size of the PCR product are listed in Table II - 6.

Amplifications of UBQ10 were used as control (Harari-Steinberg et al., 2001). In the case of the RT-PCR for COP1, RNaseH treatment was necessary. An example for the difference between no treatment and treatment is shown in the attachment A M-2. RNaseH treatment was done according to the manufacturers instructions.

Table II - 6: Used primer and conditions for RT-PCR including the expected size of the PCR products with CDNA as a template or in case of contamination with genomic DNA, with genomic DNA. *CHS* primer were obtained from AG Höcker, primer for *EF1α* and *UBQ10* were used before (Harari-Steinberg et al., 2001; Kirik et al., 2007; Sun et al., 1997).

gene	primer 1	primer 2	annealing [°C]	elongation	cycle	size genomic	size cDNA
CHS	330	331	66	35	23/26/29/32	392	392
EF1α	167	168	60	30	17/20/23/26/29	809	709
UBQ10	326	327	66	35	20/23/26/29	633	633
COP1	238	329	59	30	28/31/34/37	976	228

2.2. Yeast methods

2.2.1. LiAc-transformation

Competent yeast cells were made according to a modified protocol of Schiestl und Gietz 1989. 10 ml of YPAD medium were inoculated with a single colony of a freshly plated yeast strain. The preparatory culture was incubated o/n at 30 °C and 200 rpm.

1 ml of the preparatory culture was used for inoculation of the main culture (V = 50 ml) which was incubated four to five hours at 30 °C and 200 rpm until an OD_{600} of 0,6 - 1,2 was reached. Cells were harvested for 5 min at 3500 x g. The yeast pellet was resuspended in 25 ml of sterile water, centrifuged as before, the washed cells were resuspended in 1 ml of sterile water and again spun down. The cell pellet was resolved in 550 µl 100 mM LiAc and 100 mM LiAc. The cell suspension was portioned to 50 µl aliquots and centrifuged as described above.

Yeast transformation was performed using a modified LiAc method of Gietz et al. (Gietz and Woods, 2006). In order, 240 µl PEG-4000 (50 %), 36 µl 1M LiAc, 25 µl single stranded herring sperm DNA (10mg/ml), as well as 50 µl of the DNA solution (200 - 500 ng DNA) were added per aliquot of copetent yeast cells. The sample was mixed and incubated for 25 min at 30 °C with occasional shaking followed by incubation for 25 min at 42 °C without shaking. After centrifugation for 1 min at 3500 x g, the transformed yeast cells were resuspended in 200 µl of sterile water. 50 and 150 µl of the cell suspension was streaked out on selective SD agar plates and incubated for 2 to 3 days at 30 °C.

2.2.2. Yeast Two-Hybrid screen and interaction analysis

The GAL4 BD-fused COP1 protein was used as a bait protein to screen an *Arabidopsis thaliana* cDNA prey library (suspension culture) (Nemeth et al., 1998). Yeast two-hybrid screens were performed according to Soellick and Uhrig, 2001. Interaction candidates were verified by gap repair (*in vivo* recombination). For Yeast-Two Hybrid interaction analysis a double transformation with a bait and prey plasmid was performed as described before (Gietz and Schiestl, 2007). All used constructs were tested for autoactivation. GFP was used as a negative control.

2.2.3. Yeast Two-Hybrid by co-transformation

The YTH screening is used for verification of interactions between two proteins (Fields and Song, 1989). *S. cerevisiae* AH109 was co-transformed with two plasmids: one coding for the bait protein and mediating leucin synthesis, the other coding for the prey protein and mediating tryptophan synthesis. Yeast harboring both plasmids after transformation was selected on SD medium lacking L and W. Bait and prey proteins are fused to the DNA binding and activation domains of the Gal4 transcription factor. In case of interaction and thus reassembly of the Gal4 transcription factor, a histidin reporter gene (*HIS3*) under the control of the *Gal4* promoter is activated. pCD2 and pACT2, coding solely for the Gal4-BD and -AD, functioned as negative controls, whereas pAS-SNF1 and pACT-SNF4 were used as positive controls (interaction proven by Celenza et al. 1989). Transformation of the yeast cells was performed as described above (see II.2.2.1). 500 - 800 ng DNA were used of each plasmid and transformed yeast was streaked out on SD-LW agar plates. After 2 days of incubation at 30 °C, 10 single colonies were resuspended in 100 µl water each and streaked out on interaction medium (SD-LWH plus 3 mM 3-AT, a competitive inhibitor of the *HIS3* gene). After 4 to 6 days of incubation at 30 °C, the first transgenic interacting yeast clones showed up.

2.2.4. Yeast Two-Hybrid screening with Gerite media

YTH screenings with Gelrite media were performed using a modified method of MacFarlane and Uhrig (2008). An S. cerevisiae bait culture (V = 50 ml) was grown up to an OD_{600} of 0.6 - 0.8. An *S. cerevisiae* bait starter culture (V = 50 ml), based on a single colony of a freshly streaked out yeast strain, was grown in SD-W medium with a final concentration of 4 % glucose. A 1.5 ml aliquot of a frozen yeast library culture was thawed at 42 °C and shaken for 1 hour in 25 ml YPAD at 30 °C up to an OD_{600} of 0.4 to 0.5. Volumes corresponding to an OD_{600} = 10 of the bait and library cultures were mixed and centrifuged for 5 min at 3500 x g. The cell sediment was resuspended in 10 ml YPAD plus

10 % PEG-6000 (Duchefa). Mating, fusion of the yeast cells due to different mating types, was performed o/n in a 100 ml Erlenmeyer flask at 30 °C and gentle shaking at 80 rpm. The mating culture was harvested by centrifugation for 4 min at 3500 rpm. After resuspension of the cell pellet in 15 ml SD-LWH Gelrite medium this suspension was mixed with further 500 ml of the same medium. To determine the mating titer (number of mated yeast clones) of the YTH screening, 10 µl of the Gelrite cell suspension was streaked out on a SD-LW agar plate. The titer plate was analysed after 2 days. The Gelrite cell suspension was portioned to 15 Petri dishes and incubated 1 to 2 weeks until yeast colonies showed up. The colonies were carefully transferred from the Gelrite medium to an SD-LWH agar plate and incubated 3 to 4 days at 30 °C until the yeast colonies were big enough for further analysis by colony PCR (see II.2.2.5).

2.2.5. Yeast colony PCR

This method was used for direct amplification of DNA fragments derived from on single yeast colonies. Cells from a single yeast colony were picked with a pipet tip and used as the template. The colony PCR was performed using Bio*taq*® polymerase (Bioline). 2 mM MgCl was added to the PCR sample (V = 50 µl) as well as primers ADXL3 and ADXXL5 for amplification of the prey cDNA obtained in the YTH screening. The following PCR program was used: 94°C 2 min [94°C 45 sec, 54°C 45s, 72°C 2 min] x 40, 72°C 5 min.

2.2.6. Sequencing of colony PCR products

Prior to sequencing, the colony PCR products were digested with *Taq*I and analysed by Agarose gel electrophoresis to identify redundant prey clones. Those PCR products with a unique restriction pattern were analysed by DNA sequencing (see II.2.1.4).

2.2.7. Auto activation

In some cases, the *HIS3* reporter gene is activated by the bait protein itself independent from a specific interaction with the prey. The auto activating properties of a bait have to be tested prior to YTH screenings. In analogy to the YTH screening method (see II.2.2.4), yeast was co-transformed with 500 to 800 ng of the bait plasmid as well as pACT-SNF4 or pAS-SNF1, respectively. Transformed yeast cells were streaked out on SD-LWH agar plates with 3 to 20 mM 3-AT. pCD2 and pCACT2 served as negative controls, pAS-SNF1 and pACT-SNF4 as positive controls.

2.2.8. Gap repair cloning

This method is based on the yeasts ability of homologous recombination of DNA fragments (e.g. a PCR product) into a linear vector. For successful recombination, the ends of the PCR product (ca. 40 nt) had to be homologous to the target vector pCACT2. The help of specifically designed primers, which added homologous overhangs to the PCR product, achieved this. pCACT2 was digested with *EcoR*I and *Xho*I and dephosphorylated with CIAP (1 h at 37 °C, heat inactivation 10 min at 65 °C). 1 µg of the purified PCR product and 25 ng of the purified linearised vector were transferred into *S. cerevisiae* AH109 (see II. 2.2.1.) and the transformed yeast was streaked out on SD-LW agar medium. A transformation solely with the linearised vector without PCR product served as negative control. After 2 to 3 days of incubation at 30 °C, ca. 10 colonies were transferred to SD-LWH agar medium and further incubated at 30 °C for another 4 to 5 days.

2.2.9. Yeast Three-Hybrid

Yeast three hybrid assays were performed using a modified method of the Clontech system (Tirode et al., 1997). pBRIDGE served as additional vector and expression was controlled by the methionin suppressable promoter Pro*Met25*. Methionin was used in concentrations of 0, 100, 200 and 500 µM.

2.2.10. GARFILD

GARFILD = Gateway®-compatible random fragments YTH in frame library screening for domain mapping

template PCR

Polymerase: Phusion™ High-Fidelity DNA Polymerase

Primer: 81 PAP2 attB1 + 111 PAP2 ns attB2 / 20 ANS COP1 attB1 + 21 ANS COP1 attB2

Template: pENTR4-PAP2 / pDONR207-COP1

Programm: 98°C 5 min [98°C 2min, 65°C 30 sec, 72°C20 sec] x 30 72°C 7 min

annealing PCR

Polymerase: Bio*taq*™ DNA Polymerase

Primer: Figure III-5, Table III - 6

Template: gelextracted template PCR product

Programm: 94°C 2 min [94°C 1 min, 40°C 5 min, 72°C 2 min] x 2

tag PCR

Polymerase: Bio*taq*™ DNA Polymerase

Primer: Figure III-5, Table III - 6

Template: ROCHE purified annealing PCR product

Programm: 94°C 2 min [94°C 1 min, 60°C (gradient) 1 min, 72°C 2 min] x 40 72°C 5 min

Gradient: temperatures between 53.6°C and 66.4°C / 50.0°C and 70.5°C

purification: pel extraction MinElute, Quiagen, purificationHigh Pure PCR Product Purification Kit, ROCHE

BP reaction was performed according to the manufacturs insructions. For the used amount of PCR product see III 2.3.1..

Library LR reaction for GARFILD:

First day:

C-termini: ~600ng Library-entry, 200 ng cut pAD-GATE1-3 each (sum: 600 ng), 2µl LR Clonase, 2µl buffer, 1 µl TE buffer. o/n 25°C

N-termini: pAD-GATE2, 2µl LR Clonase, 2µl buffer, 1 µl TE buffer. o/n 25°C

Second day:

add 2µl buffer, 2µl LR clonase, ad 24 µl with TE. o/n 25 °C

Third day:

add 4 µl Proteinase K, 37°C 10 min

add 24 µl 7,5M NH_4Ac, 1µl gycogen (1mg/ml), 165 µl EtOH, incubate 20 min on dry ice, spin 30 min at 4°C, 13 000 and wash two times with 70% EtOH.

Finally the pelleted DNA is resuspended in 10 µl water. *E.coli* transformation does only differ in the used LB medium that is supplemented with 40% glycerol.

The library was transformed to yeast (Y187) as describbed elsewehere. The screeing procedure resembled the procedure with cDNA libraries. Differences are named in III 2.3.

2.3. Transient and stable transformation of plants

2.3.1. *A. tumefaciens* transformation

Chemically competent Agrobacteria: A 5 ml YEB-overnight culture with 20 mg/ml Rif is used to inoculat amain culture of 500 ml YEB with 20 mg/ml Rif. The culture is harvested at an OD600 of 0.5-0.6 (5min 7000g, 4°C). The supernatant is removed and 25 ml icecold 0,15M NaCl are added and incubated on ice for 15 min. After subsequent pelleting 5 ml of icecold 20 mM CaCl2 are added and aliquots are frozen in liquid nitrogen.

Transformation of *A. tumefaciens*: 1-2 µl of DNA were added to a thawn aliquot of chemically competent cells and frozen again in liquid nitrogene. When thawn again, a heatshock of 42°C for two minutes is applied. After adding 800µl Yeb medium and shaking for 2h at 28°C 100l are plated on appropriate plates.

Transformants were verified by restriction analysis. For this, a liquid culture, based on a single colony, was grown for 2 days at 28 °C and 220 rpm, followed by plasmid isolation (QIAprep® Miniprep), digestion with appropriate restriction endonucleases and gel electrophoresis.

2.3.2. Tobacco infiltration

Leaves of *Nicotina benthamiana* were transiently co-infiltrated with supervirulent *A. tumefaciens* strain LBA4404.pBBR1MCS.virGN54D (MIDpEGATE 104) or LBA4404pBBR1MCS-5.virGN54D (for all other plasmids) (van der Fits et al., 2000) harboring the different plasmids and the antisilencing *Agrobacteria* strain 19K (Voinnet et al., 1999) as described earlier (Gigolashvili et al., 2007). Plants were kept for 4 days at 24°C at long day conditions after infiltration and prior to protein analysis.

2.3.3. *A. thaliana* cell suspension culture transformation

The transformations have been described before (Berger et al., 2007). The same *A. tumefaciens* strains as for tobacco infiltration were used to transform dark-grown white cell suspension cultures.

2.3.4. Floral dip transformation

Stable transformation of *A. thaliana* was achieved using the floral dip method (Clough and Bent, 1998).

2.3.5. Biolistic transformation, localization, co-localization and BiFC (Bimolecular Fluorescence Complementation)

Epidermal cells of the adaxial part of the white leaf bases of leek (*Allium porrum*) were transiently transformed by biolistic transformation with plasmids coding for fusion proteins of the N- and C-terminal half of YFP for BiFC experiments or for whole fluorescence tags in case of localisation and co-localisation. For biolistic transformation, 300 µg of 1 µm gold particles were coated with 300 ng of each (BiFC) plasmid (e.g. COP1pCL112 and MIDpCL113) and 200 ng of the transformation control CFP-TALIN in case of BiFC (Saedler et al., 2004) according to the manufacturer´s instructions. 900 psi rupture discs were used to accelerate the coated gold particles for 6 cm under a vacuum of 26 inches of Hg with a biolistic PDS-1000/He instrument (Bio-Rad, München, Germany). The bombarded leaf bases were incubated at room temperature on a filter soaked with water in the dark and analysed after 24 h. 80 to 200 different transformed cells of at least two independent transformations were microscopically analysed with a Leica DMRB fluorescence microscope equipped with 500/20 YFP selective BP excitation filter (AHF, Tuebingen, Germany) and a 436/20 CFP BP excitation filter (Leica, Wetzlar, Germany) or Ds-red filter. Alternatively CLSM was performed

2.4. Protein methods

2.4.1. Determination of total protein

The total protein concentration in plant extracts was determined by the method of Bradford (Bradford 1976), using the Bio Rad protein assay kit with bovine serum albumin as a standard. Plant extracts were prepared by homogenising plant tissue with the tissue–lyzer (see II.2.1.3) using 100 µl of cracking buffer instead of magic buffer. Samples were stored on ice and wrapped in aluminium foil until they were analysed.

2.4.2. SDS-PAGE (Sodium Dodecyl sulfate-polyacrylamide gel electrophoresis)

Prior to immuno-blotting, the proteins were separated by SDS-PAGE (Davis, 1964; Ornstein, 1964; Sambroock and Russell, 2001). The 0.5 cm-thick gels composed of a 12.5% stacking- gel and a 12.5% separation gel were run with a Hoefer electrophoresis system at 20 mA (Mighty small II 8 x 7 cm^2-gels). The molecular weight of the proteins was estimated by using a calibrated molecular weight marker (PageRuler™ Prestained Protein Ladder; Fermentas)

Table II - 7: 12.5% SDS-PAGE-gel. Separating and stacking gel for four small 12.5% SDS-PAGE-geles

	separating gel	stacking gel
Acrylamid/Bisacrylamid	6.25 ml	1 ml
Tris pH 8.8 / pH 6.8	1.9 ml	630 µl
Water (sterile)	6.62 ml	5.75 ml
10% SDS	150 µl	75 µl
10% APS	75 µl	40 µl
TEMED	5 µl	5 µl

2.4.3. Coomassie staining

SDS-PAGE-gels wer stained with Coomassie solution to additionally estimate and compare the relative amounts of loaded protein. Gels were incubated for 20 min in Coomassie solution and subsequently destained with a destainig solution. (Fazakes de St. Groth, 1963; Meyer and Lamberts, 1965).

2.4.4. Antibodies

For immunodetection in IP and Co-IP experiments, the following antibodies were used:

Table II - 8: Used antibodies. Name of antibody, antigen, organism in which the antibody was raised and used dilution. All antibodies ar for HRP **(horse raddish peroxidase)** detection.

antibodies	antigen	raised in	dilution
anti-HA	HA (YPYDVPDYA)	rat	2:3000
anti-GFP	GFP	mouse	1:1000
anti-ubiquitin	ubiquitin	mouse	1:500
anti-β–tubulin	tubulin	mouse	2:3000
anti- mouse (HRP-conjugated)	mouse IgG (H+L)	goat	1.3000
anti-Rat (HRP-conjugated)	Rat IgG (H+L)	goat	1:3000

2.4.5. IP from *A. thaliana* cell suspension culture - homogenisation

The IP was essentially performed as described in II 2.6.6 for the Co-IP. Only the homogenisation was done differently. Dark grown white cell suspension culture established and maintained by Irene klinkhammer from Pro35S:*MID-YFP* (mid-1) line (Kirik et al., 2007) and Col-0 were homogenised as follows: cultures were harvested by vacuum filtration and freezed directly in liquid nitrogen. Same weight for both samples were used and the double amount of homogenisation buffer was added. The frozen culture and buffer slowly thawed on ice in the dark. This mixture was homogenised with the help of a french press. All parts that had contact to the culture were pre-cooled. Triton X-100 was added after the french press step. Cell debris were removed by centrifugation and 0.1% SDS, 10 mM DTT and Complete (ROCHE, protease inhibitor) were added to the supernatant. After an incubation of at 4°C for 20 minutes the possibly remaining debris were pelleted and the supernatant was used for the IP with Miltenyi beads as described for the Co-IPs.

2.4.6. IP/Co-IP

Protein extracts were prepared from co-infiltrated leaves of *N. benthamiana* expressing YFP-PAP2 or MID and RFP-HA-COP1 fusions under control of the cauliflower mosaic virus 35S promoter. 4 days after infiltration, 530 - 540 mg of the successfully infiltrated leave areas (determined with a Leica MZ FL III fluorescence binocular) were lysed as described before (Kirik et al., 2007). A 570 µl aliquot of this lysate was used with 50 µL of anti-GFP MicroBeads (Miltenyi Biotec, Bergisch Gladbach, Germany) according to the manufacturer's instructions. RFP-HA and YFP fusion proteins were visualised by protein gel blotting using a monoclonal rat anti-HA antibody or a mouse anti-GFP antibody (Roche, Mannheim, Germany) and a horseradish peroxidase–conjugated goat anti-rat antibody or goat anti-mouse antibody, respectively (Jackson, Suffolk, UK). Chemiluminescence signals were visualised with a LAS-4000 mini luminescent image analyser (Fujifilm Europe, Düsseldorf, Germany). As controls YFP-MID and RFP-HA-COP1 were expressed alone or in combination with RFP-HA-attB1 or YFP-attB1 (both in pBatTL-B-p35s), respectively. RK19 alone was also infiltrated and tested. See Figure II - 1 for a detailed flow chart of this procedure.

In case of Co-IP from transformed *A. thaliana* cell suspension culture protoplast were prepared as described before (Mathur and Koncz, 1998c). See Figure II - 2 for a detailed flow chart of the procedure.

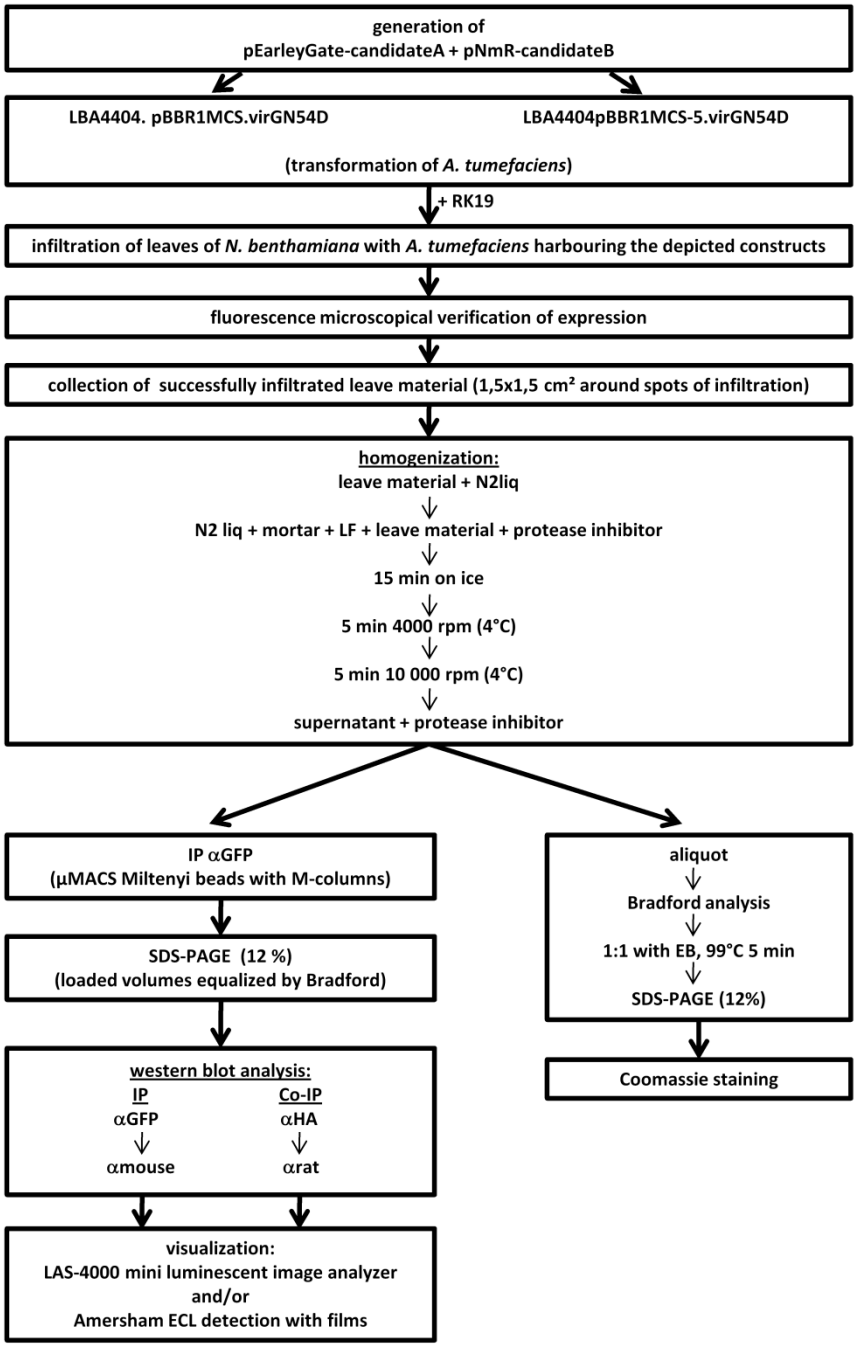

Figure II - 1: Flow chart for CoIPs from *N. benthamiana* infiltrated. SDS-PAGE gels had a concentration of 12.5% and not of 12% as indicated.

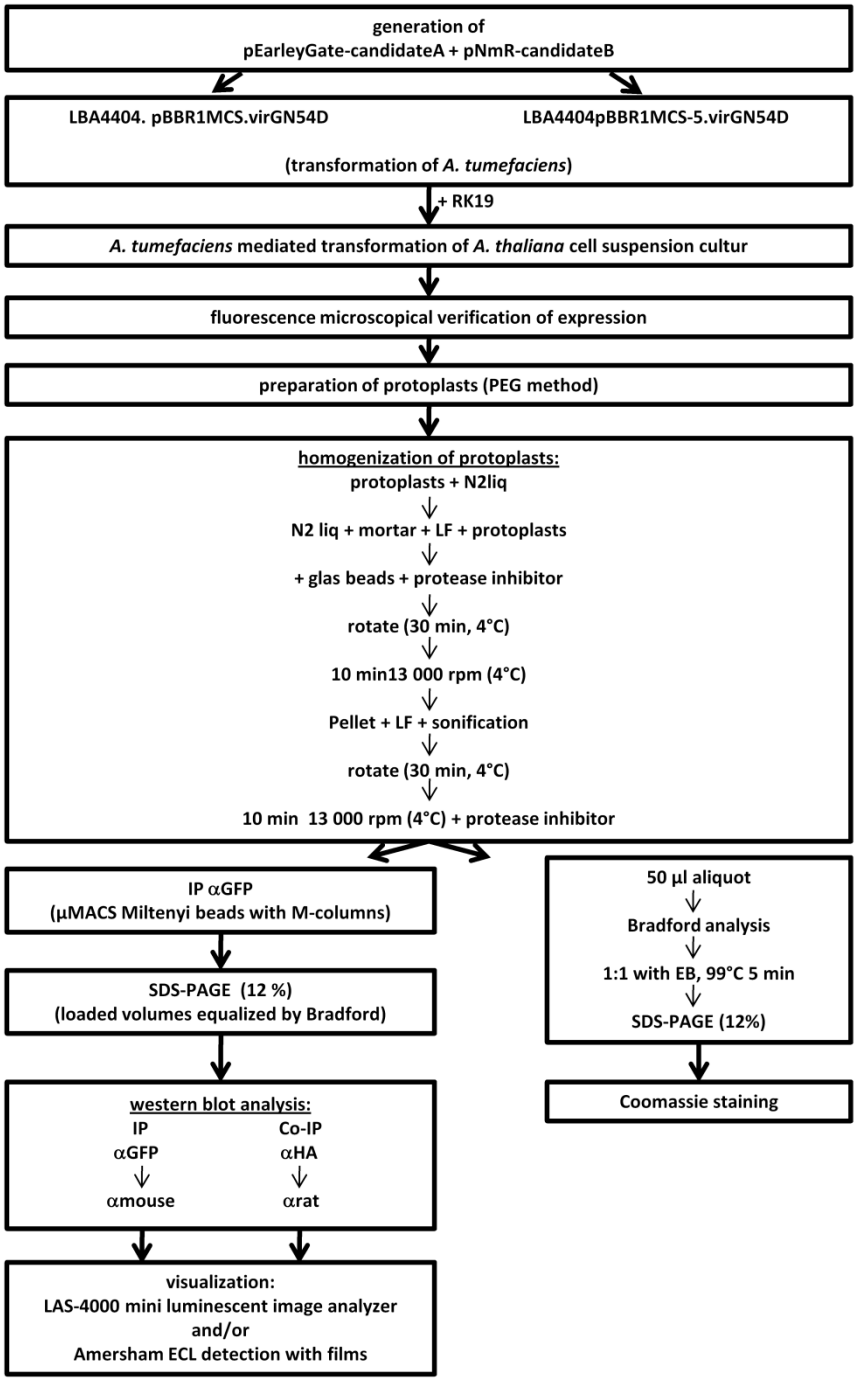

Figure II - 2: Flow chart for Co-IPs from transformed *A. thaliana* cell suspension culture. SDS-PAGE gels had a concentration of 12.5% and not of 12% as indicated.

2.4.7. Ubiquitin western blot analysis:

For ubiquitin detection an additional step was included in the western blotting procedure. The PVDF membrane was denatured. After blotting the membrane was incubated for 30 min in denaturation buffer at 4°C. Subsequently three washing steps for 10 sec, three steps for 5 min and three steps for 10 sec were done with PBST. Blocking and all following steps were performed as for all other western blot analysis, except that 3% BSA was used instead of Sucofin milk powder.

2.4.8. Stripping:

For stripping the probed membrane was ioncubated with stripping buffer for 30 min at RT. After washing the membrane with PBST the membrane was tested for remaining fluorescence. Subsequent analysis with another anti-body was performed as described for normal western blotting analysis using 3% BSA instead of Sucofin milk powder.

2.5. Plant methods

2.5.1. Growth conditions

After sawing, seeds were stratified for two days at 4°C. Seedlings were grown under LD conditions (16h light, 8h dark), SD (8h light, 16h dark) under constant white light (Wc), blue (Bc), red (Rc), far-red FR (FRc) light or in the dark. Seed were sterilised for growth on plates or sawn on soil.

To obtain "dark" conditions the plates were wrapped at least twice with aluminium foil. Two plant rooms were used for bolting experiments: one at 24°C (light bulbs: a mix of one Osram Cool White (L58W/21-840Lumilux Plus Eco) and one Natura de Luxe (L58W/76) providing on average 31-46 $\mu mol*m^{-2}*s^{-1}$) and the other at 21°C (light bulbs: providing on average 125 $\mu mol*m^{-2}*s^{-1}$) For protein stability tests, the plates were placed in a PERCIVAL incubator at different light conditions: Light conditions were measured with Bc: 5 $\mu mol*m^{-2}*s^{-1}$; Rc: 30 $\mu mol*m^{-2}*s^{-1}$; FRc 1 $\mu mol*m^{-2}*s^{-1}$.

2.5.2. Sterilisation

Seeds were sterilised with 70% [v/v] ethanol followed by 2% NaOCl for 3 min, subsequently washed with water, twice, and placed on agar-solidified plates containing 1x MS (pH 5,8) with 0, 1 or 3% sucrose. After cold treatment for 2-3 days at 4 °C, the plates were placed into white light for 4 h to induce germination and kept in at the depited light conditions at 21 °C for 7 days, if not quoted otherwise.

2.5.3. Cossings

Crossing was done as described before (Koornneef et al., 1992).

2.5.4. Genetic analysis

PCR for genotyping

Lines carrying multiple mutations were generated as described earlier (Kirik et al., 2007) with one modification. In the case of *mid-1*, F2 progeny was BASTA selected to analyse only resistant plants that carry at least one *mid-1* allele. Several primers were used to determine the genotype of the F2 and F3 progeny (see Table II - 5).

In general two different types of PCR were performed for TDNA insertion and EMS mutants examplified by *mid-1* and *cop1-4*. For the other genotypes see Table II - 5. *mid-1*: 5`-GTATCTGCCTGATAAATGGATTGTATTG-3` was used with SKI015 RB (Weigel et al., 2000) to identify the *mid-1* allele and with 5`-CTGCATGATAGAGGAACCGTTACATTAC-3` to detect the wild-type *MID* gene. In the case of *cop1-4*: the primer combination of 5`-CCAAAGAAGGATGCGCTGAGTGGGTCAGATACG-3` and 5`-TCTCGAGCTGTCAATCCAGATGACCAAG-3` creates a *Sna*BI restriction enzyme digestion site in the *cop1-4* allele but not in the wild-type *COP1* allele.

Segregation analysis:

T1 or F2 plants were planted and the segregation was determined according to their BASTA restistance when they carryes a construct conferring BASTA resistance. Otherwise plants were counted according to their phenotype or genotype. Homozygous lines were identified by a lack of segregation and tested for the number of insertation by the segragation analysis.

2.5.5. Measurements of hypocotyl length, petiole and lamina angles

Col-0, single mutant and the corresponding double mutant seedlings were grown on the same plate. Seedlings from 2-4 independent plates were measured (in total at least 40 plants for Col-0 and single mutants and 11 plants for double mutants). Hypocotyl length was measured using the segmented lines measurement tool of image J 1.41o (Wayne Rasband, NIH, USA). For *mid-1 cop1-4* a homozygous line (F4 plants), for *mid-1 cop1*^{eid6} a segregating line was analysed (F2 and F3 plants) and the genotypes were determined by PCR.

Petiole and lamina angles of the cotyledons were measured manually with photographs of the same seedlings. The petiole angle was defined as the angle between two lines that were drawn through the centers of the two petioles of the cotyledons. The centers were defined by two points close to the SAM in the middle of the petiole visible on a photograph. The lamina angle was defined as the angle between two lines drawn through the base and tip of the lamina of the cotyledons marked on a photograph. This angle was only measured for plants in which the two cotyledons could be seen from the side.

2.5.6. Determination of anthocyanin accumulation

Seedlings were grown on agar-solidified plates with 1x MS and 2% Sucrose for 3 days. 190 - 240 mg seedlings were harvested under green light and transferred to 1 ml extraction buffer (18% [v/v] 1-propanol and 1% [v/v] concentrated HCl) for anthocyanin extraction. The samples were incubated for 24h at room temperature in the dark and centrifuged. Total anthocyanin in the supernatant was determined spectroscopically using a NovaSpecII Spectrophotometer (Pharmacia LKB Biotech). The relative amount of anthocyanin per g freshweight was determined by calculating the difference of A_{535} and A_{650}. At least two independent experiments were performed. (Hoecker et al., 1998; Lange et al., 1971; Schmidt and Mohr, 1981)

2.5.7. Ploidy measurements

The C-content of epidermal cells of the hypocotyl of 7-day-old dark-grown seedlings was determined by DAPI staining using a Leica DMRB fluorescence microscope, a 360/40 DAPI BP excitation filter (Leica, Wetzlar, Germany) and DISCUS software package (Carl H. Hilgers-Technisches Büro, Königswinter, Germany). DAPI staining was done as described in Gendreau et al. (1997) with the following modifications: after staining, the seedlings were transferred for 45 min to 70% ethanol prior to mounting them in water. Four representative dark-grown seedlings from two independent 1x MS plates without sucrose were analysed. The intensity of the DAPI-fluorescence of the nuclei of 25-35 epidermal cells along the hypocotyl (no stomata guard cells) and of 15-22 stomata guard cells of the cotyledons was determined per plant. Fluorescence intensity was measured with the DISCUS software by adding up the intensity for all pixels of the marked nucleus minus the background of the cytoplasm. For each nucleus the mean of three measurements was calculated. The mean intensity of the stomata guard cells served as a 2C reference for the corresponding plant. The value for an epidermal nucleus was divided by the intensity of the 2C control and the result was doubled again

(=x). Classes for the corresponding C-contents were defined by the following half-open intervals: (0,3] (=2C); (3,6] (=4C); (6,12] (= 8C); (12,24] (=16C); (24,48] (=32C).

2.6. Microscopy, Image acquisition and processing

Confocal laser-scanning microscopy (CLSM) was performed using a Leica TCS-SP2 confocal microscope (DMRE7) equipped with the Leica software Lite 2.05 (LCS, Leica Microsystems). For two different fluorescence channels sequential scanning was applied starting with the laser with a higher wavelength. Z-stacks were merged for representation using the named software.

For fluorescence microscopy a Leica DMRB fluorescence microscope was used.

Two fluorescece binoculars were used in this work: Leica MZ10F fluorescence binocular and Leica MZFLIII fluorescence binocular (Scion Corporation Digitalkamera).

Photographs were taken with a Canon EOS 5D Mark II, Panasonic DMC-FZ50 or a TRAVELER Super Slim XS 8 digital camera and processed with Adobe Photoshop Elements 7.0.1 and IrfanView 4.25. Only brightness and contrast were changed simultaneously for all parts of one picture.

DNA gels were captured with a BioRad documenter and the geldoc programme Quantity one 4.5.0.

2.7. Software

Table II - 9 lists all used software.

Table II - 9: All software, programms and databases used in this work.

DISCUS software package	Carl H. Hilgers-Technisches Büro, Königswinter, Germany
Leica Application Suite (LAS)	Leica Microsystems
Leica Software Lite 2.05 (LCS)	Leica Microsystems
Leica Application Suit V3 Version 3.5.0	Leica Microsystems
ImageJ 1.41o	Wayne Rasband, NIH, USA
Cytoscape software (version 2.6.3)	(Shannon et al., 2003)
CLC DNA workbench 5.5	CLC bio A/S
SOPMA	(Geourjon and Deleage, 1995)
BioGrid	(Stark et al., 2006)
TAIR	(Swarbreck et al., 2008)
SMART	(Letunic et al., 2009; Schultz et al., 1998)
PSORT	(Robbins et al., 1991)
NCBI BLASTN and BLASTP	(Altschul et al., 1997)
Entrez Gene	(Maglott et al., 2005)
UniProt	Jain et al. 2009, The UniProt Consortium, 2010
MASCOT	(Perkins et al., 1999)
EndNote	Thomson Reuters
Microsoft Office 2007	Microsoft Corporation
Adobe Acrobat Reader 7.1.0	Adobe Systems Incorporated
Adobe Photoshop Elements 7.0.1	Adobe Systems Incorporated
IrfanView 4.25	http://www.irfanview.com/

III. Results

This work aimed at the identification of new regulators of COP1-controlled morphogenesis in *A. thaliana*. For this purpose, 32 new interaction candidates for COP1 were identified in yeast two hybrid (YTH) screenings and integrated together with screening results for DET1 into an interaction network of already published COP1 and DET1 interactors. (part 1)

Out of the network and the screening results, A putative new target of COP1, PAP2, and a putative new regulator of COP1, MID (= MIDGET), were chosen for further analysis. (part 2 and 3)

The interaction with COP1 was verified for both candidates using a bimolecular fluorescence complementation (BiFC) assay. Co-immunoprecipitation (Co-IP) showed that both candidates can share a complex with COP1 *in planta*. In addition, a new YTH-based domain mapping method was developed and used to identify specific domains of PAP2 and COP1 interacting with COP1 or MID, respectively. Evidence was gathered for PAP2 being a target of COP1. The functional relevance of the MID-COP1 interaction could be proven by analysing phenotypes of the single mutants and genetic interaction. New aspects of COP1 function and regulation depending on the interaction with MID could be unravelled regarding the stabilisation of COP1. First evidence positioning MID in a SPA1 and phyA dependent complex or pathway were obtained by the verification of the SPA1-MID interaction via BiFC, co-purification of MID with phyA and analysis of the protein stability of MID depending on light quality.

1. New putative targets and regulators of COP1 - screening and selection

1.1. Screening for new COP1 interactors

Prior to YTH screening COP1 has been tested for auto-activation (II.2.2.7.). COP1 is not auto-activating (Figure III - 5). Hoecker and Quail (2001) also reported this for the combination of pGBKT7-COP1 with the empty activation domain vector. The libraries listed in Table III - 1 were screened with COP1 as bait. Mating titres (number of yeast colonies that originated from a successful mating event) ranged between $2.1*10^6$ and 1.27*107 (Table III - 1; II.2.2.4.).

Table III - 1: Libraries used for the bait COP1 YTH screenings. Given is the name of the library, the origin of the included cDNA and mating titres of the performed screenings (number of yeast colonies that originated from a successful mating event).

bait	library	origin of the cDNA in the library	titre
COP1	Clontech	cDNA, green leaf material, 3 week old vegetative tissue (*A. thaliana* ecotype Col-0)	$2.1*10^6$
COP1	1699	cDNA suspension culture (*A. thaliana*) (Nemeth et al., 1998)	$4.65*10^6$
COP1	HS	cDNA, whole plant (*A. thaliana* ecotype Col-0)	$1.27*10^7$
COP1	REGIA	transcription factors (*A. thaliana*) based on cDNA from the REGIA project (Paz-Ares , The Regia Consortium; 2002)	$9*10^6$

Table III - 2 lists the COP1 screening results. Interaction candidates are sorted related to their already published functions and annotated domains. False positive classification was decided by using a database provided by J. F. Uhrig (unpublished data). A candidate is rated as false positive when it also appeared with other functional and structural independent baits in YTH screenings. Nevertheless, it cannot be ruled out that a false positive prey obtained from a YTH screening is a real interactor of the used bait. All colony PCR products with the same sequence or *Taq*I digestion pattern contributed to the absolute frequency of an interaction candidate in the performed screenings (Table III - 2). An example for the *Taq*I selection is shown in Figure III - 1.

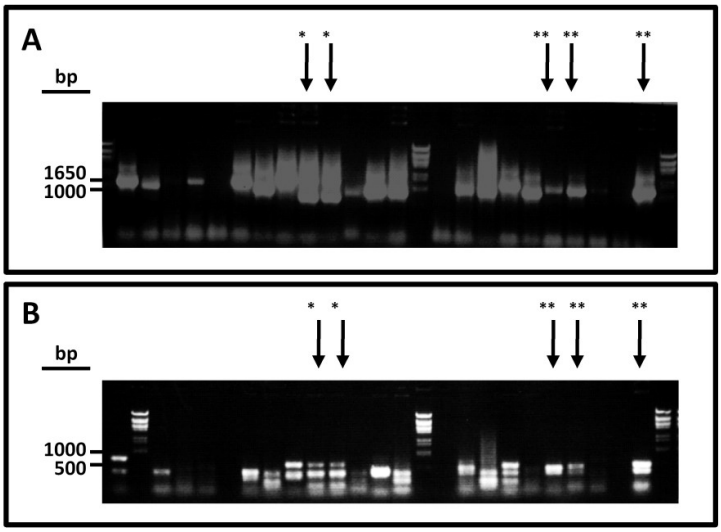

Figure III - 1: Example for the selection of amplicons from colony PCR by applying *Taq*I restriction.
(A) Colony-PCR amplicons after gel - electrophoresis. **(B)** Samples from (A) with additional *Taq*I digestion. Arrows point to examples that were defined as the same prey after *Taq*I digestion. Amplicons of two different preys are highlighted with one or two asterisks, respectively.

In order to verify the interaction with COP1, all interaction candidates from the 1699 library were tested by in vivo recombination (gap repair) prior to sequencing (II.2.2.8.) In case of YTH screenings with the Clontech, HS and REGIA libraries, at least one representative colony PCR product for each interaction candidates was used for verification of the interaction by gap repair (Table III - 2).

Table III - 2: Results of the COP1 YTH-screening. AGI codes of interaction candidates were identified using NCBI BLASTN (Altschul et al., 1997). The gene symbol, synonyms and the full name were obtained from TAIR (www.arabidopsis.org). All listed characterising data (predicted function and domains) for the interaction candidates were obtained from TAIR (www.arabidopsis.org). For At5g51730 a homology to an annotated domain was found that was not listed at TAIR (for the alignment see attachment A R-1). Additionally used sources are named in the fourth column from the right. In the last three columns the library from which the interaction candidate was identified, the frequency and the result of gap repair are given. Frequency: number of colony PCR products with the same sequence or digestion pattern. + / - indicate if an interaction could be verified by gap repair or not; n. d.: not determined. * false positive according to a database provided by J. F. Uhrig. Published interactors are greyed out.

AGI	symbol	synonyms	full name	predicted function / involed in	predicted domains	additional source	library	frequency	gap repair
DNA replication and modification									
At5g24630	MID	BIN4	MIDGET	part of DNA topoisomerase complex (ATP-hydrolyzing)	AT-hook	Kirik, V. *et al.* (2007)	1699	6	+
At2g30620	H1.2	-	HISTONE H1.2	nucleosome assembly	histone H1/H5, cellular component: nucleosome	-	HS	1	+
At4g02060	PRL*	MCM7	PROLIFERA	DNA replication initiation, DNA unwinding during replication, sugar mediated signaling pathway	DNA-dependent ATPase MCM, MCM protein 7	-	HS	5	+
At3g47490	-	-	-	endonuclease activity	HNH endonuclease	-	1699	2	+
At1g01690	PRD3	-	PUTATIVE RECOMBINATION INITIATION DEFECTS 3	necessary for creating DSBs	-	De Muyt, A. *et al.* (2009)	1699	1	+
Transcription									
At1g02340	HFR1	RSF1, FBI1, REP1	LONG HYPOCOTYL IN FAR-RED	transcription factor activity	helix-loop-helix DNA-binding, basic helix-loop-helix dimerisation region bHLH	-	HS	1	+
At1g66390	PAP2	MYB90	PRODUCTION OF ANTHOCYANIN PIGMENT 2	transcription factor activity	myb, DNA-binding, SANT, DNA-binding	-	REGIA	>90	+
At1g06040	STO	-	SALT TOLERANCE	transcription factor activity	zinc finger, CONSTANS-type	-	Clontech	6	+
At2g31380	STH	-	SALT TOLERANCE HOMOLOGUE	transcription factor activity	zinc finger, CONSTANS-type	-	Clontech, 1699	25	+
Development									
At3g02170	LNG2	-	LONGIFOLIA2	monopolar cell growth	-	-	HS	1	+
At1g71440	PFI	TFC E	PFIFFERLING	tubulin complex assembly, embryonic development ending in seed dormancy, cytokinesis	cytoskeleton-associated protein	-	HS	3	+
Protein modification									
At2g32950	COP1	-	CONSTITUTIVE PHOTOMORPHOGENIC1	E3 ubiquitin ligase	zinc finger (RING-type), WD40 repeat, coiled coil, homology to TAFII80	-	HS	14	+
At3g48330	PIMT1	-	PROTEIN-L-ISOASPARTATE METHYLTRANSFERASE 1	protein-L-isoaspartate (D-aspartate) O-methyltransferase activity, aging, response to salt stress, seed germination, abscisic acid	protein-L-isoaspartate(D-aspartate) O-methyltransferase	-	1699	1	+
Response to biotic / abiotic stress / signal transduction									
At5g42900	COR27	-	COLD REGULATED GENE 27	-	Evening Element in the promoter confers cold-induced gene expression	Mikkelsen, M. D. *et al.* (2009)	1699	3	+
At4g12720	NUDT7	GFG1, ATNUDX7	NUDIX HYDROLASE HOMOLOG 7	ADP-ribose hydrolase activity, negatively regulates EDS1-conditioned plant defense and programmed cell death	anti-sense to fibroblast growth factor protein, NUDIX hydrolase	-	HS	1	+
At4g16860	RPP4	-	RECOGNITION OF PERONOSPORA PARASITICA 4	defense response, defense response to fungi	leucine-rich repeat, disease resistance protein, Toll-Interleukin receptor, NB-ARC, ATP binding	-	HS	1	+
At2g20990	SYT1	SYTA, NTMC2T1.1	SYNAPTOTAGMIN 1	response to cold, plasma membrane repair, protein targeting to membrane	C2 calcium-dependent membrane targeting, C2 calcium/lipid-binding region	-	HS	2	+
At5g37740	-	-	-	-	C2 calcium-dependent membrane targeting, C2 calcium/lipid-binding region	-	1699	2	+
Transport									
At5g13450	ATPS DELTA	-	DELTA SUBUNIT OF MT ATP SYNTHASE	ATP synthesis coupled proton transport	ATPase, F1 complex, OSCP/delta subunit	-	1699, HS	6	+
At4g02510	TOC159	TOC86, TOC160, PPI2	TRANSLOCON AT THE OUTER ENVELOPE MEMBRANE OF CHLOROPLASTS 159	protein targeting to chloroplast	chloroplast protein import component Toc86/159, AIG1 (GTP binding)	-	HS	5	+
At4g11790	-	-	-	intracellular transport	Ran Binding Protein 1, pleckstrin homology-type	-	HS	1	n.d.

TABLE III - 2 (continued)

AGI	symbol	synonyms	full name	predicted function / involed in	predicted domains	additional source	library	frequency	gap repair
Metabolic processes									
At5g19550	ASP2	AAT2, ASPAT	ASPARTATE AMINOTRANSFERASE 2	nitrogen metabolism, major cytosolic isoenzyme controlling aspartate biosynthesis in the light	pyridoxal phosphate-dependent transferase, major, aspartate/other aminotransferase	-	1699	1	+
At1g79530	GAPCP-1	-	GLYCERALDEHYDE-3-PHOSPHATE DEHYDROGENASE OF PLASTID 1	carbohydrate metabolic process, glycolysis, primary root development	glyceraldehyde 3-phosphate dehydrogenase, NAD(P)-binding; Molecular Function: catalytic activ	-	1699	1	+
At4g26910	-	-	-	dihydrolipoyllysine-residue succinyltransferase activity, acyltransferase activity	2-oxoacid dehydrogenase acyltransferase, catalytic, biotin/lipoyl attachment, dihydrolipoamide succinyltransferase	-	HS	1	-
At5g55070	-	-	-	2-oxoacid dehydrogenase family protein, response to oxidative stress	2-oxoacid dehydrogenase acyltransferase, catalytic, biotin/lipoyl attachment, dihydrolipoamide succinyltransferase	-	HS	13	+
At5g61450	-	-	-	2-phosphoglycerate kinase-related	-	-	HS	1	+
Cell wall biogenesis									
At5g65730	-	-	-	xyloglucosyl transferase, response to water deprivation	xyloglucan endotransglucosylase/hydrolase	-	Clontech	1	+
Photosynthetic protein									
At2g30570	PSWII	-	PHOTOSYSTEM II REACTION CENTER W	protein similar to photosystem II reaction center subunit W	Photosystem II protein PsbW, class	-	Clontech	1	+
Ribosomal proteins/translation									
At3g49080	-*	-	-	translation, structural constituent of ribosome	ribosomal protein S5 domain 2-type fold	-	1699	1	+
At3g53430	RPL12B*	-	60S ribosomal protein L12	translation, structural constituent of ribosome	ribosomal protein L11	-	1699	1	+
At5g60670	RPL12C*	-	60S ribosomal protein L12	translation, structural constituent of ribosome	ribosomal protein L11	-	HS	3	+
At3g26400	EIF4B1	-	EUKARYOTIC TRANSLATION INITIATION FACTOR 4B1	translation initiation factor activity	plant specific eukaryotic initiation factor 4B	-	1699	1	+
Others									
At1g21740	-	-	-	N-terminal protein myristoylation	protein of unknown function DUF 630 and DUF632	-	HS	2	+
At1g30070	-	-	-	domains: SGS, CS, HSP20-like chaperone; SGT1-like protein, Sgt1p is a highly conserved eukaryotic protein that is required for both SCF (Skp1p/Cdc53p-Cullin-F-box)-mediated ubiquitination and kinetochore function in yeast and also plays a role in the cAMP pathway.		InterPro (EMBL-EBI)	1699	1	+
At1g49850	-	-	-	protein / zinc ion binding, possibly E3-ubiquitin-protein ligase	zinc finger, RING-type, C3HC4 type RING finger	PROSITE (Hulo, N. *et al.* (2007))	1699	2	+
At3g54760	-	-	-	-	description (TAIR): dentin sialophosphoprotein-related	-	1699	2	+
At4g33980	-	-	-	unknown, best BLAST result from Arabidopsis thaliana for COR27	-	-	1699	2	+
At5g47690	-	-	-	binding	armadillo-type fold	BLASTp (NCBI)	HS	1	+
At5g51730	-	-	-	best hit (BLASTp): ATNUC-L2 (ATRANGAP1 at Entrez Gene), AtNUC-L1 for their RRM (RNA recognition motif)/RBD (RNA binding domain)/RNP (ribonucleoprotein domain), a highly abundant domain in eukaryotes in proteins involved in post-transcriptional gene expression processes: mRNA and rRNA processing, RNA export, and RNA stability,interacts with ssRNA, ssDNA + proteins		this work, attachment	1699	5	+

The classical selection of an interesting interaction candidate identified by YTH screening is based on literature research and grouping of YTH screening results according to (predicted) functions of the interaction candidates. In a first step this type of analysis was conducted. Highly abundant metabolic and ribosomal proteins are often found as false positives in YTH screenings (personal observation). The ribosomal proteins listed in Table III - 2 were also rated as false positives by the used database (J. F. Uhrig, unpublished data). In this regard, three groups remain in which four or five interaction candidates could be grouped: "transcription", "response to biotic / abiotic stress / signal transduction", "DNA replication and modification".

Transcription:

The identification of already published interactors of COP1 –STO, STH and HFR1 – in addition to COP1 itself, indicates that the screenings were successful for all used libraries except for the REGIA library (Duek et al., 2004, McNellis et al., 1996, Holm et al., 2001). In case of the REGIA library consisting of transcription factors, only one interaction candidate was found that has not been published as an interactor of COP1 before. The only new candidate in this group – PAP2 – is a promising candidate for a putative target of COP1.

Response to biotic / abiotic stress / signal transduction:

All listed proteins are involved in signal transduction pathways and therefore of high interest for further analysis. At the time of candidate selection, four proteins were described as unknown proteins in the TAIR database. At this time, no strong evidence indicated that one of these interaction candidates regulates COP1 function and no candidate was chosen from this group for further analysis. Only RPP4 (RECOGNITION OF PERONOSPORA PARASITICA 4) was annotated by TAIR, a protein involved in pathogene response.

DNA replication and modification:

MID, a component of the TOPOVI complex, is essential for endoreduplication (Breuer et al., 2007; Kirik et al., 2007). PRD3 (PUTATIVE RECOMBINATION INITIATION DEFECTS 3) was recently (after the selection was done) described to be necessary for creating DSBs (De Muyt et al., 2009). *Mid* mutants as well as *cop1* mutants exhibit an increase in DSBs (Breuer et al., 2007; Dohmann et al., 2008). Histone H1.2 could link COP1 to chromatin and therefore position COP1 in an interesting context concerning regulation of transcription. For *MID*-mutants, chromatin remodelling as well as silencing defects were observed (Breuer et al., 2007; Kirik et al., 2007).

In concert with one of the interactors of this group COP1 might directly be involved in DNA modifying processes and cell cycle progression.

Unknown or less characterised proteins are often neglected when selecting a candidate. To obtain a selection criterion that is also suitable for these proteins, properties of already published interactors were used.

1.2. Selection of a new putative target of COP1

In the presented YTH screening, a huge number of so far unknown putative COP1 interactors were identified. In addition, already known interactors were found and subsequently used to develop a quick and cheap method to classify the interaction candidates. STO (At1g06040) and STH (At2g31380) share a conserved interaction motif (Holm et al., 2001). Holm and co-workers (2001) could show that a salt bridge between Lys^{550} of COP1 and an aspartate e.g. located in the conserved motif in STO, STH is necessary for the interaction with COP1.

Gap repair with $COP1^{K550E}$, was applied in order to classify the interaction candidates identified in the screening. In parallel, gap repair with COP1 as a bait and the same selected amplicons served as a positive control. It was expected that yeast harbouring STO and STH would grow on interaction media (SD-LWH_3: selective drop out media lacking leucine, tryptophan and histidine, supplemented with 3mM 3-AT see II.1.11) in combination with COP1 but not with $COP1^{K550E}$. If a candidate would bind to the WD40 domain of COP1 in the same way like STO and STH, it is likely to be a target of COP1. Candidates with the same gap repair result as expected for STO and STH were classified as a putative target of COP1. It has to be mentioned that typically no selection for negative growth is used in yeast experiments. Therefore, the result of this experiment can only give a hint and reduce the number of interaction candidates to be analysed. Further verification is needed. In Table III - 3 only those interaction candidates are listed that grew in combination with COP1 after the gap repair experiment. This experiment has been performed once. Verification, e.g. by full length YTH experiments is necessary. Beside the published protein STO, PAP2, an unknown protein (At2g30570), a xyloglucane endotransglycosylase (At5g65730) and two probably false positive candidates (PRL and a structural constituent of the ribosome) could be identified as putative targets of COP1. The majority of described COP1 functions and interactions take place in the nucleus (Seo et al., 2003; Wang et al., 2001; Yu et al., 2008). Since PAP2 is the only putative nuclear protein in this group, it is the most promising putative target that has been identified in the presented YTH screenings. PAP2 will hence be analysed in more detail in part 2 of this work concerning its interaction with COP1.

COP1 has been shown to interact with itself via its coiled-coil domain (Torii et al., 1998). The result that COP1 interacts with itself and with $COP1^{K550E}$ in gap repair experiments together with the expected results for STO underlines that at least the coiled-coil and WD40 domain are folded properly for the interaction in yeast. Therefore, the reliability of this method has been proven. In the case of the proteins of the second group listed in Table III - 3, Lys^{550} of COP1 does not seem to be essential for the interaction or they are false positives.

Table III - 3: Classification of putative COP1 interactors in regard to their ability to bind to $COP1^{K550E}$ in yeast by comparative gap repair. + / - describes the growth on interaction media of yeast harbouring the depicted bait and prey constructs after gap repair. Only interaction candidates that grew in combination with COP1 in this experiment are listed. Candidates were grouped according to their ability to interact with $COP1^{K550E}$ or not. An asterisk marks candidates that were categorised as false positives. SD-LWH_3: selective drop out media lacking leucine, tryptophan and histidine, supplemented with 3mM 3-AT.

AGI	prey	bait	growth on SD-LWH_3		bait
At1g06040	STO	COP1	+	-	$COP1^{K550E}$
At1g66390	PAP2 = (MYB 90)	COP1	+	-	$COP1^{K550E}$
At4g02060	PRL*	COP1	+	-	$COP1^{K550E}$
At2g30570	PSWII	COP1	+	-	$COP1^{K550E}$
At5g65730	Xyloglucan Endotransglycosylase	COP1	+	-	$COP1^{K550E}$
At5g60670	structural constituent of ribosome*	COP1	+	-	$COP1^{K550E}$
At2g32950	COP1	COP1	+	+	$COP1^{K550E}$
At5g42900	COR27	COP1	+	+	$COP1^{K550E}$
At1g01690	PRD3	COP1	+	+	$COP1^{K550E}$
At1g49850	zinc finger (C3HC4-type RING finger) family protein	COP1	+	+	$COP1^{K550E}$
At4g33980	unknown protein	COP1	+	+	$COP1^{K550E}$
At5g19550	ASP2	COP1	+	+	$COP1^{K550E}$
At1g79530	glyceraldehyd-3-phosphat-dehydrogenase	COP1	+	+	$COP1^{K550E}$

1.3. Screening for new DET1 interactors

According to genetic evidences and complex formation with other COP1 regulators, DET1 is thought to act upstream or in concert with COP1 (Ang and Deng, 1994; Chen et al., 2010; Chen et al., 2006; Nixdorf and Hoecker, 2010; Yanagawa et al., 2004). In order to identify a new putative regulator of COP1, putative DET1 interactors obtained from YTH screenings were integrated together with the COP1 interaction candidates in a generated interaction network of published COP1 interactors (Figure III - 3).

For this purpose, DET1 YTH screenings were performed in analogy to the COP1 screenings. In the frame of this work, no gap repair verification has been conducted due to time limitation. The

putative DET1 interactors only served for the network-based selection of a putative regulator. Five to ten days after mating, yeast colonies can be transferred from the Gelrite interaction medium to agar plates for further analysis. In the case of DET1, the first distinct colonies were transferred after ten days. The mating titres (number of yeast colonies that originated from a successful mating event) were comparable with those of the COP1 screenings.

Table III - 4: Libraries used with the baits DET1, $DET1^{1-277}$, $DET1^{150-452}$ and $DET1^{277-543}$ and mating titre (number of yeast colonies that originated from a successful mating event) of the YTH screenings.

bait	library	titre
DET1	Clontech	$1.23*10^7$
DET1	1699	$7.5*10^6$
DET1	HS	$5.15*10^6$
DET1	REGIA	$1.52*10^7$
$DET1^{1-277}$	Clontech	$1.32*10^7$
$DET1^{1-277}$	1699	$1.43*10^7$
$DET1^{1-277}$	HS	$1.91*10^7$
$DET1^{1-277}$	REGIA	$4.35*10^6$
$DET1^{150-452}$	Clontech	$2.6*10^6$
$DET1^{150-452}$	1699	$1.27*10^7$
$DET1^{150-452}$	HS	n.d.
$DET1^{150-452}$	REGIA	$3.3*10^6$
$DET1^{277-543}$	Clontech	$4.6*10^6$
$DET1^{277-543}$	1699	$1.28*10^7$
$DET1^{277-543}$	HS	$1.42*10^7$
$DET1^{277-543}$	REGIA	$4.25*10^7$

In Table III - 5 22 amplicons could be grouped for five different preys after *Taq*I digestion and sequencing. 73% coded for ARP1 (ARABIDOPSIS RIBOSOMAL PROTEIN 1), the most common artefact within the libraries. This indicates (1) that DET1 is either toxic for yeast, (2) that the N-terminal fusion with the GAL4-activation domain prevents the proper folding of DET1 which is sufficient for interactions or (3) that there is only a very low number of DET1 interactors.

To improve the screening efficiency, fragments of DET1 were generated. DET1 is a protein of 543 aa with no functional domains characterised so far. In order to avoid that any sheet or helix is destroyed, the secondary structure was predicted using the SOPMA program (Geourjon and Deleage, 1995). $DET1^{1-277}$, $DET1^{150-452}$ and $DET1^{277-543}$ start and/or end in coiled coil domains. All fragments have a size of 150-350 aa to allow proper folding of probably existing interaction domains within the sequence. (Figure III - 2)

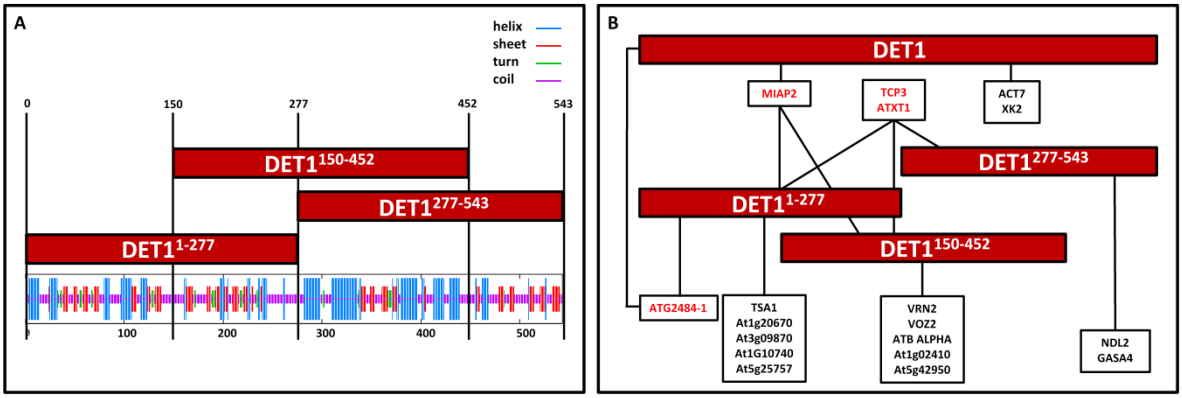

Figure III - 2: Fragmentation of DET1 and YTH screening results.
(A) Secondary structure of DET predicted by the SOPMA program (Geourjon and Deleage, 1995). Numbers indicate amino acid positions of DET1. Note: the three generated DET1 fragments (DET1$^{1-277}$, DET1$^{150-452}$ and DET1$^{277-543}$) start and/or end in coiled coil domains. **(B)** Interaction candidates for DET1 identified in YTH screenings with the full length DET1 or the three fragments. No false positives or candidates that appeared with all three fragments are shown. Note that two putative interactors were found in screenings that interacted with two and two putative candidates that interacted with all different DET1 baits (red).

Mating titres (number of yeast colonies that originated from a successful mating event) and growth behaviour of the yeast cells were comparable to those of the full length protein. The number of different obtained interaction candidates from YTH screenings increased to 17 for all fragments in comparison to five for full length DET1. 58% of the amplicons coded for ARP1. Beside ARP1, two candidates were identified in screenings with all three different fragments. It is likely that these interactions are artificial, although it is possible that an interaction candidate can bind to two domains within one protein. Interestingly, in the case of tomato DET1 it has been shown that the nonacetylated N-terminal tail of H2B can bind to TDET1$^{1-448}$ and to TDET1$^{374-523}$ (Benvenuto et al., 2002). Therefore, these candidates were included in the network in the next chapter, although they might be false-positives.

Table III - 5: Results of the DET1 YTH-screening. AGI codes of interaction candidates were identified using NCBI BLASTN (Altschul et al., 1997). The gene symbol, synonyms and the full name were obtained from TAIR (www.arabidopsis.org), except the name MIAP2 that was designated in my diploma thesis for (At2g45680). All listed characterising data (predicted function and domains) for the interaction candidates were obtained from TAIR (www.arabidopsis.org). Additionally used sources are named in the sixth column from the right. In the last five columns the library from which the interaction candidate was identified, the frequency in total and for the three DET1 fragments DET1$^{1\text{-}277}$, DET1$^{150\text{-}452}$ and DET1$^{277\text{-}543}$ is given. Frequency: number of colony PCR products with the same sequence or digestion pattern. * false positive according to a database provided by J. F. Uhrig. Published interactors are greyed out.

							frequency					
AGI	symbol	synonyms	full name	predicted function / involed in	predicted domains	additional source	library	total	DET1$^{1\text{-}543}$	DET1$^{1\text{-}277}$	DET1$^{150\text{-}452}$	DET1$^{277\text{-}543}$
DNA replication and modification												
At4g16845	VRN2		REDUCED VERNALIZATION RESPONSE2	response to cold, regulation of gene expression by genetic imprinting, vernalization response	zinc finger protein with similarity to Polycomb group (PcG) proteins of plants and animals	Gendall, A. R. *et al.* (2001)	HS	1	0	0	1	0
Transcription												
At1g53230	TCP3		TEOSINTE BRANCHED1, CYCLOIDEA AND PCF TRANSCRIPTION FACTOR 3	transcription factor	Transcription factor, TCP		REGIA	28	0	21	4	3
At2g45680	MIAP2	-	MIDGET ASSOCIATED 2	(TCP family transcription factor)	Transcription factor, TCP	my diploma thesis	REGIA	4	2	1	1	0
At1g20670	-	-	-	(protein-protein binding, assembly or activity of multi-component complexes involved in transcriptional activation)	Bromodomain	Tamkun, J. W. (1995)	HS	2	0	2	0	0
At2g42400	VOZ2	-	VASCULAR PLANT ONE ZINC FINGER PROTEIN 2	transcription activator activity, DNA binding, dimerization	Domain-A and Domain-B (functional novel zinc coordinating motif and a conserved basic region)	Mitsuda, N. *et al.* (2004)	HS	1	0	0	1	0
Cell cycle												
At1g52410	TSA1	-	TSK-ASSOCIATING PROTEIN 1	(mitosis, calcium ion binding)	novel calcium-binding repeat	Suzuki, T. *et al.* (2005)	HS	1	0	1	0	0
RNA binding proteins												
At4g17330	ATG2484-1	-	ARABIDOPSIS THALIANA G2484-1 PROTEIN	(RNA binding)	Tudor-like, plant, Agenet; , RNA binding		HS	2	1	1	0	0
Response to biotic / abiotic stress / signal transduction												
At3g09870	-	-	-	(response to auxin stimulus)	Auxin responsive SAUR protein		HS	3	0	3	0	0
At5g11790	NDL2		N-MYC DOWNREGULATED-LIKE2	acts in a signaling pathway that modulates root auxin transport, auxin gradients, affects levels of at least two auxin transport facilitators	Pollen specific protein SF21	Mudgil, Y. *et al.* (2009)	HS	1	0	0	0	1
At5g15230	GASA4		GAST1 PROTEIN HOMOLOG 4	response to gibberellin stimulus, gibberellic acid mediated signaling pathway, regulates flowering and seed development	Gibberellin regulated protein	Roxrud, I. (2007)	HS	1	0	0	0	1
At1g51690	ATB ALPHA		PROTEIN PHOSPHATASE 2A 55 KDA REGULATORY SUBUNIT B ALPHA ISOFORM	(protein phosphatase type 2A complex, nucleotide binding, signal transduction)	Protein phosphatase 2A, regulatory subunit PR55, WD40 repeat		HS	3	0	0	3	0
Cytoskeleton												
At5g09810	ACT7	-	ACTIN7	structural constituent of cytoskeleton	ACTIN domains: ATP and protein binding		HS	1	1	0	0	0
Metabolic processes												
At1g10740	-	-	unknown protein	(glycerol biosynthetic process)	-		1699	1	0	1	0	0
At3g62720	ATXT1	XT1, XXT1	ARABIDOPSIS THALIANA XYLOSYLTRANSFERASE 1	polysaccharide biosynthetic process,xyloglucan biosynthetic process, root hair elongation	galactosyl transferase		HS	16	0	2	9	5
At5g49650	XK2	XK-2	XYLULOSE KINASE 2	phosphorylating xylulose and deoxy-xylulose, most likely plays a role in producing precursors for isoprenoid biosynthesis	Carbohydrate kinase, FGGY		1699	2	2	0	0	0
Assembly of proteins												
At1g02410	-	-	-	(protein complex assembly, copper ion binding)	Cytochrome c oxidase assembly protein CtaG/Cox11		Clontech, HS	6	0	0	6	0
Ribosomal proteins												
At1g43170	ARP1*		ARABIDOPSIS RIBOSOMAL PROTEIN 1	cytoplasmic ribosomal protein	Ribosomal protein L3; Translation elongation and initiation		HS, 1699	118	16	21	28	53
Others												
At5g25757	-	-	-	-	-		HS	2	0	2	0	0
At5g42950	-	-	-	(GYF domain-containing protein)	GYF		HS	4	0	0	4	0

1.4. Generation of an interaction network for COP1 and DET1

All proteins of the presented network in this chapter are either direct interactors of COP1 or DET1 or they are interactors of these direct interactors. In the graphical visualisation of an interaction network, nodes represent proteins that are connected by lines or edges in the case of interaction. A protein with lots of interactors is called a hub, whereas for the determination of a threshold for a hub varying criteria are used (Aragues et al., 2007; Ekman et al., 2006; Han et al., 2004).

The interaction network for COP1 and DET1 was generated by assembling results from Cytoscape (version 2.6.3) database screenings, additional screening of the EntrezGene and BioGRID database and literature research for new results that are not included in the databases yet (Maglott et al., 2005; Stark et al., 2006). All interactions were traced back to the original paper. Only interactions that were found by YTH or a reconstituted complex (BioGRID nomenclature (www.thebiogrid.org): An interaction is detected between purified proteins in vitro.) were selected and are shown in the network in Figure III - 3 with black, purple or green solid lines. Results from Co-IP experiments with plant material were neglected. Therefore, the network can be called YTH-based.

Finally, own results from YTH screenings with COP1, DET1, DET1-fragmnets, MID and RHL1 as baits (this work and my diploma thesis) were integrated into the network (Figure III - 3, dotted purple, blue and green lines). The interaction of MID with MIAP1 (MIDGET ASSOCIATED PROTEIN1, DRIP2) and ACT7 (ACTIN 7) was additionally verified by BiFC experiments in leek (*Allium porrum*). The interaction of GRF1 and MIAP2 was shown in a full length YTH experiment and BiFC in leek in the same work (Figure III - 3, both: solid green lines). (sources for all interactions can be found in A R-2 in the attachment)

One structural network element can easily be recognised: a clique in which every node is connected to all other nodes. The COP9 signalosome in the presented interaction network represents such a motif (black solid lines in Figure III - 3). Another example might be SPA1, SPA2, SPA3, SPA4, DDB1A, DDB1B, COP1 and CO or SPA1, SPA2, SPA3 and SPA4. Multibody structures like protein complexes or dynamic functional modules have a high structural significance (Spirin and Mirny, 2003; Yeger-Lotem et al., 2004). The COP9 signalosome shows that these structures can be identified in this small network. Hubs with eight and more solid edges in the presented network are COP1, DDB1A, COP10 phyB, phyA, DDB1A, CO, CSN1, CSN3, CSN4, SPA1 and HFR1. Nodes are listed according to their degree (number of edges), starting with the highest.

The generated protein interaction network will be used in the next chapter for the selection of a putative new regulator of COP1.

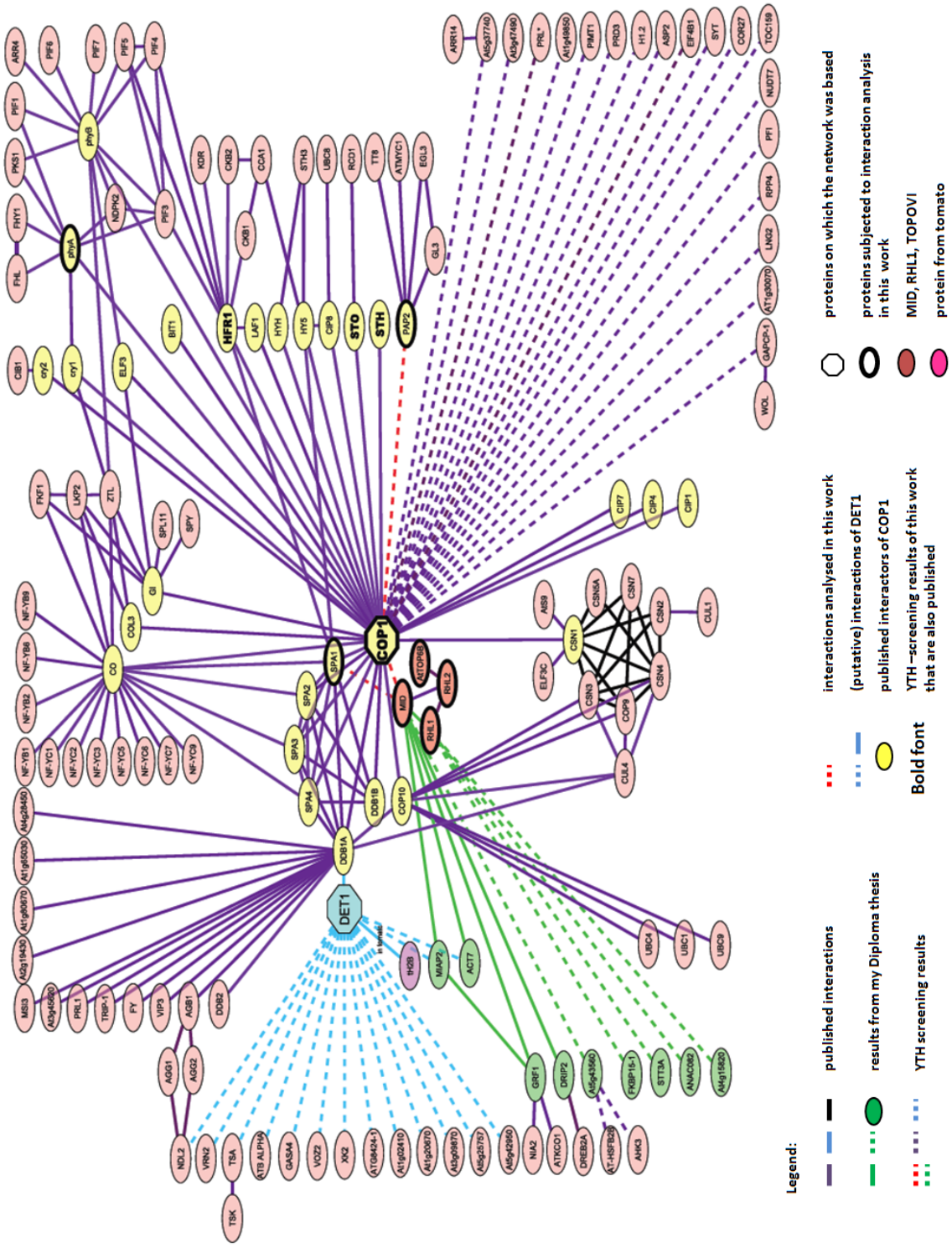

Figure III - 3: COP1 and DET1 interaction network. This network was created using the Cytoscape software (version 2.6.3), (Shannon et al., 2003), Entrez (Maglott et al., 2005), UniProt (Jain et al. 2009, The UniProt Consortium, 2010), BioGRID (Stark et al., 2006), TAIR (Swarbreck et al., 2008). The displayed components and interactions in this network are based on three criteria: 1) Interactions needed to be shown at least in yeast. 2) Shown interactors are interactors of COP1 or DET1 or the interactors of these. 3) All interactions represented by purple, black or blue solid lines are supported by a publication. A list for all interactions can be found in the attachment (A R-2).
Proteins are nodes, interactions are represented by edges in this network; octagonal shape: proteins from which this network was developed; solid lines: published interactions; dashed lines: YTH screening results; solid green lines: YTH screening results (for GRF1-MIAP2: full length YTH) that were verified by BiFC in my Diploma thesis; bold font: interactors that were published and also identified in the YTH screens of this work; red lines: interactions analysed in this work; thick frame: interactors in the centre of analysis in this work; yellow filling: (putative) interactors of COP1; blue lines: (putative) interactors of DET1; green filling and lines: results of my Diploma thesis; pink filling: interactors from other species, in the case of DET1 the conserved *Solanum lycopersicum* version was used; red filling: TOPOVI, MID and RHL1. MIAP2: At2g45680.

1.5. Selection of a new putative regulator of COP1

MID is the only putative COP1 interactor connecting to other proteins in the COP1-DET1-interaction-network presented in the previous chapter. In the case of MID, the generated network shows a direct link not only with COP1 but also with SPA1 and two indirect links with DET1 via MIAP2 and ACT7. This positions MID in a frame of two COP1 function modifying proteins that share complexes with COP1 (Ang et al., 1998; Fittinghoff et al., 2006; Nixdorf and Hoecker, 2010; Pick et al., 2007; Saijo et al., 2003; Saijo et al., 2008; Seo et al., 2003; Yanagawa et al., 2004; Zhu et al., 2008).

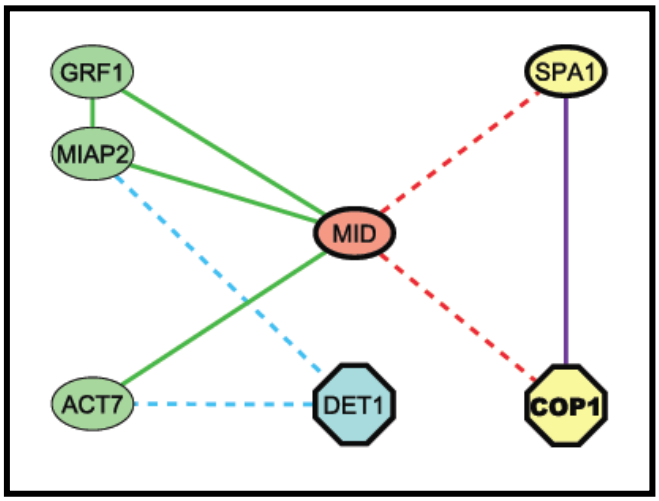

Figure III - 4: Extract from the COP1 and DET1 interaction network presented in FIgure III - 3. The graphic was created using Cytoscape software (version 2.6.3) (Shannon et al., 2003).
octagonal shape: proteins from which this network in Figure III - 3 was developed; solid purple line: published interaction (evidence according to verified BioGRID database data: by YTH, reconstituted complex, affinity capture-Western and -MS, co-purification; Hoecker and Quail, 2001; Saijo et al., 2003; Saijo et al., 2008; Stark et al., 2006; Zhu et al., 2008); dashed blue lines: YTH screening results; solid green lines: YTH screening (GRF1-MIAP2: full length YTH) results that were verified by BiFC in my Diploma thesis; bold font: interactors that were published and also identified in the YTH screens of this work; dashed red lines: interactions analysed in this work; thick frame: interactors in the centre of analysis in this work; yellow filling: interactors of COP1; green filling and lines: results of my Diploma thesis; red filling: MID.

Figure III - 4 shows that MID, COP1 and SPA1 form a triangle, the simplest geometrical form that can be found in an interaction network (Milo et al., 2002). 92% of the triangles in the yeast interactome represent known protein complexes (Yeger-Lotem et al., 2004).

To place MID in one or several different complexes or pathways with COP1, SPA1 and DET1, the direct interaction of MID with COP1 and the functional relevance of the interaction was investigated in this work. First experiments concerning the physical and functional interaction or dependency of MID and SPA1 were performed.

2. PAP2 - a new putative target of COP1

PAP2 (At1g66390) was selected as putative target of COP1 in I-2. Several hints have already indicated that PAP2, a putative interactor of COP1, is probably a transcription factor marked for degradation by COP1:

First, PAP2 as a R2R3-MYB protein has the ability to bind to DNA (Klempnauer and Sippel, 1987; Sakura et al., 1989) and can activate the *DFR* promoter in concert with EGL3, GL3 or TT8 (Zimmermann et al., 2004). Second, it has already been shown that overexpression of PAP2 leads to accumulation of anthocyanin in *A. thaliana* and *Nicotiana tabacum* cv. Xanthi (Borevitz et al., 2000). Third, amongst others, HY5, LAF1 or HFR1 are targets of COP1 and are involved in the regulation of anthocyanin biosynthesis (Duek et al., 2004; Jang et al., 2005; Saijo et al., 2003; Seo et al., 2003). PAP2 would fit in such a regulative context. And fourth, no interaction of PAP2 with $COP1^{K550E}$ could be concluded from a gap repair experiment with the mutated $COP1^{K550E}$, indicating that PAP2 behaves similar to STO, STH and HY5 in YTH experiments (compare III. 1.2).

Taken together, these functional properties strongly suggest that PAP2 is a target of COP1. Further experiments presented in this chapter will substantiate that the selective gap repair experiment described in III.1.2. identified a so far unknown target of COP1.

2.1. PAP2 interacts with COP1

2.1.1. The PAP2 - COP1 interaction in yeast

PAP2 interacts with COP1 in the selective gap repair experiment (chapter III.I.2) but no interaction could be shown with the $COP1^{K550E}$ mutant. This result was verified with full length constructs in a double transformation YTH experiment (Figure III - 5 - A, B). Because the PAP2 GAL4-binding domain fusion is auto-activating in yeast (E), only PAP2 GAL4-activation domain fusions could be used for further yeast experiments. GFP served as a negative control and no growth was observed in the combination with PAP2 as a prey (C, D, to show specific interaction).

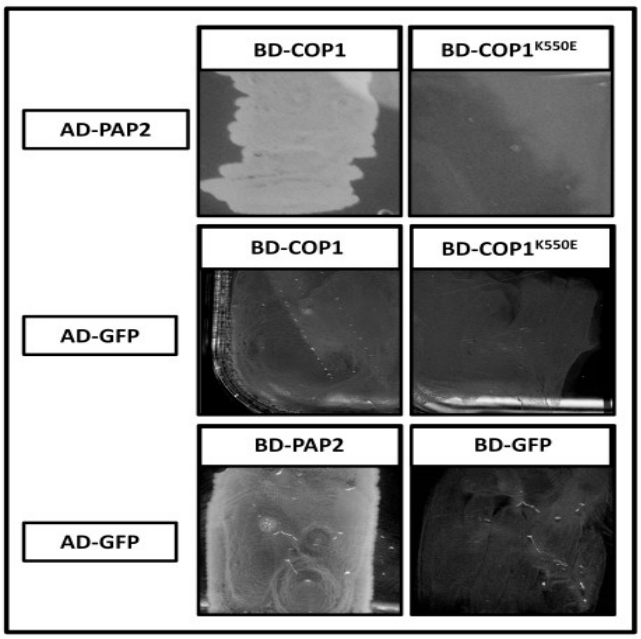

Figure III - 5: PAP2 interacts with COP1 but not with COP1^{K550E} in yeast. *Saccharomyces cerevisiae* AH109 were transformed with two constructs coding for the depicted fusion proteins (pAS2-1-attR-COP1, pAS2-1-attR-COP1^{K550E}, pAS2-1-attR-PAP2, pAS2-1-attR-GFP, pACT-attR-PAP2, pACT-attR-GFP). Double transformed cells were first selected on on SD-LW medium and then tested for interaction on SD-LWH medium supplemented with 3 mM 3-AT. Combinations with GFP served as negative controls. BD: GAL4-binding domain; AD: GAL4-activation domain

2.1.2. PAP2 and COP1 colocalise and interact *in planta*

Growth in the presented YTH experiment is a result of an interaction of two proteins (or complex formation) in the yeast nucleus. A prerequisite for the interaction of two proteins *in planta* is their colocalisation. To answer the question, if COP1 and PAP2 colocalise in plant cells, plasmids for the expression of YFP-tagged PAP2 and for RFP-tagged COP1 were generated.

2.1.2.1. YFP-PAP2 and RFP-HA-COP1 are functional fusion proteins *in planta*.

PAP2 was recombined into pEarleyGate104 using Gateway® Technology resulting in an N-terminal YFP-fusion (Earley et al., 2006). The vector pNmR (N-terminal mono RFP) was constructed for the fusion of RFP-HA to the N-terminus of COP1. A fusion to the N-terminus was preferred, as the C-terminus of COP1 might be more sensitive to structural changes (McNellis et al., 1994a). The C-terminus (amino acids 374-670) consists of seven WD40 repeats with a total number of 28 predicted β-sheets which most likely folds as a seven bladed β-propeller (Holm et al., 2001; Sondek et al., 1996).

pNmR is based on the vector pBatTL-B-p35S. Figure III - 6 illustrates that pBatTL-B-p35s allows a Pro35S:Pro35S-driven expression with a translational enhancer. The vector was obtained by cutting

out (*Spe*I) the N-terminal portion of *YFP* that was located downstream of the Gateway® cassette of pBatTL-B-sYFP-N (J. F. Uhrig, unpublished). The accuracy of the sequence of the religated vector was confirmed by sequencing at the restriction site. Finally, pNmR was created for N-terminal fusions of RFP-HA under Pro35S:Pro35S regulation with a translational enhancer in plants using pGJ2811 containing mRFP1-Q66T (Jach et al., 2006) as a template. RFP-HA was amplified with the primers JU339 and JU340 (designed by J. F. Uhrig) and cut with *Bam*HI and *Bgl*II. pBatTL-B-p35s was linearised with *Bgl*II. RFP-HA was ligated upstream of the Gateway® cassette as verified by sequencing. Both binary vectors confer BASTA resistance in plants and a spectinomycin resistance in bacteria. (Figure III - 6)

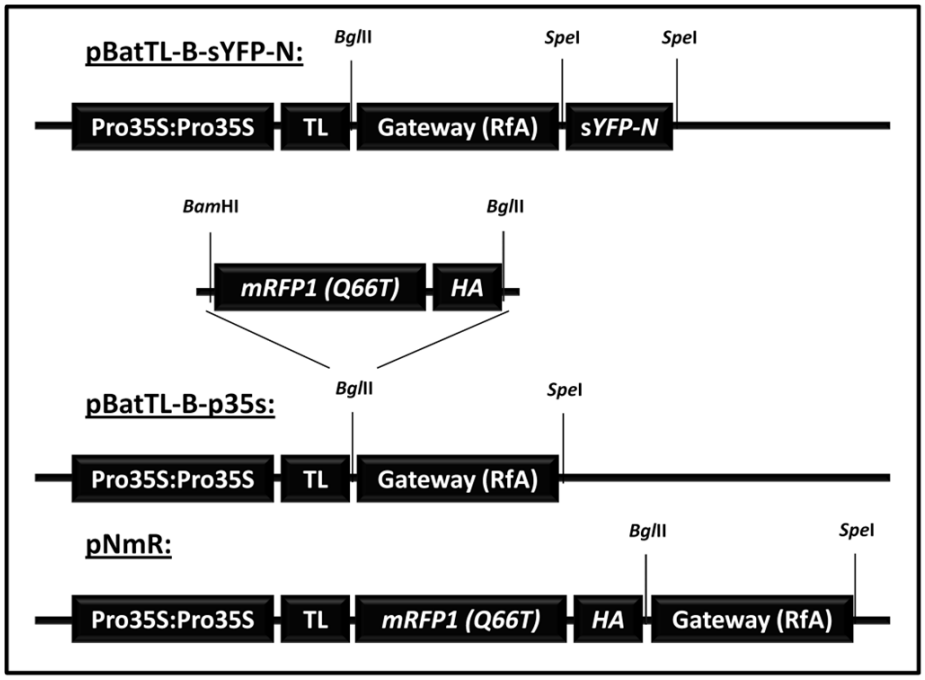

Figure III - 6: Construction of pNmR. Vectors used for constructing pNmR, as well as pNmR itself, are shown schematically. Pro35S: Cauliflower Mosaic Virus 35s promoter; TL: translational enhancer; mRFP1 (Q66T): optimised mono RFP from Jach et al. (2006); HA: hemagglutinin tag; sYFPN: N-terminal portion of YFP; RfA reading frame A; *Bgl*II and *Spe*I: restriction sites. A vector map of pBatTL-B-p35s and pNmR can be found in attachment A R-3.

To test the functionality of Pro35SYFP-PAP2, no complementation test could be done because in the case of *PAP2* no *A. thaliana* mutant was available. Stable BASTA selected T2 *A. thaliana* plants expressing PAP2 under the control of Pro35S in Col-0 background, were purple in comparison to Col-0, indicating that probably anthocyanin or comparable derivatives accumulated (Figure III - 8-A), which reflects the described overexpressing phenotype (Borevitz et al., 2000). A very weak YFP-signal was visible in some cells but could not be documented. Further analysis of *A. thaliana* overexpression lines and generation of other (maybe C-terminal) fusion proteins will be necessary in the future to further analyse the PAP2 localisation in *A. thaliana*.

In contrast to the observations in *A. thaliana*, YFP-PAP2 was easily detectable in the nuclei of transformed *Nicotiana benthamiana* leaf epidermal cells (Figure III - 7). Three different localisation patterns were observed (Figure III - 7): PAP2 localises in *N. benthamiana* to the whole nucleus with a highlighted dot, in some rare cases in several subnuclear foci or to the whole nucleus. Additionally a faint signal was visible in some cases in the cytoplasm.

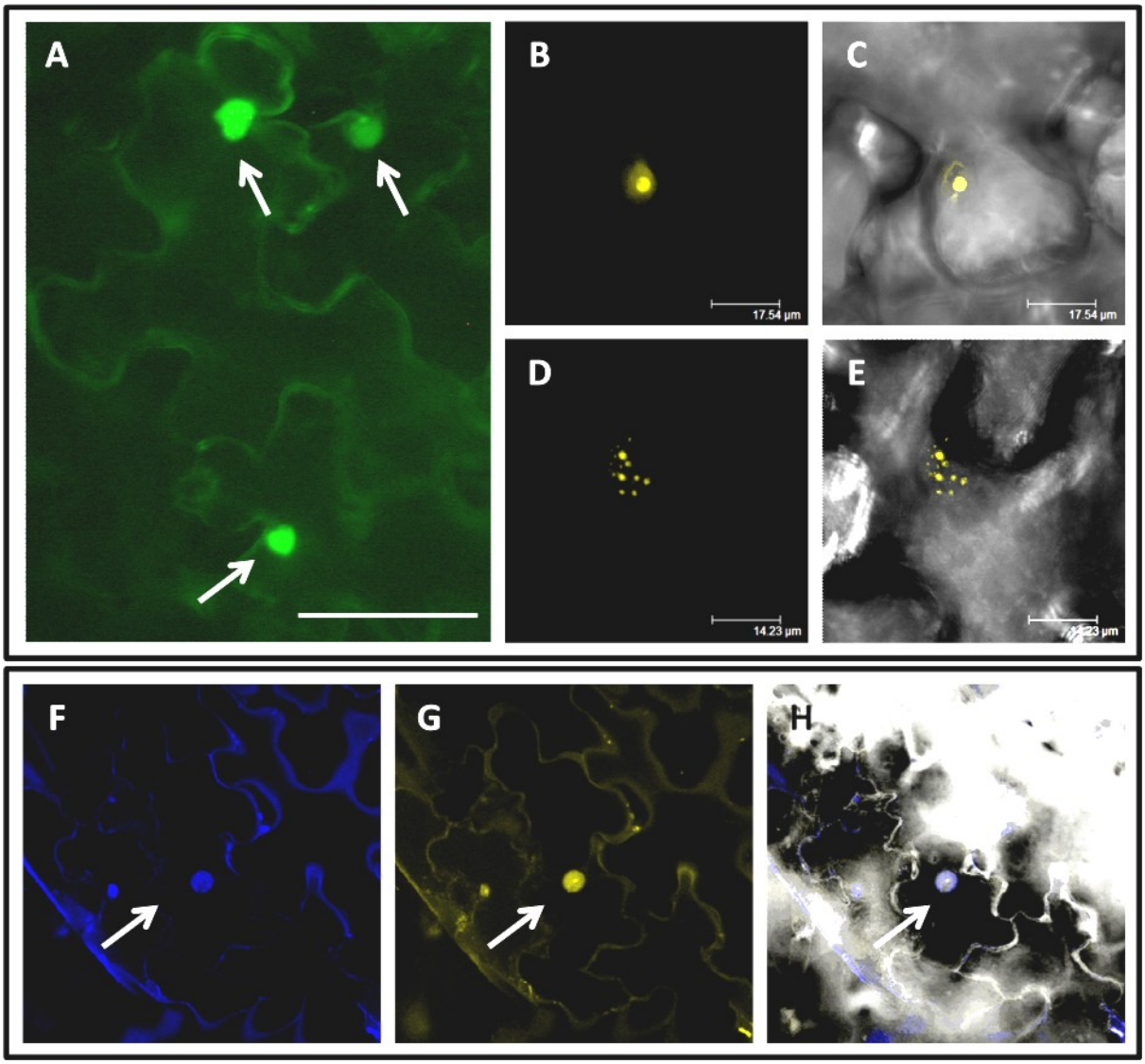

Figure III - 7: YFP-PAP2 localises to the nucleus in *Nicotiana benthamiana*.
Leaves of *N. benthamiana* were transiently transformed by co-infiltration with *A. tumefaciens* LBA4404.pBBR1MCS. virGN54D pEarleyGate104-PAP2 and the anti silencing strain RK19. Pictures were taken three days after infiltration (dai).
(A) fluorescence microscopy; **(B-H)** Confocal Laser Scanning Microscopy (CLSM); **(B, D, G)** YFP-channel; **(F)** DAPI staining; **(C, E, H)** merged picture with transmission picture. Bar equals 100 µm in (A), 17,53 µm in (B-C) and 14,53 µm in (D-E). Arrows point to nuclei.

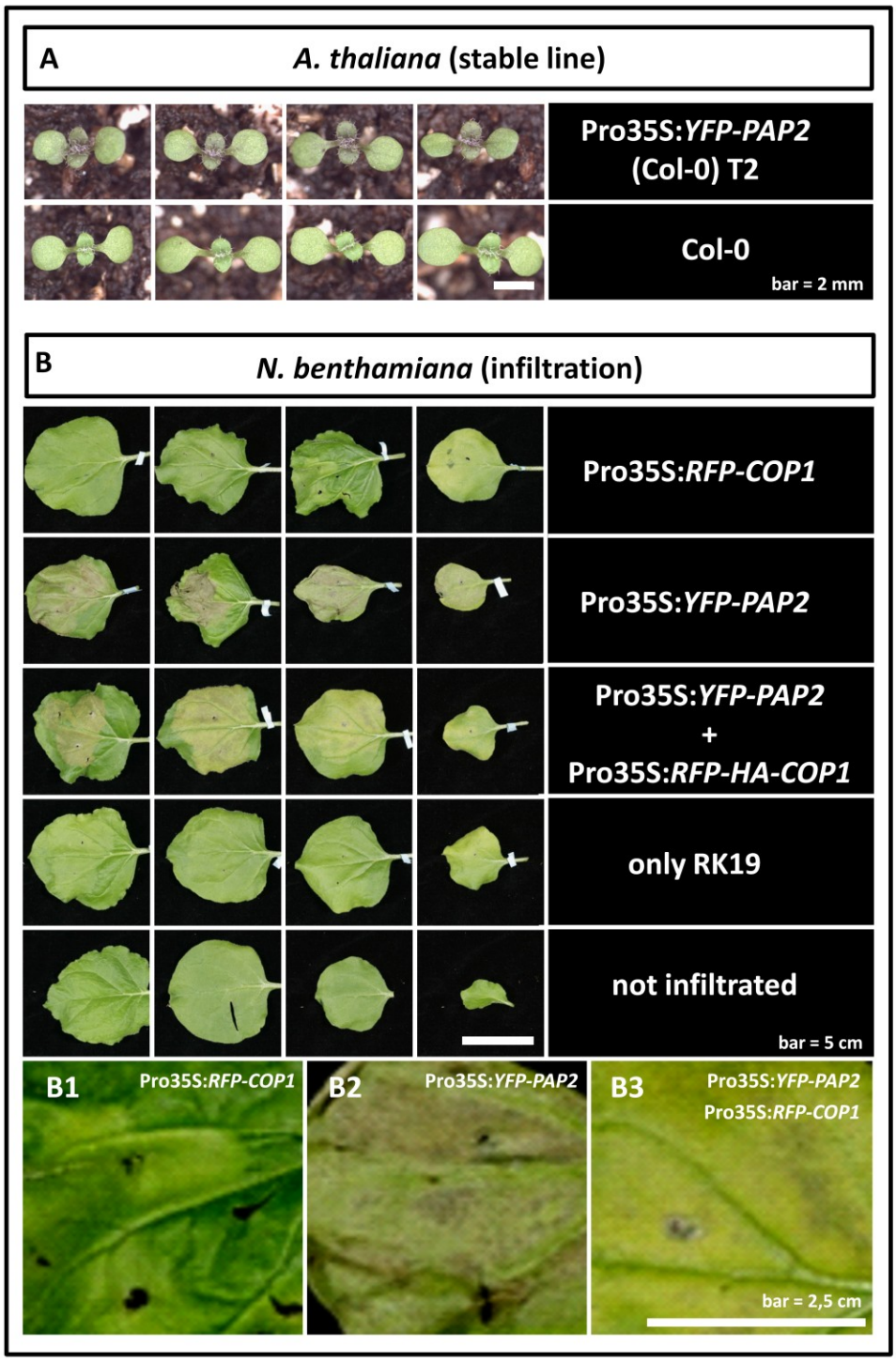

Figure III - 8: Functionality of Pro35S:Y*FP-PAP2* and functional connectivity of COP1 and PAP2 *in planta*.
(A) Upper row: Pro35S:Y*FP-PAP2* (Col-0) (T_2), floral dip transformation *A. thaliana* Col-0 by *Agrobacterium tumefaciens* GV3101, selection with BASTA. Col-0 plants of the same age and growth conditions are shown as a comparison. Pictures were captured nine days after germination (dag). Growth conditions: seeds were stratified for two days at 4°C and transferred to LD conditions at 21°C. **(B)** Five leaves per *N. benthamiana* plant were transiently transformed by infiltration with *A. tumefaciens*. Co-infiltration with combinations of *A. tumefaciens* harbouring the depicted constructs and *A. tumefaciens* RK19: first three rows. Infiltration with *A. tumefaciens* RK19 alone: fourth row. No infiltration: last row. **(B1-B3)** Enlargement of the corresponding third leaf from the left. pEarleyGate104-PAP2 in LBA4404.pBBR1MCS.virGN54D; pNmR-COP1 in LBA4404pBBR1MCS-5.virGN54D; RK19 = anti silencing strain.

N. benthamiana leaves co-infiltrated with *A. tumefaciens* RK19 and *A. tumefaciens* LBA4404.pBBR1MCS.virGN54D harbouring pEarleyGate104-PAP2 turned purple at the sites of infiltration at least three days after infiltration (dai) and finally got necrotic (dry and dead leaf material around the spots of infiltration). Co-expression of YFP-PAP2 and RFP-HA-COP1 led to a phenotype not as severe as in case of sole YFP- PAP2 expression (Figure III - 8) or of combined expression of YFP-PAP2 with RFP-attB1 (personal observation, RFP-HA-attB1 is described in III 2.1.3.). The colour of leaves expressing both fusion proteins five to seven dai was equivalent to the colour of leaves expressing YFP-PAP2 alone or in combination with RFP-HA-attB1 after three days (Figure III - 8 and personal observation). No quantification has been performed. Leaves infiltrated with *A. tumefaciens* RK19 and *A. tumefaciens* LBA4404pBBR1MCS-5.virGN54D harbouring RFP-HA-COP1 or with *A. tumefaciens* RK19 alone served as negative controls. The described phenotype occurred in all transformation events. At least three independent transformations were performed per combination. It can be concluded that YFP-PAP2 is functional in *A. thaliana* and *N. benthamiana* concerning the accumulation of anthocyanin.

It has already been shown that COP1 localises to subnuclear foci in the dark (von Arnim and Deng, 1994; von Arnim et al., 1997). In the light, the protein is depleted from the nucleus to the cytoplasm (von Arnim and Deng, 1994). This process needs several hours (von Arnim et al., 1997), so that it is possible to observe the nuclear localisation in COP1-overexpressing plants during the day.

Figure III - 9 shows that RFP-HA-COP1 in Col-0 background localises in subnuclear foci of a mature trichome under the control of Pro35S. Characteristically aggregates are visible in the cytoplasm which has previously been observed for overexpression of GUS-COP1 or GFP-COP1, respectively (Ang et al., 1998; von Arnim et al., 1997). The trichome was chosen as a cell type that completed several rounds of endoreduplication whereas the second example, the stomata guard cell, does not endoreduplicate at all. A subnuclear localisation could not be resolved for the latter so far (Figure III - 9). Therefore, other objectives or probably oil immersion in combination with DAPI staining to identify the nuclei should be used to assure that the observed localisation is in the nucleus and does not belong to cytoplasmic RFP-HA-COP1-aggregates localised close to the nucleus. Beside the characteristic localisation, the functionality of the Pro35S:Pro35S:*RFP-HA-COP1* construct was proven by a rescue experiment. In Figure III - 9 it can be seen that stable transformed *cop1-4* plants could be rescued with pNmR-COP1. Older plants showed all aspects of phenotypes: from the *COP1*-mutant phenotype (silencing) to an over-complementation phenotype with bigger leaves (see A R-4 in the attachment) and a longer shoot compared to the Col-0 wildtype. This was not observed for the

overexpression in Col-0 background. The segregation ratio of two lines per background was determined. BASTA resistance served as a marker for successful transformation. For the Col-0 background 75.8% and 74.2% of the plants were BASTA-resistant, for the *cop1-4* background the percentages were 75% and 74.7%, respectively. The observed segregation ratios indicate that the analysed plants carried only one T-DNA insertion coding for RFP-HA-COP1. Taken together, it can be concluded that the RFP-HA-COP1 fusion protein exhibits typical COP1 functions *in planta*.

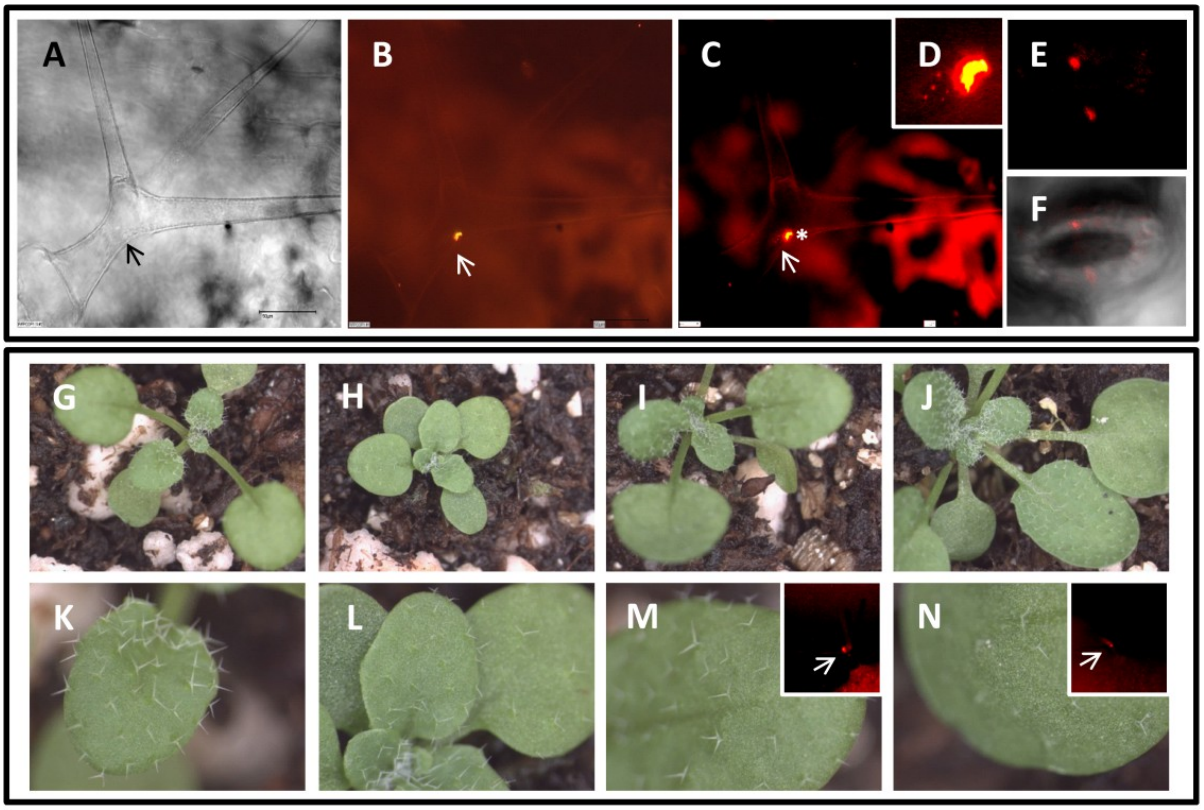

Figure III - 9: Functionality of Pro35S:Pro35S:*RFP-HA-COP1 in planta*.
(A-F) RFP-HA-COP1 expression in Pro35S:Pro35S:*RFP-HA-COP1* (Col-0) T_1 *A. thaliana* plants. **(A-C)** Mature trichome; **(E-F)** stomata guard cells; **(A)** bright-field image; **(B-D)** fluorescence microscopy with DS-red filter; **(E-F)** CLSM; **(F)** transmission picture. Note the localisation to subnuclear foci in the trichome nucleus in the close-up image in (D). In (C) brightness and contrast were modified in comparison to B to visualise the subnuclear localisation. Arrows point to nuclei. *: an aggregate in the cytoplasm resulting from COP1-overexpression that can also be seen in D.
(G-N) 15-day-old plants grown on soil under LD conditions at 21°C. (G-J) and (K-N) have the same magnification. **(K-J)** Enlargements of (G-J). Insets in (M-N): RFP-fluorescence in a trichome of the corresponding plant. All pictures were captured with a fluorescence binocular. **(G, K)** Col-0; **(H, L)** *cop1-4*; **(I, M)** Pro35S:Pro35S:*RFP-HA-COP1*(Col-0) T_1; **(J, N)** Pro35S:Pro35S:*RFP-HA-COP1* (*cop1-4*) T_1.

2.1.2.2. PAP2 and COP1 colocalise *in planta*

The prerequisite for interaction is the colocalisation of two proteins. The colocalisation of PAP2 and COP1 could be shown in epidermal cells of *Allium porrum*, leaf epidermal cells of *N. benthamiana* and cells of *A. thaliana* cell suspension culture. For colocalisation in the monocotyledon *Allium porrum* an N-terminal CFP-fusion protein of COP1 was expressed using pENSG-CFP (N. Medina-Escobar, unpublished, MPIZ Cologne) and YFP-PAP2 using pEarleyGate104. Both proteins colocalise in distinct subnuclear foci (Figure III - 10-A-D).

The functional constructs coding for RFP-HA-COP1 and YFP-PAP2 described in III. 2.1.2.1. were used for colocalisation experiments in cells of *A. thaliana* cell suspension culture. Transformation efficiency was low and for YFP-PAP2 only a weak, almost not presentable YFP-signal, possibly due to degradation of the protein, was visible in a fluorescence microscope. Pictures could not be captured with a Confocal Laser Scanning Microscope because of bleaching effects. Colocalisation was also observed in subnuclear foci (Figure III - 10-M-P).

In order to increase the number of analysed cells and to obtain a stronger YFP-signal, the colocalisation was also analysed in *N. benthamiana* as another example of a dicotyledon in comparison to the monocotyledon *Allium porrum*. It could be shown that RFP-COP1 colocalises with YFP-PAP2 in one or more subnuclear foci (Figure III - 10-E-L). Nuclei of leaf epidermal cells of *N. benthamiana* were much larger than nuclei of *A. thaliana* cell suspension culture cells and detection of fluorescence signals of transformed cells was improved. For *N. benthamiana*, additional DAPI staining was performed to identify the nuclei (attachment A R-5). Thereby the localisation of both proteins to the nucleus could be confirmed. All localisation experiments described in this work were repeated at least once.

Figure III - 10: PAP2 and COP1 colocalise in subnuclear foci *in planta*. (see next page)

(A-D) Colocalisation of CFP-COP1 and YFP-PAP2 in biolistically transformed leek epidermal cells. Pictures on the right are close-up images of the nucleus in A-D; **(E-L)** Colocalisation of RFP-HA-COP1 and YFP-PAP2 in infiltrated epidermal leaf cells of *N. benthamiana* **(M-P)** Colocalisation of RFP-HA-COP1 and YFP-PAP2 in an *A. thaliana* cell suspension culture cell. Leaves were co-infiltrated and the suspension culture cells were co-transformed with a combination of *A. tumefaciens* harbouring pNmR-COP1, pEGATE104-PAP2 and *A. tumefaciens* RK19. *N. benthamiana* plants were kept at 24°C at LD conditions. *A. thaliana* cell suspension cultures were kept with constant shaking in the dark. Pictures were taken three dai or five days after transformation, respectively.
(A, M) bright-field images, (M) was rendered to greyscale for a better visualisation; **(B-C), (N-O)** fluorescence microscopy; **(E-L)** CLSM (independent scanning, displayed pictures are merged z-stacks), **(I-L)** close-up images of the marked area visualised in E; **(E, I)** transmission picture; **(F, J)** RFP-channel; **(G, K)** YFP channel; **(D, H, L, P)** merged pictures; arrows point to nuclei, red structures outside the nuclei are typical cytoplasmic COP1-overexpression-aggegates; bar equals 50 µm in (A-D) and 25 µm in (P). CFP-COP1: pENSG-CFP-COP1; YFP-PAP2: pEarleyGate104-PAP2 (LBA4404. pBBR1MCS.virGN54D); RFP-HA-COP1: pNmR-COP1 (LBA4404pBBR1MCS-5.virGN54D); RK19 = anti silencing strain.

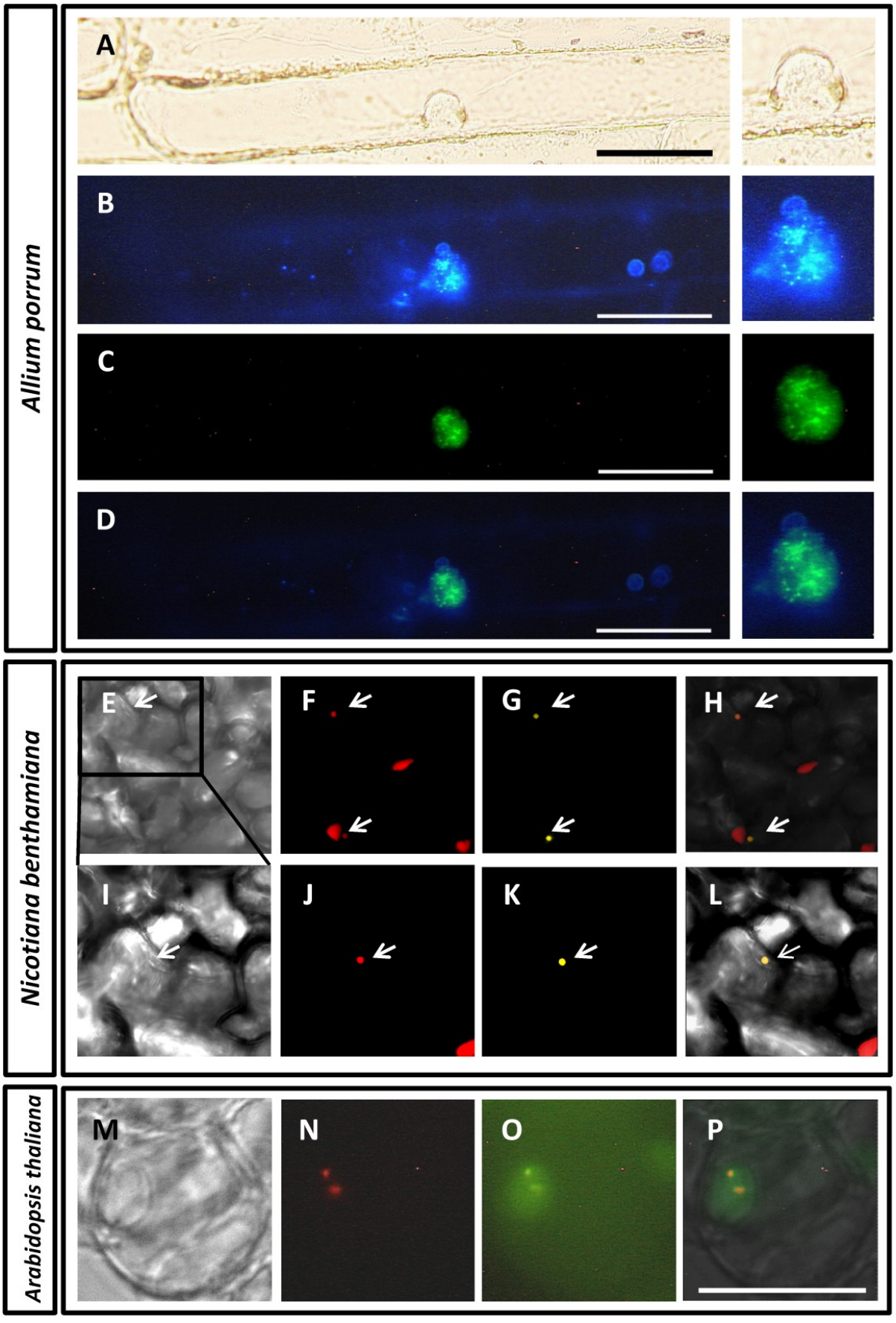
Allium porrum
A
B
C
D
Nicotiana benthamiana
E
F
G
H
I
J
K
L
Arabidopsis thaliana
M
N
O
P

2.1.2.3. PAP2 and COP1 interact in *Allium porrum*

The direct PAP2 - COP1 interaction was further verified *in planta* by BiFC experiments. The N- and C-terminal halves of YFP were fused to PAP2 and COP1. Constructs coding for the fusion proteins were biolistically transferred into epidermal cells of *Allium porrum*. The YFP molecule is only reconstituted if the two fusion proteins interact. The cytoskeleton marker CFP-TALIN was co-bombarded as a transformation control. The experiment was performed twice. Cytoplasmic aggregates or putative inclusion bodies were observed for all COP1 combinations analysed via BiFC, as reported elsewhere (Ang et al., 1998; von Arnim et al., 1997).

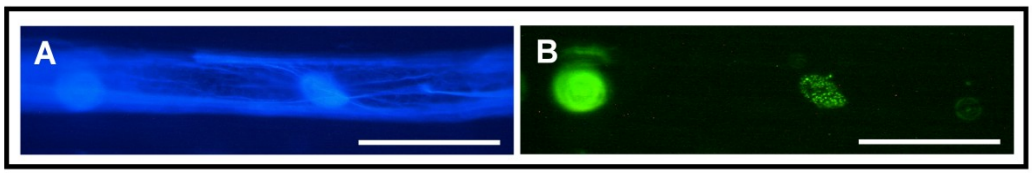

Figure III - 11: BiFC assay for PAP2 and COP1. Plasmids encoding BiFC fusion constructs of PAP2 and COP1 with the N- or C-terminal part of YFP were co-bombarded into leek cells (*Allium porrum*). **(A)** CFP-TALIN served as a transformation control. **(B)** YFP fluorescence indicates interaction between PAP2 and COP1. The interaction was localised to subnuclear foci. Bar equals 100 µm. BiFC-constructs: pCL112-COP1, pCL113-PAP2.

2.1.3. PAP2 and COP1 share one complex *in vivo*

If PAP2 is a target of COP1 it needs to be present in a complex with COP1 *in planta*. The abilities of RFP-HA-COP1 and YFP-PAP2 to share a complex in a dicotyledon were tested by a Co-IP experiment. The constructs used for this experiment were the same as for the co-localisation studies. Their functionalities *in planta* have already been shown in III. 2.1.2.1. COP1 is known to be part of different complexes (Chen et al., 2010; Chen et al., 2006; Saijo et al., 2008; Zhu et al., 2008) and a huge number of interactors has already been identified (see Figure III - 3). Therefore, YFP-PAP2 was immunoprecipitated with Miltenyi αGFP µMACS beads whereas RFP-HA-COP1 was detected by western blot analysis with an αHA-antibody in case of successful Co-IP. The Miltenyi based Co-IP from proteins expressed in cells of *A. thaliana* cell suspension culture and infiltrated *N. benthamiana* leaf material was established and optimised (see II.2.4.6. for details).

Transformed dark grown cells of *A. thaliana* suspension culture were used for the Co-IP experiment. Transformation efficiency was low and for YFP-PAP2 only a weak YFP-signal, possibly due to degradation of the protein, was visible in a fluorescence microscope that could not be captured because of bleaching effects.

The Co IP experiments were furthermore performed by infiltration of *N. benthamiana* leaves in order to increase YFP-PAP2 concentration. The expression and colocalisation in leave epidermal cells of *N. benthamiana* has already been shown for RFP-HA-COP1 and YFP-PAP2 in III.2.1.2.2. An advantage of fluorescence tagged proteins is that their expression and proper localisation can be tested prior to the Co-IP experiment. Making use of this property, the concentrations of the fusion proteins in the input fraction were adjusted. Only successfully infiltrated leaf material of a defined size around the infiltration spots was selected, cut out and weighed. The same fresh weight was used for all samples of one Co-IP experiment Total protein concentrations of the input fractions were comparable. (see Bradford analysis in the attachment, A R-6)

Immunoprecipitated YFP-PAP2 from infiltrated *N. benthamiana* leaves was detectable in western blot analysis. The corresponding flow diagram of the experimental procedures is shown in chapter II.2.4.6., figure II - 1.

In contrast to the advantage of expression control, the large size of fluorescence tags in comparison to a small tag like HA might be a disadvantage. Unspecific binding to the tag is possible. The Gateway® *att*B1-sites give rise to several amino acids that are translated together with N-terminal tags. These amino acids are also translated in the negative controls for the Co-IP experiment RFP-HA-attB1 and YFP-attB1 that are encoded by pBatTL-B-p35s-RFP-HA-attB1 and pBatTL-B-p35s-YFP-attB1. In order to construct these vectors, *RFP-HA-att*B1 and *YFP-att*B1 were amplified from pEarleyGate104-MID and pNmR-COP1 by using the Gateway®-compatible primers ANS235 either with ANS234 or ANS236. The silent mutations in the modified *att*B1 sequence (see Figure III - 12) of pDONR207-YFP-attB1 and pDONR207-RFP-HA-attB1 allowed a correct Gateway® recombination in pBatTL-B-p35s as verified by sequencing. Both fluorescence proteins localised to the cytoplasm and the nucleus in *Allium cepa* (RFP-HA-attB1) or *Allium porrum* (YFP-attB1), respectively. (Figure III - 12)

Especially for small proteins, interaction domains or peptides, the amino acids encoded by the Gateway® *att*B1 site could be relevant and the generated controls can also be used in this context in the future.

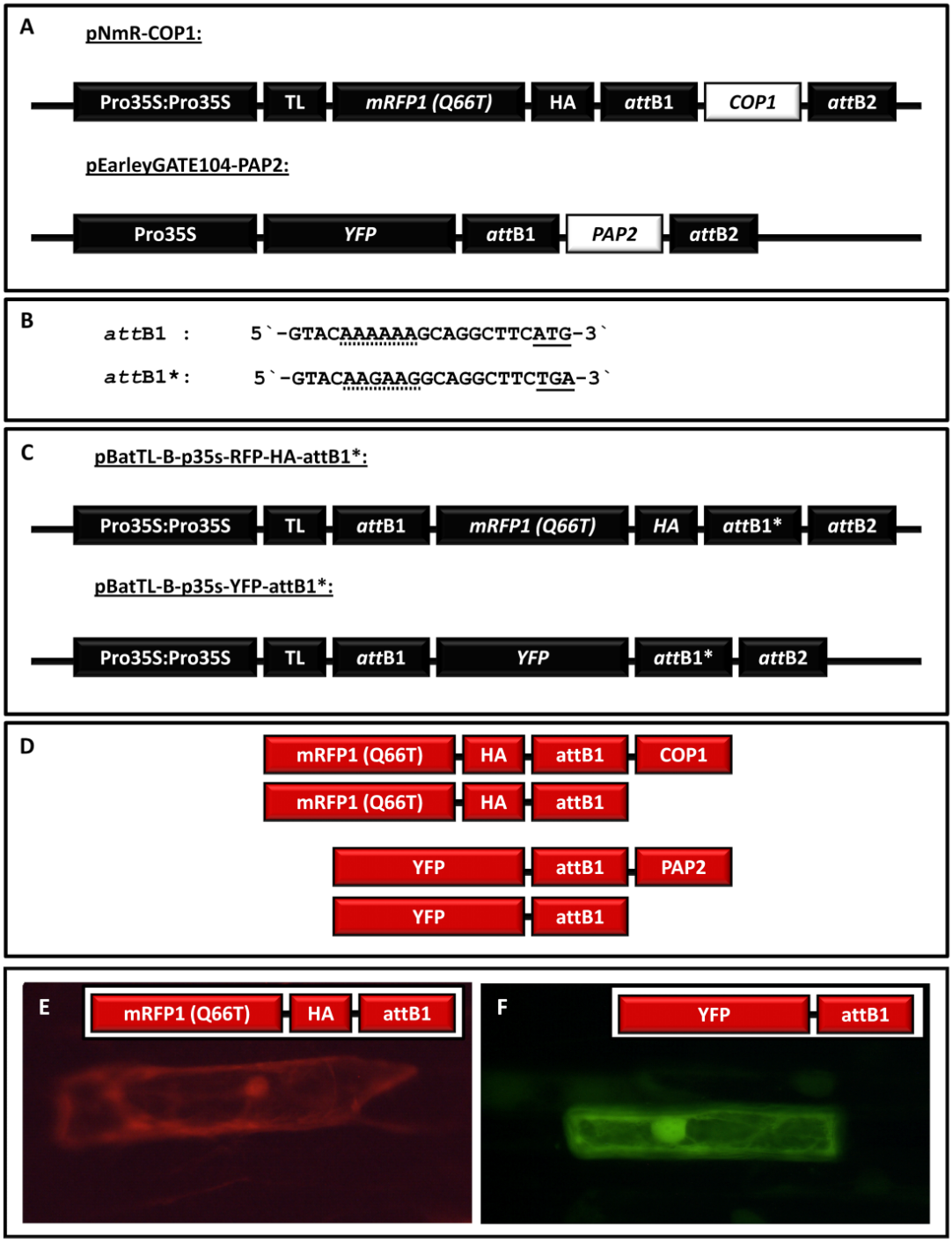

Figure III - 12: Construction of controls for the Co-IP experiment.
(A) Schematic representation of pNmR-COP1 and pEarleyGate104-PAP2. **(B)** Nucleotide sequence comparison of the 3` end of the *att*B1 site and the mutated *att*B1 site (*att*B1*). Start or stop-codons are underlined. Nucleotides coding for Leu-Leu are marked with a dotted line. **(C)** Schematic representation of expression vectors coding for RFP-HA-attB1 and YFP-attB1 after Gateway® LR recombination. **(D)** Proteins used for Co-IP experiments. **(E)** Biolistic transformation. RFP-HA-attB1 is expressed in *Allium cepa*. YFP-attB1 is expressed in *Allium porrum*. Both proteins localise to the nucleus and cytoplasm. Pictures were captured with a fluorescence binocular (E) or fluorescence microscope (F), respectively.Pro35S: Cauliflower Mosaic Virus 35S promoter; TL: translational enhancer; mRFP1 (Q66T): optimised mono RFP form Jach et al. (2006); HA: hemagglutinin tag; *att*B1 and *att*B2 sites for Gateway® recombination.

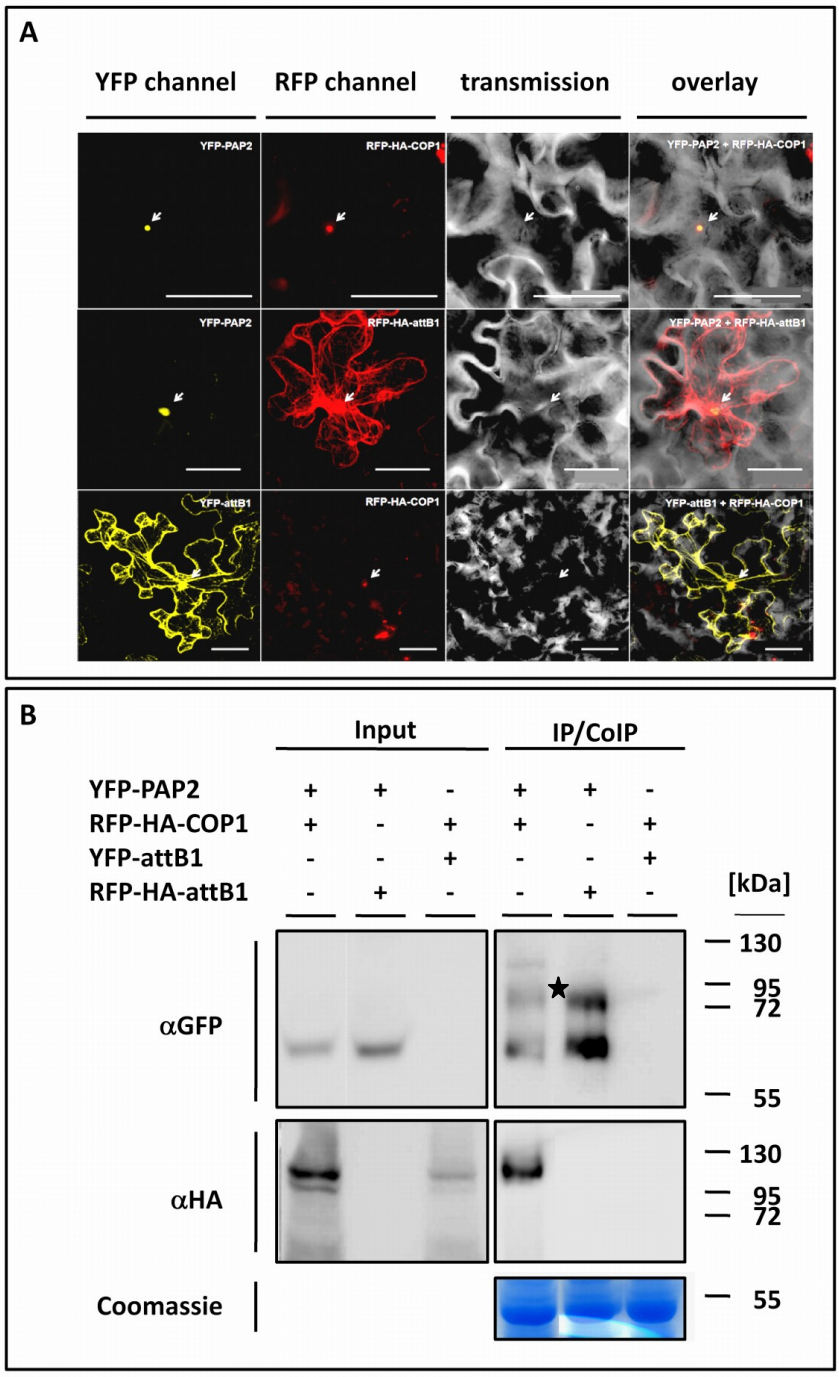

Figure III - 13: PAP2 shares one complex with COP1.
(A) Analysis of infiltrated epidermal leaf cells of *N. benthamiana* with the depicted constructs and the anti-silencing strain RK19. Pictures in one row correspond to one co-infiltration event. The pictures show a typical leaf epidermal cell three dai. The fluorescing fusion proteins are visualised with CLSM in the different channels and a merged picture is shown at the right. Sequentially scanned z-stacks were merged with Leica Confocal software. Bar equals 75 µm.**(B)** Co-IP. Infiltrated leaves from (A) were homogenised three dai. The IP of YFP-PAP2 or YFP-attB1 was performed using Miltenyi αGFP beads (Kirik, V. et al., 2007). Total protein concentrations were equalised by Bradford analysis. The Coomassie gel of input fractions served as an additional loading control. Proteins were separated by SDS-PAGE, blotted and detected with the depicted antibodies. * possibly an unspecific Miltenyi band. Note the two bands after immunoprecipitation of YFP-PAP2.
YFP-PAP2: pEarleyGate104-PAP2 (LBA4404. pBBR1MCS.virGN54D); RFP-HA-COP1: pNmR-COP1 (LBA4404pBBR1MCS-5.virGN54D); RFP-HA-attB1: pBatTL-B-p35s-RFP-HA-attB1 (LBA4404pBBR1MCS-5.virGN54D); YFP-attB1: pBatTL-B-p35s-YFP-attB1 (LBA4404pBBR1MCS-5.virGN54D); RK19 = anti silencing strain.

The Co-IP of YFP-PAP2 and RFP-HA-COP1 was successfully performed (IP: αGFP) with all negative controls (Figure III - 13). This experiment has been repeated at least three times for all shown combinations. RFP-HA-attB1 did not co-immunoprecipitate with YFP-PAP2 and no detectable RFP-HA-COP1 was co-immunoprecipitated with YFP-attB1. Figure III - 13-B shows that the immunoprecipitation was successful for all tested combinations. Several bands could be observed after western blot analysis corresponding to the incompletely translated or degraded fusion protein or probably to split off YFP-attB1 or RFP-HA-attB1. Bands with the same pattern as for the YFP-attB1 or RFP-HA-attB1 overexpression samples were also present in samples expressing YFP-PAP2 or RFP-HA-COP1, respectively (western blots see attachment A R-7).

In case of the YFP-PAP2/RFP-HA-COP1 and YFP-PAP2/RFP-HA-attB1 combination, more than one band was visible after western blot analysis using an αGFP antibody to visualise immunoprecipitated YFP-PAP2. This result was repeatedly observed. A protein mass of 58 kDa was calculated with the Compute pI/Mw tool for YFP-PAP2 (Bjellqvist et al., 1994; Bjellqvist et al., 1993; Gasteiger E., 2005). The difference in size between the first two bands corresponds to ~17 kDa. Since one molecule of ubiquitin has a molecular mass of only 8.5 kD, there must be other modifications like Small Ubiquitin-like Modifiers (SUMO, 11-12 kDa for SUMO 1, 2, 3 or 5 in *A. thaliana*) or Related to Ubiquitin (RUB, 17 kDa). The third, upper band in the sample from leaves expressing RFP-HA-COP1 and YFP-PAP2 might be an unspecific band that occured while using Miltenyi beads in combination with a goat-anti-mouse secondary antibody, as described in my diploma thesis (see Figure III - 31).

If the modification corresponding to the second band is due to ubiquitin, it is likely that PAP2 is pluri-ubiquitylated (multiple mono-ubiquitylations) with at least two ubiquitin molecules. To test this suggestion the elution fractions of the Co-IP experiment presented in Figure III - 13 were analysed by SDS-PAGE and western blot using an ubiquitin antibody for mono- and poly-ubiquitylated proteins (Figure III - 14). At the corresponding size of the presumably di-ubiquitylated PAP2 a band was detected by the anti-ubiquitin antibody. Interestingly, for both RFP-HA-COP1 bands visible in Figure III - 13 and Figure III - 14 a band of the corresponding size was visible on the western blot using anti-ubiquitin antibody. This notion was substantiated by stripping the ubiquitin blot and detecting the two RFP-HA-COP1 bands by the use of an HA antibody. No other signal was visible on the stripped blot and on the HA blot, indicating that the stripping procedure was successful. The visible smear above the two distinct bands probably belonging to RFP-HA-COP1 might be due to poly-ubiquitylated COP1 (see attachment A R-6, -8 for the whole blot). The presence of two distinct RFP-HA-COP1 bands lacking a smaller detectable RFP-HA band suggests that RFP-HA-COP1 is mono- or di-ubiquitylated

and additionally modified and thereby stabilised. It is likely that the RFP-HA tag is not modified as the band pattern of overexpressed COP1 protein on other, published western blots looks similar e.g. in Yu et al. (2008).

Still, it has to be tested if the upper lower band in the ubiquitin blot belongs to a modified PAP2, an ubiquitylated RFP-HA-COP1 or if it is the previously described unspecific Miltenyi band. The detected protein should be subjected to mass spectroscopy analysis in order to identify the modification and the linkage type concerning a possible ubiquitylation. 2D-gel electrophoresis could help to separate overlapping bands. It has to be pointed out that rubylation of YFP-PAP2 and an ubiquitylated YFP-PAP2-complex component that migrates at approximately 75 kDa can also explain the results of the GFP- and ubiquitin-blot in Figure III - 14. It is worth to verify and specify these results.

Another observation supports the notion that COP1 mediates the ubiquitylation or modification correlating with the degradation of YFP-PAP2: Less detectable YFP-PAP2 was present in all tested input fractions and the difference was even stronger in the elution fractions after IP. In addition, there was no 75 kDa band visible in the input fraction when detected with the LAS device and a very faint band on a classical Amersham film (see attachment A R-9).

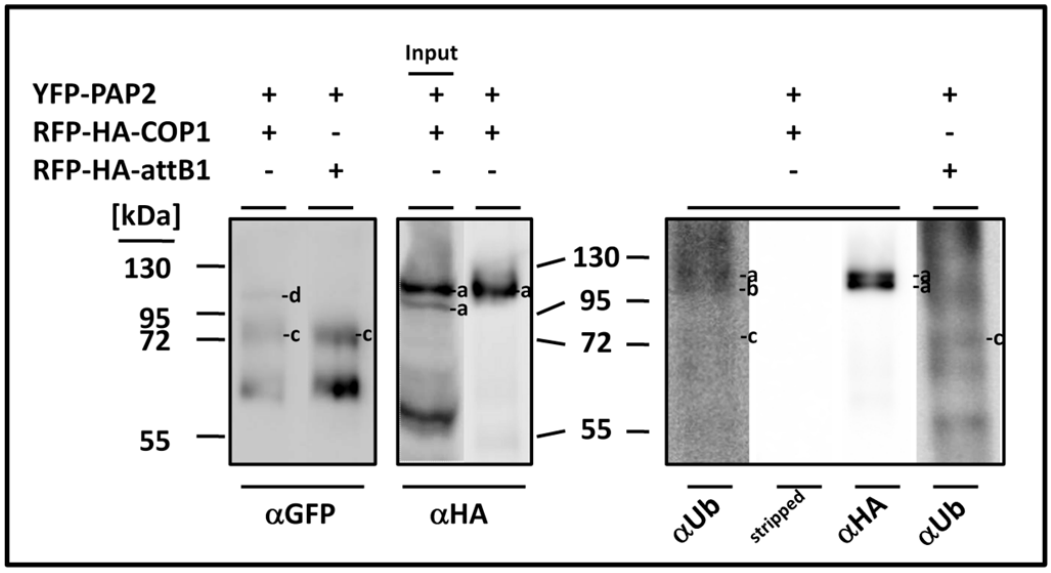

Figure III - 14: Analysis of the ubiquitylation of YFP-PAP2 and RFP-HA-COP1 expressed in *N. benthamiana* leave cells after an *A. tumefaciens* mediated transient transformation. Left part of the figure: bands are shown from the Co-IP in Figure III - 13. Combinations and procedure as described in Figure III - 13. Right side of the figure: The IP-elution fractions of the Co-IP from the left side were subjected to SDS-PAGE followed by an αUbiquitin Western blot analysis (αUb). Subsequently the blot was stripped and tested by exposing it again (stripped). Finally the same blot was tested with an αHA antibody (αHA). Only the shown bands were visible after the last treatment. αUb (P4D1), a mono-clonal antibody detects ubiquitin, polyubiquitin and ubiquitinated proteins. In all cases proteins were separated after IP, except one depicted case; a: band belongs to RFP-HA-COP1; b: band might be long to RFP-HA-COP1, a heavily modificated YFP-PAP2 or is the unspecific Miltenyi band;c: size of the modified YFP-PAP2 band. d: probably unspecific Miltenyi band described in my diploma thesis

It can be concluded that probably ubiquitylated PAP2 can share a complex in vivo with ubiquitylated COP1.

2.2. PAP2 competes with a conserved COP1-WD40-domain interacting motif

All proteins interacting with the WD40 domain have been shown to be targets of COP1. Holm et al. (2001) also found out that a salt bridge between Lys^{550} of COP1 and Asp^{246} of STO is necessary for the interaction of both proteins. This finding was already used for the selective gap repair experiment in I. 1.2. Negative results from YTH experiments need further experimental evidence to be interpreted. Therefore, a competition experiment was performed to test if the conserved motif defined by Holm et al. can compete with PAP2 for the interaction with COP1. The COP1 interacting domain of STO, named CID (COP1 Interacting Domain) in this work, was fused to the C-terminus of GFP. CID comprises of amino acids 236 to 248 of STO (Figure III - 15-A) and includes the conserved motif "VPD/EΦG" (Φ being a hydrophobe amino acid) identified by Holm et al. (2001). This motif mediates the interaction of COP1 with CID-containing proteins (STO, STH, HY5, HYH). GFP served as scaffold to allow proper folding of this small domain. In addition, GFP fluorescence could prove the expression of the protein in yeast (Figure III - 15-D).

First, the interaction of the GFP-CID fusion protein with COP1 was tested in yeast. Therefore, GFP-CID^{D246K} was constructed in analogy to STO^{D246K} to serve as a negative control (Figure III - 15-C). STH^{D236K} that corresponds to STO^{D246K} did no longer interact with COP1 (Holm et al., 2001). Figure III - 15-B shows the expected result, GFP-CID interacts with COP1, for GFP-CID^{D246K} no growth was observed on interaction plates.

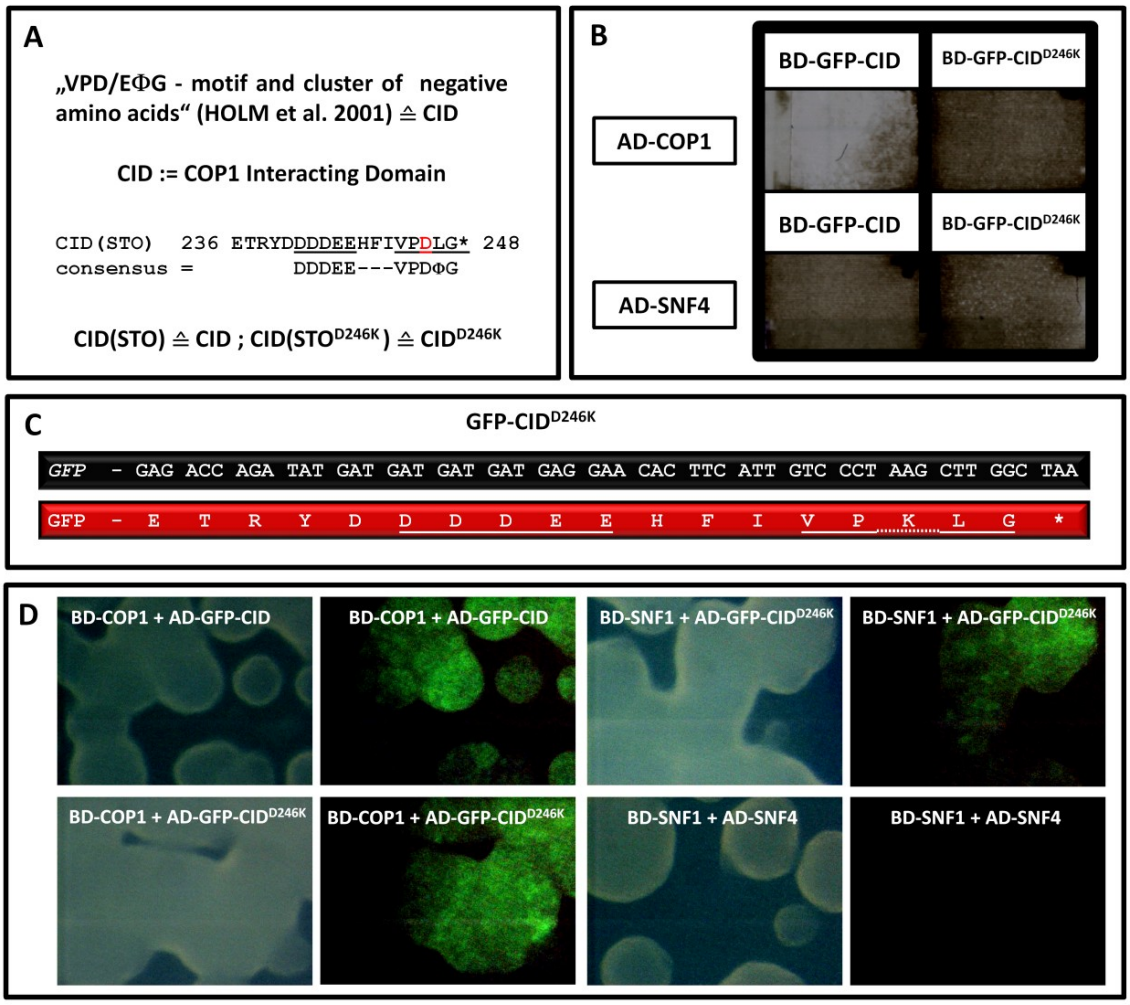

Figure III - 15: Definition, cloning and YTH analysis of the GFP-CID construct. **(A)** Definition of COP1 interacting domain (CID) that comprises of amino acids 236 to 248 of STO and includes the conserved motif "VPD/EΦG" (Φ being a hydrophobe amino acid) identified by Holm et al. (2001). **(B)** *S. cerevisiae* AH109 growing on interaction medium after YTH experiment (double transformation) with the depicted constructs. SNF4 served as a negative control. **(C)** DNA and protein sequence of CID^{D246K}. **(D)** GFP fluorescence visualised with a fluorescence binocular of yeast transformed with different combinations of GFP-CID or $GFP\text{-}CID^{D236K}$ and grown on SD-LW plates. Yeast cells harbouring BD-SNF1 and AD- SNF4 constructs served as a negative control for fluorescence analysis.

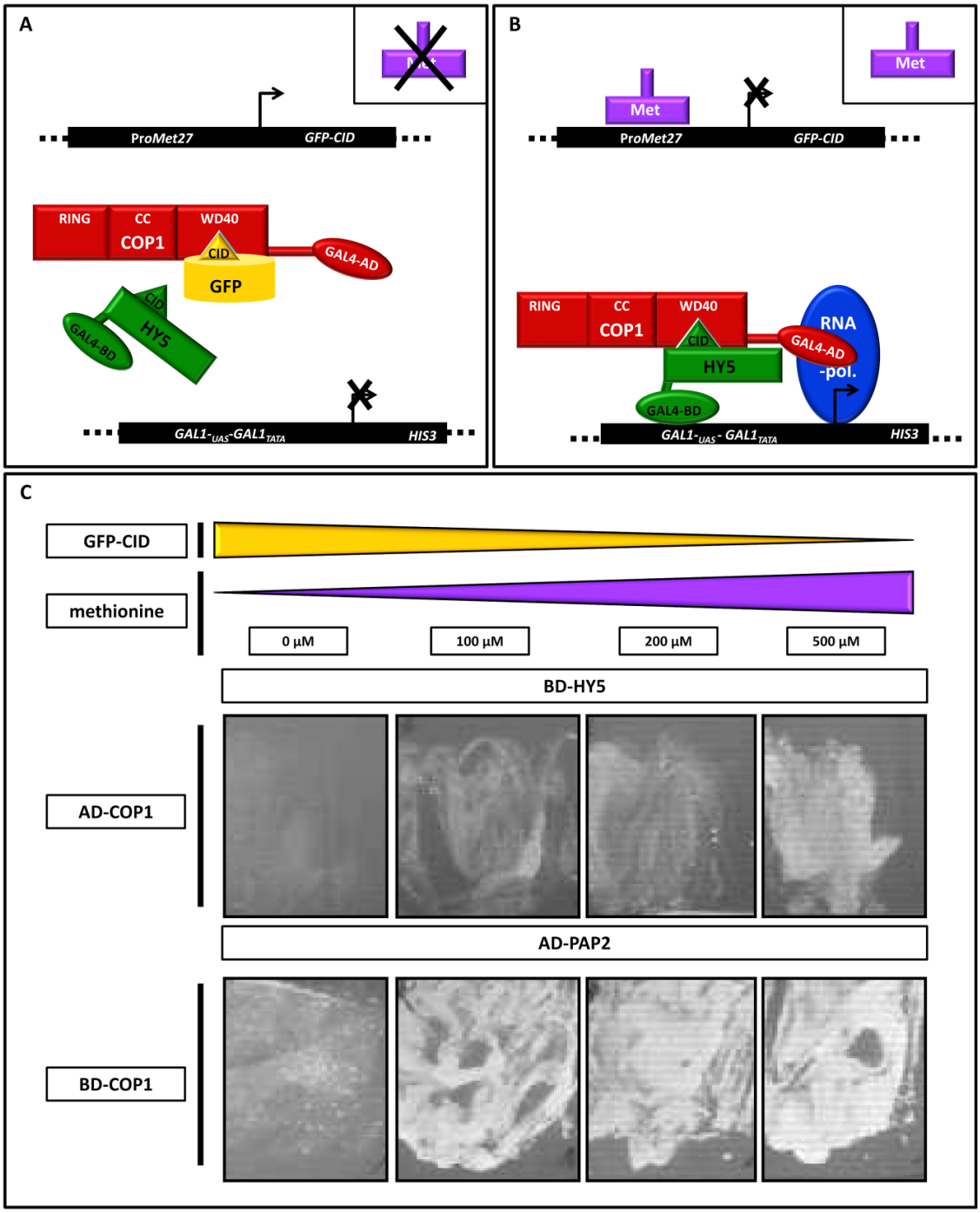

Figure III - 16: GFP-CID competes with AD-PAP2 for binding to BD-COP1.
(A-B) Mechanism of competition in the yeast three hybrid assay: An active (A) or methionine-suppressed (B) Pro*Met25* regulates expression of *GFP-CID*. (A) The competitor GFP-CID supersedes HY5. Consequently the *HIS3* gene is not expressed and yeast cannot grow on SD media lacking histidine. (B) HY5 interacts with COP1. The *HIS3* gene is accordingly expressed and enables growth of the yeast on SD media lacking histidine. **(C)** Yeast three hybrid experiment with COP1 in combination with HY5 or PAP2 (each as BD or AD fusion protein). *GFP-CID* expression is regulated in a dosage dependent manner by methionine. (C) shows SD-LWH2 plates supplemented with the depicted amounts of methionine. In one row, the same amounts of yeast cells were streaked on each plate. SD-LWH2: selective dropout media lacking leucine, tryptophan and histidine, supplemented with 2 mM 3-AT. pBridge constructs were also tested in combination with pACT-GFP as negative control (see A R-10). No growth was observed on interaction media.

Second, the interaction of COP1 with GFP-CID was used to conduct a competition experiment. In this yeast three hybrid experiment, PAP2 as GAL4-AD fusion (pACT-PAP2) and COP1 as GAL4-BD fusion (pBRIDGE-COP1/GFP-CID) were co-expressed under the control of the ADH promoter in yeast while GFP-CID expression was controlled by the methionine suppressable promoter ProMet25 (pBRIDGE-COP1/GFP-CID). Both constructs were transformed into *Saccharomyces cerevisiae* AH109 that is able to grow on SD media lacking methionine. GFP-CID is expressed by the transgenic yeast cells in the absence of methionine (Figure III - 16-A). Supplementation of methionine to the SD media results in suppression of the GFP-CID expression in a dosage dependent manner (Figur III - 16-B). Figur III - 16-C suggests that GFP-CID competes with AD-PAP2 for the binding to BD-COP1. This effect was stronger than the positive control HY5 as was visible by the growth behaviour of the transgenic yeast cells. In case of PAP2, the maximal cell density was already reached by addition of 100 µM methionine while it increased gradually for HY5 when the media was supplemented with 0 to 500 µM methionine. One could conclude that the binding of PAP2 to the WD40 domain of COP1 is much stronger than that of HY5. Nevertheless one more control is necessary. Instead of GFP-CID, GFP alone or an empty Gateway cassette should be tested to rule out the possibility that lack of methionine inhibits the growth of AH109 in general. In addition also methionine concentrations between 0 and 100 µM should be tested and the OD_{600} of both samples should be adjusted when plating to also allow a direct comparison between the different plasmid combinations. The minimal COP1 domain sufficient for the interaction with PAP2 still needs to be identified. This might be performed by using defined COP1 domains or by applying GARFILD (Gateway®-compatible random fragments YTH in frame library screening for domain mapping), a method developed in this work (see next chapter).

2.3. Identification of a PAP2 domain sufficient for PAP2 - COP1 interaction

The structure of the N-terminal part of PAP2 consisting of the R2R3 domain is well analysed (Figure IV - 2). In contrast, little is known about the C-terminal part of the protein. R2R3 MYB domains have been described as plant specific (Braun and Grotewold, 1999; Kranz et al., 2000). Probably PAP2 has more domains with plant-specific functions, therefore, a new identified COP1 interaction domain might also have the potential to be plant specific and to further dissect plant specific functions of COP1.

2.3.1. A new approach for domain mapping - a Gateway®-compatible random fragments method

The development and use of a yeast based domain mapping method is described in this chapter and named according to its properties: Gateway®-compatible random fragments YTH in frame library screening for domain mapping (GARFILD). GARFILD provides a tool for rapid domain mapping of two interactors. N-terminal and C-terminal libraries of the corresponding protein comprising of PCR-based random CDS fragments are screened in YTH screenings against the interactor to be analysed. An overlap of interacting N-terminal and C-terminal fragments maps the interaction domain sufficient for interaction of the two analysed proteins. Subsequently, this fragment can be mapped further, be analysed for existing motifs or mutated to further identify the crucial interacting amino acids. On the one hand, random fragment based domain mapping can redefine and specify published interaction domains that are often correlated to known predicted domains. On the other hand, this method is a powerful tool to identify so far unknown domains in proteins that were not predicted before. For both applications an example will be given.

The domain mapping of PAP2 based on the published interaction with EGL3 was chosen for a proof of principle experiment for GARFILD (Zimmermann et al., 2004). For the close PAP2 homologue - PAP1 - the R3 MYB repeat was identified as the interaction domain for EGL3. Random fragments of the PAP2-CDS were generated by combining different PCRs with random-, tag- and gene specific primers resulting in directed recombination of the amplicons via Gateway® technology. Figure III - 17 F shows a flow diagram of the whole method and Figure III - 17 A-E gives an overview of the applied PCR strategy for the generation of N-terminal libraries. Detailed PCR and reaction conditions as well as other applied methods are described in II.2.2.10.

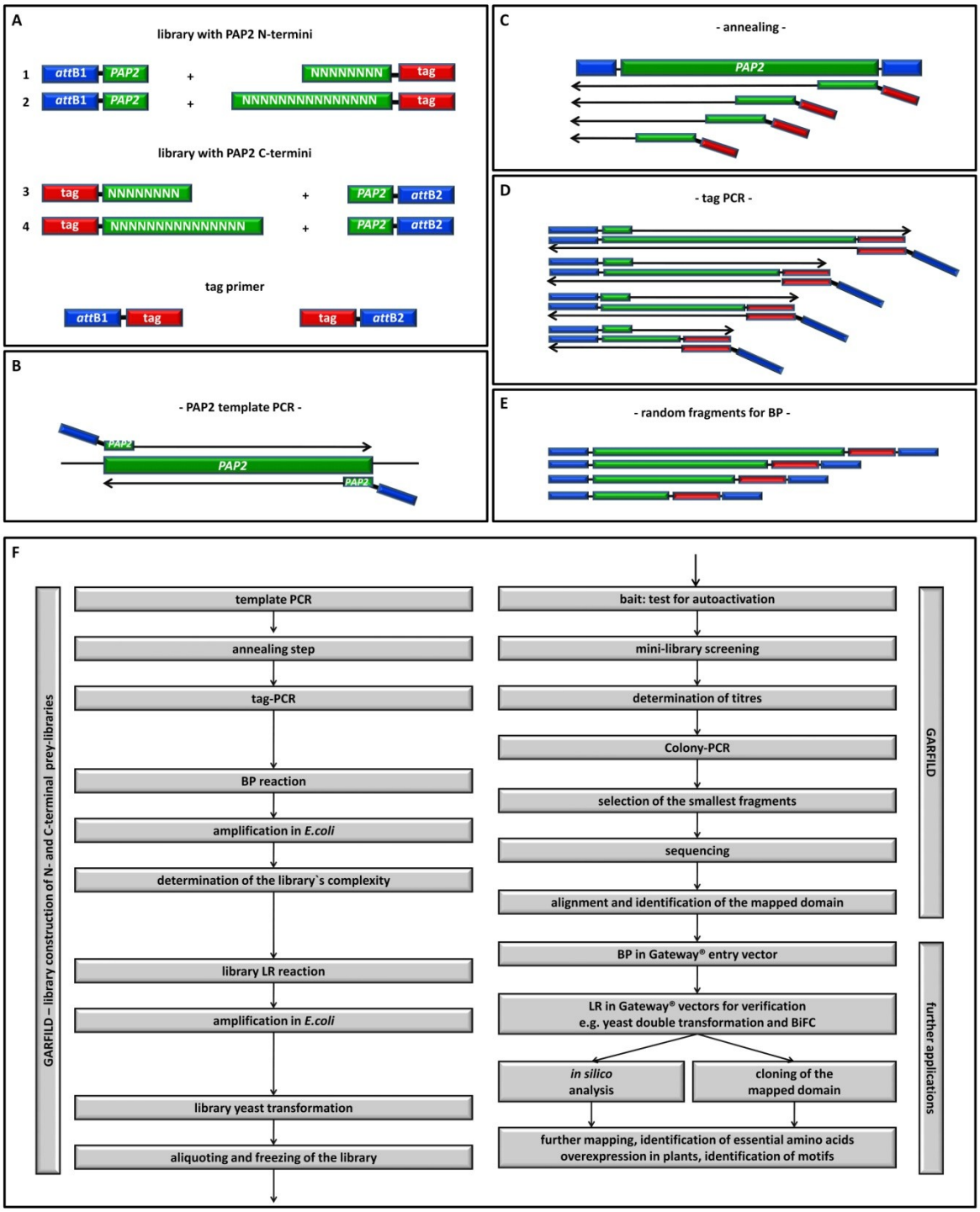

Figure III -17: GARFILD - strategy and flow diagram for library construction of N-terminal PAP2 library.
(A) Primers for the construction of random fragments of PAP2. Primer combinations for the construction of a library consisting of N-termini (1,2) or C-termini (3,4), respectively. One *PAP2*-specific and one random primer are combined. Two random primers with 8 or 15 random nucleotides were constructed for N- and C-termini, respectively. Tags in sense and antisense primers are not identical. **(B)** Template PCR with *PAP2*-specific primers. **(C**) Template from B is used for annealing and elongation with anti-sense random primers from (A) at different temperatures. **(D)** Amplification of products from (C) with *PAP2*-specific *att*B1-*PAP2* primer (sense) and *att*B2-tag primer (antisense) **(E)** Products of (D) that can be subsequently used for BP reactions. Products were purified after steps B-E. blue: *att*B1- or *att*B2-site, red: tag, green: nucleotide or *PAP2*. (F) GARFILD flow diagram of the library construction steps, GARFILD and further possible applications. For details see the text.

GARFILD - library construction - template PCR

The CDS of PAP2 was amplified with Phusion® High-Fidelity DNA Polymerase, a proof reading DNA polymerase from an entry-plasmid with Gateway® gene-specific attB1 and attB2 primers. Primers were removed by gelextraction (MinElute, Quiagen). The purified PCR product served as template for the next PCR - the annealing step.

GARFILD-library construction - annealing step

The annealing step was performed as described before (Kawasaki and Inagaki, 2001). Low temperatures allow for random priming events. A non-proof reading *Taq* Polymerase (BIOTAQ DNA polymerase, Bioline) was used which accepts primer mismatches that are necessary for the random priming events. In the annealing step, both primers give rise to PCR fragments of sense and antisense orientation in relation to the *PAP2* CDS. In comparison to Kawasaki and Inagaki (2001), modified primers were used that are shown in Table III- 6. These primers consist of 8 or 15 random nucleotides and a specific tag of known sequence. The tag is used in the next essential PCR step (tag PCR) to specify the orientation of the fragments by selectively adding an *att*B1 or *att*B2 site to the amplicons, respectively.

Table III - 6: Primers used for GARFILD template- PCR, annealing step and tag-PCR.

name	sequence
*PAP2-att*B1	GGGGACAAGTTTGTACAAAAAAGCAGGCTTAATGGAGGGTTCGTCCAAA
*PAP2-att*B2	GGGGACCACTTTGTACAAGAAAGCTGGGTAATCAAGTTCAACAGTCTC
random(8)-tag(rev)	CTAGTCCATGCGACACCATGGNNNNNNNN
random(15)-tag(rev)	CTAGTCCATGCGACACCATGGNNNNNNNNNNNNNNN
random(8)-tag(fw)	GACCATGATTACGCCCTCGAGNNNNNNNN
random(15)-tag(fw)	GACCATGATTACGCCCTCGAGNNNNNNNNNNNNNNN
*att*B2-tag(rev)	GGGGACCACTTTGTACAAGAAAGCTGGGTCGTAGTCCATGCGACACCATGG
*att*B1-tag(fw)	GGGGACAAGTTTGTACAAAAAAGCAGGCTTCGACCATTATTACGCCCTCGAG

GARFILD - library construction - tag PCR

The products of the annealing step were purified to remove primers (High Pure PCR Product Purification Kit, ROCHE) and used as a template for the next PCR step - the tag PCR. Purification steps were essential to avoid primer oligomer. DNA fragments corresponding to N-termini were amplified by tag-PCR using a *PAP2*-specific *att*B1 primer in combination with a tag-specific *att*B2 primer. For

the generation of C-termini, the tag-specific *att*B1 and *PAP2*-specific *att*B2 primer were used. As the optimal primer annealing temperatures for the different sized templates (possible dimerisation) were not known, a gradient PCR was performed with eight different annealing temperatures between 53.6°C and 66.4°C. The PCR products were visualised by gel electrophoresis (Figure III - 18) which is the first quality control of the libraries to be generated. A smear is a sign for multiple successful random priming events in the annealing step. Distinct bands appearing in PCR products for C-terminal fragments indicate that some random primers matched better than others or that the corresponding part of the CDS was less accessible for the primers at 40°C (dimerisation). A PCR product at 750 bps for the N-terminal fragments corresponds to the size of the full length *PAP2* CDS. It is possible that the *PAP2*-specific *att*B2 and *att*B1 tag primers preferentially amplified the full length template. If too much template would have been used in the first step, the band should also be visible in the C-terminal PCR products.

GARFILD - library construction - BP reaction

Prior to the BP reaction, the tag-PCR product was treated in three different ways. (1) 6 µl of the purified tag-PCR product were used; (2) the remaining volume of the purified PCR product was five-fold concentrated and 5 µl were used for the BP reaction; (3) the tag PCR was repeated using the purified PCR product from (1) as a template. 3 µl of the direct purified (High Pure PCR Product Purification Kit, ROCHE) and five-fold concentrated PCR products were used for the BP reaction. Best results were achieved for the N-terminal libraries with treatment (3) and the C-terminal libraries with treatment (2) (Table III - 7). The library was amplified in *Escherichia coli* DH5α. The numbers of primary clones - the number of transformed cells after BP-reaction - characterising the complexity of the library, are listed in Table III - 7.

Table III - 7: GARFILD - library construction: efficiency of BP, LR recombination reactions and *E. coli* transformations. Number of colonies counted after transformation in *E. coli* DH5α or *S.cerevisiae* Y187, respectively. All transformants were selected for the corresponding plasmids. Number of colonies after the BP reaction is the number of primary clones characterising the complexity of the library. > number of colonies was estimated to be at least 20 000. -: no LR recombination reaction or yeast transformation. See the text for details on the three treatments prior to BP (1, 2, 3). Type 1-4: compare to Figure III - 17.

template	library	type	number of colonies					
			BP (*E.coli*)				LR (*E.coli*)	library transformation (*S. cerevisiae*)
			total	1	2	3		
PAP2	N-termini	1	421	1	110	310	773	2500
		2	149	0	65	84	1300	2200
	C-termini	3	1202	2	750	450	800	> 20 000
		4	258	3	155	100	1100	> 20 000
COP1	N-termini	1	865	0	65	800	2550	2500
		2	541	1	40	500	2740	2300
	C-termini	3	157	-	151	6	-	-
		4	27	-	26	1	-	-

GARFILD - library construction - determination of complexity

GARFILD-N-terminal libraries constructed with random(8)-tag(rev) and random(15)-tag(rev) primers were numbered 1 and 2 and GARFILD-C-terminal libraries constructed with random(8)-tag(fw) and random(15)-tag(fw) primers were numbered 3 and 4, in analogy. Prior to the LR recombination reaction, the complexity of the libraries was tested.

Plasmids were prepared from 20 (eight for COP1-4) randomly chosen colonies. Entry-vectors were subsequently cut with *Bsr*GI in the Gateway® *att* sites. The size of the resulting restriction fragment corresponding to the insert of the entry vector. On average, it exceeds the actual *PAP2*-CDS fragment`s size with 64 unspecific bp due to primer attachments including a portion of the Gateway® sites. The fragments were separated by agarose gel electrophoresis and stained with EtBr. No restriction pattern corresponding to an empty entry plasmid was observed. For some plasmids (one for PAP2-4, COP1-1; two for PAP2-1, -2, COP1-2,-4; 5 for COP1-3), there was only the pattern for the vector backbone but neither for the Gateway® cassette nor for a fragment. Probably the fragments were very small and the concentration was too low to allow visualisation on an EtBr stained agarose gel. All fragments were categorised and sorted into size defined classes (0-100 bp, 100-200 bp, etc. corresponding to 0-36 bp, 37-136 bp, etc. of *PAP2* CDS, see attachment A R-11). The percentage representation of each class is visualised in Figure III - 18.

GARFILD - library construction - LR recombination reaction

E. coli colonies were pooled and plasmids were prepared. One disadvantage of other random fragmentation methods is that approximately two-thirds of all C-terminal fragments are cloned out of frame. To circumvent this loss of library complexity, YTH vectors for all three frames (pAD-Gate1, pAD-Gate2, pAD-Gate3) were used for the C-terminal GARFILD - libraries (Maier et al., 2008). All destination vectors were cut prior to the library LR recombination reaction (see II.2.2.10.). For the GARFILD-C-terminal libraries 200 ng of each cut vector and 600 ng of DNA were used. The reaction products were amplified in *E. coli* DH5α and plasmids were prepared. The number of colonies is listed in Table III - 7.

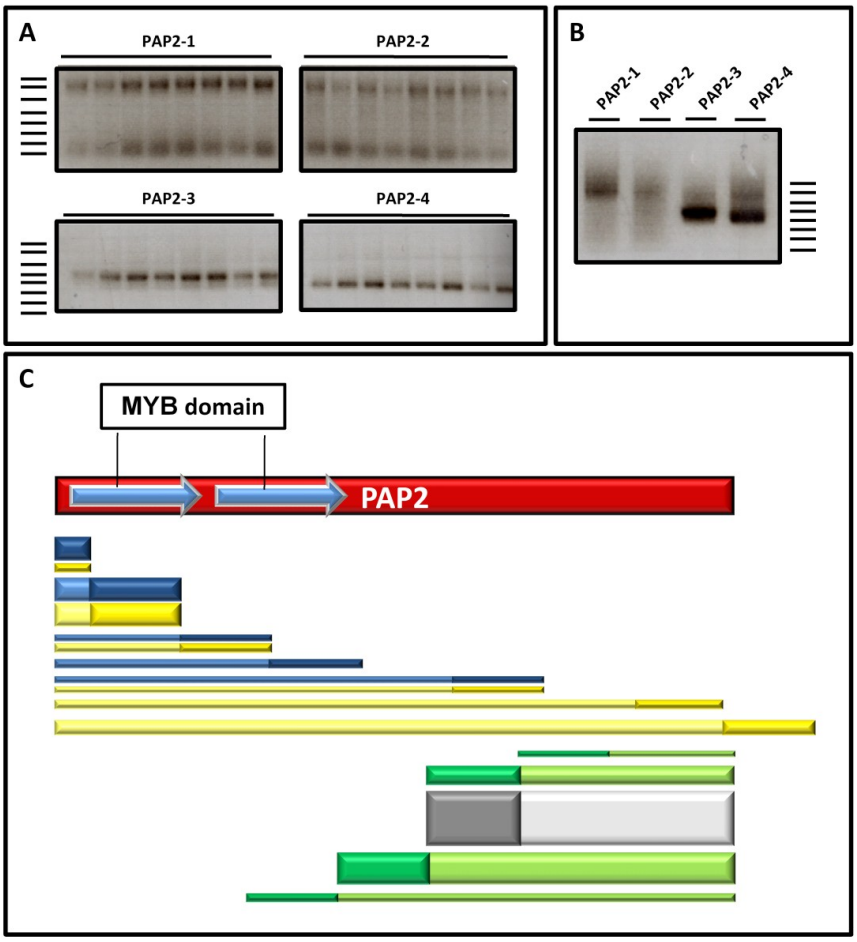

Figure III - 18: Characterisation of the PAP2 GARFILD library complexity.
(A) EtBr stained agarose gel loaded with 5 µl of DNA after the tag-PCR gradient with eight different annealing temperatures between 53.6°C and 66.4°C. **(B)** EtBr stained agarose gel loaded with 5 µl of pooled DNA after repetition of the tag-PCR gradient (for BP treatment 3). **(C)** Percentage representation of size defined fragment classes. Plasmids from 18-20 randomly chosen primary clones (clones after BP) were prepared and digested with *Bsr*GI. Thickness of the bars correlates with their abundance in this test. The table with all results can be found in the attachment A R-11 dark: range of the fragments classes` borders. blue: PAP2-1; yellow: PAP2-2; green: PAP2-3; grey: PAP2-4. Marker: 1kb+ ladder (Fermentas). Lines correspond to (from the bottom to the top): 100, 200, 300, 400, 500, 650, 850, 1000 bp, Number 1-4: compare to Figur III - 17.

GARFILD - library transformation in *S. cerevisiae* Y187

An established protocol was used to transform 200 ng of each library in *S. cerevisiae* Y187 with a 10x transformation assay (MacFarlane and Uhrig, 2008). The culture was harvested in the exponential phase at an OD_{600} of 0.7 and a microscopically determined density (Neubauer chamber) of $2.73*10^7$ cells per ml. After two days at 30°C the number of transformed yeast cells on selective dropout media lacking leucine was determined (Table III - 7). Only successfully transformed yeast cells were able to grow on this media as pAD-Gate1-3 carries the *LEU2* gene that enables *S. cerevisiae* Y187 to produce leucine. All transformed yeast cells were pooled and different volumes (10 µl, 100µl and 1 ml) of the library were frozen at a final OD_{600} of 1 as described before (MacFarlane and Uhrig, 2008).

Two factors have an influence on the complexity of a library: the number of different generated PCR fragments (characterised by the DNA smear on the agarose gel visible after tag-PCR, Figure III - 18, Figure III - 19) and the efficiency of BP-, LR recombination reaction and *E. coli* and yeast transformations (characterised by the number of colonies listed in Table III - 7). Additionally, the number of fragments in the correct frame after LR reaction needs to be mentioned for C-terminal libraries. The size of PAP2 and COP1 is 750 bp and 2028 bp. This corresponds to 747 and 2025 nucleotides coding for amino acids. In theory 747 or 2025 constructs can be obtained coding for a maximum of 269 or 675 different N- or C- terminal COP1 fragments. The number of primary clones of the PAP2-GARFILD libraries ranged between 149 and 1202. Numbers of colonies increased from step to step (BP to LR recombination, LR recombination to yeast transformation). Taken into consideration that some fragments in the primary clones exist in several copies (Figure III - 18), it can be concluded that there was no severe loss of complexity by LR recombination and yeast transformation. As the PAP2 and COP1 libraries are used in this work, the range of resulting identified fragments will give informations about the final complexity in yeast. Otherwise one should determine the complexity after yeast transformation by randomly choosing yeast colonies for a colony PCR. The size of the resulting products can give informations about the complexity in yeast.

Preparation of GARFILD-N-terminal libraries for COP1

GARFILD N- and C-terminal libraries for COP1 were constructed as described above with the corresponding COP1-specific *att*B1 and *att*B2 primers. In Figure III - 19 the characterising properties of the COP1-GARFILD libraries are shown (range of DNA smear after tag-PCR and the complexity of the libraries after BP recombination reaction). The gradient tag-PCR was performed with five different annealing temperatures between 50.0°C and 70.5°C. In Table III - 7 the numbers of primary

clones (after BP recombination), LR recombination reaction efficiency and yeast transformation efficiency are given. The C-terminal libraries were not considered as complex enough to contribute to a domain mapping of COP1. No LR recombination reaction was performed with these libraries.

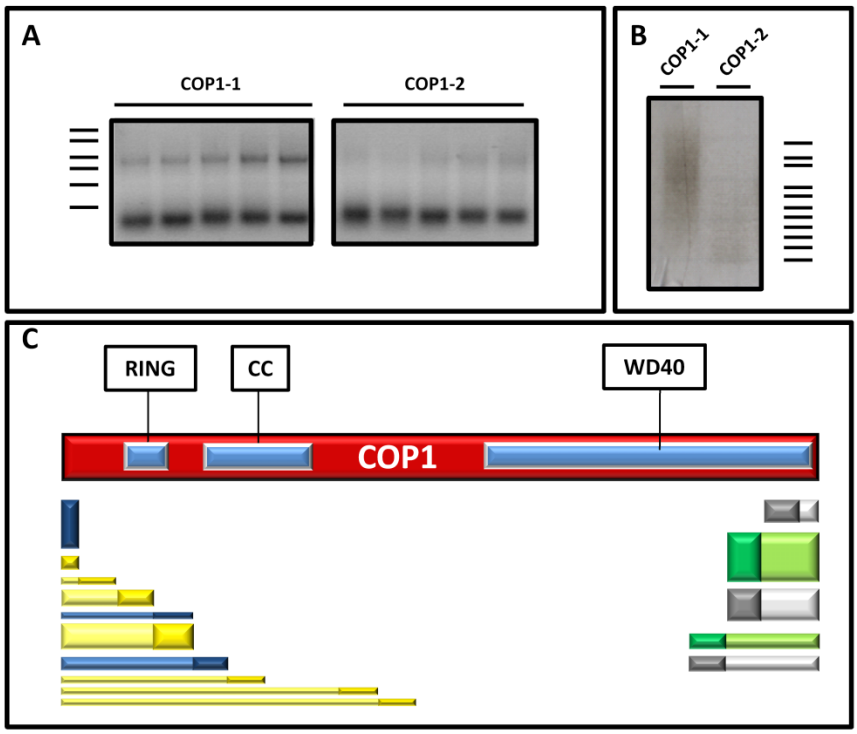

Figure III - 19: Characterisation of the COP1 GARFILD library complexity.
(A) EtBr stained agarose gel loaded with 5 µl of DNA after the tag-PCR gradient with five different annealing temperatures between 50°C and 70.5°C. **(B)** EtBr stained agarose gel loaded with 5 µl of pooled DNA after repetition of the tag-PCR gradient (for BP treatment 3). **(C)** Percentage representation of size defined fragment classes. Plasmids from 6 (C-termini) to 19 randomly chosen primary clones (clones after BP) were prepared and digested with *Bsr*GI. Thickness of the bars correlates with their abundance in this test. The table with all results can be found in the attachment A R-11) dark: range of the fragments classes` borders. blue: COP1-1; yellow: COP1-2; green: COP1-3; grey: COP1-4. Marker in (A): 1kb GeneRuler (Fermentas). Lines correspond to (from the bottom to the top): 250, 500, 750, 1000, 1500, 2000 bp; marker in (B): 1kb+ ladder (Fermentas). Lines correspond to (from the bottom to the top): 100, 200, 300, 400, 500, 650, 850, 1000, 1650, 2000, 3000 bp. Number 1-4: compare to Figure III - 17.

2.3.2. Proof of principle and applications of the random fragments method - screening

Several combinations of baits and GARFILD libraries were used for the first GARFILDs in this work: (1) EGL3 as a bait and PAP2 GARFILD libraries to provide a prove of principle experiment; (2) GFP as a bait and PAP2 GARFILD libraries as a negative control for the libraries; (3) COP1 as a bait and PAP2 GARFILD libraries to provide a first application of the method and to map the interaction domain of PAP2 for the interaction with COP1; (4) COP1 as a bait and COP1 GARFILD libraries to test the COP1 N-terminal libraries; (5) GFP as a bait and COP1 GARFILD libraries as a negative control for the libraries; (6) $COP1^{K550E}$ as a bait and COP1 GARFILD libraries to test if interactions of the protein via

other domains than the WD40 domain are impaired by the mutation - in this case the self-association of COP1 via the coiled coil domain. All used baits did not show auto-activation.

To determine the amount of library and bait culture for the GARFILD mating step the following rule was applied: The number of independent successful matings (mating titres) should be five times higher than the number of independent clones in the library (Sambroock and Russell, 2001). The primary clones of the constructed GARFILD libraries do not correspond to independent clones as several fragment lengths were represented more than once. Best complexity was reached for the PAP2-2 and COP1-2 library corresponding to a maximum of theoretically 149 and 541 independent clones (Table III - 7, Figure III - 18, Figure III - 19). For coverage a mating-titre corresponding to approximately 2500 mating events would be needed in comparison to $5 * 10^6$ mating events for which a standardized protocol was developed by Soellick and Uhrig (2001). Therefore, a factor of 2000 was determined for downscaling.

GARFILD was performed in analogy to the established YTH screening procedure (II.2.2.2.) with minor modifications. The used OD_{600} of the library and of the bait was scaled down with the factor of 2000 to OD_{600}=0.01 for GARFILD. The frozen aliquots were smaller than for normal YTH screenings. Therefore, the frozen libraries were thawn and transferred with pre-warmed YPAD. Finally, the volume of the gelrite screening media was reduced to 200 ml.

In the first screenings with PAP2 GARFILD libraries with an OD_{600} of 0.1 and 1 were used in addition to an OD_{600} of 0.01. The volume of the gelrite screening media was reduced to 25, 100 and 200 ml, respectively. In regard to the desired mating titres an OD_{600}=0.01 proved to be optimal (Table III - 8). Titre plates for screenings with a library and bait OD_{600} of 1 were too dense to be counted. Therefore, 200 ml of screening media were used for subsequent GARFILDs.

For COP1 as a bait and for the combinations with COP1 GARFILD libraries, only combinations of OD_{600}=0.01 were used. In Table III - 8 the mating titres of the different screenings are listed. The mating titres lead to the conclusion that they are high enough to cover the libraries at least five-fold. Due to a lower density of yeast cells in the mating solution that was not equally scaled down, not only the mating events might have contributed to the observed mating titres but also subsequent cell divisions. The latter effect has to be minimized. If the mating titres stay stable when minimising the volume of the mating solution than one can conclude that mating titres in these first screenings represent mating efficiency coupled with cell divisions. The results of the colony PCRs after screening supported this notion as most colony PCR products showed the same size. Six to 17 colony PCR

products per library were sequenced in this first application (with GARFILD-specific forward and reverse primers, see attachment A M-1). In further applications this number can be reduced as only the shortest interacting fragments are of interest for the mapping. There is also optimisation potential in the used volume of gelrite screening media. Further downscaling will also allow for performing more screenings in parallel in the future.

Table III - 8: Screened libraries with the baits EGL3, COP1, COP1^{K550E} and GFP and mating-titre (number of yeast colonies that originated from a successful mating event) of the mating for the YTH screenings. The library types are described in the text or in Figure III - 17. OD_{600} corresponds to the OD_{600} of 1ml library or bait culture that was used for the YTH screenings. Number 1-4: compare to Figure III - 17.

bait	library	type	titre	
			OD_{600}=0.01	OD_{600}=0.1
EGL3	PAP2	1	$1*10^4$	$1.93*10^6$
		2	$3.73*10^4$	$1.32*10^6$
		3	$4.5*10^4$	$1.38*10^6$
		4	$2.5*10^4$	$1.54*10^6$
GFP	PAP2	1	$2.25*10^4$	$9*10^5$
		2	$5*10^4$	$1.3*10^6$
		3	$8.5*10^4$	$1.34*10^6$
		4	$3.5*10^4$	$1.42*10^6$
COP1	PAP2	1	$2.6*10^4$	-
		2	$1.8*10^4$	-
		3	$2*10^4$	-
		4	$1.8*10^4$	-
COP1	COP1	1	$4.6*10^4$	-
		2	$4*10^4$	-
GFP	COP1	31	$1.82*10^5$	-
		42	$1.18*10^5$	-
COP1^{K550E}	COP1	1	$4*10^4$	-
		2	$4*10^4$	-

2.3.3. Proof of principle and applications of the random fragments method - identification of interaction domains.

The R2R3 domain is located between base pairs 22 and 333 of the PAP2-CDS (Figure IV - 2). The minimal N-terminal fragment of PAP2 identified with GARFILD for EGL3 as bait ends at base pair 375 of the *PAP2*-CDS (Table III - 9). This nicely correlates with the finding of Zimmermann and co-workers (2004), that the R3 MYB repeat of PAP1, a close homologue of PAP2, confers the interaction with EGL3. No C-terminal fragment was identified. This might be due to the lack of fragments comprising the whole R3 repeat.

A small peptide including the amino acids of the *att*B1 site and additional random amino acids was identified by GARFILD with EGL3 but not with GFP or COP1 as baits. Another fragment starting at base pair 430 of the *PAP2*-CDS was identified as a nonsense protein because it was not in frame. Sequences that could not be analysed resulted from mixed yeast colonies or colonies harbouring more than one plasmid. (Table III - 9)

For COP1 the interaction domain of PAP2 could be mapped to base pairs 439 to 663 of the *PAP2*-CDS by the shortest N- and C-terminal fragments (Table III - 9, attachment A R-12). Figure III - 20-A schematically shows the identified domains for EGL3 and COP1.

The shortest fragment sufficient for the interaction of COP1 with full length COP1 in yeast ended after 462 base pairs (Table III - 9). This covers only the first third of the coiled-coil domain that has previously been identified as the self-association domain for COP1 (Torii et al., 1998). COP1^{K550E} behaved similar in GARFILD and comparable fragments were identified (Table III - 9). Figure III - 20-C schematically shows the identified domains for COP1 and COP1^{K550E}.

Table III - 9: Overview of the sequencing results after a GARFILD with PAP2 and COP1 libraries. COP1, EGL3 and COP1K550E were used as baits. GFP served as a negative control. Only the size of the fragment that corresponds to base pairs that matches 100% of the PAP2 and COP1 amino acids are given. Number 1-4 of the libraries: compare to Figure III - 17. After the BP recombination of the fragments in Figure III - 17-E the fragments were recombined in yeast vectors with the GAL4 activation domain that were available in three frames (Maier et al., 2008). yellow: minimal fragment, in the case of the PAP2 fragment 454-747 two amino acids differed (NN) from 439-747 (DD) due to two different nucleotides in the random priming region. *: minimal fragment used for verification that was cloned in pAD-Gate2. The sequences of the shortest CDS fragments, PAP2 fragment 454-747 and COP1 fragment 1-479 can be found in the attachment (A R-12).

bait	fragment [bp] corresponding to the CDS	frequency	library				gate		
			N-termini		C-termini				
			1	2	3	4	1	2	3
PAP2 - GARFILD									
EGL3	1-747	5	4	1	-	-	-	5	-
EGL3	1-709	1	0	1	-	-	-	1	-
EGL3	1-700	1	0	1	-	-	-	1	-
EGL3	1-417	1	1	0	-	-	-	1	-
EGL3	1-394	1	0	1	-	-	-	1	-
EGL3	1-375*	1	0	1	-	-	-	1	-
EGL3	bad sequence	3	2	1	-	-	-	-	-
EGL3	small peptide, attB1	6	-	-	6	0	0	6	0
EGL3	small peptide, 430- frameshift	6	-	-	0	6	0	6	0
COP1	1-747	12	4	9	-	-	-	12	-
COP1	1-709	1	0	1	-	-	-	1	-
COP1	1-700	1	0	1	-	-	-	1	-
COP1	1-699	3	2	1	-	-	-	3	-
COP1	1-663*	1	0	1	-	-	-	1	-
COP1	bad sequence	2	2	0	-	-	-	-	-
COP1	276-747	2	-	-	2	0	0	0	2
COP1	328-747*	17	-	-	17	0	10	2	5
COP1	430-747	2	-	-	0	2	0	0	2
COP1	439-747	14	-	-	0	14	1	0	13
COP1	454-747	1	-	-	0	1	0	0	1
COP1 – GARFILD									
COP1	1-468	8	0	8	-	-	-	8	-
COP1	1-479*	1	0	1	-	-	-	1	-
COP1	1-792*	1	0	1	-	-	-	1	-
COP1^{K550E}	1-468	11	0	11	-	-	-	11	-
COP1^{K550E}	1-789	1	1	0	-	-	-	1	-
COP1^{K550E}	1-792*	1	0	1	-	-	-	1	-
COP1^{K550E}	attB1+peptide	1	1	0	-	-	-	1	-
COP1^{K550E}	bad sequence	2	1	1	-	-	-	2	-
COP1^{K550E}	random peptide	1	0	1	-	-	-	1	-

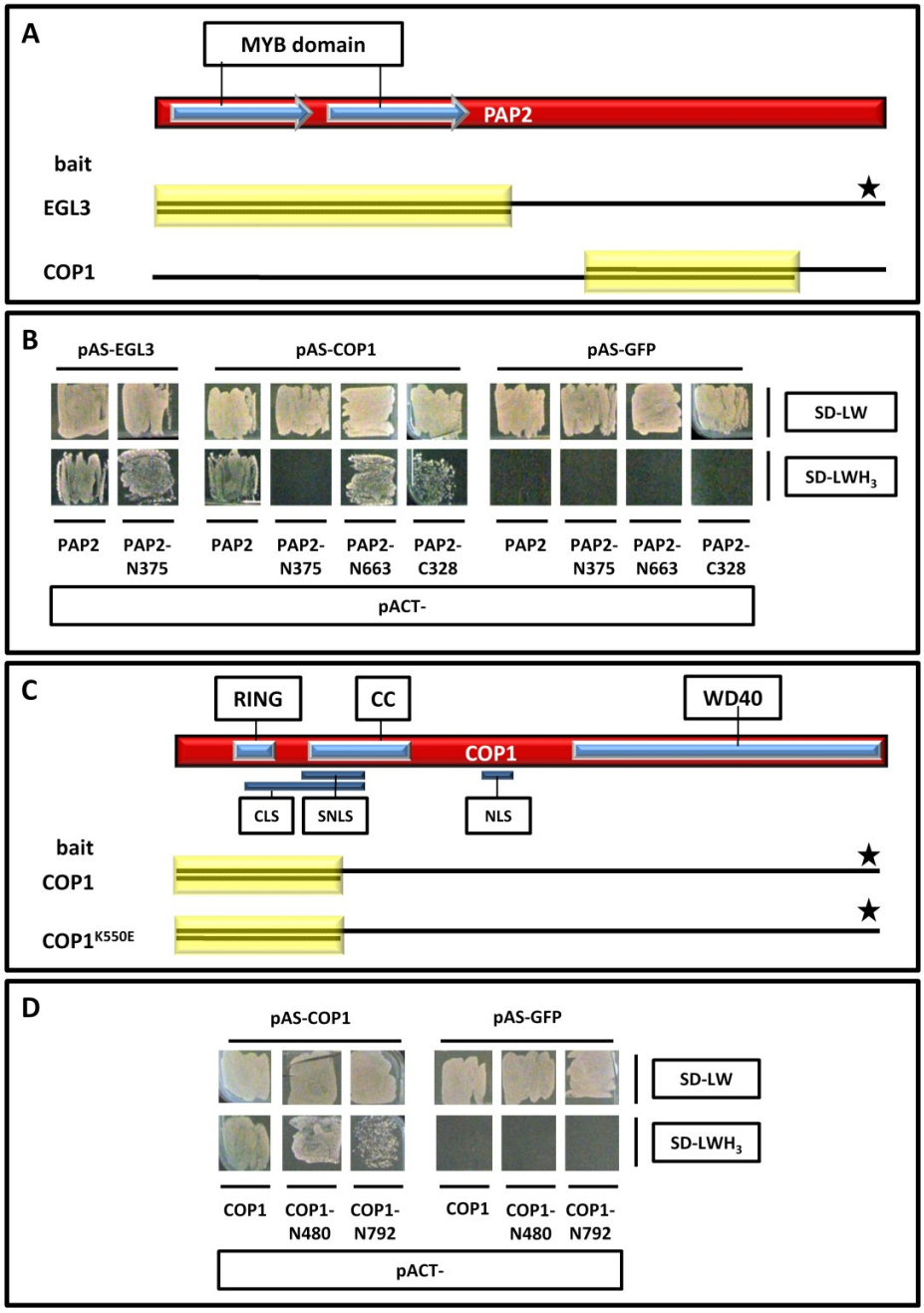

Figure III - 20: Schematic representation and verification of the GARFILD results.
(A, C) Schematic representation of the GARFILD results with PAP2 libraries (A) and COP1 libraries (C). red: PAP2 or COP1 protein with known domains. black: minimal interacting N- or C-terminal fragments, yellow (transparent): minimal fragment of PAP2 or COP1 that is sufficient for the interaction. * No result from the GARFILD screenings available. Given is the full length of the protein for which the interaction has been shown before (Torii et al., 1998; Zimmermann et al., 2004). MYB domain: R2 R3 MYB domain, RING: REALLY INTERESTING NEW GENE, CC: coiled coil domain, WD40: WD40 domain, CLS: cytoplasmic localisation signal, SNLS: subnuclear localization signal, NLS: nuclear localization signal **(B,D)** Verification of the interaction of selected GARFILD fragments with the corresponding bait. *S. cerevisiae* AH109 was transformed with two constructs coding for the depicted constructs. After selection on SD-LW media, several yeast colonies were streaked out on SD-LWH media supplemented with 3 mM 3-AT. Combinations with GFP served as negative controls. Fragments are described by the first or last corresponding base pair from Table III - 9. N: N-terminal fragment, C: C-terminal fragment. Chosen were the smallest fragments that were cloned in pAD-Gate2. COP1-N480 was chosen as the sequence ends with a direct stop and no additional amino acids.

No expression vectors in all frames for verification experiments have been generated so far. Therefore, only the smallest N- and C-terminal fragments in pAD-Gate2 were recombined into Gateway® entry vectors. COP1$^{1-480}$ was chosen instead of COP1$^{1-462}$ as the sequence ends with a direct stop and no additional amino acids are translated. A first verification with the yeast vector pACT-attR in YTH double transformation experiment is shown in Figure III - 20-B, D. The pACT-attR vector has a T7 promoter and can also be used for subsequent in vitro translation Co-IP experiments. BiFC experiments will follow.

2.3.4. *In silico* analysis of the PAP2 domain sufficient for PAP2 - COP1 interaction

In silico analysis of the PAP2 domain that interacts with COP1 revealed that the published, conserved CID motif that confers interaction of HY5, HYH, STO and STH with COP1 probably needs to be redefined (Holm et al., 2001). Holm and co-workers (2001) describe the conserved motif as "a novel motif, with the core sequence V-P-E/D-Φ-G (Φ = hydrophobic residue) in conjugation with an upstream stretch of 4-5 negatively charged residues". A modified motif was not only found in PAP2 but also in PAP1 by alignment (Figure III - 21). The protein sequence of all published interactors and interaction candidates of COP1 and DET1 presented in the network in Figure III - 3 were analysed. All proteins exhibiting the minimal sequence VP[D/E] are included in the alignment in Figure III - 21.

The alignment suggests a redefined motif for the putative *Arabidopsis thaliana* - COP1 Interacting Domain (AtCID): [D/E]X2[D/E]X4VP[D/E]Φ (Φ = hydrophobic residue). Provided that COP1 interacts with the AtCID of PAP2, the last glycine does not seem to be necessary. Interestingly the last amino acid of this new modified motif was the last amino acid of the minimal GARFILD N-terminal fragment. (Figure III - 21 and Table III - 9)

The alignment of human and *A. thaliana* COP1 showed that Lys^{550} is conserved (see attachment A R-13). Therefore it is possible that there are also human proteins that interact with hCOP1 in the same way like it was shown for STO, STH, HY5 and HYH in *A. thaliana* (Holm et al., 2001). The same search as described in the last paragraph was performed for all interactors of human COP1 listed at EntrezGene (Maglott et al., 2005). Three of these (c-Jun, c-Fos and JUND) showed a further modified motif: [D/E]X4VP[D/E]Φ (Φ = hydrophobic residue) probably located in a human - COP1 Interacting Domain (hCID). This finding further supports that the glycine can be neglected for the consensus motif and not all four to five negatively charged amino acids upstream of the core sequence are necessary. Interestingly, all *A. thaliana* proteins showed one conserved amino acid more than the human proteins in this alignment. Maybe the first aspartate or glutamate is plant-specific.

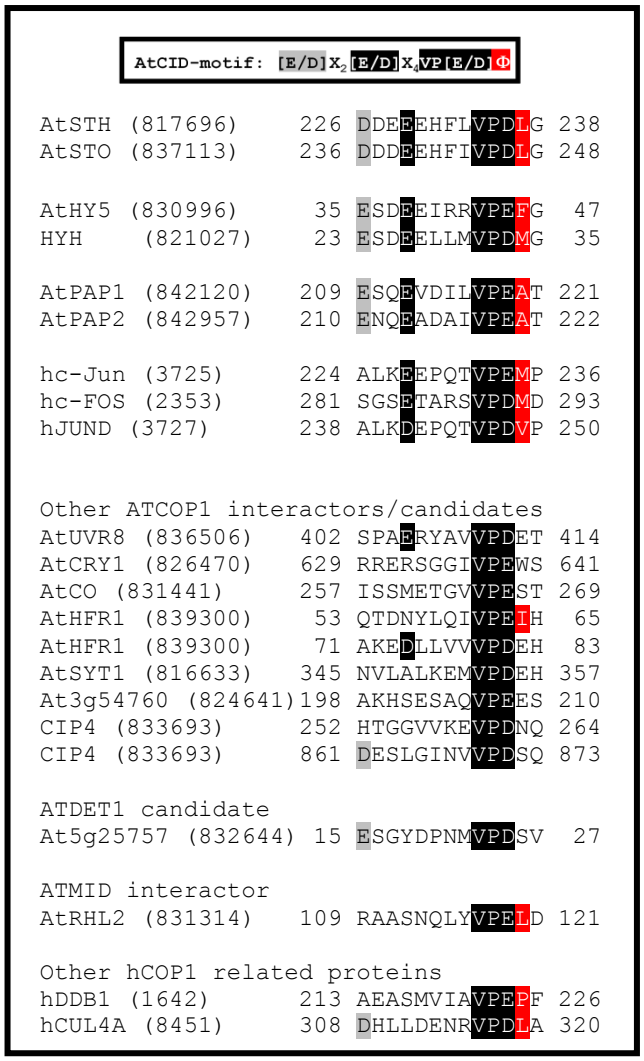

Figure III - 21: Alignment of the *Arabidopsis thaliana* - COP1 Interacting Domain (AtCID). red: hydrophobe amino acid, black: conserved amino acids, grey: conserved in *A. thaliana* COP1 interactors. For further details see the text. In brackets: GeneID listed at EntrezGene.

On the one hand it will be of great interest to test if the conserved motif is essential for interactions with AtCOP1 and hCOP1 and on the other hand if the hCOP1 can interact with the AtCOP1 interactors and vice versa. It is tempting to speculate that the existence of this motif in a protein correlates with the protein`s ability to interact with COP1 as the motif seems to have withstood evolutionary pressure.

One would expect that beside the motif also functions are conserved between the human and *A. thaliana* COP1 protein. In human, COP1 regulates aspects and transcription factors that are involved in the cell cycle and DNA damage response. In plants, so far, no direct connection to the cell cycle or DNA modifying proteins has been unravelled for COP1, despite the progress presented in this work

concerning MID (part 3). There might be two reasons for this gap of knowledge: (1) it is no gap of knowledge as these functions are not directly fulfilled by the COP1 protein in plants; (2) the corresponding targets and interactors have not been identified yet. Probably they were not present in YTH libraries that are typically screened to identify new interactors, or they are toxic to yeast. Another possibility is that mutants are lethal and therefore no phenotypical comparisons can be drawn to the *COP1* mutants.

It is possible that the identified motif can help to close this gap. Therefore, *A. thaliana* and human databases were searched via BLASTP (NCBI) for the AtCID (Figure III - 22) or for the hCID (Figure III - 23) and A R-14 in the attachment) motif, respectively. Glycine was also admitted at the position of the hydrophobic residue. Some of the human proteins also share the AtCID sequence (Figure III - 23 - upper group).

Indeed, several proteins were identified that modify DNA, are involved in DNA repair or cell cycle progression or are associated to chromatin (e.g. anaphase promoting complex subunit 1 and 2 from human (ANAPC1, ANAPC2) , B double prime 1 (BDP1), dedicator of cytokinesis 11 (DOCK11) or FASCIATA1 (AtFAS1)) (Figure III - 22 and Figure III - 23). AtCID might also appear by chance in some proteins, the kind of hydrophobic residue might be essential or AtCID might be masked in some proteins. Randomly chosen proteins form Figure III - 22 and Figure III - 23 should be tested for their ability to interact with COP1 (via the hCID or AtCID) in the future to elucidate whether the redefined motif was able to predict new COP1 interactors or not.

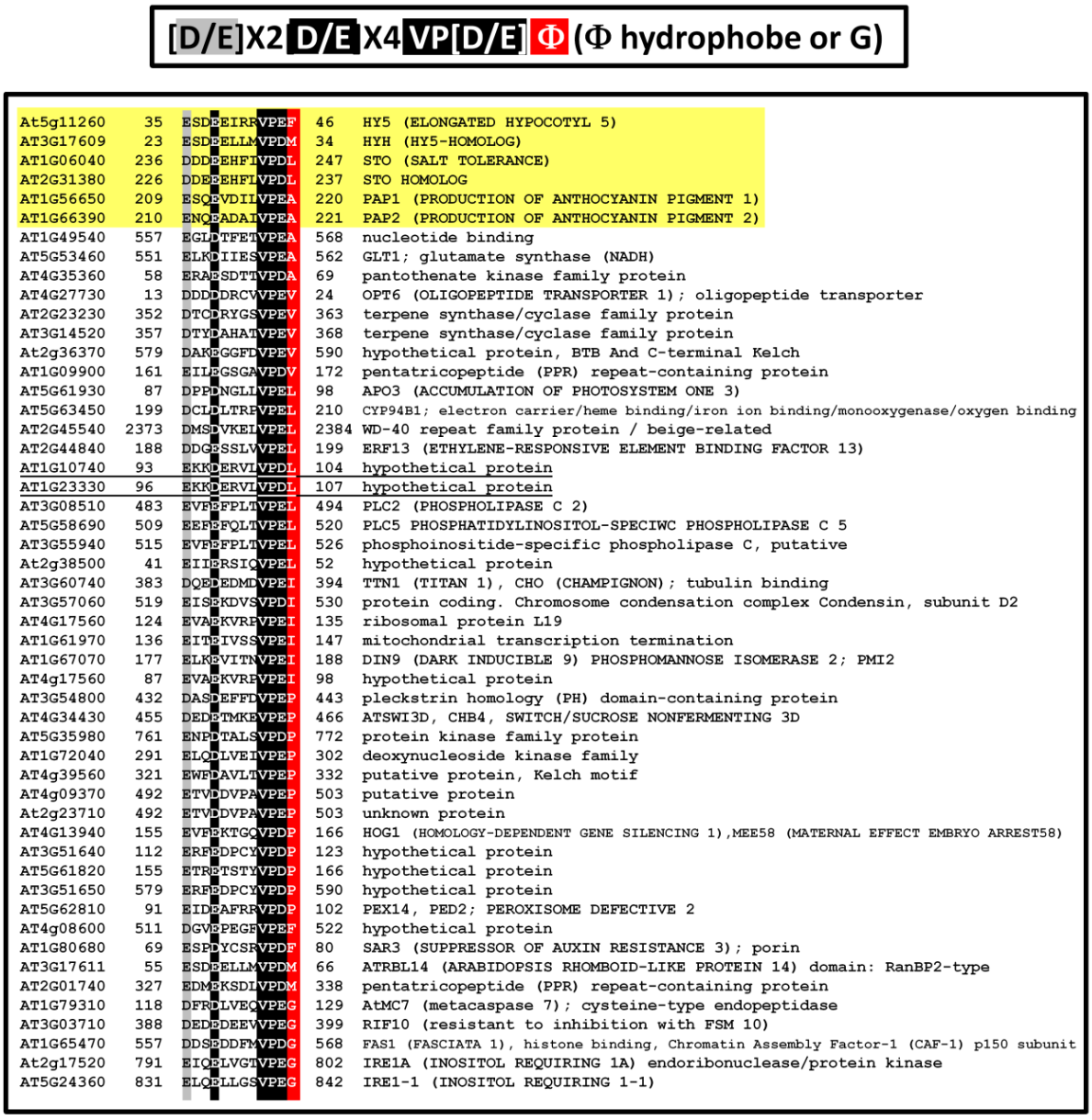

Figure III - 22: Alignment of BLASTP (NCBI) *A. thaliana* results the *Arabidopsis thaliana* - COP1 Interacting Domain (AtCID). The blasted consensus sequence is given above the alignment. Genes are identified by their AGI code (left) and a short description extracted from the BLASTP results. Numbers correspond to base pairs of the gene or CDS provided by the BLASTP results with no further validation. (Altschul et al., 1997) grey: *A. thaliana*-specific conserved amino acid, black: highly conserved amino acids, red: hydrophobe amino acids or glycine, yellow: published interactors ad PAP1 and PAP2 from the alignments in this work. Underlined: Two proteins that also were found in the alignment of the protein sequence that is code by At5g51730 (see attachment A R-1 and Table III - 2, Figure III - 21).

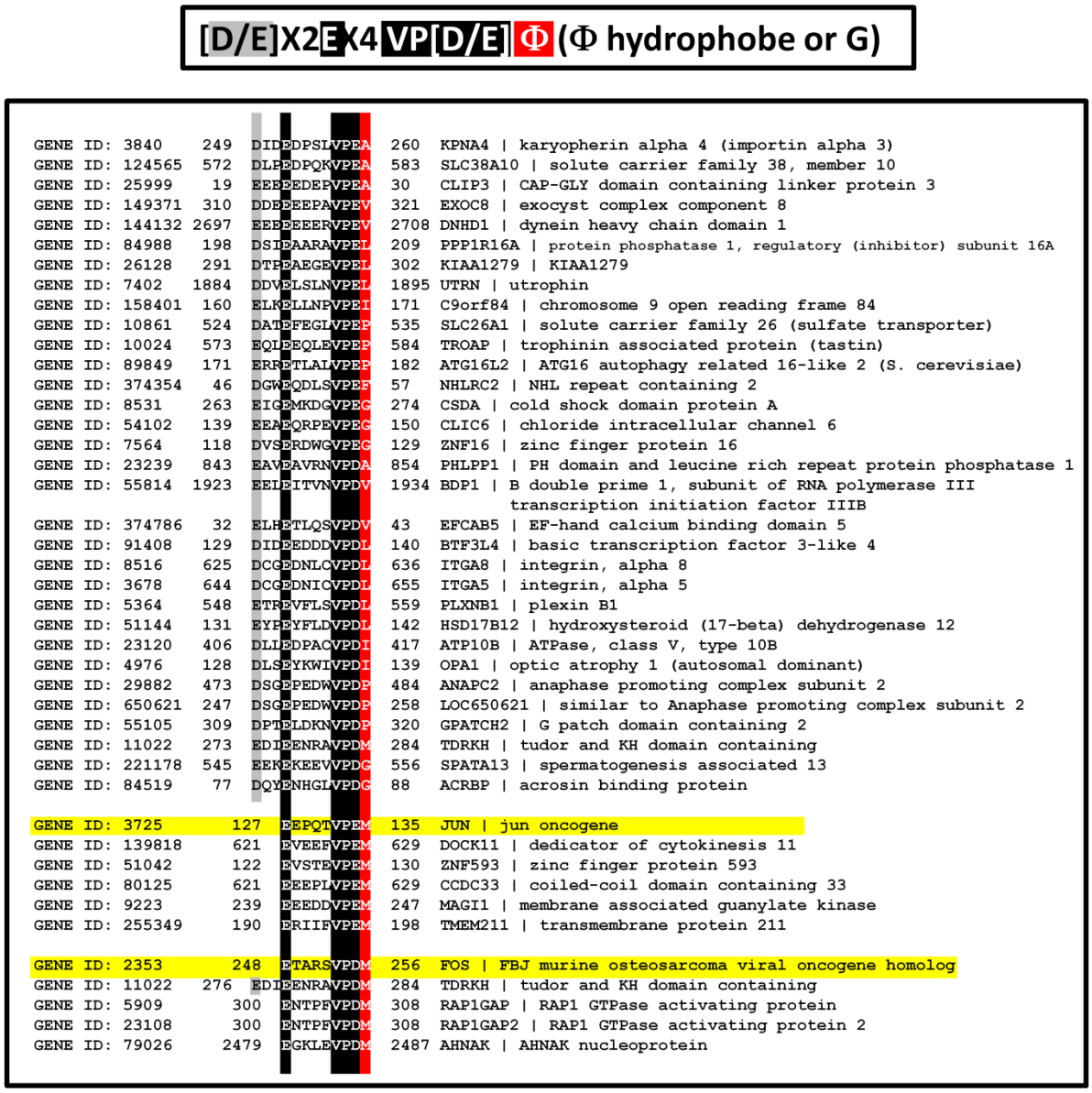

Figure III - 23 Extracts from an alignment of BLASTP (NCBI) *homo sapiens* results for the EX2VP[D/E]Φ sequence. The blasted consensus sequence is given above the alignment. In the first part of the alignment all proteins are shown that also exhibit the corresponding AtCID. In the second pat proteins with the same hydrophobic residue as cJun and cFos are listed. Genes are identified by their AGI code (left) and a short description extracted from the BLASTP results. Numbers correspond to base pairs of the gene or CDS provided by the BLASTP results with no further validation. (Altschul et al., 1997) grey: *A. thaliana*-specific conserved amino acid, black: highly conserved amino acids, red: hydrophobe amino acids or glycin, yellow: published interactors that are mentioned in the text and in Figure III - 21. The complete BLASTP results are listed in A R-14 in the attachment.

3. MIDGET - a new putative regulator of COP1

MID, COP1 and SPA1 form a triangle in the interaction network presented in 1.4 (Figure III - 3). In yeast it has been shown that it is likely for three proteins of such a triangle to be part of one complex (Yeger-Lotem et al., 2004).

This interaction network (Figure III - 4) positioned MID in the frame of SPA1 and also of DET1, two COP1-function-modifying proteins that share complexes with COP1 (Ang et al., 1998; Fittinghoff et al., 2006; Nixdorf and Hoecker, 2010; Pick et al., 2007; Saijo et al., 2003; Saijo et al., 2008; Seo et al., 2003; Yanagawa et al., 2004; Zhu et al., 2008).

The physical and functional interaction of MID with COP1 was verified in this work and will be presented in this part. Furthermore, first results concerning the physical and functional interaction or dependency of MID and SPA1 will be shown.

3.1. MIDGET interacts with COP1 and SPA1

3.1.1. The *MIDGET*-Col-0 CDS

BRASSINOSTEROID INSENSITIVE4 (*BIN4*) is identical to *MIDGET* (*MID*) (At5g23640), a plant specific, single copy gene coding for a DNA binding nuclear protein (Breuer et al., 2007; Kirik et al., 2007). In 2007 Breuer and co-workers did not present a sequence for the *BIN4*-CDS and therefore referred to the annotated sequence at TAIR (www.arabiddopsis.org) at this time. In contrast, Kirik and co-workers presented a cDNA sequence for *MID* obtained from a 5`RACE experiment that differed from the TAIR sequence at that time. In 2009, this difference was also observed by Forterre and Gadell. Alignments showed that the sequence from Kirik et al. (2007) matches with only one mismatch to the CDS At5g23640.3 and At5g23640.4 two of six splicing variants that are annotated at TAIR since June 2009 (attachment figure A R-15). Subsequent multiple sequencing of L*er* cDNA (a kind gift of M. Pesch) revealed that the one differing nucleotide can also be found in the CDS of *MID*-L*er*. Therefore, all constructs based on the sequence published in Kirik at al. (2007) will be referred to as *MID*-L*er*.

For the cloning of *MID*-Col-0 two independent cDNA preparations from dark grown seedlings and plant material grown under long day conditions (LD, 16h light, 8h dark cycles, a kind gift of C. Jörgens) were sequenced several times with different primers. The sequences corresponded in all

cases to the annotated splicing variants At5g23640.3 and At5g23640. (www.arabidopsis.org). *MID*-Col-0 was amplified from Col-0 cDNA and verified by sequencing. All constructs based on the Col-0 sequence are referred to as *MID*-Col-0 or *MID* in this work. The *MID*-Col-0 sequence can be found in the attachment (A R- 16). Further analysis concerning the so far not observed splicing variants of *MID* is necessary in the future.

The differing nucleotide between *MID*-L*er* and *MID*-Col-0 leads to an amino acid exchange (Figure III - 24). Figure III - 24 also shows the predicted AT-hook, a bipartite NLS and direct repeats (with more than 80% homology) published in Kirik et al. (2007). Additionally, the M-phase inducer phosphatase domain that was predicted by SMART with a probability of $9.2*e^{-1}$ is indicated (Letunic et al., 2009; Schultz et al., 1998).

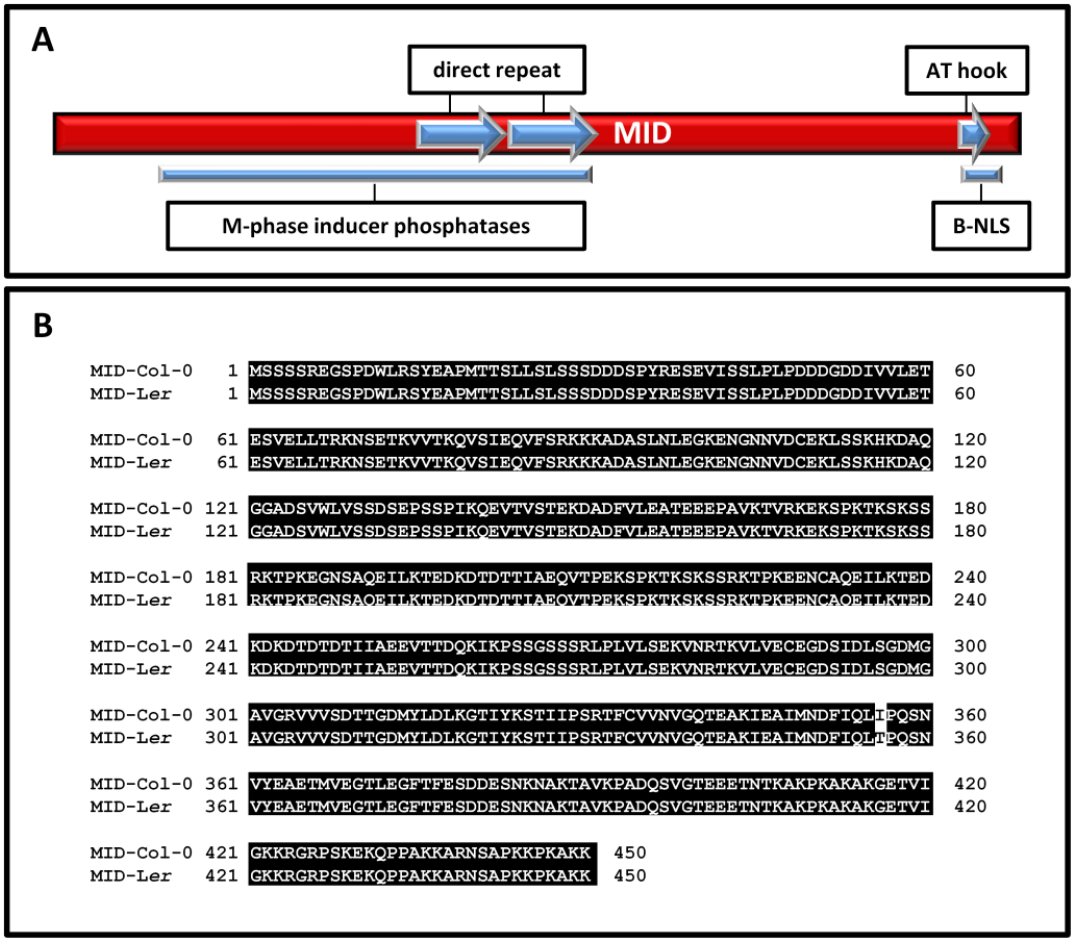

Figure III - 24: MID-Col-0 and MID-L*er* sequence and domains.
(A) Schematic representation of MID with predicted domains. Direct repeats share a homology of more than 80% (aa 170-210 and 212-256). M-phase inducer phosphatase domain (aa 50-250) and HMG DNA binding domain preferring A/T-rich DNA regions (aa 421-433, AT-hook) were predicted by SMART, a bipartite nuclear localization signal (aa 423-439, B-NLS) was predicted by PSORT in Kirik et. al (2007) (Kirik et al., 2007; Letunic et al., 2009; Robbins et al., 1991; Schultz et al., 1998).
(B) Amino acid alignment of MID-Col-0 (sequence corresponds to the sequence encoded by At5g23640.3 and At5g23640.4 annotated at TAIR) and MID-L*er* (Kirik et al., 2007). black boxes: identical amino acids.

The rescue of the *mid*-mutant phenotype with the Pro35S:*MID*-L*er*-*YFP* construct was already reported by Kirik et al. (2007). The phenotype of the used mutants in this work, *mid-1* (Col-0) and *mid2* (Col-0), was characterised by Kirik et al. (2007) and will be described in more detail in III.3.

Beside the characteristic localisation, the functionality of the Pro35S:*YFP-MID*-Col-0 construct was proven by a rescue experiment. Figure III - 25 shows that stable transformed *mid-2* plants could be rescued with pEarleyGate-MID-Col-0 concerning the size of the plant, the shoot length and the trichome phenotype. Leaf area and petiole length for all Pro35S:*YFP-MID* (*mid-2*) plants in the T_3 generation from two independent lines were reduced in comparison to the wildtype (Figure III - 25). This might be due to the used promoter, the fused YFP-tag or the relevance of one of the other splicing variants. The YFP fluorescence and specific localisation of YFP-MID to the nucleus proved that the fusion protein is expressed and no significant portions of YFP are cleaved from YFP-MID *in planta.* No significant over-complementation phenotypes were observed.

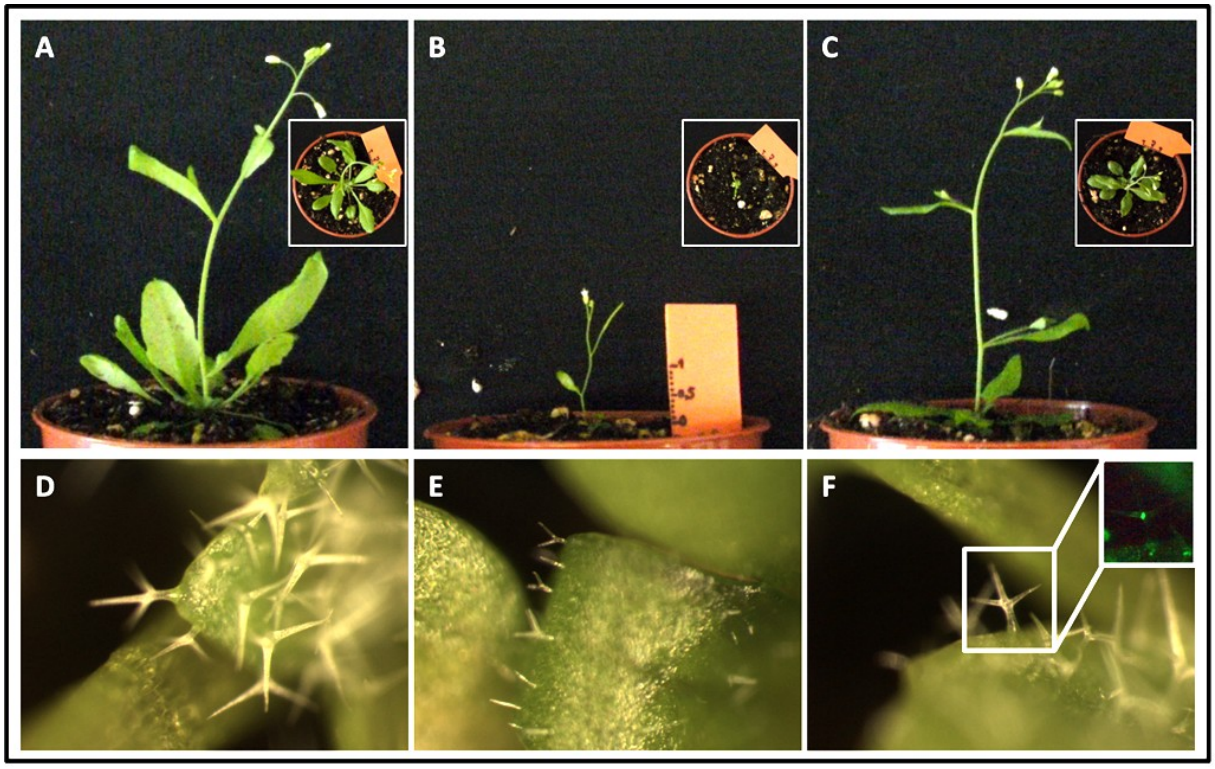

Figure III - 25: (A-C) Pictures of 29-day-old plants that were grown under LD conditions at 21°C. Pictures were taken from the side with a digital camera. The unit is cm on the orange ruler. Insets are pictures from the same plant taken from the top. **(D-F)** Trichomes of 9-day-old plants grown under LD conditions at 21°C. Pictures were taken with a Leica MZ10F fluorescence binocular and the Leica Application Suit V3 Version 3.5.0. All pictures have the same magnification. Inset in (F) was taken with a YFP filter at the same magnification. Note the YFP fluorescence in the nucleus of the trichome.
(A, D) Col-0; (B, E) *mid-2* (Col-0); (C, F) pEarleyGate104-MID-Col-0 (*mid-2*), T_3 plant, BASTA selected.

The segregation ratio of four lines in the T_2 generation was determined. BASTA resistance served as a marker for successful transformation. Over 100 plants were analysed per line to determine the segregation. 74.6%, 68.5%, 74.7% and 75.5% of the plants were BASTA-resistant. The observed segregation ratios indicate that the analysed plants carried only one T-DNA insertion coding for YFP-MID-Col-0. Plants from the first and third line were used for the analysis of the phenotype in the T_3 generation.

Taken together, it can be concluded that the YFP-MID-Col-0 fusion protein exhibits typical MID functions *in planta*.

3.1.2. The MIDGET - COP1 interaction in yeast

The Colony PCR products corresponding to *MID* from YTH screenings with COP1 (I. 1.1.) contained an unspecific sequence upstream of the *MID* sequence (attachment A R-17). For YTH analysis with full length MID-L*er* pCD2-attR-MID-L*er* and pcACT2-MID-L*er* -attR were available. The pAS-2-1-attR and pcACT2-attR versions were created. Three fragments of *MID*-L*er*-CDS were already cloned in my diploma thesis: $MID^{1\text{-}798}$, $MID^{781\text{-}1353}$ and $MID^{661\text{-}990}$.

Figure III - 26 shows a successful verification of the COP1-MID interaction with full length MID-L*er* constructs. It has to be mentioned that yeast harbouring MIDGET and COP1 YTH constructs proved to be problematic in regard to their growth behaviour. MID seems to be toxic to yeast cells as different sizes of colonies were observed for yeast co-transformed with MID constructs on selection media (e.g. Figure III - 27) and growth was delayed for more than two days in comparison to other unproblematic combinations. This growth behaviour was suppressed by co-transformation with pACT-attR-$MID^{260\text{-}450}$. Additionally, the temperature for growth on interaction media was critical. Yeast harbouring a COP1 and MID YTH constructs grew better at 24°C or 28°C in comparison to 30°C (Figure III - 27). This hints at folding or stability problems for MID. For other COP1 combination nothing similar was observed. In this context it is also possible that MID interacts with COP1 via another domain than all other tested interactors or that a plant-specific modification is necessary for the MID-COP1 interaction. Plasmids coding for negative controls, pAS2-1-SNF1 and pACT-SNF4, were replaced by pAS2-1-GFP and pACT-GFP as single colonies were visible after prolonged incubation (necessary for MID) at 30°C (Figure III - 27).

MIDGET is a co-factor of the *A. thaliana* topoisomerase VI (TOPOVI) consisting of ROOT HAIRLESS 2 (RHL2) and topoisomerase 6 subunit B (AtTOP6B) (Kirik et al., 2007). MID interacts with RHL1 and

RHL1 has been shown to be an essential component of the TOPOVI complex (Kirik et al., 2007; Sugimoto-Shirasu et al., 2005). Therefore, also RHL1, RHL2 and AtTOP6B were tested in the YTH experiment for their interaction with COP1. As single colonies grew for the negative controls for RHL2, no conclusions could be drawn for the RHL2-COP1 interaction. Increasing concentrations of 3-AT might show in the future if RHL2 and COP1 interact in yeast. In the case of the combination COP1-AtTOP6B, very few colonies grew on interaction media. There might be a weak interaction of AtTOP6B with COP1 in yeast but from the performed YTH experiments no interaction of TOPOVI components with COP1 can be concluded. (Figure III - 26)

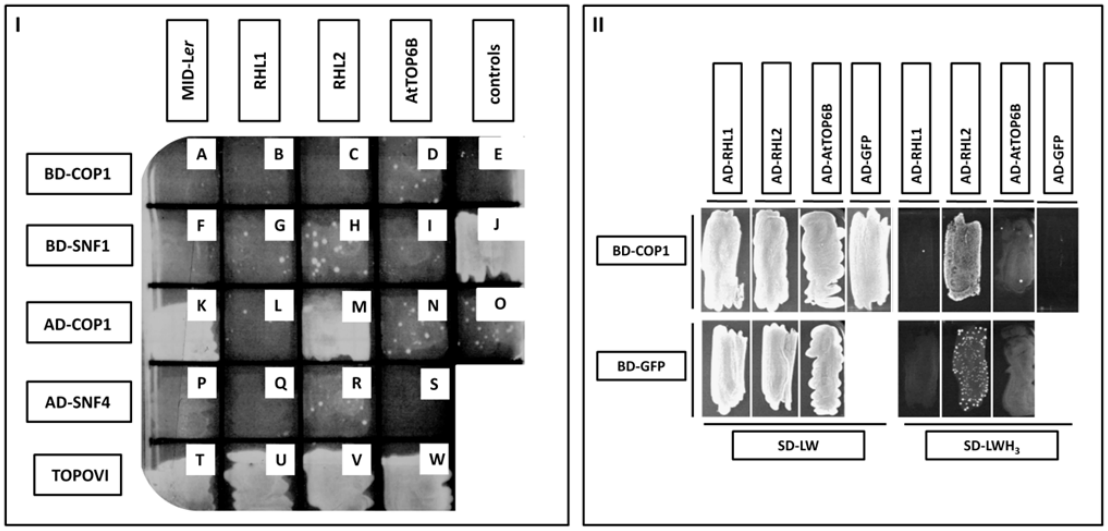

Figure III - 26: MID interacts with COP1 in yeast.
(I) Interaction plate of a YTH double transformation experiment using *S. cerevisiae* AH109. SNF1 and SNF4 were used as negative controls. (A-D, F-I) BD-COP1 and BD-SNF1 with AD-fusions of the depicted proteins. In (E) AD-SNF4 was used as a negative control for BD-COP1. (I) is the positive control BD-SNF1 with AD-SNF4 (Celenza et al., 1989). (K-N, P-S) AD-COP1 and AD-SNF4 with BD-fusions of the depicted proteins. In (O) BD-SNF1 was used as a negative control for AD-COP1. (T) BD-MID + AD-RHL1; (U) BD-RHL1 + AD-MID; (V) BD-RHL2 + AD-AtTOP6B; (W) BD-AtTOP6B + AD-RHL2. (T-W) show the functionality concerning interactions in yeast for the used constructs. **(II)** Selection and interaction plate for YTH combinations of BD-COP1 and BD-GFP with the TOPOVI components RHL1, RHL2, AtTOP6B and GFP as a negative control in *S. cerevisiae* AH109. BD: GAL4-binding domain, AD: GAL4-activation domain. pAS2-1 was used for COP1, GFP and SNF1; pACT was used for COP1, GFP and SNF4; pCD2 and pcACT2 were used for MID-L*er*, RHL1, RHL2 and AtTOP6B. SD-LW: selection plates, selective drop out plates lacking leucine and tryptophan. SD-LWH3: interaction plates, selective drop out plates lacking leucine, tryptophan and histidine supplemented with 3mM 3-AT.

As the MID-RHL1 interaction can be shown in YTH experiments under all tested conditions it was speculated that RHL1 might stabilise MID. Therefore, RHL1 was co-expressed with BD-MID and AD-COP1 in a dosage dependent manner by the application of the pBRIDGE system (II. 2.2.9.). No influence by RHL1 on COP1 self-association was observed indicating that the lack of methionine did not impair growth of the used yeast strain AH109. The interaction of MID and RHL1 served as a control for the suppression of Pro*Met25* by the methionine present in the interaction plates. Yeast harbouring pBRIDGE-MID/RHL1 (*BD-MID*, Pro*Met25*:*RHL1*) and pcACT2-RHL1 grew significantly

better on interaction media with 100µM methionine (suppression of Pro*Met25* expressed RHL1) in comparison to interaction media lacking methionine. No influence on the MID/COP1 interaction by the presence of RHL1 was observed. In the same experiment the MID/COP1^{K550E} interaction was tested. Both proteins interact in yeast independent of the presence and absence of RHL1 indicating that MID interacts with COP1 in another way than STO, STH, HY5 or HYH (Holm et al., 2001).

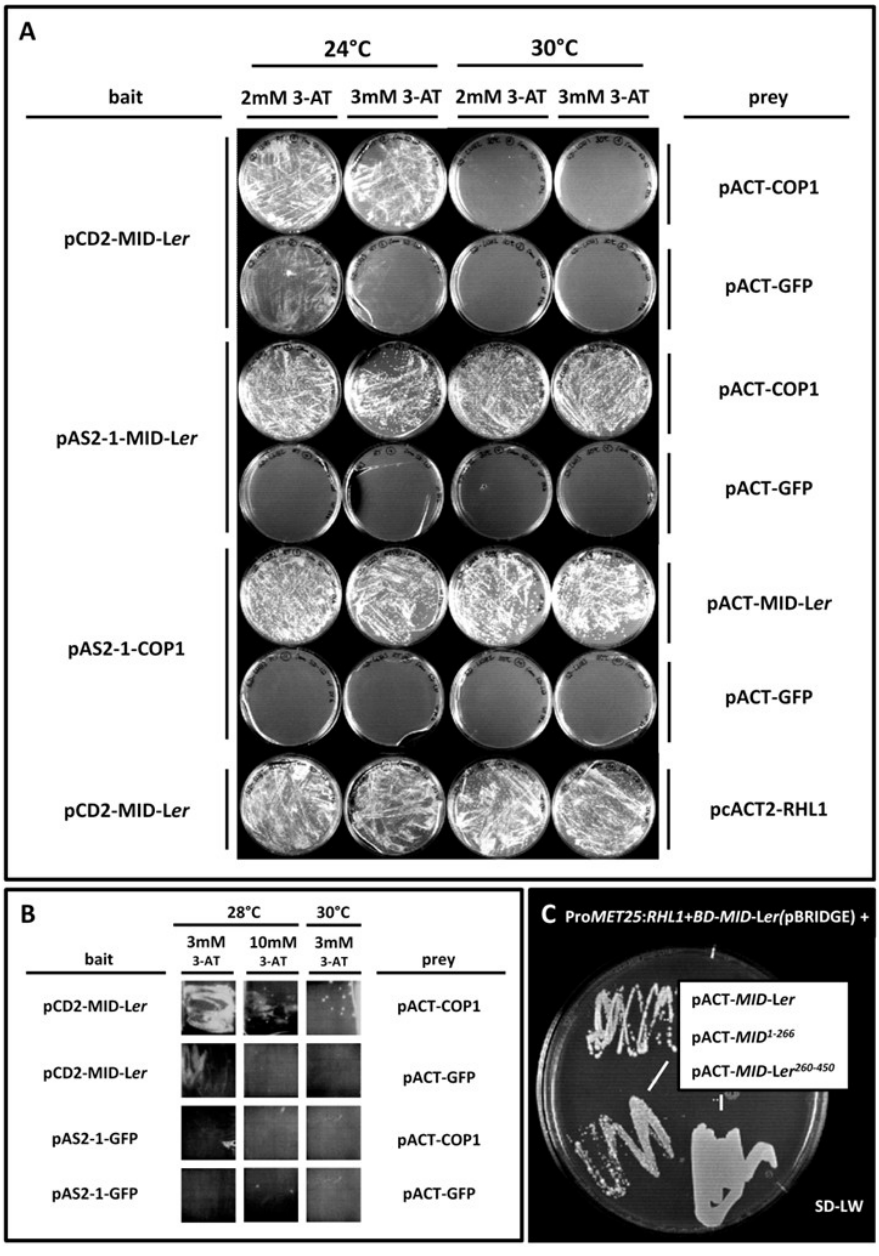

Figure III - 27: The MID-COP1 interaction in yeast is temperature sensitive and MID is toxic to yeast.
(A, B) *S. cerevisiae* AH109 that were double transformed with a bait construct depicted at the left and a prey construct depicted as a prey construct and selected for the plasmids. Same amounts of double transformed yeast cells were plated on four plates containing 2 or 3 (A) or 3 or 10 (B) mM 3-AT Yeast were subsequently incubated at 24°C (A), 28°C (B) or 30°C (A, B). GFP served as a negative control. **(C)** *S. cerevisiae* AH109 double transformed with pBRIDGE-MID/RHL1 (*BD-MID*, ProMet25:*RHL1*) and pACT-MID-L*er*, pACT-MID$^{1-266}$ or pACT-MID-L*er*$^{260-450}$ growing on a selection plate. Note the different growth behaviour of the yeast. SD-LW: selection plates, selective drop out plates lacking leucine and tryptophan.

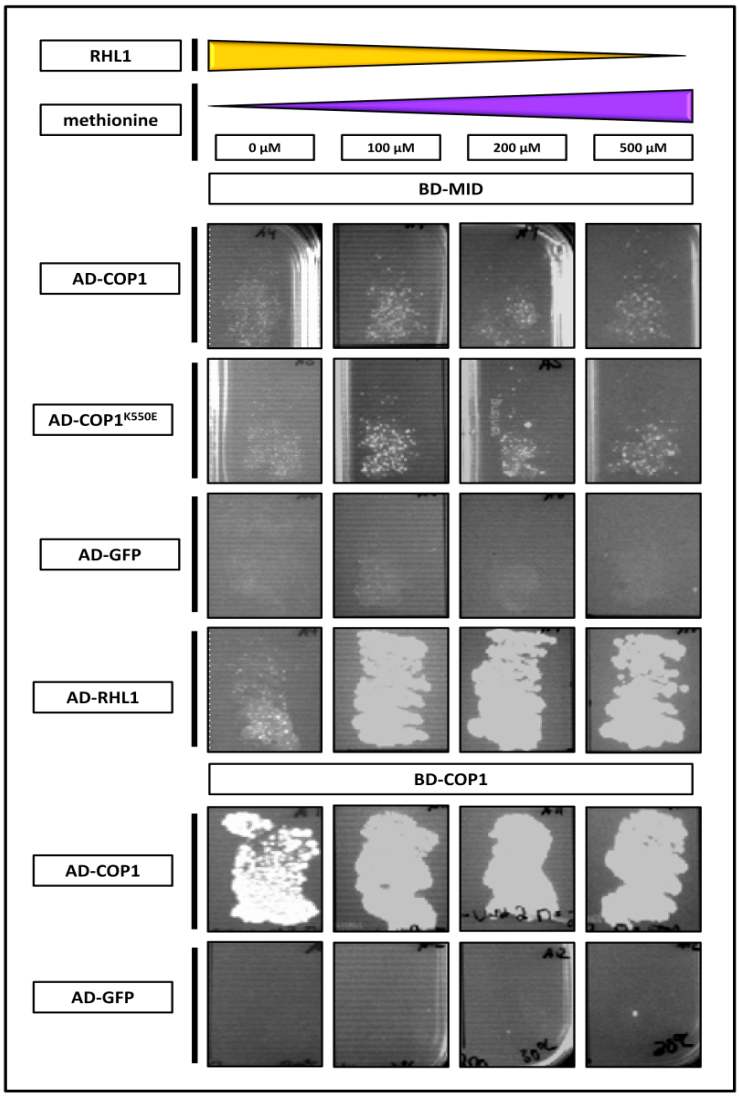

Figure III - 28: Influence of RHL1 co-expression on the MID-COP1 interaction.
Cells of *S. cerevisiae* AH109 were double transformed with the depicted constructs on the left and pBRIDGE-MID/RHL1 (*BD-MID*, Pro*Met25*:*RHL1)* (BD-MID) or pBRIDGE-COP1/RHL1 (*BD-COP1*, Pro*Met25*:*RHL1*) (BD-COP1). The same volume of selected double transformed yeast cells was spread for each combination on four different interaction plates supplemented with 0, 100, 200 or 500 µM methionine. Purple and yellow gradient: schematic representation of the methionine concentration in the plates and RHL1 expression, respectively. Weak growth can be observed on all plates for BD-MID and AD-COP1 or AD-COP1^{K550E}. Note the difference for the AD-RHL1 combination between 0 and 100 µM methionine. GFP served as a negative control. BD: GAL4-binding domain, AD: GAL4-activation domain.

3.1.3. MIDGET and COP1 colocalise and interact *in planta*

MIDGET and COP1 colocalise in planta as was shown by biolistic transformation of leek (*Allium porrum*) epidermal cells, transformation of cells of *A. thaliana* cell suspension culture and infiltration of *N. benthamiana* leaves (Figure III - 29). CFP-COP1 (*Allium porrum*) or RFP-HA-COP1 localised to subnuclear foci whereas YFP-MID-Col-0 was visible in the whole nucleus. The functionality of

Pro35S:Pro35S:RFP-HA-COP1 and Pro35S-YFP-MID was shown in this work (Figure III - 9, Figure III - 25).

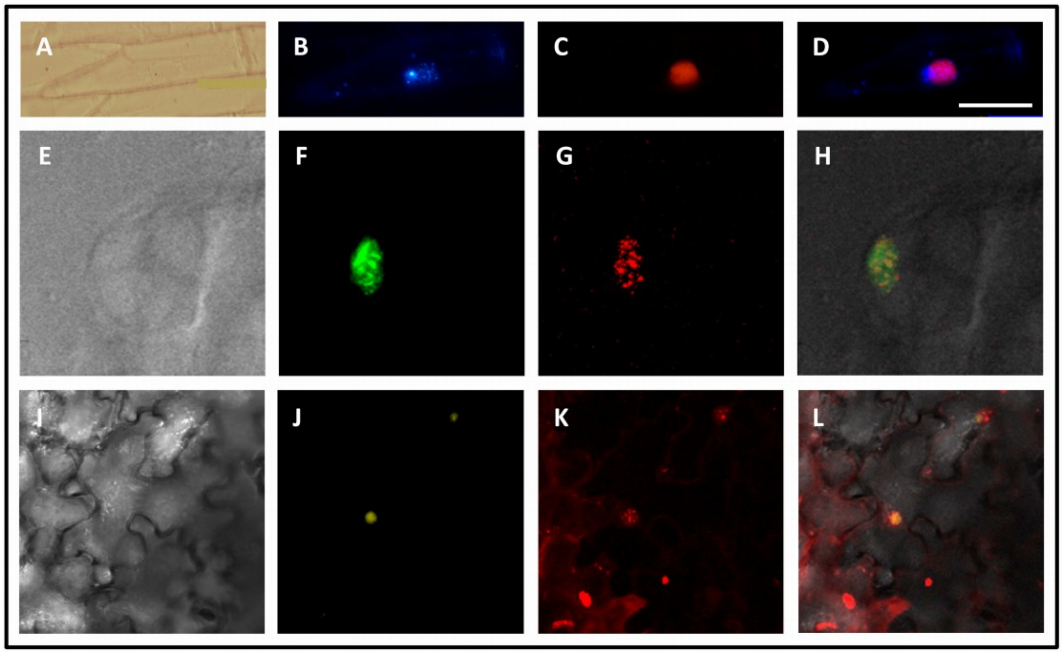

Figure III - 29: MID-L*er* and COP1 colocalise in the nucleus *in planta*.
(A-D) Co-localisation of CFP-COP1 and RFP-MID-L*er* in biolistically transformed leek (*Allium porrum*) epidermal cells. (E-H) Co-localisation of YFP-MID-L*er* and RFP-HA-COP1 in a cell of dark grown *A. thaliana* cell suspension culture. (I-L) Co-localisation of YFP-MID-L*er* and RFP-HA-COP1 in infiltrated epidermal leaf cells of *N. benthamiana*. Leaves were co-infiltrated and the suspension culture cells were co-transformed with a combination of *A. tumefaciens* harbouring pEGATE104-MID-L*er*, pNmR-COP1 and *A. tumefaciens* RK19. *N. benthamiana* plants were kept at 24°C at LD conditions. *A. thaliana* cell suspension cultures were kept with constant shaking in the dark. Pictures were taken three dai or five days after transformation, respectively. (A) bright-field image, (B-C) fluorescence microscopy; (F-G, J-K) CLSM (independent scanning, in F and G, sequential scanning in J and K, displayed pictures are merged z-stacks), (E, I) transmission picture; (F, J) YFP channel; (G, K) RFP-channel; (D, H, L) merged pictures. Bar equals 50 µm in (A-D) An 10-fold water objective was used in (E-H) and an 40-fold APO objective in (I-L). Pictures in one row (E-L) were taken at the same magnification. CFP-COP1: pENSG-CFP-COP1; YFP-MID: pEarleyGate104-MID (LBA4404. pBBR1MCS.virGN54D); RFP-HA-COP1: pNmR-COP1 (LBA4404pBBR1MCS-5.virGN54D); RK19 = anti silencing strain.

BiFC experiments revealed that MIDGET and COP1 interact in subnuclear foci in epidermal cells of *Allium porrum* and in leaf epidermal cells of *N. benthamiana* (Figure III - 29). N-terminal fusions of MIDGET and COP1 were generated with the N- and C-terminal portions of a split YFP- molecule using the vectors pCL112 and pCL113. The cytoskeleton marker CFP-TALIN served as a transformation control. For both possible combinations a minimum of two experiments was performed with at least fifty cells that showed a CFP-TALIN signal and an YFP-signal. After 24h protein aggregates formed in the cytoplasm in cells expressing COP1-fusion-proteins as was also seen for COP1 and PAP2 (Figure III - 11) and reported in Ang et al. (1998) or von Arnim et al (1997). Self-association of the used COP1 BiFC constructs occurred in subnuclear foci as was expected. The MIDGET constructs were already

tested in my Diploma thesis. As DET1 did not show a signal in the BiFC experiment with COP1, it served as a negative control.

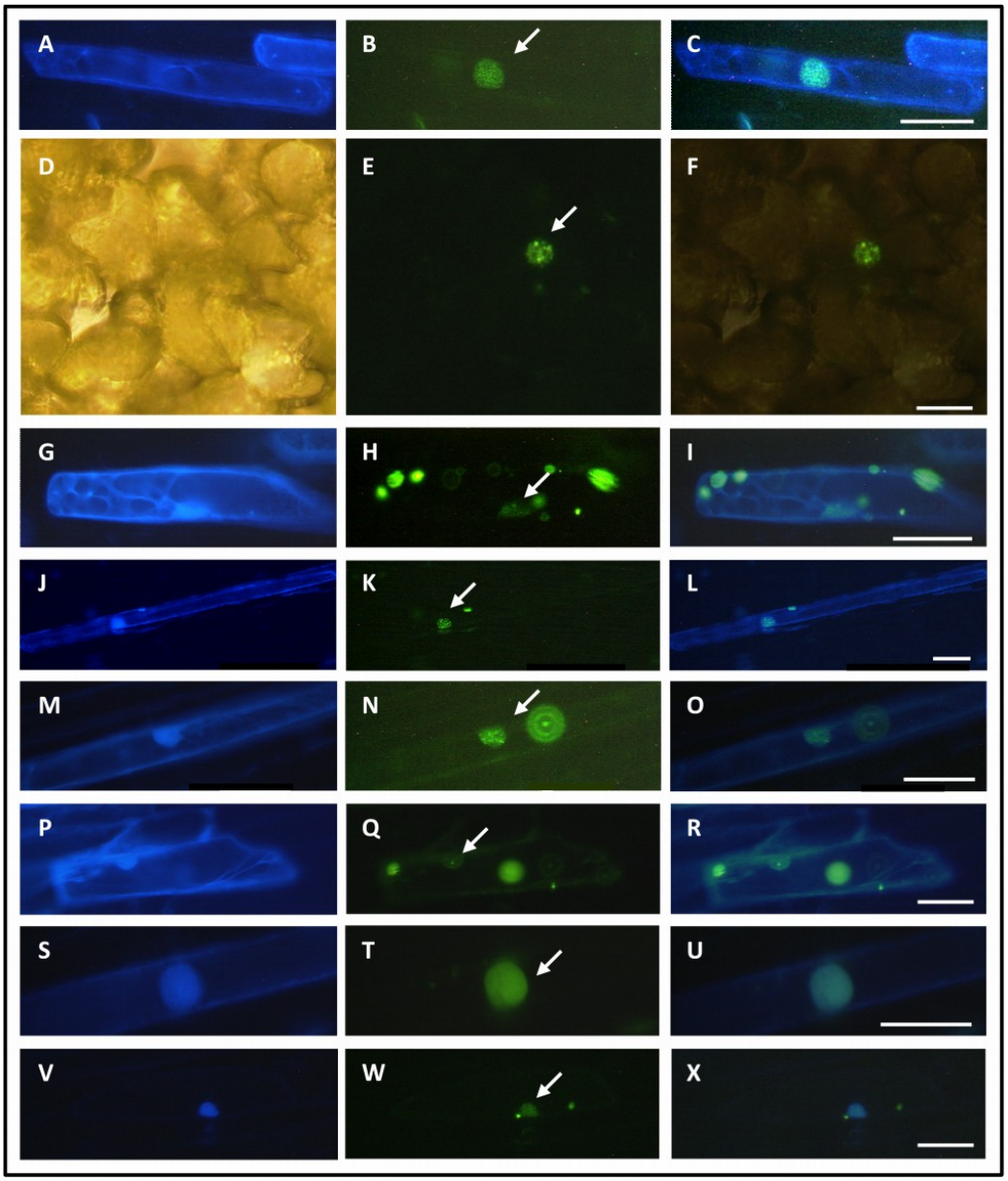

Figure III - 30: BiFC assay for COP1 with MID, TOPOVI components and fragments of MID. **(A-C, G-X)** Plasmids encoding BiFC fusion constructs of COP1 and the interaction partner to be tested with the N- or C-terminal part of YFP were co-bombarded into leek cells (*Allium porrum*) or co-infiltrated into *N. benthamiana* (as described in Figure III - 29). **(D-F)** The interaction partners are in the first and second row: MID-L*er*, in the third row: RHL1 in the fourth row: AtTOP6B (Note that not all transformed cells showed YFP fluorescence.), in the fifth row: COP1; in the sixth row: MID$^{1\text{-}266}$; in the seventh row: MID-L*er*$^{260\text{-}450}$; and in the last row: MID-L*er*$^{260\text{-}450}$. **(A, G, J, M, P)** CFP-TALIN or **(V)** CFP-GL3 served as a transformation control. **(B, E, H, K, N, Q, T, W)** YFP fluorescence indicates interaction with COP1 in the BiFC assay. Most interaction were localised to subnuclear foci, despite in (T) for MID$^{260\text{-}450}$. Pictures in the right column are merged pictures of the two pictures to the left. Arrows point to the nucleus. All pictures were taken with a fluorescence microscope. Bar equals 50 µm. BiFC-constructs and transgenic *A. tumefaciens* strains: pCL112-COP1, pCL113-COP1, pCL113-MID-L*er*, pCL112-RHL1, pCL112-AtTOP6B, pCL113-MID$^{1\text{-}266}$, pCL112-MID-L*er*$^{260\text{-}450}$, pCL113-MID$^{220\text{-}330}$, pCL112-COP1 (LBA4404pBBR1MCS-5.virGN54D), pCL113-MID (LBA4404pBBR1MCS-5.virGN54D) RK19 = anti silencing strain.

A signal did not appear for all transformed cells for BiFC of COP1 and AtTOP6B. But when a signal was visible it was localised to subnucear foci. The YFP signal for RHL1-COP1 was weak in subnuclear foci but also in cytoplasmic aggregates or inclusion bodies. The N-terminal and middle part of MID (MID^{1-266} and $MID^{220-330}$) was able to interact with COP1 in subnuclear foci. This was not the case for the C-terminal portion of MIDGET ($MID^{260-450}$) for which a weak signal in the whole nuclear was detected in the BiFC assay with COP1. MID^{1-266} and $MID^{220-330}$ cover both or one direct repeats and the whole or parts of the predicted M-phase inducer phosphatase domain (Figure III - 24).

3.1.4. MIDGET and COP1 share one complex *in vivo*

Co-IP experiments were performed in analogy to the PAP2-COP1 Co-IP (III. 2.1.3.). In contrast to YFP-PAP2, YFP-MID was easily detectable in cells of *A. thaliana* cell suspension culture (Figure III - 29). YFP-MID was immunoprecipitated from double transformed cells of *A. thaliana* cell suspension culture. An RFP-HA-COP1 was subsequently detected with an anti-HA antibody. Beside the bands corresponding to the tagged protein, the anti-GFP antibody also detected unspecific bands resulting from the use of Miltenyi anti-GFP beads antibody (~130, 50 and 20 kDa). These bands were already described in my diploma thesis. For the anti-HA antibody only the band corresponding to the small antibody chain was detected as an RFP-HA-unspecific band (~20 kDa.)

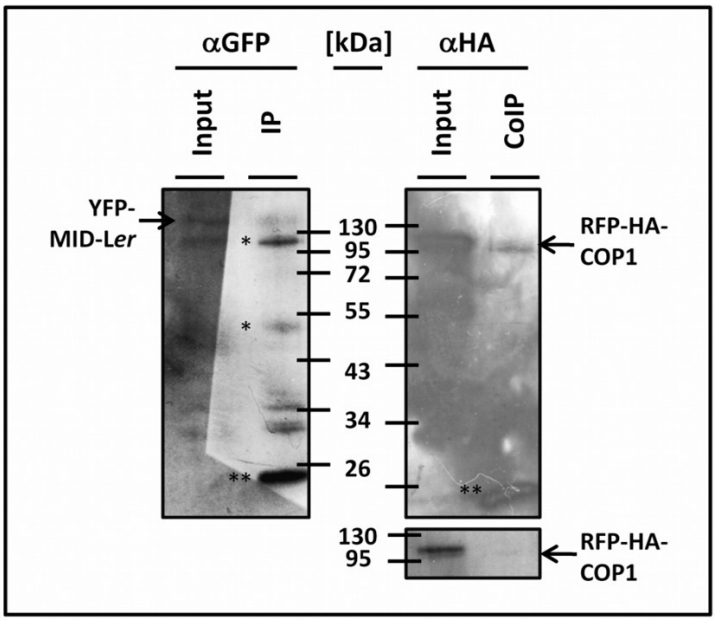

Figure III - 31: Co-IP of RFP-HA-COP1 and YFP-MID. Co-transformed *A. thaliana* cell suspension culture with YFP-MID-L*er* and RFP-HA-COP1 (big blot) or RFP-HA-COP1 alone (small blot) and the anti-silencing strain RK19 was homogenised five days after transformation. The IP of YFP-MID was performed using Miltenyi αGFP beads (Kirik, V. et al., 2007). Proteins were separated by SDS-PAGE, blotted and detected with the depicted antibodies. * unspecific Miltenyi bands already described in my diploma thesis. ** Miltenyi band, small antibody chain. YFP-MID-L*er*: pEarleyGate104-MID-L*er* (LBA4404. pBBR1MCS.virGN54D); RFP-HA-COP1: pNmR-COP1 (LBA4404pBBR1MCS-5.virGN54D); RK19 = anti silencing strain.

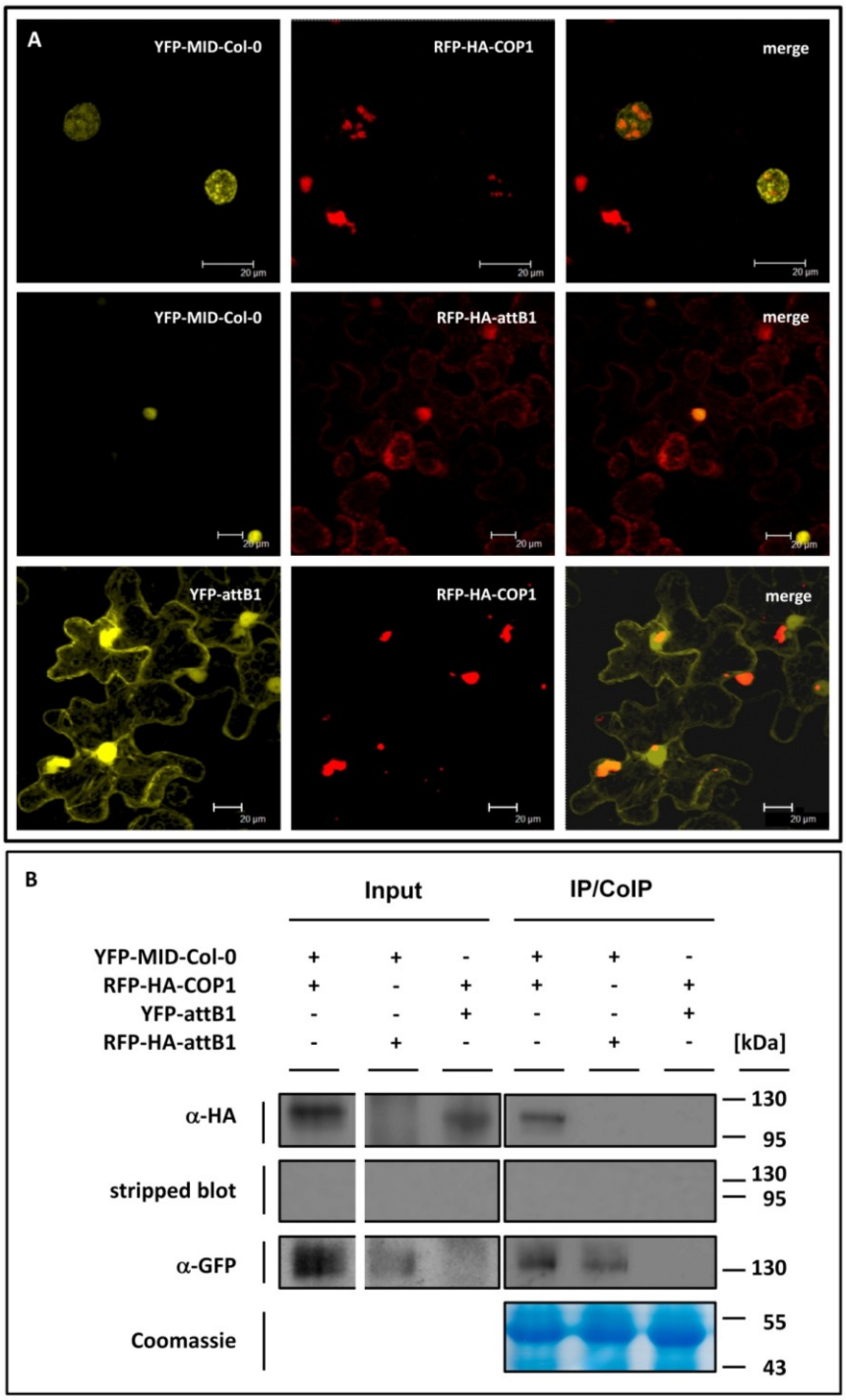

Figure III - 32: MID shares one complex with COP1.
(A) Analysis of infiltrated epidermal leaf cells of *N. benthamiana* with the depicted constructs and the anti-silencing strain RK19. Pictures in one row correspond to one co-infiltration event. The pictures show a typical leaf epidermal cell three dai. The fluorescing fusion proteins are visualised with CLSM in the different channels and a merged picture is shown at the right. Sequentially scanned z-stacks were merged with Leica Confocal software. Bar equals 20 µm.
(B) Co-IP. Infiltrated leaves from (A) were homogenised three dai. The IP of YFP-MID or YFP-attB1 was performed using Miltenyi αGFP beads (Kirik, V. et al., 2007). Total protein concentrations were equalised by Bradford analysis. The Coomassie gel of input fractions served as an additional loading control.
YFP-MID: pEarleyGate104-MID (LBA4404. pBBR1MCS.virGN54D); RFP-HA-COP1: pNmR-COP1 (LBA4404pBBR1MCS-5.virGN54D); RFP-HA-attB1: pBatTL-B-p35s-RFP-HA-attB1 (LBA4404pBBR1MCS-5.virGN54D); YFP-attB1: pBatTL-B-p35s-YFP-attB1 (LBA4404pBBR1MCS-5.virGN54D); RK19 = anti silencing strain.

As the concentrations of immunoprecipitated YFP-MID-L*er* remained low with this method, a Co-IP from infiltrated *N. benthamiana* leaves was conducted. The Co-IP of YFP-MID-Col-0 and RFP-HA-COP1 was successfully performed with all controls (IP: αGFP, Figure III – 32). This experiment has been repeated for all shown combinations. RFP-HA-COP1 did not co-immunoprecipitate with YFP-MID-Col-0 and no detectable RFP-HA-COP1 was co-immunoprecipitated with YFP-attB1. The used beads were saturated as equal amounts of protein were detected after IP. For the band of YFP-attB1 see the attachment A R-18 and A R-19 for the whole blot.

It can be concluded that YFP-MID and RFP-HA COP1 interact in the nucleus of *N. benthamiana* epidermal leaf cells in subnuclear foci and both protein can share one complex *in planta*. Furthermore, a possibly modificated form of RFP-HA-COP1 (second band) is visible on the blots which means that, if this is a modification of COP1 and not of the RFP-HA-tag, that the unmodified and modified form are in one complex with YFP-MID. It has to be pointed out that the result might not reflect the *in vivo* situation as proteins from all organelles and from all cells are present in the input fraction for the Co-IP.

3.1.5. First experiments *in planta* verify the MIDGET - SPA1 interaction

SPA1 was found as a putative interactor in YTH screenings with MIDGET as a bait (Joachim F. Uhrig, unpublished data). The *spa1*-mutant was identified as a suppressor of *phyA-105* (Hoecker et al., 1998) and shown to interact with COP1 (Hoecker and Quail, 2001).

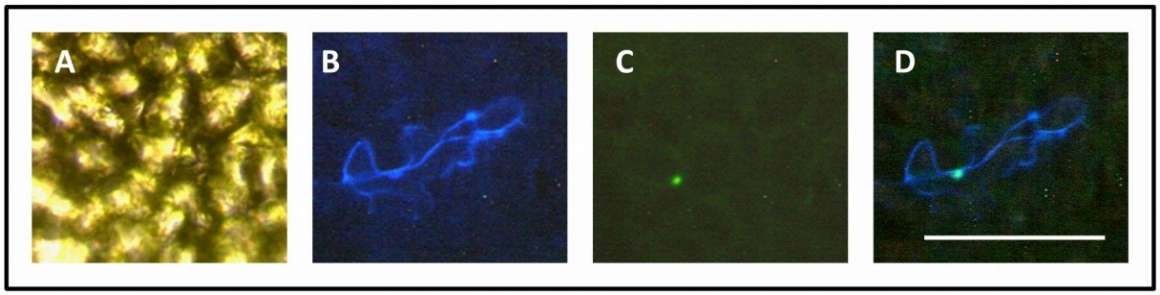

Figure III - 33: BiFC assay for SPA1 with MID-L*er*. Plasmids encoding BiFC fusion constructs, pCL113-SPA1 and pCL112-MID-L*er* with the N- or C-terminal part of YFP were co-bombarded into leaf epidermal cells of *A. thaliana* seedlings that have developed their third and fourth true leaf. CFP-TALIN served as a transformation control (B). (A) bright-field image; (B) CFP filter; (D) YFP-selective filter; (D) merged picture of (B) and (C). YFP fluorescence (C) indicates interaction with SPA1 in the BiFC assay in an leaf epidermal cell. All pictures have the same magnification and were taken with a fluorescence microscope. Only few cells were hit in this experiment. Bar equals 100 µm.

The interaction of MID-L*er* and SPA1 - was verified by a BiFC assay in epidermal cells of *A. thaliana* and *Allium porrum* using biolistic transformation (Figure III - 33, Figure III - 34). The interacting

proteins localised to the whole nucleus. For both experiments the cytoskeleton marker CFP-TALIN was used as a transformation control. In the case of *A. thaliana*, plants grown on MS plates showing their third and fourth true leave were biolistically transformed. The number of analysed transformed cells was very low; therefore, an additional BiFC assay in *Allium porrum* was conducted.

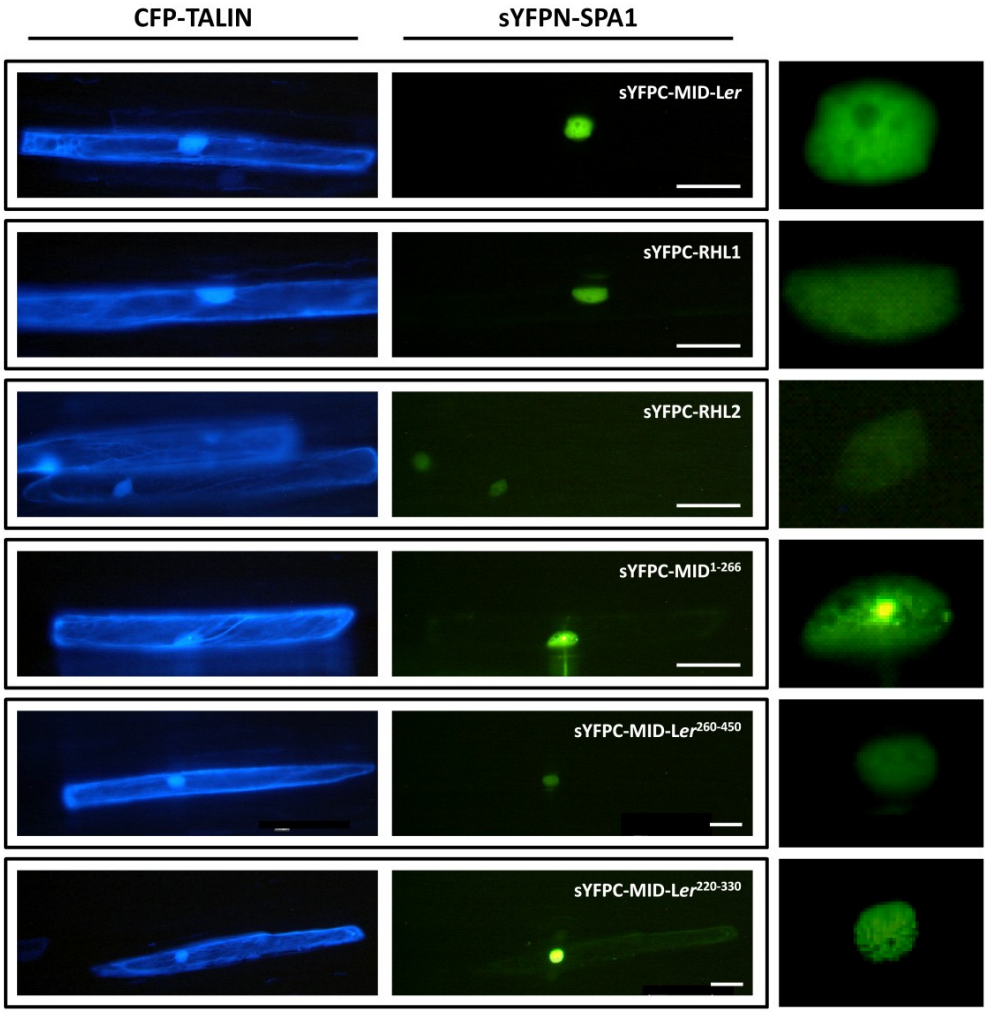

Figure III - 34: BiFC assay for SPA1 with MID, TOPOVI components and fragments of MID. Plasmids encoding BiFC fusion constructs of SPA1 and the depicted interaction partner with the N- or C-terminal part of YFP were co-bombarded into leek cells (*Allium porrum*). CFP-TALIN served as a transformation control (in the left column). YFP fluorescence in the middle column indicates interaction with SPA1 in the BiFC assay. Pictures in the right column are close-ups of the nuclei from the middle column. All pictures were taken with a fluorescence microscope and the DISCUS software using an integration of 1, except for the picture with sYFPC-RHL1 (integration of 2). Bar equals 50 µm. BiFC-constructs and transgenic *A. tumefaciens* strains: pCL112-SPA1, pCL113-MID-L*er*, pCL113-RHL1, pCL113-RHL2, pCL113-MID$^{1-266}$, pCL113-MID-L*er*$^{260-450}$, pCL113-MID$^{220-330}$.

Additionally, the interaction of the three MID-L*er* fragments with SPA1 was tested. Fluorescence in the nucleus was detected for all three fragments but was comparably weak throughout the whole nucleus for the C-terminal fragment. The strongest and most distinct signal was observed for

MID$^{220-330}$ and SPA1 in subnuclear foci a characteristical localisation of SPA1 (Zhu et al., 2008). Interestingly, the fluorescence for the BiFC assay of MID$^{1-266}$ and SPA1 was visible in subnuclear foci often concentrating at the envelope, leaving several black holes and one or more bright fluorescing dots are present in the centre of the nucleus. For the described BiFC experiments fluorescence microscopy was used. In further experiments CLSM should be applied to improve the resolution of such three dimensional distributions of interacting proteins. The direct repeats of MID, present in MID$^{1-266}$ and MID$^{220-330}$ (one repeat) should be subjected to interaction studies with COP1 and SPA1.

Beside MID, RHL2 and RHL1 showed to interact with SPA1 in lots of subnuclear foci in the BiFC assay whereas the signal for AtTOP6B and SPA1 was too weak and not reliable (23 of 68 cells showed a weak signal to conclude interaction.

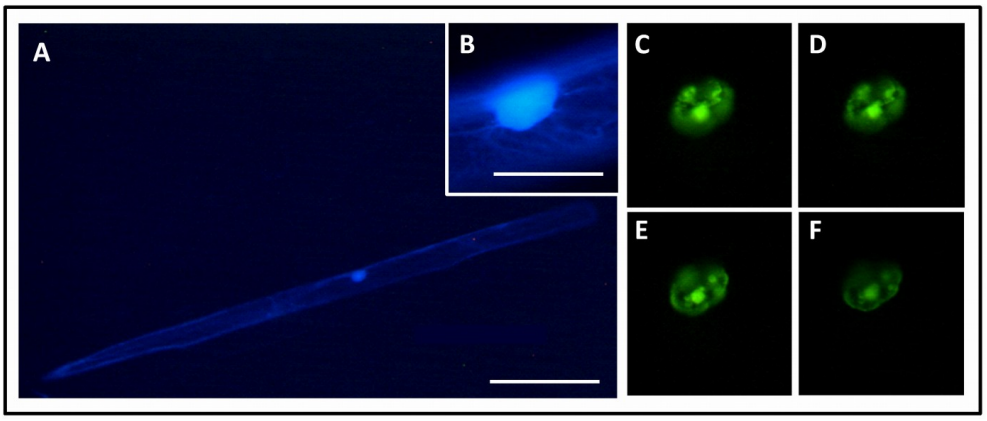

Figure III - 35: BiFC assay for SPA1 with MIAP2. Plasmids encoding BiFC fusion constructs, pCL112-SPA1 and pCL113-MIAP2 with the N- or C-terminal part of YFP were co-bombarded into leek cells (*Allium porrum*). CFP-TALIN served as a transformation control (A, B). YFP fluorescence (C-F) indicates interaction with SPA1 in the BiFC assay. (B-F) have the same magnification and are close-ups of (A). Pictures in (C-F) were made in different focused layers of the nucleus, beginning from the top. All pictures were taken with a fluorescence microscope. Note the subnuclear localisation characteristical for MIAP2. Bar equals 200 µm in (A) and 50 µm for (B-F).

MIAP2 was identified in an YTH screening with DET1 as a putative interactor. SPA1 shares a complex with DET1 (Nixdorf and Hoecker, 2010). A BiFC experiment for MIAP2 and SPA1 showed a MIAP2-specific subnuclear localisation that was also observed in my diploma thesis and is shown in Figure III - 35. The YFP fluorescence resulting from the interaction of MIAP2 and SPA1 also localises to the nuclear envelop.

3.2. First results suggest that MIDGET is not a target of COP1

3.2.1. Identification of a COP1 domain sufficient for the interaction with MID and AtTOP6B

Targets of COP1 typically bind to the WD40 domain of COP1 (HY5, STO, STH) (Holm et al., 2001). As the interaction of COP1 and MID was not as easily detectable in yeast as e.g. the interaction of MID with RHL1 or COP1 with COP1, it was suggested that the interaction is weak, MID is toxic for yeast, MID needs to be modified or MID is not properly folded in yeast for specific interactions. GARFILD (III. 2.3.) provides a possibility to identify the smallest fragment present in the used COP1 libraries that allows an interaction in the yeast nucleus. It was reported previously that truncations of COP1 completely lacking the WD40 domain could rescue more aspects of the COP1 function than those in which parts of the WD40 domain were present (McNellis et al., 1996; McNellis et al., 1994b). This underlines an advantage of GARFILD: minimal fragments that are capable to fold as it is needed for the interaction can be found with GARFILD, although the precisely determined domains might not show an interaction in an YTH assay with the tested bait.

In order to identify the interaction domain of COP1 for the MID-COP1 interaction, the N-terminal COP1 GARFILD libraries (III. 2.3.) were screened against MID as a bait. An OD_{600} of 0.01 was used for bait and library. The titres were $8.6*10^5$ and $7.06*10^5$ yeast colonies that originated from a successful mating event. Only the first two cysteines of the COP1 RING finger motif (CPIC) are included in the shortest identified COP1 fragment, $COP1^{1-67}$ (Table III - 10, Figures III - 36).

Table III - 10: Overview of the sequencing results after a GARFILD with COP1 libraries and MID as a bait.
GFP served as a negative control. Only the size of the fragment that corresponds to base pairs that matches 100% to the COP1 amino acids are given. Number 1-2 of the libraries: compare to Figure III - 17. yellow: minimal COP1-specific fragment, COP1N1-274 exhibited a frame shift close to the start codon. The sequence for COP1N1-202 did not cover the start codon (see attachment A R-12 for details). Artificial sequence: several *att*B1 sites were detected in the sequence, probably due to primer oligomerisation. Fragments encoding the artificial sequence were very short and not distinguishable from the size of a theoretically empty plasmid on an Et-Br gel (that as not observed).

bait	fragment [bp] corresponding to the CDS	frequency	library	
			N-termini	
			1	2
COP1 - GARFILD				
MID	1-202	2	2	0
MID	1-274	2	2	0
MID	artificial sequence (multiple *att*B1)	12	3	9

Another interactor of MIDGET, the E3-ubiquitin ligase DRIP2 (At2g30580, named MIAP1 in my diploma thesis) also exhibits a RING finger domain (my diploma thesis and Qin et al., 2008). Still it is possible that MIDGET also interacts with the complete RING finger domain. Due to the lack of a COP1

C-terminal GARFILD library at this time point of the project, with this method, it cannot be ruled out that MID also interacts with other parts of COP1.

In case of verification, this is the first time that this part of COP1 has been shown to be relevant for protein-protein interaction. *COP1*$^{1-201}$ was successfully amplified with specific Gateway® primers and recombined in frame into pDONR207 as was verified by sequencing. COP1$^{1-67}$ showed to be auto-activating when expressed as a GAL4-BD fusion protein (Figure III - 36). Only few colonies grew when the interaction of MID-Col-0 and COP1$^{1-67}$ was tested in an YTH experiment, similar to the results for full length COP1 with MID-L*er* (Figure III - 36). BiFC constructs have been prepared and will be tested in the future. The identified new interaction domain has to be verified *in planta* and subsequent interaction analysis of the known interaction domains of COP1, the identified random fragments and the use of corresponding deletion-constructs might shed a new light on the COP1 interaction domains. In contrast to MID, for AtTOP6B the interaction with COP1$^{1-67}$ in yeast could be concluded from the performed YTH experiments. A repetition to verify the RHL1-COP1$^{1-67}$ interaction is needed. (Figure III - 36)

A target of COP1 would be expected to interact with the RING or WD40 domain of COP1. Therefore, the identification of an interaction domain for MIDGET and probably TOPOVI components in the N-terminal region upstream of the RING finger and ending before the CLS is a strong hint for MIDGET being not or not only a target of COP1.

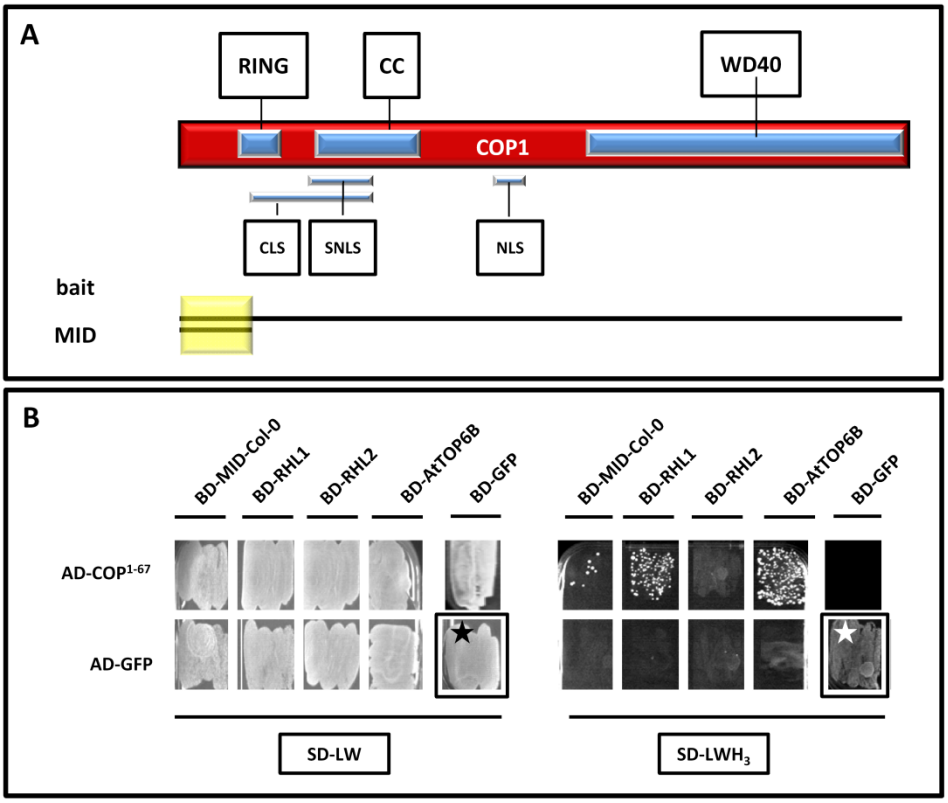

Figure III - 36: Schematic representation and verification of the GARFILD results.
(A) Schematic representation of the GARFILD results with COP1 libraries. Red: COP1 protein with known domains. Black: minimal interacting N- or C-terminal fragments, yellow (transparent): minimal fragment of COP1 that is sufficient for the interaction. For the C-terminal fragment the full length of the protein is given as no result from the GARFILD screenings available. The interaction is shown in this work. RING: REALLY INTERESTING NEW GENE, CC: coiled coil domain, WD40: WD40 domain, CLS: cytoplasmic localisation signal, SNLS: subnuclear localisation signal, NLS: nuclear localisation signal
(B) Verification and analysis of the interaction of the shortest GARFILD fragment with the depicted baits. *S. cerevisiae* AH109 was transformed with two constructs coding for the depicted fusion proteins. Chosen was the smallest fragment that was cloned with specific primers with a direct stop codon. Asterisk: Combination of BD-COP1$^{1-67}$ and GFP shows that BD-COP1$^{1-67}$ is auto-activating. After selection on SD-LW media, several yeast colonies were streaked out on SD-LWH media supplemented with 3 mM 3-AT. Combinations with GFP served as negative controls. BD: GAL4-binding domain, AD: GAL4-activation domain. pACT was used for COP1$^{1-67}$ and GFP, pAS2-1 was used for MID-Col-0, GFP and COP1 $^{1-67}$ and pcACT2 was used for RHL1, RHL2 and AtTOP6B.

3.2.2. MID-L*er* co-purifies with phyA and IWS2

MID is problematic in YTH experiments. This might be due to a modification of the protein that does not occur in yeast. In addition, it would be expected that MID is ubiquitylated if it was a target of COP1. To identify possible modifications of MID, overexpressed YFP-tagged MID was immunoprecipitated from a dark grown cell suspension line. The cell suspension culture line of a stable homozygous line of MID-L*er*-YFP (*mid-1*) (Kirik et al., 2007) was established and maintained with the help of Irene Klinkhammer. Cells of the cell suspension culture were tested for nuclear YFP fluorescence prior to harvesting. This is the expected localisation of MID-L*er*-YFP. In addition to this it was observed that the cells of the Pro35S:*MID-YFP* (*mid-1*) cell culture line were bigger than that of a

Col-0 line of the same age (figure III - 37). The dark grown cell suspension culture was collected by vacuum filtration, immediately frozen in liquid nitrogen and exposed to daylight during this short procedure allowing complexes to be present that are characteristic for dark grown plant cells and for an early light answer. After homogenisation using a french press an IP was performed with Miltenyi anti-GFP beads. Col-0 cell suspension culture was treated in the same way to serve as a negative control but total protein concentrations were lower than for the transgenic line according to Bradford analysis although same amounts of harvested cells were used (attachment A R-20). The size of *MID-YFP* cloned by V. Kirik is about 2100 bp. Western blot analysis with an anti-GFP antibody showed that the IP was successful. YFP-MID showed to migrate higher as theoretically determined as already was also observed in my diploma thesis. Also in other western blot analysis with anti-GFP antibody, the three unspecific Miltenyi bands were visible that were described in my diploma thesis (Figure III - 31). A band above and the band corresponding to the size of the YFP detected MID-YFP band from western blot analysis was cut from a Coomassie stained SDS-PAGE gel. Proteins that were present in these bands were analysed for possible modifications in the group of Jürgen Schmidt at the MPIZ, cologne, by Thomas Colby. Thomas Colby could not identify a SUMO-, Nedd- or ubiquitin-modification of MIDGET with mass spectrometric methods using trypsin digested proteins, so far. Mascot analysis of the resulting peptide mass fingerprints from both bands revealed that YFP and MID was manly present in the lower band. Traces of MID were also detected in the upper band as would be expected without applying 2D electrophoresis to two bands that are as close together as the selected ones in this work (personal information of Thomas Colby). Interestingly, the upper band contained CHR11 and phyA was present in the lower band. The MASCOT scores were 124 for CHR11 with a threshold of 34 to be rated as significant. For the lower band the MASCOT scores were 341 for phyA, 151 for MID and 95 for GFP with a threshold of 57 to be rated as significant. (MASCOT data obtained from Thomas Colby are shown in the attachment, A R-21)

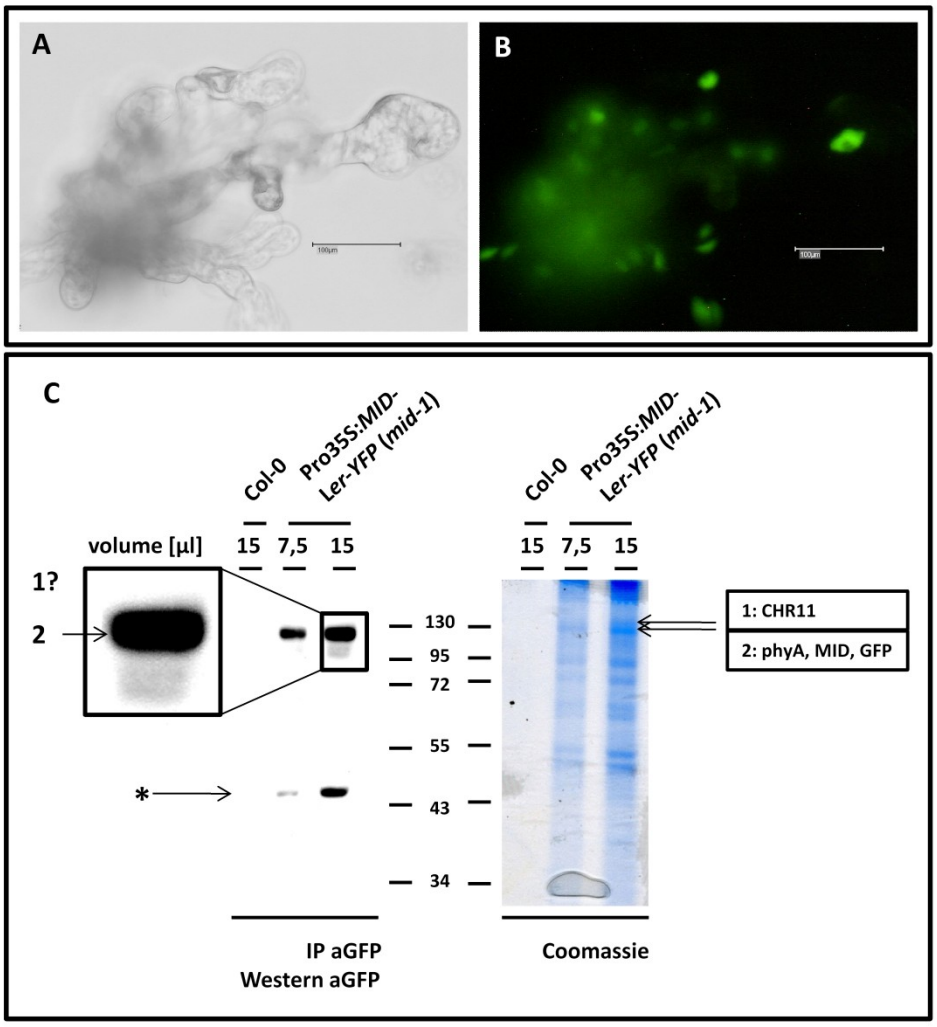

Figure III - 37: Co-purification of CHR11 and phyA with immunoprecipitated MID-YFP from Pro35S:MID-YFP (mid-1) cell suspension culture.
(A) Bright field image rendered to grey scale for better visualisation of Pro35S:MID-YFP (mid-1) cell suspension culture. **(B)** Fluorescence microscopy of MID-YFP expression in the same cells visualised in (A). Bars equal 100µm. (C) Pro35S:MID-YFP (mid-1) cell suspension culture was homogenised. The IP of YFP-MID was performed using Miltenyi αGFP beads (Kirik, V. et al., 2007). According to Bradford analysis 15 µl of the Col-0 sample corresponds to 7.5 µl of the Pro35S:*MID-YFP* (*mid-1*) sample. Proteins were separated by SDS-PAGE, blotted and detected with the depicted antibodies or the gel was stained with Coomassie. Band 2 was detectable in western blot analysis using an anti-GFP antibody suggesting that it corresponds to MID-YFP. Boxes to the right of the Coomassie stained gel show the proteins that were identified from the cut bands No 1 and 2 by Thomas Colby (MPIZ cologne, group Jürgen Schmidt). The MASCOT data for both bands can be found in the attachment, A R-21. * unspecific Miltenyi band.

It is important to note, that unspecific binding that was not observed for Col-0 cannot be ruled out for the identified and co-purified proteins due to the lower amount of used Col-0 total protein. The negative control needs to be optimised and the ability of the identified proteins to interact or to share a complex with MID needs to be verified in the future.

3.2.3. MID-L*er* stability is impaired in red and far red light

The probably shared complex with phyA and the interaction with SPA1 suggested that MID might be involved in red or far-red mediated light signalling. One question that arises is, if the MID protein`s stability is influenced by different light qualities.

To answer this question, a homozygous line with proven Pro35s-driven HA-MID expression in homozygous *mid-1* background was established. In the T1 generation, only plants looking like the wildtype were selected as a BASTA selection was not possible because the mutant was BASTA resistant and the construct also encoded the BASTA resistance gene. A phenotypical rescued line in the T_2 generation was selected. Finally the HA-expression was verified by Western blot analysis with homogenised leave material using cracking buffer. (Figure III - 38)

To test the stability of HA-MID under different light conditions, seeds of this line and of Col-0 were sterilised, spread on the two halves of five MS plates (1% sucrose), kept in the dark for 3 days at 4°C and exposed to white light for 4h to induce germination. After 4 more days in the dark at 21°C the seedlings were exposed for 4 h to blue, red, far-red, white light or darkness at 21°C. The same amount of plant material of pEarleygate201-MID-L*er* (*mid-1*) and Col-0 seedlings was harvested from all plates under green safety light, homogenised with glass beads and 2xLaemmli buffer and subjected to SDS-PAGE. Western blot analysis revealed that less protein was present in the seedlings exposed to red or far-red light (Figure III - 38). Detection with an anti-β-Tubulin antibody (Figure III - 38) proved that the same amounts of total protein were loaded except in the case of the white light treated pEarleygate201-MID-L*er* (*mid-1*) seedlings.

This experiment should be repeated several times and the loading of the samples should be varied to prevent an influence of different blotting behaviour or the experimental setup on the signal strength.

A change in protein concentration detected by Western blot analysis with this experimental setup can only be explained by regulation on the protein degradation or stabilisation level but not by a change in transcription levels because of the chosen time frame. Therefore, this experiment substantiates the suggestion that MIDGET might be involved in red / far-red light signalling. Possibly the stabilisation of the MIDGET protein is directly regulated by phyA. This result shows that MIDGET might be a target of COP1 under these specific light conditions. Therefore, genetical analysis under these light conditions will be needed in the future.

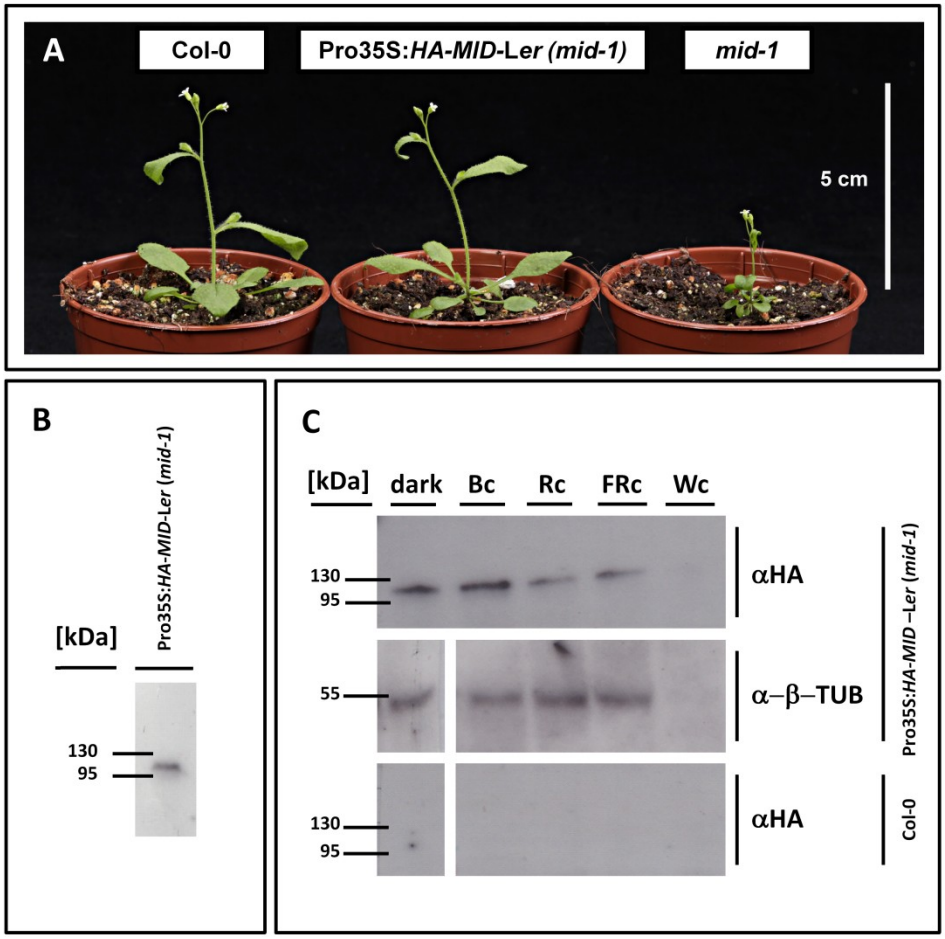

Figure III - 38: (A) Rescue of *mid-1* with Pro35S:*HA-MID.* **(B)** HA-MID is expressed in Pro35S:*HA-MID* (*mid-1*). The chosen line was homozygous for the mutant and for the construct. Leave material was homogenised in 2x laemmli buffer and subjected to SDS-PAGE (12.5%). Subsequently, western blot analysis with an anti-HA antibody detected HA-MID expressed in Pro35S:*HA-MID* (*mid-1*). **(C)** Western blot analysis of 4-day-old dark-grown Pro35S:*HA-MID* (*mid-1*) and Col-0 seedlings that were transferred to the indicated light conditions for four hours. Proteins were separated by SDS-PAGE, blotted and detected with the depicted antibodies. Temperature: 21°C; Bc: 5 µmol*m^{-2}*s^{-1}; Rc: 30 µmol*m^{-2}*s^{-1}; FRc 1 µmol*m^{-2}*s^{-1} Samples for other experiments were tested on the same blot to the right of the white light sample that showed distinct bands at the same position on the blot, indicating that no blotting problem occurred.

3.2.4. YFP-MID-L*er* cannot rescue the *cop1-4*-mutant phenotype

In order to test if MID is downstream of COP1, YFP-MID-L*er* was overexpressed using pEarleyGate104-MID-L*er* in *cop1-4, mid-1* and Col-0 (Figure III - 39). So far, plants in the T_1 generation have been selected with BASTA and were analysed under LD conditions. Under these conditions no significant influence on Col-0 and *cop1-4* plants was observed. *Mid-1* was rescued by the used construct indicating the functionality of the overexpressed fusion protein. The expression of the protein was tested using a Leica MZ10F fluorescence binocular. Comparison of the YFP intensity of a typical T_1-plant for each transformation did not show significant differences between the different backgrounds under LD-conditions (Figure III - 39). *Spa1-100* was also included in this first analysis. At

least ten T_1 plants have been analysed for their phenotype and for the YFP-signal. One can conclude that under LD conditions MID is no or not only a target of COP1. Analysis of these plants in the dark and after exposure to different light qualities should be performed in the next generation.

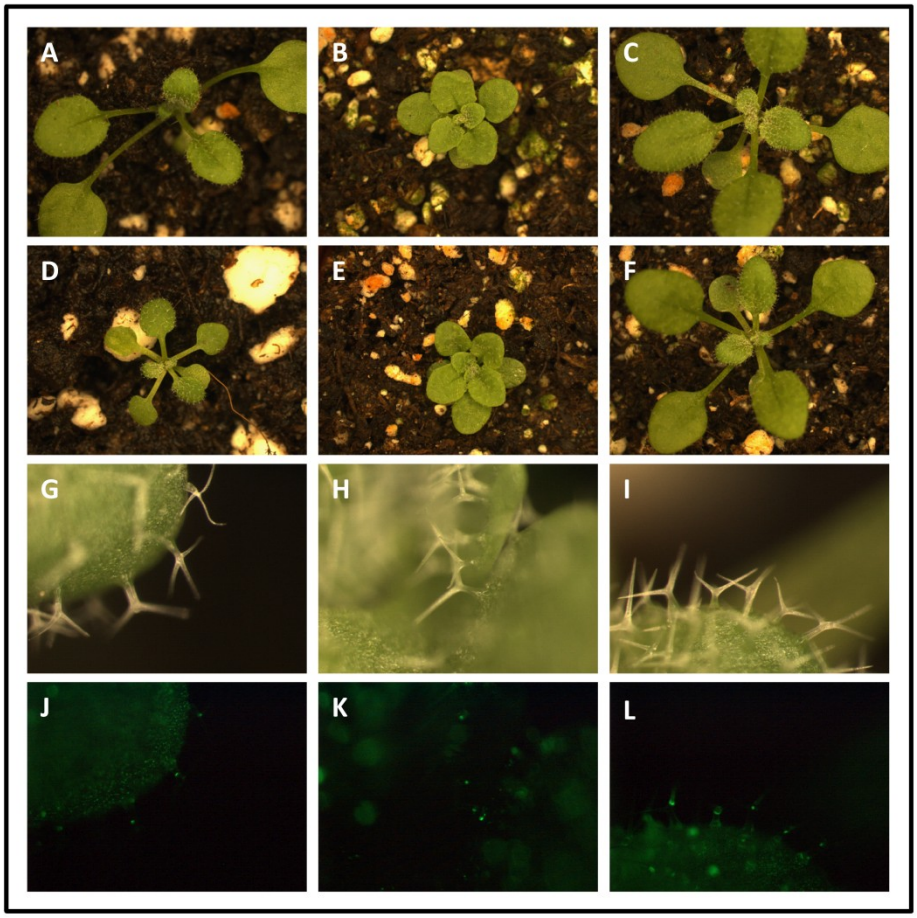

Figure III - 39: YFP-MID-L*er* cannot rescue the *cop1-4*-mutant phenotype.
In the first row **(A-C)** the untransformed background is shown. (A) Col-0, (B) *cop1-4*; (C) *spa1-100*. **(D-L)** BASTA-selected plants over-expressing YFP-MID-L*er*. Second row: rosette of the transgenic plants; third row: trichomes of the transgenic plants and last row: fluorescence image of the trichomes of the fifth or sixth true leave in the row above. Pictures in one row have the same magnification; pictures in one column starting in the second row correspond to the same 20-day-old T1 plant. First column: Pro35S:*MID*-L*er*-*YFP* (Col-0), second column: T1 plant Pro35S:*MID*-L*er*-*YFP* (*cop1-4*), third column: T1 plant Pro35S:*MID*-L*er*-*YFP* (*spa1-100*). Note that all plants were BASTA selected but not the wild type and *cop1-4*. YFP fluorescence is located in the nuclei. All pictures were acquired with a Leica MZ10F fluorescence binocular and the Leica Application Suit V3 Version 3.5.0.

3.3. *MID*- and *TOPOVI* mutants exhibit *COP1*-mutant phenotypes

After the verification of the COP1-MID-interaction the question rose if this interaction is of functional relevance. Therefore, the mutant phenotypes were analysed focusing on aspects of photomorphogenesis and the bolting behaviour. Not only *mid*-mutants were analysed but also *topoVI*-mutants. *TopoVI* mutants were included in the analysis to find out if the observed mutant

phenotypes are MID-specific or related to the TOPOVI function. Additionally, further hints can be obtained if MIDGET is another target of COP1 or a regulator of COP1.

As *mid-2* (Col-0), *rhl2* (Col-0) and *hyp6* (Col-0) are very small plants they produce only small amounts of seeds per plant. Additionally less seeds of these mutants germinate in comparison to the wild type (Figure III - 55). This is the reason why *hyp6* had to be excluded for most experiments.

In this chapter results of the following experiments are presented: comparison of the phenotypes of the *mid-* and *topoVI* mutants with *cop1-4* in the dark (III-3.1.1.) and in the light (III-3.3.2), determination of anthocyanin levels in *mid-2* and *rhl2* (III-3.3.3.), comparison of *CHS* transcription levels of *mid-2* and *rhl2* with *cop1-4* (III-3.3.4.), analysis of the bolting behaviour of *MID-* and *TOPOVI* mutants under LD and SD conditions and the observation that the time of bolting is temperature dependent (III-3.3.5).

3.3.1. Phenotype of *MID* and *TOPOVI* mutant seedlings in the dark

Mid and *topoVI* mutants show morphological aspects of photomorphogenesis when grow in the dark. The hypocotyl of the seedlings is much shorter than in the wild-type and slightly longer than in *cop1-4* (see also Figure III - 53). The cotyledons are open and no apical hook is visible for 7-day-old seedlings. (Figure III - 40)

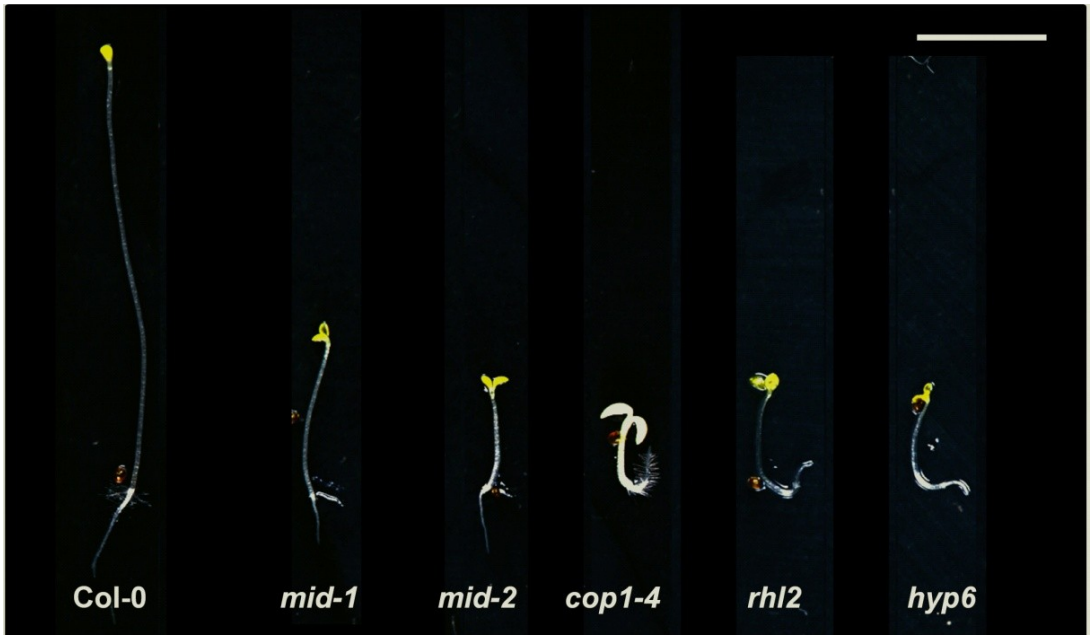

Figure III - 40: Morphogenetic comparison of 7-day-old dark-grown *mid-2* and *topoVI* mutant seedlings with Col-0 and *cop1-4*. Seeds were stratified for 2 days at 4°C prior to 4h of white light for germination induction and seven days of incubation in the dark at 21°C on MS plates lacking sucrose. The pictures were taken with a Canon EOS 5D Mark II by Siegfried Werth. Bar equals 5 mm.

It was decided to analyse 7-day-old seedlings as *mid* and *topoVI* mutants might develop slower than e.g. *cop1-4* or Col-0 in the dark (Figure III - 41). In Figure III - 41 three- and 7-day-old seedlings of *mid-2*, *rhl2*, *cop1-4*, another *cop1* mutant - *cop1*^{eid6} - and the *spa1* mutant *spa1-100* are compared. Three days after light induction Col-0, *cop1*^{eid6} and *spa1-100* showed an apical hook. To a lower extend, this was also visible for *rhl2* and *mid-2* seedlings. After three days, *cop1-4* mutants exhibited open cotyledons. After seven days of darkness, the *cop1*^{eid6} seedlings had open cotyledons while the *spa1-100* mutant still looked like the wild-type with a shorter hypocotyl. A short hypocotyl was also observed for *mid-2* and *rhl2*. These mutants have opened their cotyledons after seven days in the dark. In the case of *cop1-4* the cotyledons` lamina angle was larger than 180°C for 7-day-old seedlings in comparison to 3-day-old seedlings (Figure III - 41, see Figure III - 53 for a definition of the lamina angel). Between day three and seven, the hypocotyl of Col-0 and *spa1-100* elongates more than for the other mutants, indicating that the hypocotyls of *cop1-4*, *mid-2* and *rhl2* can be analysed and compared after three or seven days. Probably *mid-2* and *rhl2* are delayed in several aspects of seedling development (e.g. opening of cotyledons). A statistical analysis of the described phenotypes after three, four, five, six, seven and eight days should be conducted in the future.

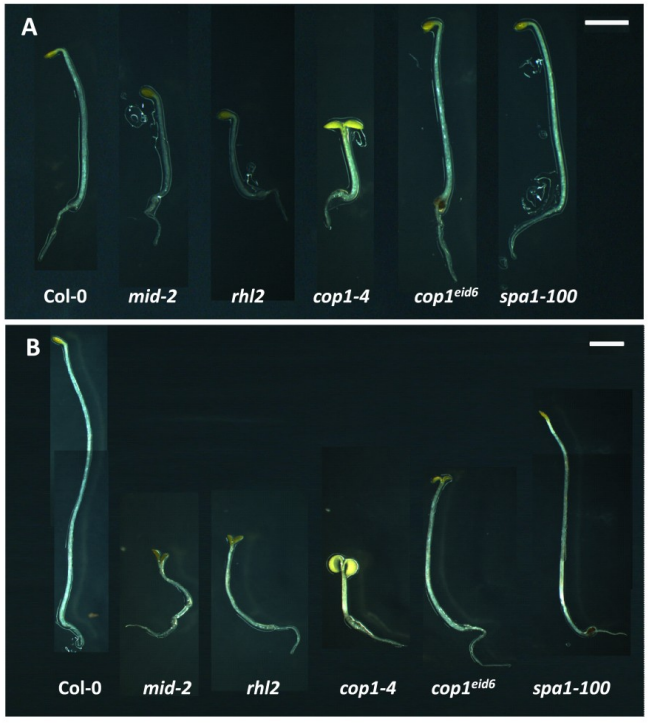

Figure III -41: Morphogenetic comparison of 3- **(A)** and 7- **(B)** day-old dark-grown *mid-2* and *rhl2* seedlings with Col-0, *cop1-4, cop1*^{eid6} and *spa1-100*. Seeds were stratified for 2 days at 4°C prior to 4h of white light for induction of germination and seven days of incubation in the dark at 21°C on MS plates lacking sucrose. The pictures were captured with a Leica MZFLIII. Bars equal 2 mm.

The seed coat mucilage of *mid* mutants exhibits a defect as was shown in Kirik et al. (2007). Seeds of these mutants lack a columella. Not only *mid-1* and *mid-2* but also *rhl2* and *hyp6* seeds are darker in colour than the wildtype (for *mid-1* see Figure III - 55) and the sterilisation solution colours yellowish. These phenotypes were not observed for cop1-4 seeds leading to the question if early seedling development of these mutants is comparable under stress conditions. Photomorphogenesis of dark grown seedlings is analysed using MS plates lacking sucrose to avoid the observation of an additional effect of sugar and not of photomorphogenesis alone. In the case of the *mid* and *topoVI* mutants, one might also analyse a germination defect or a developmental delay on these plates. Therefore, it was decided to compare the phenotype of dark grown seedlings also on MS plates supplemented with 1% sucrose (Figure III - 42). 7-day-old dark-grown seedlings showed the same hypocotyl phenotype under these conditions in comparison to MS plates lacking sucrose. For the cotyledon phenotype a clear difference was observed. Cotyledons opened wider and the first true leaves were already visible on MS plates supplemented with 1% sucrose.

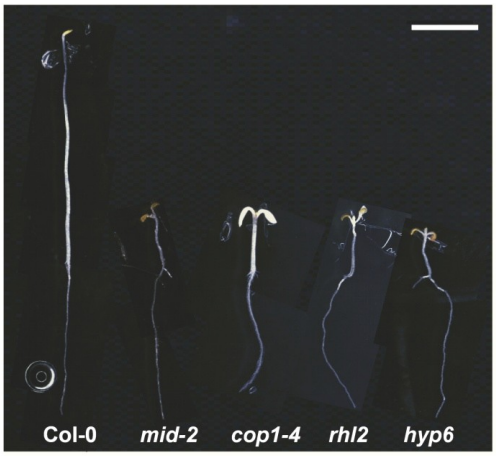

Figure III - 42: Morphogenetic comparison of 7-day-old dark-grown *topoVI*-mutant seedlings with Col-0 and *cop1-4*. Seeds were stratified for 2 days at 4°C prior to 4h of white light for induction of germination and seven days of incubation in the dark at 21°C on MS plates supplemented with 1% sucrose. The pictures were taken with a Leica MZFLIII binocular. Bar equals 5 mm.

3.3.2. Phenotype of *MID* and *TOPOVI* mutant seedlings in the light

Only slight differences to the wildtype are observed for 7-day-old *cop1-4* seedlings grown under constant light conditions (e.g. Figure III - 43) In contrast, adult *cop1-4* plants grown under LD or SD conditions varies strongly from the wildtype (e.g. Figure III - 45, Figure III - 51). Therefore, the morphology of *mid* and *topoVI* mutants was also tested under constant light, LD and SD conditions, the latter in regard to bolting.

Figure III - 43 gives an impression of the different germination and growth behaviour under constant light conditions (40 µmol*m^{-2}*s^{-1}). Seedlings of *mid-1*, *mid-2*, *rhl2* and *hyp6*, respectively, exhibited a smaller overall plant size, shorter root and a reduced germination efficiency than the wildtype and *cop1-4* with *hyp6* showing the most severe phenotypes (Figure III - 43, Figure III - 55). Values for the lamina angle are higher than 180°C, as can be seen in Figure III - 43 and Figure III - 44, whereas it is close to 180°C for *cop1-4* and Col-0 (for a definition of the lamina angle see Figure III - 53). In Figure III - 44 the root hairs of *cop1-4* can be seen. *Mid* and *topoVI* mutants have shorter and less root hairs than the wildtype (Kirik et al., 2007; Sugimoto-Shirasu et al., 2002). In Figure III - 43 - B it is obvious that the shown *mid-1* seedlings did not germinate simultaneously. These observations were made especially for seedlings that grew on MS media without sucrose. For further experiments a milder sterilisation procedure was applied (described in III.3.3.3) and the period of stratification was elongated from two to three days. As a consequence of the above mentioned observed differences, 7-day-old seedlings were used for morphological comparisons under constant light conditions.

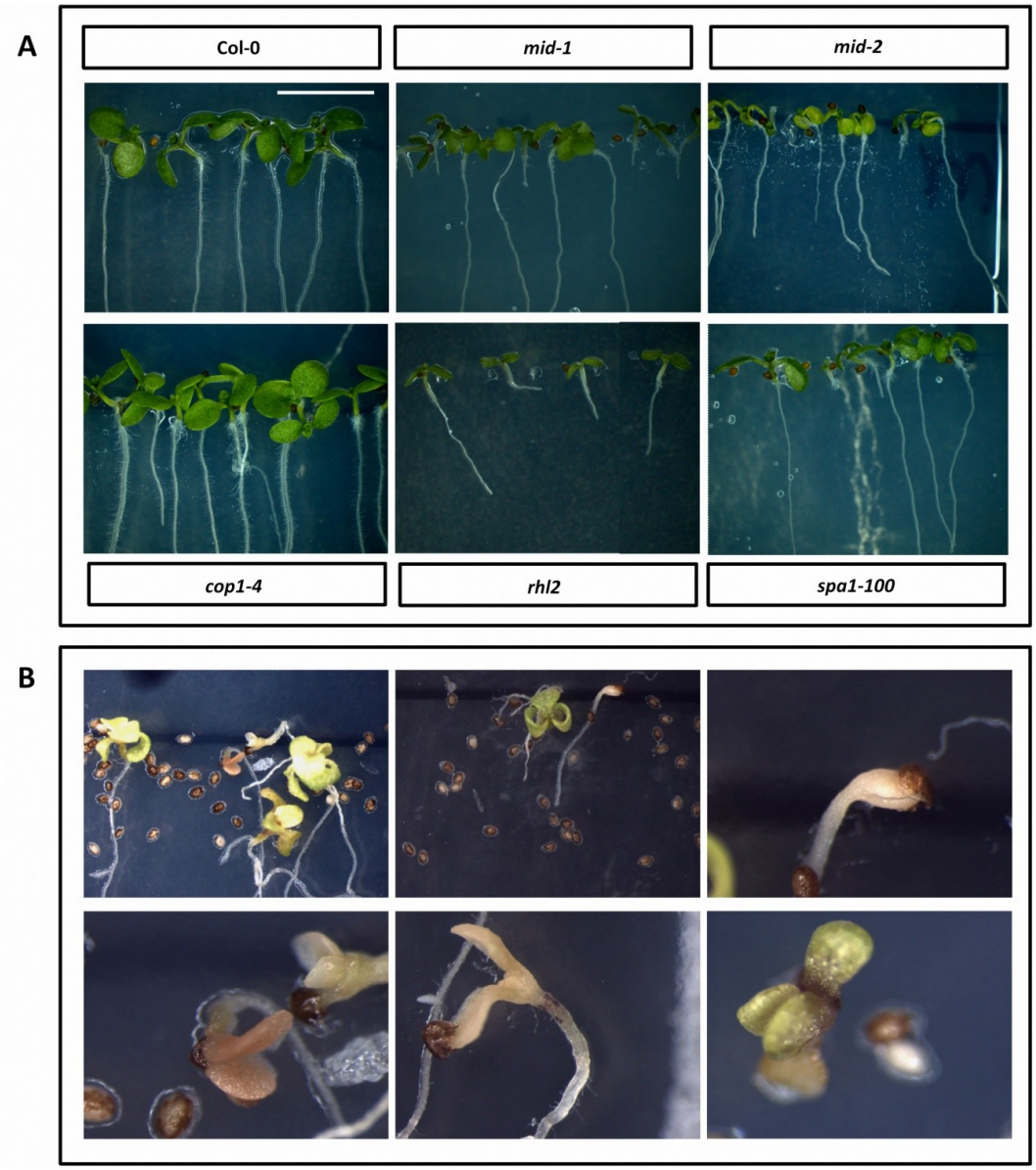

Figure III - 43: Germination defect and possible developmental delay of MID- and TOPOVI mutants.
(A) Col-0, *mid-1*, *mid-2*, *rhl2*, *hyp6* and *cop1-4* seeds were placed on MS plates without sucrose and the plates were kept for 7 days in constant white light (40 µmol*m^{-2}*s^{-1}) at 21 °C after two days of stratification at 4°C. Note the different length of the roots observable for all mutants. The pictures were taken with a Panasonic DMC-FZ50. Bar equals 5 mm. **(B)** 11-day-old *mid-1* mutants that were shifted after 4 days of darkness to LD conditions for 7 more days. Upper row: 0.8-fold magnification, lower row: 3.2-fold magnification. The pictures were taken with a Leica MZFLIII binocular.

To follow one criteria for the selection of representative single plants shown in Figure III - 44, *MID*- and *TOPOVI* mutant seedlings with the longest hypocotyl, biggest leaves and longest roots were chosen. In addition, 3-day-old seedlings are presented on the most stringent plates - MS without sucrose (Figure III - 44 -a, C). This criterion was an exception for this work, applied due to the observations of the germination differences described above. The observed phenotype of the *mid* and *topoVI* mutants resembled an enhanced photomorphogenesis phenotype. Roots of *rhl2* and

hyp6 were even shorter than those of *mid-1* and *mid-2* under all tested conditions whereas the lamina angle (compare Figure III - 53) seems to be larger for mid-1 and mid-2. These observations should be supported by statistical analysis in the future.

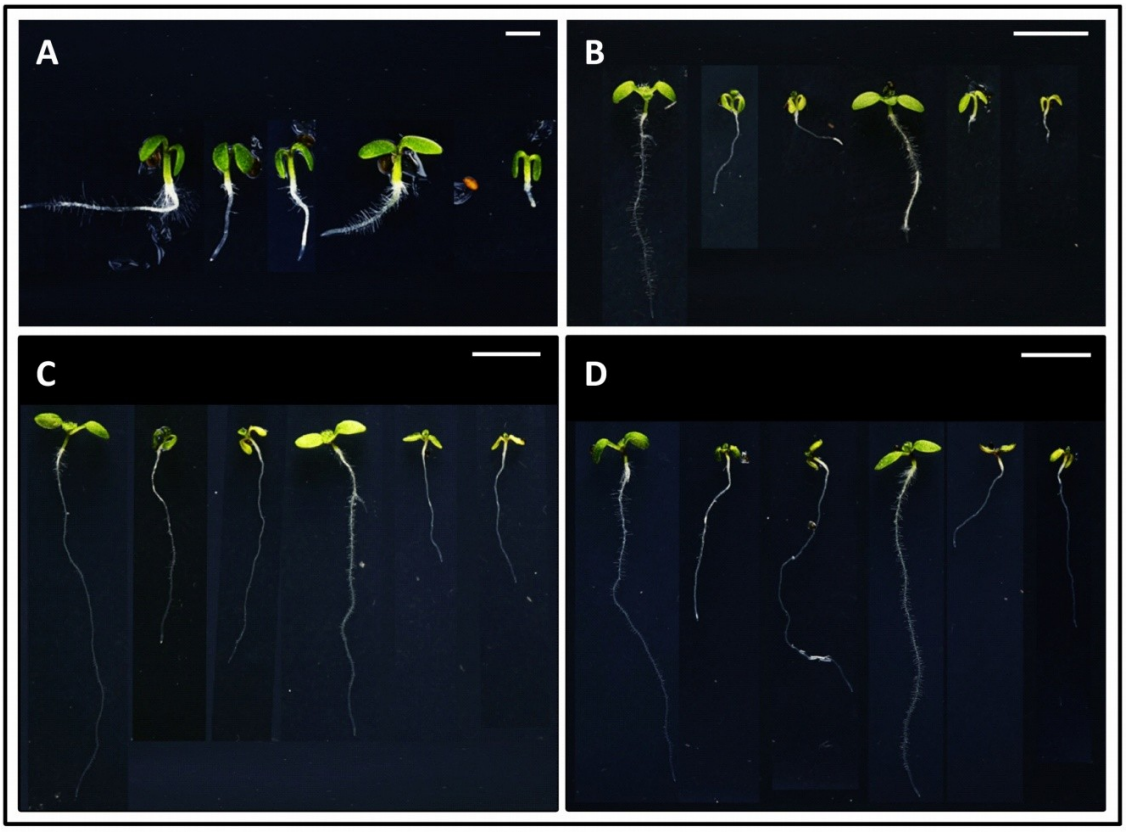

Figure III - 44: Morphogenetic comparison of 3- **(A)** and 7- **(B-D)** day-old light-grown seedlings grown on MS plates lacking sucrose **(A,B)** or supplemented with 1% sucrose **(C)** or 3% sucrose **(D)**. Seeds were stratified for 2 days at 4°C prior to 4h of white light for germination induction and three or seven days of incubation in constant light (40 µmol*m^{-2}*s^{-1}) at 21°C From the left to the right: Col-0, *mid-1*, *mid-2*, *cop1-4*, *rhl2*, *hyp6*. Note that no plant germinated for the experiment in (A) Only the best developed plants out of four plants were compared in this picture as a germination defect was observed for the *mid* and *topoVI* mutants. All genotypes for each condition were grown on one MS-plate. Pictures were taken with a Canon EOS 5D Mark II by Siegfried Werth. Bar equals 1 mm in (A) and 5 mm in (B-D).

12-day-old *mid-1* and *mid-2* plants grown under LD conditions on soil also showed a difference in hypocotyl length in comparison to the wildtype (Figure III - 45) as was already statistically analysed for 23-day-old *mid-1* plants in my diploma thesis. The rosettes and trichomes of older plants that grew under the same conditions are shown in Figure III - 45. The rosettes of different mutants were compared for 27-day-old plants, just before *hyp6* bolted and shortly after bolting of *mid-2*. At this age the rosettes of *mid-2*, *rhl2* and *hyp6* did not reach half the diameter of those of *cop1-4* or *cop1*^{eid6} for which the same holds true in comparison with Col-0 and *spa1-100*. Trichome branching and trichome size of *cop1-4*, cop1^{eid6} and *spa1-100* resembled the Col-0 phenotype. It has to be pointed out that the branching and number of trichomes per leaf has not been statistically analysed, yet. *Mid*

and *topoVI* mutants have underbranched and smaller trichomes than the wildtype as was shown before (Kirik et al., 2007; Sugimoto-Shirasu et al., 2002).

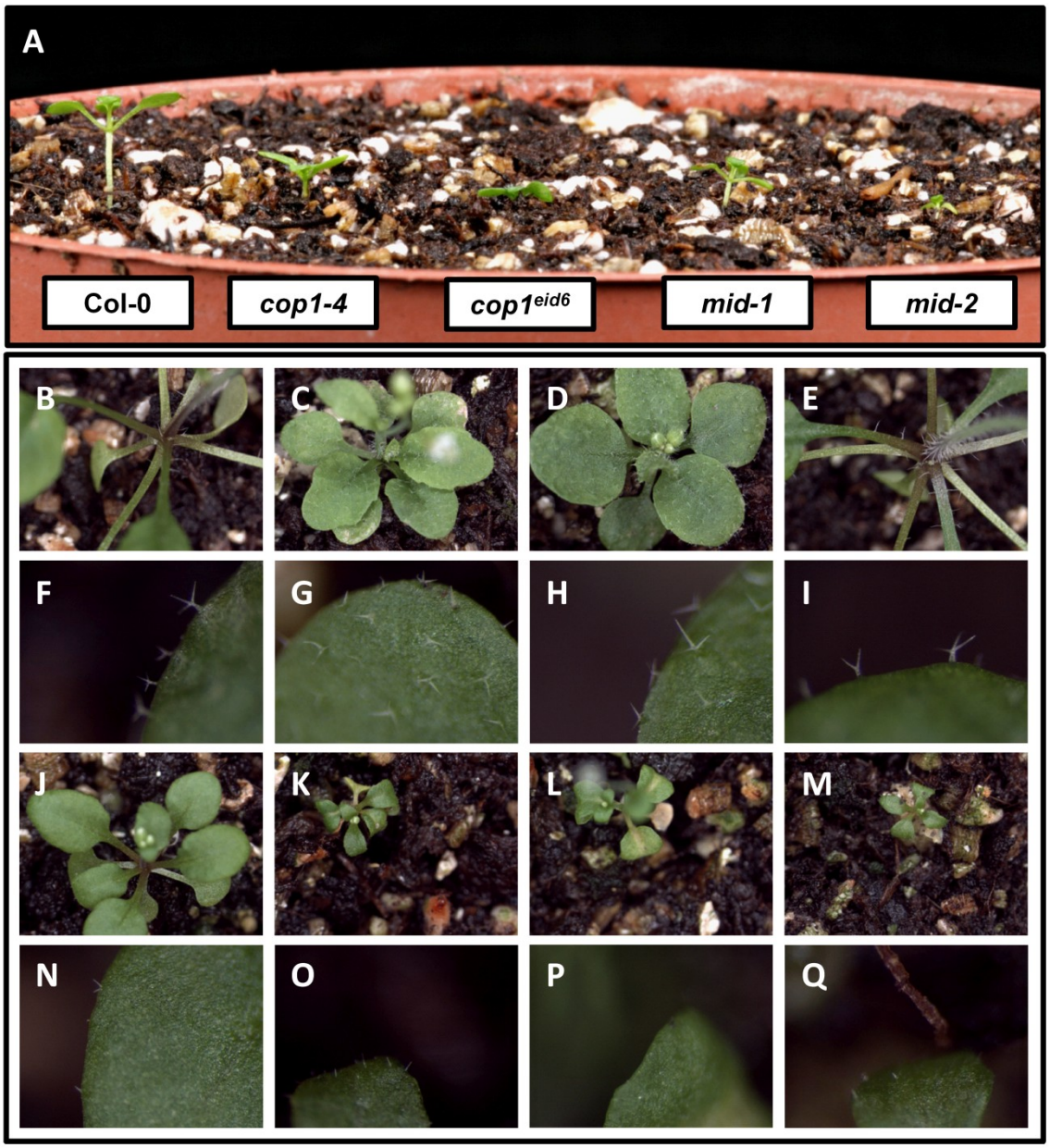

Figure III - 45: Morphogenetic comparison of 12-day-old *mid* and *cop1* mutant seedlings with Col-0 and rosettes and trichomes of 27-day-old plants.
(A) Morphogenetic comparison of 12-day-old *mid* and *cop1* mutant seedlings with Col-0. Seeds were stratified for 3 days at 4°C and kept on soil at 21°C at LD conditions in the greenhouse. The picture was taken with a Canon EOS 5D Mark II by Siegfried Werth. **(B-P)** Comparison of rosettes and trichomes of adult plants. **(B-E, J-M)** pictures of rosettes of 27-day-old plants taken with a 0.8 fold magnification. **(F-I, N-Q)** are pictures of trichomes of the third or fourth true leaf from the plant shown above taken with a 5-fold magnification. (B, F) Col-0, (C, G) *cop1-4*, (D, H) *cop1*^{eid6}, (E, I) *spa1-100*, (J, N) *mid-1,* (K, O) *mid-2*, (L, P) *rhl2*, (M, Q) *hyp6*. Pictures were taken just before *hyp6* bolted and shortly after bolting of *mid-2* with a Leica MZFLIII binocular.

Figure III - 46 shows the dwarf phenotype of an adult *mid-2* plant (52-day-old) compared to a wildtype plant of the same age. Yin et al. (2002) observed a reduced senescence phenotype or *bin3*

and *bin5* but did not specify it. For *hyp6* in this work, the most sever senescence phenotype was observed. Even after four month, when the wildype was already harvested, *hyp6* plants still produced new flowers (Figure III - 46 shows a picture of a more than 3-month-old plant).

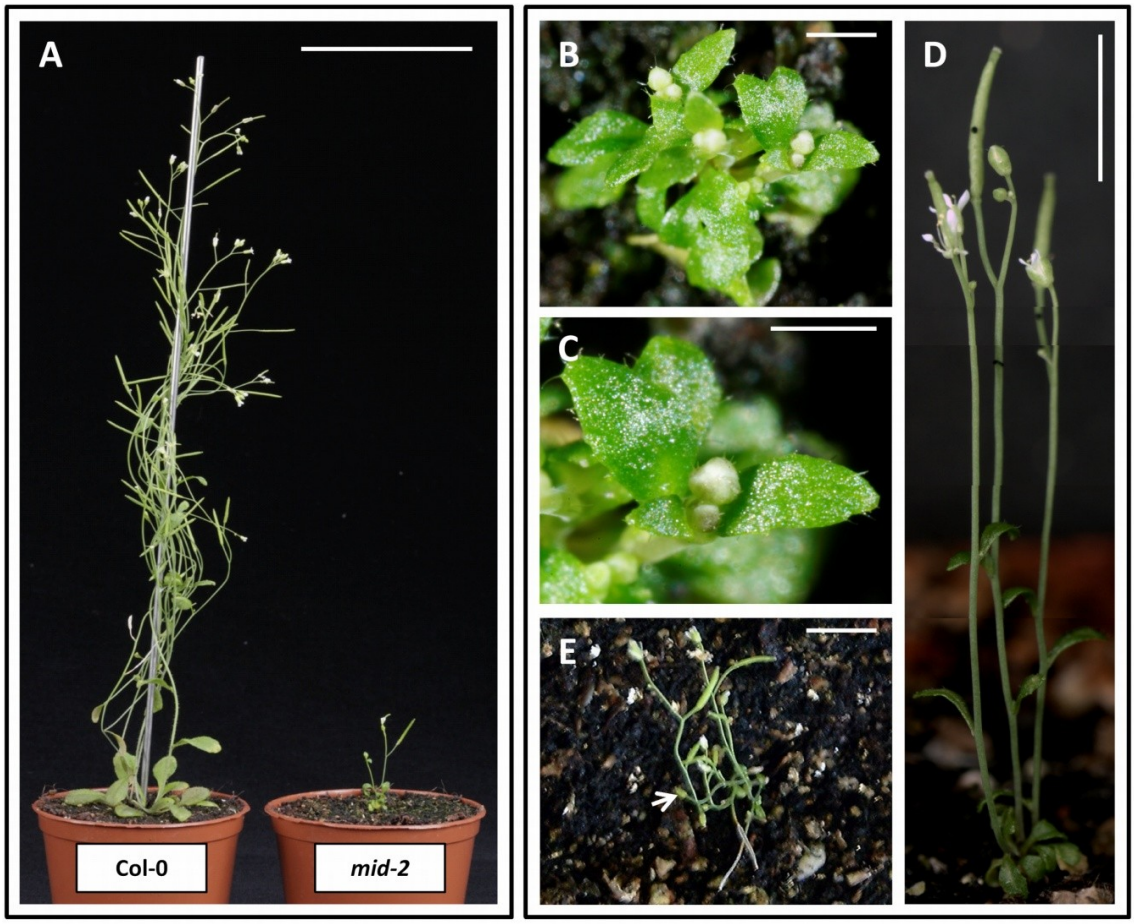

Figure III - 46: Adult phenotypes of *mid-2* and *hyp6*.
(A) 52-day-old Col-0 and *mid-2* plant. **(B-C)** Parallel initiation of three shoots of a 70-day-old *hyp6* mutant. **(C)** is a close-up of (B). **(D)** Adult 79-day-old *hyp6* plant. **(E)** A 99-day-old hyp6 plant still developing new flowers (arrow). (B-E) show the same plant. Pictures (A-D) were captured with a Canon EOS 5D Mark II by Siegfried Werth. Picture (E) was taken with a TRAVELER Super Slim XS 8 digital camera. Bar equals 5 cm in (A), 1 mm in (B) and (C), 1 cm in (D) and 5mm in (E).

3.3.3. Anthocyanin accumulates in *MID*- and *RHL2* mutants

It is thought that lack of COP1 leads to an accumulation of photomorphogenesis-specific transcription factors such as HY5, HFR1 or LAF1, due to a decrease of COP1-mediated degradation especially in the dark (Duek et al., 2004; Jang et al., 2005; Saijo et al., 2003; Seo et al., 2003). This in turn leads to increased anthocyanin levels as e.g. HY5 activates the transcription of *CHALCONE SYNTHASE* (*CHS*) a key enzyme for anthocyanin biosynthesis (Ang et al., 1998; Feinbaum and Ausubel, 1988). Therefore, *cop1* mutants accumulate anthocyanin as was shown e.g. in Ang and Deng (1994).

In this work, it was tested if also *mid-2* and *rhl2* exhibit an elevated anthocyanin level in comparison to Col-0.

The limited seed material and the small size of *MID*- and *TOPOVI* mutants made it necessary to optimise the germination in a pre-test. This optimisation had to face two essential criteria: first contamination needed to be avoided and second the number of germinating seeds should be optimised. An easily observable yellowish colour was observed for all solutions in which these seeds were sterilised. This might be due to the reported seed coat mucilage defect (Kirik et al., 2007). Mere Cl_2 gas treatment proved to abolish germination. Therefore, the sterilisation process to choose should be as quick and mild as possible. EtOH treatment was not sufficient in the case of *mid-1* and *mid-2* seeds to constantly avoid contamination. Finally different incubation times for the NaOCl treatment were tested. Three minutes of incubation with 2% NaOCl avoided contamination and gave the best germination efficiency tested for *mid-1* seeds (Figure III - 47).

For the anthocyanin test, approximately 50 seeds are used per replica and the anthocyanin content has been determined before per seedling (Hoecker et al., 1998) or per gram fresh weight (Datta et al., 2007). Col-0 and *cop1-4* seedlings have a longer hypocotyl or more leaf area than *mid-2* and *rhl2* seedlings, respectively. Therefore, it is likely that the number of cells or the size of the cell organelles that can contribute to the production and storage of anthocyanin is different and not comparable. To compare the weight per seedling and the difference between the two calculation possibilities, the following experiment was conducted. 50 seedlings of Col-0, *cop1-4*, *mid-2* and *rhl2* were sterilised for anthocyanin detection in Figure III - 47. Plates were exposed to darkness or LD conditions for 7 days. The number of germinated seedlings and the fresh weight was determined when harvesting under protective green light. Table III - 11 shows the different weight per seedling in this experiment. Interestingly, the weight per *cop1-4* seedling in the dark equals the weight in the light. In the case of mid-1 the two weights are almost equal. This would be expected for seedlings exhibiting a photomorphogenesis phenotype. In the dark, wild-type seedlings weighed only half of the light-grown seedlings. This corresponds nicely to the different developmental program - skotomorphogenesis - in the dark. It has to be pointed out that the low weights of *mid-1* and *rhl2* might be close to the detection limit of the use balance. 50 *mid-1* seedlings weighed only 25% of 50 *cop1-4* seedlings. This explains the differences visible in Figure III - 47 - A and B. In this pre-test *mid-1* showed an elevated anthocyanin content per seedling (Figure III - 47 - A) and per gram fresh weight (Figure III - 47 - B) under LD conditions and in the dark in comparison to the wild-type. When calculated per gram fresh weight it was even higher under LD conditions than for *cop1-4*. Based on

these results, the anthocyanin content per gram fresh weight was determined in subsequent experiments. For *rhl2* no elevated anthocyanin levels were detectable in this pre-test. This might be explained by a lack of anthocyanin accumulation or the low amount of plant material. As a consequence of the latter, the detection threshold of the photometer was probably not reached. To avoid this problem, higher amounts of plant material were taken in subsequent experiments.

Table III - 11: Comparison of the weight per seedling in anthocyanin experiments of light-grown and dark-grown seedlings. The number of harvested seedlings and the fresh weight [g] were determined for the anthocyanin experiment in Figure III - 47 - A and B. Note that there is no difference for *cop1-4* in the light and in the dark and that *mid-1* weights much less than *cop1-4*.

sample	light			dark		
	No. of seedlings	fresh weight [g]	fresh weight / seedling [mg]	No. of seedlings	fresh weight [g]	fresh weight / seedling [mg]
Col-0	50	0.06	1.2	50	0.03	0.6
cop1-4	50	0.04	0.8	50	0.04	0.8
mid-1	39	0.01	0.26	50	0.01	0.2
rhl2	47	0.02	0.43	34	0.005	0.15

Due to a lack of seed material only the values for dark-grown seedlings were determined in the optimised experiment (Figure III - 47). At least three replicas of 7-day-old dark-grown seedlings of Col-0, *mid-2*, *rhl2* and *cop1-4* were analysed. For Col-0, *mid-2* and *cop1-4* 190-240 mg, for *rhl2* 40-160 mg of seedlings could be harvested. In the dark, the anthocyanin accumulation is higher in *mid-2* and *rhl2* seedlings than in the wild-type but lower than in *cop1-4*.

As a next step, the plant material for *rhl2* should be increased in another replica to reduce STDEV values and to conclude if there is more anthocyanin in *rhl2* than in *mid-2* in the dark. Additionally the anthocyanin content of light grown seedlings should be analysed.

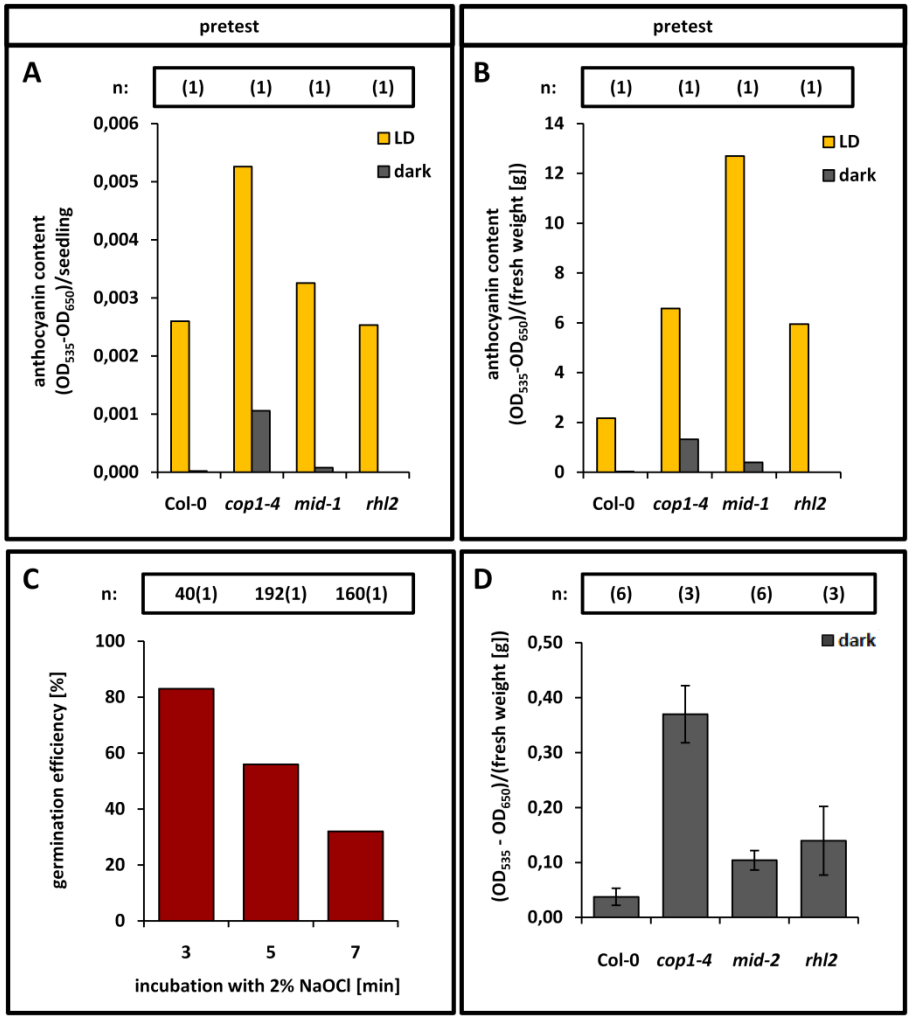

Figure III - 47: Increased anthocyanin content of *mid* mutants and *rhl2*. (A, B, D) The anthocyanin content of 7-day-old seedlings was determined in a pre-test per seedling (A), per gram fresh weight (B) and in the final experiment with at least three independent replicas per gram fresh weight (D). (C) Determination of the NaOCl-treatment dependent germination efficiency. Growth conditions: (A-B) Seedlings were kept for 7 days at 21°C under LD conditions or darkness, respectively. (C) *mid-1* seeds were sterilised with 2% NaOCl for 3, 5 or 7 minutes, respectively, and placed on MS 1%. After three days of stratification, the plates were incubated under LD conditions at 21°C. (D) Seedlings were kept for 7 days at darkness at 21°C. For *rhl2*, only 40, 60 and 160 mg of seedlings could be harvested for three independent assays. Error bars in (D): SE of the mean. n: number of analysed seeds, in brackets: number of replicas, LD: long day, SD: short day. Raw data in attachment A R-22.

3.3.4. CHS transcription is up-regulated in *mid-2* and *rhl2*

In *cop1-4* the expression of light-responsive genes like *CHLOROPHYLL A/B BINDING PROTEIN* (*CAB*), *RBC*, *PSAA/B* and *CHS* is up-regulated. This has also been show for the mutant *bin5 (RHL2*-mutant*)* concerning *CAB*, *RBC* and *PSAA/B* (Yin et al., 2002). The elevated anthocyanin levels of *mid-2* and *rhl2* suggest that genes of the anthocyanin biosynthesis pathway might be up-regulated. Therefore, the

transcription of *CHS* has been chosen to be analysed in this work for *mid-2* and *rhl2* in comparison to Col-0 and *cop1-4*.

Several considerations were made to choose the proper control for this sqRT-PCR-analysis. *ACTIN* was excluded as a control because ACT7 interacts with MID on the protein level as I could show in my diploma thesis applying YTH and BiFC and the used mutants have a morphogenesis defect. *EF1αA4* has already been used for RT-PCR with *midget* cDNA from light-grown plants in my diploma thesis and in Kirik et al. (2007) as a control. It is not known if *EF1αA4* is applicable as a control for dark-grown seedlings. *UBQ10* has been established as a control for RT-PCR especially with dark-grown seedlings before: Sun et al. (1997) showed that *UBQ10* is constitutively expressed in the light and in the dark. Harari-Steinberg et al. (2001) could prove that the steady state levels of *UBQ10* are not influenced by the state of development. The *EF1αA4* and *UBQ10* sqRT-PCRs were performed in parallel with Col-0, *mid-2*, *rhl2* and *cop1-4* cDNA that was prepared from 3-day-old dark-grown plants. Interestingly *UBQ10* transcript-levels were not comparable when levels of *EF1αA4* transcripts were equal (Figure III - 48). It has to be mentioned that for equal *EF1αA4* transcript-levels the amount of template needed to be adjusted after cDNA preparation with comparable amounts of total RNA. This was not or not in this extent the case for *UBQ10*. Therefore, the published control for dark-grown seedlings*, UBQ10*, was selected for further RT-PCR analysis. This means that one can conclude that *EF1αA4* is up-regulated in *mid-2*, *rhl2* and *cop1-4* in 3-day-old dark grown seedlings. A verification of this RT-PCR is needed. Other controls like *TUBULIN* or *HSP70* should additionally be applied in experiments in the future.

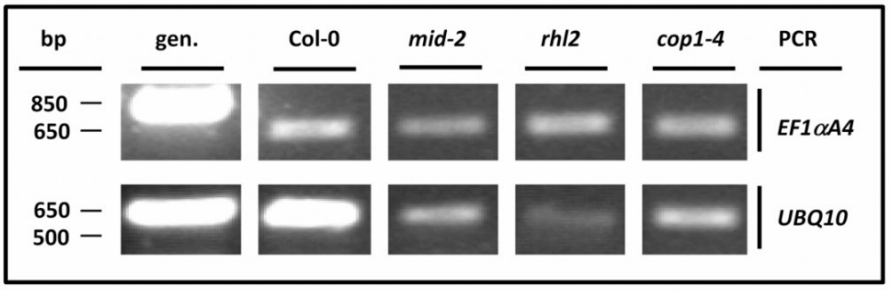

Figure III - 48: Different levels of EF1αA4 and UBQ10 in the dark. RT-PCR was performed on dark-grown seedlings that were kept for 3 days on MS media lacking sucrose after induction of germination. cDNA synthesis reaction with water instead of reverse transcriptase gave no visible transcript amplification. The exponential phase was determined before. The amount of template was adjusted to comparable EF1αA4-levels. The RT-PCR mixes differ only in the primer. EF1αA4: 26 cycles, UBQ10: 29 cycles. gen.: genomic DNA (Col-0).

All shown sqRT-PCRs in Figure III - 49 and the COP1 RT PCR described in III. 3.5. were performed with the same cDNA. Genomic DNA contamination could be excluded by different sizes of *EF1αA4* and *COP1* PCR-products for cDNA and genomic DNA (Table II - 6, Figure III - 48) in addition to this the negative control marked in the right column of Figure III - 49 (in which a cDNA synthesis without reverse transcriptase served as a template for the subsequent PCR) could not only exclude a genomic contamination but also a RNA contamination of the template. The latter is discussed in II. 2.1.5. in more detail.

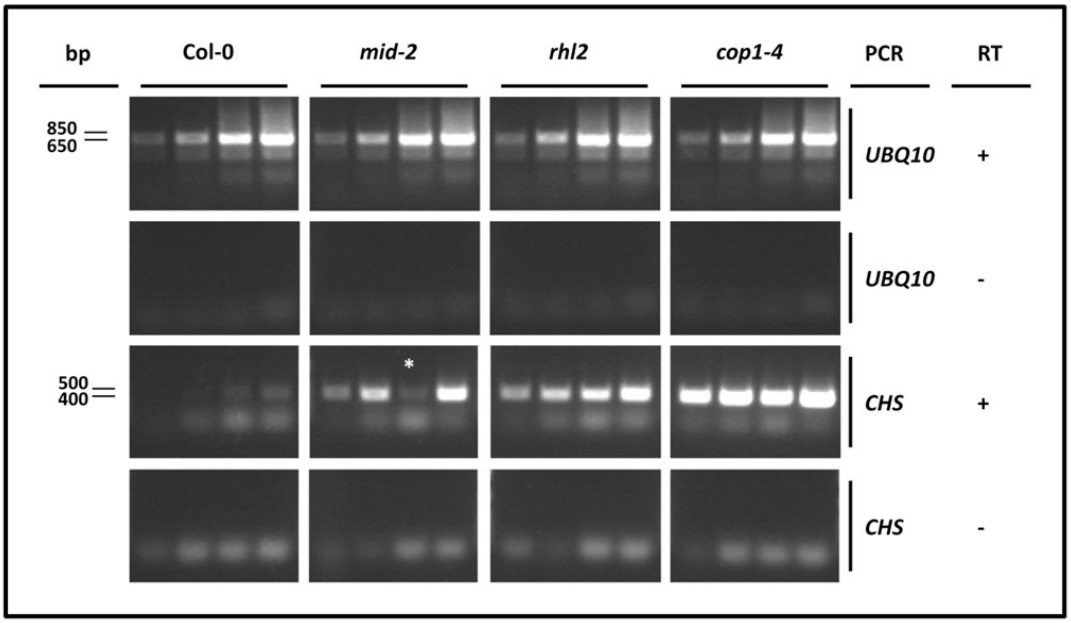

Figure III - 49: *CHALCONE SYNTHASE* (*CHS*) transcription is up-regulated in *mid-2* and *rhl2*. RT-PCR was performed on dark-grown seedlings that were kept for 3 days on MS media lacking sucrose after induction of germination. RT-PCR of *UBIQUITIN10* (*UBQ10*) underlines that same amounts of RNA were used. cDNA synthesis reaction with water instead of reverse transcriptase served as a negative control. Note that CHS transcript levels are much higher in *cop1-4* than in *mid-2* and *rhl2*. In the right column, + and - depict the presence and absence of reverse transcriptase in the cDNA synthesis reaction. *CHS*: 29, 32, 35 and 38 cycles, *UBQ10*: 23, 26, 29 and 32 cycles. * the slot of the gel was defect, RT: reverse transcriptase. The same portions of the gels are shown for the negative controls.

Figure III - 49 shows that *CHS*-expression is up-regulated in 3-day-old dark-grown *mid-2* and *rhl2* seedlings. *UBQ10* RT-PCR analysis proves that equal amounts of cDNA were used. In *cop1-4* the highest transcript accumulation could be observed. It has to be pointed out that this experiment has been performed once for *mid-2* and twice for *rhl2*. This result is in agreement with the elevated anthocyanin levels in both mutants described in III.3.3.3.

3.3.5. *MID*- and *TOPOVI* mutants bolt earlier under LD conditions

Another *cop1* mutant phenotype beside the aspects of photomorphogenesis is that the *cop1* mutants bolt earlier than the wildtype under LD and SD conditions. This *cop1* mutant phenotype could also be

observed in *mid*- and *topoVI*-mutants. The time point of bolting was determined by counting the number of rosette leaves when the first bud was visible. It could be shown that *mid-1* (7.7 +/-1.0 leaves), *mid-2* (5.5 +/- 0.6 leaves), *rhl2* (4.7 +/- 0.6 leaves) and *hyp6* (5.5 +/- 1.0 leaves) bolt significantly earlier that the wild type (10.7 +/- 0.9) under LD conditions at 21 °C in autumn and spring in the greenhouse (Figure III - 50). Only one experiment could be performed for *mid-2* and *hyp6* due to the lack of homozygous seed material and to time restriction. For *rhl2* two and for Col-0 and *mid-1* three independent experiments were conducted.

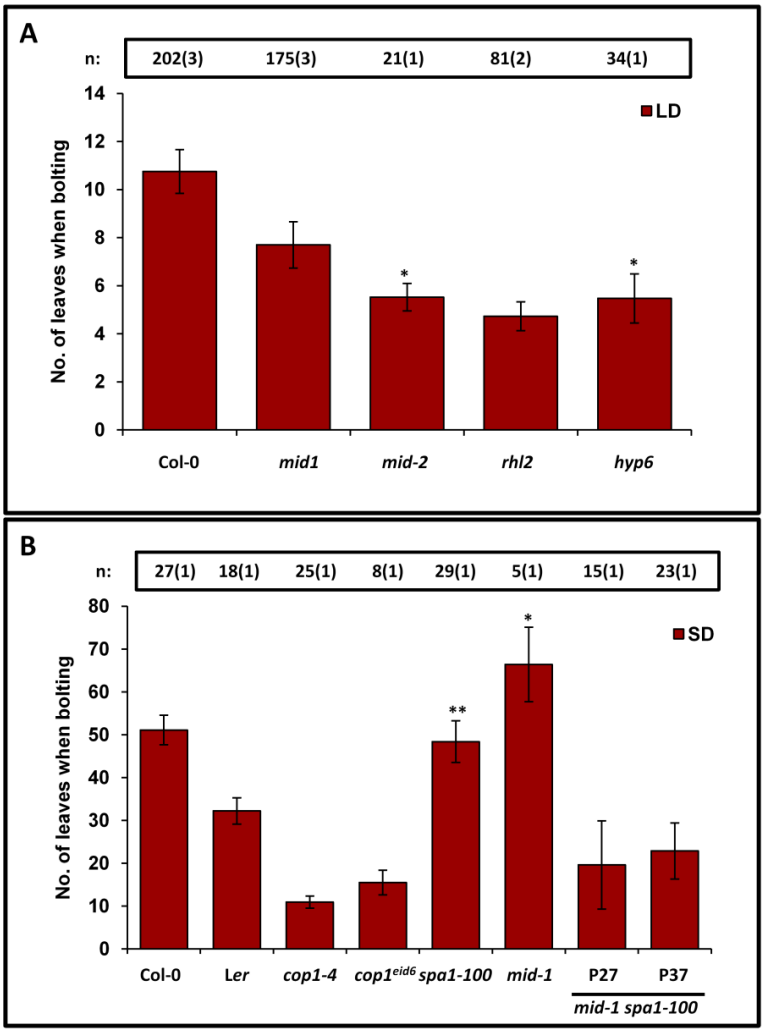

Figure III - 50: *Mid*- and *topoVI* mutants bolt early under LD conditions; *mid-1* bolts late under SD conditions.
(A) Single seeds were placed on soil in 77er trays and placed in the greenhouse under LD conditions at 21°C after stratification. The tray position were exchanged regularly. All trays in one assay were positioned under one pair of light sources. **(B)** Single seeds were placed on soil in single pots and randomised throughout a whole plant room. The plants were kept under SD-conditions at 21°C after stratification. The same type of light sources was used like in the greenhouse. Error bars = SE of the mean. *: Student's *t* test; P< 0.001, the difference to *rhl2* was subject of the *t*-test in (A); in (B) the difference to the wildtype was tested by t-test. **: Student`s *t* test; P= 0.0196. n: number of analysed plants, in brackets: number of replicas, LD = long day, SD = short day. The number of leaves was determined when the first bud was visible. Raw data in attachment A R-23.

Bolting under SD conditions was tested in a 21°C warm plant room. 51.1 (+/- 3.5) leaves were counted for Col-0 plants when bolting. *Cop1-4* (10.9 +/- 1.4) bolted significantly earlier than the wild-type. Interestingly *mid-1* (66.4 +/- 8.7) bolted significantly later than the wild type and therefore differed from the *cop1-4* mutant phenotype under these conditions, whereas two lines of the *mid-1 spa1-100* double mutant (19.6 +/- 10.3 and 22.9 +/- 6.5) bolted much earlier than the wildtype. These double mutants were generated in this work. Plants were randomised and distributed on three levels in all parts of a plant room. (Figure III - 50) This experiment could only be performed once due time limitations. The *mid-1 cop1-4* double mutants (III. 3.4) did not germinate for the SD experiment and has not been generated at the time of the LD experiments as well as all other double mutants generated in this work that are presented in III. 3.4. When this thesis was written, the bolting experiment for *mid-1* has not been finished. Therefore only five plants could be included in the graph in Figure III - 50-B. Up to ten more *mid-1* plants already showed more leaves than the wildtype but did not bolt at this time (after 110 days). In Figure III - 51 the phenotypes of the analysed mutant of the SD experiment are shown. *Mid-2* and *rhl2* plants did not survive.

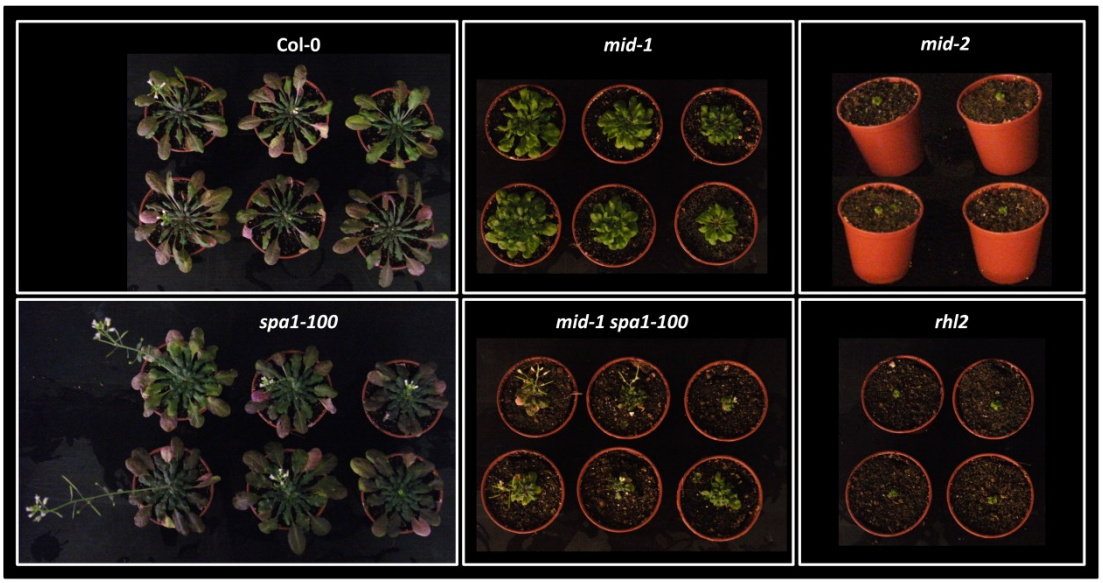

Figure III - 51: Phenotype of 87-day-old-plants grown on soil under SD conditions at 21°C. The *mid-2* and *rhl2* plants on the right died before bolting. All plants originate from the bolting experiment in Figure III - 50. Pictures were taken with a TRAVELER Super Slim XS 8 digital camera. Light intensity: 31-46 µmol*m^{-2}*s^{-1}. Pots have a diameter of 6 cm.

A very high significant shift to an even earlier bolting was observed for all plants except *mid-2* when performing the LD bolting experiment at 24°C in a plant room instead of 21°C in the nursery (Figure III - 52). The same types of light sources were used. It has to be taken into consideration that additional sunlight was present in the greenhouse. The used light bulbs for all experiments were a mix of one Osram Cool White (L58W/21-840Lumilux Plus Eco) and one Natura de Luxe (L58W/76),

above each tray. In the used plant chamber a light intensity of 31-46 µmol*m^{-2}*s^{-1} was measured. A higher light intensity of 125 µmol*m^{-2}*s^{-1} was applied for a first experiment in another plant chamber at 21°C. Col-0, *mid-1*, *spa1-100* and two lines of *mid-1 spa1-100* (Figure III - 50) were tested and similar results for Col-0 and mid-1 in comparison to the experiments in the nursery were obtained (Figure III - 52).

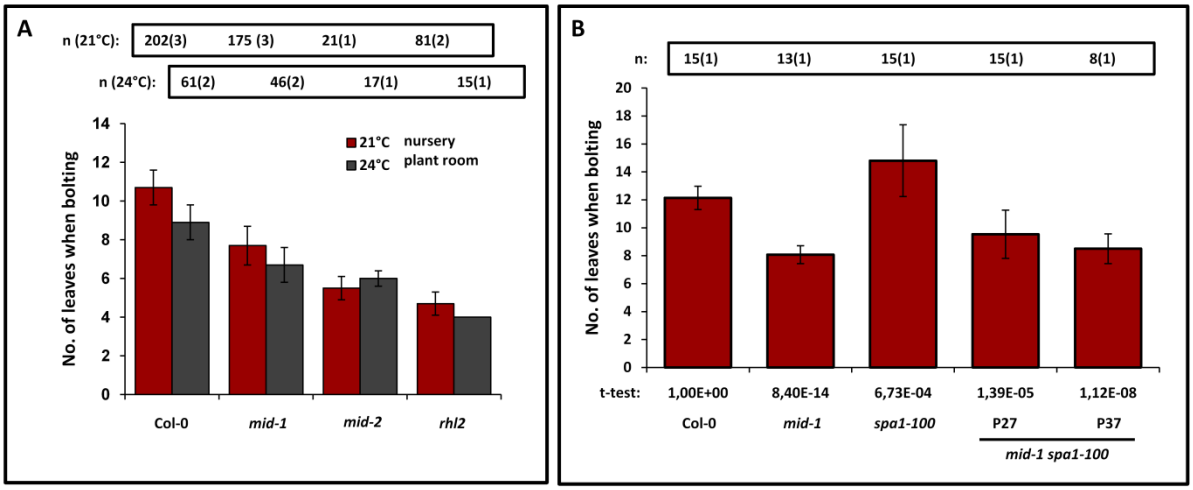

Figure III - 52: Influence of temperature and light intensity on bolting.
(A) Col-0, *mid-1* and *rhl2* bolt earlier at 24°C than at 21°C. Comparison of the bolting experiment from Figure III - 50 (at 21°C in a nursery) and a bolting experiment at 24°C in a plant chamber. For the first experiment see Figure III - 50 and the text, for the second experiment: Single seeds were placed on soil in pots with 6 cm diameter and placed in a plant chamber under LD conditions at 24°C after stratification. Col-0: 8.9 +/-0.9; *mid-1*: 6.7 +/- 0.9; *mid-2*: 6 +/- 0.4 and *rhl2*: 4 +/- 0. **(B)** *Mid-1* and *mid-1 spa1-100* bolt earlier than the wildtype under LD conditions and at high light intensities. *Spa1-100* bolts slightly later than the wildtype at high light intensities. Single seeds were placed on soil in pots with 6 cm diameter and placed in a plant chamber under LD conditions at 21°C after stratification. Col-0: 12.1 +/- 0.83; *mid-1*: 8 +/- 1; *spa1-100*: 14.8 +/- 2.57; *mid-1 spa1-100* (P27): 10 +/- 2; *mid-1 spa1-100* (P32): 8.5 +/- 1.1. Light intensity: 31-46 µmol*m^{-2}*s^{-1} (A, plant room) and 125 µmol*m^{-2}*s^{-1} (B). Error bars = SE of the mean. In (B) the t-test results are shown below the bars. n: number of analysed plants, in brackets: number of replicas. The number of leaves was determined when the first bud was visible. Raw data in attachment A R-24.

It will be of great interest to examine the response of *mid* and *topoVI*-mutants to different light qualities and quantities in the future and to concentrate on the differences to the *cop1*-mutant phenotypes as there are the bolting behaviour under short day conditions, trichome, root, petiole and the enhanced photomorphogenesis phenotype of *mid* in the light.

3.4. MID- and TOPOVI components interact genetically with COP1

A genetic analysis was performed to answer the question if MID is a target or a regulator of COP1. For this analysis a weak (lack-of-function) allele of *MID* - *mid-1* (Col-0) - and two weak alleles of *COP1* - *cop1-4* (Col-0) and *cop1*^{eid6} (L*er*) - were chosen to be crossed. As *mid-1* is BASTA resistant due to a

activation tagging T-DNA insertion in exon III of *MID*, the double mutants could also be selected with BASTA. Additionally, the parents and its progeny used for the morphogenetic analysis presented in Figure III - 53 were tested by PCR for their genotype. In the case of *mid-1 cop1-4* the parent and its progeny were all homozygous for both mutants. For *mid-1 cop1^{eid6}* three parents were heterozygous for both mutants.

In cop1-4 mutants a truncated N-terminus of COP1 is expressed (COP1$^{1-282}$) due to a point mutation caused by EMS mutagenesis at position 847 of the *COP1* CDS that leads to a stop codon (McNellis et al., 1994a). The phenotype of *cop1^{eid6}*-L*er* in the dark is less severe than for *cop1-4* but the mutant showed to be hypersensitive in far-red light (eid = "empfindlicher im dunkelroten Licht") (Dieterle et al., 2003). In cop1^{eid6} the amino acid His^{69} located in the RING finger of COP1-L*er* is exchanged by Tyr.

For targets of COP1 a (partial) rescue of the *cop1* mutant phenotype is expected. In the case of a regulator a (partial) enhancement of the cop1 mutant phenotype would be the expected result. Therefore, seedlings of double mutants of *mid-1* and *cop1-4* or *cop1^{eid6}* were analysed in the dark in regard to aspects of photomorphogenesis. 32 seeds of each parent were used to obtain on average two seedlings that are homozygous for both mutants for mid-1 cop1^{eid6}. Both double mutants show an enhanced cop1 mutant phenotype with a significantly reduced hypocotyl length in comparison to the single mutants (Figure III - 53). The "open cotyledon" phenotype has been measured with an so called cotyledon angle before (Boccalandro et al., 2004) but unfortunately the authors did not describe the angle. From the mutants analysed in the cited paper one can conclude that this angle is the angle between the laminas of the cotyledons named "lamina angle" in this work. As cotyledons are leaves and a leave consists of a petiole and a lamina, in this work, the petiole and lamina angle will be determined to characterise the "open cotyledon" phenotype. The cotyledons of seven-day-old *cop1-4* and *cop1^{eid6}* seedlings have almost parallel petioles in the dark. This is not the case for stronger alleles of *COP1* as there are *cop1-1* or *cop1-5* shown e.g. in Ang and Deng (1994) that exhibit a wider cotyledon angle.

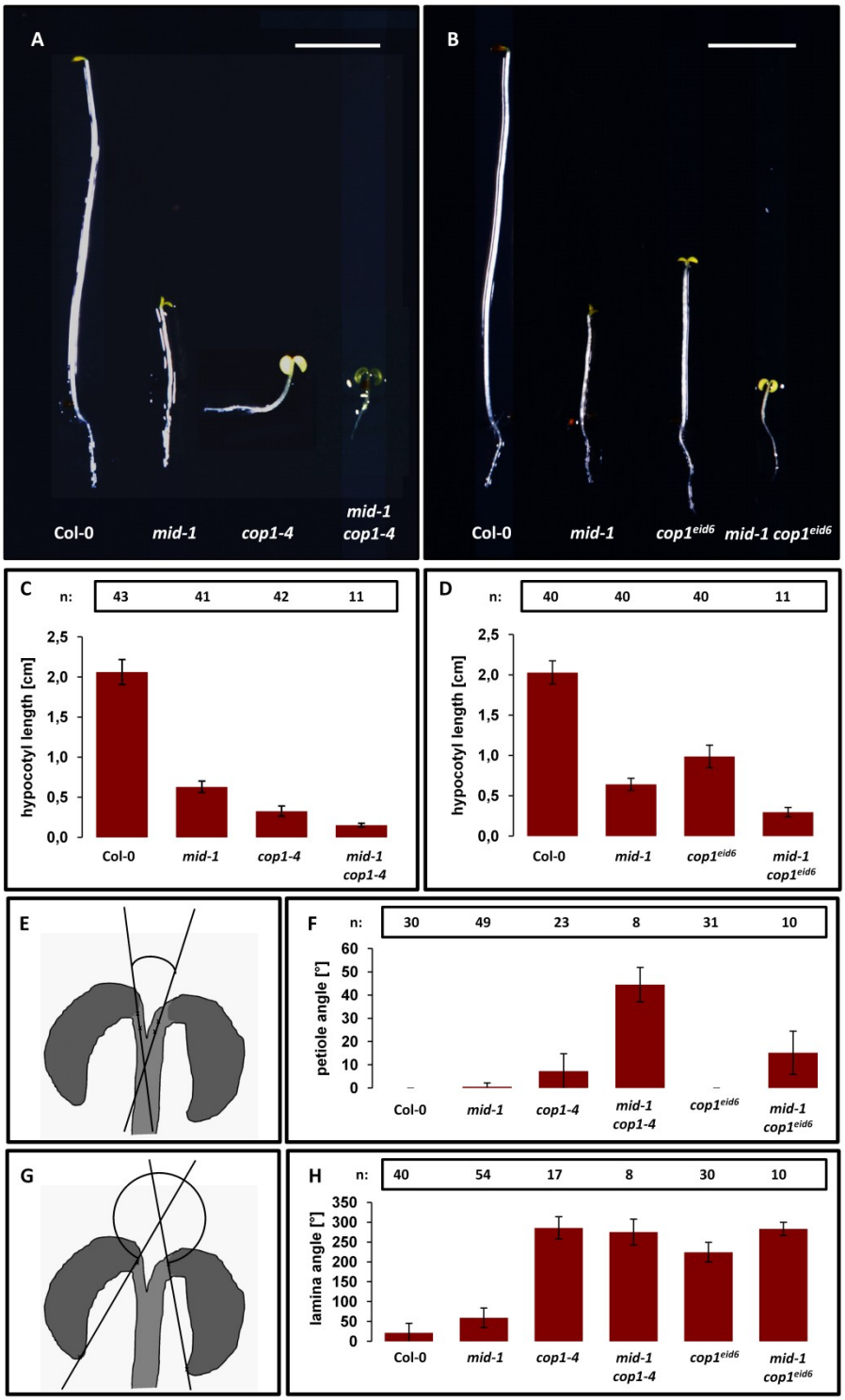

Figure III - 53: MIDGET and COP1 interact genetically in the dark. **(A) - (B)** Enhanced *cop1* mutant phenotype of 7-day-old dark-grown double mutant seedlings of *mid-1 cop1-4* and *mid-1 cop1*^{eid6}, respectively. **(C) and (D)** Reduced hypocotyl length in the double mutants *mid-1 cop1-4* and *mid-1 cop1*^{eid6}. Hypocotyl length was measured with imageJ. **(E) and (G)** Schematic example for the measurement of the petiole and lamina angle. The dark grey color represents the yellow to white color of the cotyledons in dark grown seedlings. **(F) and (H)** Enhanced opening of cotyledons is caused by a larger petiole angle in the double mutants in comparison to the single mutants and the wildtype. (E) petiole angle. (G) lamina angle. n: the number of analysed seedlings is depicted above the corresponding column in the diagrams. All analysed double mutants were verified by PCR. Bar equals 5 mm in (A) and (B). Error bars in (C), (D), (F) and (H) are STDEV. Pictures in A and B were taken with a Canon EOS 5D Mark II by Siegfried Werth. Raw data in attachment A R-25, A R-26.

In this work, the petiole angle was defined as the angle between two lines that were drawn through the centres of the two petioles of the cotyledons. The centres were defined by two points close to the SAM in the middle of the petiole visible on a photograph. The lamina angle was defined as the angle between two lines drawn through the base and tip of the lamina of the cotyledons marked on a photograph. This angle was measured only for plants in which the two cotyledons could be seen from the side. Figure III - 53 and *t*-test analysis show that the petiole angle is significantly larger in the double mutants than in the single mutants. It could also be shown that this phenotype is also less severe in the *cop1*^{eid6} mutants than in *cop1-4*. Lamina angles for *mid-1 cop1-4* and *mid-1 cop1*^{eid6} were comparable to the angle for *cop1-4*, whereas the lamina angle for *cop*^{eid6} is smaller in comparison to these mutants. Pictures for further statistical analysis have been taken and will compare other morphological aspects as cotyledon leaf area index, petiole length, complexity of the cotyledon epidermal cells, the "open stomata in the dark" phenotype and the root length. Nevertheless, the presented phenotypical comparison already reveals that MID and COP1 interact genetically.

For double mutants of *cop1-4* with *mid-2* and the *topoVI* components, representative seedlings under different growth conditions were chosen and are presented in Figure III - 54 and Figure III - 56. When grown for seven days under constant light, mid-1 differs from Col-0 and *cop1-4* by the *mid-1*-trichome phenotype and by a larger lamina angle. For cop1-4 the reduced petiole length might be the most severe difference to the wildtype upon statistical analysis. The double mutant *mid-1 cop1-4* showed reduced germination efficiency Figure III - 55 and therefore might be delayed in development in comparison to the single mutants.

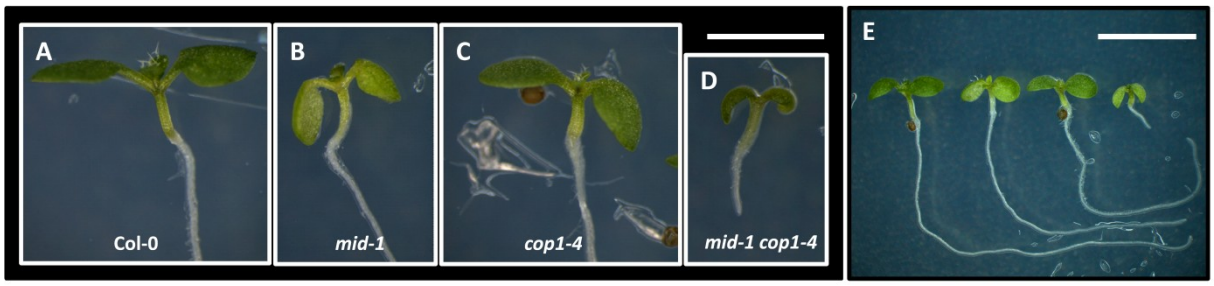

Figure III - 54: MIDGET and COP1 interact genetically in the light. **(A) - (D)** Enhanced *cop1* mutant phenotype of seven days old light-grown double mutant seedlings of *mid-1 cop1-4* and **(E)** *mid-1 cop1*^{eid6}, respectively. Seedlings in (E) are (from the left to the right): Col-0, *mid-1*, *cop1*^{eid6} and *mid-1 cop1*^{eid6}. All seeds were sterilised and kept on MS plates lacking sucrose under constant white light (40 µmol*m^{-2}*s^{-1}). All analysed double mutants were verified by PCR. Bars equal 5 mm. Pictures in (A-D) and (E) were taken at the same magnification with a Leica MZFLIII binocular.

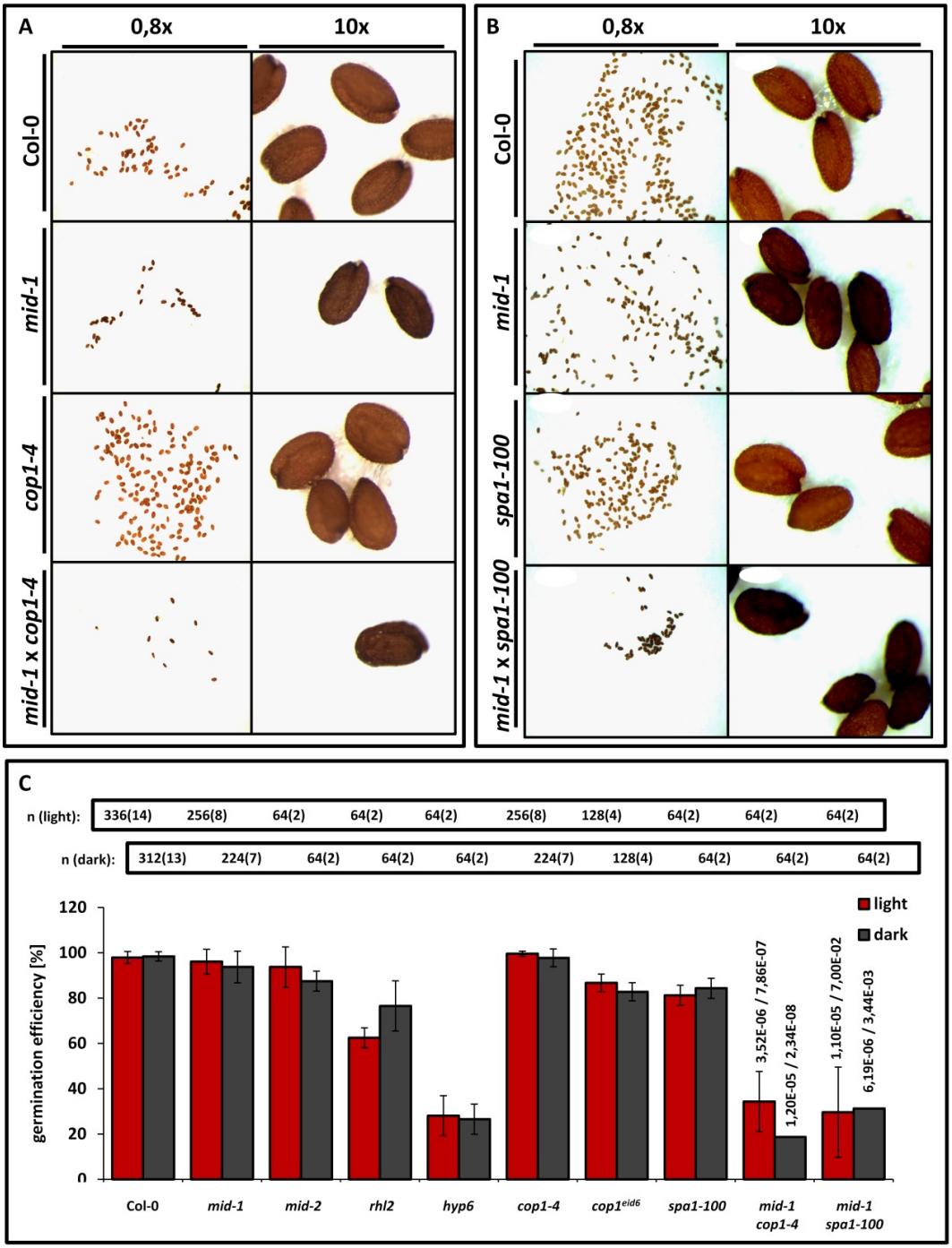

Figure III - 55: Seed and germination analysis of *mid-1 cop1-4* and *mid-1 spa1-100* and germination analysis of *topoVI* single mutants.

(A, B) Pictures of dried seeds of the depicted genotypes were taken with a Leica MZFLIII binocular. Seeds of plants that were ripened and harvested under the same condition are boxed. All pictures in one column were changed in parallel concerning brightness and contrast. Note that *mid-1* and doublemutant seeds were darker - almost black - smaller and narrower than all other seeds. **(C)** Determination of the germination efficiency for various single mutants, Col-0, *mid-1 cop1-4* and *mid-1 spa1-100*. For each assay, 32 seeds (24 seeds for Col-0) were placed on MS plates lacking sucrose after sterilisation, were exhibited to 4h of white light for induction of germination and were kept for seven days in darkness or in constant white light (40 µmol*m^{-2}*s^{-1}). The t-test results are shown for the comparison of the mean of the double mutants with mid-1 (first value) and *cop1-4* or *spa1-100* (second value), respectively. Differences between germination efficiency in the light and in the dark were not significant. (P<0.05: difference is significant) n: number of analysed plants, in brackets: number of replicas. Note, that for several mutants only two independent assays were performed yet. Error bars in (C) are STDEV. raw data in attachment A R-27.

Figure III - 54 shows that the roots of both analysed double mutants are shorter than the corresponding single mutants under constant white light. For *mid-1 cop1*^{eid6} statistical analysis might reveal in the future that the hypocotyl length is significantly reduced in comparison to the single mutants and to the wildtype.

Beside the trichome and root hair phenotype the seed phenotype of *mid-1* is epistatic to *cop1-4* and *spa1-100* (Figure III - 55). Seeds of *mid-1* and of these double mutants are darker (almost black) and narrower in appearance than seeds of the wildtype. Whereas *mid-1* seeds are narrow, *cop1-4* seeds appear roundish. Not only *mid-1 cop1-4* but also *mid-1 spa1-100*, *rhl2* and *hyp6* were shown to exhibit a defect in germination efficiency (Figure III - 55).

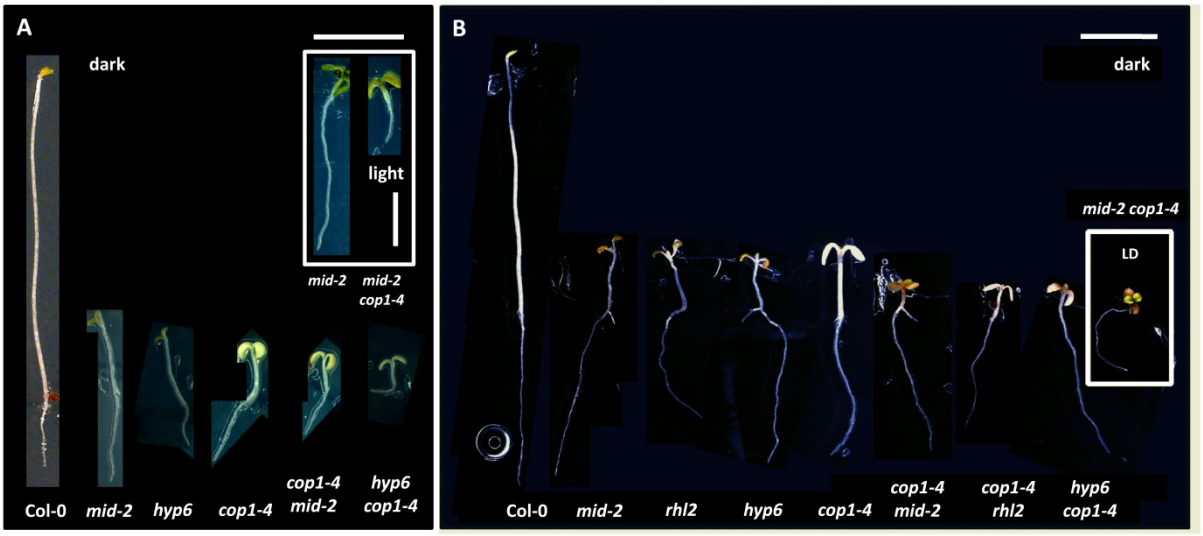

Figure III - 56: TOPOVI and COP1 interact genetically in the dark. Enhanced *cop1* mutant phenotype of 7-day-old dark-grown double mutant seedlings *cop1-4 mid-2*, *hyp6 cop1-4* and *cop1-4 rhl2*. *S*eeds were placed on MS plates lacking sucrose (A) or supplemented with 1% sucrose (B) after sterilisation, were exhibited to 4h of white light for induction of germination and were kept for seven days in darkness (A, B), at LD conditions (inset in (B)) or in constant white light (40 µmol*m^{-2}*s^{-1}) (inset in (A)). Note that the double mutants grown on MS plates with 1% sucrose look similar to the corresponding light-grown seedlings. Bars equal 5 mm in (A) and (B) and 2.5 mm in the inset. For segregation analysis see Table III - 12.

Phenotypical analysis of double mutants (*cop1-4 mid-2*, *hyp6 cop1-4* and *cop1-4 rhl2*) underlined that not only MID but also TOPVI interacts genetically with COP1 (Figure III - 56). For *hyp6 cop1-4* and to a lower extent for *cop1-4 mid-2* an enhanced *cop1* mutant phenotype was observed in the dark on MS plates lacking sucrose. For *cop1-4 mid-2* this enhancement was strikingly increased when grown under constant light conditions on plates lacking sucrose. When using plates supplemented with 1% sucrose an interesting observation could be made. For all three analysed double mutants in Figure III - 56 the phenotype in the darkness resembled their phenotype in the light, whereas the phenotype of the single mutants was characterised by a comparably longer hypocotyl, longer petioles and

smaller cotyledon leaf laminas. The overall phenotype of the single mutants was similar to the *det1-1* phenotype (Pepper et al., 1994). All analysed double mutants in Figure III - 56 were subjected to a phenotypical segregation analysis. The genotype of the parents was determined by PCR. Segregation ratios were in the expected ranges and therefore supported the phenotypical selection for the seedlings in Figure III - 56 (Table III - 12).

Table III - 12: Segregation analysis of progeny of one or two lines of double mutants of *cop1-4* and *topoVI* mutants. The seeds were sterilised and kept for seven days on MS plates lacking sucrose in the darkness or under constant light or for 8 days on plates supplemented with 1% sucrose in the darkness or under LD conditions. The number of plants exhibiting the indicated phenotype corresponding to the named mutant or doublemutant is listed (brackets: number of independent analysis) and the percentage was calculated on the basis of seeds that were sawn. For plates with 1% sucrose all seeds germinated, for plates lacking sucrose see Figure III - 55 (32 seeds were used per assay). Rows describing different analysis are separated by red boxes. For a description of the double mutant phenotypes, see the text. According to prior PCR analysis, two parents were heterozygous for *cop1-4* and *hyp6* (0% sucrose) or *rhl2* (1% sucrose), respectively. All other analysed seedlings are the progeny of plants that were homozygous for *cop1-4* and heterozygous for *hyp6* or *mid-2*, respectively. In the case of *cop1-4 rhl2,* the genotype was additionally determined by PCR. The expected percentage according to the genotype of the parent is given in the right column.

	phenotype	No. of plants	percentage – determined [%]	percentage-expected [%]
MS 0% sucrose				
dark	*hyp6 cop1-4*	4(2)	6.25	6.25
	cop1-4 mid-2	14 (2)	21.9	25
light	*cop1-4 mid-2*	14 (2)	21.9	25
MS 1% sucrose				
dark	*cop1-4*	14	73.7	75
	hyp6 cop1-4	5	26.3	25
	Col-0	57	57	56.25
	cop1-4	17	17	18.75
	rhl2	21	21	18.75
	cop1-4 rhl2	5	5	6.25
	cop1-4	16	72.7	75
	cop1-4 mid-2	6	27.3	25
LD	*cop1-4*	29	78.4	75
	cop1-4 mid-2	8	21.6	25

3.5. MID is necessary for COP1 stabilisation

MID and COP1 interact, co-localise in the nucleus, a so far unknown possible interaction domain has been identified by the use of the MID-COP1 interaction and the interaction is of functional relevance as can be concluded from genetic analysis. The phenotypes of the *mid* mutants and of the *topoVI* mutants could be explained by a reduced level of COP1 protein in the dark. This could be the result of

reduced levels of *COP1* transcripts or of COP1 protein. A sqRT-PCR analysis was conducted to determine *COP1* transcript levels in mid-2 and rhl2 mutants in comparison to the wildtype using 3-day-old dark-grown seedlings. Figure III - 57 shows that no significant differences in *COP1* transcript-levels between the two mutants and the wildtype could be observed.

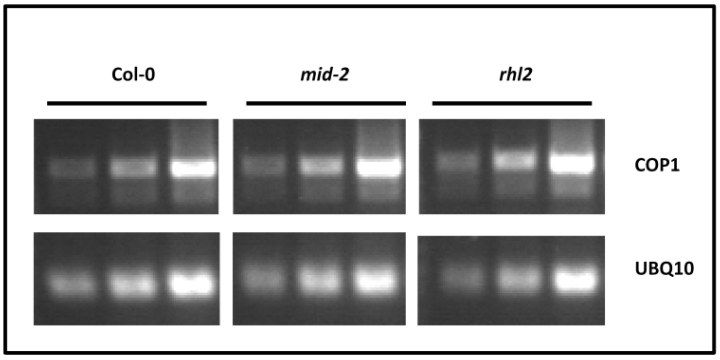

Figure III - 57: No significant change in *COP1* transcript-levels in *mid-2* and *rhl2*.
RT-PCR analysis of *COP1* and *UBQ10* transcripts in 3-day-old dark-grown seedlings, grown on MS plates lacking sucrose. RT-PCR with *Ubiquitin10* (*UBQ10*) underlines that same amounts of RNA were used. *COP1*: 31, 34 and 37 cycles, *UBQ10*: 23, 26 and 29 cycles. The negative controls are shown in A M-2.

A hint for a regulative influence of the MID protein on the COP1 protein *in planta* was found in the *N. benthamiana* infiltration experiments (Figure III - 58). When RFP-HA-COP1 was expressed alone or in combination with YFP-attB1 the characteristic subnuclear foci that are observed in *Allium cepa* and *A. thaliana* for this construct and that has been published could not be observed (von Arnim and Deng, 1994; von Arnim et al., 1997). In most transformed cells only one subnuclear focus was visible, in some other cells up to three subnuclear foci where observed.

This changed, when YFP-MID was co-expressed. In Figure III - 58 the minimal countable number of subnuclear foci in the two described scenario is presented. For counting, one experiment using CLSM was conducted and foci were counted while scanning through the different layers of captured z-stacks (four examples of merged z-stacks are shown in Figure III - 58). In a second experiment fluorescence microscopy was applied to count the subnuclear foci. In Figure III - 58 the significant difference in the number of subnuclear foci in dependence on the presence or absence of YFP-MID in both experiments is depicted. Alexander Maier (group Ute Höcker, university of cologne) used his COP1 antibody to show that the COP1 protein levels in 3-day-old dark-grown seedlings of *rhl2* and *mid-2* and in adult mid-2 plants grown under LD conditions are reduced in comparison to the wild type (Alexander Maier, preliminary, unpublished data).

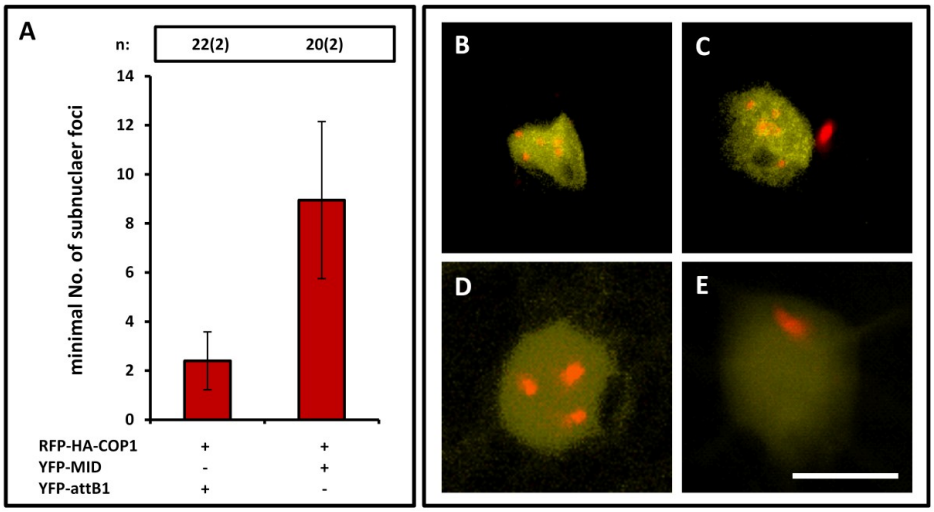

Figure III - 58: Overexpression of YFP-MID increases the number of subnuclear foci of RFP-HA-COP1.
Analysis of infiltrated epidermal leaf cells of *N. benthamiana* with the depicted constructs and the anti-silencing strain RK19. The fluorescing fusion proteins were visualised with CLSM by sequential scanning of the different channels. Merged pictures of nuclei of cells expressing YFP-MID and RFP-HA-COP1 (B, C) and YFP-attB1 and RFP-HA-COP1 (D,E) are shown at the right. Sequentially scanned z-stacks were merged with Leica Confocal software. The number of subnuclear foci was determined by scanning through the nucleus, analysis of the merged pictures or by fluorescence microscopy. As still some foci might have been too small to be detected or were covered by others, the determined number is name "minimal No. of subnuclear foci".. Bar equals 20 µm. n: number of analysed plants, in brackets: number of replicas. In C a cytoplasmic aggregate can be seen close to the nucleus. Raw data in attachment A R-28.
YFP-MID: pEarleyGate104-MID (LBA4404. pBBR1MCS.virGN54D); RFP-HA-COP1: pNmR-COP1 (LBA4404pBBR1MCS-5.virGN54D); YFP-attB1: pBatTL-B-p35s-YFP-attB1 (LBA4404pBBR1MCS-5.virGN54D); RK19 = anti silencing strain.

3.6. MID, RHL2 COP1 and HY5 are necessary for proper endoreduplication in dark-grown hypocotyls

The photomorphogenesis phenotype of *mid* and *topoVI* mutants in the dark might be explained by reduced COP1 stability in these mutants. MID and the TOPVI have been shown to be essential for endoreduplication (Kirik et al., 2007; Sugimoto-Shirasu et al., 2002). In 1998 Gendreau et al. reported that the hypocotyl cells of dark-grown *cop1* mutant seedlings have a lower C-content than the wildtype.

Hypocotyl elongation is a component of the skotomorphogenetic development in *A. thaliana*. Often cell elongation correlates with endoreduplication and elongated dark-grown hypocotyls also have elongated cells. Is the endoreduplication defect in *mid* and *topoVI* mutants independent of the endoreduplication defect in *cop1* mutants in dark-grown hypocotyls? COP1 could influence endoreduplication in a direct manner (e.g. through a MID/TOPOVI-specific pathway or in an indirect manner, e.g. by the degradation of transcription factors that inhibit endoreduplication in dark-grown hypocotyls.

HY5 is one of the best characterised targets of COP1 (I. 2). The hypocotyls of dark-grown *hy5 cop1-4* double mutants are longer than those of *cop1-4* (see e.g. Ang and Deng, 1994; personal observation) If HY5 is involved in the regulation of endoreduplication one would expect that HY5 inhibits endoreduplication that is often correlated with cell elongation and would correlate nicely with the observed differences in hypocotyl length. Instead, endoreduplication analysis of 7-day-old dark-grown hypocotyl epidermal cells based on DAPI staining in this work revealed that the C-content of *hy5-215* is reduced in comparison to the wildtype and the C-content of *hy5-215 cop1-4* is even lower than that of *cop1-4* (Figure III - 59) suggesting a G2 arrest in the analysed cells of *hy5-215*. Additionally, it was observed that hypocotyl epidermal cells of 7-day-old dark-grown *hy5-215* and *hy5-215 cop1-4* seedlings are smaller than the wildtype (personal observation) indicating that HY5 inhibits cell division and promotes endoreduplication in the dark-grown hypocotyl. A statistical analysis has to be conducted. DAPI fluorescence was at the lower threshold for analysed *hy5-215* and *hy5-215 cop1-4* nuclei; this might improve when repeating the experiment with 5 instead of 0.5 µg/ml DAPI for the staining.

C-contents for pooled hypocotyl epidermal and cortex cells in comparison to pooled hypocotyl cells in and around the central cylinder varied for one round of endoreduplication (Gendreau et al., 1998). As the morphology of epidermal hypocotyl cells of dark-grown seedlings varies from cortex cells (Gendreau et al., 1997) only epidermal cells were analysed. All epidermal cells of the two opposing sided of the hypocotyl were analysed for which a picture of the nucleus could be captured without underlying fluorescence of other cells. Only one epidermal cell type was examined. Stomata guard cells were excluded. One assay consisted of three to four seedlings from two experimental replicas with a total number of 57 to 121 analysed epidermal cells per assay. In regard to the same harvest and therefore to the same light conditions for ripening of the used seeds, Col-0/*hy5-215*, *hy5-215 cop1-4/cop1-4* and Col-0/*mid-2*/*rhl2* were comparable. Beside the percentage distribution of C-content classes (see II. 2.5.7.), the percentage of cells with more than 8C - corresponding to more than two rounds of endoreduplication - were compared. Reduced C-contents of *mid-2*, *rhl2* and *cop1-4* that have been reported before, were also observed in the performed experiment. Values for three independent assays with Col-0 seedlings were comparable. These results indicate the reliability of the experimental setup and the obtained data.

Seeds for *mid-1 cop1-4* did not germinate for this experiment. In the future double mutants of *mid* and *topoVI* mutants with *cop1* mutants should be analysed as well as double mutants of *cop1* mutants with lack- or loss-of-function mutants of other targets of COP1

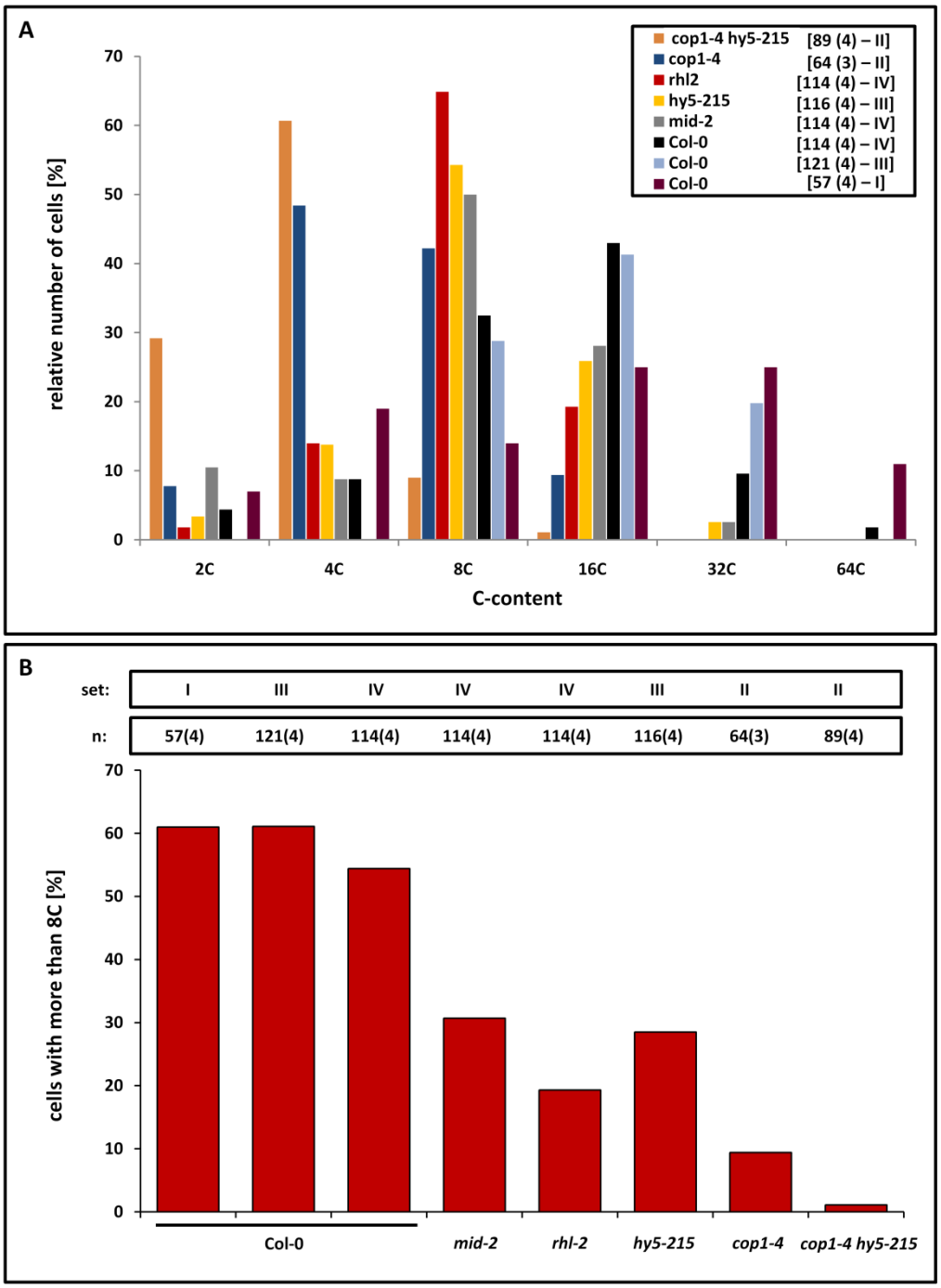

Figure III - 59: TOPOVI, COP1 and HY5 are necessary for endoreduplication in epidermal cells of the hypocotyl in the dark. Analysis of nuclear DNA-content of epidermal cells of 7-day-old dark-grown seedling by measuring the fluorescence of DAPI-stained nuclei. The relative amount of cells per mutant with the corresponding fluorescence-intensity-defined C-content is indicated. 20 nuclei of stomata guard cells were used to define the DNA-content of 2C. From two cell files at the opposing sides of the hypocotyl all nuclei were analysed that could be focused on (except stomata guard cells). Fluorescence intensity was determined using the DISCUS program (see II. 2.7.7.). n: No. of epidermal cells analysed. In brackets: number of seedlings analysed. At least two independent experimental setups were used. Roman numbers correspond to seed sets that were harvested at the same time from plants that ripened at the same light conditions. Sets I and II were stained with 0.5 µg/ml DAPI, for sets III and IV 5 µg/ml DAPI were used. (B) Visualisation of the differences between the mutants and the wildtype was improved when comparing the relative number of cells that exhibit a DNA-content of 8C or more. Raw data in attachment A R-29, A R-30.

IV. Discussion

This work aimed at the identification of regulators of COP1-controlled morphogenesis in *A. thaliana*. Candidates from YTH-screening were selected according to their potential of being a target, co-factor or regulator of COP1. A target specific gap repair approach and the generation of a COP1 and DET1 based network indeed identified a new target of COP1 – PAP2 - involved in anthocyanin biosynthesis and MID, a regulator of COP1 connecting photomorphogenesis and endoreduplication by physical and genetical interaction with COP1.

PAP2 and MID were the only interaction candidates of COP1 that were analysed in detail out of the screening results and for which a function was predicted that could be supported with strong evidence presented in this work. The screening results revealed three other fields that should be subjected to detailed analysis in the future as they also have the potential to contribute to a more general understanding of the COP1 function:

(1) Brown and co-workers (2005) showed that UVB-RESISTANCE 8 (UVR8) associates with chromatin. COP1 interacts with UVR8 (Favory et al., 2009). In humans, COP1 regulates for example the stability and function of MTA1 (Metastasis-associated protein 1), a component of the nucleosome remodelling and histone deacetylation complex (NuRD) (Li et al., 2009). There is also evidence for tomato DET1 binding to the N-terminal tail of histone H2B and an involvement in chromatin remodelling was proposed (Benvenuto et al., 2002). For *MID*-mutants, chromatin remodelling as well as silencing defects were observed (Breuer et al., 2007; Kirik et al., 2007). Binding of COP1 to histone H1.2 and MID might therefore position COP1 in a new interesting context. The generation and repair of double strand breaks (DSBs) is also a promising aspect to be investigated in the future. PRD3 (PUTATIVE RECOMBINATION INITIATION DEFECTS 3) was recently described to be necessary for creating DSBs (De Muyt et al., 2009) as well as RHL2 (ROOT HAIRLESS 2, AT5g02820) or SPO11-3 a constituent of TOPOVI whose homologues SPO11-1 and SPO11-2 functions during meiosis. *Mid* mutants exhibit, like *cop1*-mutants, an increase in DSBs (Breuer et al., 2007; Dohmann et al., 2008). In concert with one of the interactors of this group, COP1 might directly be involved in DNA modifying processes and cell cycle progression. This involvement of COP1 might be by marking essential proteins for degradation or by being regulated by cell cycle associated proteins. Thereby, COP1 could contribute to the communication between cell cycle and photomorphogenesis *in planta*.

(2) Most likely new signal transduction functions of COP1 in the light will also be found by interactions with cytoplasmatic proteins as COP1 is localised to the cytoplasm in the light. RPP4 with its Toll-Interleukin receptor domain (van der Biezen et al., 2002) might be involved in one of these aspects in concert with COP1 in pathogen response and the corresponding transcriptional regulation. Beside RPP4, COR27, SYT1 and NUDIX7 might be involved in signal transduction pathways differing from the light-signal transduction but also being regulated by COP1, thereby suggesting that COP1 is a factor integrating different signal transduction pathways.

(3) An essential step to be unravelled in future studies will also be the light dependent nuclear export and import of COP1. For COP1 it is known that the protein follows a mechanism of nucleocytoplasmic partitioning that by far lags the speed of COP1-inactivation. In rice, importin α 1B has been identified as a protein being involved in the nuclear import of COP1 (Jiang et al., 2001). For *A. thaliana* it is suggested that importins do not play a major role in nuclear import but rather cytoskeleton associated proteins are involved. CIP1, a cytoplasmatic, cytoskeleton associated interactor of COP1 is a candidate for mediating the nuclear import of COP1 in *A. thaliana* (Matsui et al., 1995). Finally, the COP9-signalosom has been shown to be essential for the nuclear localisation of COP1 with CSN1 that has recently been reported to directly interact with COP1 (Wang et al., 2009). As an example, for two screening candidates a literature based prediction of their function is presented to show the potential of careful candidate selection from YTH screening results:

1. COP1 interaction candidates connect COP1 to the Ran-cycle

Small proteins can diffuse through nuclear pores, whereas large proteins need to be recognised by their nuclear localisation signal and can diffuse with the help of nucleoporins into or out of the nucleus. This is organised by the Ran (Ras-related nuclear protein), a protein of the Ras superfamily, that has been well analysed in euklaryotes. Ras were first identified as oncogenes responsible for cancer-causing activity of two viruses (Harvey and Kirsten virus) (Chang et al., 1982). Previously, Jennifer Harvey and Werner Kirsten found these viruses originally in rats resulting in the name for Ras from Rat sarcoma (Harvey, 1964; Kirsten et al., 1970).

The small GTPase (Guanosine-triphosphate) Ran is a soluble G-protein that is homologous to the alpha subunit of G-proteins. In contrast to the latter, it can function on its own. G proteins are in their active state, when bound to GTP. Hydrolysation of GTP to GDP (Guanosine-diphosphate) renders the G protein inactive. GDP is finally exchanged to GTP and the cycle can begin anew.

Therefore, G proteins can be considered as molecular switches. Ran, as well as other G proteins, has a very low intrinsic GTPase activity and needs the help of GAPs (GTPase activating proteins) and GEFs (Guanine nucleotide exchange factors) for GTP hydrolysis and GTP exchange, respectively. (Berg et al., 2002; Bischoff et al., 1994; Bischoff and Ponstingl, 1991).

RanGAPs in turn are activated by RanBP1 (Ran-binding protein 1) (Takai et al., 2001). In mammalia and mouse. RanBP1 inhibits the GEF activity of RCC1 (Regulator of chromosome condensation 1) (Bischoff et al., 1995). AtUVR8 exhibits homology to RCC1 but did not show GEF activity with the tested Ran proteins (Brown et al., 2005).

RCC1 is localised to chromatin and converts RanGDP to RanGTP (Ohtsubo et al., 1989). In contrast, RanGAP acts in the cytoplasma and is associated to the nuclear pore complex (NPC). This creates a RanGTP/RanGDP gradient across the nuclear envelope (Gorlich and Kutay, 1999; Kalab et al., 2006). For nuclear import, a cytoplasmic cargo protein harbouring a NLS is bound by importin α, that in turn is bound by importin β that mediates the recognition by the NPC. With the help of chaperonins the cargo/importin α/β trimer is relocalised to the inner part of the nuclear envelop where RanGTP competes with importin α for the binding to importin β and succeeds as it is highly abundant in the nucleus. The importin α/RanGTP heterodimer diffuses to the cytoplasm where RanGAP activates the intrinsic GTPase activity of Ran with the help of RanBP1. Conformational changes releases importin α. RanGDP is recycled to the nucleus and GEFs convert RanGDP to RanGTP. A new cycle can begin. The mechanism for nuclear export is similar. It begins with a cargo/exportin/RanGTP trimer that diffuses to the cytoplasm. RanGAP releases the cargo and exportin and RanGDP are recycled back to the nucleus where Ran-GDP is converted by GEFs to RanGTP. (Figure IV - 1)

Ran not only functions in transporting RNA and proteins through the NPC but is also involved mitotic spindle assembly and nuclear envelope reassembly after separation of chromosomes in mitosis. In case of the function in cell cycle progression, RanBP1 and RanGAP facilitate the attachment of spindle fibres to the chromosomes in an indirect manner. Importin binding inhibits spindle assembly factors. RanGTP releases them in a similar mechanism to cargo release in the nuclear im- and export cycle. (Gorlich and Kutay, 1999; Moore and Blobel, 1993; Zhang and Clarke, 2000; Zhang and Clarke, 2001; Zhang et al., 2002)

Most elements of the Ran-cycle are conserved and functional in plants. (Ballas and Citovsky, 1997; Haizel et al., 1997; Hicks et al., 1996; Jiang et al., 1998a; Jiang et al., 1998b; Nemeth et al., 1998; Smith et al., 1997; Smith and Raikhel, 1999; Vernoud et al., 2003) (Ma and coworkers (2007)).

AtRanBP1 interacts with Ran (Haizel et al., 1997). RanBP1c is involved in auxin-induced mitotic progression (Kim et al., 2001), is primarily localised to the cytosol, is a co-activator for RanGAP in vitro and inhibits EDTA induced release of GTP from Ran (Kim and Roux, 2003). Finally AtRanGAP showed differences to its animal counterparts. The binding domain to the nuclear envelope differs and is localised to the N-terminus instead of the C-terminus and it localises to the cell plate during division that is not present in animals (Jeong et al., 2005; Matunis et al., 1996). AtRanGAP1 has been shown to localise to the mitotic spindle during cell division (Matunis et al., 1996). A functional RCC1 has so far not been identified in *A. thaliana*. One can summarise that the Ran-cycle-coupled nucleocytoplasmic transport is conserved in plants during interphase with some modifications and probably differing functions of Ran due to the different cell division procedure in plants.

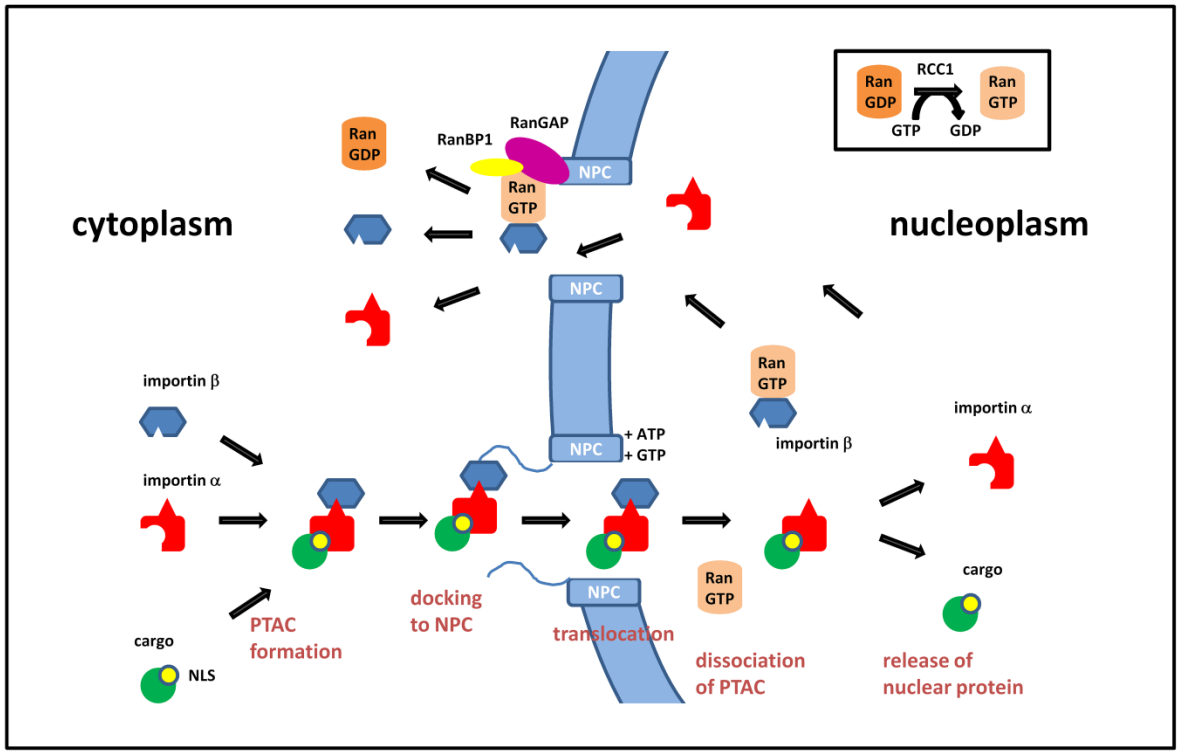

Figure IV - 1: Schematic representation of nuclear import as an example of the Ran cycle. Inset: Predominant conversion of RanGDP to RanGTP by RCC1 in the nucleus. PTAC: nuclear pore-targeting complex; NPC: nuclear pore complex; NLS: nuclear localisation signal; RanGAP: Ran GTPase activating proteins; RanBP1: Ran BINDING PROTEIN 1; RCC1: Regulator of chromosome condensation 1. See text for details. Modified from Yamamoto and Deng, 1999.

A so far uncharacterised candidate for a COP1-associated RanGAP - At5g51730 with homology to AtRanGAP1 (alignment is shown in A R-1) – and a candidate harbouring a RanBP1 domain - At4g11790 - have been identified in the COP1 YTH screenings. In addition alignments for At5g51730 have shown similarity to two other proteins harbouring the reduced AtCID-motif identified in this work and are therefore also putative interactors of COP1 (At1g10740 and At1g23330 in Figure III – 22

and attachment A R-1). In the alignments of human proteins carrying the AtCID motif Importin α 3 has for example been found as a candidate for the nuclear import of COP1.

The *A. thaliana* candidates should not only be analysed as putative nuclear export or import factors for COP1 but also as factors that might be involved in spindle assembly during mitosis. If these proteins are targets of COP1 the consequence of their degradation would be a reduced release of spindle assembly factors and therefore an inhibition of mitosis can be concluded providing COP1 with a link to the cell cycle. If a halt in the cell cycle also correlates with the alternative of endoreduplication for the cell, this could explain endoreduplication defects of the *cop1* mutants, exhibiting less endocycles in the dark grown hypocotyls (Gendreau, 1997).

2. PRODUCTION OF ANTHOCYANIN PIGMENT 2 (PAP2)

Accumulation of anthocyanin has been observed in response to stress conditions such as UV-light, nutrient depletion and low temperature (Cominelli et al., 2008; Lillo et al., 2008; Olsen et al., 2009; Rowan et al., 2009; Teng et al., 2005; Winkel-Shirley, 2001). Anthocyanin protects cells from high light damage and mediates tolerance of limiting nitrogen conditions (Peng et al., 2008; Takahashi et al., 1991). At least four classes of transcription factors are involved in the regulation of anthocyanin biosynthesis in *A. thaliana*: bZIP, MYB, bHLH and WD-40-repeat.

PAP2 (At1g66390) is a R2R3-MYB protein with high homology to PAP1 (PRODUCTION OF ANTHOCYANIN PIGMENT 1, At1g56650). Both proteins exhibit 93% identity in their MYB domain and, 77% overall identity (Figure IV - 2; Borevitz et al. 2000). MYB domains in c-Myb from vertebrates consist of up to three imperfect repeats named R1, R2 and R3 (Ogata et al., 1994). Repeats in other species are referred to according to their sequence similarity to one of the three repeats. The R2R3 repeat represents the minimum DNA-binding domain and has been described as plant specific (Braun and Grotewold, 1999; Klempnauer and Sippel, 1987; Kranz et al., 2000; Sakura et al., 1989). Stracke et al. (2001) found a consensus motif present in most R2R3-type MYB domains from *A. thaliana* (Figure IV - 2).

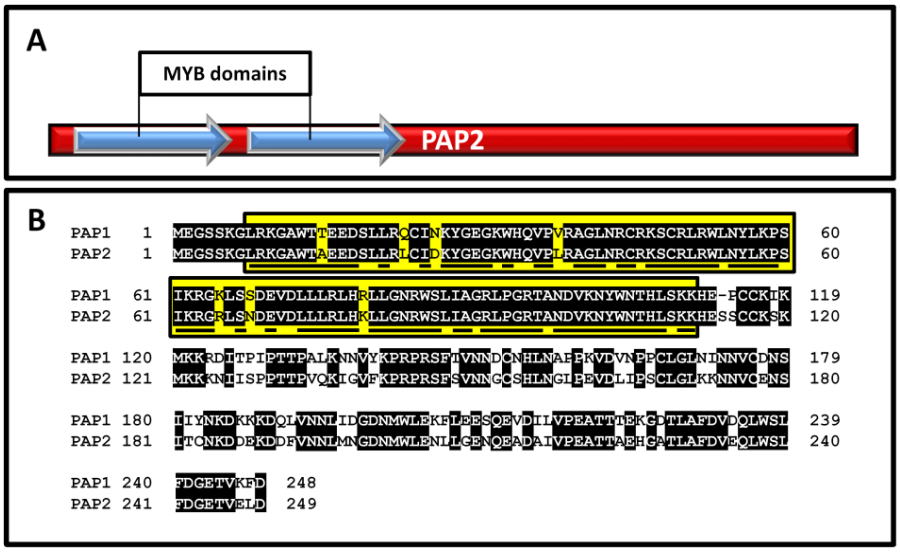

Figure IV – 2: R2R3 MYB domain of PAP1 and PAP2. (A) Schematic representation of the R2R3 MYB domain of PAP2. Blue arrows: R2 or R3 MYB repeat (B) Amino acid sequence alignment of PAP1 and PAP2. Sequences were obtained from TAIR (www.arabidopsis.org). Black boxes: identical amino acids; yellow boxes: R2 or R3 MYB repeat determined by the consensus sequence (underlined) given by Stracke et al. (2001).

PAP1 and PAP2 activate the *DIHYDROFLAVONOL 4-REDUCTASE* (*DFR*) promoter in concert with ENHANCER OF GLABRA3 (EGL3), GLABRA3 (GL3) or TRANSPARENT TESTA8 (TT8) (Zimmermann et al., 2004). *DFR* is one of the late genes in anthocyanin biosynthesis (Nesi et al., 2000).

PAP1 was originally identified through activation tagging experiments. The *pap1-D* line from the Weigel collection overexpressed PAP1 and showed an up-regulation of a broad range of activated late and early anthocyanin biosynthesis genes (Borevitz et al., 2000; Weigel et al., 2000). PAP2 was identified by sequence comparison. Plants over-expressing PAP2 exhibited a similar but milder phenotype than the *pap1-D* mutant (Borevitz et al., 2000). Recently, Gonzales and coworkers (2008) showed that overexpression of MYB113 and MYB114 leads to a *pap1-D*-like phenotype. In RNAi lines targeting all four mentioned MYB-genes, the TTG1/EGL3 regulated anthocyanin biosynthesis genes and the targeted Myb genes were down-regulated (Gonzalez et al., 2008). Genetic analysis revealed that the function of PAP1, PAP2, MYB113 and MYB114 is dependent on bHLH transcription factors - predominantly on EGL3 - and TTG1 (Gonzalez et al., 2008) suggesting that they act in a WD40/bHLH/MYB complex.

Here, PAP2 has been identified as an interactor of COP1. PAP2 can share a complex with COP1 *in planta* as was shown by Co-IP from infiltrated *N. benthamiana* leaves. A modification of YFP-PAP2 resulting in a 17 kDa shift on an SDS-PAGE gel was shown to be most likely due to ubiquitin. Because of the size it is expected that PAP2 is di-ubiquitylated. Mono-ubiquitylation has been reported to be

able to stabilise proteins. In case of PAP2, this does not seem to be true. When expressed together with RFP-HA-COP1 the concentration of YFP-PAP2 in the input fractions and after IP was always lower than when co-expressed with RFP-HA-attB1. This points to a possible ubiquitylation by COP1, thereby indicating that PAP2 is a target of COP1. In the case of COP1, two bands on the western blot were identified that correspond to RFP-HA-COP1 and are ubiquitylated. An unubiquitylated species of COP1 has not been identified, suggesting that COP1 is either mono- and di-ubiquitylated or mono-ubiquitylated and carries an additional modification while interacting with PAP2. Taken together, if the ubiquitylating activity of COP1 towards PAP2 can be proven in the future, one can conclude that COP1 is ubiquitylated in its active state concerning ubiquitylation of PAP2. The modifications should be identified by mass spectroscopy in further experiments.

The used constructs showed to be functional according to the enhanced production of anthocyanin when overexpressing YFP-PAP2 in *A. thaliana* or *N. benthamiana* but detection by the means of fluorescence microscopy was difficult in *A. thaliana* because of weak YFP signals. Surprisingly, YFP-PAP2 exhibited different types of localisation in infiltrated leaves of *N. benthamiana* indicating that subnuclear YFP-PAP2 is complex regulated.

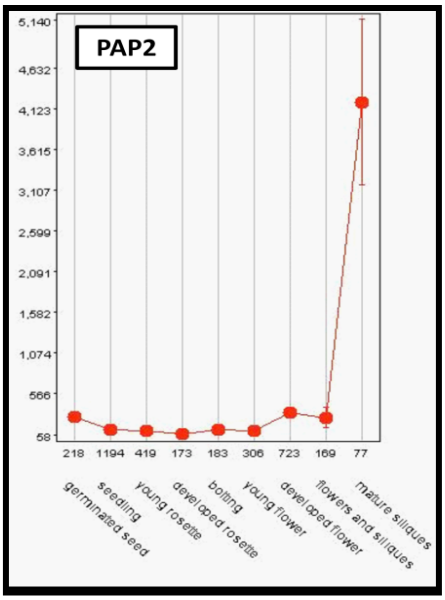

Figure IV - 3: Expression profiles of PAP1 and PAP2 in the different depicted developmental stages. Vertical axis: expression intensity in arbitrary units. The expression profiles were obtained from GENEVESTIGATOR (Hruz et al., 2008; Schmid et al., 2005).

Also expression of *PAP2* seems to be strictly suppressed in most stages of plant development and increases dramatically in the senescence and seed maturation stage of plant development (Figure IV - 3). Nitrogen depletion induces a strong up-regulation of *PAP2* (900-fold in leaves in comparison to 6-fold for *PAP1*) (Lea et al., 2007). In seedlings, a strong induction of transcription by white light was

found for *PAP1* and *PAP2* with *PAP1* preceding *PAP2* concerning to kinetics (Cominelli et al., 2008). Although much progress has been made in determining transcriptional regulation of *PAP1* and *PAP2*, so far, nothing has been known before about the post-translational regulation of these proteins in contrast, for example, to the bZIP transcription factors HY5 and HYH, as was described before.

Domain mapping with GARFILD identified the PAP2 domain responsible for the interaction with COP1. This domain contained the AtCID sequence at its C-terminus. The functionality and applicability of the GARFILD method has been shown by the mapping of the R2R3 MYB repeat of PAP2 for the published interaction with EGL3. As PAP2 is autoactivating in yeast, GARFILD bait libraries of COP1 have to be constructed for domain mapping, existing COP1 fragments from other screenings could be recombined into bait vectors alternatively or defined domains could be selected in the case of COP1 as a well characterized protein in contrast to PAP2 providing a rough mapping.

In contrast to the other AtCID-motif containing transcriptionfactors (HY5, HYH, STO, STH) PAP2 seems predominantly to respond to lack of nitrogen than to light. It will be of great interest to elucidate the role of COP1 in the post-transcriptional regulation of this senescence and nitrogen-response-specific protein adding a stage of plant development to the COP1-controlled morphogenesis that has not been investigated intensively before.

3. GARFILD - Gateway®-compatible random fragments YTH in frame library screening for domain mapping

Several methods for random fragmentation of DNA have been developed and applied, so far. DNA is fragmented by the use of enzymatic, physical or PCR-based methods for example DNaseI digestion (Anderson, 1981), exonuclease III (Exo III) truncation (Henikoff, 1984), hydrodynamic shearing (Oefner et al., 1996) or the use of tagged random primers (Grothues et al., 1993; Kawasaki and Inagaki, 2001). Typically, the obtained fragments are ligated into vectors for subsequent screening procedures or vectors are religated after fragmentation. For example, J. Hackbusch has developed a vector for expression in yeast, named pACT-Del, which uses Exo III truncation (Hackbusch, 2004). This vector allows selective generation of N- or C-terminal fragments of the corresponding protein.

Concerning domain mapping, these methods exhibit several weak points that were the criteria for the development of GARFILD: (1) All methods are based on ligation steps and therefore primer design is necessary for subsequent Gateway® recombination. This is of particular interest as a growing number of vectors that can be used for *in planta* verification are Gateway® based. In

addition, the Gateway recombination is a fast and reliable method for simultaneous recombination of several DNA fragments. (2) Two third of all C-terminal fragments are lost due to frame shifts. This would reduce the complexity of the generated libraries. (3) For some methods, cloning has to be undirected. Again, this would result in reduced library complexity. (4) Ligation can produce combinations of more than one fragment in one vector. The domain might not be properly mapped in such a case. (5) In most cases, additional amino acids are added to the C-terminus of the protein due to lacking stop codons. The additional sequence might influence the binding behaviour especially of small fragments. (6) Only the use of primers allows further flexible attachment of small tags, restriction sites or stop codons. GARFILD already proved to be a flexible method that can circumvent these disadvantages of existing methods for random fragmentation in regard of domain mapping.

Several modifications of GARFILD have already been successfully applied following the experiments of this thesis: Random primers with a short *att*L1 or *att*L2 tag were created that allow a direct LR recombination reaction and therefore supersedes the BP-reaction in which complexity can be lost. Additionally stop codons in all three frames have been attached with these primers. GARFILD middle libraries have been constructed by preparing C-terminal fragments from N-terminal libraries and vice versa. The volume of the mating culture has been successfully reduced to 400 µl in plastic 24 well-plates. Bait libraries have been constructed by the use of 5`FOA and a yeast strain that eliminates auto-activating fragments from the library. The listed modifications still need optimisation. Especially the construction of libraries from long templates needs to be optimised. In the future, BiFC and Co-IP vectors for verification *in planta* should be constructed in all three reading frames, probably with *att*P-sites to allow a direct BP from the Colony PCR product of the shortest identified fragment. A second round of domain mapping should be applied with the so far rough mapped interaction domains. In the case of PAP2 site directed mutagenesis experiments should be performed as a next steps concentrating on Glu^{220} that corresponds to Asp^{246} of STO. Taken together, GARFILD has proven to be able to overcome most problems for random fragments based domain mapping.

All four applications of GARFILD in this work were successful although the mapping is still rough in some cases. The application of EGL3 with PAP2 libraries provided a proof of principle. In the case of MID, the interaction domain of COP1, a so far well characterised protein, has never been proposed before to mediate interactions. For the self association of COP1 it has been shown that isolated domains are not necessarily needed as a whole. Finally, mapping of the PAP2 domain responsible for interaction with COP1 exemplified how a so far unknown protein region can be quickly mapped with

this method. On the one side, the reliability of the method was show and on the other side the power of combining GARFILD and *in silico* analysis was proven.

The identified reduced conserved motif named AtCID motif in PAP2 has been found in several other proteins from *A. thaliana* and also in the human interactor of hCOP1 cJun. (III. 2.3.4) In addition a transcription factor that associates with cJun, cFos, has been shown to carry the hCID motif. One of the most interesting *A. thaliana* proteins carrying the AtCID is FAS1 which is part of a chromatin assembly factor. *FAS1* has been shown to genetically interact with *MIDGET* (Kirik et al., 2007). But also the other proteins are worth to be tested for their interaction with COP1. ARABIDOPSIS RHOMBOID-LIKE PROTEIN 14 (ATRBL14) surprised for example by carrying exactly the same AtCID like HYH. Proteins from different functional processes were identified that exhibit the AtCID or hCID motif. Several proteins involved in GTPase signalling were found like ATRBL14 (with a RanBP2 domain), the human proteins RAP1 (Ras-proximate-1) GTPase activating protein (RAP1GAP), RAP1 GTPase activating protein 2 (RAP1GAP2) Rho GTPase activating protein 31 and 32 (ARHGAP31, ARHGAP32) and DOCK11 (a member of a GEF (guanine nucleotide exchange factor) family). Even if the domain can mediate interaction in all these proteins, the possibility of masking has to be taken into consideration. Further interaction analysis will show if this reduced motives (AtCID and hCID) are functional not only in *A. thaliana* but also in human and if these motives are sufficient to predict new COP1 interactors maybe with restrictions of the hydrophobe amino acid.

Screening of random fragment libraries for domain mapping has the advantage that in a living eukaryotic system only those fragments wil appear as interacting fragments that are properly folded in the cell and mediate interaction. This cannot be planned easily by in silico analysis especial for proteins with no annotated domains. In case of the cop1 mutants the problem of proper folding is exemplified by two *cop1* mutants. A mutant, which has an amino acid substitution in the WD40 domain, was classified a strong mutant. A weak mutant turned out to have a truncated COP1 protein that lacks the complete WD40 domain. Another striking advantage of GARFILD is the combination of YTH screening results of a hub in an interaction network in combination with GARFILD libraries of this hub protein, tremendously speeding up the procedure from the identification of candidates to the domain mapping of the interaction domains and finally to the verification *in planta* for various candidates in parallel.

4. MIDGET and TOPOVI regulate COP1 activity

MID is an essential component of the TOPOVI that is essential for endoreduplication in *A. thaliana* (Breuer et al., 2007; Kirik et al., 2007). TOPOVI exhibits a structurally based homology to archaea type II B topoisomerase that can induce double strand breaks (DSB) and religate the DNA after the passage is completed (Bates and Maxwell, 2005). TOPOVI of *A. thaliana* consist of an A_2B_2 heterodimer that is homologous to the type II B class topoisomerases of archaea (Bergerat et al., 1997; Champoux, 2001). The homology was mainly based on structural homology determined by Corbett and Berger (2003) for TOPOVI. The A subunit in *A. thaliana* - RHL2 - harbours the domain for DNA cleavage, whereas in the B subunit - AtTOP6B - the ATPase domain can be found. It was shown that AtTOP6B and RHL2 can interact and thereby form a functional TOPOVI (Hartung et al., 2002; Hartung and Puchta, 2001). Interaction analysis revealed that MID is connected with the core TOPOVI components RHL2 and AtTOP6B via RHL1 and probably can directly interact with RHL2 (Breuer et al., 2007; Kirik et al., 2007).

Based on YTH screenings with COP1 and DET1 a network was created in this work positioning MID in a frame with SPA1 and DET1, two COP1 function modifying proteins, that share complexes with COP1 (Zhu et al., 2010; Nixdorf and Hoecker, 2010). MID is the only candidate obtain from YTH screenings in this work that connected to other proteins in the COP1-DET1-interaction-network.

Figure III - 4 shows that MID, COP1 and SPA1 form a triangle, the simplest geometrical form that can be found in an interaction network (Milo et al., 2002). 92% of the triangles in the yeast interactome represent known protein complexes (Yeger-Lotem et al., 2004). In plants the percentage will be much lower due to localisation to different cell compartments and due to different expression profiles of proteins, that interact in yeast but do not necessarily need to colocalise and thereby might never interact with each other *in planta*. Therefore additional analysis *in planta* is needed.

In the network, MID is not only connected with COP1 and SPA1 but also indirectly connected with DET1 via ACT7 and MIAP2. Based on results from this work the network can be extended by providing links for COP1 and SPA1 with MID, RHL1 and AtTOP6B, whereas the interaction of MID with COP1 has been verified *in planta* and in this work.

YTH results with full length COP1 or with $COP1^{1-67}$ that was first identified in a GARFILD screening with MID – and additional BiFC results could connect COP1 with MID, RHL1 and AtTOP6B. Due to auto-activation of the RHL2 construct, results from yeast for RHL2 could not be evaluated in this

work. Connection of SPA1 with MID and RHL1 was solely based on BiFC results so far. Mass spectroscopy analysis indicated that MID can share a complex with phyA as well as with CHR11

BiFC signal localization to distinct subnuclear foci of MID-fragments in combination with COP1 and SPA1 indicating that the most essential portion of MID mediating the interaction with COP1 and SPA1 is located in the overlap of MID^{1-260} and $MID^{220-330}$ (Figure III - 34).

As expected, MID interacts with COP1 and $COP1^{K550E}$ indicating that it is no target that interacts with COP1 in a STO/STH like manner (Holm et al., 2001). This was further substantiated by the identification of the first 67 amino acids of COP1 as the interaction domain for MID. This N-terminus does not include any known domain of COP1 and thereby has the potential to unravel new functions or regulative aspects of COP1. RHL1, that interacts with MID, probably stabilises COP1 or shows a bridging effect in the Yeast Three Hybrid assay as yeast harboring Gal4-BD and AD-fusions of COP1 grew similarly on plates lacking methionine. This was not observed for any other combination. GFP expressed by the Pro*Met25* in combination with all tested candidates in the Yeast Three Hybrid assay is needed to allow a reliable interpretation of the results.

Mid and *topoVI* mutants exhibit several *cop1* mutant phenotyps. Especially *rhl2* and *hyp 6* have shown a germination effect. In the darkness, they have shorter hypocotyls, slightly open cotyledons, accumulate anthocyanin and express CHS a light-regulated gene. In contrast to cop1-4 the cotyledons are yellowish and not almost white as in cop1-4. When grow on MS lacking sucrose *mid* and *topVI* mutants have wide open cotelydons and they develop their first true leaves on MS plates supplemented with 1% MS. This might not simply be a sugar effect but also might be due to the seedcoat defect observed for *mid* mutants that leads to a reduced germination efficiency of the seeds. Three other overexpressor lines and a mutant, respectively, have been found in literature exhibiting a very similar when grown in the dark on plates. Unfortunately, the authors did not give the sucrose concentration used for these plates. The mutant is *det1-1* and the overexpressor lines are CCT1 and CCT2 the lines overexpressing the C-terminus of CRY1 and CRY2 that constitutively inhibits COP1. This leads to the conclusion that these proteins might act in similar pathways with MID/TOPOVI together or as antagonists. The phenotype caused by constitutive inhibition of COP1 by the CRYPTOCHROMES resembles the phenotype of the loss of function *mid* and *topoVI* mutants in the dark. Indicating that MID/TOPOVI are needed for sufficient COP1 activity. Together with the enhancement of the *cop1* mutant phenotype in double mutants with *mid, rhl2* and *hyp6*, one can conclude that MID and the TOPOVI are essential for proper COP1 activity in the dark. Interaction

studies showed that these proteins can be in one complex in the plant cell with SPA1 and / or DET1 also contributing to this complex / these complexes and cryptochromes possibly inhibiting the same activity of COP1 that is activated by DET1 and MID. In further experiment the possibility of complex formation and genetic analysis should be performed for CRY1, CRY2, DET1, MID and the TOPOVI proteins and genes. This is another hint positioning MID upstream of COP1 in a regulative context.

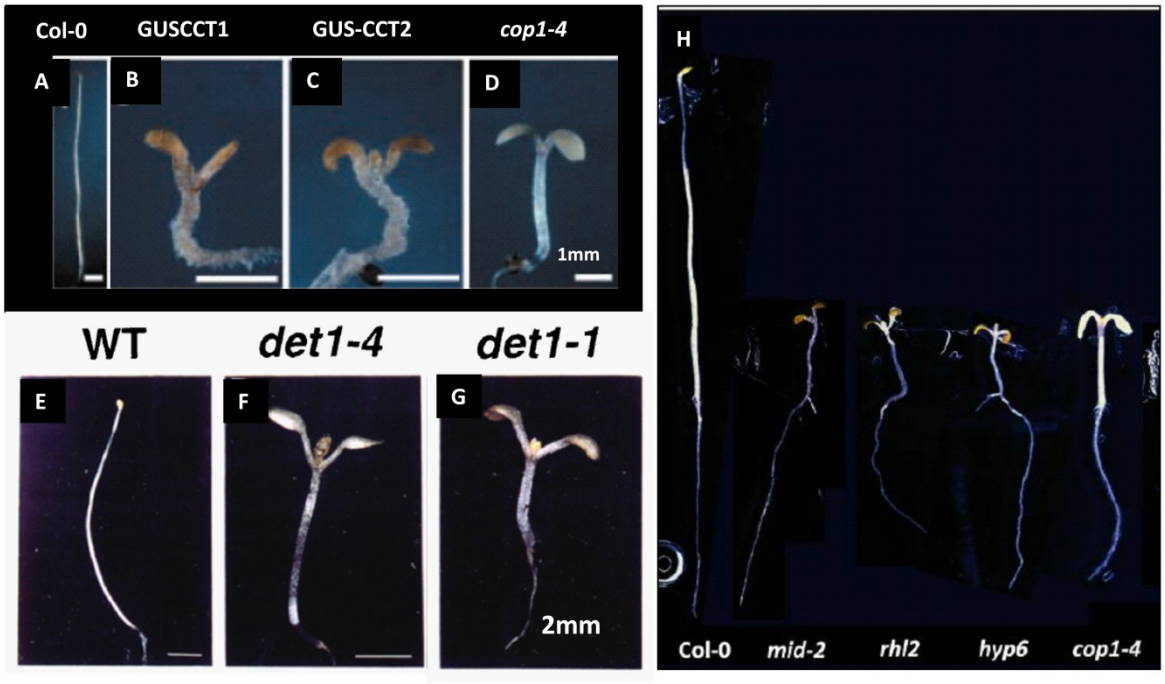

Figure IV-4: CCT1: Comparison of dark grown seedlings. **(H)** 1% MS for the other seedlings no sugar conditions were given. C-terminus of CRY1 , CCT2: C-terminus of CRY2 **(A-D)** were taken from Wang et al. (2001); **(E-G)** were taken from Pepper et al. (1994); (H) see Figure III - 42; plants in F and G have the same magnification; all seedlings in H were photographed at the same magnification.

Strikingly, Alexander Maier could detect only very low concentrations of COP1 in *mid* mutants in dark-grown seedlings and light-grown adult plants (personal, preliminary information) although the expression levels were not significantly altered in comparison to the wildtype (Figure III-57). This leads to the conclusion that MID is essential to stabilise COP1 and provides an explanation for the *cop1* mutant phenotypes in *mid* and the *topoVI*. As also the *topoVI* mutants exhibit this phenotype it can be concluded that the function of MID in stabilising COP1 is in a TOPOVI-dependent context.

5. Linking endoreduplication with photomorphogenesis

Endoreduplication is the main function that is attributed to the TOPOVI today. The *mid* mutants are dwarf with small organs (Breuer et al., 2007; Kirik et al., 2007). Small organ size can be due to a reduced cell expansion or to cell proliferation. No severe difference in the cell number but in cell size

was observed especially for endoreduplicating cell types (Breuer et al., 2007). This results in a shortened hypocotyl, small leaves, reduced trichome size and branching as well as less and shorter root hairs in comparison to the wild type (Kirik et al., 2007). FACS (fluorescence activated cell sorting) analysis revealed an endoreduplication defect (Breuer et al., 2007; Kirik et al., 2007). Leaf cells of *mid* mutants grown under LD conditions complete a maximum of two endocycles (8C) whereas in the wildtype three to four endocycles (16C, 32C) can be observed (Kirik et al., 2007). Tetraploidy of *bin* mutants achieved by colchicine treatment could only partially rescue the organ size (Breuer et al., 2007). This indicates that the dwarfism is partially due to the reduced DNA content in *mid/bin* mutants.

Already during germination two endocycles take place in the dark-grown hypocotyl and the third cycle, that is specific to dark-grown hypocotyls, is completed very early during cell growth. PhyA inhibits the third endocycle in dark-grown hypocotyls (Gendreau et al., 1997). In plants, a correlation between cell size and endoreduplication has been observed (Melaragno et al., 1993). In contrast, the *cry*1 mutants exhibits a three-fold longer hypocotyl in B than the wildtype without significant change in DNA-content, indicating that cell size and endoreduplication is not strictly coupled. (Gendreau et al., 1998) This could also explain why the CRY overexpressor lines shown in Figure IV - 4 are eve smaller than *cop1-4*. Hypocotyls of cop1-4 mutants have a short hypocotyl and reduced endocycle number and therefore C-content in the dark (Gendreau et al. 1997 and Figure III - 53, 59). Cry mutants in contrast, have a longer hypocotyl than the wildtype but no enhance C-contents. In the cry mutants the opposing effect might take place. No change in endocycles in comparison to *cop1-4* but reduced cell-expansion. A longer hypocotyl does not necessarily consist of longer cells. This was also shown in this work for the *hy5-215* mutants that exhibit hypocotyl length as the wildtype but have very low C-contents. It was observed, but needs to be statistically analysed in further experiments, that the cells were much dramatically shorter than in the wildtype, suggesting that HY5 inhibits cell division in the wildtype. The low C-contents in the mutant might be due to time restrictions that do not allow endocycles to complete in rapidly dividing cells in the *hy5-215* hypocotyl. Dohmann et al (2008) stated a G2 arrest for *csn* mutants. This is not the case in *mid* and *topoVI* mutants, indicating together with the results of *hy5-215* around the COP1 protein different types of endoreduplication and cell cycle modulation are present. One can suggest, that COP1 might have a checkpoint function in the decision for or against endoreduplication. Endoreduplication might be indirectly activated by a change in transcription factor activity or by MID and TOPOVI allowed to take place even above 2 rounds of endocycles. It is tempting to speculate that interaction of a functional TOPOVI complex might activate or stabilize COP1 and therefore change the abundance of endocycle-specific

transcription factors. If COP1 in turn stabilizes TOPOVI or degrades its components upon receiving other signal possibly vie the DNA-damage response pathway, it could act as such a checkpoint and allow endoreduplication only when the level of DSB is not too high. Nevertheless, a secondary effect of DNA-damage occurring as a result of inproper endocycle-related DNA packaging is more likely in the *mid* mutant:

Plants have a mechanism to arrest their cell cycle upon DNA stress. Activation of this checkpoint results in activation of DNA-damage response genes and inactivation of genes responsible for mitosis and cytokinesis (Chen et al., 2003; Culligan et al., 2006). As an exception, CYCB1;1 is up-regulated in response to DNA-damage probably to titrate cell cycle components necessary for proceeding into mitosis (Chen et al., 2003; Culligan et al., 2006; De Veylder et al., 2007). ATM (ataxia-telangiectasia-mutated) activates the transcriptional induction, ATR (ATM- and Rad3-related) stabilises the CYCB1;1 protein (Culligan et al., 2006).

ATM/ATR dependent DNA-damage response is triggered in post-mitotic cells of *mid* mutants. DNA double strand breaks (DSB) were observed in leaves of light grown plants but not in mitotic cells of the root apical meristem. DSB-inducible genes are up-regulated in an ATM/ATR-dependent manner. Especially in differentiated post-proliferating cells, an increase of ProPARP2:GUS activity was observed. The G2/M phase specific cyclin CYCB1;1 is ectopically expressed in trichomes and elongated hypocotyl cells, cell types that do not divide anymore. This correlates with RT-PCR results showing an up-regulation of CYCB1;1. A predominant G2 arrest was concluded. A *mid* mutant trichome can overcome the cell cycle arrest by expression of CYCB1;2 under the control of the ProGL2 indicating that cells need to be in the mitotic cycle to undergo endoreduplication. It was concluded that loss of MID or the TOPOVI activate an ATM/ATR-dependent cell cycle or endoreduplication specific checkpoint. (Breuer et al., 2007; Kirik et al., 2007)

A second line of evidence supports a function of MID in chromatin condensation possibly with DET1 in one complex that has been shown to bind to the N-terminus of H2B (Benvenuto et al., 2001). A functional role in chromatin organisation and gene silencing of MID and TOPOVI was shown by Kirik and coworkers (2007). Interphase nuclei in *mid* mutants lack the typical formation of chromocenters that are highly condensed heterochromatic DNA consisting of centromeric and pericentromeric repeats and rDNA genes (Fransz et al., 2002). A synergistic phenotype of *mid* mutants and *fas1* (*fasciata*) was observed. FAS1 is the p150 subunit of chromatin assembly factor1. The mutant is affected in heterochromatin formation in non-mitotic cells (Kirik et al., 2006). Additionally the *TSI*

(*TRANSCRIPTIONALLY SILENCING INFORMATION A*) locus, normally located in a heterochromatic region, is expressed in 7-day-old *mid* seedlings (Kirik et al., 2007; Steimer et al., 2000). Breuer and coworkers (2007) did not observe an up-regulation for two week old plants. An additional link for a role in chromatin remodelling has been provided in this work by the identification of CHR11 (by Thomas Colby, group Jürgen Schmidt, MPIZ) as one of the proteins that were co-purified with MID-L*er*-YFP from dark-grown cell-suspension culture.

Taken together, it is not very likely that the only function of MID is to stabilise COP1 and the reduced levels of COP1 in the *mid/topoVI* mutant explains the photomorphogenesis-specific phenotypes but does not explain all *mid/topoVI* phenotypes - especially the trichome and roothair phenotypes that cannot be observed in *cop1* mutants (see the model in Figure IV-5).

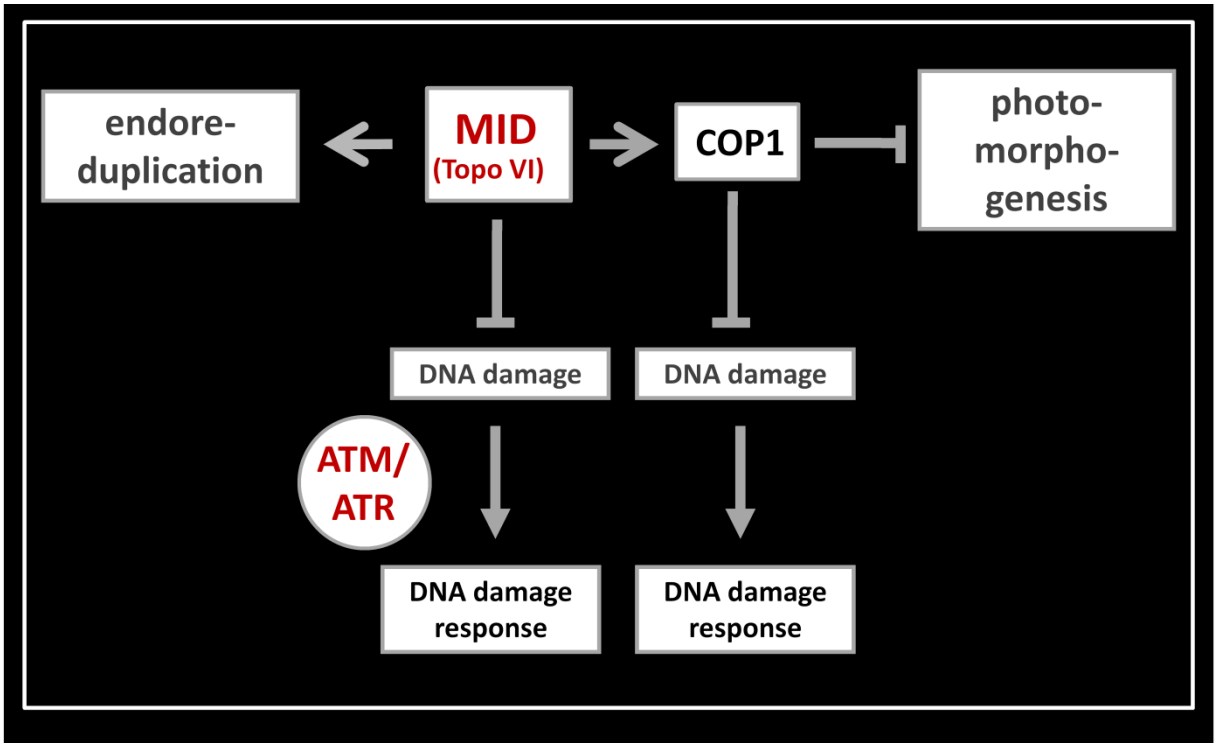

Figure IV - 5: MID stabilizes COP1. MID and the TOPOVI are essential for endoreduplication (Sugimoto-Shirasu, et al. 2005; Kirik et al., 2007) whereas COP1 suppresses photomorphogenesis. In *mid* mutants the COp1 level is decreased and therefore photomorphogenesis is not sufficiently inhibited. It has not been shown jet, if COP1 in turn can modulate TOPOVI activity or if the endoreduplication defect in *cop1* hypocotyls in the dark is *mid/topoVI* - dependent. For mutants of MID and of COP1 an up-regulation of DNA damage response has been shown. In the case of *mid* this is ATM/ATR dependent. (Dohmann et al. 2008; Breuer et al., 2007)

Probably phyA plays a role in MID-dependent endoreduplication. Similar to the situation in the mid-mutant, phyA functions in the dark grown hypocotyl to repress the third endocycle. Repression of the third endocycle is exactly what is seen for *mid* and *topoVI* mutants under different conditions.

Probably phyA is involved in the R, FR-dependent reduction of HA-MID-levels that were observed in this work for the first time and need to be verified in the future. Another influence of phyA might happen during germination as but the reduced germination efficiency might also be explained by the lacking columella of *mid* seeds (Kirik et al., 2007). This phenotype sowed to be epistatic to *cop1-4* and *spa1-100*.

Interestingly, MID expression rises at the time of bolting (Genevestigator, Hruz, etal. 2008) suggesting a function of MID in this process, that also correlates with an increase in endoreduplication in the shoot. This work showed that *mid-1* flowers early under LD conditions and late under SD conditions, whereas the double mutants with *spa1-100* flower early under both conditions.

6. MID is involved in the regulation of COP1/SPA1 controlled flowering

Under LD conditions *mid* and *topoVI* mutants flower earlier than the wildtype. This is consistent with the dependency of the COP1 stability on MID and the TOPOVI. Reduced levels of COP1 degrade less CO in the dark and therefore CO promotes flowering by enhanced FT expression. In contrast to this finding the late flowering of *mid-1* and early flowering of the double mutant *mid-1 spa1-100* under SD conditions challenges the model based solely on COP1 stability.

COP1 is thought to be predominantly active in the nucleus. In the light, GUS-COP1 is depleted from the nucleus. But also light-grown *cop1* mutant seedlings show aspects of enhanced photomorphogenesis suggesting a function of COP1 also in the light. Low levels of fluorescence tagged RFP-HA-COP1 are visible in the nucleus of overexpressing lines grown under LD conditions (Figure III-9) correlating with the observation that the nucleocytoplasmic partitioning of COP1 is a slow process. Taken together, the activity of probably small portions of nuclear COP1 in the light can be concluded.

One can assume that a very low level of COP1 can suppress bolting with some defined lower threshold. During the day, upon activation by blue light, the C-termini of activated and dimerized cry1 binds to the WD40 domain of COP1 and thereby inhibit COP1 probably by blocking the access to the WD40 domain for COP1 targets. PhyA can phosphorylate cry1. It is tempting to speculate that phyA thereby desensitizes cry1 signalling and probably could release COP1 from its cry1 dependent inhibition. Nevertheless, new COP1 is also synthesised and not all molecules will be inhibited by cry when the light intensities are reduced and in the dark. MID is needed to concentrate COP1 in

subnuclear foci in tobacco. Subnuclear foci have been discussed as reservoirs of proteins. Possibly this also holds true for *A. thaliana*. If this is the case, MID provides a reservoir of active and probably inactive (CRY1-bound) COP1 ready to be activated. In such a scenario it would be expected that COP1 constantly can dissociates from these reservoirs but also associates again, reaching a steady state level. With degradation, nucleocytoplasmic partitioning, additional activation (SPA1) and inactivation (CRY) this would provide another mode of COP1 regulation. Activation by release from CRY could release large portions of COP1 as a response to a signal, probably a light signal mediated by phyA. It is also possible that SPA1 can activate not only free COP1 but also CRY-bound COP1 by detecting targets with its WD40 domain. This process would be much less effective than with free COP1 as can be concluded from the sever phenotypes of lines over expressing CCT1 or CCT2 (Wang et al.; 2001; Figure IV - 4). Taken together this might explain the late flowering phenotype of *mid-1* mutants in contrast to the early flowering of *mid-1 spa1-100* double mutants and add to the upcoming result concerning cross-talk between cryptochromes and phytochromes.

During the day, cry is activated by blue light, dimerises and inhibits COP1. COP1 is predominantly shuttled in the cytoplasm but as this is a slow process free COP1 and cry-COP1 can be found in the nucleus. One or both forms are stabilized by MID probably by concentrating COP1 in subnuclear foci and preventing thereby a quick depletion of COP1 from the nucleus. Some COP1 molecules will dissociate from the complex and fulfil their function probably also in concert with MID but the effect is not comparable to the situation in darkness. At the end of the day no new activated cry titrates active COP1 from the nuclear COP1 pool and concentrated nuclear COP1 might be released from cry or from the subnuclear foci upon changing light signals via phyA and probably SPA1. This leads to higher active amounts of COP1 protein in the dark that acts in concert with SPA1 to degrade CO and thereby inhibit flowering. The regulation in the morning will not be considered in this model. In mutants lacking MID (*mid-2*) or expressing only its N-terminus (*mid-1*) COP1 levels are reduced and therefore the nuclear available COP1-pool might be close to the threshold for the suppression of CO activity. Under LD conditions a higher amount of COP1 is inactivated by cry during the day. A release during dusk at the onset of the night is reduced or does not happen as MID is not concentrating COP1 in subnuclear foci. Therefore *mid-1* mutants bolt early under LD conditions. An additional lack of SPA1 protein enhances the described effects or contributes equally to them when SPA1 is acting in concert with MID in its presence. This explains the early flowering phenotype of the double mutants at LD conditions. The situation under SD conditions is different. The available time for inactivating COP1 is much shorter for cry in comparison to LD conditions and therefore less molecules in total are inactivated in a cry-dependent manner. This leads to a higher nuclear pool of free COP1 than under

LD conditions. It has to be assumed that low amounts of free COP1 are sufficient for its function in suppressing flowering. Comparably higher levels of free COP1 might be reached in *mid-1* than in the wildtype although the total COP1 levels are much reduced in the mutant due to lack of titrating activity of MID that is present in the wildtype. Consequently, this results in late flowering for *mid-1*. The earl flowering of *mid-1 spa1-100* can be explained by an essential role of SPA1 activating low levels of COP1 to reach levels of active COP1 protein above the discussed threshold. Another possibility is that SPA1 acts by its proposed role in releasing COP1 from the cry dimers in co-action with phyA. A residual activity of cry-COP1 by the help of SPA1 could also contribute the repression of flowering. A high relevance of the cry-COP1 release to elevate the nuclear free COP1 levels can not only explain the bolting phenotypes but also why in darkness no elevated levels of COP1 can be achieved as the pseudo-reservoir of CRY-COP1 is not established in the absence of light. It will be of great interest to test all aspects of this hypothetical model in the future and to analyse the expression of clock specific genes in detail to enhance the understanding of the MID-function in the clock context.

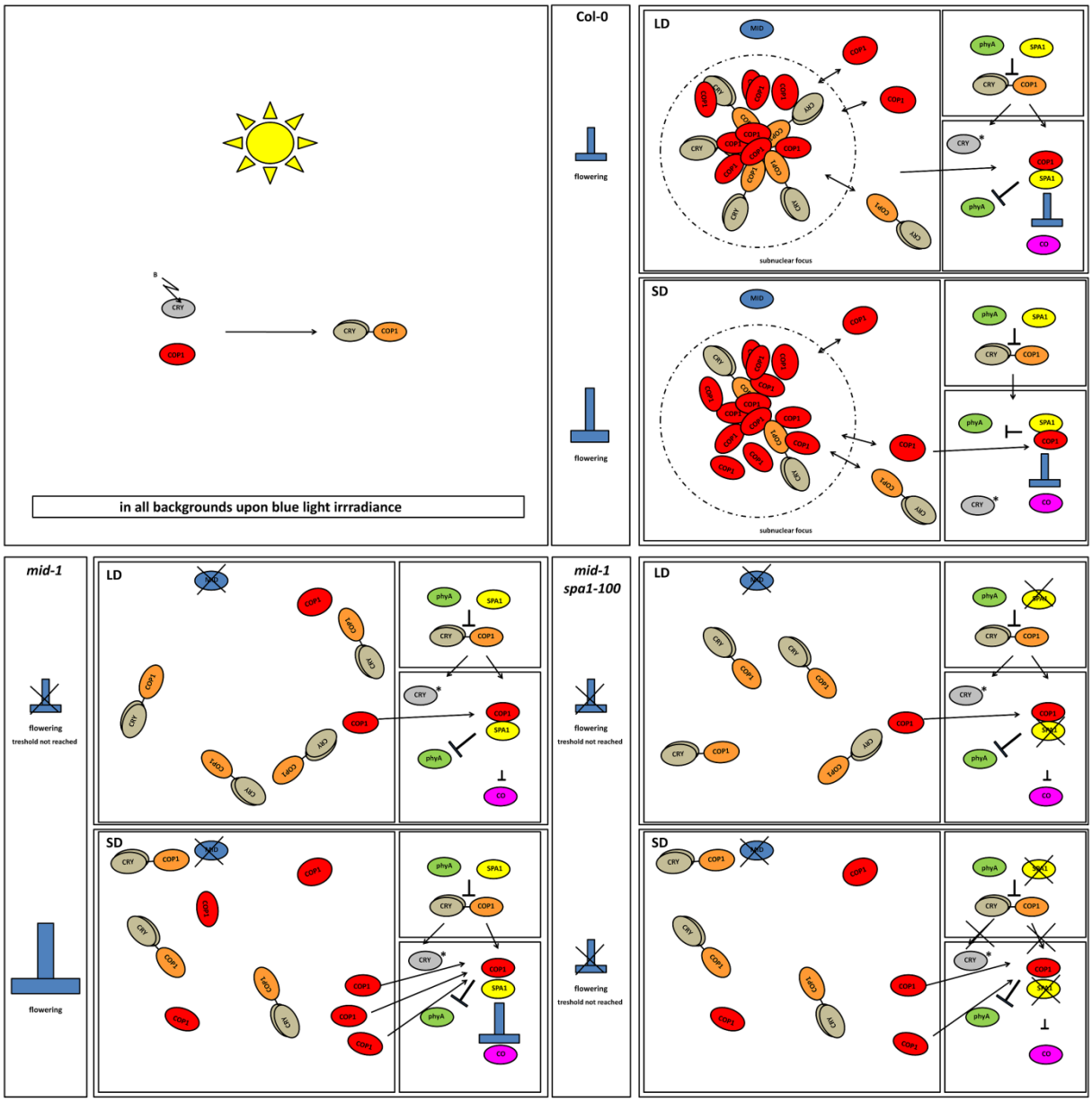

Figure IV - 6: Model for the MID-dependent regulation of COP1/SPA1-controlled flowering. For details see the text of this chapter. "threshold" means COP1 threshold, the amount of active free COP1 that is necessary to suppress flowering.

V. Attachment

All attachments first mentioned in material and methods part are marked with an "M" and in the results part with an "R".

A M-1 List of all used primers with nucleotide sequence in 5'-3'-orientation. GW: Gateway®.

primer name	type of PCR	nucleotide sequence
1 DET1 attB1 sense	GW-cloning	GGGGACAAGTTTGTACAAAAAAGCAGGCTTCATGTTCACAAGCGGTAACGTCA
2 DET1 attB2 antisense	GW-cloning	GGGGACCACTTTGTACAAGAAAGCTGGGTCTCATCGCCTAAAATGGAT
3 5`GAD	sequencing after Colony-PCR	CTGTATGGCTTACCCATACGATGTTCC
4 seq DET1 middle sense	sequencing, cloning of DET1	TGACGCTGTTCCTGGTGTTCCTTCCATTG
5 JU342-COP-Apt-attL	inverse PCR, cloning of GFP-CID	ACACTTCATTGTCCCTGATCTTGGCTAAACCCAGCTTTAAAGTTGGCATTATA
7 JU344-COP-Apt-GFP-revers	inverse PCR, cloning of GFP-CID/GFP-CID^{D246K}	TCCTCATCATCATCATCATATCTGGTCTCTTTGTATAGTTCATCCATGCCATG
8 ANS-COP-Apt-attL-D236K	inverse PCR, cloning of GFP-CID^{D246K}	ACACTTCATTGTCCCTAAGCTTGGCTAAACCCAGCTTTAAAGTTGGCATTATA
9 ANS-GFP-attB1-s	GW-cloning	GGGGACAAGTTTGTACAAAAAAGCAGGCTTCATGGGTAAAGGAGAAGAACTTT
29 ANS GFP stop attB2	GW-cloning	GGGGACCACTTTGTACAAGAAAGCTGGGTATTATTTGTATAGTTCATC
11 ANS seq attR2 Spe1 site pBatTL-B s	sequencing of pBatTL-B-p35s after ligation	CGGGGAAGAAGTGGCTGATCTCAGC
12 ANS HY5 as	amplification from cDNA	ACATGATAATTATTGATACAATTCTCTG
13 ANS HY5 s	amplification from cDNA	CACCAGCTTCGCTACTAAGACAACAAATC
14 ANS HY5 attB1	GW-cloning	GGGGACAAGTTTGTACAAAAAAGCAGGCTTCATGCAGGAACAAGCGACT
15 ANS HY5 attB2	GW-cloning	GGGGACCACTTTGTACAAGAAAGCTGGGTATCAAAGGCTTGCATCAGCAT
20 ANS COP1 attB1	GW-cloning	GGGGACAAGTTTGTACAAAAAAGCAGGCTTCATGGAAGAGATTTCGACGGATCC
21 ANS COP1 attB2	GW-cloning	GGGGACCACTTTGTACAAGAAAGCTGGGTATCACGCAGCGAGTACCAGA
52 ANS COP1 K550E s	Inverse PCR, cloning of COP1^{K550E}	TCTTCAGTGGACACAAGGAGGCAGTTTCCTATG
23 ANS COP1 K550E as + COP1 seq as	Inverse PCR, cloning of COP1^{K550E}	CATGAAGTGGTTGGCTTATGTTTCTTAGATCG
26 ANS GFP-seq-s-attL2	Sequencing GFP-CID/GFP-CID^{D246K}	GCGTTCAACTAGCAGACCATTATCAAC
30 ANS COP1 seq s Mitte	sequencing, COP1/COP1^{K550E}	TGAGAGGAACATGCAGATACTTTTGGAC
31 ANS AD 5 seq	Sequencing of yeast with prey plasmid	GGATGTTTAATACCACTACAA
32 ANS-DET1$^{1-277}$-attB2	GW-cloning	GGGGACCACTTTGTACAAGAAAGCTGGGTATCACTGACTTAGACTA

V. Attachment

		TGACG
33 ANS-DET1$^{277-543}$-attB1	GW-cloning	GGGGACAAGTTTGTACAAAAAAGCAGGCTTCATGCCAAGTGGTTC GAATTCG
34 ANS-DET1$^{150-452}$-attB1	GW-cloning	GGGGACAAGTTTGTACAAAAAAGCAGGCTTCATGAATGACGCTGTT CCTGGT
35 ANS-DET1$^{150-452}$-attB1	GW-cloning	GGGGACCACTTTGTACAAGAAAGCTGGGTATCATGGGGAGGGACTT TGTGA
JU340 N-mRFP-N fw	generating pNmR	GAGAGAGGATCCAAACCATGGCCTCCTCCGAGGACGTC
JU339 N-mRFP-C-HA rev	generating pNmR	GAGAGAAGATCTGTCGACAGCGTAATCTGGAACATCGTATGGGTA GGCGCCGGTGGAGTGGCGGCCCTC
51 ANS COP1 as end	sequencing, COP1/COP1^{K550E}	CACGCAGCGAGTACCAGAACTTTGATG
50 ANS HA sense pEGATE201	genotyping	GTACCCATACGATGTTCCAGATTACGC
62 ANS YFP seq sense pEGATE104	genotyping	GCACAAGCTGGAGTACAACTACAACAGC
63 MID attB1	GW-cloning	GGGGACAAGTTTGTACAAAAAAGCAGGCTTCAACATGAGCAGCAG CTCTAG
81 PAP2 attB1	GW-cloning, GARFILD	GGGGACAAGTTTGTACAAAAAAGCAGGCTTAATGGAGGGTTCGTCCA AA
82 PAP2 attB2	GW-cloning	GGGGACCACTTTGTACAAGAAAGCTGGGTACTAATCAAGTTCAACA GT
99 seq s pDONR207	sequencing of entry constructs	CTCAGGAGAGCGTTCACCGACAAACAAC
100 seq as pDONR207	sequencing of entry constructs	CAGAGCTGCAGCTGGATGGCAAATAATG
111 PAP2 ns attB2	GW-cloning, GARFILD	GGGGACCACTTTGTACAAGAAAGCTGGGTAATCAAGTTCAACAGTC TC
113 MID CTAB start s	genotyping	ATGAGCAGCAGCTCTAGAGAGGGATC
115 LBa1 (SALK)	genotyping	TGGTTCACGTAGTGGGCCATCG
117 372-as4	genotyping	TATGCTTGCTAGAGAGTTTTTCAC
167 EF1a-UP	RT-PCR	ATGCCCCAGGACATCGTGATTTCAT
168 EF1a-RP	RT-PCR	TTGGCGGCACCCTTAGCTGGATCA
171 Weigel SKI015 RB	genotyping	AGATCCGAAACTATCAGTG
172 mid-1 genotyping mit Weigel 170 171	genotyping	GTATCTGCCTGATAAATGGATTGTATTG
176 MOE5F	genotyping	GCTCGAGCTTCCTTTGCTAACCTTTTC
178 HYP6dCAP-M	genotyping	CGAATTTTGAATTGTGGATCTCATCG
179 SPO3-3F	genotyping	CCTTATCCACCAACTCTGCCTCAGGAAC
180 rhl2CAPS-R	genotyping	CCCATCTTTGTGCAATCTATCATATCTCC
181 COP1dCAPS	genotyping	attaaagatgctttcctcacgacttgtggt
182 cop1-eid6 genotyping as	genotyping	AAAGCTAAGGACCAAACACAAATTACGAGT
183 COP1dCAPS cop1-4 BsaAI/SnaBI	genotyping	ccaaagaaggatgcgctgagtgggtcagatacg
184 cop1-4 genotyping as genomic	genotyping	TCTCGAGCTGTCAATCCAGATGACCAAG
186 mid-1 genotyping as	genotyping	CTGCATGATAGAGGAACCGTTACATTAC
208 LB3 SAIL	genotyping	TAGCATCTGAATTTCATAACCA
217 mid-2 genotyping s Intron	genotyping	gaaattaacaattgaaagtggatgg
226 SPA1 behind SAIL as 2	Genotyping	GCATTCATAATACTATTCTCACCAGCTGC
228 Spa1 Intron 1 s3	genotyping	GTATATGATTTAAGGTATGGAGGCTGTAG

V. Attachment

234 RFP-HA-attB1 fw	genotyping	GGGGACAAGTTTGTACAAAAAAGCAGGCTTCATGGCCTCCTCCGAGGAC
235 RFP-HA-attB1 rev	genotyping	GGGGACCACTTTGTACAAGAAAGCTGGGTCTCAGAAGCCTGCCTTCTTGTAC
236 YFP-attB1	genotyping	GGGGACAAGTTTGTACAAAAAAGCAGGCTTCATGGGCAAGGGCGAGGAGCTG
237 COP1dCAPs elong	genotyping	gtatgcagattattaaagatgctttcctcacgacttgtggt
238 cop1-eid6 genotyping as 2	genotyping	GTTTCAATACACTATCATTCCTATAAACATGCTTC
249 ADH-term-seq-as	Sequencing of yeast with prey and bait plasmid	CTATACCTGAGAAAGCAACCTGACCTAC
250 pMet-seq-s	sequencing, pBRIDGE	GTAATACAGGGTCGTCAGATACATAG
251 pMet-term-seq-as	sequencing, pBRIDGE	CGGATAAGAAAGCAACACCTGGC
ANS252-attB1-Tag-XhoI	tag primer GARFILD	GGGGACAAGTTTGTACAAAAAAGCAGGCTTCGACCATTATTACGCCCTCGAG
ANS253-attB2-Tag-NcoI	tag primer GARFILD	GGGGACCACTTTGTACAAGAAAGCTGGGTCGTAGTCCATGCGACACCATGG
ANS254-pAD-Gate-seq	Sequencing of yeast with prey plasmid	CTATTCGATGATGAAGATACCCCA
ANS-259-MID EST sense1	Sequencing of MID	AGCAGTGGTATCAACGCAGAGTAC
ANS-260-MID EST sense2	Sequencing of MID	ACACTTCAATCTCTCCGCCGGCGAAATC
ANS-261-MID EST as	Sequencing of MID	GTCAACGTTGTTTCCATTCTCCTTCCCTTCAAG
ANS-262-MID EST seq as	Sequencing of MID	GATACTCACTTGCTTCGTCACAACCTTC
ANS-263-MID EST7 sense3	Sequencing of MID	GAACAAGCAGTTTATGCCCCAATCTTCTTC
264-AD5`seq start	Sequencing of yeast with prey plasmid	gatggataaagcggaattaattcccgag
265-MID-s-cloning	amplification from cDNA	ccacgtctcctcgccgggttttaacctc
266-MID-as-cloning	amplification from cDNA	CTATTTCATGGTAATAATGTCGTCTCAAAC
271 Random(08)-NcoI-Tag von J. Uhrig	GARIFLD random primer	CTAGTCCATGCGACACCATGGNNNNNNNN
272 Random(15)-NcoI-Tag von J. Uhrig	GARIFLD random primer	CTAGTCCATGCGACACCATGGNNNNNNNNNNNNNNN
273 Random(08)-XhoI-Tag von J. Uhrig	GARIFLD random primer	GACCATGATTACGCCCTCGAGNNNNNNNN
274 Random(15)-XhoI-Tag von J. Uhrig	GARFILD random primer	GACCATGATTACGCCCTCGAGNNNNNNNNNNNNNNN
291 COP1 seq N-term	Sequencing, COP1	GTGTCAATTAAGGAGGTTGATAATCTTC
292 COP1 seq as C-term	Sequencing, COP1	GACAAAAATTTAACATAGGAAACTGCTTTC
ANS pAD-GATE2 seq as	Sequencing of yeast with prey plasmid	GAGGAGTATAGTTACATAAAAGAAG
ANS AD3XL	colony PCR	GCGACCTCATGCTATACCTGAGAAAGCAACCTGACCTACAGGAAAGAG
ANS AD5XXL	colony PCR	GGACGGACCAAACTGCGTATAACGCGTTTGGAATCACTACAGGGATG
ANS 317 attL1 PAP2-COP1frag+ATG	GaW cloning, direct LR	GTACAAAAAAGCAGGCTTCatgtctgttaacaatggtt
ANS 318 attL2 PAP2-COP1frag+stopp	GaW cloning, direct LR	GTACAAGAAAGCTGGGTtcaCGCTTCAGGAACAATC
ANS 319 attL1 COP1 start +ATG	GaW cloning, direct LR	GTACAAAAAAGCAGGCTTCatggaagagatttcgacgg
ANS 320 attL2 COP1-COP1frag	GaW cloning, direct LR	GTACAAGAAAGCTGGGTtcaTTCCATTTTTCTCTTC
ANS 321 attL2 COP1-MIDfrag	GaW cloning, direct LR	GTACAAGAAAGCTGGGTtcaACAAGCCGTGAGGAAA
ANS 322 attL1 PAP2 start +ATG	GaW cloning, direct LR	GTACAAAAAAGCAGGCTTCatggagggttcgtccaaag
ANS 323 attL2 PAP2-EGL3frag	GaW cloning, direct LR	GTACAAGAAAGCTGGGTtcaTTTCTTTTTCATTTTA
ANS 326 Ubq10 RT-PCR s	RT-CR	cgattactcttgaggtggag

V. Attachment

ANS 327 Ubq RT-PCR as	**RT-PCR**	**agaccaagtgaagtgtggac**
ANS 328 COP1 RT-PCR s	**RT-PCR**	**CCTGGAGTGTTGACTTTT**
ANS 329 COP1 RT-PCR as	**RT-PCR**	**GTGGTTGGCTTATGTTTCT**
ANS 330 CHS s	**RT-PCR**	**CAATTCGGAAACGTCACATG**
ANS 331 CHS as	**RT-PCR**	**TGTGATCTCAGAGCAGACAAC**

A M-2: RT-PCR on COP1 with and without RNaseH treatment. +/-: cDNA synthesis with or without reverse transcriptase RT-PCR was performed on 3 day old dark-grown seedlings from MS plates lacking sucrose.

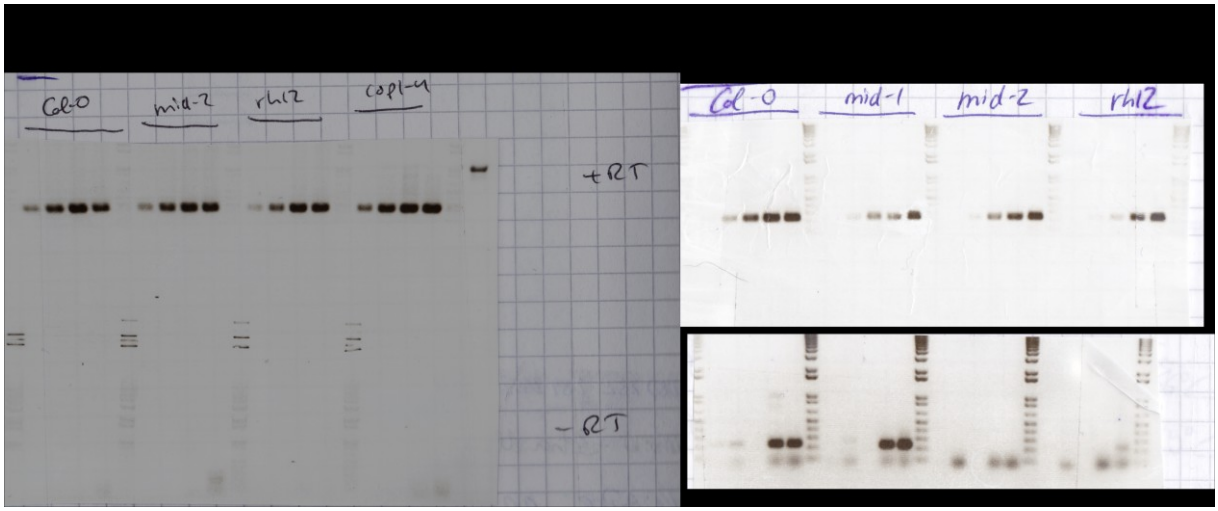

A R-1: (A) Alignment of ATNUC-L1 (=AT1G48920) with AT5g51730 after NCBIp BLAST. **(B)** Alignment of ATNUC-L2 (=ATRANGAP1 at Entrez=AT3G18610) with At5g51730 after NCBIp BLAST. **(A-B)** Identical amino acids are highlighted in red. **(C)** Alignment of At5g51730, ATNUC-L1 and ATNUC-L2 to RRM (RNA recognition motif) / RBD (RNA binding domain) / RNP (ribonucleoprotein domain). Shaded in black are amino acids that are shared by all three proteins. Aminoacids in red are aminoacids of the corresponding protein that are the same in RRM/RBD/RNP. **(A-C)** modified after NCBI BLASTp and Entrez Gene (Altschul, S.F. et al. (1997) Altschul, S.F. et al. (1997); Marchler-Bauer A et al. (2009); Marchler-Bauer A and Bryant SH (2004)) Sequences based on TAIR sequences (www.arabidopsis.org)

```
(A)
ATNUC-L1    376 GERGERPAFTP-QSGNFRSGGDGGDEKKIFVKGFDASLSEDDIKNTLREHFSSCGEIKNVSVPIDRDTGNSKGIAYLE 452
At5g51730   535 AEVGERALFIPKQGGRYDCGT-------IFVKGYDSSLGENDLARALLEHFSPCGMI-SRIYFQTNDAGEAVLKHVFI 243


ATNUC-L1    453 FSEGK--EKALE-LNGSDMGGGFYLVVDEPRPR 482
At5g51730   244 VMLQGT-EDALK-LNGSDMGGCNLEVHDATERD 274


(B)
ATNUC-L2    456 DLANERGTPRNSNPGRKGEGSQSRTIYVRGFSSSLGEDEIKKELRSHFSKCGEVTRVHVPTDRETGASRGFAYIDLTSG
At5g51730   174 AEVGERALFIPKQGGRYDCG----TIFVKGYDSSLGENDLARALLEHFSPCGMI-SRIYFQTNDAGEAVLKHVFIVMLQ


ATNUC-L2    533 FD-E-ALQLSGSEIGGGNIHVEESRPRD 560
At5g51730   248 GT-EDALKLNGSDMGGCNLEVHDATERD 274


(C)
RRM/RBD/RNP   1 TLFVGNLPPDVTEED----LRELFSKFGKVESVRIVRDKDT-KSKGFAFVEFEDEEdaEKALEaLNGKELGGRPLRVE  73
ATNUC-L1    402 KIFVKGFDASLSEDDiktLREHFSSCGEIKNVSVPIDRDTgNSKGIAYLEFSEGK--EKALE-LNGSDMGGGFYLVV 476
ATNUC-L2    480 TIYVRGFSSSLGEDEikkELRSHFSKCGEVTRVHVPTDRETGaSRGFAYIDLTSGFD-E-ALQ-LSGSEIGGGNIHVE 554
At5g51730   194 TIFVKGYDSSLGENDLARALLEHFSPCGMI-SRIYFQTNDAGEAVLKHVFIVMLQGT-EDALK-LNGSDMGGCNLEVH 268
```

V. Attachment

A R-2: List o all published interactions included in the network in FIGURE III - 3. Given is the name and AGI code of both interaction prtners as they are listed at TAIR (www.arabidopsis.org), the evidence for the interaction as listed at BioGRID (Stark et al., 2006) and the corresponding publications. All BioGRID data were validated and additional literature research results were included in the list. Results from my diploma thesis are also included. BioGRID (www.thebiogrid.org) interaction categories: **YTH; affinity capture-Western:** An interaction is inferred when a Bait protein affinity captured from cell extracts by either polyclonal antibody or epitope tag and the associated interaction partner identified by Western blot with a specific polyclonal antibody or second epitope tag. This category is also used if an interacting protein is visualized directly by dye stain or radioactivity. Note that this differs from any co-purification experiment involving affinity capture in that the co-purification experiment involves at least one extra purification step to get rid of potential contaminating proteins. **Reconstituted complex:** An interaction is detected between purified proteins in vitro. **Co-purification:** An interaction is inferred from the identification of two or more protein subunits in a purified protein complex, as obtained by classical biochemical fractionation or affinity purification and one or more additional fractionation steps. **FRET:** An interaction is inferred when close proximity of interaction partners is detected by fluorescence resonance energy transfer between pairs of fluorophore-labeled molecules, such as occurs between CFP (donor) and YFP (acceptor) fusion proteins. **PCA:** A protein-protein interaction assay in which a bait protein is expressed as fusion to one of the either N- or C- terminal peptide fragments of a reporter protein and prey protein is expressed as fusion to the complementary N- or C- terminal fragment of the same reporter protein. Interaction of bait and prey proteins bring together complementary fragments, which can then fold into an active reporter. **Biochemical activity:** An interaction is inferred from the biochemical effect of one protein upon another, for example, GTP-GDP exchange activity or phosphorylation of a substrate by a kinase. The "bait" protein executes the activity on the substrate "hit" protein. Completed with the differenciation **YTH-screen; Co-IP (for the Miltenyi Co-IP from my diploma thesis), BiFC** and Bioluminescence Resonance Energy Transfer (**BRET).**

V. Attachment

interactor 1		interactor 2			
name	AGI	name	AGI	evidence	source
COP1	At2g32950	DDB1A	At4g05420	reconstituted complex	(Chen et al., 2010)
COP1	At2g32950	DDB1B	At4g21100	reconstituted complex	(Chen et al., 2010)
COP1	At2g32950	COP10	At3g13550	YTH; affinity capture-western	(Suzuki et al., 2002; Yanagawa et al., 2004)
COP1	At2g32950	CSN1	At3g61140	YTH	(Wang et al., 2009)
COP1	At2g32950	SPA1	At2g46340	YTH; reconstituted complex; affinity capture-western; co-purification; affinity capture-MS	(Hoecker and Quail, 2001; Saijo et al., 2003; Saijo et al., 2008)
COP1	At2g32950	SPA2	At4g11110	affinity capture- western; reconstituted complex	(Laubinger et al., 2004; Zhu et al., 2008)
COP1	At2g32950	SPA3	At3g15354	YTH; reconstituted complex; affinity capture-western	(Laubinger and Hoecker, 2003; Zhu et al., 2008)
COP1	At2g32950	SPA4	At1g53090	YTH; reconstituted complex; affinity capture-western	(Laubinger and Hoecker, 2003; Zhu et al., 2008)
COP1	At2g32950	CO	At5g15840	YTH (CO C-term); reconstituted complex; FRET; biochemical activity	(Liu et al., 2008b)
COP1	At2g32950	COL3	At2g24790	YTH	(Datta et al., 2006)
COP1	At2g32950	GI	At1g22770	YTH (COP1 RING- and CC-domain); PCA	(Yu et al., 2008)
COP1	At2g32950	cry1	At4g08920	YTH; reconstituted complex; affinity capture-Western	(Yang et al., 2001)
COP1	At2g32950	cry2	At1g04400	YTH; affinity capture-Western	(Wang et al., 2001)
COP1	At2g32950	CIP8	At5g64920	YTH; reconstituted complex; affinity capture-Western	(Hardtke et al., 2002; Torii et al., 1999)
COP1	At2g32950	HY5	At5g11260	YTH; reconstituted complex; biochemical activity	(Ang et al., 1998; Saijo et al., 2003)
COP1	At2g32950	HFR1	At1g02340	YTH; reconstituted complex; affinity capture-western; biochemical activity	(Duek et al., 2004; Jang et al., 2005; Yang et al., 2005)
COP1	At2g32950	HYH	At3g17609	YTH	(Holm et al., 2002)
COP1	At2g32950	phyB	At2g18790	YTH	(Yang et al., 2001)
COP1	At2g32950	STH	At2g31380	YTH; BRET	(Holm et al., 2001; Subramanian et al., 2006)
COP1	At2g32950	STO	At1g06040	YTH	(Holm et al., 2001)
COP1	At2g32950	LAF1	At4g25560	reconstituted complex; affinity capture-western; biochemical activity	(Seo et al., 2003)
COP1	At2g32950	BIT1	At2g36890	YTH; BiFC; Co-IP	(Hong et al., 2008)
COP1	At2g32950	CIP4	AT5g37190	reconstituted complex	(Yamamoto et al., 2001)
COP1	At2g32950	phyA	At1g09570	reconstituted complex; biochemical activity; affinity capture-western	(Saijo et al., 2008; Seo et al., 2004)
COP1	At2g32950	CIP7	At4g27430	YTH; reconstituted complex	(Yamamoto et al., 1998)
COP1	At2g32950	CIP1	At5g41790	Reconstituted complex	(Matsui et al., 1995)
COP1	At2g32950	ELF3	At2g25930	YTH; biochemical activity; affinity capture-western; PCA	(Yu et al., 2008)
DET1	At4g10180	DDB1A	At4g05420	YTH; affinity capture-Western	(Bernhardt et al., 2006; Chen et al., 2010)
DET1	At4g10180	tH2B	tomato	Reconstituted complex, histone association for AtH2B shown	(Benvenuto et al., 2002)
SPA1	At2g46340	SPA2	At4g11110	reconstituted complex, Co-fractionation, Affinity Capture-Western	(Zhu et al., 2008)
SPA1	At2g46340	SPA3	At3g15354	reconstituted complex, Co-fractionation, Affinity Capture-Western	(Zhu et al., 2008)

V. Attachment

SPA1	At2g46340	SPA4	At1g53090	reconstituted complex, Co-fractionation, Affinity Capture-Western	(Zhu et al., 2008)
SPA1	At2g46340	DDB1A	At4g05420	reconstituted complex	(Chen et al., 2010)
SPA1	At2g46340	CO	At5g15840	reconstituted complex; FRET	(Laubinger et al., 2006)
SPA1	At2g46340	HFR1	At1g02340	YTH; reconstituted complex	(Yang et al., 2005)
SPA1	At2g46340	HY5	At5g11260	YTH	(Saijo et al., 2003)
SPA2	At4g11110	SPA3	At3g15354	reconstituted complex, Co-fractionation, Affinity Capture-Western	(Zhu et al., 2008)
SPA2	At4g11110	SPA4	At1g53090	reconstituted complex, Co-fractionation, Affinity Capture-Western	(Zhu et al., 2008)
SPA2	At4g11110	DDB1A	At4g05420	reconstituted complex	(Chen et al., 2010)
SPA2	At4g11110	DDB1B	At4g21100	reconstituted complex	(Chen et al., 2010)
SPA2	At4g11110	CO	At5g15840	reconstituted complex	(Laubinger et al., 2006)
SPA3	At3g15354	SPA4	At1g53090	reconstituted complex, Co-fractionation, Affinity Capture-Western	(Zhu et al., 2008)
SPA3	At3g15354	DDB1A	At4g05420	reconstituted complex	(Chen et al., 2010)
SPA3	At3g15354	DDB1B	At4g21100	reconstituted complex	(Chen et al., 2010)
SPA3	At3g15354	CO	At5g15840	reconstituted complex	(Laubinger et al., 2006)
SPA4	At1g53090	DDB1A	At4g05420	reconstituted complex	(Chen et al., 2010)
SPA4	At1g53090	DDB1B	At4g21100	reconstituted complex	(Chen et al., 2010)
SPA4	At1g53090	CO	At5g15840	reconstituted complex	(Laubinger et al., 2006)
CO	At5g15840	ZTL	At5g57360	YTH	(Fukamatsu et al., 2005)
CO	At5g15840	LKP2	At2g18915	YTH	(Fukamatsu et al., 2005)
CO	At5g15840	FKF1	At1g68050	YTH	(Fukamatsu et al., 2005)
CO	At5g15840	NF-YB1	At2g38880	YTH (with CO CCT domain); reconstituted complex; FRET	(Wenkel et al., 2006)
CO	At5g15840	NF-YB2	At5g47640	YTH (with CO CCT domain)	(Wenkel et al., 2006)
CO	At5g15840	NF-YB6	At5g47670	YTH (with CO CCT domain)	(Wenkel et al., 2006)
CO	At5g15840	NF-YB9	At1g21970	YTH (with CO CCT domain)	(Wenkel et al., 2006)
CO	At5g15840	NF-YC1	At3g48590	YTH (with CO CCT domain); reconstituted complex; FRET	(Wenkel et al., 2006)
CO	At5g15840	NF-YC2	At1g56170	YTH (with CO CCT domain)	(Wenkel et al., 2006)
CO	At5g15840	NF-YC3	At1g54830	YTH (with CO CCT domain)	(Wenkel et al., 2006)
CO	At5g15840	NF-YC5	At5g50490	YTH (with CO CCT domain)	(Wenkel et al., 2006)
CO	At5g15840	NF-YC6	At5g50480	YTH (with CO CCT domain)	(Wenkel et al., 2006)
CO	At5g15840	NF-YC7	At5g50470	YTH (with CO CCT domain)	(Wenkel et al., 2006)
CO	At5g15840	NF-YC9	At1g08970	YTH (with CO CCT domain)	(Wenkel et al., 2006)
COL3	At2g24790	ZTL	At5g57360	YTH	(Fukamatsu et al., 2005)
COL3	At2g24790	LKP2	At2g18915	YTH	(Fukamatsu et al., 2005)
GI	At1g22770	ZTL	At5g57360	YTH; reconstituted complex; affinity capture-Western	(Kim et al., 2007)
GI	At1g22771	LKP2	At2g18915	YTH; reconstituted complex	(Kim et al., 2007)

V. Attachment

GI	At1g22770	FKF1	At1g68050	YTH; reconstituted complex; affinity capture-Western	(Kim et al., 2007; Sawa et al., 2007)
GI	At1g22770	ELF3	At2g25930	YTH; PCA	(Yu et al., 2008)
GI	At1g22770	SPY	At3g11540	YTH; reconstituted complex (Co-purification from *E. coli*)	(Tseng et al., 2004)
GI	At1g22770	SPL11	At1g27360	reconstituted complex	(Kim et al., 2007)
LKP2	At2g18915	ZTL	At5g57360	YTH	(Yasuhara et al., 2004)
LKP2	At2g18915	FKF1	At1g68050	YTH	(Yasuhara et al., 2004)
CRY1	At4g08920	ZTL	At5g57360	YTH; reconstituted complex	(Jarillo et al., 2001)
CRY1	At4g08920	phyA	At1g09570	YTH	(Ahmad et al., 1998)
CRY2	At1g04400	CIB1	At4g34530	YTH; affinity capture-Western	(Liu et al., 2008a)
phyA	At1g09570	FHY1	AT2G37678	YTH; reconstituted complex	(Hiltbrunner et al., 2006)
phyA	At1g09570	FHL	At5g02200	YTH; reconstituted complex	(Hiltbrunner et al., 2006)
phyA	At1g09570	PIF1	At2g20180	reconstituted complex	(Huq et al., 2004)
phyA	At1g09570	PIF3	At1g09530	YTH; reconstituted complex; affinity capture-western	(Fairchild et al., 2000; Ni et al., 1998; Phee et al., 2006)
phyA	At1g09570	PKS1	At2g02950	YTH; reconstituted complex	(Fankhauser et al., 1999)
phyA	At1g09570	NDPK2	At5g63310	reconstituted complex; affinity capture-western	(Im et al., 2004)
phyB	At2g18790	ZTL	At5g57360	YTH; reconstituted complex	(Jarillo et al., 2001; Kevei et al., 2006)
phyB	At2g18790	ELF3	At2g25930	YTH; reconstituted complex	(Liu et al., 2001)
phyB	At2g18790	PIF1	At2g20180	reconstituted complex	(Huq et al., 2004)
phyB	At2g18790	PIF3	At1g09530	YTH; reconstituted complex; affinity capture-western	(Ni et al., 1998; Phee et al., 2006)
phyB	At2g18790	PIF4	At2g43010	reconstituted complex	(Huq et al., 2004)
phyB	At2g18790	PIF5	At3g59060	YTH; reconstituted complex	(Khanna et al., 2004; Shen et al., 2007)
phyB	At2g18790	PIF6	At3g62090	reconstituted complex	(Khanna et al., 2004)
phyB	At2g18790	PIF7	At5g61270	reconstituted complex	(Leivar et al., 2008)
phyB	At2g18790	NDPK2	At5g63310	reconstituted complex; affinity capture-western	(Phee et al., 2006; Shen et al., 2005)
phyB	At2g18790	PKS1	At2g02950	YTH; reconstituted complex	(Fankhauser et al., 1999)
phyB	At2g18790	ARR4	At1g10470	YTH; affinity capture-Western	(Sweere et al., 2001)
FHY1	AT2G37678	FHL	At5g02200	reconstituted complex	(Zhou et al., 2005)
DDB1A	At4g05420	DDB2	At5g58760	YTH	(Bernhardt et al., 2006)
DDB1A	At4g05420	COP10	At3g13550	YTH; affinity capture-Western	(Chen et al., 2006; Yanagawa et al., 2004)
DDB1A	At4g05420	CUL4	At5g46210	YTH; reconstituted complex; affinity capture-Western	(Bernhardt et al., 2006; Chen et al., 2010; Chen et al., 2006; Lee et al., 2008)
DDB1A	At4g05420	AGB1	At4g34460	YTH	(Lee et al., 2008)
DDB1A	At4g05420	TRIP-1	At2g46280	YTH; affinity capture-Western	(Lee et al., 2008)
DDB1A	At4g05420	-	At1g80670	YTH	(Lee et al., 2008)

V. Attachment

DDB1A	At4g05420	-	At2g19430	YTH	(Lee et al., 2008)
DDB1A	At4g05420	-	At3g45620	YTH	(Lee et al., 2008)
DDB1A	At4g05420	FY	At5g13480	YTH; affinity capture-Western	(Lee et al., 2008)
DDB1A	At4g05420	MSI3	At4g35050	YTH	(Lee et al., 2008)
DDB1A	At4g05420	-	At4g28450	YTH	(Lee et al., 2008)
DDB1A	At4g05420	-	At1g65030	YTH	(Lee et al., 2008)
DDB1A	At4g05420	PRL1	At4g15900	YTH; affinity capture-Western	(Lee et al., 2008)
DDB1A	At4g05420	VIP3	At4g29830	YTH	(Lee et al., 2008)
COP10	At3g13550	CUL4	At5g46210	YTH; affinity capture-Western	(Chen et al., 2006)
COP10	At3g13550	CSN3	At5g14250	YTH; affinity capture-Western	(Suzuki et al., 2002; Yanagawa et al., 2004)
COP10	At3g13550	CSN4	At5g42970	YTH	(Suzuki et al., 2002)
COP10	At3g13550	COP9	At4g14110	YTH	(Suzuki et al., 2002)
COP10	At3g13550	UBC1	At1g14400	reconstituted complex	(Lau and Deng, 2009)
COP10	At3g13550	UBC4	At5g41340	reconstituted complex	(Lau and Deng, 2009)
COP10	At3g13550	UBC9	At4g27960	reconstituted complex	(Lau and Deng, 2009)
CUL1		CSN2	At2g26990	YTH, affinity capture-Western	(Serino and Deng, 2003)
CUL4	At5g46210	COP9	At4g14110	YTH	(Chen et al., 2006)
CUL4	At5g46210	CSN3	At5g14250	YTH; affinity capture-Western	(Chen et al., 2006)
CUL4	At5g46210	CSN4	At5g42970	YTH; affinity capture-Western	(Chen et al., 2006)
CSN1	At3g61140	CSN2	At2g26990	YTH	(Serino et al., 2003)
CSN1	At3g61140	CSN3	At5g14250	YTH, affinity capture-Western, co-purification	(Peng et al., 2001; Serino et al., 2003)
CSN1	At3g61140	CSN4	At5g42970	YTH	(Serino et al., 2003)
CSN1	At3g61140	CSN5A	At1g22920	YTH, affinity capture-Western	(Kwok et al., 1998)
CSN1	At3g61140	CSN7	At1g02090	YTH, reconstituted complex	(Dessau et al., 2008; Karniol et al., 1999)
CSN1	At3g61140	COP9	At4g14110	YTH, affinity capture-Western, co-purification	(Serino et al., 2003; Staub et al., 1996)
CSN1	At3g61140	AtS9	At1g29150	YTH	(Kwok et al., 1999)
CSN1	At3g61140	EIF3C	At3g56150	YTH, affinity capture-Western	(Kim et al., 2004; Yahalom et al., 2001)
CSN2	At2g26990	CSN3	At5g14250	YTH	(Serino et al., 2003)
CSN2	At2g26990	CSN4	At5g42970	YTH, affinity capture-Western, co-purification	(Serino et al., 2003)
CSN3	At5g14250	CSN4	At5g42970	YTH, affinity capture-Western	(Feng et al., 2003; Serino and Deng, 2003)
CSN3	At5g14250	CSN7	At1g02090	YTH	(Serino et al., 2003)
CSN3	At5g14250	COP9	At4g14110	YHT	(Serino et al., 2003)
CSN4	At5g42970	CSN5A	At1g22920	YTH	(Serino et al., 2003)
CSN4	At5g42970	CSN7	At1g02090	YTH	(Serino et al., 2003)
CSN4	At5g42970	COP9	At4g14110	YTH	(Serino et al., 2003)

V. Attachment

CSN7	At1g02090	COP9	At4g14110	YTH, reconstituted complex	(Dessau et al., 2008; Karniol et al., 1999)
HY5	At5g11260	CIP8	At5g64920	reconstituted complex	(Hardtke et al., 2002)
HY5	At5g11260	STH3	AT1G78600	YTH, FRET	(Datta et al., 2008)
HY5	At5g11260	CCA1	AT2G46830	YTH; reconstituted complex	(Andronis et al., 2008)
CIP8	At5g64920	UBC8	At5g41700	reconstituted complex	(Hardtke et al., 2002)
STO	At1g06040	RCD1	At1g32230	YTH	(Belles-Boix et al., 2000)
HYH	At3g17609	STH3	AT1G78600	YTH	(Datta et al., 2008)
HFR1	At1g02340	LAF1	At4g25560	reconstituted complex; affinity capture-Western	(Jang et al., 2007)
HFR1	At1g02340	PIF3	At1g09530	reconstituted complex	(Fairchild et al., 2000)
HFR1	At1g02340	CKB1	At5g47080	YTH	(Park et al., 2008)
HFR1	At1g02340	CKB2	At4g17640	YTH	(Park et al., 2008)
HFR1	At1g02340	PIF5	At3g59060	reconstituted complex, PCA, affinity capture-western	(Hornitschek et al., 2009)
HFR1	At1g02340	PIF4	At2g43010	Reconstiuted complex, PCA	(Hornitschek et al., 2009)
HFR1	At1g02340	KDR	At1g26945	YTH	(Hyun and Lee, 2006)
CCA1	AT2G46830	CKB1	At5g47080	YTH, reconstituted complex	(Sugano et al., 1998)
CCA1	AT2G46830	CKB2	At4g17640	YTH	(Sugano et al., 1998)
PIF3	At1g09530	PIF4		YTH, reconstituted complex	(Toledo-Ortiz et al., 2003)
PIF3	At1g09530	PIF5	At3g59060	YTH	(Fujimori et al., 2004)
PIF3	At1g09530	NDPK2	At5g63310	affinity capture-western	(Phee et al., 2006)
MID	At5g24630	RHL1	At1g48380	YTH; BiFC	my diploma thesis, (Kirik et al., 2007)
MID	At5g24630	RHL2	At5g02820	YTH	(Breuer et al., 2007)
MID	At5g24630	SPA1	At2g46340	YTH-screen	J. F. Uhrig (unpublished data)
MID	At5g24630	GRF1	At4g09000	YTH-screen, BiFC	my diploma thesis
MID	At5g24630	ACT7	At5g09810	YTH-screen; BiFC	my diploma thesis
MID	At5g24630	DRIP2	At2g30580	YTH; BiFC	my diploma thesis
MID	At5g24630	MIAP2	At2g45680	YTH, BiFC	my diploma thesis
MID	At5g24630	-	At5g43560	YTH	my diploma thesis
GRF1	At4g09000	MIAP2	At2g45680	YTH; BiFC	my diploma thesis
GRF1	At4g09000	ATKCO1	At5g55630	reconstituted complex	(Latz et al., 2007)
GRF1	At4g09000	NIA2	At1g37130	YTH	(Kanamaru et al., 1999)
DRIP2	At2g30580	DREB2A	At5g05410	YTH	(Qin et al., 2008)
-	At5g43560	AHK3	At1g27320	YTH-Screen	(Dortay et al., 2008)

-	At5g43560	AT-HSFB2B	At4g11660	YTH-screen	(Li et al., 2010)
RHL2	At5g02820	AtTOP6B	At3g20780	YTH; BiFC	(Hartung and Puchta, 2001); my diploma thesis
RHL1	At1g48380	RHL2	At5g02820	YTH; BiFC; affinity-capture-Western	(Kirik et al., 2007; Sugimoto-Shirasu et al., 2005) my diploma thesis
RHL1	At1g48380	ANAC082	At5g09330	YTH-screen	my diploma thesis
RHL1	At1g48380	-	At4g15820	YTH-screen	my diploma thesis
RHL1	At1g48380	FKBP15-1	At3g25220	YTH-screen	my diploma thesis
RHL1	At1g48380	STT3A	At5g19690	YTH-screen	my diploma thesis
PAP2	At1g66390	EGL3	At1g63650	YTH; reconstituted complex	(Zimmermann et al., 2004)
PAP2	At1g66390	GL3	At5g41315	reconstituted complex	(Zimmermann et al., 2004)
PAP2	At1g66390	TT8	At4g09820	YTH; reconstituted complex	(Zimmermann et al., 2004)
PAP2	At1g66390	AtMYC1	At4g00480	YTH; reconstituted complex	(Zimmermann et al., 2004)
GL3	At5g41315	EGL3	At1g63650	YTH	(Zhang et al., 2003)
AGB1	At4g34460	AGG1	At3g63420	YTH, reconstituted complex	(Mason and Botella, 2000)
AGB1	At4g34460	AGG2	At3g22942	YTH, reconstituted complex	(Mason and Botella, 2001)
NDL2	AT5G11790	AGG1	At3g63420	Yeast Three Hybrid with AGB Pro*Met25*:AGG1	(Mudgil et al., 2009)
NDL2	AT5G11790	AGG2	At3g22942	Yeast Three Hybrid with AGB Pro*Met25*:AGG2	(Mudgil et al., 2009)
TSA	At1g52410	TSK	At3g18730	YTH, reconstituted complex	(Suzuki et al., 2005)
GAPCP-1	At1g79530	WOL	At2g01830	YTH-screen	(Dortay et al., 2008)
-	At5g37740	ARR14	At2g01760	YTH-screen	(Dortay et al., 2008)

V. Attachment

A R-3: Vector map of **(A)** pNmR-RfA (pNmR) and **(B)** pBatTL-B-35s-attR (pBatTL-B-p35s). p35S: Cauliflower Mosaic Virus (CaMV) 35s promoter; TL: translational enhancer; RFP (Q66T) no stop: optimized mono RFP from Jach et al. (2006) without stop codon ; HA: hemagglutinin tag; attR1,attR2: Gateway® sites for recombination with the Gateway® LR reaction ;CmR: ; ccdB: ccdB-Gen for selection after BP reaction, toxic for DH5α (*E.coli*) ; 35S-pA: polyadenylation signal of the CaMV *35S* gene; LB,RB: left and right border for the *A. tumefaciens* mediated insertion in the plant genome ; stA: ensures stability of the plasmid; rep: origin of replication; BaR: gene conferring resistance against the herbicide BASTA; *Spe*I, *Bgl*II: restriction sites for the depicted enzymes; RfA: reading frame A. Vector maps were generated with CLC DNA Workbench (CLC bio).

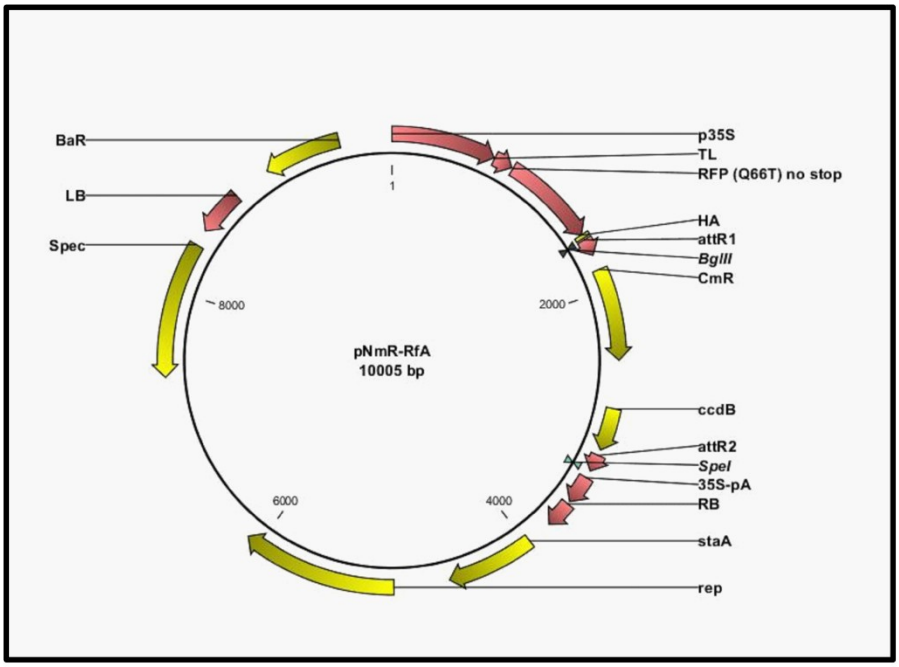

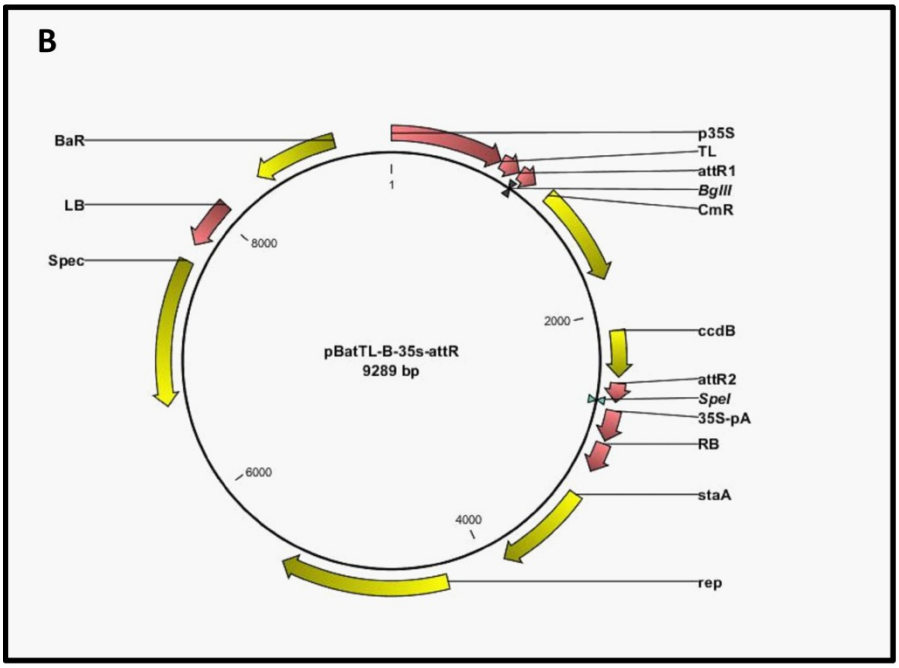

V. Attachment

A R-4: (A, C): pNmR-COP1 (*cop1-4*) T1, BASTA selected on MS – agar plates; Plants on soil were kept at 21°C at LD conditions. **(B,D)** pNmR-COP1 (Col-0) plants in the left (B) or last (D) third of the tray are Col-0 wildtype. Note the different sizes of plants in both cases (probably due to silencing and overcomplementation) but that no leave phenotype is visible for the wildtype background. Pictures of adult plants after bolting or around the time point of bolting. Plants in (B) and (D) are one week older than plants in (A, C). Pictures were taken with a TRAVELER Super Slim XS 8 digital camera.

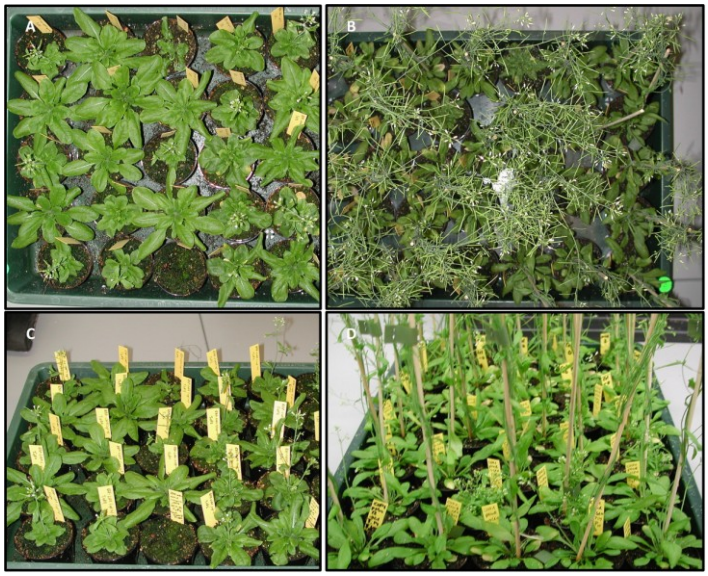

A R-5: DAPI staining verifies the nuclear localization of RFP-HA-COP1, YFP-PAP2, YFP-MID or the co-localizaton with RFP-HA-COP1. Leaves of *N. benthamiana* were co-infiltrated with different combination of *A. tumefaciens* harbouring pNmR-COP1, pEGATE104-PAP2, pEGATE104-MID and RK19 (depicted at the right). The plants were kept at 24°C at LD conditions. Pictures were taken three dai. DAPI: Fluorescence microscopy of DAPI stained nuclei. YFP; RFP: YFP or RFP channel. Merge: Pictures from the left were merged using Adobe photoshop software. Arrows point to nuclei. Bar equals 50 µm.
YFP-PAP2 = pEarleyGate104-PAP2 (LBA4404. pBBR1MCS.virGN54D); YFP-MID = pEarleyGate104-MID (LBA4404. pBBR1MCS.virGN54D); RFP-HA-COP1 = pNmR-COP1 (LBA4404pBBR1MCS-5.virGN54D); RK19 = anti silencing strain.

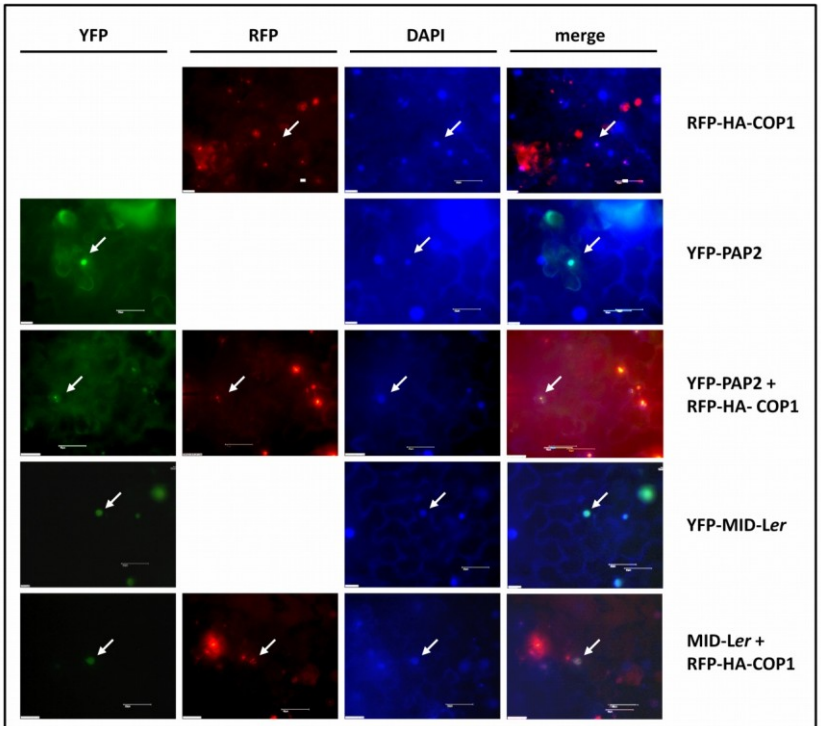

V. Attachment

A R-6: Bradford analysis and original LAS picture from ubiquitin western blot analysis.
(A-C) Bradford analysis of the input fraction for the Co-IP presented in Figure III-13. (A) Results of three independent measurements to obtain mean values for the Bradford calibration curve. The same proportion of the used lysis buffer was present in the analysed sample as in (C). (B) Bradford calibration curve (C) Threefold measurement of the input fractions and calculation of total protein concentration. The last column gives the volume that was loaded on the SDS-PAGE gels used for western blot analysis and Coomassie staining.
(D) Results of werstern blot analysis with an aubiquitin antibody. Left: original LAS picture (increment mode) right: modified picture with the Multi Gauge software (Fujifilm).
Leaves of *N. benthamiana* were infiltrated with the depicted constructs. Expression of the fusion proteins was verified by CLSM prior to homogenization three dai. The IP of YFP-PAP2 or YFP-attB1 (Kirik, V. et al., 2007) was performed using Miltenyi αGFP beads. Total protein concentrations were equalize by Bradford analysis (see A-C).
Band of the marker correspond to (from the bottom to the top): 26, 34, 43, 55, 72, 95, 130, 170 kDa.
Imaged were visualized with a LAS-4000 mini luminescent image analyzer (Fujifilm) in increment mode. YFP-PAP2 = pEarleyGate104-PAP2 (LBA4404. pBBR1MCS.virGN54D); RFP-HA-COP1 = pNmR-COP1 (LBA4404pBBR1MCS-5.virGN54D); RFP-HA-attB1 = pBatTL-B-p35s-RFP-HA-attB1 (LBA4404pBBR1MCS-5.virGN54D); YFP-attB1= pBatTL-B-p35s-YFP-attB1 (LBA4404pBBR1MCS-5.virGN54D); RK19 = anti silencing strain.

A

	BSA [µg]					
	0	2	4	6	8	10
assay 1	0	0,164	0,292	0,381	0,49	0,577
assay 2	0	0,14	0,27	0,398	0,507	0,596
assay 3	0	0,158	0,286	0,404	0,494	0,576
mean	0,000	0,154	0,283	0,394	0,497	0,583

B

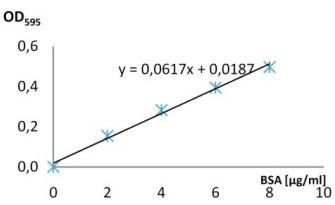

C

	OD595				total protein	loaded volume of input [µl]
sample	1	2	3	mean	[µg/µl]	total protein = 60 µg
YFP-PAP2 RFP-HA-COP1 (+RK19)	0,242	0,24	0,239	0,240	4,198	14,3
YFP-PAP2 RFP-HA-attB1 (+RK19)	0,232	0,227	0,226	0,228	4,004	15,0
YFP-attB1 RFP-HA-COP1 (+RK19)	0,254	0,202	0,259	0,238	4,166	14,4

D

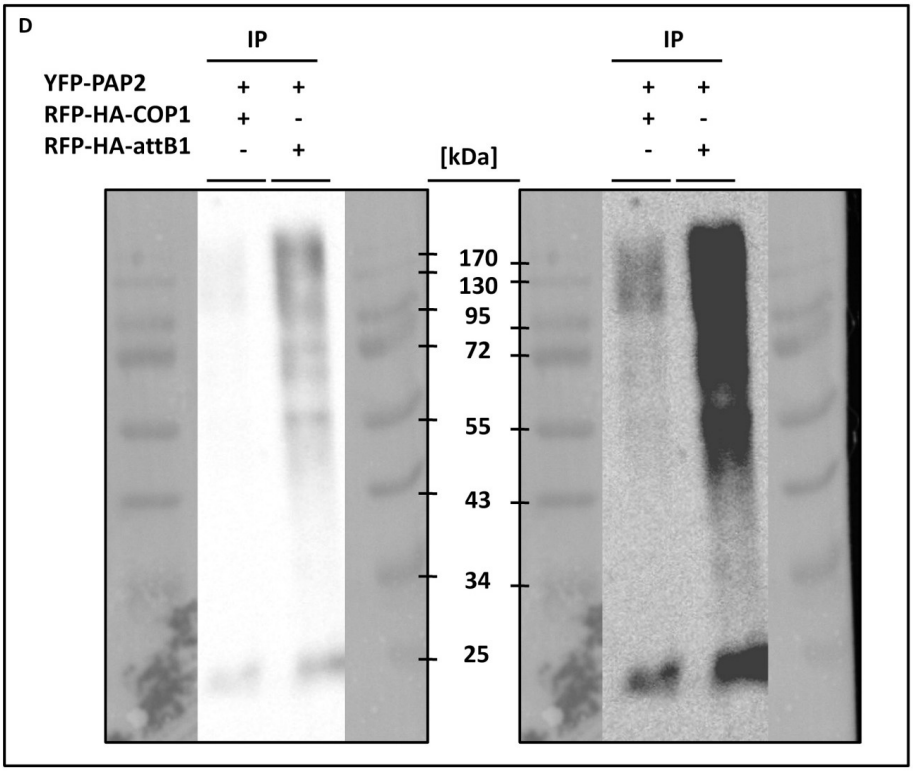

V. Attachment

A R-7: Co-IP. Leaves of *N. benthamiana* were infiltrated with the depicted constructs. Expression of the fusion proteins was verified by Confocal laser-scanning microscopy prior to homogenization three dai. The IP of YFP-PAP2 or YFP-attB1 (Kirik, V. et al., 2007) was performed using Miltenyi αGFP beads. Total protein concentrations were equalized by Bradford analysis. Proteins were separated by SDS-PAGE, blotted and detected with the depicted antibodies. The white area in the fourth band from the left in the lower blot resulted from oversaturation. Bands of the marker (M) corresponds to (from the bottom to the top): 26, 34, 43, 55, 72, 95, 130, 170 kDa.
Images were visualized with a LAS-4000 mini luminescent image analyzer (Fujifilm) in increment mode. YFP-PAP2 = pEarleyGate104-PAP2 (LBA4404. pBBR1MCS.virGN54D); RFP-HA-COP1 = pNmR-COP1 (LBA4404pBBR1MCS-5.virGN54D); RFP-HA-attB1 = pBatTL-B-p35s-RFP-HA-attB1 (LBA4404pBBR1MCS-5.virGN54D); YFP-attB1= pBatTL-B-p35s-YFP-attB1 (LBA4404pBBR1MCS-5.virGN54D); RK19 = anti silencing strain.

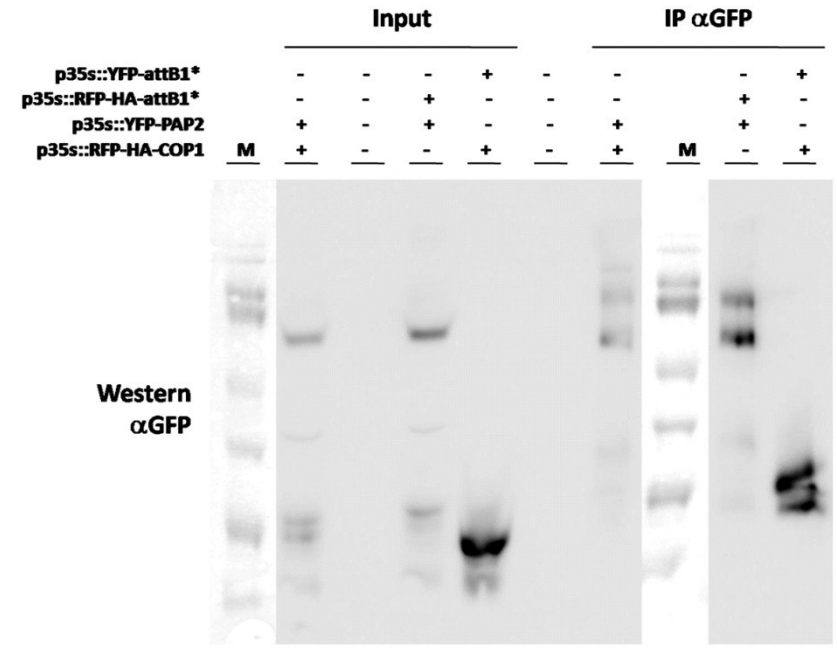

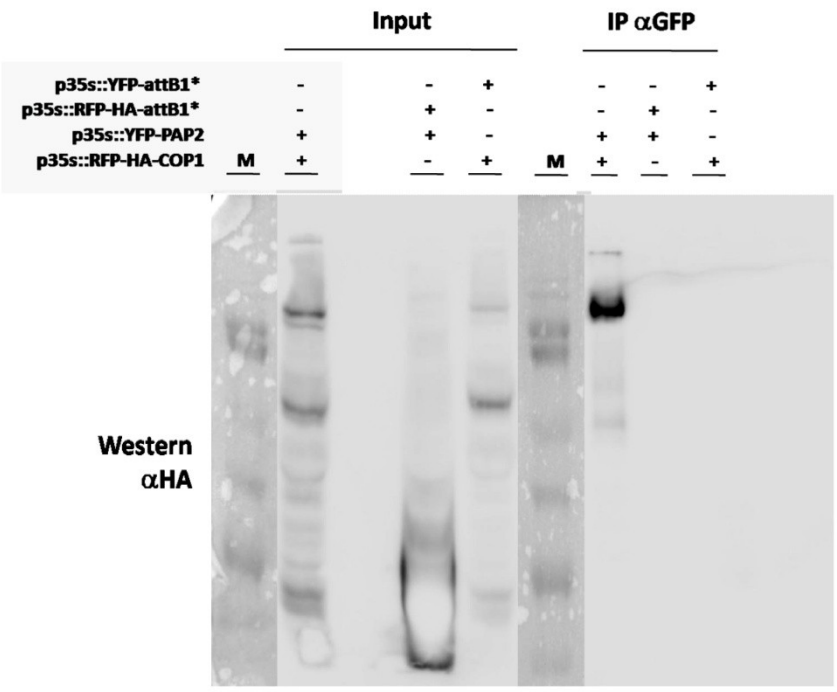

V. Attachment

A R-8: Detection of ubiquitylated proteins in the IP fraction of the Co-IP presented e.g. in Figure III-13. Leaves of *N. benthamiana* were infiltrated with the depicted constructs. Expression of the fusion proteins was verified by CLSM prior to homogenization three dai. The IP of YFP-PAP2 or YFP-attB1 (Kirik, V. et al., 2007) was performed using Miltenyi αGFP beads. Total protein concentrations were equalized by Bradford analysis. Input and IP of leaves infiltrated with RK19 alone served as controls. Proteins were separated by SDS-PAGE, blottest and detected with the depicted antibodies.
Blot from Figure III-14 (upper picture, detection with αUb) subjected to a stripping procedure, detection (middle picture) shows that the stripping was successful. Picture at the bottom shows the same blot after treatment with an αHA and appropiate secondary antibody. Bands of the marker (M) correspond to (from the bottom to the top): 26, 34, 43, 55, 72, 95, 130, 170 kDa. Imaged were visualized with a LAS-4000 mini luminescent image analyzer (Fujifilm) in increment mode. Upper picture was modified with the Multi Gauge program (Fujifilm). YFP-PAP2 = pEarleyGate104-PAP2 (LBA4404. pBBR1MCS.virGN54D); RFP-HA-COP1 = pNmR-COP1 (LBA4404pBBR1MCS-5.virGN54D); RFP-HA-attB1 = pBatTL-B-p35s-RFP-HA-attB1 (LBA4404pBBR1MCS-5.virGN54D); YFP-attB1= pBatTL-B-p35s-YFP-attB1 (LBA4404pBBR1MCS-5.virGN54D); RK19 = anti silencing strain.

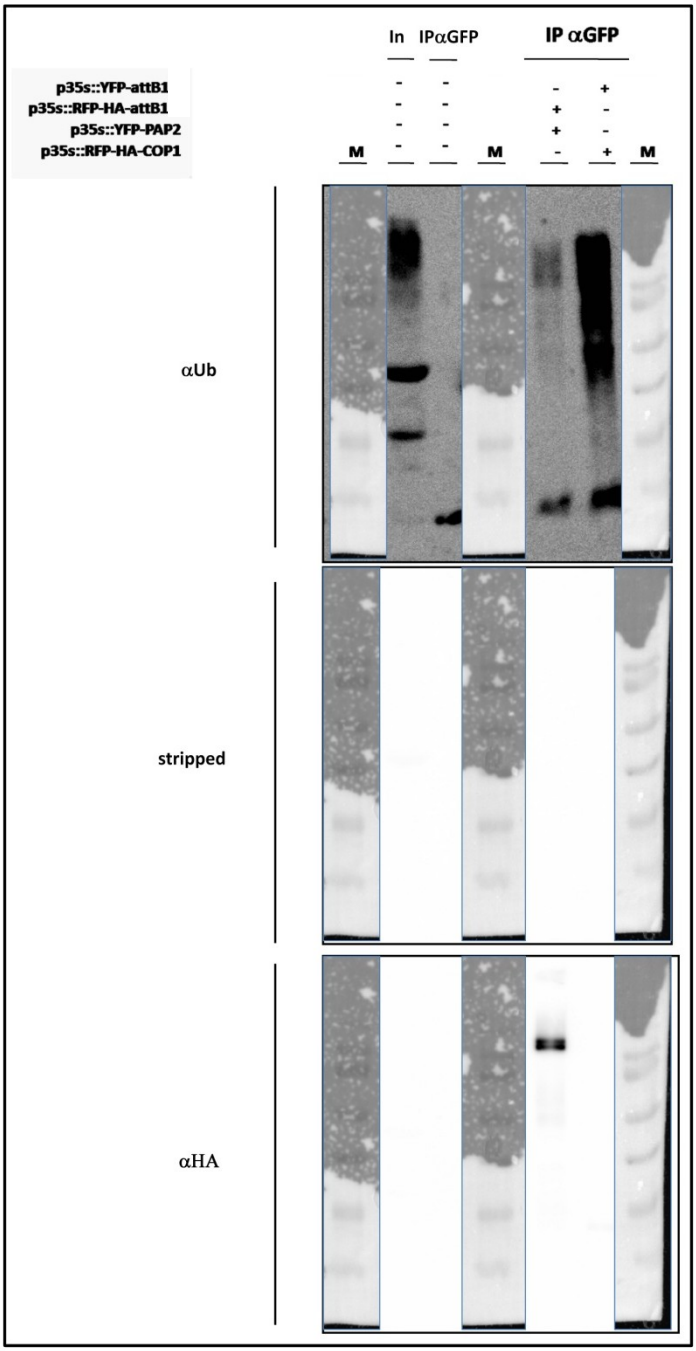

V. Attachment

A R-9: Amersham film of the whole blot presented in Figure II-13 and A R-7. * This band was not detectable with the LAS device. For details see Figure II-xy and A R-7. Detection anti-GFP.

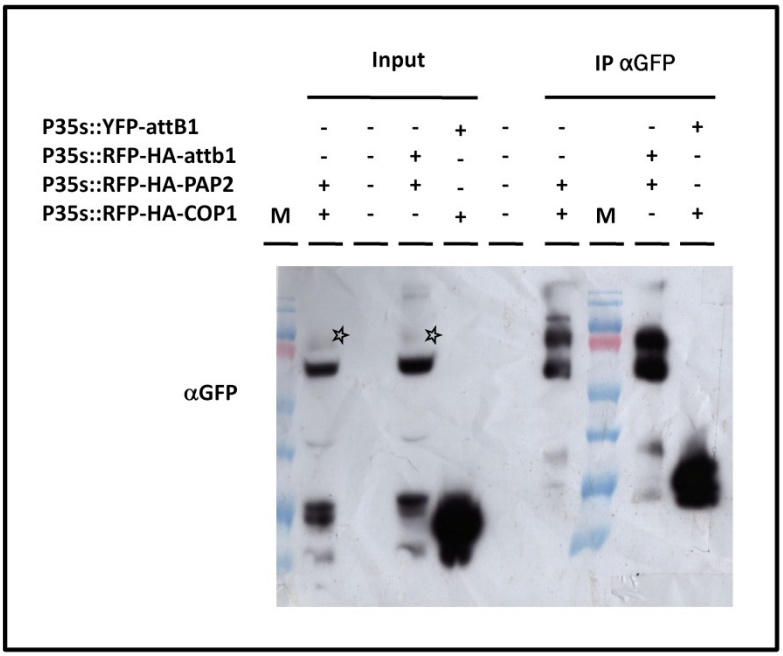

A R-10: Negative controls for the experiment shown in figure III - 16. Combinations with pACT-GFP. For a detailed description see Figure III-16.

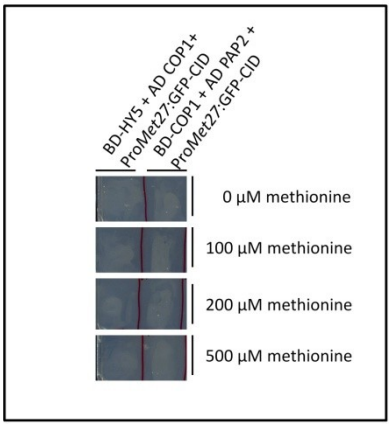

V. Attachment

A R-11: Marker for GARFILD library complexity: 6 to 20 randomly chosen colonies were used for plasmid preparation. Subsequent *Bsr*GI digestion resultet in several fragments comprising of the amplified fragment with 64 bp on average from the primers (64 on average). All fragments were categorized and sorted into size defined classes (0-36 bp, 37-136 bp, etc.) of *PAP2* CDS. In brackets percentage in relation to of all tested fargments of the corresponding library. For more details see Figure III - 18 or Figure III - 19.

template	library	type	No. of fragments of the corresponding size [bp]									
			0-36	37-136	137-236	237-336	337-436	437-536	537-636	637-736	737-836	837-936
PAP2	N-termini	1	7 (39)	7 (39)	1 (6)	2 (11)	0	1 (6)	0	0	0	0
		2	2 (11)	7 (39)	2 (11)	0	0	1 (6)	0	2 (11)	4 (22)	0
	C-termini	3	0	0	1 (5)	6 (30)	11 (55)	2 (10)	0	0	0	0
		4	0	0	0	19 (100)	0	0	0	0	0	0
COP1	N-termini	1	15 (79)	0	0	1 (5)	3 (16)	0	0	0	0	0
		2	3 (17)	1 (6)	4 (22)	7 (39)	0	1 (6)	0	0	1 (6)	1 (6)
	C-termini	3	0	0	12 (80)	3 (20)	0	0	0	0	0	0
		4	0	2 (33)	3 (50)	1 (17)	0	0	0	0	0	0

A R-12: Amino acid sequences of fragments of PAP2 and COP1 identified with GARFILD. Give is the bait, the used library the base pairs coding for the fragment (CDS), the amino acids of the fragment of PAP2 or COP1. Gate: fragment was in the corresponding pAD-Gatex1-3 vector that determines the frame of the *att*B1 site and the fragment. amino acid sequence: black and underlined: aa coded by the *att*B1 site in the given frame and by the random sense primer sequence; black, not underlined: aa coded by the *att*B2 site and by the random antisense primer sequence; blue: aa of PAP2 or COP1, respectively; red: amino acids coded by nucleotides that differ from the PAP2 sequence and were added by a random primers; * bp 480 differed from the PAP2-CDS but the corresponding triplett codes for the same aa; # possibly a frame shift close to the start. Given is the sequence for in frame translation.

bait	library	fragment [bp] of CDS	aa	gate	sequence [aa]
EGL3	PAP2-2	1-375	1-125	2	STSLYKKAGLM^{1}...KKN^{125}AMVSHGLRPSF*
COP1	PAP2-2	1-663	1-221	2	STSLYKKAGLM^{1}...VPEA^{221}DVPWCPHGLRPSFLVQSG*
COP1	PAP2-3	328-747	110-249	2	STSLYKKAGFDHYYALEK^{110}KH...VELD^{249}YPAFLYKVVDGWASIRDPSSSSCR*
COP1	PAP2-4	439-747	147-249	3	SNKFVQKSRLRPLLRPRGF^{147}SVNNG...VELD^{249}VPAFLYKVVRWVGIDTGSIELELQMNRRY*
COP1	PAP2-4	454-737	152-249	3	SNKFVQKSRLRPLLRPRGF^{147}SVDDG^{152}...VELD^{249}VPAFLYKVVRWVGIDTGSIELELQMNRRY*
COP1	COP1-2	1-479*	1-160	2	STSLYKKAGLM^{1}...QEEA^{160}*
COP1/ COP1^{K550E}	COP1-2	1-468	1-156	2	STSLYKKAGLM^{1}...KRKME^{156}PEEPMVSHGLRPSFLVQSQ*
MID	COP1-1	1-202	1-67	2	STSLYKKAGLM^{1}...LTAC^{67}DGPWCRMDYDPAFLYKVVDGWASIRDPSSSSCR*
MID	COP1-1	1-274	1-91	2	STSLYKKAGLM^{1}...CCSQ^{91}PLTFHGVAWTTTQLSCTKWLMGGHRYGIHRARAADES*

V. Attachment

A R-13: NCBI "BLAST2seq" (Altschul et al. 1997 (gapped) results for the alignment of *Arabidopsis thaliana* COP1 and human COP1 Isoform1 with sequences from the Uniprot website (www.uniprot.org). The amino acids that were analysed for the AtCOP1 in Holm et al. (2001) are coloured according to the results presented in the cited paper. Results are given for YTH experiments. green - K422E: significant stronger binding for HY5 in comparison to AtCOP1, weaker for STO and STH; R465E: sligly stronger binding for HY5 in comparison to AtCOP1 and weaker for STO and STH. red - E592R: stronger binding for all interaction partners in comparison to AtCOP1. yellow - K550E and W467A: no binding for all interaction partners.

Query: *Arabidopsis thaliana* COP1 vs. Sbjct: human COP1 Isoform1

Score = 459 bits (1180), Expect = 2e-133, Method: Compositional matrix adjust.
Identities = 259/650 (39%), Positives = 383/650 (58%), Gaps = 69/650 (10%)

```
Query  45   DLDKDLLCPICMQIIKDAFLTACGHSFCYMCIITHLRNKSDCPCCSQHLTN-NQLYPNFL  103
            D   D +CPIC  +I++A++T CGHSFCY CI   L + + CP C+  + N + LYPNFL
Sbjct  129  DKSNDFVCPICFDMIEEAYMTKCGHSFCYKCIHQSLEDNNRCPKCNYVVDNIDHLYPNFL  188

Query  104  LDKLLKKTSARH----------VSKTASPLDQ-FREALQRGCD-VSIKEVDNLLTLLAER  151
            +++L+ K   R           VS T     Q F++ L    D + +  V+ +L LL ++
Sbjct  189  VNELILKQKQRFEEKRFKLDHSVSSTNGHRWQIFQDWLGTDQDNLDLANVNLMLELLVQK  248

Query  152  KRKMEQEEAERNMQILLDFLHCLRKQKVDELNEVQTDLQYIKEDINAVERHRIDLYRARD  211
            K+++E E     +QIL++FL   R+ K ++L ++Q +L  ++EDI  VE     LY
Sbjct  249  KKQLEAESHAAQLQILMEFLKVARRNKREQLEQIQKELSVLEEDIKRVEEMS-GLYSPVS  307

Query  212  RYSVKLRMLGDDPSTRNAWPHEKNQIGFNSNSLSIRGGNFVGNYQNKKVEGKAQGSSHGL  271
              S   +     PS  +           +S   S   G F G+ Q KK
Sbjct  308  EDSTVPQFEAPSPSHSSI---------IDSTEYSQPPG-FSGSSQTKK------------  345

Query  272  PKKDALSGSDSQSLNQSTVSMARKKRIHAQFNDLQECYLQKRRQLADQPNSKQENDKSVV  331
                       Q    ST++ +R+KR+ A F DL++CY   R        S+  +D
Sbjct  346  -----------QPWYNSTLA-SRRKRLTAHFEDLEQCYFSTRM-------SRISDDSRTA  386

Query  332  RREGYSNGLADFQSVLTTFTRYSRLRVIAEIRHG-DIFHSANIVSSIEFDRDDELFATAG  390
             +      L +FQ  L+ FTRY+ +R +A + +  D+++ ++IVSSIEFDRD + FA AG
Sbjct  387  SQ------LDEFQECLSKFTRYNSVRPLATLSYASDLYNGSSIVSSIEFDRDCDYFAIAG  440

Query  391  VSRCIKVFDFSSVVNEPADMQCPIVEMSTRSKLSCLSWNKHEKNHIASSDYEGIVTVWDV  450
            V++ IKV+++ +V+ +  D+  P  EM+  SK+SC+SW+ + KN +ASSDYEG V +WD
Sbjct  441  VTKKIKVYEYDTVIQDAVDIHYPENEMTCNSKISCISWSSYHKNLLASSDYEGTVILWDG  500

Query  451  TTRQSLMEYEEHEKRAWSVDFSRTEPSMLVSGSDDCKVKVWCTRQEASVINIDMKANICC  510
             T Q    Y+EHEKR WSVDF+  +P +L SGSDD KVK+W T  + SV +I+ KAN+CC
Sbjct  501  FTGQRSKVYQEHEKRCWSVDFNLMDPKLLASGSDDAKVKLWSTNLDNSVASIEAKANVCC  560

Query  511  VKYNPGSSNYIAVGSADHHIHYYDLRNISQPLHVFSGHKKAVSYVKFLSNNELASASTDS  570
            VK++P S  ++A G ADH +HYYDLRN  QP+ VF GH+KAVSY KF+S  E+ SASTDS
Sbjct  561  VKFSPSSSRYHLAFGCADHCVHYYDLRNTKQPIMVFKGHRKAVSYAKFVSGEEIVSASTDS  620

Query  571  TLRLWDVKDNLPVRTFRGHTNEKNFVGLTVNSEYLACGSETNEVYVYHKEITRPVTSHRF  630
             L+LW+V     +R+F+GH NEKNFVGL  N +Y+ACGSE N +Y+Y+K +++ + + +F
Sbjct  621  QLKLWNVGKPYCLRSFKGHINEKNFVGLASNGDYIACGSENNSLYLYYKGLSKTLLTFKF  680

Query  631  GSPDM---DDAEEEAGSYFISAVCWKS----DSPTMLTANSQGTIKVLVL  673
             +       D +E+  + F+SAVCW++    +S  ++ ANSQGTIKVL L
Sbjct  681  DTVKSVLDKDRKEDDTNEFVSAVCWRALPDGESNVLIAANSQGTIKVLEL  730
```

A R-14.: NCBI BLASTP results for all possible hCID sequences (Altschul et al. 1997). For a detailed description see Figure II-23. Highlighted in yellow: proteins that also show the AtCID. For all abbrevations see the corresponding Gene-ID at EntrezGene. (Entrez: Maglott et al., 2005)

```
GENE ID: 100287738    76  EDQSQVPEA  84   LOC100287738 | hypothetical protein LOC100287738
GENE ID: 57514       558  EDAKAVPEA  566  ARHGAP31 | Rho GTPase activating protein 31
GENE ID: 284379        8  ESPACVPEA  16   LOC284379 | solute carrier family 7 (cationic amino
                                           acid transporter, y+ system)
```

V. Attachment

GENE ID: 203197	272	ELHQLVPEA	280	C9orf91 | chromosome 9 open reading frame 91
GENE ID: 2037	160	EREEAVPEA	168	EPB41L2 | erythrocyte membrane protein band 4.1-like 2
GENE ID: 57221	1745	EKTIQVPEA	1753	KIAA1244 | KIAA1244
GENE ID: 124565	575	EDPQKVPEA	583	SLC38A10 | solute carrier family 38, member 10
GENE ID: 5764	267	ELDNLVPEA	275	PTN |
GENE ID: 63971	761	EWKEKVPEA	769	KIF13A | kinesin family member 13A
GENE ID: 23013	2307	ETSHSVPEA	2315	SPEN | spen homolog, transcriptional regulator (Drosophila)
GENE ID: 3726	241	EEPQTVPEA	249	JUNB | jun B proto-oncogene
GENE ID: 79024	76	EDQSQVPEA	84	MGC5590 | hypothetical protein
GENE ID: 51246	69	EERCAVPEA	77	SHISA5 | shisa homolog 5 (Xenopus laevis
GENE ID: 9274	185	EPVPPVPEA	193	BCL7C | B-cell CLL/lymphoma
GENE ID: 8807	104	EWEVSVPEA	112	IL18RAP | interleukin 18 receptor accessory protein
GENE ID: 25999	22	EEDEPVPEA	30	CLIP3 | CAP-GLY domain containing linker protein 3
GENE ID: 3840	252	EDPSLVPEA	260	KPNA4 | karyopherin alpha 4 (importin alpha 3)
GENE ID: 100288781	210	ELEDVVPEV	218	LOC100288781 | similar to hCG1994130
GENE ID: 7273	9256	EVSVTVPEV	9264	TTN | titin
	10464	EPPAKVPEV	10472	
GENE ID: 144132	2700	EEEERVPEV	2708	DNHD1 | dynein heavy chain domain 1
GENE ID: 2199	556	EEPLIVPEV	564	FBLN2 | fibulin 2
GENE ID: 2199	582	EEPLIVPEV	590	FBLN2 | fibulin 2
GENE ID: 54578	55	EIVVVVPEV	63	UGT1A6 | UDP glucuronosyltransferase 1 family, polypeptide A6
GENE ID: 79026	595	EGKVKVPEV	603	AHNAK | AHNAK nucleoprotein
GENE ID: 1981	536	EANPAVPEV	544	EIF4G1 | eukaryotic translation initiation factor 4 gamma, 1
GENE ID: 23112	34	EQKTKVPEV	42	TNRC6B | trinucleotide repeat containing 6B
GENE ID: 23228	862	ELQGIVPEV	870	PLCL2 | phospholipase C-like 2
GENE ID: 149371	313	EEEPAVPEV	321	EXOC8 | exocyst complex component 8
GENE ID: 6524	342	EVACVVPEV	350	SLC5A2 | solute carrier family 5 (sodium/glucose cotransporter
GENE ID: 26173	1812	ELRVPVPEV	1820	INTS1 | integrator complex subunit 1
GENE ID: 54578	55	EIVVVVPEV	63	UGT1A6 | UDP glucuronosyltransferase 1 family, polypeptide A6
GENE ID: 55879	30	EFSSAVPEV	38	GABRQ | gamma-aminobutyric acid (GABA) receptor, theta
GENE ID: 653220	31	EPATRVPEV	39	XAGE1B | X antigen family, member 1
GENE ID: 1401	99	EILFEVPEV	107	CRP | C-reactive protein, pentraxin-related
GENE ID: 80233	330	ESGKLVPEL	338	C17orf70 | chromosome 17 open reading frame 70
GENE ID: 100133982	190	ETEPIVPEL	198	LOC100133982 | similar to anaphase promoting complex subunit1
GENE ID: 84988	198	EAARAVPEL	209	PPP1R16A | protein phosphatase 1, regulatory (inhibitor) subunit 16A
GENE ID: 7273	9283	EPPPKVPEL	9291	TTN | titin
GENE ID: 55359	390	EAVLQVPEL	398	STYK1 | serine/threonine/tyrosine kinase 1
GENE ID: 54677	544	EEGLPVPEL	552	CROT | carnitine O-octanoyltransferase
GENE ID: 10178	1001	ERGTIVPEL	1009	ODZ1 | odz, odd Oz/ten-m homolog 1(Drosophila)
GENE ID: 10128	906	EVPFDVPEL	914	LRPPRC | leucine-rich PPR-motif containing
GENE ID: 56181	225	ETEVEVPEL	233	FAM54B | family with sequence similarity 54, member B
GENE ID: 54856	788	ESVLSVPEL	796	GON4L | gon-4-like (C. elegans)
GENE ID: 26128	294	EAEGEVPEL	302	KIAA1279 | KIAA1279 [Homo sapiens]
GENE ID: 9743	48	EEDDFVPEL	56	ARHGAP32 | Rho GTPase activating protein 32
GENE ID: 79026	1798	EIDASVPEL	1806	AHNAK | AHNAK
GENE ID: 22927	134	ESPAKVPEL	142	HABP4 | hyaluronan binding protein 4
GENE ID: 84838	311	ENEPRVPEL	319	ZNF496 | zinc finger protein 496
GENE ID: 64682	399	ETEPIVPEL	407	ANAPC1 | anaphase promoting complex subunit 1
GENE ID: 57731	1105	ELEARVPEL	1113	SPTBN4 | spectrin, beta, non-erythrocytic 4
GENE ID: 7402	1887	ELSLNVPEL	1895	UTRN
GENE ID: 9724	389	EDPEQVPEL	397	UTP14C | UTP14, U3 small nucleolar ribonucleoprotein, homolog C(yeast)
GENE ID: 84182	243	EESRKVPEL	251	FAM188B | family with sequence similarity 188, member B
GENE ID: 115653	46	EDGMPVPEL	54	KIR3DL3 | killer cell immunoglobulin-like receptor
GENE ID: 64601	187	EDSYLVPEL	195	VPS16 | vacuolar protein sorting 16 homolog (S. cerevisiae)
GENE ID: 57125	197	EIPMSVPEI	205	PLXDC1 | plexin domain containing 1
GENE ID: 10645	415	ESRIVVPEI	423	CAMKK2 | calcium/calmodulin-dependent protein kinase kinase 2,beta
GENE ID: 7415	723	EEDDPVPEI	731	VCP | valosin-containing protein
GENE ID: 115701	2003	EGFGEVPEI	2011	ALPK2 | alpha-kinase
GENE ID: 158401	163	ELLNPVPEI	171	C9orf84 | chromosome 9 open reading frame 84
GENE ID: 338	1534	EQGFTVPEI	1542	APOB | apolipoprotein B (including Ag(x) antigen)
GENE ID: 91748	941	EGEEEVPEI	949	C14orf43 | chromosome 14 open reading frame
GENE ID: 26011	1037	EKGPIVPEI	1045	ODZ4 | odz, odd Oz/ten-m homolog 4 (Drosophila)
GENE ID: 389151	140	EFCASVPEI	148	PRR23B | proline rich 23B
GENE ID: 389152	140	EVCASVPEI	148	PRR23C | proline rich 23C
GENE ID: 23281	478	ENKTEVPEP	486	MTUS2 | microtubule associated tumor suppressor candidate 2
GENE ID: 147138	10	ERAPGVPEP	18	TMC8 | transmembrane channel-like 8
GENE ID: 1201	15	EGEETVPEP	23	CLN3 | ceroid-lipofuscinosis, neuronal 3
GENE ID: 6651	464	EPPQEVPEP	472	SON | SON DNA binding protein
	1243	**EAAVTVPEP**	**1251**	
GENE ID: 166614	771	EPEPGVPEP	779	DCLK2 | doublecortin-like kinase 2

V. Attachment

GENE ID: 10861	527	EFEGLVPEP	535	SLC26A1 | solute carrier family 26 (sulfate transporter)
GENE ID: 65249	54	ERFSRVPEP	62	ZSWIM4 | zinc finger, SWIM-type containing 4
GENE ID: 1201	15	EGEETVPEP	23	CLN3 | ceroid-lipofuscinosis, neuronal
GENE ID: 10024	576	EEQLEVPEP	584	TROAP | trophinin associated protein (tastin)
GENE ID: 64151	974	ESDHEVPEP	982	NCAPG | non-SMC condensin I complex, subunit G
GENE ID: 140856	23	EVLGSVPEP	31	C20orf79 | chromosome 20 open reading frame 79
GENE ID: 89849	174	ETLALVPEP	182	ATG16L2 | ATG16 autophagy related 16-like 2 (S. cerevisiae)
GENE ID: 30062	94	EYEGVVPEP	102	RAX | retina and anterior neural fold homeobox
GENE ID: 7040	139	ELREAVPEP	147	TGFB1 | transforming growth factor, beta 1
GENE ID: 64151	394	ESDHEVPEP	402	NCAPG | non-SMC condensin I complex, subunit G
GENE ID: 1633	46	EDWEVVPEP	54	DCK | deoxycytidine kinase
GENE ID: 55086	82	EPRDTVPEP	90	CXorf57 | chromosome X open reading frame 57
GENE ID: 80854	215	ETVIDVPEP	223	SETD7 | SET domain containing (lysine methyltransferase) 7
GENE ID: 54704	118	EYSFKVPEF	126	PDP1 | pyruvate dehyrogenase phosphatase catalytic subunit 1
GENE ID: 8731	121	EGVVDVPEF	129	RNMT | RNA (guanine-7-)
GENE ID: 84263	166	ESTGAVPEF	174	HSDL2 | hydroxysteroid dehydrogenase like 2
GENE ID: 22820	351	EQLAAVPEF	359	COPG | coatomer protein complex, subunit gamma
GENE ID: 29109	148	EDKDLVPEF	156	FHOD1 | formin homology 2 domain containing 1
GENE ID: 374354	49	EQDLSVPEF	57	NHLRC2 | NHL repeat containing 2
GENE ID: 9223	239	EEEDDVPEM	247	MAGI1 | membrane associated guanylate kinase
GENE ID: 80125	621	EEEPLVPEM	629	CCDC33 | coiled-coil domain containing 33
GENE ID: 255349	190	ERIIFVPEM	198	TMEM211 | transmembrane protein 211
GENE ID: 139818	621	EVEEFVPEM	629	DOCK11 | dedicator of cytokinesis 11
GENE ID: 3725	127	EEPQTVPEM	135	JUN | jun oncogene
GENE ID: 51042	122	EVSTEVPEM	130	ZNF593 | zinc finger protein 593
GENE ID: 2735	385	ESRLTVPEG	393	GLI1 | GLI family zinc finger 1
GENE ID: 100287170	36	ELLELVPEG	44	LOC100287170 | hypothetical protein LOC100287170
GENE ID: 6397	456	ECMCEVPEG	464	SEC14L1 | SEC14-like 1 (S. cerevisiae)
GENE ID: 1950	509	EEGVDVPEG	517	EGF | epidermal growth factor (beta-urogastrone)
GENE ID: 57017	169	EEDRPVPEG	177	COQ9 | coenzyme Q9 homolog (S. cerevisiae)
GENE ID: 441239	521	EPHRGVPEG	529	LOC441239 | hypothetical protein LOC441239
GENE ID: 55596	324	ELDLPVPEG	332	ZCCHC8 | zinc finger, CCHC domain containing 8
GENE ID: 651746	70	ESAESVPEG	78	ANKRD33B | ankyrin repeat domain 33B
GENE ID: 147912	590	ETAISVPEG	598	SIX5 | SIX homeobox
GENE ID: 161176	846	ELEARVPEG	854	C14orf49 | chromosome 14 open reading frame 49
GENE ID: 6614	1450	EPGLDVPEG	1458	SIGLEC1 | sialic acid binding Ig-like lectin 1, sialoadhesin
GENE ID: 84678	469	ENKKCVPEG	477	KDM2B | lysine (K)-specific demethylase 2B
GENE ID: 84314	17	ETAALVPEG	25	TMEM107 | transmembrane protein 107
GENE ID: 84925	254	ETVYPVPEG	262	DIRC2 | disrupted in renal carcinoma 2
GENE ID: 9717	477	ESVCNVPEG	485	SEC14L5 | SEC14-like 5 (S. cerevisiae)
GENE ID: 1950	551	EEGVDVPEG	559	EGF | epidermal growth factor (beta-urogastrone)
GENE ID: 7564	121	ERDWGVPEG	129	ZNF16 | zinc finger protein 16
GENE ID: 8531	266	EMKDGVPEG	274	CSDA | cold shock domain protein A
GENE ID: 147912	9	ETAISVPEG	17	SIX5 | SIX homeobox 5
GENE ID: 126823	253	EQWAGVPEG	261	KLHDC9 | kelch domain containing 9
GENE ID: 54102	142	EQRPEVPEG	150	CLIC6 | chloride intracellular channel 6
GENE ID: 158471	1921	ENPALVPDA	1929	PRUNE2 | prune homolog 2 (Drosophila)
GENE ID: 5175	710	EVRKAVPDA	718	PECAM1 | platelet/endothelial cell adhesion molecule
GENE ID: 3681	132	EIIQTVPDA	140	ITGAD | integrin, alpha D
GENE ID: 8395	286	ETPQNVPDA	294	PIP5K1B | phosphatidylinositol-4-phosphate 5-kinase, type I, beta
GENE ID: 155400	53	ENEDMVPDA	61	NSUN5P1 | NOP2/Sun domain family, member 5 pseudogene 1
GENE ID: 3560	500	EAGEEVPDA	508	IL2RB | interleukin 2 receptor, beta
GENE ID: 6584	47	EHRCRVPDA	55	SLC22A5 | solute carrier family 22 (organic cation/carnitine transporter), member 5
GENE ID: 79635	89	ELQTQVPDA	97	CCDC121 | coiled-coil domain containing 121
GENE ID: 11099	759	EPKAHVPDA	767	PTPN21 | protein tyrosine phosphatase, non-receptor type 21
GENE ID: 27143	742	EELVSVPDA	750	KIAA1274 |
GENE ID: 23239	846	EAVRNVPDA	854	PHLPP1 | PH domain and leucine rich repeat protein phosphatase 1
GENE ID: 388666	108	ETDVCVPDA	116	FLJ36116 | hypothetical locus LOC388666
GENE ID: 9603	176	EPTAQVPDA	184	NFE2L3 | nuclear factor (erythroid-derived 2)-like 3
GENE ID: 374383	412	EHSDAVPDA	420	DKFZp686O24166 | hypothetical protein DKFZp686O24166
GENE ID: 7273	2419	ECKVSVPDV	2427	TTN | titin
GENE ID: 79026	844	ESEIKVPDV	852	AHNAK | AHNAK nucleoprotein
GENE ID: 79960	712	ENDGYVPDV	720	PHF17 | PHD finger protein 17
GENE ID: 55814	1926	EITVNVPDV	1934	BDP1 | B double prime 1, subunit of RNA polymerase III transcription initiation factor IIIB
GENE ID: 122402	449	ESSVTVPDV	457	TDRD9 | tudor domain containing 9
GENE ID: 63893	878	EKMEAVPDV	886	UBE2O | ubiquitin-conjugating enzyme E2O
GENE ID: 374786	35	ETLQSVPDV	43	EFCAB5 | EF-hand calcium binding domain 5
GENE ID: 64969	246	EPEDEVPDV	254	MRPS5 | mitochondrial ribosomal protein S5
GENE ID: 374666	228	ENYFYVPDL	236	WASH3P | WAS protein family homolog 3 pseudogene
GENE ID: 100287171	247	ENYFYVPDL	255	WASH1 | WAS protein family homolog 1

V. Attachment

GENE ID: 8516	628	EDNLCVPDL	636	ITGA8 | integrin, alpha 8
GENE ID: 51144	134	EYFLDVPDL	142	HSD17B12 | hydroxysteroid (17-beta) dehydrogenase 12
GENE ID: 3678	647	EDNICVPDL	655	ITGA5 | integrin, alpha 5 (fibronectin receptor, alpha polypeptide)
GENE ID: 57469	284	EDKNGVPDL	292	PNMAL2 | PNMA-like 2
GENE ID: 653440	175	ENYFYVPDL	183	WASH6P | WAS protein family homolog 6 pseudogene
GENE ID: 22801	783	EDEHCVPDL	791	ITGA11 | integrin, alpha 11
GENE ID: 85441	490	EEQLVVPDL	498	PRIC285 | peroxisomal proliferator-activated receptor A interacting complex 285
GENE ID: 79026	3899	EGDMQVPDL	3907	AHNAK | AHNAK nucleoprotein
GENE ID: 400793	194	EVSLSVPDL	202	C1orf226 | chromosome 1 open reading frame 226
GENE ID: 9110	848	EQLSSVPDL	856	MTMR4 | myotubularin related protein 4
GENE ID: 100131401	136	EEDDDVPDL	144	LOC100131401 | similar to hCG2008008
GENE ID: 54997	98	ENFNNVPDL	106	TESC | tescalcin
GENE ID: 51289	23	ELFSLVPDL	31	RXFP3 | relaxin/insulin-like family peptide receptor 3
GENE ID: 91408	132	EEDDDVPDL	140	BTF3L4 | basic transcription factor 3-like 4
GENE ID: 375260	29	ENYFYVPDL	37	WASH2P | WAS protein family homolog 2 pseudogene
GENE ID: 5364	551	EVFLSVPDL	559	PLXNB1 | plexin B1
GENE ID: 653635	29	ENYFYVPDL	37	WASH5P | WAS protein family homolog 5 pseudogene
GENE ID: 5545	200	ETSPEVPDL	208	PRB4 | proline-rich protein BstNI subfamily 4
GENE ID: 100286910	65	EQGTDVPDI	73	LOC100286910 | hypothetical protein LOC100286910
GENE ID: 23095	755	EFLNLVPDI	763	KIF1B | kinesin family member 1B
GENE ID: 7753	292	EEEPWVPDI	300	ZNF202 | zinc finger protein 202
GENE ID: 9590	1024	EVEGGVPDI	1032	AKAP12 | A kinase (PRKA) anchor protein 12
GENE ID: 55187	125	EISHTVPDI	133	VPS13D | vacuolar protein sorting 13 homolog D (S. cerevisiae)
GENE ID: 84254	433	ETRIGVPDI	441	CAMKK1 | calcium/calmodulin-dependent protein kinase kinase 1,alpha
GENE ID: 79712	193	ETFTDVPDI	201	GTDC1 | glycosyltransferase-like domain containing 1
GENE ID: 4976	131	EYKWIVPDI	139	OPA1 | optic atrophy 1 (autosomal dominant)
GENE ID: 338	1635	ELQWPVPDI	1643	APOB | apolipoprotein B (including Ag(x) antigen)
GENE ID: 23120	838	EDPACVPDI	846	ATP10B | ATPase, class V, type 10B
GENE ID: 64780	809	EGAGPVPDP	817	MICAL1 | microtubule associated monoxygenase, calponin and LIM domain containing 1
GENE ID: 29882	476	EPEDWVPDP	484	ANAPC2 | anaphase promoting complex subunit 2
GENE ID: 650621	247	EPEDWVPDP	258	LOC650621 | similar to Anaphase promoting complex subunit 2
GENE ID: 11176	87	EVSVLVPDP	95	BAZ2A | bromodomain adjacent to zinc finger domain, 2A
GENE ID: 441457	518	EAAREVPDP	526	FAM22G | family with sequence similarity 22, member G
GENE ID: 63892	427	EGADFVPDP	435	THADA | thyroid adenoma associated
GENE ID: 55105	312	ELDKNVPDP	320	GPATCH2 | G patch domain containing 2
GENE ID: 100288570	167	EELRGVPDP	175	LOC100288570 | similar to glycosylphosphatidyl-inositol anchor attachment protein 1 homolog (yeast)
GENE ID: 65989	153	ELVLPVPDP	161	DLK2 | delta-like 2 homolog (Drosophila)
GENE ID: 5493	936	EVLKKVPDP	944	PPL | periplakin
GENE ID: 4942	77	EAGVVVPDP	85	OAT | ornithine aminotransferase
GENE ID: 4939	578	EQGSGVPDF	586	OAS2 | 2'-5'-oligoadenylate synthetase 2, 69/71kDa
GENE ID: 5257	203	ERVYRVPDF	211	PHKB | phosphorylase kinase, beta
GENE ID: 2353	248	ETARSVPDM	256	FOS | FBJ murine osteosarcoma viral oncogene homolog
GENE ID: 11022	276	EENRAVPDM	284	TDRKH | tudor and KH domain containing
GENE ID: 5909	300	ENTPFVPDM	308	RAP1GAP | RAP1 GTPase activating protein
GENE ID: 23108	300	ENTPFVPDM	308	RAP1GAP2 | RAP1 GTPase activating protein 2
GENE ID: 79026	2479	EGKLEVPDM	2487	AHNAK | AHNAK nucleoprotein
GENE ID: 51374	222	ENGSCVPDG	230	C2orf28 | chromosome 2 open reading frame 28
GENE ID: 389333	203	EAQRLVPDG	211	LOC389333 | hypothetical protein LOC389333
GENE ID: 84519	80	ENHGLVPDG	88	ACRBP | acrosin binding protein
GENE ID: 284207	44	ELRLLVPDG	52	METRNL | meteorin, glial cell differentiation regulator-like
GENE ID: 221178	548	EKEEVVPDG	556	SPATA13 | spermatogenesis associated 13
GENE ID: 9203	67	EKDPGVPDG	75	ZMYM3 | zinc finger, MYM-type 3
GENE ID: 3973	34	EPCNCVPDG	42	LHCGR | luteinizing hormone/choriogonadotropin receptor
GENE ID: 3973	34	EPCNCVPDG	42	LHCGR | luteinizing hormone/choriogonadotropin receptor
GENE ID: 54726	2	EAAVGVPDG	10	OTUD4 | OTU domain containing 4
GENE ID: 81622	20	EDLLGVPDG	28	UNC93B1 | unc-93 homolog B1 (C. elegans)
GENE ID: 2068	502	EMSAVVPDG	510	ERCC2 | excision repair cross-complementing rodent repair deficiency, complementation group 2
GENE ID: 57761	333	EAAQVVPDG	341	TRIB3 | tribbles homolog 3 (Drosophila)
GENE ID: 79147	124	EFVALVPDG	132	FKRP | fukutin related protein

V. Attachment

A R-15: Aignment of of *MID*-CDS (Ler) (the sequence published in Kirik et al. (2007)), *MID*-CDS (Col-0) (the sequenced used in this work and verified by sequencing) and six splicing variants annotated by TAIR (www.arabidopsis.org) for *BIN4* that is a synonym for *MID*. Coloured are all differences between the sequences. Note that *MID*-CDS (Col-0), *BIN4.3*-CDS and *BIN4.4*-CDS match 100%. The aligment was done using CLC DNA Workbench (CLC bio A/S).

V. Attachment

```
MID CDS (Ler)    ATGAGCAGCA GCTCTAGAGA GGGATCTCCA GATTGGCTTC 40
MID CDS (Col-0)  ATGAGCAGCA GCTCTAGAGA GGGATCTCCA GATTGGCTTC 40
BIN4.1-CDS       ATGAGCAGCA GCTCTAGAGA GGGATCTCCA GATTGGCTTC 40
BIN4.2-CDS       ATGAGCAGCA GCTCTAGAGA GGGATCTCCA GATTGGCTTC 40
BIN4.3-CDS       ATGAGCAGCA GCTCTAGAGA GGGATCTCCA GATTGGCTTC 40
BIN4.4-CDS       ATGAGCAGCA GCTCTAGAGA GGGATCTCCA GATTGGCTTC 40
BIN4.5-CDS       ATGAGCAGCA GCTCTAGAGA GGGATCTCCA GATTGGCTTC 40
BIN4.6-CDS       ATGAGCAGCA GCTCTAGAGA GGGATCTCCA GATTGGCTTC 40

MID CDS (Ler)    GCTCTTACGA GGCACCCATG ACTACTTCAT TGTTGTCGCT 80
MID CDS (Col-0)  GCTCTTACGA GGCACCCATG ACTACTTCAT TGTTGTCGCT 80
BIN4.1-CDS       GCTCTTACGA GGCACCCATG ACTACTTCAT TGTTGTCGCT 80
BIN4.2-CDS       GCTCTTACGA GGCACCCATG ACTACTTCAT TGTTGTCGCT 80
BIN4.3-CDS       GCTCTTACGA GGCACCCATG ACTACTTCAT TGTTGTCGCT 80
BIN4.4-CDS       GCTCTTACGA GGCACCCATG ACTACTTCAT TGTTGTCGCT 80
BIN4.5-CDS       GCTCTTACGA GGCACCCATG ACTACTTCAT TGTTGTCGCT 80
BIN4.6-CDS       GCTCTTACGA GGCACCCATG ACTACTTCAT TGTTGTCGCT 80

MID CDS (Ler)    ATCATCTTCA GATGATGATA GTCCTTATAG GGAATCTGAA 120
MID CDS (Col-0)  ATCATCTTCA GATGATGATA GTCCTTATAG GGAATCTGAA 120
BIN4.1-CDS       ATCATCTTCA GATGATGATA GTCCTTATAG GGAATCTGAA 120
BIN4.2-CDS       ATCATCTTCA GATGATGATA GTCCTTATAG GGAATCTGAA 120
BIN4.3-CDS       ATCATCTTCA GATGATGATA GTCCTTATAG GGAATCTGAA 120
BIN4.4-CDS       ATCATCTTCA GATGATGATA GTCCTTATAG GGAATCTGAA 120
BIN4.5-CDS       ATCATCTTCA GATGATGATA GTCCTTATAG GGAATCTGAA 120
BIN4.6-CDS       ATCATCTTCA GATGATGATA GTCCTTATAG GGAATCTGAA 120

MID CDS (Ler)    GTCATTTCGT CTCTTCCTTT GCCTGATGAT GACGGTGACG 160
MID CDS (Col-0)  GTCATTTCGT CTCTTCCTTT GCCTGATGAT GACGGTGACG 160
BIN4.1-CDS       GTCATTTCGT CTCTTCCTTT GCCTGATGAT GACGGTGACG 160
BIN4.2-CDS       GTCATTTCGT CTCTTCCTTT GCCTGATGAT GACGGTGACG 160
BIN4.3-CDS       GTCATTTCGT CTCTTCCTTT GCCTGATGAT GACGGTGACG 160
BIN4.4-CDS       GTCATTTCGT CTCTTCCTTT GCCTGATGAT GACGGTGACG 160
BIN4.5-CDS       GTCATTTCGT CTCTTCCTTT GCCTGATGAT GACGGTGACG 160
BIN4.6-CDS       GTCATTTCGT CTCTTCCTTT GCCTGATGAT GACGGTGACG 160

MID CDS (Ler)    ACATTGTGGT TCTTGAGACA GAATCTGTGG AGTTACTGAC 200
MID CDS (Col-0)  ACATTGTGGT TCTTGAGACA GAATCTGTGG AGTTACTGAC 200
BIN4.1-CDS       ACATTGTGGT TCTTGAGACA GAATCTGTGG AGTTACTGAC 200
BIN4.2-CDS       ACATTGTGGT TCTTGAGACA GAATCTGTGG AGTTACTGAC 200
BIN4.3-CDS       ACATTGTGGT TCTTGAGACA GAATCTGTGG AGTTACTGAC 200
BIN4.4-CDS       ACATTGTGGT TCTTGAGACA GAATCTGTGG AGTTACTGAC 200
BIN4.5-CDS       ACATTGTGGT TCTTGAGACA GAATCTGTGG AGTTACTGAC 200
BIN4.6-CDS       ACATTGTGGT TCTTGAGACA GAATCTGTGG AGTTACTGAC 200

MID CDS (Ler)    TAGGAAGAAT TCCGAAACGA AGGTTGTGAC GAAGCAAGTG 240
MID CDS (Col-0)  TAGGAAGAAT TCCGAAACGA AGGTTGTGAC GAAGCAAGTG 240
BIN4.1-CDS       TAGGAAGAAT TCCGAAACGA AGGTTGTGAC GAAGCAAGTG 240
BIN4.2-CDS       TAGGAAGAAT TCCGAAACGA AGGTTGTGAC GAAGCAAGTG 240
BIN4.3-CDS       TAGGAAGAAT TCCGAAACGA AGGTTGTGAC GAAGCAAGTG 240
BIN4.4-CDS       TAGGAAGAAT TCCGAAACGA AGGTTGTGAC GAAGCAAGTG 240
BIN4.5-CDS       TAGGAAGAAT TCCGAAACGA AGGTTGTGAC GAAGCAAGTG 240
BIN4.6-CDS       TAGGAAGAAT TCCGAAACGA AGGTTGTGAC GAAGCAAGTG 240

MID CDS (Ler)    AGTATCGAGC AGGTGTTTTC TAGAAAGAAG AAAGCAGATG 280
MID CDS (Col-0)  AGTATCGAGC AGGTGTTTTC TAGAAAGAAG AAAGCAGATG 280
BIN4.1-CDS       AGTATCGAGC AGGTGTTTTC TAGAAAGAAG AAAGCAGATG 280
BIN4.2-CDS       AGTATCGAGC AGGTGTTTTC TAGAAAGAAG AAAGCAGATG 280
BIN4.3-CDS       AGTATCGAGC AGGTGTTTTC TAGAAAGAAG AAAGCAGATG 280
BIN4.4-CDS       AGTATCGAGC AGGTGTTTTC TAGAAAGAAG AAAGCAGATG 280
BIN4.5-CDS       AGTATCGAGC AGGTGTTTTC TAGAAAGAAG AAAGCAGATG 280
BIN4.6-CDS       AGTATCGAGC AGGTGTTTTC TAGAAAGAAG AAAGCAGATG 280

MID CDS (Ler)    CTAGTCTCAA CCTTGAAG-- ---------- GGAAGGAGAA 308
MID CDS (Col-0)  CTAGTCTCAA CCTTGAAG-- ---------- GGAAGGAGAA 308
BIN4.1-CDS       CTAGTCTCAA CCTTGAAG-- ---------- GGAAGGAGAA 308
BIN4.2-CDS       CTAGTCTCAA CCTTGAAG-- ---------- GGAAGGAGAA 308
BIN4.3-CDS       CTAGTCTCAA CCTTGAAG-- ---------- GGAAGGAGAA 308
BIN4.4-CDS       CTAGTCTCAA CCTTGAAG-- ---------- GGAAGGAGAA 308
BIN4.5-CDS       CTAGTCTCAA CCTTGAAG-- ---------- GGAAGGAGAA 308
BIN4.6-CDS       CTAGTCTCAA CCTTGAAGAT TCGTGTGCAG GGAAGGAGAA 320

MID CDS (Ler)    TGGAAACAAC GTTGACTGTG AAAAACTCTC TAGCAAGCAT 348
MID CDS (Col-0)  TGGAAACAAC GTTGACTGTG AAAAACTCTC TAGCAAGCAT 348
BIN4.1-CDS       TGGAAACAAC GTTGACTGTG AAAAACTCTC TAGCAAGCAT 348
BIN4.2-CDS       TGGAAACAAC GTTGACTGTG AAAAACTCTC TAGCAAGCAT 348
BIN4.3-CDS       TGGAAACAAC GTTGACTGTG AAAAACTCTC TAGCAAGCAT 348
BIN4.4-CDS       TGGAAACAAC GTTGACTGTG AAAAACTCTC TAGCAAGCAT 348
BIN4.5-CDS       TGGAAACAAC GTTGACTGTG AAAAACTCTC TAGCAAGCAT 348
BIN4.6-CDS       TGGAAACAAC GTTGACTGTG AAAAACTCTC TAGCAAGCAT 360

MID CDS (Ler)    AAGGATGCTC AA---GGAGG AGCTGATTCT GTATGGCTTG 385
MID CDS (Col-0)  AAGGATGCTC AA---GGAGG AGCTGATTCT GTATGGCTTG 385
BIN4.1-CDS       AAGGATGCTC AACAGGGAGG AGCTGATTCT GTATGGCTTG 388
BIN4.2-CDS       AAGGATGCTC AA---GGAGG AGCTGATTCT GTATGGCTTG 385
BIN4.3-CDS       AAGGATGCTC AA---GGAGG AGCTGATTCT GTATGGCTTG 385
BIN4.4-CDS       AAGGATGCTC AA---GGAGG AGCTGATTCT GTATGGCTTG 385
BIN4.5-CDS       AAGGATGCTC AA---GGAGG AGCTGATTCT GTATGGCTTG 385
BIN4.6-CDS       AAGGATGCTC AA---GGAGG AGCTGATTCT GTATGGCTTG 397

MID CDS (Ler)    TCTCATCTGA TTCTGAGCCA TCCTCTCCTA TAAAGCAGGA 425
MID CDS (Col-0)  TCTCATCTGA TTCTGAGCCA TCCTCTCCTA TAAAGCAGGA 425
BIN4.1-CDS       TCTCATCTGA TTCTGAGCCA TCCTCTCCTA TAAAGCAGGA 428
BIN4.2-CDS       TCTCATCTGA TTCTGAGCCA TCCTCTCCTA TAAAGCAGGA 425
BIN4.3-CDS       TCTCATCTGA TTCTGAGCCA TCCTCTCCTA TAAAGCAGGA 425
BIN4.4-CDS       TCTCATCTGA TTCTGAGCCA TCCTCTCCTA TAAAGCAGGA 425
BIN4.5-CDS       TCTCATCTGA TTCTGAGCCA TCCTCTCCTA TAAAGCAGGA 425
BIN4.6-CDS       TCTCATCTGA TTCTGAGCCA TCCTCTCCTA TAAAGCAGGA 437
```

V. Attachment

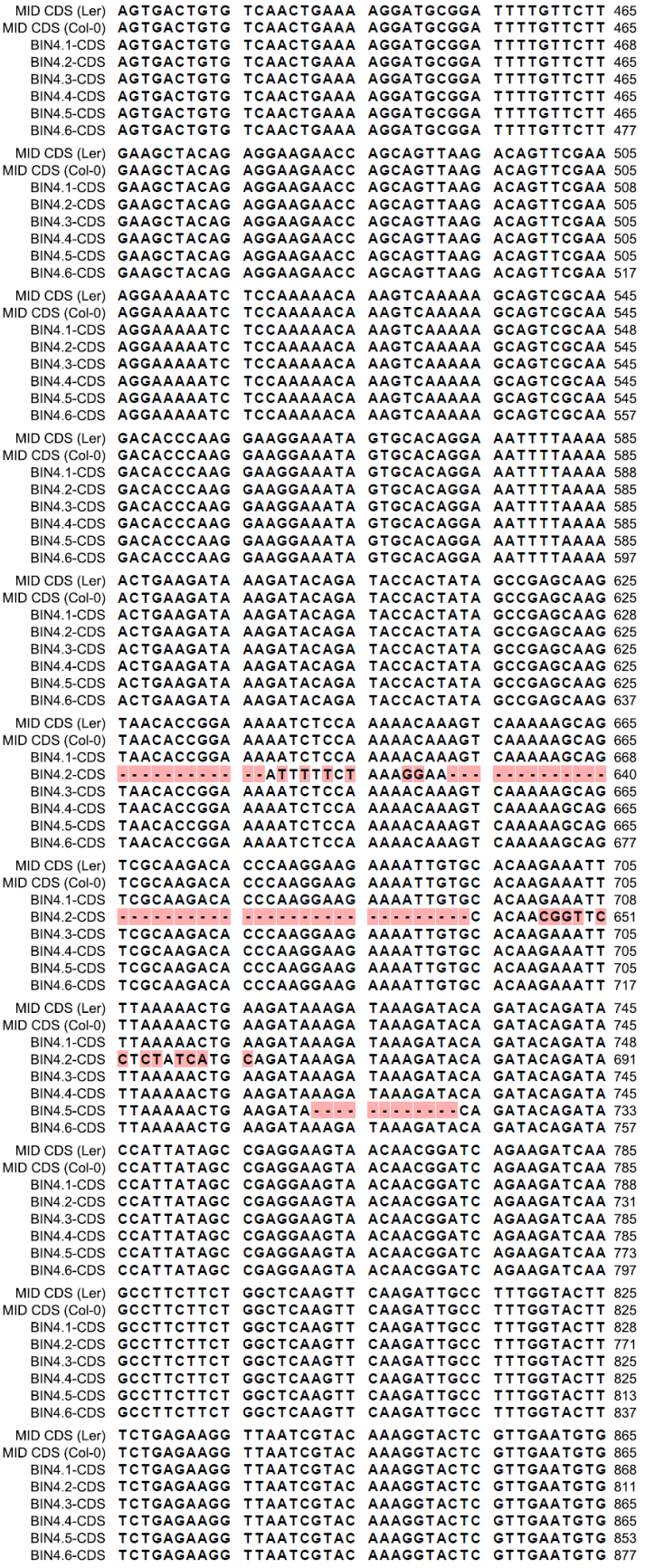

V. Attachment

```
MID CDS (Ler)  AAGGTGACTC GATAGATTTG AGTGGAGACA TGGGGGCTGT 905
MID CDS (Col-0) AAGGTGACTC GATAGATTTG AGTGGAGACA TGGGGGCTGT 905
BIN4.1-CDS     AAGGTGACTC GATAGATTTG AGTGGAGACA TGGGGGCTGT 908
BIN4.2-CDS     AAGGTGACTC GATAGATTTG AGTGGAGACA TGGGGGCTGT 851
BIN4.3-CDS     AAGGTGACTC GATAGATTTG AGTGGAGACA TGGGGGCTGT 905
BIN4.4-CDS     AAGGTGACTC GATAGATTTG AGTGGAGACA TGGGGGCTGT 905
BIN4.5-CDS     AAGGTGACTC GATAGATTTG AGTGGAGACA TGGGGGCTGT 893
BIN4.6-CDS     AAGGTGACTC GATAGATTTG AGTGGAGACA TGGGGGCTGT 917

MID CDS (Ler)  TGGACGCGTG GTTGTTTCAG ACACAACCGG GGACATGTAC 945
MID CDS (Col-0) TGGACGCGTG GTTGTTTCAG ACACAACCGG GGACATGTAC 945
BIN4.1-CDS     TGGACGCGTG GTTGTTTCAG ACACAACCGG GGACATGTAC 948
BIN4.2-CDS     TGGACGCGTG GTTGTTTCAG ACACAACCGG GGACATGTAC 891
BIN4.3-CDS     TGGACGCGTG GTTGTTTCAG ACACAACCGG GGACATGTAC 945
BIN4.4-CDS     TGGACGCGTG GTTGTTTCAG ACACAACCGG GGACATGTAC 945
BIN4.5-CDS     TGGACGCGTG GTTGTTTCAG ACACAACCGG GGACATGTAC 933
BIN4.6-CDS     TGGACGCGTG GTTGTTTCAG ACACAACCGG GGACATGTAC 957

MID CDS (Ler)  TTGGACTTGA AAGGAACCAT ATATAAATCA ACAATCATTC 985
MID CDS (Col-0) TTGGACTTGA AAGGAACCAT ATATAAATCA ACAATCATTC 985
BIN4.1-CDS     TTGGACTTGA AAGGAACCAT ATATAAATCA ACAATCATTC 988
BIN4.2-CDS     TTGGACTTGA AAGGAACCAT ATATAAATCA ACAATCATTC 931
BIN4.3-CDS     TTGGACTTGA AAGGAACCAT ATATAAATCA ACAATCATTC 985
BIN4.4-CDS     TTGGACTTGA AAGGAACCAT ATATAAATCA ACAATCATTC 985
BIN4.5-CDS     TTGGACTTGA AAGGAACCAT ATATAAATCA ACAATCATTC 973
BIN4.6-CDS     TTGGACTTGA AAGGAACCAT ATATAAATCA ACAATCATTC 997

MID CDS (Ler)  CATCCAGAAC ATTTTGCGTT GTTAACGTAG GTCAGACAGA 1025
MID CDS (Col-0) CATCCAGAAC ATTTTGCGTT GTTAACGTAG GTCAGACAGA 1025
BIN4.1-CDS     CATCCAGAAC ATTTTGCGTT GTTAACGTAG GTCAGACAGA 1028
BIN4.2-CDS     CATCCAGAAC ATTTTGCGTT GTTAACGTAG GTCAGACAGA 971
BIN4.3-CDS     CATCCAGAAC ATTTTGCGTT GTTAACGTAG GTCAGACAGA 1025
BIN4.4-CDS     CATCCAGAAC ATTTTGCGTT GTTAACGTAG GTCAGACAGA 1025
BIN4.5-CDS     CATCCAGAAC ATTTTGCGTT GTTAACGTAG GTCAGACAGA 1013
BIN4.6-CDS     CATCCAGAAC ATTTTGCGTT GTTAACGTAG GTCAGACAGA 1037

MID CDS (Ler)  GGCTAAGATT GAAGCTATTA TGAATGACTT CATACAGCTG 1065
MID CDS (Col-0) GGCTAAGATT GAAGCTATTA TGAATGACTT CATACAGCTG 1065
BIN4.1-CDS     GGCTAAGATT GAAGCTATTA TGAATGACTT CATACAGCTG 1068
BIN4.2-CDS     GGCTAAGATT GAAGCTATTA TGAATGACTT CATACAGCTG 1011
BIN4.3-CDS     GGCTAAGATT GAAGCTATTA TGAATGACTT CATACAGCTG 1065
BIN4.4-CDS     GGCTAAGATT GAAGCTATTA TGAATGACTT CATACAGCTG 1065
BIN4.5-CDS     GGCTAAGATT GAAGCTATTA TGAATGACTT CATACAGCTG 1053
BIN4.6-CDS     GGCTAAGATT GAAGCTATTA TGAATGACTT CATACAGCTG 1077

MID CDS (Ler)  ACACCACAAT CTAATGTCTA CGAGGCAGAA ACAATGGTGG 1105
MID CDS (Col-0) ATACCACAAT CTAATGTCTA CGAGGCAGAA ACAATGGTGG 1105
BIN4.1-CDS     ATACCACAAT CTAATGTCTA CGAGGCAGAA ACAATGGTGG 1108
BIN4.2-CDS     ATACCACAAT CTAATGTCTA CGAGGCAGAA ACAATGGTGG 1051
BIN4.3-CDS     ATACCACAAT CTAATGTCTA CGAGGCAGAA ACAATGGTGG 1105
BIN4.4-CDS     ATACCACAAT CTAATGTCTA CGAGGCAGAA ACAATGGTGG 1105
BIN4.5-CDS     ATACCACAAT CTAATGTCTA CGAGGCAGAA ACAATGGTGG 1093
BIN4.6-CDS     ATACCACAAT CTAATGTCTA CGAGGCAGAA ACAATGGTGG 1117

MID CDS (Ler)  AAGGCACTCT GGAAGGATTT ACGTTCGAAT CAGATGATGA 1145
MID CDS (Col-0) AAGGCACTCT GGAAGGATTT ACGTTCGAAT CAGATGATGA 1145
BIN4.1-CDS     AAGGCACTCT GGAAGGATTT ACGTTCGAAT CAGATGATGA 1148
BIN4.2-CDS     AAGGCACTCT GGAAGGATTT ACGTTCGAAT CAGATGATGA 1091
BIN4.3-CDS     AAGGCACTCT GGAAGGATTT ACGTTCGAAT CAGATGATGA 1145
BIN4.4-CDS     AAGGCACTCT GGAAGGATTT ACGTTCGAAT CAGATGATGA 1145
BIN4.5-CDS     AAGGCACTCT GGAAGGATTT ACGTTCGAAT CAGATGATGA 1133
BIN4.6-CDS     AAGGCACTCT GGAAGGATTT ACGTTCGAAT CAGATGATGA 1157

MID CDS (Ler)  AAGTAACAAA AACGCCAAGA CTGCTGTAAA GCCAGCTGAT 1185
MID CDS (Col-0) AAGTAACAAA AACGCCAAGA CTGCTGTAAA GCCAGCTGAT 1185
BIN4.1-CDS     AAGTAACAAA AACGCCAAGA CTGCTGTAAA GCCAGCTGAT 1188
BIN4.2-CDS     AAGTAACAAA AACGCCAAGA CTGCTGTAAA GCCAGCTGAT 1131
BIN4.3-CDS     AAGTAACAAA AACGCCAAGA CTGCTGTAAA GCCAGCTGAT 1185
BIN4.4-CDS     AAGTAACAAA AACGCCAAGA CTGCTGTAAA GCCAGCTGAT 1185
BIN4.5-CDS     AAGTAACAAA AACGCCAAGA CTGCTGTAAA GCCAGCTGAT 1173
BIN4.6-CDS     AAGTAACAAA AACGCCAAGA CTGCTGTAAA GCCAGCTGAT 1197

MID CDS (Ler)  CAAAGTGTAG GCACAGAGGA AGAAACCAAC ACAAAAGCCA 1225
MID CDS (Col-0) CAAAGTGTAG GCACAGAGGA AGAAACCAAC ACAAAAGCCA 1225
BIN4.1-CDS     CAAAGTGTAG GCACAGAGGA AGAAACCAAC ACAAAAGCCA 1228
BIN4.2-CDS     CAAAGTGTAG GCACAGAGGA AGAAACCAAC ACAAAAGCCA 1171
BIN4.3-CDS     CAAAGTGTAG GCACAGAGGA AGAAACCAAC ACAAAAGCCA 1225
BIN4.4-CDS     CAAAGTGTAG GCACAGAGGA AGAAACCAAC ACAAAAGCCA 1225
BIN4.5-CDS     CAAAGTGTAG GCACAGAGGA AGAAACCAAC ACAAAAGCCA 1213
BIN4.6-CDS     CAAAGTGTAG GCACAGAGGA AGAAACCAAC ACAAAAGCCA 1237

MID CDS (Ler)  AACCCAAAGC CAAAGCAAAA GGCGAAACTG TTATAGGAAA 1265
MID CDS (Col-0) AACCCAAAGC CAAAGCAAAA GGCGAAACTG TTATAGGAAA 1265
BIN4.1-CDS     AACCCAAAGC CAAAGCAAAA GGCGAAACTG TTATAGGAAA 1268
BIN4.2-CDS     AACCCAAAGC CAAAGCAAAA GGCGAAACTG TTATAGGAAA 1211
BIN4.3-CDS     AACCCAAAGC CAAAGCAAAA GGCGAAACTG TTATAGGAAA 1265
BIN4.4-CDS     AACCCAAAGC CAAAGCAAAA GGCGAAACTG TTATAGGAAA 1265
BIN4.5-CDS     AACCCAAAGC CAAAGCAAAA GGCGAAACTG TTATAGGAAA 1253
BIN4.6-CDS     AACCCAAAGC CAAAGCAAAA GGCGAAACTG TTATAGGAAA 1277

MID CDS (Ler)  AAAGAGAGGA AGACCATCTA AAGAGAAGCA GCCACCAGCA 1305
MID CDS (Col-0) AAAGAGAGGA AGACCATCTA AAGAGAAGCA GCCACCAGCA 1305
BIN4.1-CDS     AAAGAGAGGA AGACCATCTA AAGAGAAGCA GCCACCAGCA 1308
BIN4.2-CDS     AAAGAGAGGA AGACCATCTA AAGAGAAGCA GCCACCAGCA 1251
BIN4.3-CDS     AAAGAGAGGA AGACCATCTA AAGAGAAGCA GCCACCAGCA 1305
BIN4.4-CDS     AAAGAGAGGA AGACCATCTA AAGAGAAGCA GCCACCAGCA 1305
BIN4.5-CDS     AAAGAGAGGA AGACCATCTA AAGAGAAGCA GCCACCAGCA 1293
BIN4.6-CDS     AAAGAGAGGA AGACCATCTA AAGAGAAGCA GCCACCAGCA 1317
```

V. Attachment

```
MID CDS (Ler)  AAGAAGGCTA GAAATTCTGC CCCTAAGAAG CCAAAAGCCA 1345
MID CDS (Col-0) AAGAAGGCTA GAAATTCTGC CCCTAAGAAG CCAAAAGCCA 1345
BIN4.1-CDS     AAGAAGGCTA GAAATTCTGC CCCTAAGAAG CCAAAAGCCA 1348
BIN4.2-CDS     AAGAAGGCTA GAAATTCTGC CCCTAAGAAG CCAAAAGCCA 1291
BIN4.3-CDS     AAGAAGGCTA GAAATTCTGC CCCTAAGAAG CCAAAAGCCA 1345
BIN4.4-CDS     AAGAAGGCTA GAAATTCTGC CCCTAAGAAG CCAAAAGCCA 1345
BIN4.5-CDS     AAGAAGGCTA GAAATTCTGC CCCTAAGAAG CCAAAAGCCA 1333
BIN4.6-CDS     AAGAAGGCTA GAAATTCTGC CCCTAAGAAG CCAAAAGCCA 1357

MID CDS (Ler)  AGAAATGA 1353
MID CDS (Col-0) AGAAATGA 1353
BIN4.1-CDS     AGAAATGA 1356
BIN4.2-CDS     AGAAATGA 1299
BIN4.3-CDS     AGAAATGA 1353
BIN4.4-CDS     AGAAATGA 1353
BIN4.5-CDS     AGAAATGA 1341
BIN4.6-CDS     AGAAATGA 1365
```

A R-16: *MID*-Col-0 CDS. Sequence corresponds to the CDS of *BIN4.3*-CDS and *BIN4.4*-CDS shown in A R-15, two splicing variants annotated by TAIR (www.arabidopsis.org). The red boxed nucteotide is a C in MID-L*er* and the published sequence in Kirik et al. (2007).

```
                                   20                  40
MID (Col-0) CDS《ATGAGCAGCAGCTCTAGAGAGGGATCTCCAGATTGGCTTCGCTCTTACGAGGCA
                 60                  80                 100
MID (Col-0) CDS CCCATGACTACTTCATTGTTGTCGCTATCATCTTCAGATGATGATAGTCCTTAT
                          120                 140                 160
MID (Col-0) CDS AGGGAATCTGAAGTCATTTCGTCTCTTCCTTTGCCTGATGATGACGGTGACGAC
                                   180                 200
MID (Col-0) CDS ATTGTGGTTCTTGAGACAGAATCTGTGGAGTTACTGACTAGGAAGAATTCCGAA
                 220                 240                 260
MID (Col-0) CDS ACGAAGGTTGTGACGAAGCAAGTGAGTATCGAGCAGGTGTTTTCTAGAAAGAAG
                          280                 300                 320
MID (Col-0) CDS AAAGCAGATGCTAGTCTCAACCTTGAAGGGAAGGAGAATGGAAACAACGTTGAC
                                   340                 360
MID (Col-0) CDS TGTGAAAAACTCTCTAGCAAGCATAAGGATGCTCAAGGAGGAGCTGATTCTGTA
                 380                 400                 420
MID (Col-0) CDS TGGCTTGTCTCATCTGATTCTGAGCCATCCTCTCCTATAAAGCAGGAAGTGACT
                          440                 460                 480
MID (Col-0) CDS GTGTCAACTGAAAAGGATGCGGATTTTGTTCTTGAAGCTACAGAGGAAGAACCA
                                   500                 520                 540
MID (Col-0) CDS GCAGTTAAGACAGTTCGAAAGGAAAAATCTCCAAAAACAAAGTCAAAAAGCAGT
                                            560                 580
MID (Col-0) CDS CGCAAGACACCCAAGGAAGGAAATAGTGCACAGGAAATTTTAAAAACTGAAGAT
                          600                 620                 640
MID (Col-0) CDS AAAGATACAGATACCACTATAGCCGAGCAAGTAACACCGGAAAAATCTCCAAAA
                                   660                 680                 700
MID (Col-0) CDS ACAAAGTCAAAAAGCAGTCGCAAGACACCCAAGGAAGAAAATTGTGCACAAGAA
                                            720                 740
MID (Col-0) CDS ATTTTAAAAACTGAAGATAAAGATAAAGATACAGATACAGATACCATTATAGCC
                 760                 780                 800
MID (Col-0) CDS GAGGAAGTAACAACGGATCAGAAGATCAAGCCTTCTTCTGGCTCAAGTTCAAGA
                          820                 840                 860
MID (Col-0) CDS TTGCCTTTGGTACTTTCTGAGAAGGTTAATCGTACAAAGGTACTCGTTGAATGT
                                   880                 900
MID (Col-0) CDS GAAGGTGACTCGATAGATTTGAGTGGAGACATGGGGGCTGTTGGACGCGTGGTT
                 920                 940                 960
MID (Col-0) CDS GTTTCAGACACAACCGGGGACATGTACTTGGACTTGAAAGGAACCATATATAAA
                          980                1.000               1.020
MID (Col-0) CDS TCAACAATCATTCCATCCAGAACATTTTGCGTTGTTAACGTAGGTCAGACAGAG
                                  1.040               1.060               1.080
MID (Col-0) CDS GCTAAGATTGAAGCTATTATGAATGACTTCATACAGCTGAT[C]ACCACAATCTAAT
                                           1.100               1.120
MID (Col-0) CDS GTCTACGAGGCAGAAACAATGGTGGAAGGCACTCTGGAAGGATTTACGTTCGAA
                         1.140               1.160               1.180
MID (Col-0) CDS TCAGATGATGAAAGTAACAAAAACGCCAAGACTGCTGTAAAGCCAGCTGATCAA
                                  1.200               1.220               1.240
MID (Col-0) CDS AGTGTAGGCACAGAGGAAGAAACCAACACAAAAGCCAAACCCAAAGCCAAAGCA
                                           1.260               1.280
MID (Col-0) CDS AAAGGCGAAACTGTTATAGGAAAAAAGAGAGGAAGACCATCTAAAGAGAAGCAG
                         1.300               1.320               1.340
MID (Col-0) CDS CCACCAGCAAAGAAGGCTAGAAATTCTGCCCCTAAGAAGCCAAAAGCCAAGAAA

MID (Col-0) CDS TGA》
```

V. Attachment

A R-17: Results of the sequencing reaction of the Colony PCR on the clones harbouring fragments of *MID* cDNA. Shown are the results generated with NCBI BLASTN blast2seq for two sequences (A) and (B) (Altschule et al. 1997). yellow: the aligned sequence in the NCBI BLASTN results. Note the GAGA-sequence that only occured for sequences with *MID*-fragments and appeared for all sequences with *MID*-fragments.

```
(A)
ANCCTTNCTTNGGGTGGCATANGCCANGANGCCCCGGGGTATCCGAATTCGGCTCGAGGCAGNGAGAGAGAGAGAGAGAG
AGAGAGTAGAGAGAGAGAGAGAGAGAGAGAGAGAGAGAGANAGAGAGAGAGANAGAGAGANAGAGAGANAGAGAGANACN
ANAGANAGAGANAGAGNGANNNANAGAGAGAGAGAGAGCCTNATNGNGAATCTGAAGTCNTTTCGNCNCNTCNTTTTCTC
TCATNTNTGACGGTGACGTCTTTGTGTTTCTTGAGACACAATCTNTTNTCTTACTGACTNGGAAGAATTCCNATACTTNC
GTTGTGACTCTATCAAGTGAGTNTCGCGCANGTGTTTTCTAGCAAAGAAGAAACCAGATGCTATNTCTCAACCTTGAAGG
GAANCNAGAATGGANTCNNCNTTGACTGTGNNANNCTCTCTNGCAAGCNTNANGATGCTCAAGGANGAGCTGNTTCTGTA
TGGCTTNTCTCATCTGATTCTGAGCCATCCTCTCCTATAAAGCNNGAAGTGACTGTGTCAACTCANANGGATGCTGATTT
TGTTCTTGAAGCTACAGAGGAACAACCTGTCTTTANNGCGGTTCGACAGGAAAANTCTCCAAANACAAAGTCACANAGCA
NTCNCNAGACACCCANGTATGGATCTCGTGCTCNGGAAATTTTAAAACTGAAGATAAAGATNCACATCC

Alignment NCBI BLASTn "Align two or more sequences": Query: MID-Col-0 CDS
Query   301  GAATCTGAAGTCATTTCGTCTCTTCCTTTGC-CTGAT-GATGACGGTGACGACATTGTGG  358
             |||||||||||| |||||  |  |  ||  |||  |  ||  ||   |||||||||||  |  |||||
Sbjct1  208  GAATCTGAAGTCNTTTCGNCNCNTCNTTTTCTCTCATNTNTGACGGTGACGTCTTTGTGT  267
Query   359  TTCTTGAGACAGAATCTGTGGAGTTACTGACTAGGAAGAATTCCGAAACGAAGGTTGTGA  418
             ||||||||||| |||||  |     |||||||||  ||||||||||  |  ||     |||||||
Sbjct1  268  TTCTTGAGACACAATCTNTTNTCTTACTGACTNGGAAGAATTCCNATACTTNCGTTGTGA  327
Query   419  C-GAAGCAAGTGAGTATCGAGCAGGTGTTTTCTAG-AAAGAAGAAAGCAGATGCTA-GTC  475
             |   | |||||||||  |||  |||  ||||||||||  ||||||||||  |||||||||   ||
Sbjct1  328  CTCTATCAAGTGAGTNTCGCGCANGTGTTTTCTAGCAAAGAAGAAACCAGATGCTATNTC  387
Query   476  TCAACCTTGAAGGGAA-GGAGAATGGAAACAACGTTGACTGTGAAAAACTCTCTAGCAAG  534
             ||||||||||||||||   ||||||||  |  | |||||||||  |  ||||||  |||||
Sbjct1  388  TCAACCTTGAAGGGAANCNAGAATGGANTCNNCNTTGACTGTGNNANNCTCTCTNGCAAG  447
Query   535  CATAAGGATGCTCAAGGAGGAGCTGATTCTGTATGGCTTGTCTCATCTGATTCTGAGCCA  594
             | | | ||||||||||||| ||||||  |||||||||||||  ||||||||||||||||||||
Sbjct1  448  CNTNANGATGCTCAAGGANGAGCTGNTTCTGTATGGCTTNTCTCATCTGATTCTGAGCCA  507
Query   595  TCCTCTCCTATAAAGCAGGAAGTGACTGTGTCAACTGAAAAGGATGCGGATTTTGTTCTT  654
             ||||||||||||||||  ||||||||||||||||||  |  |  ||||||  |||||||||||||
Sbjct1  508  TCCTCTCCTATAAAGCNNGAAGTGACTGTGTCAACTCANANGGATGCTGATTTTGTTCTT  567
Query   655  GAAGCTACAGAGGAAGAACCAG-CAGTTAA-GACAGTTCGaaaggaaaaatctccaaaaa  712
             ||||||||||||||| ||||  |  |   |||   |  |  ||||||  |||||||  ||||||||  |
Sbjct1  568  GAAGCTACAGAGGAACAACCTGTCT-TTANNG-CGGTTCGACAGGAAAANTCTCCAAANA  625
Query   713  caaagtcaaaaaGCAGTCGCAAGACACCCAAGGAAGGAAATAGTGCACAGGAAATTTTAA  772
             ||||||||  |  ||||  ||  |  |||||||||  |  |  |||   |  ||||  |  ||||||||||
Sbjct1  626  CAAAGTCACANAGCANTCNCNAGACACCCANGTATGGATCTCGTGCTCNGGAAATTTTAA  685
Query   773  AAACTGAAGATAAAGAT  789
             ||  |||||||||||||
Sbjct1  686  AA-CTGAAGATAAAGAT  701


(B)
TAANTCNNNNGNTTTNTTNTCNNNNNNAAANCCATCNTNGGGNGNCATATGGCCATGGAGGCCCCGCGGGATATCCGAAA
TTCGGCNCGCAGTCAGANNAGATTANANNGAGAGAAGNGAGGAGTANCAGAGAGAGAGAGCAGAGNNAGAGAGAGAGACA
NNGAGNTAGAGTTCAGATCATTNGCAGAGGANACCCATANNTACCNTCGNTNNTGACNCNATCAGTCTTCAGATGNTNAT
ANTCCTTATAGGGAATCTGAAGTCATTTCGTCNTCTTCCTTTGCCTGATGATGACGGTGNCGACATTGTGGTTCTTGAGA
CNGAATCTGTGGAGTTACTGACTAGGAAGAATTCCGAAACGAANGTTGTGACGAAGCAAGTNAGTATCGAGCAGGTGTTT
TCTAGAAAGAAGANAGCAGATGCTAGTCTCAACCTTGAAGGGCAGNAGAATGGAANCAACGTTGACTGTGAAAAAACTCT
CTAGCAAGCATAAGGATGCTCAAAGGAGGGAGCTGATTCTGTATGGCTTGTCTCATCTGATTCTGAGCCATCCTCTCCTA
TAAAGCAGGAAGTGACTGTNTCAACTGAAAAAGGAATGCGGATTTTTNTTCTTTGAAGCTACCAGAGNAAGNAACCCAGC
AGTTTAAGNACNATTTCNGAAAGGAAAAAATCTTCCAAAAACAAAANTCAAAAAAGNCANTCCGCCAGACNCCCCNNGGC
AAGGGAAATTAATGCCCACNGGNAATTTTNAAAANCTGAAGGATAAANNTTTCGANNNTNCCCCCTNTTAGGNCGGNNAA
ATT



Query   270  ATCA-TCTTCAGATGATGATAGTCCTTATAGGGAATCTGAAGTCATTTCGTC-TCTTCCT  327
             ||||  ||||||||||  |  |||  ||||||||||||||||||||||||||||||  |||||||
Sbjct2  221  ATCAGTCTTCAGATGNTNATANTCCTTATAGGGAATCTGAAGTCATTTCGTCNTCTTCCT  280
Query   328  TTGCCTGATGATGACGGTGACGACATTGTGGTTCTTGAGACAGAATCTGTGGAGTTACTG  387
```

V. Attachment

```
                ||||||||||||||||||| |||||||||||||||||||| ||||||||||||||||||
Sbjct2  281  TTGCCTGATGATGACGGTGNCGACATTGTGGTTCTTGAGACNGAATCTGTGGAGTTACTG  340
Query   388  ACTAGGAAGAATTCCGAAACGAAGGTTGTGACGAAGCAAGTGAGTATCGAGCAGGTGTTT  447
                ||||||||||||||||||||||| |||||||||||||||| ||||||||||||||||||
Sbjct2  341  ACTAGGAAGAATTCCGAAACGAANGTTGTGACGAAGCAAGTNAGTATCGAGCAGGTGTTT  400
Query   448  TCTAGAAAGAAGAAAGCAGATGCTAGTCTCAACCTTGAAGGGAAGGAGAATGGAAACAAC  507
                |||||||||||||| |||||||||||||||||||||||||||| || ||||||||| ||||
Sbjct2  401  TCTAGAAAGAAGANAGCAGATGCTAGTCTCAACCTTGAAGGGCAGNAGAATGGAANCAAC  460
Query   508  GTTGACTGTGAAAAA-CTCTCTAGCAAGCATAAGGATGCTCAA-GGAGG-AGCTGATTCT  564
                ||||||||||||||| |||||||||||||||||||||||||||| ||||| ||||||||||
Sbjct2  461  GTTGACTGTGAAAAAACTCTCTAGCAAGCATAAGGATGCTCAAAGGAGGGAGCTGATTCT  520
Query   565  GTATGGCTTGTCTCATCTGATTCTGAGCCATCCTCTCCTATAAAGCAGGAAGTGACTGTG  624
                ||||||||||||||||||||||||||||||||||||||||||||||||||||||||||||
Sbjct2  521  GTATGGCTTGTCTCATCTGATTCTGAGCCATCCTCTCCTATAAAGCAGGAAGTGACTGTN  580
Query   625  TCAACTGAAAA-GGA-TGCGGATTTTG-TTCTT-GAAGCTAC-AGAGGAAG-AACC-AGC  677
                |||||||||||  ||| ||||||||||  |||||  |||||||| |||| ||| |||| |||
Sbjct2  581  TCAACTGAAAAAGGAATGCGGATTTTTNTTCTTTGAAGCTACCAGAGNAAGNAACCCAGC  640
Query   678  AGTT-AAG-AC-AGTTC-Gaaaggaaaaa-tct-ccaaaaacaaag-tcaaaaa-G-CAG  728
                ||||  |||  ||  |  |||  ||||||||||| |||  ||||||||||  |||||||  |  ||
Sbjct2  641  AGTTTAAGNACNATTTCNGAAAGGAAAAAATCTTCCAAAAACAAAANTCAAAAAAGNCAN  700
Query   729  TC-GCAAGACACCCAA-GG-AAGG-AAAT-AGTGCACA--GGAAATTTTAAAAA-CTGAA  780
                ||  ||  ||||  |||   ||  ||||  ||||  |  |||  ||  ||  ||||||  ||||  |||||
Sbjct2  701  TCCGCCAGACNCCCCNNGGCAAGGGAAATTAATGCCCACNGGNAATTTTNAAAANCTGAA  760
Query   781  G-ATAAA  786
                |  |||||
Sbjct2  761  GGATAAA  767
```

A R-18: (A) Whole blots of Figure III-31. For details see figure III-31. **(B)** Whole blots of figure III-32. Note that this is a repeated Western blot analysis of the samples from A R-19. For better visualization this blot was stripped after detection with an anti-HA antibody. Second (lower) anti-GFP western-blot is over-exposed. For details see figure III-32 or A R-19. The ladder for (A) and (B) is the same as in A R-19 with the red or thick band representing 72 kDa. The uppermost band above 130 kDa is 170 kDa.

V. Attachment

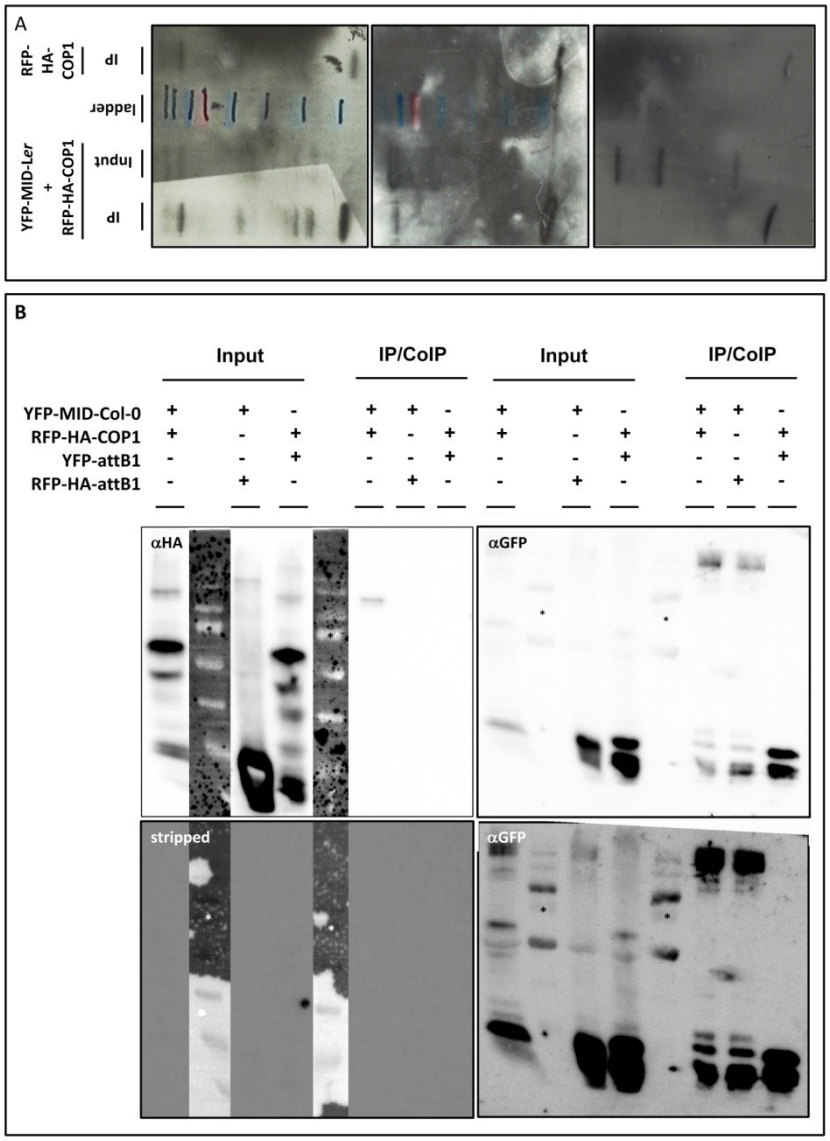

A R-19: Co-Immunoprecipiation of RFP-HA-COP1 with YFP-MID with all controls and bradford analysis.
(A) Measurements for Bradford calibration curve. The table shows the threefold independent measurements at OD_{595} to determine a mean for a bradford calibration curve. 0, 2, 4, 6, 8 and 10 µg of BSA were used. The absorption ranged between 0,194 and 0,843. Therefore, most measurements were in the linear range of the photometre and for the bradford test. Same amounts of sample buffer that was used for the measurements in C was included for every sample of the calibration curve measurements. **(B)** Bradford calibration curve. The resulting calibratiopn curve is showen with the x-aches giving the amount of BSA in µg and the y-achsis with the corresponding means of the OD595 values presented in (A). The formula for the resulting trendline is given. **(C)** Bradford analysis for the input samples used for immunoprecipitation. Leaves of N. benthamiana that were coinfiltrated with constructs coding for the proteins in the first column and the antisilencing strain RK19 (in brackets) were homgenized for further immunoprecipitation analysis. For bradford analysis, the input samples were diluted 1:10 with water and 10 µl were used for a total of 1 ml in the bradford assay. This resulted in a 1:1000 dilution. Three independent measurements per sample were done (column 2-4). The resulting mean (column 5) was used as the y-value to determine the x value in the formula gioven in (B) and the result was multiplied wth 1000 (dilution). This gives the total protein concentration per µl in the sample (column 6) The last column gives thevolume that was loaded on the gel for Western blot analysis and coomasie staining shown in (D). The maximum volume to be loaded was 18 µl. This corresponds to 33,365 µg of total protein in the limiting sample.
(D) Co-Immunoprecipitation of RFP-HA-COP1 with YFP-MID. Leaves of N. benthamiana were co-infiltrated with the depicted combinations of Agrobacteria harboring one of the following constructs: pNmR-COP1, pEarleyGATE104-MID, pBat-TL-B-p35s-RFP-HA-attB1 and pBat-TL-B-p35s-YFP-attB1. In all cases RK19 – an anti-silenciong strain – was (co-)infiltrated. The transformation was confirmed by fluorescence microscopy. 530 to 540 mg of transformed leave material was homogenized.The loading control (Coomassie staining) shows that equal amounts of total protein were loaded. In addition the samples were adjusted to the same total protein content of the input according to bradford analysis prior to loading. Immunoprecipitation (IP) of proteins from plant extract was performed with 50 µl anti-GFP beads. Proteins were separated

by SDS-PAGE, blottest and detected with the depicted antibodies. Combinations with RFP-HA-attB1 and YFP-attB1 served as negative controls. Note the smallest visible band on the GFP IP blot of the small antibody chain and the incomplete translation products or degradation products or free YFP –attB1 or RFP-Ha-attB1.

A

	BSA [µg]					
	0	2	4	6	8	10
assay 1	0	0,242	0,391	0,562	0,703	0,835
assay 2	0	0,205	0,372	0,525	0,678	0,829
assay 3	0	0,194	0,410	0,538	0,686	0,843
mean	0	0,214	0,391	0,542	0,689	0,836

B

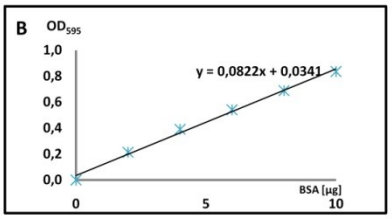

C

sample	OD595 1	2	3	mean	total protein [µg/µl]	loaded volume of input [µl] total protein = 33,365 µg
YFP-MID-Col-0 + RFP-HA-COP1 (+RK19)	0,212	0,205	0,222	**0,213**	2,176	15,4
YFP-MID (Col-0) + RFP-HA-attB1 (+RK19)	0,207	0,191	0,194	**0,197**	1,986	16,8
YFP-attB1 + RFP-HA-COP1 (+RK19)	0,221	0,208	0,205	**0,211**	2,156	15,5
YFP-MID (Col-0) (+RK19)	0,225	0,171	0,194	**0,197**	1,978	16,9
RFP-HA-COP1 (+RK19)	0,199	0,198	0,219	**0,205**	2,083	16,0
(RK19)	0,192	0,178	0,19	**0,187**	1,856	18,0

D

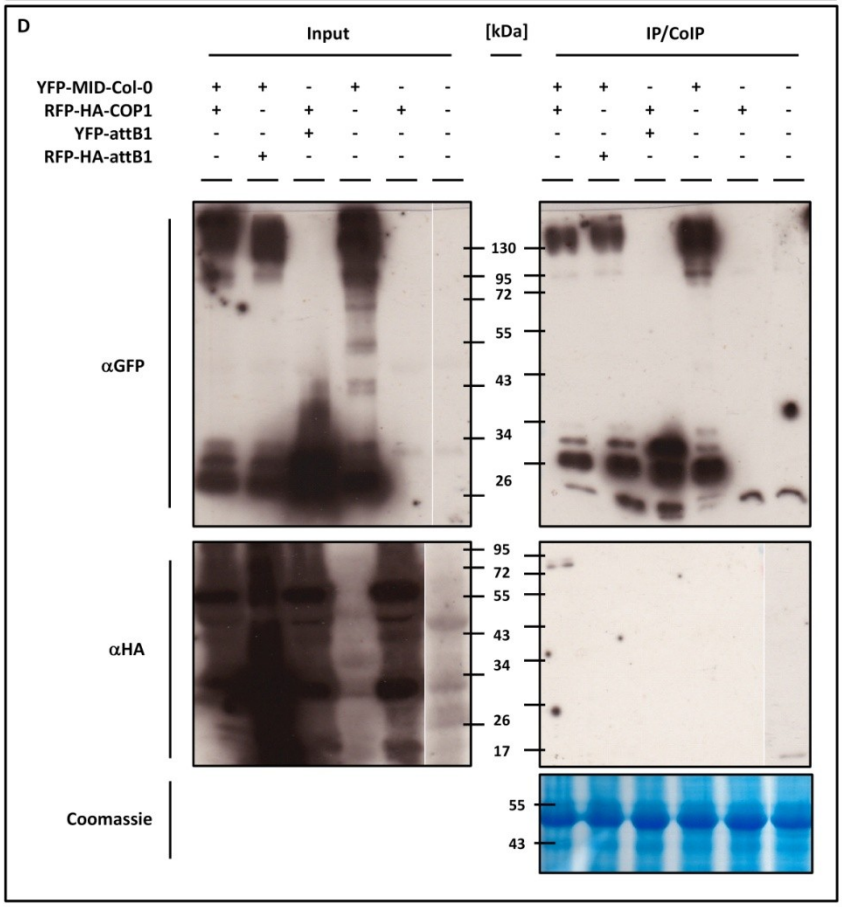

V. Attachment

A R-20: Bradford co-purification. See Figure III-37 for details. The 1:10 dilution of sample "MID-YFP" was only measured once. Note that 10 µl of the sample were used meaning that a dilution of 1:10 is in fact no dilution in the final calculation.

A

	BSA [µg]					
	0	2	4	6	8	10
assay 1	0	0,136	0,194	0,295	0,369	0,504
assay 2	0	0,132	0,186	0,293	0,385	0,495
assay 3	0	0,073	0,156	0,275	0,387	0,492
mean	0,000	0,114	0,179	0,288	0,380	0,497

B

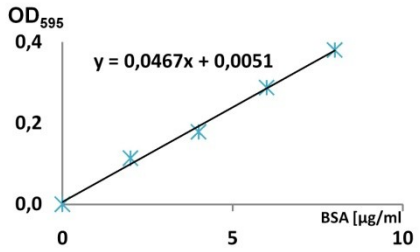

C

sample	OD_{595} 1	2	3	mean (undiluted)	total protein [µg/µl]	total protein used for IP [µg]
Col-0 no dilution	0,426	0,322	0,328	0,036	0,659	3294,1
MID-YFP 1:10	0,088			0,088	1,775	8875,8
MID-YFP no dilution	0,716	0,778	0,768	0,075	1,505	7526,8
MID-YFP 1:5	0,149	0,153	0,156	0,076	1,525	7626,7

V. Attachment

A R-21: Mascot results obtained from Thomas Colby group Jürgen Schmitz, MPIZ. See Figure III-37 for details. (A) band1 (B) band2 (C) band2 only *A. thaliana*.

(A)

Mascot Search Results

```
User            : colby
Email           : colby@mpiz-koeln.mpg.de
Search title    : Andrea S band 1 1-d LC no ker no tryp arabidopsis
MS data file    : AndreaS_Band1_1d.mgf
Database        : NCBInr 20100306 (10551781 sequences; 3596151245 residues)
Taxonomy        : Arabidopsis thaliana (thale cress) (62500 sequences)
Timestamp       : 10 Mar 2010 at 10:04:01 GMT
Protein hits    : gi|20259462 putative ATPase (ISW2) [Arabidopsis thaliana]
                  gi|10177863 unnamed protein product [Arabidopsis thaliana]
                  gi|7228247  putative protein [Arabidopsis thaliana]
```

Probability Based Mowse Score

Ions score is -10*Log(P), where P is the probability that the observed match is a random event.
Individual ions scores > 35 indicate identity or extensive homology (p<0.05).
Protein scores are derived from ions scores as a non-probabilistic basis for ranking protein hits.

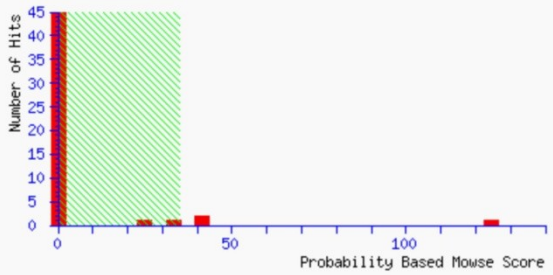

Peptide Summary Report

Format As: Peptide Summary — Help
Significance threshold p< 0.05 — Max. number of hits AUTO
Standard scoring / MudPIT scoring — Ions score or expect cut-off 0 — Show sub-sets 0
Show pop-ups / Suppress pop-ups — Sort unassigned: Decreasing Score — Require bold red
Select All | Select None | Search Selected | Error tolerant

1. gi|20259462 Mass: 122993 Score: 124 Queries matched: 5 emPAI: 0.13
putative ATPase (ISW2) [Arabidopsis thaliana]
Check to include this hit in error tolerant search

Query	Observed	Mr(expt)	Mr(calc)	Delta	Miss	Score	Expect	Rank	Peptide
109	463.2100	924.4054	923.4205	0.9850	0	6	61	3	K.VGMSQMQK.Q + Oxidation (M)
☑ 134	565.7400	1129.4654	1129.5363	-0.0709	0	55	0.0008	1	K.DLEAVNAGGER.K
☑ 135	567.2800	1132.5454	1132.5248	0.0207	0	74	1e-05	1	K.GEEATAELDAK.M
☑ 145	640.3000	1278.5854	1278.5576	0.0279	0	61	0.00018	1	K.DSTITDEDIDR.I
☑ 163	754.8800	1507.7454	1507.7154	0.0300	0	16	5.7	1	R.DASIEAYNKPGSEK.F

V. Attachment

Proteins matching the same set of peptides:
gi|22330875 Mass: 122979 Score: 124 Queries matched: 5
CHR11 (CHROMATIN-REMODELING PROTEIN 11); ATP binding / DNA binding / DNA-dependent ATPase/ helicase/ hydrolase,
gi|68568746 Mass: 123180 Score: 124 Queries matched: 5
RecName: Full=Putative chromatin-remodeling complex ATPase chain; AltName: Full=ISW2-like; AltName: Full=Sucros

---

2. gi|10177863 Mass: 58756 Score: 44 Queries matched: 2 emPAI: 0.13
unnamed protein product [Arabidopsis thaliana]
☐ Check to include this hit in error tolerant search

Query	Observed	Mr(expt)	Mr(calc)	Delta	Miss	Score	Expect	Rank	Peptide
☑ 196	1002.9700	2003.9254	2003.9647	-0.0393	0	(19)	2	1	K.TAVKPADQSVGTEEETNTK.A
☑ 197	668.9900	2003.9482	2003.9647	-0.0166	0	41	0.011	1	K.TAVKPADQSVGTEEETNTK.A

Proteins matching the same set of peptides:
gi|238481365 Mass: 47318 Score: 44 Queries matched: 2
BIN4 (brassinosteroid-insensitive4); double-stranded DNA binding [Arabidopsis thaliana]
gi|238481367 Mass: 49307 Score: 44 Queries matched: 2
BIN4 (brassinosteroid-insensitive4); double-stranded DNA binding [Arabidopsis thaliana]
gi|238481371 Mass: 48821 Score: 44 Queries matched: 2
BIN4 (brassinosteroid-insensitive4); double-stranded DNA binding [Arabidopsis thaliana]
gi|238481373 Mass: 49740 Score: 44 Queries matched: 2
BIN4 (brassinosteroid-insensitive4); double-stranded DNA binding [Arabidopsis thaliana]
gi|240256338 Mass: 49435 Score: 44 Queries matched: 2
BIN4 (brassinosteroid-insensitive4); double-stranded DNA binding [Arabidopsis thaliana]

---

3. gi|7228247 Mass: 70800 Score: 39 Queries matched: 1 emPAI: 0.05
putative protein [Arabidopsis thaliana]
☐ Check to include this hit in error tolerant search

Query	Observed	Mr(expt)	Mr(calc)	Delta	Miss	Score	Expect	Rank	Peptide
☑ 112	471.7500	941.4854	941.5182	-0.0327	0	39	0.032	1	R.GVNLDPLSK.W

Proteins matching the same set of peptides:
gi|22328952 Mass: 75781 Score: 39 Queries matched: 1
nucleolar protein, putative [Arabidopsis thaliana]
gi|30696661 Mass: 77014 Score: 39 Queries matched: 1
nucleolar protein, putative [Arabidopsis thaliana]
gi|222423014 Mass: 70084 Score: 39 Queries matched: 1
AT5G55920 [Arabidopsis thaliana]

V. Attachment

(B)

Mascot Search Results

```
User           : colby
Email          : colby@mpiz-koeln.mpg.de
Search title   : Andrea S band 2 1-d LC
MS data file   : AndreaSBand2_1d.mgf
Database       : NCBInr 20100306 (10551781 sequences; 3596151245 residues)
Timestamp      : 10 Mar 2010 at 10:10:25 GMT
Protein hits   : gi|16421      unnamed protein product [Arabidopsis thaliana]
                 gi|238481365 BIN4 (brassinosteroid-insensitive4); double-stranded DNA binding [Arabidopsis thaliana]
                 gi|130188    RecName: Full=Phytochrome A
                 gi|155663    green-fluorescent protein [Aequorea victoria]
```

Probability Based Mowse Score

Ions score is -10*Log(P), where P is the probability that the observed match is a random event.
Individual ions scores > 56 indicate identity or extensive homology (p<0.05).
Protein scores are derived from ions scores as a non-probabilistic basis for ranking protein hits.

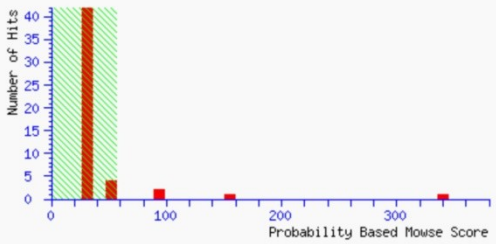

Peptide Summary Report

Format As: Peptide Summary — Help
Significance threshold p< 0.05 — Max. number of hits AUTO
Standard scoring / MudPIT scoring — Ions score or expect cut-off 0 — Show sub-sets 0
Show pop-ups / Suppress pop-ups — Sort unassigned: Decreasing Score — Require bold red
Select All | Select None | Search Selected | Error tolerant

1. gi|16421 Mass: 125661 Score: 341 Queries matched: 7 emPAI: 0.12
unnamed protein product [Arabidopsis thaliana]
Check to include this hit in error tolerant search

Query	Observed	Mr(expt)	Mr(calc)	Delta	Miss	Score	Expect	Rank	Peptide
120	475.7000	949.3854	949.4361	-0.0507	0	18	5.3e+02	6	R.MIVDCNAK.H
☑ 148	530.3300	1058.6454	1058.5972	0.0483	0	45	1	1	R.IIAQTTVDAK.L
☑ 159	568.3300	1134.6454	1134.5856	0.0599	0	35	11	1	R.NPLSGIMFTR.K
☑ 184	646.8700	1291.7254	1291.6885	0.0370	0	78	0.00045	1	R.VTGPVVENQPPR.S
☑ 192	660.8900	1319.7654	1319.7085	0.0570	0	39	4	1	R.SLFTAPSASALQK.A
☑ 194	667.3400	1332.6654	1332.6231	0.0423	0	67	0.0069	1	K.EVELDNQMVEK.N
☑ 196	680.3600	1358.7054	1358.6500	0.0555	0	58	0.052	1	K.MIEGTELGPEQR.R

V. Attachment

Proteins matching the same set of peptides:
gi|15217562 Mass: 125676 Score: 341 Queries matched: 7
PHYA (PHYTOCHROME A); G-protein coupled photoreceptor/ protein histidine kinase/ red or far-red light photoreceptor/

---

2. gi|238481365 Mass: 47318 Score: 151 Queries matched: 3 emPAI: 0.26
BIN4 (brassinosteroid-insensitive4); double-stranded DNA binding [Arabidopsis thaliana]
Check to include this hit in error tolerant search

Query	Observed	Mr(expt)	Mr(calc)	Delta	Miss	Score	Expect	Rank	Peptide
207	726.8800	1451.7454	1451.7079	0.0376	0	70	0.0027	1	R.TFCVVNVGQTEAK.I
257	1002.9300	2003.8454	2003.9647	-0.1193	0	80	0.00016	1	K.TAVKPADQSVGTEEETNTK.A
258	669.0100	2004.0082	2003.9647	0.0434	0	(48)	0.35	1	K.TAVKPADQSVGTEEETNTK.A

Proteins matching the same set of peptides:
gi|238481367 Mass: 49307 Score: 151 Queries matched: 3
BIN4 (brassinosteroid-insensitive4); double-stranded DNA binding [Arabidopsis thaliana]
gi|238481371 Mass: 48821 Score: 151 Queries matched: 3
BIN4 (brassinosteroid-insensitive4); double-stranded DNA binding [Arabidopsis thaliana]
gi|238481373 Mass: 49740 Score: 151 Queries matched: 3
BIN4 (brassinosteroid-insensitive4); double-stranded DNA binding [Arabidopsis thaliana]
gi|240256338 Mass: 49435 Score: 151 Queries matched: 3
BIN4 (brassinosteroid-insensitive4); double-stranded DNA binding [Arabidopsis thaliana]

---

3. gi|130188 Mass: 125146 Score: 102 Queries matched: 3 emPAI: 0.03
RecName: Full=Phytochrome A
Check to include this hit in error tolerant search

Query	Observed	Mr(expt)	Mr(calc)	Delta	Miss	Score	Expect	Rank	Peptide
120	475.7000	949.3854	949.4361	-0.0507	0	18	5.3e+02	6	R.MIVDCNAK.H
148	530.3300	1058.6454	1058.5972	0.0483	0	45	1	1	R.IIAQTTVDAK.L
192	660.8900	1319.7654	1319.7085	0.0569	0	38	5.2	2	R.TVFTAPSASALQK.A

Proteins matching the same set of peptides:
gi|2499555 Mass: 125369 Score: 99 Queries matched: 3
RecName: Full=Phytochrome type A

---

4. gi|155663 Mass: 27017 Score: 95 Queries matched: 2 emPAI: 0.14
green-fluorescent protein [Aequorea victoria]
Check to include this hit in error tolerant search

Query	Observed	Mr(expt)	Mr(calc)	Delta	Miss	Score	Expect	Rank	Peptide
82	413.7200	825.4254	825.4055	0.0200	0	19	3.2e+02	1	K.FICTTGK.L
146	525.8200	1049.6254	1049.5142	0.1113	0	76	0.00096	1	K.FEGDTLVNR.I

V. Attachment

(C)

Mascot Search Results

```
User           : colby
Email          : colby@mpiz-koeln.mpg.de
Search title   : Andrea S band 2 1-d LC
MS data file   : AndreaSBand2_1d.mgf
Database       : NCBInr 20100306 (10551781 sequences; 3596151245 residues)
Taxonomy       : Arabidopsis thaliana (thale cress) (62500 sequences)
Timestamp      : 10 Mar 2010 at 10:11:08 GMT
Protein hits   : gi|16421     unnamed protein product [Arabidopsis thaliana]
                 gi|238481365 BIN4 (brassinosteroid-insensitive4); double-stranded DNA binding [Arabidopsis thaliana]
```

Probability Based Mowse Score

Ions score is -10*Log(P), where P is the probability that the observed match is a random event.
Individual ions scores > 35 indicate identity or extensive homology (p<0.05).
Protein scores are derived from ions scores as a non-probabilistic basis for ranking protein hits.

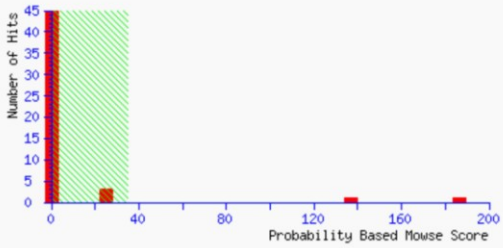

Peptide Summary Report

Format As: Peptide Summary			Help
	Significance threshold p< 0.05	Max. number of hits AUTO	
	Standard scoring ○ MudPIT scoring ◉	Ions score or expect cut-off 0	Show sub-sets 0
	Show pop-ups ◉ Suppress pop-ups ○	Sort unassigned Decreasing Score	Require bold red ☐

Select All | Select None | Search Selected | ☐ **Error tolerant**

```
1.    gi|16421    Mass: 125661    Score: 186    Queries matched: 10    emPAI: 0.19
      unnamed protein product [Arabidopsis thaliana]
   ☐ Check to include this hit in error tolerant search
```

V. Attachment

Query	Observed	Mr(expt)	Mr(calc)	Delta	Miss	Score	Expect	Rank	Peptide
68	403.2400	804.4654	804.4745	-0.0091	0	21	3	2	K.AFLEVVK.T
☑ 104	438.2700	874.5254	874.5065	0.0189	0	22	2.3	1	R.FVPFPLR.Y
☑ 120	475.7000	949.3854	949.4361	-0.0507	0	18	4.4	1	R.MIVDCNAK.H
☑ 148	530.3300	1058.6454	1058.5972	0.0483	0	45	0.0074	1	R.IIAQTTVDAK.L
☑ 159	568.3300	1134.6454	1134.5856	0.0599	0	35	0.08	1	R.NPLSGIMFTR.K
☑ 169	602.8100	1203.6054	1203.5918	0.0137	0	20	2.7	1	R.LQSLPSGSMER.L
☑ 184	646.8700	1291.7254	1291.6885	0.0370	0	78	3.5e-06	1	R.VTGPVVENQPPR.S
☑ 192	660.8900	1319.7654	1319.7085	0.0570	0	39	0.03	1	R.SLFTAPSASALQR.A
☑ 194	667.3400	1332.6654	1332.6231	0.0423	0	67	5.5e-05	1	K.EVELDNQMVEK.N
☑ 196	680.3600	1358.7054	1358.6500	0.0555	0	58	0.00038	1	K.MIEGTELGPEQR.R

Proteins matching the same set of peptides:
gi|15217562 Mass: 125676 Score: 186 Queries matched: 10
PHYA (PHYTOCHROME A); G-protein coupled photoreceptor/ protein histidine kinase/ red or far-red light photoreceptor/

---

2. gi|238481365 Mass: 47318 Score: 140 Queries matched: 5 emPAI: 0.26
BIN4 (brassinosteroid-insensitive4); double-stranded DNA binding [Arabidopsis thaliana]
☐ Check to include this hit in error tolerant search

Query	Observed	Mr(expt)	Mr(calc)	Delta	Miss	Score	Expect	Rank	Peptide
☑ 140	510.7700	1019.5254	1019.5135	0.0119	0	20	2.8	1	K.QEVTVSTEK.D
☑ 152	544.7900	1087.5654	1087.5509	0.0145	0	9	31	1	K.EGNSAQEILK.T
☑ 207	726.8800	1451.7454	1451.7079	0.0376	0	70	2.1e-05	1	R.TFCVVNVGQTEAK.I
☑ 257	1002.9300	2003.8454	2003.9647	-0.1193	0	80	1.2e-06	1	K.TAVKPADQSVGTEEETNTK.A
☑ 258	669.0100	2004.0082	2003.9647	0.0434	0	(48)	0.0026	1	K.TAVKPADQSVGTEEETNTK.A

Proteins matching the same set of peptides:
gi|238481367 Mass: 49307 Score: 140 Queries matched: 5
BIN4 (brassinosteroid-insensitive4); double-stranded DNA binding [Arabidopsis thaliana]
gi|238481371 Mass: 48821 Score: 140 Queries matched: 5
BIN4 (brassinosteroid-insensitive4); double-stranded DNA binding [Arabidopsis thaliana]
gi|238481373 Mass: 49740 Score: 140 Queries matched: 5
BIN4 (brassinosteroid-insensitive4); double-stranded DNA binding [Arabidopsis thaliana]
gi|240256338 Mass: 49435 Score: 140 Queries matched: 5
BIN4 (brassinosteroid-insensitive4); double-stranded DNA binding [Arabidopsis thaliana]

V. Attachment

A R-22: Data that were used for figure III-47. See figure III - 47 for details. A-D correspond to A-D of figure III-47.

A + B

sample	condition	No. of seedlings	fresh weight [g]	dilution factor	A_{535}	A_{650}	$corrA_{535}$	corrA535/g	corrA535/seedling
Col-0	light	50	0,06	2,97	0,145	0,015	0,13	2,1667	0,0026
cop1-4	light	50	0,04	2,94	0,29	0,027	0,263	6,5750	0,0053
mid-1	light	39	0,01	2,97	0,136	0,009	0,127	12,7000	0,0033
rhl2	light	47	0,02	2,94	0,142	0,023	0,119	5,9500	0,0025
Col-0	dark	50	0,03	2,94	0,005	0,004	0,001	0,0333	0,0000
cop1-4	dark	50	0,04	2,94	0,057	0,005	0,053	1,3250	0,0011
mid-1	dark	50	0,01	2,94	0,015	0,011	0,004	0,4000	0,0001
rhl2	dark	34	0,005	2,94	0,01	0,01	0	0,0000	0,0000

C

NaOCl treatment [min]	no of seeds	germinated after 2 days [%]
3	40	83
5	192	56
7	160	32

D

	seed set	experimental set	fresh weight [g]	OD_{535}	OD_{650}	$OD_{535} - OD_{650}$	$(O_{D535} - OD_{650})$ / freshweight [g]	range of fresh weight [g]	mean: $(O_{D535} - OD_{650})$ / freshweight [g]	STDEV: $(O_{D535} - OD_{650})$ / freshweight [g]
Col-0	1	A	0,21	0,012	0,005	0,007	0,033	0,2-0,21	0,028	0,006
Col-0	1	B	0,2	0,011	0,005	0,006	0,030			
Col-0	2	A	0,2	0,01	0,004	0,006	0,030			
Col-0	2	B	0,2	0,011	0,007	0,004	0,020			
cop1-4	1	A	0,2	0,094	0,008	0,086	0,430	0,2	0,385	0,064
cop1-4	1	B	0,2	0,071	0,003	0,068	0,340			
mid-2	1	A	0,2	0,031	0,01	0,021	0,105	0,2-0,24	0,096	0,012
mid-2	1	B	0,22	0,029	0,012	0,017	0,077			
mid-2	2	A	0,24	0,034	0,01	0,024	0,100			
mid-2	2	B	0,24	0,031	0,007	0,024	0,100			
rhl2	1	A	0,04	0,013	0,01	0,003	0,075	0,04-0,08	0,138	0,088
rhl2	2	A	0,08	0,022	0,006	0,016	0,200			

A R-23: Data that were used for figure III-50. See figure III - 50 for details. A,B correspond to A, B of figure III-50.

A

No. of leaves when bolting	Col-0	*mid-1*	*mid-2*	*rhl2*	*hyp6*
	No. of plants				
	assay 1	assay 1	assay 1	assay 1	assay 1
4	-	-	-	-	-
5	-	-	-	-	-
6	-	-	-	-	-
7	-	3	-	-	-
8	-	27	-	-	-
9	-	9	-	-	-
10	12	1	-	-	-
11	32	1	-	-	-
12	11	-	-	-	-
13	1	-	-	-	-
	assay 2	assay 2	assay 2	2 x assay 2	assay 2
4	-	-	-	27	-
5	-	-	-	49	-
6	-	-	-	5	-
7	-	22	-	-	-
8	-	20	-	-	-
9	2	16	-	-	-
10	17	1	-	-	-
11	34	-	-	-	-
12	14	-	-	-	-
13	5	-	-	-	-
	assay 3	assay 3	assay 3	assay 3	assay 3
4	-	-	1	-	6
5	-	1	8	-	12
6	-	15	12	-	11
7	-	33	-	-	4
8	1	21	-	-	1
9	12	4	-	-	-
10	33	1	-	-	-
11	23	-	-	-	-
12	5	-	-	-	-
13	-	-	-	-	-
No. of assays	3	3	1	2	1
No. of plants	202	175	21	81	34
mean	10,7	7,7	5,5	4,7	5,5
STDEV	0,9	1,0	0,6	0,6	1,0
t-test (Col-0)	1	5,88E-108	3,41E-153	2,67E-68	3,98E-84
t-test (rhl2)	-	-	1	1,64E-07	2,46E-06

B

	Col-0	*Ler*	*cop1-4*	*cop1*^{eid6}	spa1-100	mid-1	*mid-1 spa1-100-P27*	*mid-1 spa1-100-P32*
							P27	P32
1	46	35	12	12	37	81	14	17
2	47	29	9	13	40	67	18	14
3	50	31	11	13	40	64	17	19
4	48	34	11	15	44	61	19	15
5	47	30	10	15	48	59	23	15
6	48	30	11	20	48		25	17
7	46	29	11	18	47		28	18
8	46	34	9	18	50		18	18
9	48	30	12		43		26	17
10	58	40	10		47		30	26
11	51	30	10		46		32	25
12	53	32	12		43		21	15
13	54	37	12		46		30	20
14	50	33	11		47		25	37
15	56	30	11		52		27	32
16	52	35	11		50			30
17	52	31	12		53			26
18	50	30	11		52			26
19	52		11		52			26
20	54		10		46			31
21	55		9		52			28
22	52		10		53			27
23	54		10		52			27
24	58		11		49			
25	51		16		47			
26	50				53			
27	52				56			
28					53			
29					57			
n	27	18	25	8	29	5	15	23
mean	51,1	32,2	10,9	15,5	48,4	66,4	19,6	22,9
STDEV	3,5	3,1	1,4	2,9	4,9	8,7	10,3	6,5
t-Test (Col-0)	1,00E+00	2,62E-22	5,66E-46		1,96E-02	1,07E-07	1,93E-18	2,03E-24
t-Test (*Ler*)		1,00E+00		2,04E-12				

V. Attachment

A R-24: Data that were used for figure III-52. See figure III - 52 for details. A, B correspond to A,B of figure III-52. Data for the nursery are data from A III-23.

A

No. of leaves when bolting	No. of plants			
	Col-0	*mid-1*	*mid-2*	*rhl2*
	assay 1	assay 1	assay 1	assay 1
4	-	-	-	19
5	-	1	1	-
6	-	17	15	-
7	1	10	1	-
8	15	-	-	-
9	18	-	-	-
10	-	-	-	-
11	-	-	-	-
	assay 2	assay 2	assay 2	assay 2
4	-	-	-	2
5	-	-	-	-
6	-	4	1	-
7	-	7	-	-
8	7	5	-	-
9	9	2	-	-
10	7	-	-	-
11	4	-	-	-
assay	2	2	1	1
n	61	46	17	19
mean	8,9	6,7	6,0	4,0
STDEV	0,9	0,9	0,4	0,0
t-test plant room - nursery	1,05E-34	5,40E-77	5,25E-03	6,79E-08

B

	Col-0	mid-1	spa1-100	mid-1 spa1-100 (27)	mid-1 spa1-100 (32)
	No. of leaves	No. of leaves	No. of leaves	No. of leaves	No. of leaves
1	13	8	12	7	9
2	11	8	13	8	8
3	12	8	15	8	8
4	12	8	14	8	8
5	12	8	13	8	7
6	12	8	17	9	8
7	12	7	15	9	10
8	13	8	13	11	10
9	13	8	14	11	-
10	13	8	17	9	-
11	11	8	14	11	-
12	11	8	13	9	-
13	13	10	13	12	-
14	11	-	22	10	-
15	13	-	17	13	-
n	15	13	15	15	8
mean (leaves)	12,1	8	14,8	10	8,5
STDEV	0,83	1	2,57	2	1,1
t-test	1,00E+00	8,40E-14	6,73E-04	1,39E-05	1,12E-08

A R-25: Data that were used for figure III-53. See figure III - 53 for details. C, D correspond to C, D of figure III-53.

C

plant No.	hypocotyl length [cm]			
	Col-0	*mid-1*	*cop1-4*	*mid-1 cop1-4*
1	1,885	0,732	0,411	0,114
2	2,026	0,789	0,033	0,118
3	1,878	0,631	0,310	0,161
4	2,112	0,583	0,333	0,142
5	2,022	0,595	0,277	0,153
6	2,062	0,654	0,326	0,179
7	1,980	0,616	0,405	0,172
8	2,123	0,611	0,273	0,134
9	2,182	0,628	0,285	0,142
10	1,755	0,677	0,305	0,181
11	2,041	0,627	0,301	0,176
12	2,093	0,593	0,250	
13	2,130	0,567	0,319	
14	2,164	0,493	0,337	
15	1,884	0,657	0,215	
16	2,167	0,667	0,329	
17	2,149	0,538	0,328	
18	2,128	0,526	0,373	
19	2,251	0,673	0,353	
20	2,067	0,467	0,374	
21	2,092	0,564	0,334	
22	2,178	0,733	0,322	
23	1,886	0,618	0,369	
24	1,832	0,594	0,383	
25	2,474	0,642	0,293	
26	2,070	0,678	0,347	
27	1,942	0,629	0,289	
28	2,047	0,720	0,448	
29	2,005	0,628	0,351	
30	2,015	0,610	0,372	
31	2,276	0,523	0,356	
32	2,091	0,545	0,358	
33	1,854	0,704	0,344	
34	1,991	0,641	0,300	
35	2,206	0,731	0,330	
36	1,858	0,638	0,372	
37	2,223	0,696	0,254	
38	2,280	0,626	0,338	
39	2,392	0,625	0,355	
40	1,864	0,749	0,310	
41	1,974	0,595	0,395	
42	2,151		0,335	
43	1,856			
n	43	41	42	11
mean	2,062	0,630	0,326	0,152
STDEV	0,156	0,070	0,065	0,024

D

plant No.	hypocotyl length [cm]			
	Col-0	*mid-1*	*cop1-eid6*	*mid-1 cop1-eid6*
1	2,146	0,607	0,964	0,265
2	1,977	0,636	0,896	0,38
3	2,169	0,593	0,734	0,292
4	2,200	0,462	1,011	0,277
5	1,913	0,672	0,955	0,393
6	2,051	0,606	1,042	0,344
7	1,871	0,649	0,991	0,333
8	1,995	0,527	1,094	0,223
9	1,566	0,556	0,929	0,273
10	2,092	0,645	1,081	0,263
11	2,019	0,481	0,809	0,215
12	1,892	0,639	0,831	
13	2,099	0,686	0,926	
14	2,047	0,709	1,054	
15	2,022	0,629	1,199	
16	1,941	0,627	0,893	
17	1,784	0,636	1,071	
18	2,142	0,814	0,926	
19	2,013	0,555	0,855	
20	2,121	0,648	0,756	
21	1,968	0,541	1,218	
22	2,199	0,738	1,009	
23	1,962	0,717	0,849	
24	1,901	0,67	1,057	
25	1,997	0,648	1,134	
26	1,985	0,719	1,088	
27	2,094	0,573	1,127	
28	1,805	0,63	1,015	
29	2,184	0,648	0,971	
30	2,197	0,667	1,103	
31	2,219	0,67	0,955	
32	2,268	0,657	1,081	
33	2,100	0,74	1,225	
34	1,836	0,665	0,883	
35	2,016	0,587	1,002	
36	1,925	0,792	0,700	
37	2,169	0,737	1,309	
38	2,196	0,611	1,034	
39	1,992	0,703	0,976	
40	2,127	0,58	0,747	
n	40	40	40	11
mean	2,030	0,642	0,988	0,296
STDEV	0,144	0,075	0,140	0,059

V. Attachment

A R-26: Data that were used for figure III-53. See figure III - 53 for details. F, H correspond to F, H of figure III-53.

	F			petiole angle			H			lamina angle		
	Col-0	*mid-1*	*cop1-4*	*mid-1 cop1-4*	*cop1-eid6*	*mid-1 cop1-eid6*	Col-0	*mid-1*	*cop1-4*	*mid-1 cop1-4*	*cop1-eid6*	*mid-1 cop1-eid6*
1	0	0	7	50	0	11	0	94	256	328	221	260
2	0	0	13	57	0	18	39	81	266	306	210	266
3	0	0	4	33	0	17	72	44	254	266	221	308
4	0	0	15	41	0	26	7	91	302	234	213	290
5	0	3	5	45	0	7	83	87	272	260	203	304
6	0	0	6	45	0	0	23	52	331	298	264	298
7	0	0	8	47	0	19	64	65	334	242	224	313
8	0	0	8	38	0	12	2	29	264	269	251	180
9	0	3	6		0	10	39	74,5	318		215	269
10	0	0	0		0	32	60	31	309		224	347
11	0	5	3		0		12	110	268		228	
12	0	8	15		0		14	53	308		221	
13	0	0	6		0		51	90	300		188	
14	0	2,5	11		0		4	79	265		194	
15	0	0	0		0		0	69	263		168	
16	0	0	0		0		26	27	252		195	
17	0	0	2		0		12	12	299		231	
18	0	0	4		0		14	66			241	
19	0	0	20		0		1,5	74			225	
20	0	0	4,5		0		38	30			233	
21	0	4	0		0		72	59,5			225	
22	0	2,5	30		0		0	82			236	
23	0	0	0		0		0	30			229	
24	0	0			0		15	68			212	
25	0	0			0		0	53			291	
26	0	0			0		29	111			259	
27	0	0			0		5	57			257	
28	0	0			0		2	32			241	
29	0	0			0		13	36			219	
30	0	0			0		5	49			198	
31		0			0		34	71				
32		0					4	25				
33		0					3	37				
34		0					7	37				
35		1,5					3	61				
36		0					2	80				
37		0					0	57				
38		0					31	78				
39		0					36	49				
40		0					49	61				
41		0						25				
42		0						30				
43		0						23				
44		0						93				
45		0						97				
46		0						58				
47		0						87				
48		0						32				
49		0						64				
50								38				
51								77				
52								81				
53								66				
54								51				
n	30	49	23	8	31	10	40	54	17	8	30	10
mean	0	0,6	7,3	44,5	0	15,2	21,8	59,5	285,9	275,4	224,6	283,5
STDEV	0	1,6	7,4	7,4	0	9,3	23,9	24,5	27,9	32,5	24,8	16,5

V. Attachment

A R-27: Data that were used for figure III-55. See figure III - 55 for details. 24 seeds were tested for Col-0 and 55 seeds for all mutants and double mutants.

light																		
		STEDV	mean [%]	n		germinated seeds												
		2,6	97,9	14	Col-0	23	24	24	23	22	24	24	24	24	24	24	23	24
		5,5	96,1	8	*mid-1*	32	31	32	32	27	30	30	32					
		8,8	93,8	2	*mid-2*	32	28											
		4,4	62,5	2	*rhl2*	21	19											
		8,8	28,1	2	*hyp6*	11	7											
		1,1	99,6	8	*cop1-4*	32	32	32	32	32	32	32	31					
		3,9	86,7	4	*cop1-eid6*	26	29	28	28									
t-test (*mid-1*)	t-test (*cop1-4/spa1-100*)	4,4	81,3	2	*spa1-100*	25	27											
3,52E-06	7,86E-07	13,3	34,4	2	*mid-1 cop1-4*	14	8											
1,10E-05	7,00E-02	19,9	29,7	2	*mid-1 spa1-100*	5	14											
dark																		
		STEDV	mean [%]	n		germinated seeds												
		2,1	98,4	13	Col-0	24	24	23	24	23	24	23	24	23	24	24	24	23
		7,0	93,8	7	*mid-1*	31	32	31	32	26	28	30						
		4,4	87,5	2	*mid-2*	27	29											
		11,0	76,6	2	*rhl2*	27	22											
		6,6	26,6	2	*hyp6*	7	10											
		3,9	97,8	7	*cop1-4*	32	32	29	32	30	32	32						
		4,0	82,8	4	*cop1-eid6*	27	25	28	26									
t-test (*mid-1*)	t-test (*cop1-4/spa1-100*)	4,4	84,4	2	*spa1-100*	28	26											
1,20E-05	2,34E-08	0,0	18,8	2	*mid-1 cop1-4*	6	6											
6,19E-06	3,44E-03	0,0	31,3	2	*mid-1 spa1-100*	10	10											

A R-28: Data that were used for figure III-58. See figure III - 58 for details.

p35s::YFP-MID	-	+
p35s::YFP-attB1	+	-
p35s::RFP-HA-COP1	+	+
	minimal No. of dots	
	assay 1	assay 1
1	3	6
2	1	4
3	1	8
4	3	5
5	1	6
6	1	6
7	3	12
8	3	6
9	2	5
10	4	6
11	1	
12	1	

	assay 2	assay 2
1	2	14
2	2	11
3	2	16
4	1	5
5	4	8
6	4	6
7	2	12
8	3	18
9	5	13
10	3	12
n (1)	12	10
average (1)	2	2,8
n (2)	10	6,4
average (2)	2,8	11,5
n (1+2)	22	20
average (1+2)	2,4	8,95
STDEV (1+2)	1,18	3,2

V. Attachment

A R-29: Data that were used for figure III-36. See figure III - 59 for details. Percentage of cells in the depicted C-classes.

	Col-0	*mid-2*	*rhl2*	*hy5-215*	*cop1-4*	*cop1-4 hy5-215*	Col-0	Col-0
seed set	IV	IV	IV	III	II	II	III	I
2C	4,4	10,5	1,8	3,4	7,8	29,2	0,0	7,0
4C	8,8	8,8	14,0	13,8	48,4	60,7	0,0	19,0
8C	32,5	50,0	64,9	54,3	42,2	9,0	28,8	14,0
16C	43,0	28,1	19,3	25,9	9,4	1,1	41,3	25,0
32C	9,6	2,6	0,0	2,6	0,0	0,0	19,8	25,0
64C	1,8	0,0	0,0	0,0	0,0	0,0	0,0	11,0
n	114	114	114	116	64	89	121	57
> 8C	54,4	30,7	19,3	28,5	9,4	1,1	61,1	61
n	62	35	22	33	6	1	74	35

A R-30: Data that were used for A R-29 and figure III-59. See figure III - 59 for details. Meas.: measurement. Three measurements per nucleus were done. The average of stomata of the same plants were used to determine the C-content that was sorted into classes (see II 2.5.7). Values of stomata of one seedlings are arranged above the values for the hypocotyl epidermal cells, except for the last seedling for *cop1-4 hy5-215* that are given side by side. Several tables, above each table the corresponding seed batch of the wildtype, the mutant or double mutant is given. int: used integration of the DISCUS programme. av.: average. Klasse: class

Col-0 (I)

stomata (cotyledons) (int 1/2)

No	Meas. 1	Meas. 2	Meas. 3	average	STBDEV (per nucleus)				No	Meas. 1	Meas. 2	Meas. 3	average	STBDEV (per nucleus)			
1	1346	1239	1136	1240,3	105,0				1	1980	1901	2046	1975,7	72,6			
2	1735	1650	1499	1628,0	119,5				2	1544	1445	1570	1519,7	66,0			
3	1825	1851	1648	1774,7	110,5				3	1469	1544	1517	1510,0	38,0			
4	1906	1795	2128	1943,0	169,6				4	1221	1251	1148	1206,7	53,0			
5	1614	1831	1654	1699,7	115,5				5	1902	1783	1813	1832,7	61,9			
6	1360	1239	1003	1200,7	181,6				6	2050	1934	1794	1926,0	128,2			
7	1222	1305	1484	1337,0	133,9				7	1981	1642	1756	1793,0	172,5			
8	1508	1562	1708	1592,7	103,5				8	1257	1249	1303	1269,7	29,1			
9	1539	1247	1392	1392,7	146,0				9	1449	1300	1496	1415,0	102,3			
10	1929	1990	1700	1873,0	152,9				10	2023	1958	1990	1990,3	32,5			
11	1316	1388	1144	1282,7	125,4				11	1444	1344	1259	1349,0	92,6			
12	1192	1304	1105	1200,3	99,8				12	1275	1420	1153	1282,7	133,7			
13	1434	1128	1245	1269,0	154,4				13	1654	1943	1658	1751,7	165,7			
14	1200	1242	1213	1218,3	21,5				14	1239	1348	1390	1325,7	77,9			
15	1400	1163	1315	1292,7	120,1				15	1718	1894	1683	1765,0	113,1			
16	1576	1471	1546	1531,0	54,1				16	1418	1584	1312	1438,0	137,1			
17	1490	1603	1277	1456,7	165,5				17	1386	1226	1006	1206,0	190,8			
18	1217	1812	1810	1613,0	342,9				18	1677	1763	1813	1751,0	68,8			
			av.	1474,7	134,5				19	1650	1746	1879	1758,3	115,0			
			STDEV	241,0								av.	1582,4	97,4			
												STDEV	270,4				

hypocotyl epidermal cells (int 1/2)

No	Meas. 1	Meas. 2	Meas. 3	average	STBDEV	C-content			No	Meas. 1	Meas. 2	Meas. 3	average	STBDEV	C-content	
1	25478	24692	28229	26133,0	1857,2	35,4	32		1	14006	12874	12487	13122,3	789,4	16,6	16
2	19743	18039	17804	18528,7	1058,2	25,1	32		2	5731	5076	6365	5724,0	644,5	7,2	8
3	20677	20250	20106	20344,3	297,0	27,6	32		3	10962	10434	11147	10847,7	370,0	13,7	16
4	23630	24507	28157	25431,3	2400,9	34,5	32		4	9973	9274	8696	9314,3	639,5	11,8	8
5	5693	6350	6621	6221,3	477,2	8,4	8		5	8428	9067	8854	8783,0	325,4	11,1	8
6	3176	2732	2706	2871,3	264,2	3,9	4		6	2493	2194	2185	2290,7	175,3	2,9	2*
	3710	4189	3641	3846,7	298,5	5,2	4		7	1354	1995	1866	1738,3	339,0	2,2	2*
7	21006	18521	19577	19701,3	1247,2	26,7	32		8	4998	4571	4615	4728,0	234,9	6,0	4
8	4327	3869	3622	3939,3	357,7	5,3	4		9	13817	14846	14984	14549,0	637,7	18,4	16
9	3136	3387	4070	3531,0	483,4	4,8	4		10	8556	9416	9280	9084,0	462,3	11,5	8
10	21772	22493	24394	22886,3	1354,5	31,0	32		11	21075	19303	19070	19816,0	1096,5	25,0	32
11	28539	23534	26869	26314,0	2548,2	35,7	32		12	27894	26215	25868	26659,0	1083,5	33,7	32
12	9354	7986	7339	8226,3	1028,8	11,2	8		13	17479	18854	17625	17986,0	755,2	22,7	16
13	27753	27282	26926	27320,3	414,8	37,1	32		14	6665	7915	7148	7242,7	630,4	9,2	8
14	20699	18542	19298	19513,0	1094,5	26,5	32		15	16322	16368	16157	16282,3	111,0	20,6	16
15	14886	15708	15618	15404,0	450,9	20,9	16		16	3316	3595	2918	3276,3	340,2	4,1	4
16	15836	16404	17229	16489,7	700,4	22,4	16		17	2829	2549	2657	2678,3	141,2	3,4	4
17	40812	38979	43151	40980,7	2091,1	55,6	64		18	1963	2212	2241	2138,7	152,8	2,7	2
18	13469	12139	14644	13417,3	1253,3	18,2	16		19	8003	9495	7718	8405,3	954,4	10,6	8
19	37846	34272	35821	35979,7	1792,3	48,8	64		20	34955	32591	34355	33967,0	1228,8	42,9	32
20	14080	14643	13860	14194,3	403,8	19,3	16		21	19590	19424	19257	19423,7	166,5	24,5	32
21	39397	38181	36150	37909,3	1640,5	51,4	64		22	61461	61519	62534	61838,0	603,5	78,2	64
22	15957	14937	14886	15260,0	604,2	20,7	16		23	13278	12720	13913	13303,7	596,9	16,8	16
23	45230	47717	46331	46426,0	1246,2	63,0	64		24	10842	12754	12707	12101,0	1090,6	15,3	16
24	55994	54537	53231	54587,3	1382,2	74,0	64		25	1138	1536	1455	1376,3	210,3	1,7	2
25	2249	2156	1857	2087,3	204,8	2,8	2		26	3816	3142	3206	3388,0	372,0	4,3	4
26	3321	2380	3000	2900,3	478,4	3,9	4		27	10175	10692	10517	10461,3	263,0	13,2	16
27	36795	37817	36251	36954,3	795,1	50,1	64		28	2069	1947	1616	1877,3	234,4	2,4	2
28	35141	34274	34737	34717,3	433,8	47,1	32		29	4282	4021	3792	4031,7	245,2	5,1	4
29	12385	12274	12356	12338,3	57,6	16,7	16		30	4058	3554	3338	3650,0	369,5	4,6	4

V. Attachment

cop1-4

stomata (cotyledons) (int 1/8)

No	Meas. 1	Meas. 2	Meas. 3	average	STBDEV
1	2918	2266	1781	2321,7	570,5
2	3216	3135	2842	3064,3	196,8
3	2900	2999	2909	2936,0	54,7
4	3203	3476	3998	3559,0	403,9
5	4723	4466	4039	4409,3	345,5
6	3644	3272	4565	3827,0	665,6
7	3654	3967	3403	3674,7	282,6
8	4828	4067	4177	4357,3	411,3
9	3584	4331	3757	3890,7	391,0
10	4287	3502	3936	3908,3	393,2
11	3161	3409	3627	3399,0	233,2
12	5203	4327	4756	4762,0	438,0
13	5641	5711	6195	5849,0	301,7
14	2729	3471	2619	2939,7	463,4
15	3922	3467	4346	3911,7	439,6
16	3210	3365	3688	3421,0	243,9
17	3485	3553	3418	3485,3	67,5
18	3637	4034	4290	3987,0	329,0
19	2579	2899	2617	2698,3	174,8
20	4125	4281	3699	4035,0	301,3
			av.	3721,8	
			STDEV	785,1	

No	Meas. 1	Meas. 2	Meas. 3	average	STBDEV
1	4561	5291	4300	4717,3	513,7
2	4518	4635	4789	4647,3	135,9
3	3425	2951	2543	2973,0	441,4
4	4780	32886	3281	13649,0	16676,6
5	4448	3651	3932	4010,3	404,2
6	2643	2583	2035	2420,3	335,1
7	2760	3361	3001	3040,7	302,5
8	2294	2415	2741	2483,3	231,2
9	4469	4462	3183	4038,0	740,5
10	3673	4071	3443	3729,0	317,7
11	3038	4872	4365	4091,7	947,1
12	2300	2444	3281	2675,0	529,7
13	3250	4284	3403	3645,7	558,1
14	2928	2099	2636	2554,3	420,5
15	3659	3517	3849	3675,0	166,6
16	2634	3545	3737	3305,3	589,3
17	2797	2390	3417	2868,0	517,2
18	2872	2657	2766	2765,0	107,5
19	2664	2719	2734	2705,7	36,9
			av.	4030,8	
			STDEV	2582,6	

hypocotyl epidermal cells (int 1/8)

No	Meas. 1	Meas. 2	Meas. 3	average	STBDEV	C-content	Klasse
1	9077	12025	12178	11093,3	1747,9	6,0	4
2	9975	11793	11042	10936,7	913,6	5,9	4
3	4077	5639	6793	5503,0	1363,1	3,0	2
4	4485	4337	3940	4254,0	281,8	2,3	2
5	4197	4156	6087	4813,3	1103,2	2,6	2
6	4439	4898	5837	5058,0	712,6	2,7	2
7	9700	11348	9792	10280,0	926,1	5,5	4
8	5865	6045	7017	6309,0	619,7	3,4	4
9	10535	8071	9889	9498,3	1277,6	5,1	4
10	14938	17206	14633	15592,3	1405,8	8,4	8
11	9065	5637	8539	7747,0	1846,1	4,2	4
12	15135	11703	14557	13798,3	1837,5	7,4	8
13	5340	7452	7975	6922,3	1395,1	3,7	4
14	3904	6861	4811	5192,0	1514,9	2,8	2
15	9660	6521	7796	7992,3	1578,7	4,3	4
16	12029	10201	13271	11833,7	1544,3	6,4	8
17	6762	9170	6540	7490,7	1458,6	4,0	4
18	7337	8613	6533	7494,3	1048,9	4,0	4
19	6579	7401	6527	6835,7	490,3	3,7	4
20	9707	12246	11995	11316,0	1399,1	6,1	8
21	7201	6536	5925	6554,0	638,2	3,5	4
22	10929	14026	10894	11949,7	1798,2	6,4	8
23	7528	11084	9911	9507,7	1812,0	5,1	4
24	7439	8915	7136	7830,0	951,8	4,2	4
25	8811	6832	6728	7457,0	1173,8	4,0	4
26	2381	3758	3685	3274,7	774,8	1,8	2*
27	3104	3768	3391	3421,0	333,0	1,8	2*

No	Meas. 1	Meas. 2	Meas. 3	average	STBDEV	C-content	Klasse
1	14872	14361	13023	14085,3	954,8	7,0	8
2	12021	19061	26203	19095,0	7091,1	9,5	8
3	17200	15036	15119	15785,0	1226,1	7,8	8
4	15199	21040	16655	17631,3	3040,4	8,7	8
5	10513	11765	13426	11901,3	1461,3	5,9	4
6	14424	12804	14773	14000,3	1050,6	6,9	8
7	6604	8155	7216	7325,0	781,2	3,6	4
8	6241	5998	8063	6767,3	1128,6	3,4	4
9	17782	18180	14485	16815,7	2028,2	8,3	8
10	7246	8894	7051	7730,3	1012,5	3,8	4
11	9200	11145	9639	9994,7	1020,1	5,0	4
12	15670	13952	18250	15957,3	2163,4	7,9	8
13	19670	17696	18176	18514,0	1029,5	9,2	8
14	8812	11398	9567	9925,7	1329,8	4,9	4
15	11832	11627	9224	10894,3	1450,2	5,4	4
16	5003	8623	6585	6737,0	1814,8	3,3	4
17	17896	14944	16165	16335,0	1483,3	8,1	8
18	11072	15315	14650	13679,0	2282,1	6,8	8
19	11757	13079	12602	12479,3	669,5	6,2	8
20	13175	18005	16357	15845,7	2455,3	7,9	8
21	18557	16500	17588	17548,3	1029,1	8,7	8
22	12577	13639	14355	13523,7	894,6	6,7	8
23	13784	16308	11809	13967,0	2255,1	6,9	8
24	14024	9117	11794	11645,0	2456,9	5,8	4

stomata (cotyledons) (int 1/8)

No	Meas. 1	Meas. 2	Meas. 3	average	STBDEV
1	2275	2273	2045	2197,7	132,2
2	2450	3348	3553	3117,0	586,7
3	2397	1959	2970	2442,0	507,0
4	3143	3347	2788	3092,7	282,9
5	2160	2840	3010	2670,0	449,8
6	3393	3453	3119	3321,7	178,1
7	2331	3227	2511	2689,7	474,0
8	2095	3327	2491	2637,7	629,0
9	2444	2259	2796	2499,7	272,8
10	3214	3433	2698	3115,0	377,4
11	3915	4448	3599	3987,3	429,1
12	3699	4612	4176	4162,3	456,7
13	4146	4005	4132	4094,3	77,7
14	2960	2611	3444	3005,0	418,3
15	3120	2907	2789	2938,7	167,8
16	2746	3562	2865	3057,7	440,8
17	2217	3222	3039	2826,0	535,3
18	3381	4347	3363	3697,0	563,0
19	2838	3472	2605	2971,7	448,7
			av.	3080,2	
			STDEV	558,1	

hypocotyl epidermal cells (int 1/8)

No	Meas. 1	Meas. 2	Meas. 3	average	STBDEV	C-content	Klasse
1	3855	4910	3831	4198,7	616,1	2,7	2*
2	5172	6238	6306	5905,3	636,0	3,8	4
3	5431	6245	6567	6081,0	585,5	3,9	4
4	6234	5219	6354	5935,7	623,5	3,9	4
5	27512	23144	27931	26195,7	2651,1	17,0	16
6	17335	19249	16435	17673,0	1437,1	11,5	8
7	13008	16355	21435	16932,7	4243,1	11,0	8
8	13071	12854	13008	12977,7	111,6	8,4	8
9	23603	28347	19717	23889,0	4322,1	15,5	16
10	28177	26827	26516	27173,3	883,0	17,6	16
11	24118	17399	19820	20445,7	3402,9	13,3	16
12	13147	17501	15515	15387,7	2179,8	10,0	8
13	20984	28344	19806	23044,7	4627,0	15,0	16
14	22657	20101	23962	22240,0	1964,0	14,4	16
15	4065	4655	5241	4653,7	588,0	3,0	4
16	9958	10818	9151	10072,0	833,6	6,5	8
17	5464	4955	4988	5135,7	284,8	3,3	4
18	15620	13568	19706	16298,0	3124,7	10,6	8
19	11610	11276	14857	12581,0	1978,1	8,2	8
20	3389	3982	3031	3467,3	480,3	2,3	2*
21	4567	3840	3303	3903,3	634,4	2,5	2*
22	6453	4840	5215	5502,7	844,1	3,6	4
23	7152	5293	5085	5843,3	1138,1	3,8	4

V. Attachment

cop1-4 hy5-215

stomata (cotyledons) (int 1/8)

No	Meas. 1	Meas. 2	Meas. 3	average	STBDEV
1	2044	1769	2502	2105,0	370,3
2	1592	1269	2149	1670,0	445,2
3	1593	2019	2543	2051,7	475,8
4	1805	2339	1898	2014,0	285,3
5	2166	2603	2437	2402,0	220,6
6	1382	1743	1684	1603,0	193,7
7	2513	2249	2206	2322,7	166,2
8	2432	2052	2013	2165,7	231,5
9	1445	2105	1936	1828,7	342,8
10	1592	1394	1445	1477,0	102,8
11	1741	1868	1862	1823,7	71,7
12	1948	1939	2052	1979,7	62,8
13	2005	1545	1943	1831,0	249,6
14	1581	2161	1779	1840,3	294,8
15	2243	1625	2319	2062,3	380,6
16	2102	2199	1713	2004,7	257,2
17	1203	1889	1828	1640,0	379,7
18	1709	1756	1805	1756,7	48,0
19	1818	1626	1788	1744,0	103,3
20	1720	1631	1940	1763,7	159,1
			av.	1904,3	
			STDEV	239,8	

No	Meas. 1	Meas. 2	Meas. 3	average	STBDEV
1	2482	2365	2168	2338,3	158,7
2	2378	2039	2718	2378,3	339,5
3	1665	1977	2134	1925,3	238,7
4	2287	2396	3283	2655,3	546,3
5	2668	2228	2742	2546,0	277,9
6	2327	2482	2817	2542,0	250,4
7	2571	3304	2747	2874,0	382,6
8	3031	3083	2752	2955,3	178,0
9	2474	2019	2325	2272,7	232,0
10	1776	2630	1627	2011,0	541,2
11	2167	1716	2026	1969,7	230,7
12	1423	1756	1695	1624,7	177,3
13	1520	2236	1806	1854,0	360,4
14	2799	2739	[illegible]	[illegible]	43,3
15	1790	2066	[illegible]	[illegible]	240,4
16	1802	2043	[illegible]	[illegible]	220,8
17	1821	1352	1781	1651,3	260,0
			av.	2249,5	
			STDEV	427,0	
			av.	2153,6	
			STDEV	580,4	

hypocotyl epidermal cells (int 1/8)

No	Meas. 1	Meas. 2	Meas. 3	average	STBDEV	C-content	Klasse
1	11564	11143	10290	10999,0	649,1	11,6	8
2	11914	13300	10862	12025,3	1222,8	12,6	16
3	12578	11637	15443	13219,3	1982,4	13,9	16
4	19000	17031	19355	18462,0	1251,9	19,4	16
5	20548	20207	19421	20058,7	578,0	21,1	16
6	16203	15718	17285	16402,0	802,2	17,2	16
7	13891	18635	14783	15769,7	2521,2	16,6	16
8	7223	8389	7305	7639,0	650,8	8,0	8
9	7617	6286	5483	6462,0	1077,8	6,8	8
10	6406	4854	4125	5128,3	1165,0	5,4	4
11	4573	3837	2814	3741,3	883,4	3,9	4
12	4288	5777	4176	4747,0	893,8	5,0	4
13	3478	3823	3390	3563,7	228,9	3,7	4
14	1847	2227	2334	2136,0	255,9	2,2	2
15	3545	4295	3229	3689,7	547,5	3,9	4
16	4045	4979	3320	4114,7	831,7	4,3	4
17	9665	11746	8518	9976,3	1636,4	10,5	8
18	6385	6050	6898	6444,3	427,1	6,8	8
19	13831	14546	14305	14227,3	363,8	14,9	16
20	8029	7449	7550	7676,0	309,8	8,1	8
21	12307	14030	13431	13256,0	874,7	13,9	16
22	7425	6379	7454	7086,0	612,5	7,4	8
23	17548	14769	16230	16182,3	1390,1	17,0	16
24	14133	12646	11941	12906,7	1119,0	13,6	16
25	18764	14398	16239	16467,0	2191,9	17,3	16
26	29760	40690	35441	35297,0	5466,4	37,1	32
27	2602	1476	1718	1932,0	592,7	2,0	2
28	5955	5398	5498	5617,0	297,0	5,9	4
29	1729	1393	1197	1439,7	269,1	1,5	2*
30	1247	1824	1326	1465,7	312,8	1,5	2*

No	Meas. 1	Meas. 2	Meas. 3	average	STBDEV	C-content	Klasse
1	4262	2939	3523	3574,7	663,0	3,2	
2	4444	5304	5093	4947,0	448,2	4,4	
3	3260	2229	2805	2764,7	516,7	2,5	
4	2600	2889	3036	2841,7	221,8	2,5	
5	5298	4927	4019	4748,0	658,0	4,2	
6	4893	5176	4951	5006,7	149,5	4,5	
7	3207	4199	3124	3510,0	598,1	3,1	
8	3661	3956	3963	3860,0	172,4	3,4	
9	3818	3458	3590	3622,0	182,1	3,2	
10	6865	6334	6145	6448,0	373,3	5,7	
11	2621	2745	2752	2706,0	73,7	2,4	
12	1325	1411	2098	1611,3	423,7	1,4	
13	1953	1820	1544	1772,3	208,6	1,6	
14	2008	2441	2374	2274,3	233,1	2,0	
15	5180	4418	5296	4964,7	477,0	4,4	
16	5057	5273	5391	5240,3	169,4	4,7	
17	5321	4620	5989	5310,0	684,6	4,7	
18	5195	5467	6770	5810,7	841,9	5,2	
19	14237	13034	13920	13730,3	623,5	12,2	
20	2876	2395	2308	2526,3	305,9	2,2	
21	3066	3521	3825	3470,7	382,0	3,1	
22	9137	8150	9001	8762,7	534,9	7,8	

stomata (cotyledons) (int 1/8)

No	Meas. 1	Meas. 2	Meas. 3	average	STBDEV
1	2795	3229	3830	3284,7	519,7
2	3324	3535	3553	3470,7	127,3
3	2443	3188	2623	2751,3	388,7
4	2356	2344	2932	2544,0	336,1
5	2888	3035	3002	2975,0	77,1
6	2919	3676	3056	3217,0	403,4
7	2884	3106	3055	3015,0	116,3
8	3017	3453	3663	3377,7	329,5
9	3090	3418	3022	3176,7	211,7
10	3276	3537	2842	3218,3	351,1
11	3693	2919	3548	3386,7	411,4
12	2796	3344	3058	3066,0	274,1
13	2747	2537	2888	2724,0	176,6
14	3033	3222	3188	3147,7	100,7
15	2521	2846	2773	2713,3	170,5
16	2893	2301	2519	2571,0	299,4
17	2265	2687	2661	2537,7	236,5
18	3498	3779	3116	3464,3	332,8
			av.	3010,4	
			STDEV	313,4	

No	Meas. 1	Meas. 2	Meas. 3	average	STBDEV
1	2003	1905	1559	1822,3	233,3
2	2512	2613	2614	2579,7	58,6
4	2025	2105	2236	2122,0	106,5
5	2243	2060	1953	2085,3	146,7
6	1512	1672	1453	1545,7	113,3
7	1586	1338	1418	1447,3	126,6
8	1448	1558	1608	1538,0	81,9
9	2007	1650	1711	1789,3	191,0
10	1678	1789	2034	1833,7	182,2
11	1841	1632	1570	1681,0	142,0
12	2045	1674	1841	1853,3	185,8
13	1994	1876	2022	1964,0	77,5
14	2163	1933	1896	1997,3	144,7
15	1865	1712	1647	1741,3	111,9
16	1279	1424	1492	1398,3	108,8
			av.	1826,6	
			STDEV	303,5	

hypocotyl epidermal cells (int 1/8)

No	Meas. 1	Meas. 2	Meas. 3	average	STBDEV	C-content	Klasse
1	7117	7661	7362	7380,0	272,4	4,9	4
2	6878	8961	7763	7867,3	1045,4	5,2	4
3	5049	5452	6169	5556,7	567,3	3,7	4
4	6594	6646	6589	6609,7	31,6	4,4	4
5	5425	6121	5054	5533,3	541,7	3,7	4
6	6087	5881	5336	5768,0	388,0	3,8	4
7	6742	5451	6531	6241,3	692,5	4,1	4
8	3419	3288	3766	3491,0	247,0	2,3	2
9	6336	6028	7189	6517,7	601,4	4,3	4
10	5954	5929	5000	5627,7	543,7	3,7	4
11	5456	5000	4971	5142,3	272,0	3,4	4
12	4834	4567	4525	4642,0	167,6	3,1	4
13	19487	15968	15489	16981,3	2183,1	11,3	8
14	2930	3575	3287	3264,0	323,1	2,2	2
15	1914	1939	2025	1959,3	58,2	1,3	2
16	2694	3350	3757	3267,0	536,3	2,2	2
17	5911	8226	7653	7263,3	1205,7	4,8	4
18	6425	6227	7475	6709,0	670,7	4,5	4
19	5649	4927	4333	4969,7	659,0	3,3	4
20	1844	1503	1459	1602,0	210,7	1,1	2*
21	6335	7463	6943	6913,7	564,6	4,6	4
22	2712	2503	2250	2488,3	231,3	1,7	2
23	5157	4921	3892	4656,7	672,7	3,1	4
24	5091	5475	5834	5466,7	371,6	3,6	4

No	Meas. 1	Meas. 2	Meas. 3	average	STBDEV	C-content
1	3265	2896	4192	3451,0	667,7	3,8
2	6018	5508	5789	5771,7	255,4	6,3
3	3814	3357	3448	3539,7	241,9	3,9
4	2051	3092	3591	2911,3	785,7	3,2
5	1971	1046	1565	1527,3	463,6	1,7
6	1514	1486	1892	1630,7	226,8	1,8
7	3872	3468	4393	3911,0	463,7	4,3
8	4797	4228	4852	4625,7	345,5	5,1
9	6517	5528	6243	6096,0	510,6	6,7
10	3344	3091	2582	3005,7	388,1	3,3
11	1326	1022	1051	1133,0	167,8	1,2
12	3175	3445	4499	3706,3	699,6	4,1
13	3956	3376	3671	3667,7	290,0	4,0
14	6657	6603	6127	6462,3	291,7	7,1
15	2136	1987	2053	2058,7	74,7	2,3
16	2784	3659	3709	3384,0	520,2	3,7
17	1100	1303	1421	1274,7	162,4	1,4

V. Attachment

cop1-4 hy5-215 continued

stomata (cotyledons) (int 1/8)							
No	Meas. 1	Meas. 2	Meas. 3	average	STBDEV		
1	1482	1575	1796	1617,7	161,3		
2	1569	1791	1556	1638,7	132,1		
3	1642	1671	1494	1602,3	94,9		
4	2148	1982	2099	2076,3	85,3		
5	2095	1641	1921	1885,7	229,1		
6	1958	2060	1954	1990,7	60,1		
7	1674	1893	1678	1748,3	125,3		
10	1944	2161	1919	2008,0	133,1		
11	1835	2142	2212	2063,0	200,5		
12	1993	2074	1972	2013,0	53,9		
13	2097	2236	2286	2206,3	97,9		
14	1502	1978	1413	1631,0	303,8		
15	2219	2248	2032	2166,3	117,2		
16	2121	2357	2154	2210,7	127,8		
17	1855	1584	1834	1757,7	150,8		
			av.	1907,7			
			STDEV	224,1			

hypocotyl epidermal cells (int 1/8)						
No	Meas. 1	Meas. 2	Meas. 3	average	STBDEV	C-content
1	4354	4819	3881	4351,3	469,0	4,6
2	4208	4128	4537	4291,0	216,8	4,5
3	3781	4427	4510	4239,3	399,1	4,4
4	3604	3330	2793	3242,3	412,5	3,4
5	2836	3201	3319	3118,7	251,8	3,3
6	3205	3689	3945	3613,0	375,8	3,8
7	2412	2219	2302	2311,0	96,8	2,4
8	3038	4473	3636	3715,7	720,8	3,9
9	1774	1203	1593	1523,3	291,8	1,6
10	1631	1980	1367	1659,3	307,5	1,7
11	1727	2094	2297	2039,3	288,9	2,1
12	2378	1679	1894	1983,7	358,0	2,1
13	2906	2725	2701	2777,3	112,1	2,9
14	1759	1926	1832	1839,0	83,7	1,9
15	7199	6194	5123	6172,0	1038,2	6,5
16	3388	4676	4902	4322,0	816,7	4,5
17	2047	2190	2227	2154,7	95,1	2,3
18	5133	6094	5530	5585,7	482,9	5,9
19	7820	6394	7438	7217,3	738,2	7,6
20	5675	5359	5680	5571,3	183,9	5,8
21	5491	5317	4722	5176,7	403,2	5,4
22	3875	4724	4233	4277,3	426,2	4,5
23	5788	5656	4755	5399,7	562,2	5,7
24	2684	2972	3170	2942,0	244,4	3,1
25	6006	5988	5189	5727,7	466,6	6,0
26	2462	1845	1914	2073,7	338,1	2,2
27	4169	4220	4757	4382,0	325,8	4,6

V. Attachment

Col-0 (III)

stomata (cotyledons) (int 1/8)

No	Meas. 1	Meas. 2	Meas. 3	average	STBDEV
1	5304	4709	4510	4841,0	413,1
2	4417	4601	5100	4706,0	353,4
3	5451	5656	4962	5356,3	356,6
4	4552	5082	5592	5075,3	520,0
5	3197	3253	3350	3266,7	77,4
6	4320	4499	4434	4417,7	90,6
7	4016	3157	3446	3539,7	437,1
8	3443	3687	4106	3745,3	335,3
9	5428	5110	5956	5498,0	427,3
10	6025	5551	6819	6131,7	640,7
11	3505	3403	3657	3521,7	127,8
12	4590	4250	5442	4760,7	614,1
13	4694	4535	4462	4563,7	118,6
14	4424	4434	4677	4511,7	143,3
15	6347	6099	6524	6323,3	213,5
16	4406	4575	4697	4559,3	146,1
17	5631	6917	6678	6408,7	684,0
18	6098	5824	6437	6119,7	307,1
19	6007	5750	5587	5781,3	211,7
			av.	4901,5	
			STDEV	916,0	

No	Meas. 1	Meas. 2	Meas. 3	average	STBDEV
1	3494	3803	3114	3470,3	345,1
2	3260	3246	3020	3175,3	134,7
3	3019	2637	3338	2998,0	351,0
4	3445	3202	3275	3307,3	124,7
5	2674	2863	3138	2891,7	233,3
6	3104	2635	2967	2902,0	241,2
7	2724	1340	2833	2299,0	832,3
8	3816	3819	3032	3555,7	453,5
9	2470	2975	2642	2695,7	256,7
10	2356	2827	2924	2702,3	303,8
			av.	2999,7	
			STDEV	387,2	

hypocotyl epidermal cells (int 1/8)

No	Meas. 1	Meas. 2	Meas. 3	average	STBDEV	C-content	Klasse
1	39631	41198	41306	40711,7	937,4	16,6	16
2	66267	67152	70610	68009,7	2295,0	27,8	32
3	31070	26718	27187	28325,0	2388,8	11,6	8
4	52464	51004	56646	53371,3	2928,4	21,8	16
5	24965	24368	24333	24555,3	355,2	10,0	8
6	61740	59879	62978	61532,3	1559,9	25,1	32
7	7402	6878	6677	6985,7	374,3	2,92*	
8	5040	6407	5982	5809,7	699,6	2,42*	
9	32174	33144	32299	32539,0	527,7	13,3	16
10	29605	30288	30989	30294,0	692,0	12,4	16
11	28995	25656	27797	27482,7	1691,5	11,2	8
12	20590	23893	23586	22689,7	1824,8	9,3	8
13	22488	27007	24165	24553,3	2284,4	10,0	8
14	26114	23214	22815	24047,7	1800,6	9,8	8
15	25976	24923	25182	25360,3	548,7	10,3	8
16	41581	40491	41266	41112,7	560,9	16,8	16
17	39479	42727	43402	41869,3	2097,4	17,1	16
18	19772	19379	19231	19460,7	279,6	7,9	8
19	24005	26384	25096	25161,7	1190,9	10,3	8
20	20041	22133	23727	21967,0	1848,6	9,0	8
21	23036	21386	22169	22197,0	825,4	9,1	8
22	24192	24680	26032	24968,0	953,2	10,2	8
23	21852	19967	22366	21395,0	1263,1	8,7	8
24	25894	26601	25484	25993,0	565,0	10,6	8
25	37256	39884	40127	39089,0	1592,1	15,9	16
26	19664	22246	20880	20930,0	1291,7	8,5	8
27	54227	51770	54065	53354,0	1374,2	21,8	16
28	20710	20480	19516	20235,3	633,5	8,3	8
29	19279	22988	20022	20763,0	1962,4	8,5	8
30	22681	22296	25150	23375,7	1548,6	9,5	8
31	38193	40131	46186	41503,3	4169,5	16,9	16
32	44234	46878	43869	44993,7	1642,1	18,4	16

No	Meas. 1	Meas. 2	Meas. 3	average	STBDEV	C-content	Klasse
1	27177	29199	31094	29156,7	1958,8	19,4	16
2	53950	54569	51337	53285,3	1715,5	35,5	32
3	22535	20025	23633	22064,3	1849,5	14,7	16
4	14021	12817	14528	13788,7	878,8	9,2	8
5	10566	10579	12051	11065,3	853,6	7,4	8
6	18270	17676	19480	18475,3	919,4	12,3	16
7	13788	14499	11362	13216,3	1644,8	8,8	8
8	49568	50754	58549	52957,0	4879,0	35,3	32
9	42438	55750	50780	49656,0	6726,8	33,1	32
10	20191	24669	26178	23679,3	3113,8	15,8	16
11	27201	26217	28342	27253,3	1063,5	18,2	16
12	25503	25563	23964	25010,0	906,4	16,7	16
13	22495	27748	25086	25109,7	2626,6	16,7	16
14	41633	40414	38781	40276,0	1431,0	26,9	32
15	52444	50577	49298	50773,0	1582,1	33,9	32
16	42704	54328	53595	50209,0	6509,8	33,5	32
17	25626	26405	24464	25498,3	976,8	17,0	16
18	20224	20506	21491	20740,3	665,2	13,8	16
19	51457	51666	50008	51043,7	903,0	34,0	32
20	52282	56957	50341	53193,3	3400,8	35,5	32
21	20706	18499	20482	19895,7	1214,7	13,3	16
22	54420	60010	60533	58321,0	3388,5	38,9	32
23	37569	38767	51235	42523,7	7568,0	28,4	32
24	37249	34663	36235	36049,0	1303,0	24,0	32
25	29838	35036	31452	32108,7	2660,5	21,4	16
26	17590	16139	18907	17545,3	1384,5	11,7	8
27	22806	18940	18822	20189,3	2266,9	13,5	16
28	16400	16287	17436	16707,7	633,3	11,1	8
29	16156	16334	19013	17167,7	1600,6	11,4	8
30	36878	29754	35376	34002,7	3755,3	22,7	16
31	34127	23279	32788	30064,7	5914,6	20,0	16

stomata (cotyledons) (int 1/8)

	Meas. 1	Meas. 2	Meas. 3	average	STBDEV
1	3431	4174	3247	3617,3	490,8
2	4181	3370	3386	3645,7	463,7
3	3814	3004	3653	3490,3	428,8
4	4262	3340	3817	3806,3	461,1
5	3414	3398	3030	3280,7	217,2
6	3448	3988	3202	3546,0	402,1
7	3743	2951	3795	3496,3	473,0
8	4890	3789	4078	4252,3	570,8
9	3624	3230	3606	3486,7	222,5
10	4232	4814	3844	4296,7	488,2
11	4376	4517	4027	4306,7	252,3
12	3995	3621	3983	3866,3	212,5
13	3034	4148	3721	3634,3	562,0
14	3008	3206	3171	3128,3	105,7
15	2647	3915	3219	3260,3	635,0
16	4129	3340	4225	3898,0	485,6
17	4451	4441	3349	4080,3	633,4
18	4187	4235	3290	3904,0	532,3
	n=17		av.	3722,0	
			STDEV	370,6	

	Meas. 1	Meas. 2	Meas. 3	average	STBDEV
1	3469	4005	3799	3757,7	270,4
2	3020	3955	3135	3370,0	509,9
3	3845	3824	3616	3761,7	126,6
4	4004	4297	4374	4225,0	195,2
5	4733	4720	5454	4969,0	420,1
6	4825	4105	4509	4479,7	360,9
7	4300	4508	4130	4312,7	189,3
8	4526	3248	3154	3642,7	766,4
9	3636	3161	3131	3309,3	283,3
10	3035	2522	3736	3097,7	609,4
11	4337	4168	4262	4255,7	84,7
12	3429	3994	4735	4052,7	655,0
13	4335	4545	5376	4752,0	550,5
14	4046	3499	3925	3823,3	287,3
15	3746	4665	3845	4085,3	504,4
			av.	3993,0	
			STDEV	590,0	

hypocotyl epidermal cells (int 1/8)

No	Meas. 1	Meas. 2	Meas. 3	average	STBDEV	C-content	Klasse
1	47494	43836	45043	45457,7	1863,9	24,4	32
2	17801	21544	21278	20207,7	2088,5	10,9	8
3	37633	49801	45342	44258,7	6155,9	23,8	16
4	22713	19772	21308	21264,3	1471,0	11,4	8
5	47325	51359	43434	47372,7	3962,7	25,5	32
6	19286	15559	23623	19489,3	4035,8	10,5	8
7	45084	55216	54397	51565,7	5628,2	27,7	32
8	23207	20732	20347	21428,7	1552,1	11,5	8
9	24942	26277	23516	24911,7	1380,7	13,4	16
10	17950	23228	16788	19322,0	3432,2	10,4	8
11	34473	37159	39308	36980,0	2422,5	19,9	16
12	50788	54292	53127	52735,7	1784,5	28,3	32
13	25960	26758	23368	25362,0	1772,4	13,6	16
14	49474	45411	43165	46016,7	3197,8	24,7	32
15	26481	28316	19995	24930,7	4371,8	13,4	16
16	15780	17730	20440	17983,3	2340,3	9,7	8
17	22712	16559	17598	18956,3	3293,7	10,2	8
18	42194	49764	37401	43119,7	6233,3	23,2	16
19	31819	35189	34355	33787,7	1755,2	18,2	16
20	21128	22480	20701	21436,3	928,7	11,5	16
21	40752	37077	48553	42127,3	5860,3	22,6	16
22	41446	43267	41259	41990,7	1109,3	22,6	16
23	17724	20589	19317	19210,0	1435,5	10,3	8
24	42902	48659	48625	46728,7	3314,0	25,1	32
25	17253	22259	20110	19874,0	2511,3	10,7	8
26	50411	41672	44817	45633,3	4426,3	24,5	32
27	24964	22865	19267	22365,3	2881,2	12,0	16
28	43448	47488	40319	43751,7	3594,1	23,5	16
29	18276	15798	19224	17766,0	1769,0	9,5	8
30	17310	15516	16500	16442,0	898,4	8,8	8

No	Meas. 1	Meas. 2	Meas. 3	average	STBDEV	C-content	Klasse
1	35244	33007	34394	34215,0	1129,2	17,1	16
2	25209	28705	27685	27199,7	1797,8	13,6	16
3	23598	27655	31770	27674,3	4086,0	13,9	16
4	26081	24819	26711	25870,3	963,4	13,0	16
5	15804	19956	24105	19955,0	4150,5	10,0	8
6	17627	17393	21236	18752,0	2154,4	9,4	8
7	58874	59215	62462	60183,7	1980,4	30,1	32
8	21912	20578	19765	20751,7	1084,0	10,4	8
9	18399	21328	16871	18866,0	2264,9	9,4	8
10	20229	17749	19228	19068,7	1247,7	9,6	8
11	28577	28063	28537	28392,3	285,9	14,2	16
12	23399	23308	25485	24064,0	1231,5	12,1	16
13	29746	32719	31940	26394,0	1541,6	13,2	16
14	20901	18832	15121	18284,7	2928,6	9,2	8
15	52304	49388	59623	53771,7	5273,0	26,9	32
16	48041	54571	53711	52107,7	3548,0	26,1	32
17	28902	30462	31069	30144,3	1117,9	15,1	16
18	42345	52541	43196	46027,3	5657,0	23,1	16
19	18801	16561	14215	16525,7	2293,2	8,3	8
20	18337	19643	19982	19320,7	868,6	9,7	8
21	28447	26884	29366	28232,3	1254,8	14,1	16
22	31317	38538	33563	34472,7	3695,4	17,3	16
23	18274	20025	22244	20181,0	1989,6	10,1	8
24	53513	41999	50287	48599,7	5939,6	24,3	32
25	31246	30627	31102	30991,7	323,9	15,5	16
26	24882	21900	25264	24015,3	1841,9	12,0	16
27	26123	23237	26670	25343,3	1844,5	12,7	16
28	18752	25556	22206	22171,3	3402,1	11,1	8
29	15888	16644	27261	19931,0	6359,2	10,0	8
30	18504	17335	15580	17139,7	1471,8	8,6	8

V. Attachment

hy5-215:

stomata (cotyledons) (int 1/8)

No	Meas. 1	Meas. 2	Meas. 3	average	STBDEV
1	5164	4019	4456	4546,333	577,8203
2	4291	4011	4713	4338,333	353,3855
3	6749	6578	6981	6769,333	202,268
4	5310	4978	4390	4892,667	465,8984
5	5403	5112	5901	5472	399
6	3495	3174	3075	3248	219,5609
7	4066	4889	5106	4687	548,6374
8	7458	6019	6521	6666	730,3759
9	6234	6092	6121	6149	75,02666
10	4128	4604	4936	4556	406,133
11	5021	4818	4945	4928	102,5622
12	5254	4546	4685	4828,333	375,1324
13	5084	6156	5317	5519	563,8253
14	4821	5260	4908	4996,333	232,4486
15	5136	4671	4893	4900	232,579
			av.	5099,8	
			STDEV	911,6	

No	Meas. 1	Meas. 2	Meas. 3	average	STBDEV
1	2627	3340	3769	3245,3	576,9
2	3396	3940	3503	3613,0	288,2
3	3953	3459	3347	3586,3	322,4
4	3543	3606	3554	3567,7	33,7
5	4023	4575	4353	4464,0	157,0
6	4566	4213	4365	4289,0	107,5
7	5202	5521	5704	5612,5	129,4
8	4243	4008	4628	4318,0	438,4
9	4279	4249	4909	4479,0	372,7
10	5854	5012	5002	5289,3	489,0
11	5205	4639	5467	5103,7	423,2
12	4121	4259	4418	4266,0	148,6
13	4471	4553	5017	4680,3	294,4
14	4845	5081	4920	4948,7	120,6
15	3412	4533	3874	3939,7	563,4
16	3694	3831	4220	3915,0	272,9
17	3636	4400	4331	4122,3	422,6
18	3766	3743	4264	3924,3	294,4
			av.	4298,0	
			STDEV	644,2	

hypocotyl epidermal cells (int 1/8)

No	Meas. 1	Meas. 2	Meas. 3	average	STBDEV	C-content	Klasse
1	25527	24359	22890	24258,7	1321,4	9,5	8
2	20851	18823	17948	19207,3	1489,2	7,5	8
3	11109	10363	10764	10745,3	373,4	4,2	4
4	19395	19346	20193	19644,7	475,5	7,7	8
5	5293	4849	5341	5161,0	271,3	2,0	2
6	26082	25942	26430	26151,3	251,3	10,3	8
7	22426	25765	24101	24097,3	1669,5	9,5	8
8	5471	5772	4846	5363,0	472,4	2,1	2
9	5382	5447	4700	5176,3	413,8	2,0	2*
10	3740	4470	5466	4558,7	866,4	1,8	2*
11	14175	12623	14729	13842,3	1091,7	5,4	4
12	22851	24195	20776	22607,3	1722,5	8,9	8
13	22103	21729	21854	21895,3	190,4	8,6	8
14	24414	24561	19379	22784,7	2950,3	8,9	8
15	8183	7827	7795	7935,0	215,4	3,1	4
16	4334	4430	4004	4256,0	223,5	1,7	2
17	21866	19378	20661	20635,0	1244,2	8,1	8
18	7098	7557	8608	7754,3	774,1	3,0	4
19	24932	20761	22041	22578,0	2136,7	8,9	8
20	25650	25518	22190	24452,7	1960,6	9,6	8
21	16467	15547	19749	17254,3	2208,9	6,8	8
22	9047	8066	8665	8592,7	494,5	3,4	4
23	20969	20204	18899	20024,0	1046,7	7,9	8
24	26215	20173	23809	23399,0	3041,8	9,2	8
25	46775	43877	41675	44109,0	2557,9	17,3	16
26	47111	43946	40100	43719,0	3511,0	17,1	16
27	50192	48716	48107	49005,0	1072,1	19,2	16
28	56939	56069	42729	51912,3	7964,9	20,4	16
29	64458	64836	69550	66281,3	2837,1	26,0	32
30	17454	17034	15839	16775,7	837,9	6,6	8

No	Meas. 1	Meas. 2	Meas. 3	average	STBDEV	C-content	Klasse
1	17387	19865	18060	18437,3	1281,4	8,6	8
2	16029	18909	20135	18357,7	2107,8	8,5	8
3	20221	21964	20420	20868,3	954,1	9,7	8
4	19581	20827	16638	19015,3	2151,0	8,8	8
5	14532	16996	16766	16098,0	1361,1	7,5	8
6	15610	17090	17389	16696,3	952,6	7,8	8
7	18357	17509	17792	17886,0	431,7	8,3	8
8	25379	22105	24859	24114,3	1759,5	11,2	8
9	31028	36415	32158	33200,3	2840,7	15,4	16
10	12563	13656	11632	12617,0	1013,1	5,9	4
11	26606	32824	36529	31986,3	5014,3	14,9	16
12	12285	14203	12359	12949,0	1086,6	6,0	8
13	13345	14567	11523	13145,0	1531,8	6,1	8
14	38295	36045	39096	37812,0	1581,8	17,6	16
15	10953	11961	10354	11089,3	812,1	5,2	4
16	27275	25306	29046	27209,0	1870,9	12,7	16
17	13868	12751	15013	13877,3	1131,0	6,5	8
18	20886	22239	21915	21680,0	706,4	10,1	8
19	27950	25617	21883	25150,0	3060,3	11,7	8
20	14203	13592	21296	16363,7	4282,4	7,6	8
21	18435	21299	20620	20118,0	1496,5	9,4	8
22	12652	11266	13832	12583,3	1284,4	5,9	4
23	15973	18104	17111	17062,7	1066,3	7,9	8
24	19763	16020	18564	18115,7	1911,4	8,4	8
25	15787	20022	15557	17122,0	2514,1	8,0	8
26	15328	15111	15829	15422,7	368,2	7,2	8
27	10408	10018	8323	9583,0	1108,5	4,5	4
28	40399	36559	40693	39217,0	2306,6	18,2	16
29	24104	18954	20767	21275,0	2612,3	9,9	8
30	28379	28672	24058	27036,3	2583,5	12,6	16

stomata (cotyledons) (int 1/8)

No	Meas. 1	Meas. 2	Meas. 3	average	STBDEV
1	3823	3434	3189	3482,0	319,7
2	3738	4457	3262	3819,0	601,6
3	3224	3350	3142	3238,7	104,8
4	4002	3505	3503	3670,0	287,5
5	3062	3142	2621	2941,7	280,6
6	3808	3296	3876	3660,0	317,1
7	2935	2425	3277	2879,0	428,8
10	2485	3246	2745	2825,3	386,8
11	3762	3975	3561	3766,0	207,0
12	3395	4220	3259	3624,7	520,0
13	2141	2556	3344	2680,3	611,1
14	3344	3107	3690	3380,3	293,2
15	2743	3027	2952	2907,3	147,2
16	4176	4172	3781	4043,0	226,9
17	4087	3561	3904	3850,7	267,0
18	3546	3616	3613	3591,7	39,6
19	4461	4543	4824	4609,3	190,4
20	4691	4348	4096	4378,3	298,7
21	3810	4015	3572	3799,0	221,7
22	3457	3368	3961	3595,3	319,8
23	3647	3281	4130	3686,0	425,8
24	3405	4005	2949	3453,0	529,6
			av.	3540,0	
			STDEV	489,4	

No	Meas. 1	Meas. 2	Meas. 3	average	STBDEV
1	4916	4200	4129	4415,0	435,3
2	4433	4122	4530	4361,7	213,1
3	5104	5357	5276	5245,7	129,2
4	4473	3909	4669	4350,3	394,6
5	4306	4841	4251	4466,0	325,9
6	4705	5068	4567	4780,0	258,8
7	3883	4123	4641	4215,7	387,4
8	3893	3799	4695	4129,0	492,4
9	3185	3088	3269	3180,7	90,6
10	3333	3055	4028	3472,0	501,2
11	4864	3732	4620	4405,3	595,7
12	4384	4259	3524	4055,7	464,7
13	3598	3179	3920	3565,7	371,6
14	3425	3558	3227	3403,3	166,6
15	3517	3924	3759	3733,3	204,7
16	3915	4323	3826	4021,3	265,0
17	3763	3973	4545	4093,7	404,7
18	4238	4682	4968	4629,3	367,8
19	3945	4217	4385	4182,3	222,0
20	4907	4306	4680	4631,0	303,5
21	3909	3589	3735	3744,3	160,2
			av.	4118,6	
			STDEV	559,9	

hypocotyl epidermal cells (int 1/8)

No	Meas. 1	Meas. 2	Meas. 3	average	STBDEV	C-content	Klasse
1	20028	17405	18140	18524,3	1353,1	10,5	8
2	36725	39767	33180	36557,3	3296,7	20,7	16
3	32320	29670	27482	29824,0	2422,7	16,8	16
4	36440	33694	35428	35187,3	1388,7	19,9	16
5	14841	20331	16831	17334,3	2779,4	9,8	8
6	37990	36929	34647	36522,0	1708,3	20,6	16
7	38710	38714	44085	40503,0	3102,1	22,9	16
8	22185	21860	19077	21040,7	1708,3	11,9	8
9	20999	20739	18051	19929,7	1632,2	11,3	8
10	23733	25137	26216	25028,7	1245,0	14,1	16
11	17164	15266	11159	14529,7	3069,5	8,2	8
12	43061	45421	52390	46957,3	4850,5	26,5	32
13	22197	18966	21371	20844,7	1678,6	11,8	8
14	30623	31284	31046	30984,3	334,8	17,5	16
15	19145	18149	20322	19205,3	1087,8	10,9	8
16	40617	44799	39331	41582,3	2859,0	23,5	16
17	11986	14113	13054	13051,0	1063,5	7,4	8
18	15465	14468	14025	14652,7	737,5	8,3	8
19	18698	19254	19455	19135,7	392,1	10,8	8
20	12244	11268	11781	11764,3	488,2	6,6	8
21	17770	21111	18844	19241,7	1705,6	10,9	8
22	34921	32510	34289	33906,7	1250,1	19,2	16
23	10580	13341	12595	12172,0	1428,3	6,9	8
24	10284	9478	11355	10372,3	941,6	5,9	4
25	3466	3011	3304	3260,3	230,6	1,8	2
26	3121	3160	2897	3059,3	141,9	1,7	2*
27	3060	2738	2694	2830,7	199,8	1,6	2*
28	14638	14462	15002	14700,7	275,4	8,3	8
29	15677	14748	13342	14589,0	1175,6	8,2	8
30	9411	8746	8107	8754,7	652,0	4,9	4

No	Meas. 1	Meas. 2	Meas. 3	average	STBDEV	C-content	Klasse
1	10093	11826	10751	10890,0	874,8	5,3	4
2	27181	29611	24019	26937,0	2804,0	13,1	16
3	20931	16365	19641	18979,0	2353,9	9,2	8
4	26399	23984	22009	24130,7	2198,7	11,7	8
5	19730	22326	24448	22168,0	2363,0	10,8	8
6	53318	44685	51312	49771,7	4517,9	24,2	32
7	22462	41680	38604	34248,7	10322,8	16,6	16
8	16753	19163	18636	18184,0	1267,0	8,8	8
9	16886	19919	17881	18228,7	1546,1	8,9	8
10	19637	21124	23993	21584,7	2214,2	10,5	8
11	11123	12305	11968	11798,7	608,9	5,7	4
12	16450	15626	18474	16850,0	1465,5	8,2	8
13	26438	25208	25902	25849,3	616,7	12,6	16
14	20068	20079	22330	20825,7	1302,8	10,1	8
15	30855	32904	31385	31714,7	1063,5	15,4	16
16	31603	26125	27971	28566,3	2787,1	13,9	16
17	8607	10703	9723	9677,7	1048,7	4,7	4
18	15030	15691	18663	16461,3	1935,1	8,0	8
19	41300	37538	37910	38916,0	2073,0	18,9	16
20	16824	21471	21922	20072,3	2822,2	9,7	8
21	12113	11427	13002	12180,7	789,7	5,9	4
22	32621	29301	30857	30926,3	1661,1	15,0	16
23	17191	16651	14192	16011,3	1598,6	7,8	8
24	29553	35985	33108	32882,0	3222,0	16,0	16
25	12383	14691	14385	13819,7	1253,6	6,7	8
26	10798	11805	13052	11885,0	1129,1	5,8	4
27	12273	11176	13889	12446,0	1364,7	6,0	8
28	28872	31736	31339	30649,0	1551,7	14,9	16
29	25884	25408	24899	25397,0	492,6	12,3	16
30	27200	31025	22973	27066,0	4027,7	13,1	16

V. Attachment

Col-0 (IV)

stomata (cotyledons) (int 1/8)

No	Meas. 1	Meas. 2	Meas. 3	average	STBDEV				Meas. 1	Meas. 2	Meas. 3	average	STBDEV		
1	8525	8651	7936	8370,7	381,7			1	6941	6133	5869	6314,3	558,5		
2	8389	8533	8605	8509,0	110,0			2	6267	6316	6650	6411,0	208,4		
3	7434	7723	7426	7527,7	169,2			3	6166	5695	6690	6183,7	497,7		
4	7149	6946	6750	6948,3	199,5			4	7976	7639	7729	7781,3	174,5		
5	6665	6684	6689	6679,3	12,7			5	5776	6538	7625	6646,3	929,2		
6	6439	6901	7028	6789,3	310,0			6	7862	7932	7604	7799,3	172,7		
7	6049	7022	6943	6671,3	540,4			7	5617	5803	5592	5670,7	115,3		
8	6444	6138	6725	6435,7	293,6			8	6062	7588	6910	6853,3	764,6		
9	6471	6861	6855	6729,0	223,5			9	5393	5797	5430	5540,0	223,3		
10	7151	6406	6193	6583,3	503,0			10	6000	5064	5767	5610,3	487,3		
11	8512	7897	8623	8344,0	391,1			11	6577	6328	6944	6616,3	309,9		
12	6991	7779	7785	7518,3	456,7			12	5825	5550	5288	5554,3	268,5		
13	7737	7845	7360	7647,3	254,6			13	5388	6435	5887	5903,3	523,7		
14	9311	9538	8745	9198,0	408,4			14	3975	4606	4006	4195,7	355,7		
15	7156	7499	8105	7586,7	480,5			15	4168	5107	4808	4694,3	479,7		
16	6794	5901	5461	6052,0	679,2			16	3988	4903	4173	4354,7	483,8		
17	7392	6606	7440	7146,0	468,3			17	6381	6841	7053	6758,3	343,5		
18	5403	4881	4865	5049,7	306,1						av.	6052,2			
19	5936	6558	6018	6170,7	337,9						STDEV	1034,2			
20	6562	5190	5614	5788,7	702,5										
21	6413	7400	7256	7023,0	533,2										
22	6262	5641	5827	5910,0	318,7										
			av.	7030,8											
			STDEV	999,4											

hypocotyl epidermal cells (int 1/8)

No	Meas. 1	Meas. 2	Meas. 3	average	STBDEV	C-content	Klasse		Meas. 1	Meas. 2	Meas. 3	average	STBDEV	C-content	Klasse
1	62549	64562	64888	63999,7	230,5	18,2	16	1	25133	30508	32550	29397,0	3831,3	9,7	8
2	7137	7186	7078	7133,7	76,4	2,0	2*	2	81814	75323	80251	79129,3	3387,8	26,1	32
3	7053	7112	6830	6998,3	199,4	2,0	2*	3	36650	35240	37339	36409,7	1069,9	12,0	16
4	6505	7087	7564	7052,0	337,3	2,0	2	4	17590	15144	14970	15901,3	1465,0	5,3	4
5	25149	26328	28369	26615,3	1443,2	7,6	8	5	28069	34092	32170	31443,7	3076,5	10,4	8
6	69125	70515	64382	68007,3	4336,7	19,3	16	6	13550	13699	13579	13609,3	79,0	4,5	4
7	29516	26696	29177	28463,0	1754,3	8,1	8	7	57078	52795	52508	54127,0	2559,7	17,9	16
8	23040	24264	24091	23798,3	122,3	6,8	8	8	28563	25146	21892	25200,3	3335,8	8,3	8
9	47443	43658	42091	44397,3	1108,0	12,6	16	9	33628	31045	33515	32729,3	1459,8	10,8	8
10	79538	77889	80405	79277,3	1779,1	22,6	16	10	31905	32288	32376	32189,7	250,4	10,6	8
11	35510	37252	33962	35574,7	2326,4	10,1	8	11	16729	17674	16423	16942,0	652,1	5,6	4
12	42156	40092	41617	41288,3	1078,3	11,7	8	12	18199	14461	19527	17395,7	2626,8	5,7	4
13	76931	81125	77896	78650,7	2283,2	22,4	16	13	42475	50476	50508	47819,7	4628,6	15,8	16
14	35140	31922	31369	32810,3	391,0	9,3	8	14	72430	77650	72472	74184,0	3001,7	24,5	32
15	14957	19496	17264	17239,0	1578,3	4,9	4	15	30852	35085	29758	31898,3	2813,4	10,5	8
16	74250	80316	79987	78184,3	232,6	22,2	16	16	39661	40730	47277	42556,0	4123,3	14,1	16
17	73506	78321	77085	76304,0	874,0	21,7	16	17	33283	35143	31580	33335,3	1782,1	11,0	8
18	89994	90984	96403	92460,3	3831,8	26,3	32	18	28646	26274	30982	28634,0	2354,0	9,5	8
19	78778	71722	78677	76392,3	4917,9	21,7	16	19	39608	36064	39229	38300,3	1946,0	12,7	16
20	82250	75474	83172	80298,7	5443,3	22,8	16	20	19016	17945	16955	17972,0	1030,8	5,9	4
21	22598	20685	25842	23041,7	3646,5	6,6	8	21	10140	12149	13058	11782,3	1493,2	3,9	4
22	8921	8830	8652	8801,0	125,9	2,5	2	22	39307	36798	38726	38277,0	1313,4	12,6	16
23	7276	7548	7822	7548,7	193,7	2,1	2*	23	37596	32728	34548	34957,3	2459,7	11,6	8
24	20221	17885	18813	18973,0	656,2	5,4	4	24	39639	40321	39989	39983,0	341,0	13,2	16
25	69247	60258	63830	64445,0	2525,8	18,3	16	25	5505	6324	6351	6060,0	480,8	2,0	2*
26	74889	79455	73260	75868,0	4380,5	21,6	16	26	5772	5900	6002	5891,3	115,2	1,9	2*
27	37431	34159	37042	36210,7	2038,6	10,3	8	27	19042	19597	22609	20416,0	1919,4	6,7	8
28	79995	74579	72221	75598,3	1667,4	21,5	16	28	4757	5418	5179	5118,0	334,7	1,7	2*
29	66912	79922	66926	71253,3	9189,6	20,3	16	29	4874	3983	5273	4710,0	660,5	1,6	2*
30	79615	78383	75927	77975,0	1736,7	22,2	16	30	29933	31067	35448	32149,3	2912,5	10,6	8
								31	85842	85322	72307	81157,0	7668,7	26,8	32

stomata (cotyledons) (int 1/8)

	Meas. 1	Meas. 2	Meas. 3	average	STBDEV				Meas. 1	Meas. 2	Meas. 3	average	STBDEV		
1	5045	4320	4882	4749,0	380,4			1	4746	4854	5365	4988,3	330,6		
2	5702	5170	5292	5388,0	278,7			2	5932	4867	4833	5210,7	624,9		
3	4684	5185	5305	5058,0	329,4			3	5141	5061	5499	5233,7	233,2		
4	4494	5010	4986	4830,0	291,2			4	6380	6310	7931	6873,7	916,3		
5	4676	5667	5468	5270,3	524,2			5	6544	5983	5961	6162,7	330,4		
6	5665	5247	5141	5351,0	277,0			6	5039	5985	6610	5878,0	790,9		
7	4147	3967	5127	4413,7	624,3			7	6156	5790	5201	5715,7	481,8		
8	5162	5292	5503	5319,0	172,1			8	4492	4378	5272	4714,0	486,6		
9	4382	4861	4074	4439,0	396,6			9	3906	4218	5963	4695,7	1108,6		
10	5565	4622	4761	4982,7	509,1			10	4478	4778	4973	4743,0	249,3		
11	5906	6658	6482	6348,7	393,3			11	4204	4013	4827	4348,0	425,7		
12	4230	4938	5630	4932,7	700,0			12	5744	4527	4735	5002,0	651,0		
13	6346	5760	6697	6267,7	473,4			13	4781	4246	5046	4691,0	407,5		
14	5963	4373	6124	5486,7	967,8			14	4879	5897	5231	5335,7	517,0		
15	5424	5703	6372	5833,0	487,2			15	6001	6243	6276	6173,3	150,2		
16	5764	5459	5157	5460,0	303,5			16	5738	5802	5695	5745,0	53,8		
17	5165	5585	4900	5216,7	345,4						av.	5344,4			
			av.	5255,6							STDEV	690,5			
			STDEV	577,3											

hypocotyl epidermal cells (int 1/8)

No	Meas. 1	Meas. 2	Meas. 3	average	STBDEV	C-content	Klasse		Meas. 1	Meas. 2	Meas. 3	average	STBDEV	C-content	Klasse
1	23323	28816	26120	26086,3	2746,7	9,9	8	1	37974	49162	45069	44068,3	5660,7	16,5	16
2	34229	35621	35673	35174,3	819,1	13,4	16	2	14079	17679	16478	16078,7	1832,9	6,0	8
3	30325	34304	33305	32644,7	2070,1	12,4	16	3	74303	73066	75257	74208,7	1098,5	27,8	32
4	29059	38231	32521	33270,3	4631,7	12,7	16	4	35897	35995	36910	36267,3	558,7	13,6	16
5	13494	14972	14112	14192,7	742,3	5,4	4	5	33919	34777	32518	33738,0	1140,3	12,6	16
6	63389	68556	78930	70291,7	7914,5	26,7	32	6	33292	39481	32965	35246,0	3671,3	13,2	16
7	40318	35608	33544	36490,0	3472,1	13,9	16	7	29090	28161	27320	28190,3	885,4	10,5	8
8	63557	65222	64689	64489,3	850,3	24,5	32	8	73825	74967	74398	74396,7	571,0	27,8	32
9	22137	27469	25759	25121,7	2722,5	9,6	8	9	34265	36038	37965	36089,3	1850,5	13,5	16
10	24493	22860	21837	20846,0	1339,6	7,9	8	10	54301	62865	58471	58545,7	4282,5	21,9	16
11	53959	53232	55860	54350,3	1357,0	20,7	16	11	29154	30906	33562	31207,3	2219,4	11,7	8
12	24878	24171	24917	24655,3	419,9	9,4	8	12	52310	50346	52201	51619,0	1103,8	19,3	16
13	57492	48189	53627	53102,7	4673,6	20,2	16	13	44383	44184	45761	44776,0	858,8	16,8	16
14	71602	66707	67418	68575,7	2644,9	26,1	32	14	28608	26742	25066	26805,3	1771,8	10,0	8
15	37555	32586	34722	34954,3	2492,6	13,3	16	15	43723	43075	40076	42291,3	1945,7	15,8	16
16	12249	11656	14525	12810,0	1514,5	4,9	4	16	50548	46734	45798	47693,3	2516,1	17,8	16
17	34876	34309	33718	34301,0	579,0	13,1	16	17	25952	25026	25420	25466,0	464,7	9,5	8
18	47265	46596	49511	47790,7	1526,9	18,2	16	18	36179	40509	45342	40676,7	4583,8	15,2	16
19	5819	5100	4638	5185,7	595,1	2,0	2	19	61784	55512	61198	59498,0	3464,4	22,3	16
20	6437	6487	6040	6321,3	244,9	2,4	2	20	33017	35230	33913	34053,3	1113,2	12,7	16
21	3913	4413	4233	4186,3	253,2	1,6	2	21	151694	158173	156935	155600,7	3439,4	58,2	64
22	67261	68323	67155	67579,7	645,9	25,7	32	22	133608	129581	137562	133583,7	3990,6	50,0	64
23	20641	23011	23907	22519,7	1687,5	8,6	8	23	31513	28575	29334	29807,3	1525,1	11,2	8
24	48710	45393	52476	48859,7	3543,9	18,6	16	24	33464	35001	38023	35496,0	2319,5	13,3	16
25	45744	41592	44026	43787,3	2086,3	16,7	16	25	82655	81239	81989	81961,0	708,4	30,7	32
26	21074	21773	20454	21100,3	659,9	8,0	8	26	27023	26795	27454	27090,7	334,7	10,1	8
27	23236	21477	23160	22624,3	994,3	8,6	8	27	27692	31646	35246	31528,0	3778,4	11,8	8
28	30466	31772	28367	30201,7	1717,8	11,5	8	28	44167	48035	44321	45507,7	2190,1	17,0	16
29	17947	17089	16860	17298,7	573,0	6,6	8	29	22868	19778	18984	20543,3	2052,0	7,7	8
30	35447	37031	37326	36601,3	1010,5	13,9	16	30	45284	47117	42078	44826,3	2550,5	16,8	16

V. Attachment

mid-2

stomata (cotyledons) (int 1/8)

No	Meas. 1	Meas. 2	Meas. 3	average	STBDEV
1	6658	6022	6720	6466,7	386,3
2	7947	7952	7241	7713,3	409,1
3	6135	5954	6282	6123,7	164,3
4	5151	5448	6051	5550,0	458,6
5	4606	5030	4424	4686,7	310,9
6	5200	5280	5298	5259,3	52,2
7	6293	6867	6733	6631,0	300,3
8	6525	6894	6756	6725,0	186,4
9	7124	6953	6808	6961,7	158,2
10	7257	7962	7573	7597,3	353,1
11	6495	6951	6484	6643,3	266,5
12	6064	5808	6107	5993,0	161,7
13	6966	7344	7045	7118,3	199,4
14	8265	7514	7655	7811,3	399,2
15	6299	5889	6174	6120,7	210,1
16	5250	5120	5884	5418,0	408,8
17	6759	6837	6363	6653,0	254,2
18	6315	6412	6385	6370,7	50,1
19	7613	7262	7386	7420,3	178,0
20	7855	7925	7294	7691,3	345,9
21	6986	6875	6845	6902,0	74,3
22	6992	6645	7075	6904,0	228,1
			av.	6580,0	
			STDEV	845,6	

No	Meas. 1	Meas. 2	Meas. 3	average	STBDEV
1	5061	5235	5039	5111,7	107,4
2	5425	5053	5693	5390,3	321,4
3	5222	5546	5450	5406,0	166,4
4	5600	5377	6272	5749,7	465,9
5	5372	6078	5364	5604,7	409,9
6	5995	5427	5773	5731,7	286,2
7	5277	5452	5050	5259,7	201,6
8	5434	5362	5642	5479,3	145,4
9	5354	5593	5861	5602,7	253,6
10	5207	4729	5529	5155,0	402,5
11	5283	4808	4992	5027,7	239,5
12	5308	5225	5699	5410,7	253,1
13	5691	5201	5296	5396,0	259,9
14	6316	5596	5108	5673,3	607,7
15	4436	4443	5074	4651,0	366,3
16	4314	4235	4189	4246,0	63,2
17	5042	5406	5498	5315,3	241,1
18	5370	5465	5906	5580,3	286,0
			av.	5321,7	
			STDEV	385,0	

hypocotyl epidermal cells (int 1/8)

No	Meas. 1	Meas. 2	Meas. 3	average	STBDEV	C-content	Klasse
1	62509	68646	68923	66692,7	3625,8	20,3	16
2	32179	31751	29531	31153,7	1421,5	9,5	8
3	69977	59867	63636	64493,3	5109,2	19,6	16
4	40891	44597	43234	42907,3	1874,5	13,0	16
5	42519	49120	49219	46952,7	3840,0	14,3	16
6	31058	30817	29169	30348,0	1028,1	9,2	8
7	36601	38189	34883	36557,7	1653,4	11,1	8
8	26123	25584	25493	25733,3	340,5	7,8	8
9	24512	21043	23359	22971,3	1766,7	7,0	8
10	75091	77162	78888	77047,0	1901,1	23,4	16
11	34457	36563	33888	34969,3	1409,2	10,6	8
12	49296	49031	50579	49635,3	827,9	15,1	16
13	47806	42400	44649	44951,7	2715,7	13,7	16
14	49495	50109	43976	47860,0	3377,6	14,5	16
15	73972	67709	75010	72230,3	3949,8	22,0	16
16	79079	86273	82083	82478,3	3613,3	25,1	32
17	45512	45570	45871	45651,0	192,7	13,9	16
18	49995	55396	53386	52925,7	2729,8	16,1	16
19	78156	80740	83515	80803,7	2680,1	24,6	32
20	37150	39509	37366	38008,3	1304,1	11,6	8
21	41925	39313	37240	39492,7	2347,7	12,0	16
22	52052	56384	56232	54889,3	2458,4	16,7	16
23	37608	36390	37216	37071,3	621,8	11,3	8
24	35944	36273	38651	36956,0	1477,1	11,2	8
25	34402	36569	37816	36262,3	1727,5	11,0	8
26	39225	35503	42324	39017,3	3415,2	11,9	8
27	78432	76763	70654	75283,0	4094,8	22,9	16
28	32337	27724	30808	30289,7	2349,8	9,2	8
29	50450	48381	46253	48361,3	2098,6	14,7	16
30	55868	46873	55922	52887,7	5208,9	16,1	16

No	Meas. 1	Meas. 2	Meas. 3	average	STBDEV	C-content	Klasse
1	35051	33463	36690	35068,0	1613,6	13,2	16
2	7777	5380	7097	6751,3	1235,3	2,5	2*
3	9727	9891	9749	9789,0	89,0	3,7	2*
4	6601	8594	8313	7836,0	1078,7	2,9	2*
5	7487	7268	7331	7362,0	112,7	2,8	2*
6	72644	63285	72006	69311,7	5229,0	26,0	32
7	6496	7803	7311	7203,3	660,1	2,7	2
8	8545	7865	7141	7850,3	702,1	3,0	2
9	34931	38142	43130	38734,3	4131,5	14,6	16
10	30969	28976	28233	29392,7	1414,8	11,0	8
11	37498	33864	38560	36640,7	2462,6	13,8	16
12	5391	6095	6249	5911,7	457,4	2,2	2
13	32192	31818	31598	31869,3	300,3	12,0	8
14	54660	57079	52568	54769,0	2257,5	20,6	16
15	35250	38453	39056	37586,3	2045,7	14,1	16
16	38827	34920	34802	36183,0	2290,5	13,6	16
17	26866	30097	29173	28712,0	1664,1	10,8	8
18	29750	29877	30453	30026,7	374,6	11,3	8
19	35461	31238	33989	33562,7	2143,5	12,6	16
20	16964	18313	15611	16962,7	1351,0	6,4	8
21	45959	56028	55439	52475,3	5651,0	19,7	16
22	21977	25972	26044	24664,3	2327,6	9,3	8
23	5849	6652	8263	6921,3	1229,3	2,6	2
24	9114	7896	8167	8392,3	639,5	3,2	4
25	23577	31581	29189	28115,7	4108,5	10,6	8
26	4652	4771	5440	4954,3	424,8	1,9	2*
27	6350	5622	7707	6559,7	1058,2	2,5	2*
28	7097	7712	6135	6981,3	794,8	2,6	2
29	9122	9102	7554	8592,7	899,6	3,2	4
30	21379	20838	29140	23785,7	4644,9	8,9	8

stomata (cotyledons) (int 1/8)

No	Meas. 1	Meas. 2	Meas. 3	average	STBDEV
1	4354	4537	4770	4553,7	208,5
2	5400	6246	5606	5750,7	441,2
3	5963	5505	5199	5555,7	384,5
4	7682	7756	8198	7878,7	279,0
5	7195	7782	6843	7273,3	474,4
6	8540	8076	7640	8085,3	450,1
7	7234	7641	8128	7667,7	447,6
8	5814	5869	5158	5613,7	395,6
9	3678	3980	3673	3777,0	175,8
10	6827	6869	6020	6572,0	478,5
11	7634	7744	7397	7591,7	177,3
12	7509	6680	7017	7068,7	416,9
13	8420	8045	8679	8381,3	318,8
14	7277	7193	7312	7260,7	61,2
15	6503	6382	6754	6546,3	189,7
16	4275	4056	4078	4136,3	120,6
17	6778	6801	6484	6687,7	176,8
18	7137	7163	7644	7314,7	285,5
19	6157	6231	5839	6075,7	208,3
20	6219	6994	6904	6705,7	423,9
21	6242	6651	6834	6575,7	303,1
22	6692	6604	6705	6667,0	54,9
			av.	6533,6	
			STDEV	1233,9	

No	Meas. 1	Meas. 2	Meas. 3	average	STBDEV
1	4021	5061	4349	4477,0	531,7
2	4114	4296	4948	4452,7	438,5
3	5543	5154	6577	5758,0	735,5
4	5425	5331	5101	5285,7	166,7
5	4655	4763	4962	4793,3	155,7
6	5520	4821	5386	5242,3	371,0
7	5735	4842	5982	5519,7	599,7
8	4528	5469	4857	4951,3	477,5
9	6690	7759	7250	7233,0	534,7
10	6863	7862	6913	7212,7	562,9
11	5802	4956	5763	5507,0	477,6
12	3819	4038	4637	4164,7	423,5
13	5499	6363	5360	5740,7	543,4
14	4697	4488	5060	4748,3	289,4
15	6238	5341	5450	5676,3	489,5
16	5721	6415	5049	5728,3	683,0
17	6479	6879	6655	6671,0	200,5
18	6798	6038	6811	6549,0	442,6
19	5558	6530	5973	6020,3	487,7
20	7663	6922	7501	7362,0	389,6
			av.	**5654,7**	
			STDEV	**953,7**	

hypocotyl epidermal cells (int 1/8)

No	Meas. 1	Meas. 2	Meas. 3	average	STBDEV	C-content	Klasse
1	32594	33330	34322	33415,3	867,2	10,2	8
2	35798	38727	40194	38239,7	2238,2	11,9	8
3	7712	8232	7339	7761,0	448,5	2,4	2
4	8852	9249	8710	8937,0	279,4	2,8	2
5	20123	18513	17502	18712,7	1321,9	5,8	4
6	28398	34673	29827	30966,0	3288,9	9,6	8
7	30766	38796	32753	34105,0	4182,2	10,6	8
8	30806	29822	28532	29720,0	1140,4	9,3	8
9	26551	31776	28959	29095,3	2615,2	9,1	8
10	20554	24090	29129	24591,0	4309,4	7,7	8
11	28033	28551	29090	28558,0	528,5	8,9	8
12	24999	22982	22185	23388,7	1450,4	7,3	8
13	5091	5646	5309	5348,7	279,6	1,7	2
14	6646	5185	7992	6607,7	1403,9	2,1	2
15	29313	28061	31768	29714,0	1885,8	9,3	8
16	25234	27376	25153	25921,0	1260,7	8,1	8
17	19194	18627	17817	18546,0	692,1	5,8	4
18	18332	21463	19784	19859,7	1566,9	6,2	8
19	18779	20402	19215	19465,3	840,0	6,1	8
20	31025	29613	27246	29294,7	1909,5	9,1	8
21	34771	33160	38476	35469,0	2725,9	11,0	8
22	28517	32345	31396	30752,7	1993,4	9,6	8
23	18112	15813	17915	17280,0	1274,3	5,4	4
24	31504	30838	27074	29805,3	2388,7	9,3	8
25	20564	21420	23515	21833,0	1518,2	6,8	8
26	25920	27147	26979	26682,0	665,2	8,3	8
27	26096	24959	30154	27069,7	2730,9	8,4	8
28	24610	23030	21051	22897,0	1783,2	7,1	8
29	28592	30028	29909	29509,7	796,9	9,2	8
30	18728	24130	19191	20683,0	2994,2	6,4	8
~~31~~	~~23429~~	~~19041~~	~~19343~~	~~20937,7~~	~~2543,5~~	~~6,4~~	~~8~~

No	Meas. 1	Meas. 2	Meas. 3	average	STBDEV	C-content	Klasse
1	39045	46193	41243	42160,3	3661,2	14,9	16
2	28166	29205	36631	31334,0	4616,7	11,1	8
3	48442	43553	63028	51674,3	10131,9	18,3	16
4	47909	51809	41701	47139,7	5097,7	16,7	16
5	39254	40692	45875	41940,3	3482,6	14,8	16
6	5744	5459	5137	5446,7	303,7	1,9	2*
7	11512	11137	11684	11444,3	279,7	4,0	4
8	16244	17385	17195	16941,3	611,3	6,0	4
9	34532	30657	32743	32644,0	1939,4	11,5	8
10	40769	49318	52901	47662,7	6233,1	16,9	16
11	24406	24828	22047	23760,3	1498,7	8,4	8
12	32539	35141	29464	32381,3	2841,8	11,5	8
13	28275	34586	29892	30917,7	3278,1	10,9	8
14	23461	32765	26127	27451,0	4791,2	9,7	8
15	34718	36341	33216	34758,3	1562,9	12,3	16
16	25214	24722	25756	25230,7	517,2	8,9	8
17	17181	17039	17909	17376,3	466,7	6,1	8
18	18130	21300	22178	20536,0	2129,4	7,3	8
19	36464	32367	29232	32687,7	3626,6	11,6	8
20	32057	30600	28833	30496,7	1614,5	10,8	8
21	7767	9128	6252	7715,7	1438,7	2,7	2
22	27286	32943	29120	29783,0	2886,2	10,5	8
23	20772	24370	23425	22855,7	1865,3	8,1	8
24	41151	41856	40501	41169,3	677,7	14,6	16
25	46804	47736	50692	48410,7	2029,9	17,1	16
26	13618	13890	11350	12952,7	1394,6	4,6	4
27	6443	7750	6486	6893,0	742,5	2,4	2
28	6870	5739	6647	6418,7	599,1	2,3	2
29	12547	11039	9067	10884,3	1745,1	3,8	4
30	12417	11271	10724	11470,7	864,0	4,1	4

V. Attachment

rhl2

stomata (cotyledons) (int 1/8)

No	Meas. 1	Meas. 2	Meas. 3	average	STBDEV
1	6881	7839	7095	7271,7	502,8
2	7939	7436	7398	7591,0	302,0
3	6026	6354	5688	6022,7	333,0
4	6059	6133	6670	6287,3	333,5
5	6656	6622	6644	6640,7	17,2
6	6482	7073	6829	6794,7	297,0
7	6210	6983	6620	6604,3	386,7
8	8373	8204	6769	7782,0	881,3
9	6578	6902	6787	6755,7	164,3
10	6453	7068	5906	6475,7	581,3
11	7049	7248	7297	7198,0	131,3
12	6388	7600	6617	6868,3	643,9
			av.	6857,7	
			STDEV	519,9	

No	Meas. 1	Meas. 2	Meas. 3	average	STBDEV
1	5310	6109	5621	5680,0	402,8
2	4480	4513	3996	4329,7	289,4
3	4578	4610	4953	4713,7	207,9
4	4018	4166	3645	3943,0	268,5
5	5145	4908	5235	5096,0	168,9
7	7645	7244	6773	7220,7	436,5
8	7160	7765	7852	7592,3	376,9
9	5135	6561	5595	5763,7	727,8
11	5695	5842	6369	5968,7	354,4
12	5822	7426	7162	6803,3	860,0
13	6703	6065	7175	6647,7	557,1
14	5956	6440	6702	6366,0	378,5
15	5006	4285	5419	4903,3	573,9
16	7154	6960	5864	6659,3	695,6
17	6424	7516	5500	6480,0	1009,2
18	5406	4741	4515	4887,3	463,2
19	4716	4016	4193	4308,3	364,0
20	4339	3664	4391	4131,3	405,6
21	4277	5027	5763	5022,3	743,0
22	6001	5343	6294	5879,3	487,0
23	5876	5345	4739	5320,0	568,9
24	4322	3897	3247	3822,0	541,4
			av.	5524,5	
			STDEV	1102,8	

hypocotyl epidermal cells (int 1/8)

No	Meas. 1	Meas. 2	Meas. 3	average	STBDEV	C-content	Klasse
1	32684	36662	38540	35962,0	2990,1	10,5	8
2	33221	34894	32071	33395,3	1419,6	9,7	8
3	32051	33672	31313	32345,3	1206,7	9,4	8
4	37690	39982	37523	38398,3	1374,0	11,2	8
5	41212	39132	38481	39608,3	1426,5	11,6	8
6	30164	37491	29314	32323,0	4495,8	9,4	8
7	31576	33520	25060	30052,0	4431,1	8,8	8
8	42872	51992	38012	44292,0	7097,4	12,9	16
9	24638	26494	32790	27974,0	4272,8	8,2	8
10	31348	36723	33204	33758,3	2730,0	9,8	8
11	27554	24526	27674	26584,7	1783,9	7,8	8
12	40589	43103	43046	42246,0	1435,3	12,3	16
13	21986	21973	19761	21240,0	1280,9	6,2	8
14	22828	23981	20978	22595,7	1514,9	6,6	8
15	64397	54522	58170	59029,7	4993,3	17,2	16
16	14118	15988	13384	14496,7	1342,7	4,2	4
17	28361	24441	23393	25398,3	2618,7	7,4	8
18	27514	36047	33268	32276,3	4352,1	9,4	8
19	34819	37120	36867	36268,7	1261,8	10,6	8
20	22191	28030	27728	25983,0	3287,4	7,6	8
21	22844	31966	29287	28032,3	4688,6	8,2	8
22	28991	28613	25850	27818,0	1714,8	8,1	8
23	12727	12444	12560	12577,0	142,3	3,7	4
24	32307	25922	29276	29168,3	3193,9	8,5	8
25	36134	35825	32712	34890,3	1892,8	10,2	8
26	41097	40210	42076	41127,7	933,4	12,0	8
27	31021	27822	31348	30063,7	1948,2	8,8	8
28	31396	38149	36454	35333,0	3513,3	10,3	8
29	31101	35284	32336	32907,0	2149,2	9,6	8
30	51422	60723	52311	54818,7	5132,6	16,0	16

No	Meas. 1	Meas. 2	Meas. 3	average	STBDEV	C-content	Klasse
1	35221	26787	28030	30012,7	4553,2	10,9	8
2	24127	31726	24227	26693,3	4358,7	9,7	8
3	24830	27377	27022	26409,7	1379,5	9,6	8
4	23818	25305	26459	25194,0	1324,0	9,1	8
5	29701	30582	35214	31832,3	2961,6	11,5	8
6	4507	4564	3695	4255,3	486,1	1,5	2
7	9470	13179	11957	11535,3	1890,1	4,2	4
8	25085	29226	33881	29397,3	4400,5	10,6	8
9	38656	39145	39839	39213,3	594,5	14,2	16
10	21851	24807	27632	24763,3	2890,7	9,0	8
11	31823	25590	26866	28093,0	3292,7	10,2	8
12	22668	22854	28049	24523,7	3054,4	8,9	8
13	32820	31565	28861	31082,0	2023,2	11,3	8
14	34325	37286	33911	35174,0	1840,7	12,7	16
15	22685	20502	31028	24738,3	5555,3	9,0	8
16	12925	13595	12588	13036,0	512,6	4,7	4
17	20551	28444	25599	24864,7	3997,4	9,0	8
18	19668	26801	24890	23786,3	3692,4	8,6	8
19	21632	24138	24595	23455,0	1595,2	8,5	8
20	26752	28943	31908	29201,0	2587,7	10,6	8
21	24402	27971	31890	28087,7	3745,4	10,2	8
22	18267	17154	20125	18515,3	1501,0	6,7	8
23	24400	24092	23239	23910,3	601,4	8,7	8
24	3394	4310	4131	3945,0	485,5	1,4	2
25	18271	14879	15992	16380,7	1729,1	5,9	4
26	29581	27574	26490	27881,7	1568,3	10,1	8
27	21282	19047	18392	19573,7	1515,3	7,1	8
28	12356	12298	13392	12682,0	615,6	4,6	4
29	17869	19057	26175	21033,7	4492,0	7,6	8
30	20029	16055	20658	18914,0	2495,9	6,8	8
31	25784	24271	25531	25195,3	810,4	9,1	8
32	26210	23372	29876	26486,0	3260,8	9,6	8
33	23743	22856	27321	24640,0	2363,8	8,9	8

stomata (cotyledons) (int 1/8)

No	Meas. 1	Meas. 2	Meas. 3	average	STBDEV
1	5463	6406	6286	6051,7	513,3
2	6471	6828	6201	6500,0	314,5
3	4479	4174	5033	4562,0	435,5
4	5453	5998	5310	5587,0	363,0
5	6864	6779	6348	6663,7	276,7
6	6354	7493	7442	7096,3	643,4
9	6465	7188	6996	6883,0	374,5
10	7597	7790	7401	7596,0	194,5
11	5313	5117	5048	5159,3	137,5
12	4708	4166	5039	4637,7	440,7
13	6056	7766	4950	6257,3	1418,8
15	9366	8950	9205	9173,7	209,8
16	5537	4707	5149	5131,0	415,3
17	7867	7278	9412	8185,7	1102,1
18	5899	5379	5938	5738,7	312,1
19	6572	7652	6233	6819,0	741,0
20	4697	5375	5816	5296,0	563,7
			av.	6314,0	
			STDEV	1256,3	

No	Meas. 1	Meas. 2	Meas. 3	average	STBDEV
1	8027	7307	7914	7749,3	387,2
2	6696	7639	7395	7243,3	489,5
3	7834	9098	7610	8180,7	802,3
4	7558	7549	7320	7475,7	134,9
5	8352	8000	8857	8403,0	430,8
6	7086	8951	8508	8181,7	974,4
7	7019	8072	8462	7851,0	746,5
8	7809	6343	9154	7768,7	1405,9
9	5906	4947	6112	5655,0	621,7
10	7224	7983	7745	7650,7	388,2
11	4692	4397	5352	4813,7	489,0
12	7296	6541	7130	6989,0	396,8
13	4775	6523	4791	5363,0	1004,6
14	5782	7668	6690	6713,3	943,2
15	5201	5066	6486	5584,3	783,8
16	4758	4176	5373	4769,0	598,6
17	5300	6210	6226	5912,0	530,1
18	4496	5054	5595	5048,3	549,5
19	5922	5007	5331	5420,0	463,9
20	4526	5543	5324	5131,0	535,3
			av.	6595,1	
			STDEV	1285,2	

hypocotyl epidermal cells (int 1/8)

No	Meas. 1	Meas. 2	Meas. 3	average	STBDEV	C-content	Klasse
1	57418	60856	51637	56637,0	4658,9	17,9	16
2	39648	30933	38826	36469,0	4811,9	11,6	8
3	31162	28647	36350	32053,0	3928,0	10,2	8
4	43918	45896	43742	44518,7	1196,0	14,1	16
5	32029	42801	36650	37160,0	5404,1	11,8	8
6	44182	39652	44778	42870,7	2803,3	13,6	16
7	41602	40360	45130	42364,0	2474,6	13,4	16
8	33750	39940	42811	38833,7	4630,7	12,3	16
9	43343	43255	36928	41175,3	3678,6	13,0	16
10	39069	32882	40300	37417,0	3975,4	11,9	8
11	26947	35420	37379	33248,7	5544,6	10,5	8
12	34436	36750	38614	36600,0	2093,0	11,6	8
13	44573	36795	42692	41353,3	4058,1	13,1	16
14	32576	34773	29154	32167,7	2831,7	10,2	8
15	39630	36577	35871	37359,3	1997,9	11,8	8
16	39750	36693	43515	39986,0	3417,1	12,7	16
17	35199	31962	28954	32038,3	3123,2	10,1	8
18	34330	38845	39092	37422,3	2680,9	11,9	8
19	32123	30840	32392	31785,0	829,4	10,1	8
20	74170	59627	69117	67638,0	7383,4	21,4	16
21	35691	42067	42061	39939,7	3679,5	12,7	16
22	56361	57927	65406	59898,0	4833,9	19,0	16
23	43926	43016	41117	42686,3	1433,2	13,5	16
24	26296	36801	40327	34474,7	7299,0	10,9	8
25	20596	18872	19079	19515,7	941,3	6,2	8
26	29227	36124	33349	32900,0	3470,4	10,4	8
27	14984	17288	14072	15448,0	1657,4	4,9	4
28	20746	16252	18026	18341,3	2263,5	5,8	4
29	16052	19412	14469	16644,3	2524,2	5,3	4

No	Meas. 1	Meas. 2	Meas. 3	average	STBDEV	C-content	Klasse
1	20521	19744	22569	20944,7	1459,4	6,4	8
2	14975	16113	14153	15080,3	984,2	4,6	4
3	18251	14751	18676	17226,0	2153,9	5,2	4
4	33262	27552	36447	32420,3	4506,8	9,8	8
5	42440	44372	37160	41324,0	3733,3	12,5	16
6	47031	51938	45651	48206,7	3304,3	14,6	16
7	49614	50979	40145	46912,7	5900,6	14,2	16
8	34384	27864	32032	31426,7	3301,9	9,5	8
9	73929	70456	67799	70728,0	3074,0	21,4	16
10	15197	16342	13811	15116,7	1267,4	4,6	4
11	25756	30146	28692	28198,0	2236,3	8,6	8
12	24065	25998	26912	25658,3	1453,6	7,8	8
13	35428	30154	31934	32505,3	2683,0	9,9	8
14	30683	37612	28618	32304,3	4711,1	9,8	8
15	36198	40292	35240	37243,3	2683,3	11,3	8
16	18573	17019	15520	17037,3	1526,6	5,2	4
17	14196	13042	12983	13407,0	683,9	4,1	4
18	15297	17631	14903	15943,7	1474,5	4,8	4
19	32243	30013	31465	31240,3	1131,8	9,5	8
20	27760	26959	29952	28223,7	1549,4	8,6	8
21	23638	23989	21783	23136,7	1185,4	7,0	8
22	11924	16328	13606	13952,7	2222,4	4,2	4

Literature

Adams J, Kelso R, Cooley L. The kelch repeat superfamily of proteins: propellers of cell function. Trends Cell Biol (2000) 10:17-24.

Ahmad M, Jarillo JA, Smirnova O, Cashmore AR. The CRY1 blue light photoreceptor of Arabidopsis interacts with phytochrome A in vitro. Mol Cell (1998) 1:939-948.

Al-Sady B, Kikis EA, Monte E, Quail PH. Mechanistic duality of transcription factor function in phytochrome signaling. Proc Natl Acad Sci U S A (2008) 105:2232-2237.

Al-Sady B, Ni W, Kircher S, Schafer E, Quail PH. Photoactivated phytochrome induces rapid PIF3 phosphorylation prior to proteasome-mediated degradation. Mol Cell (2006) 23:439-446.

Alonso JM, et al. Genome-wide insertional mutagenesis of Arabidopsis thaliana. Science (2003) 301:653-657.

Altschul SF, et al. Gapped BLAST and PSI-BLAST: a new generation of protein database search programs. Nucleic Acids Res (1997) 25:3389-3402.

Anderson S. Shotgun DNA sequencing using cloned DNase I-generated fragments. Nucleic Acids Res (1981) 9:3015-3027.

Andronis C, Barak S, Knowles SM, Sugano S, Tobin EM. The clock protein CCA1 and the bZIP transcription factor HY5 physically interact to regulate gene expression in Arabidopsis. Mol Plant (2008) 1:58-67.

Ang LH, et al. Molecular interaction between COP1 and HY5 defines a regulatory switch for light control of Arabidopsis development. Mol Cell (1998) 1:213-222.

Ang LH, Deng XW. Regulatory hierarchy of photomorphogenic loci: allele-specific and light-dependent interaction between the HY5 and COP1 loci. Plant Cell (1994) 6:613-628.

Aragues R, Sali A, Bonet J, Marti-Renom MA, Oliva B. Characterization of protein hubs by inferring interacting motifs from protein interactions. PLoS Comput Biol (2007) 3:1761-1771.

Ballas N, Citovsky V. Nuclear localization signal binding protein from Arabidopsis mediates nuclear import of Agrobacterium VirD2 protein. Proc Natl Acad Sci U S A (1997) 94:10723-10728.

Bates AD, Maxwell A. DNA Topology. (2005) 2 edn. Oxford: Oxford University Press.

Bauer D, et al. Constitutive photomorphogenesis 1 and multiple photoreceptors control degradation of phytochrome interacting factor 3, a transcription factor required for light signaling in Arabidopsis. Plant Cell (2004) 16:1433-1445.

Baumgardt RL, Oliverio KA, Casal JJ, Hoecker U. SPA1, a component of phytochrome A signal transduction, regulates the light signaling current. Planta (2002) 215:745-753.

Belles-Boix E, Babiychuk E, Van Montagu M, Inze D, Kushnir S. CEO1, a new protein from Arabidopsis thaliana, protects yeast against oxidative damage. FEBS Lett (2000) 482:19-24.

Literature

Benvenuto G, Formiggini F, Laflamme P, Malakhov M, Bowler C. The photomorphogenesis regulator DET1 binds the amino-terminal tail of histone H2B in a nucleosome context. Curr Biol (2002) 12:1529-1534.

Berg JM, Tymoczko JL, Stryer L. Biochemistry. (2002) 5 edn. New York: W. H. Freeman and Company.

Berger B, Stracke R, Yatusevich R, Weisshaar B, Flugge UI, Gigolashvili T. A simplified method for the analysis of transcription factor-promoter interactions that allows high-throughput data generation. Plant J (2007) 50:911-916.

Bergerat A, de Massy B, Gadelle D, Varoutas PC, Nicolas A, Forterre P. An atypical topoisomerase II from Archaea with implications for meiotic recombination. Nature (1997) 386:414-417.

Bernhardt A, et al. CUL4 associates with DDB1 and DET1 and its downregulation affects diverse aspects of development in Arabidopsis thaliana. Plant J (2006) 47:591-603.

Bertani G. Studies on lysogenesis. I. The mode of phage liberation by lysogenic Escherichia coli. J Bacteriol (1951) 62:293-300.

Bischoff FR, Klebe C, Kretschmer J, Wittinghofer A, Ponstingl H. RanGAP1 induces GTPase activity of nuclear Ras-related Ran. Proc Natl Acad Sci U S A (1994) 91:2587-2591.

Bischoff FR, Krebber H, Smirnova E, Dong W, Ponstingl H. Co-activation of RanGTPase and inhibition of GTP dissociation by Ran-GTP binding protein RanBP1. EMBO J (1995) 14:705-715.

Bischoff FR, Ponstingl H. Catalysis of guanine nucleotide exchange on Ran by the mitotic regulator RCC1. Nature (1991) 354:80-82.

Bjellqvist B, Basse B, Olsen E, Celis JE. Reference points for comparisons of two-dimensional maps of proteins from different human cell types defined in a pH scale where isoelectric points correlate with polypeptide compositions. Electrophoresis (1994) 15:529-539.

Bjellqvist B, et al. The focusing positions of polypeptides in immobilized pH gradients can be predicted from their amino acid sequences. Electrophoresis (1993) 14:1023-1031.

Boccalandro HE, Rossi MC, Saijo Y, Deng XW, Casal JJ. Promotion of photomorphogenesis by COP1. Plant Mol Biol (2004) 56:905-915.

Borevitz JO, Xia Y, Blount J, Dixon RA, Lamb C. Activation tagging identifies a conserved MYB regulator of phenylpropanoid biosynthesis. Plant Cell (2000) 12:2383-2394.

Borthwick HA, Hendricks SB, Parker MW, Toole EH, Toole VK. A Reversible Photoreaction Controlling Seed Germination. Proc Natl Acad Sci U S A (1952) 38:662-666.

Botto JF, Sanchez RA, Whitelam GC, Casal JJ. Phytochrome A Mediates the Promotion of Seed Germination by Very Low Fluences of Light and Canopy Shade Light in Arabidopsis. Plant Physiol (1996) 110:439-444.

Bouly JP, et al. Novel ATP-binding and autophosphorylation activity associated with Arabidopsis and human cryptochrome-1. Eur J Biochem (2003) 270:2921-2928.

Braun EL, Grotewold E. Newly discovered plant c-myb-like genes rewrite the evolution of the plant myb gene family. Plant Physiol (1999) 121:21-24.

Literature

Breuer C, et al. BIN4, a novel component of the plant DNA topoisomerase VI complex, is required for endoreduplication in Arabidopsis. Plant Cell (2007) 19:3655-3668.

Briggs WR, Christie JM. Phototropins 1 and 2: versatile plant blue-light receptors. Trends Plant Sci (2002) 7:204-210.

Briggs WR, Huala E. Blue-light photoreceptors in higher plants. Annu Rev Cell Dev Biol (1999) 15:33-62.

Brown BA, et al. A UV-B-specific signaling component orchestrates plant UV protection. Proc Natl Acad Sci U S A (2005) 102:18225-18230.

Casal JJ, Sanchez RA, Yanovsky MJ. The function of phytochrome A. Plant, Cell and Environment (1997) 20:813-819.

Cashmore AR, Jarillo JA, Wu YJ, Liu D. Cryptochromes: blue light receptors for plants and animals. Science (1999) 284:760-765.

Celenza JL, Eng FJ, Carlson M. Molecular analysis of the SNF4 gene of Saccharomyces cerevisiae: evidence for physical association of the SNF4 protein with the SNF1 protein kinase. Mol Cell Biol (1989) 9:5045-5054.

Champoux JJ. DNA topoisomerases: structure, function, and mechanism. Annu Rev Biochem (2001) 70:369-413.

Chang EH, Gonda MA, Ellis RW, Scolnick EM, Lowy DR. Human genome contains four genes homologous to transforming genes of Harvey and Kirsten murine sarcoma viruses. Proc Natl Acad Sci U S A (1982) 79:4848-4852.

Chen H, et al. Arabidopsis CULLIN4-Damaged DNA Binding Protein 1 Interacts with CONSTITUTIVELY PHOTOMORPHOGENIC1-SUPPRESSOR OF PHYA Complexes to Regulate Photomorphogenesis and Flowering Time. Plant Cell (2010).

Chen H, et al. Arabidopsis CULLIN4 Forms an E3 Ubiquitin Ligase with RBX1 and the CDD Complex in Mediating Light Control of Development. Plant Cell (2006) 18:1991-2004.

Chen IP, Haehnel U, Altschmied L, Schubert I, Puchta H. The transcriptional response of Arabidopsis to genotoxic stress - a high-density colony array study (HDCA). Plant J (2003) 35:771-786.

Chory J, Peto C, Feinbaum R, Pratt L, Ausubel F. Arabidopsis thaliana mutant that develops as a light-grown plant in the absence of light. Cell (1989) 58:991-999.

Christie JM, et al. Arabidopsis NPH1: a flavoprotein with the properties of a photoreceptor for phototropism. Science (1998) 282:1698-1701.

Clack T, Mathews S, Sharrock RA. The phytochrome apoprotein family in Arabidopsis is encoded by five genes: the sequences and expression of PHYD and PHYE. Plant Mol Biol (1994) 25:413-427.

Clack T, Shokry A, Moffet M, Liu P, Faul M, Sharrock RA. Obligate heterodimerization of Arabidopsis phytochromes C and E and interaction with the PIF3 basic helix-loop-helix transcription factor. Plant Cell (2009) 21:786-799.

Literature

Clough SJ, Bent AF. Floral dip: a simplified method for Agrobacterium-mediated transformation of Arabidopsis thaliana. Plant J (1998) 16:735-743.

Cominelli E, et al. Expression analysis of anthocyanin regulatory genes in response to different light qualities in Arabidopsis thaliana. J Plant Physiol (2008) 165:886-894.

Culligan KM, Robertson CE, Foreman J, Doerner P, Britt AB. ATR and ATM play both distinct and additive roles in response to ionizing radiation. Plant J (2006) 48:947-961.

Datta S, Hettiarachchi C, Johansson H, Holm M. SALT TOLERANCE HOMOLOG2, a B-box protein in Arabidopsis that activates transcription and positively regulates light-mediated development. Plant Cell (2007) 19:3242-3255.

Datta S, Hettiarachchi GH, Deng XW, Holm M. Arabidopsis CONSTANS-LIKE3 is a positive regulator of red light signaling and root growth. Plant Cell (2006) 18:70-84.

Datta S, et al. LZF1/SALT TOLERANCE HOMOLOG3, an Arabidopsis B-box protein involved in light-dependent development and gene expression, undergoes COP1-mediated ubiquitination. Plant Cell (2008) 20:2324-2338.

David KM, Armbruster U, Tama N, Putterill J. Arabidopsis GIGANTEA protein is post-transcriptionally regulated by light and dark. FEBS Lett (2006) 580:1193-1197.

Davis BJ. Disc Electrophoresis. Ii. Method and Application to Human Serum Proteins. Ann N Y Acad Sci (1964) 121:404-427.

De Muyt A, et al. A high throughput genetic screen identifies new early meiotic recombination functions in Arabidopsis thaliana. PLoS Genet (2009) 5:e1000654.

De Veylder L, Beeckman T, Inze D. The ins and outs of the plant cell cycle. Nat Rev Mol Cell Biol (2007) 8:655-665.

Deng XW, Caspar T, Quail PH. cop1: a regulatory locus involved in light-controlled development and gene expression in Arabidopsis. Genes Dev (1991) 5:1172-1182.

Deng XW, et al. COP1, an Arabidopsis regulatory gene, encodes a protein with both a zinc-binding motif and a G beta homologous domain. Cell (1992) 71:791-801.

Dessau M, Halimi Y, Erez T, Chomsky-Hecht O, Chamovitz DA, Hirsch JA. The Arabidopsis COP9 signalosome subunit 7 is a model PCI domain protein with subdomains involved in COP9 signalosome assembly. Plant Cell (2008) 20:2815-2834.

Devlin PF, Kay SA. Cryptochromes are required for phytochrome signaling to the circadian clock but not for rhythmicity. Plant Cell (2000) 12:2499-2510.

Devlin PF, Patel SR, Whitelam GC. Phytochrome E influences internode elongation and flowering time in Arabidopsis. Plant Cell (1998) 10:1479-1487.

Devlin PF, Robson PR, Patel SR, Goosey L, Sharrock RA, Whitelam GC. Phytochrome D acts in the shade-avoidance syndrome in Arabidopsis by controlling elongation growth and flowering time. Plant Physiol (1999) 119:909-915.

Dieterle M, Buche C, Schafer E, Kretsch T. Characterization of a novel non-constitutive photomorphogenic cop1 allele. Plant Physiol (2003) 133:1557-1564.

Literature

Dohmann EM, et al. The Arabidopsis COP9 signalosome is essential for G2 phase progression and genomic stability. Development (2008) 135:2013-2022.

Dornan D, et al. ATM engages autodegradation of the E3 ubiquitin ligase COP1 after DNA damage. Science (2006) 313:1122-1126.

Dornan D, et al. The ubiquitin ligase COP1 is a critical negative regulator of p53. Nature (2004) 429:86-92.

Dortay H, Gruhn N, Pfeifer A, Schwerdtner M, Schmulling T, Heyl A. Toward an interaction map of the two-component signaling pathway of Arabidopsis thaliana. J Proteome Res (2008) 7:3649-3660.

Duek PD, Elmer MV, van Oosten VR, Fankhauser C. The degradation of HFR1, a putative bHLH class transcription factor involved in light signaling, is regulated by phosphorylation and requires COP1. Curr Biol (2004) 14:2296-2301.

Durfee T, et al. The retinoblastoma protein associates with the protein phosphatase type 1 catalytic subunit. Genes Dev (1993) 7:555-569.

Earley KW, et al. Gateway-compatible vectors for plant functional genomics and proteomics. Plant J (2006) 45:616-629.

Ekman D, Light S, Bjorklund AK, Elofsson A. What properties characterize the hub proteins of the protein-protein interaction network of Saccharomyces cerevisiae? Genome Biol (2006) 7:R45.

Fairchild CD, Schumaker MA, Quail PH. HFR1 encodes an atypical bHLH protein that acts in phytochrome A signal transduction. Genes Dev (2000) 14:2377-2391.

Fankhauser C, Chory J. Light control of plant development. Annu Rev Cell Dev Biol (1997) 13:203-229.

Fankhauser C, Yeh KC, Lagarias JC, Zhang H, Elich TD, Chory J. PKS1, a substrate phosphorylated by phytochrome that modulates light signaling in Arabidopsis. Science (1999) 284:1539-1541.

Favory JJ, et al. Interaction of COP1 and UVR8 regulates UV-B-induced photomorphogenesis and stress acclimation in Arabidopsis. EMBO J (2009) 28:591-601.

Fazakes de St. Groth Sea. Biochim. Biophys. Acta (1963):377.

Feinbaum RL, Ausubel FM. Transcriptional regulation of the Arabidopsis thaliana chalcone synthase gene. Mol Cell Biol (1988) 8:1985-1992.

Feng S, et al. The COP9 signalosome interacts physically with SCF COI1 and modulates jasmonate responses. Plant Cell (2003) 15:1083-1094.

Fields S, Song O. A novel genetic system to detect protein-protein interactions. Nature (1989) 340:245-246.

Fittinghoff K, et al. Functional and expression analysis of Arabidopsis SPA genes during seedling photomorphogenesis and adult growth. Plant J (2006) 47:577-590.

Fowler S, et al. GIGANTEA: a circadian clock-controlled gene that regulates photoperiodic flowering in Arabidopsis and encodes a protein with several possible membrane-spanning domains. EMBO J (1999) 18:4679-4688.

Literature

Franklin KA, Quail PH. Phytochrome functions in Arabidopsis development. J Exp Bot (2010) 61:11-24.

Fransz P, De Jong JH, Lysak M, Castiglione MR, Schubert I. Interphase chromosomes in Arabidopsis are organized as well defined chromocenters from which euchromatin loops emanate. Proc Natl Acad Sci U S A (2002) 99:14584-14589.

Fujimori T, Yamashino T, Kato T, Mizuno T. Circadian-controlled basic/helix-loop-helix factor, PIL6, implicated in light-signal transduction in Arabidopsis thaliana. Plant Cell Physiol (2004) 45:1078-1086.

Fukamatsu Y, et al. Identification of LOV KELCH PROTEIN2 (LKP2)-interacting factors that can recruit LKP2 to nuclear bodies. Plant Cell Physiol (2005) 46:1340-1349.

Gasteiger E. HC, Gattiker A., Duvaud S., Wilkins M.R., Appel R.D., Bairoch A. Protein Identification and Analysis Tools on the ExPASy Server. In: The Proteomics Protocols Handbook--Walker JM, ed. (2005): Humana Press.

Gendreau E, Hofte H, Grandjean O, Brown S, Traas J. Phytochrome controls the number of endoreduplication cycles in the Arabidopsis thaliana hypocotyl. Plant J (1998) 13:221-230.

Gendreau E, Traas J, Desnos T, Grandjean O, Caboche M, Hofte H. Cellular basis of hypocotyl growth in Arabidopsis thaliana. Plant Physiol (1997) 114:295-305.

Geourjon C, Deleage G. SOPMA: significant improvements in protein secondary structure prediction by consensus prediction from multiple alignments. Comput Appl Biosci (1995) 11:681-684.

Gietz RD, Schiestl RH. High-efficiency yeast transformation using the LiAc/SS carrier DNA/PEG method. Nat Protoc (2007) 2:31-34.

Gietz RD, Woods RA. Yeast transformation by the LiAc/SS Carrier DNA/PEG method. Methods Mol Biol (2006) 313:107-120.

Gigolashvili T, Berger B, Mock HP, Muller C, Weisshaar B, Flugge UI. The transcription factor HIG1/MYB51 regulates indolic glucosinolate biosynthesis in Arabidopsis thaliana. Plant J (2007) 50:886-901.

Gonzalez A, Zhao M, Leavitt JM, Lloyd AM. Regulation of the anthocyanin biosynthetic pathway by the TTG1/bHLH/Myb transcriptional complex in Arabidopsis seedlings. Plant J (2008) 53:814-827.

Gorlich D, Kutay U. Transport between the cell nucleus and the cytoplasm. Annu Rev Cell Dev Biol (1999) 15:607-660.

Goto N, Kumagai T, Koornneef M. Flowering responses to light-breaks in photomorphogenic mutants of Arabidopsis thaliana, a long day plant. Physiologia Plantarum (1991) 83:209-215.

Grothues D, Cantor CR, Smith CL. PCR amplification of megabase DNA with tagged random primers (T-PCR). Nucleic Acids Res (1993) 21:1321-1322.

Hackbusch J. Untersuchung der TALE-Homöodomänen-Proteine in *Arabidopsis thaliana*: Identifizierung und Charakterisierung von Komponenten des TALE-Interaktions-Netzwerkes. PhD thesis Universität zu Köln (2004)

Literature

Hackbusch J, Richter K, Muller J, Salamini F, Uhrig JF. A central role of Arabidopsis thaliana ovate family proteins in networking and subcellular localization of 3-aa loop extension homeodomain proteins. Proc Natl Acad Sci U S A (2005) 102:4908-4912.

Haizel T, Merkle T, Pay A, Fejes E, Nagy F. Characterization of proteins that interact with the GTP-bound form of the regulatory GTPase Ran in Arabidopsis. Plant J (1997) 11:93-103.

Halliday KJ, Salter MG, Thingnaes E, Whitelam GC. Phytochrome control of flowering is temperature sensitive and correlates with expression of the floral integrator FT. Plant J (2003) 33:875-885.

Halliday KJ, Whitelam GC. Changes in photoperiod or temperature alter the functional relationships between phytochromes and reveal roles for phyD and phyE. Plant Physiol (2003) 131:1913-1920.

Han JD, et al. Evidence for dynamically organized modularity in the yeast protein-protein interaction network. Nature (2004) 430:88-93.

Hanahan D. Studies on transformation of Escherichia coli with plasmids. J Mol Biol (1983) 166:557-580.

Harari-Steinberg O, Ohad I, Chamovitz DA. Dissection of the light signal transduction pathways regulating the two early light-induced protein genes in Arabidopsis. Plant Physiol (2001) 127:986-997.

Hardtke CS, Okamoto H, Stoop-Myer C, Deng XW. Biochemical evidence for ubiquitin ligase activity of the Arabidopsis COP1 interacting protein 8 (CIP8). Plant J (2002) 30:385-394.

Harper JW, Adami GR, Wei N, Keyomarsi K, Elledge SJ. The p21 Cdk-interacting protein Cip1 is a potent inhibitor of G1 cyclin-dependent kinases. Cell (1993) 75:805-816.

Hartung F, Angelis KJ, Meister A, Schubert I, Melzer M, Puchta H. An archaebacterial topoisomerase homolog not present in other eukaryotes is indispensable for cell proliferation of plants. Curr Biol (2002) 12:1787-1791.

Hartung F, Puchta H. Molecular characterization of homologues of both subunits A (SPO11) and B of the archaebacterial topoisomerase 6 in plants. Gene (2001) 271:81-86.

Harvey JJ. An Unidentified Virus Which Causes the Rapid Production of Tumours in Mice. Nature (1964) 204:1104-1105.

Henikoff S. Unidirectional digestion with exonuclease III creates targeted breakpoints for DNA sequencing. Gene (1984) 28:351-359.

Hennig L, Stoddart WM, Dieterle M, Whitelam GC, Schafer E. Phytochrome E controls light-induced germination of Arabidopsis. Plant Physiol (2002) 128:194-200.

Hershko A, Ciechanover A. The ubiquitin system. Annu Rev Biochem (1998) 67:425-479.

Hicks GR, Smith HM, Lobreaux S, Raikhel NV. Nuclear import in permeabilized protoplasts from higher plants has unique features. Plant Cell (1996) 8:1337-1352.

Hiltbrunner A, Tscheuschler A, Viczian A, Kunkel T, Kircher S, Schafer E. FHY1 and FHL act together to mediate nuclear accumulation of the phytochrome A photoreceptor. Plant Cell Physiol (2006) 47:1023-1034.

Literature

Hoecker U, Quail PH. The phytochrome A-specific signaling intermediate SPA1 interacts directly with COP1, a constitutive repressor of light signaling in Arabidopsis. J Biol Chem (2001) 276:38173-38178.

Hoecker U, Tepperman JM, Quail PH. SPA1, a WD-repeat protein specific to phytochrome A signal transduction. Science (1999) 284:496-499.

Hoecker U, Xu Y, Quail PH. SPA1: a new genetic locus involved in phytochrome A-specific signal transduction. Plant Cell (1998) 10:19-33.

Holm M, Hardtke CS, Gaudet R, Deng XW. Identification of a structural motif that confers specific interaction with the WD40 repeat domain of Arabidopsis COP1. EMBO J (2001) 20:118-127.

Holm M, Ma LG, Qu LJ, Deng XW. Two interacting bZIP proteins are direct targets of COP1-mediated control of light-dependent gene expression in Arabidopsis. Genes Dev (2002) 16:1247-1259.

Hong SH, et al. CRY1 inhibits COP1-mediated degradation of BIT1, a MYB transcription factor, to activate blue light-dependent gene expression in Arabidopsis. Plant J (2008) 55:361-371.

Hornitschek P, Lorrain S, Zoete V, Michielin O, Fankhauser C. Inhibition of the shade avoidance response by formation of non-DNA binding bHLH heterodimers. EMBO J (2009) 28:3893-3902.

Hough R, Pratt G, Rechsteiner M. Purification of two high molecular weight proteases from rabbit reticulocyte lysate. J Biol Chem (1987) 262:8303-8313.

Hruz T, et al. Genevestigator v3: a reference expression database for the meta-analysis of transcriptomes. Adv Bioinformatics (2008) 2008:420747.

Huala E, Oeller PW, Liscum E, Han IS, Larsen E, Briggs WR. Arabidopsis NPH1: a protein kinase with a putative redox-sensing domain. Science (1997) 278:2120-2123.

Huq E, Al-Sady B, Hudson M, Kim C, Apel K, Quail PH. Phytochrome-interacting factor 1 is a critical bHLH regulator of chlorophyll biosynthesis. Science (2004) 305:1937-1941.

Hyun Y, Lee I. KIDARI, encoding a non-DNA Binding bHLH protein, represses light signal transduction in Arabidopsis thaliana. Plant Mol Biol (2006) 61:283-296.

Im YJ, et al. Structural analysis of Arabidopsis thaliana nucleoside diphosphate kinase-2 for phytochrome-mediated light signaling. J Mol Biol (2004) 343:659-670.

Imaizumi T, Schultz TF, Harmon FG, Ho LA, Kay SA. FKF1 F-box protein mediates cyclic degradation of a repressor of CONSTANS in Arabidopsis. Science (2005) 309:293-297.

Imaizumi T, Tran HG, Swartz TE, Briggs WR, Kay SA. FKF1 is essential for photoperiodic-specific light signalling in Arabidopsis. Nature (2003) 426:302-306.

Ishikawa M, Kiba T, Chua NH. The Arabidopsis SPA1 gene is required for circadian clock function and photoperiodic flowering. Plant J (2006) 46:736-746.

Jach G, Pesch M, Richter K, Frings S, Uhrig JF. An improved mRFP1 adds red to bimolecular fluorescence complementation. Nat Methods (2006) 3:597-600.

James P, Halladay J, Craig EA. Genomic libraries and a host strain designed for highly efficient two-hybrid selection in yeast. Genetics (1996) 144:1425-1436.

Literature

Jang IC, Yang JY, Seo HS, Chua NH. HFR1 is targeted by COP1 E3 ligase for post-translational proteolysis during phytochrome A signaling. Genes Dev (2005) 19:593-602.

Jang IC, Yang SW, Yang JY, Chua NH. Independent and interdependent functions of LAF1 and HFR1 in phytochrome A signaling. Genes Dev (2007) 21:2100-2111.

Jang S, et al. Arabidopsis COP1 shapes the temporal pattern of CO accumulation conferring a photoperiodic flowering response. EMBO J (2008) 27:1277-1288.

Jarillo JA, et al. An Arabidopsis circadian clock component interacts with both CRY1 and phyB. Nature (2001) 410:487-490.

Jeong SY, Rose A, Joseph J, Dasso M, Meier I. Plant-specific mitotic targeting of RanGAP requires a functional WPP domain. Plant J (2005) 42:270-282.

Jiang CJ, Imamoto N, Matsuki R, Yoneda Y, Yamamoto N. Functional characterization of a plant importin alpha homologue. Nuclear localization signal (NLS)-selective binding and mediation of nuclear import of nls proteins in vitro. J Biol Chem (1998a) 273:24083-24087.

Jiang CJ, Imamoto N, Matsuki R, Yoneda Y, Yamamoto N. In vitro characterization of rice importin beta1: molecular interaction with nuclear transport factors and mediation of nuclear protein import. FEBS Lett (1998b) 437:127-130.

Jiang CJ, et al. Molecular cloning of a novel importin alpha homologue from rice, by which constitutive photomorphogenic 1 (COP1) nuclear localization signal (NLS)-protein is preferentially nuclear imported. J Biol Chem (2001) 276:9322-9329.

Johnson E, Bradley M, Harberd NP, Whitelam GC. Photoresponses of Light-Grown phyA Mutants of Arabidopsis (Phytochrome A Is Required for the Perception of Daylength Extensions). Plant Physiol (1994) 105:141-149.

Kagawa T, Wada M. Blue light-induced chloroplast relocation. Plant Cell Physiol (2002) 43:367-371.

Kalab P, Pralle A, Isacoff EY, Heald R, Weis K. Analysis of a RanGTP-regulated gradient in mitotic somatic cells. Nature (2006) 440:697-701.

Kanamaru K, Wang R, Su W, Crawford NM. Ser-534 in the hinge 1 region of Arabidopsis nitrate reductase is conditionally required for binding of 14-3-3 proteins and in vitro inhibition. J Biol Chem (1999) 274:4160-4165.

Kardailsky I, et al. Activation tagging of the floral inducer FT. Science (1999) 286:1962-1965.

Karniol B, Malec P, Chamovitz DA. Arabidopsis FUSCA5 encodes a novel phosphoprotein that is a component of the COP9 complex. Plant Cell (1999) 11:839-848.

Kasahara M, Kagawa T, Oikawa K, Suetsugu N, Miyao M, Wada M. Chloroplast avoidance movement reduces photodamage in plants. Nature (2002) 420:829-832.

Kawasaki M, Inagaki F. Random PCR-based screening for soluble domains using green fluorescent protein. Biochem Biophys Res Commun (2001) 280:842-844.

Kendrick RE, Kronemberg GHM. Photomorphogenesis in Plants. (1994) Dordrecht, The Netherlands. : Kluwer Academic Publishers.

Literature

Kevei E, et al. Forward genetic analysis of the circadian clock separates the multiple functions of ZEITLUPE. Plant Physiol (2006) 140:933-945.

Khanna R, Huq E, Kikis EA, Al-Sady B, Lanzatella C, Quail PH. A novel molecular recognition motif necessary for targeting photoactivated phytochrome signaling to specific basic helix-loop-helix transcription factors. Plant Cell (2004) 16:3033-3044.

Kim SH, Arnold D, Lloyd A, Roux SJ. Antisense expression of an Arabidopsis ran binding protein renders transgenic roots hypersensitive to auxin and alters auxin-induced root growth and development by arresting mitotic progress. Plant Cell (2001) 13:2619-2630.

Kim SH, Roux SJ. An Arabidopsis Ran-binding protein, AtRanBP1c, is a co-activator of Ran GTPase-activating protein and requires the C-terminus for its cytoplasmic localization. Planta (2003) 216:1047-1052.

Kim TH, Kim BH, Yahalom A, Chamovitz DA, von Arnim AG. Translational regulation via 5' mRNA leader sequences revealed by mutational analysis of the Arabidopsis translation initiation factor subunit eIF3h. Plant Cell (2004) 16:3341-3356.

Kim WY, et al. ZEITLUPE is a circadian photoreceptor stabilized by GIGANTEA in blue light. Nature (2007) 449:356-360.

Kim YM, Woo JC, Song PS, Soh MS. HFR1, a phytochrome A-signalling component, acts in a separate pathway from HY5, downstream of COP1 in Arabidopsis thaliana. Plant J (2002) 30:711-719.

Kinoshita T, Doi M, Suetsugu N, Kagawa T, Wada M, Shimazaki K. Phot1 and phot2 mediate blue light regulation of stomatal opening. Nature (2001) 414:656-660.

Kircher S, et al. Nucleocytoplasmic partitioning of the plant photoreceptors phytochrome A, B, C, D, and E is regulated differentially by light and exhibits a diurnal rhythm. Plant Cell (2002) 14:1541-1555.

Kircher S, et al. Light quality-dependent nuclear import of the plant photoreceptors phytochrome A and B. Plant Cell (1999) 11:1445-1456.

Kirik A, Pecinka A, Wendeler E, Reiss B. The chromatin assembly factor subunit FASCIATA1 is involved in homologous recombination in plants. Plant Cell (2006) 18:2431-2442.

Kirik V, Schrader A, Uhrig JF, Hulskamp M. MIDGET unravels functions of the Arabidopsis topoisomerase VI complex in DNA endoreduplication, chromatin condensation, and transcriptional silencing. Plant Cell (2007) 19:3100-3110.

Kirsten WH, Schauf V, McCoy J. Properties of a murine sarcoma virus. Bibl Haematol (1970):246-249.

Kleiner O, Kircher S, Harter K, Batschauer A. Nuclear localization of the Arabidopsis blue light receptor cryptochrome 2. Plant J (1999) 19:289-296.

Klempnauer KH, Sippel AE. The highly conserved amino-terminal region of the protein encoded by the v-myb oncogene functions as a DNA-binding domain. EMBO J (1987) 6:2719-2725.

Kobayashi Y, Kaya H, Goto K, Iwabuchi M, Araki T. A pair of related genes with antagonistic roles in mediating flowering signals. Science (1999) 286:1960-1962.

Literature

Koncz C, Schell J. The promoter of TL-DNA gene 5 controls the tissuespecific expression of chimaeric genes carried by a novel type of Agrobacterium binary vector. Molecular and General Genetics (1986) 204:383-396.

Koornneef M, Alonso-Blanco C, Stam P. Genetic Analysis. From: Methods in Molecular Biology. (1992) Totowa, NJ: Numana Press Inc.

Koornneef M, Bentsink L, Hilhorst H. Seed dormancy and germination. Curr Opin Plant Biol (2002) 5:33-36.

Kranz H, Scholz K, Weisshaar B. c-MYB oncogene-like genes encoding three MYB repeats occur in all major plant lineages. Plant J (2000) 21:231-235.

Kwok SF, et al. Arabidopsis homologs of a c-Jun coactivator are present both in monomeric form and in the COP9 complex, and their abundance is differentially affected by the pleiotropic cop/det/fus mutations. Plant Cell (1998) 10:1779-1790.

Kwok SF, Staub JM, Deng XW. Characterization of two subunits of Arabidopsis 19S proteasome regulatory complex and its possible interaction with the COP9 complex. J Mol Biol (1999) 285:85-95.

Lagarias DM, Wu SH, Lagarias JC. Atypical phytochrome gene structure in the green alga Mesotaenium caldariorum. Plant Mol Biol (1995) 29:1127-1142.

Lange H, Shropshire J, Mohr H. An analysis of phytochrome-mediated anthocyanin synthesis. Plant Physiol (1971) 47:649-655.

Lariguet P, et al. PHYTOCHROME KINASE SUBSTRATE 1 is a phototropin 1 binding protein required for phototropism. Proc Natl Acad Sci U S A (2006) 103:10134-10139.

Latz A, et al. TPK1, a Ca(2+)-regulated Arabidopsis vacuole two-pore K(+) channel is activated by 14-3-3 proteins. Plant J (2007) 52:449-459.

Lau OS, Deng XW. Effect of Arabidopsis COP10 ubiquitin E2 enhancement activity across E2 families and functional conservation among its canonical homologues. Biochem J (2009) 418:683-690.

Laubinger S, Fittinghoff K, Hoecker U. The SPA quartet: a family of WD-repeat proteins with a central role in suppression of photomorphogenesis in arabidopsis. Plant Cell (2004) 16:2293-2306.

Laubinger S, Hoecker U. The SPA1-like proteins SPA3 and SPA4 repress photomorphogenesis in the light. Plant J (2003) 35:373-385.

Laubinger S. Die Funktion der SPA Gene in der lichtgesteuerten Entwicklung von *Arabidopsis thaliana.* PhD thesis Heinrich-Heine-Universität Düsseldorf (2006)

Laubinger S, et al. Arabidopsis SPA proteins regulate photoperiodic flowering and interact with the floral inducer CONSTANS to regulate its stability. Development (2006) 133:3213-3222.

Lea US, Slimestad R, Smedvig P, Lillo C. Nitrogen deficiency enhances expression of specific MYB and bHLH transcription factors and accumulation of end products in the flavonoid pathway. Planta (2007) 225:1245-1253.

Lee JH, et al. Characterization of Arabidopsis and rice DWD proteins and their roles as substrate receptors for CUL4-RING E3 ubiquitin ligases. Plant Cell (2008) 20:152-167.

Literature

Leivar P, et al. The Arabidopsis phytochrome-interacting factor PIF7, together with PIF3 and PIF4, regulates responses to prolonged red light by modulating phyB levels. Plant Cell (2008a) 20:337-352.

Leivar P, et al. Multiple phytochrome-interacting bHLH transcription factors repress premature seedling photomorphogenesis in darkness. Curr Biol (2008b) 18:1815-1823.

Letunic I, Doerks T, Bork P. SMART 6: recent updates and new developments. Nucleic Acids Res (2009) 37:D229-232.

Li DQ, et al. E3 ubiquitin ligase COP1 regulates the stability and functions of MTA1. Proc Natl Acad Sci U S A (2009) 106:17493-17498.

Li M, Doll J, Weckermann K, Oecking C, Berendzen KW, Schoffl F. Detection of in vivo interactions between Arabidopsis class A-HSFs, using a novel BiFC fragment, and identification of novel class B-HSF interacting proteins. Eur J Cell Biol (2010) 89:126-132.

Lillo C, Lea US, Ruoff P. Nutrient depletion as a key factor for manipulating gene expression and product formation in different branches of the flavonoid pathway. Plant Cell Environ (2008) 31:587-601.

Lin C, et al. Association of flavin adenine dinucleotide with the Arabidopsis blue light receptor CRY1. Science (1995) 269:968-970.

Liscum E, Stowe-Evans EL. Phototropism: a "simple" physiological response modulated by multiple interacting photosensory-response pathways. Photochem Photobiol (2000) 72:273-282.

Liu H, et al. Photoexcited CRY2 interacts with CIB1 to regulate transcription and floral initiation in Arabidopsis. Science (2008a) 322:1535-1539.

Liu LJ, et al. COP1-mediated ubiquitination of CONSTANS is implicated in cryptochrome regulation of flowering in Arabidopsis. Plant Cell (2008b) 20:292-306.

Liu XL, Covington MF, Fankhauser C, Chory J, Wagner DR. ELF3 encodes a circadian clock-regulated nuclear protein that functions in an Arabidopsis PHYB signal transduction pathway. Plant Cell (2001) 13:1293-1304.

Ma L, et al. Light control of Arabidopsis development entails coordinated regulation of genome expression and cellular pathways. Plant Cell (2001) 13:2589-2607.

MacFarlane SA, Uhrig JF. Yeast two-hybrid assay to identify host-virus interactions. Methods Mol Biol (2008) 451:649-672.

Magliano TA, Casal JJ. Pre-germination seed-phytochrome signals control stem extension in dark-grown Arabidopsis seedlings. Photochemical Photobiological Science (2004) 3:612-616.

Maglott D, Ostell J, Pruitt KD, Tatusova T. Entrez Gene: gene-centered information at NCBI. Nucleic Acids Res (2005) 33:D54-58.

Maier R, Brandner C, Hintner H, Bauer J, Onder K. Construction of a reading frame-independent yeast two-hybrid vector system for site-specific recombinational cloning and protein interaction screening. Biotechniques (2008) 45:235-244.

Literature

Malhotra K, Kim ST, Batschauer A, Dawut L, Sancar A. Putative blue-light photoreceptors from Arabidopsis thaliana and Sinapis alba with a high degree of sequence homology to DNA photolyase contain the two photolyase cofactors but lack DNA repair activity. Biochemistry (1995) 34:6892-6899.

Mao J, Zhang YC, Sang Y, Li QH, Yang HQ. From The Cover: A role for Arabidopsis cryptochromes and COP1 in the regulation of stomatal opening. Proc Natl Acad Sci U S A (2005) 102:12270-12275.

Martel F, Grundemann D, Schomig E. A simple method for elimination of false positive results in RT-PCR. J Biochem Mol Biol (2002) 35:248-250.

Mas P, Kim WY, Somers DE, Kay SA. Targeted degradation of TOC1 by ZTL modulates circadian function in Arabidopsis thaliana. Nature (2003) 426:567-570.

Mason MG, Botella JR. Completing the heterotrimer: isolation and characterization of an Arabidopsis thaliana G protein gamma-subunit cDNA. Proc Natl Acad Sci U S A (2000) 97:14784-14788.

Mason MG, Botella JR. Isolation of a novel G-protein gamma-subunit from Arabidopsis thaliana and its interaction with Gbeta. Biochim Biophys Acta (2001) 1520:147-153.

Mathur J, Koncz C. Callus culture and regeneration. Methods Mol Biol (1998a) 82:31-34.

Mathur J, Koncz C. Establishment and maintenance of cell suspension cultures. Methods Mol Biol (1998b) 82:27-30.

Mathur J, Koncz C. PEG-mediated protoplast transformation with naked DNA. Methods Mol Biol (1998c) 82:267-276.

Mathur J, Koncz C. Protoplast isolation, culture, and regeneration. Methods Mol Biol (1998d) 82:35-42.

Matsui M, Stoop CD, von Arnim AG, Wei N, Deng XW. Arabidopsis COP1 protein specifically interacts in vitro with a cytoskeleton-associated protein, CIP1. Proc Natl Acad Sci U S A (1995) 92:4239-4243.

Matunis MJ, Coutavas E, Blobel G. A novel ubiquitin-like modification modulates the partitioning of the Ran-GTPase-activating protein RanGAP1 between the cytosol and the nuclear pore complex. J Cell Biol (1996) 135:1457-1470.

Mayer R, Raventos D, Chua NH. det1, cop1, and cop9 mutations cause inappropriate expression of several gene sets. Plant Cell (1996) 8:1951-1959.

McClung CR. Circadian Rhythms in Plants. Annu Rev Plant Physiol Plant Mol Biol (2001) 52:139-162.

McMichael RW, Jr., Lagarias JC. Phosphopeptide mapping of Avena phytochrome phosphorylated by protein kinases in vitro. Biochemistry (1990) 29:3872-3878.

McNellis TW, Torii KU, Deng XW. Expression of an N-terminal fragment of COP1 confers a dominant-negative effect on light-regulated seedling development in Arabidopsis. Plant Cell (1996) 8:1491-1503.

Literature

McNellis TW, von Arnim AG, Araki T, Komeda Y, Misera S, Deng XW. Genetic and molecular analysis of an allelic series of cop1 mutants suggests functional roles for the multiple protein domains. Plant Cell (1994a) 6:487-500.

McNellis TW, von Arnim AG, Deng XW. Overexpression of Arabidopsis COP1 results in partial suppression of light-mediated development: evidence for a light-inactivable repressor of photomorphogenesis. Plant Cell (1994b) 6:1391-1400.

Melaragno JE, Mehrotra B, Coleman AW. Relationship between Endopolyploidy and Cell Size in Epidermal Tissue of Arabidopsis. Plant Cell (1993) 5:1661-1668.

Meyer TS, Lamberts BL. Use of coomassie brilliant blue R250 for the electrophoresis of microgram quantities of parotid saliva proteins on acrylamide-gel strips. Biochim Biophys Acta (1965) 107:144-145.

Milo R, Shen-Orr S, Itzkovitz S, Kashtan N, Chklovskii D, Alon U. Network motifs: simple building blocks of complex networks. Science (2002) 298:824-827.

Moore MS, Blobel G. The GTP-binding protein Ran/TC4 is required for protein import into the nucleus. Nature (1993) 365:661-663.

Mudgil Y, Uhrig JF, Zhou J, Temple B, Jiang K, Jones AM. Arabidopsis N-MYC DOWNREGULATED-LIKE1, a positive regulator of auxin transport in a G protein-mediated pathway. Plant Cell (2009) 21:3591-3609.

Nagatani A. Light-regulated nuclear localization of phytochromes. Curr Opin Plant Biol (2004) 7:708-711.

Nakagawa M, Komeda Y. Flowering of Arabidopsis cop1 mutants in darkness. Plant Cell Physiol (2004) 45:398-406.

Nemeth K, et al. Pleiotropic control of glucose and hormone responses by PRL1, a nuclear WD protein, in Arabidopsis. Genes Dev (1998) 12:3059-3073.

Nemhauser JL. Dawning of a new era: photomorphogenesis as an integrated molecular network. Curr Opin Plant Biol (2008) 11:4-8.

Nesi N, Debeaujon I, Jond C, Pelletier G, Caboche M, Lepiniec L. The TT8 gene encodes a basic helix-loop-helix domain protein required for expression of DFR and BAN genes in Arabidopsis siliques. Plant Cell (2000) 12:1863-1878.

Ni M, Tepperman JM, Quail PH. PIF3, a phytochrome-interacting factor necessary for normal photoinduced signal transduction, is a novel basic helix-loop-helix protein. Cell (1998) 95:657-667.

Nixdorf M, Hoecker U. SPA1 and DET1 act together to control photomorphogenesis throughout plant development. Planta (2010) 231:825-833.

Nozue K, et al. Rhythmic growth explained by coincidence between internal and external cues. Nature (2007) 448:358-361.

Oefner PJ, Hunicke-Smith SP, Chiang L, Dietrich F, Mulligan J, Davis RW. Efficient random subcloning of DNA sheared in a recirculating point-sink flow system. Nucleic Acids Res (1996) 24:3879-3886.

Literature

Ogata K, et al. Solution structure of a specific DNA complex of the Myb DNA-binding domain with cooperative recognition helices. Cell (1994) 79:639-648.

Ohtsubo M, Okazaki H, Nishimoto T. The RCC1 protein, a regulator for the onset of chromosome condensation locates in the nucleus and binds to DNA. J Cell Biol (1989) 109:1389-1397.

Olsen KM, et al. Temperature and nitrogen effects on regulators and products of the flavonoid pathway: experimental and kinetic model studies. Plant Cell Environ (2009) 32:286-299.

Ornstein L. Disc Electrophoresis. I. Background and Theory. Ann N Y Acad Sci (1964) 121:321-349.

Osterlund MT, Hardtke CS, Wei N, Deng XW. Targeted destabilization of HY5 during light-regulated development of Arabidopsis. Nature (2000a) 405:462-466.

Osterlund MT, Wei N, Deng XW. The roles of photoreceptor systems and the COP1-targeted destabilization of HY5 in light control of Arabidopsis seedling development. Plant Physiol (2000b) 124:1520-1524.

Oyama T, Shimura Y, Okada K. The Arabidopsis HY5 gene encodes a bZIP protein that regulates stimulus-induced development of root and hypocotyl. Genes Dev (1997) 11:2983-2995.

Park E, et al. Degradation of phytochrome interacting factor 3 in phytochrome-mediated light signaling. Plant Cell Physiol (2004) 45:968-975.

Park HJ, Ding L, Dai M, Lin R, Wang H. Multisite phosphorylation of Arabidopsis HFR1 by casein kinase II and a plausible role in regulating its degradation rate. J Biol Chem (2008) 283:23264-23273.

Paz-Ares J, The Regia C. REGIA, An EU Project on Functional Genomics of Transcription Factors From Arabidopsis Thaliana. Comp Funct Genomics (2002) 3:102-108.

Peng M, et al. Adaptation of Arabidopsis to nitrogen limitation involves induction of anthocyanin synthesis which is controlled by the NLA gene. J Exp Bot (2008) 59:2933-2944.

Peng Z, Serino G, Deng XW. A role of Arabidopsis COP9 signalosome in multifaceted developmental processes revealed by the characterization of its subunit 3. Development (2001) 128:4277-4288.

Peng Z, et al. Evidence for a physical association of the COP9 signalosome, the proteasome, and specific SCF E3 ligases in vivo. Curr Biol (2003) 13:R504-505.

Pepper A, Delaney T, Washburn T, Poole D, Chory J. DET1, a negative regulator of light-mediated development and gene expression in arabidopsis, encodes a novel nuclear-localized protein. Cell (1994) 78:109-116.

Pepper AE, Chory J. Extragenic suppressors of the Arabidopsis det1 mutant identify elements of flowering-time and light-response regulatory pathways. Genetics (1997) 145:1125-1137.

Perkins DN, Pappin DJ, Creasy DM, Cottrell JS. Probability-based protein identification by searching sequence databases using mass spectrometry data. Electrophoresis (1999) 20:3551-3567.

Phee BK, et al. Identification of phytochrome-interacting protein candidates in Arabidopsis thaliana by co-immunoprecipitation coupled with MALDI-TOF MS. Proteomics (2006) 6:3671-3680.

Pick E, et al. Mammalian DET1 regulates Cul4A activity and forms stable complexes with E2 ubiquitin-conjugating enzymes. Mol Cell Biol (2007) 27:4708-4719.

Literature

Qin F, et al. Arabidopsis DREB2A-interacting proteins function as RING E3 ligases and negatively regulate plant drought stress-responsive gene expression. Plant Cell (2008) 20:1693-1707.

Quail PH. Phytochrome photosensory signalling networks. Nat Rev Mol Cell Biol (2002) 3:85-93.

Reed JW. Phytochromes are Pr-ipatetic kinases. Curr Opin Plant Biol (1999) 2:393-397.

Reed JW, Nagatani A, Elich TD, Fagan M, Chory J. Phytochrome A and Phytochrome B Have Overlapping but Distinct Functions in Arabidopsis Development. Plant Physiol (1994) 104:1139-1149.

Reed JW, Nagpal P, Poole DS, Furuya M, Chory J. Mutations in the gene for the red/far-red light receptor phytochrome B alter cell elongation and physiological responses throughout Arabidopsis development. Plant Cell (1993) 5:147-157.

Robbins J, Dilworth SM, Laskey RA, Dingwall C. Two interdependent basic domains in nucleoplasmin nuclear targeting sequence: identification of a class of bipartite nuclear targeting sequence. Cell (1991) 64:615-623.

Rockwell NC, Su YS, Lagarias JC. Phytochrome structure and signaling mechanisms. Annu Rev Plant Biol (2006) 57:837-858.

Roenneberg T, Merrow M. Circadian clocks: Omnes viae Romam ducunt. Curr Biol (2000) 10:R742-745.

Rowan DD, et al. Environmental regulation of leaf colour in red 35S:PAP1 Arabidopsis thaliana. New Phytol (2009) 182:102-115.

Rudiger W, Thummler F, Cmiel E, Schneider S. Chromophore structure of the physiologically active form (P(fr)) of phytochrome. Proc Natl Acad Sci U S A (1983) 80:6244-6248.

Saedler R, Mathur N, Srinivas BP, Kernebeck B, Hulskamp M, Mathur J. Actin control over microtubules suggested by DISTORTED2 encoding the Arabidopsis ARPC2 subunit homolog. Plant Cell Physiol (2004) 45:813-822.

Saijo Y, et al. The COP1-SPA1 interaction defines a critical step in phytochrome A-mediated regulation of HY5 activity. Genes Dev (2003) 17:2642-2647.

Saijo Y, et al. Arabidopsis COP1/SPA1 complex and FHY1/FHY3 associate with distinct phosphorylated forms of phytochrome A in balancing light signaling. Mol Cell (2008) 31:607-613.

Sakai T, et al. Arabidopsis nph1 and npl1: blue light receptors that mediate both phototropism and chloroplast relocation. Proc Natl Acad Sci U S A (2001) 98:6969-6974.

Sakamoto K, Nagatani A. Nuclear localization activity of phytochrome B. Plant J (1996) 10:859-868.

Sakura H, Kanei-Ishii C, Nagase T, Nakagoshi H, Gonda TJ, Ishii S. Delineation of three functional domains of the transcriptional activator encoded by the c-myb protooncogene. Proc Natl Acad Sci U S A (1989) 86:5758-5762.

Sambroock J, Russell DW. Molecular Cloning A Laboratory Manual. (2001) 3 edn.: Cold Spring Harbor Laboratory Press.

Sancar A. Mechanisms of DNA excision repair. Science (1994) 266:1954-1956.

Literature

Sang Y, et al. N-terminal domain-mediated homodimerization is required for photoreceptor activity of Arabidopsis CRYPTOCHROME 1. Plant Cell (2005) 17:1569-1584.

Santoni V, Delarue M, Caboche M, Bellini C. A comparison of two-dimensional electrophoresis data with phenotypical traits in Arabidopsis leads to the identification of a mutant (cri1) that accumulates cytokinins. Planta (1997) 202:62-69.

Sawa M, Nusinow DA, Kay SA, Imaizumi T. FKF1 and GIGANTEA complex formation is required for day-length measurement in Arabidopsis. Science (2007) 318:261-265.

Schmid M, et al. A gene expression map of Arabidopsis thaliana development. Nat Genet (2005) 37:501-506.

Schmidt R, Mohr H. Time-dependent changes in the responsiveness to light of phytochrome-mediated anthocyanin synthesis. Plant, Cell and Environment (1981) 4:433-437.

Schneider-Poetsch HA, Braun B, Marx S, Schaumburg A. Phytochromes and bacterial sensor proteins are related by structural and functional homologies. Hypothesis on phytochrome-mediated signal-transduction. FEBS Lett (1991) 281:245-249.

Schultz J, Milpetz F, Bork P, Ponting CP. SMART, a simple modular architecture research tool: identification of signaling domains. Proc Natl Acad Sci U S A (1998) 95:5857-5864.

Sellaro R, Hoecker U, Yanovsky M, Chory J, Casal JJ. Synergism of red and blue light in the control of Arabidopsis gene expression and development. Curr Biol (2009) 19:1216-1220.

Seo HS, Watanabe E, Tokutomi S, Nagatani A, Chua NH. Photoreceptor ubiquitination by COP1 E3 ligase desensitizes phytochrome A signaling. Genes Dev (2004) 18:617-622.

Seo HS, Yang JY, Ishikawa M, Bolle C, Ballesteros ML, Chua NH. LAF1 ubiquitination by COP1 controls photomorphogenesis and is stimulated by SPA1. Nature (2003) 423:995-999.

Serino G, Deng XW. The COP9 signalosome: regulating plant development through the control of proteolysis. Annu Rev Plant Biol (2003) 54:165-182.

Serino G, et al. Characterization of the last subunit of the Arabidopsis COP9 signalosome: implications for the overall structure and origin of the complex. Plant Cell (2003) 15:719-731.

Sessions A, et al. A high-throughput Arabidopsis reverse genetics system. Plant Cell (2002) 14:2985-2994.

Shalitin D, Yu X, Maymon M, Mockler T, Lin C. Blue light-dependent in vivo and in vitro phosphorylation of Arabidopsis cryptochrome 1. Plant Cell (2003) 15:2421-2429.

Shannon P, et al. Cytoscape: a software environment for integrated models of biomolecular interaction networks. Genome Res (2003) 13:2498-2504.

Sharrock RA, Clack T. Heterodimerization of type II phytochromes in Arabidopsis. Proc Natl Acad Sci U S A (2004) 101:11500-11505.

Sharrock RA, Quail PH. Novel phytochrome sequences in Arabidopsis thaliana: structure, evolution, and differential expression of a plant regulatory photoreceptor family. Genes Dev (1989) 3:1745-1757.

Literature

Shen H, Zhu L, Castillon A, Majee M, Downie B, Huq E. Light-induced phosphorylation and degradation of the negative regulator PHYTOCHROME-INTERACTING FACTOR1 from Arabidopsis depend upon its direct physical interactions with photoactivated phytochromes. Plant Cell (2008) 20:1586-1602.

Shen Y, Khanna R, Carle CM, Quail PH. Phytochrome induces rapid PIF5 phosphorylation and degradation in response to red-light activation. Plant Physiol (2007) 145:1043-1051.

Shen Y, Kim JI, Song PS. NDPK2 as a signal transducer in the phytochrome-mediated light signaling. J Biol Chem (2005) 280:5740-5749.

Shinomura T, Nagatani A, Hanzawa H, Kubota M, Watanabe M, Furuya M. Action spectra for phytochrome A- and B-specific photoinduction of seed germination in Arabidopsis thaliana. Proc Natl Acad Sci U S A (1996) 93:8129-8133.

Shinomura T, Uchida K, Furuya M. Elementary processes of photoperception by phytochrome A for high-irradiance response of hypocotyl elongation in Arabidopsis. Plant Physiol (2000) 122:147-156.

Smith HM, Hicks GR, Raikhel NV. Importin alpha from Arabidopsis thaliana is a nuclear import receptor that recognizes three classes of import signals. Plant Physiol (1997) 114:411-417.

Smith HM, Raikhel NV. Protein targeting to the nuclear pore. What can we learn from plants? Plant Physiol (1999) 119:1157-1164.

Somers DE, Devlin PF, Kay SA. Phytochromes and cryptochromes in the entrainment of the Arabidopsis circadian clock. Science (1998) 282:1488-1490.

Sondek J, Bohm A, Lambright DG, Hamm HE, Sigler PB. Crystal structure of a G-protein beta gamma dimer at 2.1A resolution. Nature (1996) 379:369-374.

Spirin V, Mirny LA. Protein complexes and functional modules in molecular networks. Proc Natl Acad Sci U S A (2003) 100:12123-12128.

Stark C, Breitkreutz BJ, Reguly T, Boucher L, Breitkreutz A, Tyers M. BioGRID: a general repository for interaction datasets. Nucleic Acids Res (2006) 34:D535-539.

Staub JM, Wei N, Deng XW. Evidence for FUS6 as a component of the nuclear-localized COP9 complex in Arabidopsis. Plant Cell (1996) 8:2047-2056.

Steimer A, Amedeo P, Afsar K, Fransz P, Mittelsten Scheid O, Paszkowski J. Endogenous targets of transcriptional gene silencing in Arabidopsis. Plant Cell (2000) 12:1165-1178.

Suarez-Lopez P, Coupland G. Plants see the blue light. Science (1998) 279:1323-1324.

Subramanian C, Kim BH, Lyssenko NN, Xu X, Johnson CH, von Arnim AG. The Arabidopsis repressor of light signaling, COP1, is regulated by nuclear exclusion: mutational analysis by bioluminescence resonance energy transfer. Proc Natl Acad Sci U S A (2004) 101:6798-6802.

Subramanian C, et al. A suite of tools and application notes for in vivo protein interaction assays using bioluminescence resonance energy transfer (BRET). Plant J (2006) 48:138-152.

Literature

Sugano S, Andronis C, Green RM, Wang ZY, Tobin EM. Protein kinase CK2 interacts with and phosphorylates the Arabidopsis circadian clock-associated 1 protein. Proc Natl Acad Sci U S A (1998) 95:11020-11025.

Sugimoto-Shirasu K, Roberts GR, Stacey NJ, McCann MC, Maxwell A, Roberts K. RHL1 is an essential component of the plant DNA topoisomerase VI complex and is required for ploidy-dependent cell growth. Proc Natl Acad Sci U S A (2005) 102:18736-18741.

Sugimoto-Shirasu K, Stacey NJ, Corsar J, Roberts K, McCann MC. DNA topoisomerase VI is essential for endoreduplication in Arabidopsis. Curr Biol (2002) 12:1782-1786.

Sun CW, Griffen S, Callis J. A model for the evolution of polyubiquitin genes from the study of Arabidopsis thaliana ecotypes. Plant Mol Biol (1997) 34:745-758.

Suzuki G, Yanagawa Y, Kwok SF, Matsui M, Deng XW. Arabidopsis COP10 is a ubiquitin-conjugating enzyme variant that acts together with COP1 and the COP9 signalosome in repressing photomorphogenesis. Genes Dev (2002) 16:554-559.

Suzuki T, Nakajima S, Morikami A, Nakamura K. An Arabidopsis protein with a novel calcium-binding repeat sequence interacts with TONSOKU/MGOUN3/BRUSHY1 involved in meristem maintenance. Plant Cell Physiol (2005) 46:1452-1461.

Swarbreck D, et al. The Arabidopsis Information Resource (TAIR): gene structure and function annotation. Nucleic Acids Res (2008) 36:D1009-1014.

Sweere U, et al. Interaction of the response regulator ARR4 with phytochrome B in modulating red light signaling. Science (2001) 294:1108-1111.

Takahashi A, Takeda K, Ohnishi T. Light-Induced Anthocyanin Reduces the Extent of Damage to DNA in UV-Irradiated Centaurea cyanus Cells in Culture. Plant Cell Physiology (1991) 32:541-547.

Takai Y, Sasaki T, Matozaki T. Small GTP-binding proteins. Physiol Rev (2001) 81:153-208.

Taylor BL, Zhulin IB. PAS domains: internal sensors of oxygen, redox potential, and light. Microbiol Mol Biol Rev (1999) 63:479-506.

Teng S, Keurentjes J, Bentsink L, Koornneef M, Smeekens S. Sucrose-specific induction of anthocyanin biosynthesis in Arabidopsis requires the MYB75/PAP1 gene. Plant Physiol (2005) 139:1840-1852.

Tepperman JM, Zhu T, Chang HS, Wang X, Quail PH. Multiple transcription-factor genes are early targets of phytochrome A signaling. Proc Natl Acad Sci U S A (2001) 98:9437-9442.

Tirode F, Malaguti C, Romero F, Attar R, Camonis J, Egly JM. A conditionally expressed third partner stabilizes or prevents the formation of a transcriptional activator in a three-hybrid system. J Biol Chem (1997) 272:22995-22999.

Toledo-Ortiz G, Huq E, Quail PH. The Arabidopsis basic/helix-loop-helix transcription factor family. Plant Cell (2003) 15:1749-1770.

Torii KU, McNellis TW, Deng XW. Functional dissection of Arabidopsis COP1 reveals specific roles of its three structural modules in light control of seedling development. EMBO J (1998) 17:5577-5587.

Literature

Torii KU, Stoop-Myer CD, Okamoto H, Coleman JE, Matsui M, Deng XW. The RING finger motif of photomorphogenic repressor COP1 specifically interacts with the RING-H2 motif of a novel Arabidopsis protein. J Biol Chem (1999) 274:27674-27681.

Tseng TS, Salome PA, McClung CR, Olszewski NE. SPINDLY and GIGANTEA interact and act in Arabidopsis thaliana pathways involved in light responses, flowering, and rhythms in cotyledon movements. Plant Cell (2004) 16:1550-1563.

Valverde F, Mouradov A, Soppe W, Ravenscroft D, Samach A, Coupland G. Photoreceptor regulation of CONSTANS protein in photoperiodic flowering. Science (2004) 303:1003-1006.

van der Biezen EA, Freddie CT, Kahn K, Parker JE, Jones JD. Arabidopsis RPP4 is a member of the RPP5 multigene family of TIR-NB-LRR genes and confers downy mildew resistance through multiple signalling components. Plant J (2002) 29:439-451.

van der Fits L, Deakin EA, Hoge JH, Memelink J. The ternary transformation system: constitutive virG on a compatible plasmid dramatically increases Agrobacterium-mediated plant transformation. Plant Mol Biol (2000) 43:495-502.

Vernoud V, Horton AC, Yang Z, Nielsen E. Analysis of the small GTPase gene superfamily of Arabidopsis. Plant Physiol (2003) 131:1191-1208.

Vierstra RD, Quail PH. Photochemistry of 124 Kilodalton Avena Phytochrome In Vitro. Plant Physiol (1983) 72:264-267.

Voinnet O, Pinto YM, Baulcombe DC. Suppression of gene silencing: a general strategy used by diverse DNA and RNA viruses of plants. Proc Natl Acad Sci U S A (1999) 96:14147-14152.

Von Arnim A, Deng XW. Light Control of Seedling Development. Annu Rev Plant Physiol Plant Mol Biol (1996) 47:215-243.

von Arnim AG. On again-off again: COP9 signalosome turns the key on protein degradation. Curr Opin Plant Biol (2003) 6:520-529.

von Arnim AG, Deng XW. Light inactivation of Arabidopsis photomorphogenic repressor COP1 involves a cell-specific regulation of its nucleocytoplasmic partitioning. Cell (1994) 79:1035-1045.

von Arnim AG, Osterlund MT, Kwok SF, Deng XW. Genetic and developmental control of nuclear accumulation of COP1, a repressor of photomorphogenesis in Arabidopsis. Plant Physiol (1997) 114:779-788.

Wang H, Kang D, Deng XW, Wei N. Evidence for functional conservation of a mammalian homologue of the light-responsive plant protein COP1. Curr Biol (1999) 9:711-714.

Wang H, Ma LG, Li JM, Zhao HY, Deng XW. Direct interaction of Arabidopsis cryptochromes with COP1 in light control development. Science (2001) 294:154-158.

Wang X, Li W, Piqueras R, Cao K, Deng XW, Wei N. Regulation of COP1 nuclear localization by the COP9 signalosome via direct interaction with CSN1. Plant J (2009) 58:655-667.

Waxman L, Fagan JM, Goldberg AL. Demonstration of two distinct high molecular weight proteases in rabbit reticulocytes, one of which degrades ubiquitin conjugates. J Biol Chem (1987) 262:2451-2457.

Literature

Weigel D, et al. Activation tagging in Arabidopsis. Plant Physiol (2000) 122:1003-1013.

Wenkel S, et al. CONSTANS and the CCAAT box binding complex share a functionally important domain and interact to regulate flowering of Arabidopsis. Plant Cell (2006) 18:2971-2984.

Wertz IE, et al. Human De-etiolated-1 regulates c-Jun by assembling a CUL4A ubiquitin ligase. Science (2004) 303:1371-1374.

Whitelam GC, Smith H. Retention of phytochrome-mediated shade avoidance responses in phytochrome-deficient mutants of Arabidopsis, cucumber and tomato. Journal of Plant Physiology (1991) 39:119 -125.

Winkel-Shirley B. Flavonoid biosynthesis. A colorful model for genetics, biochemistry, cell biology, and biotechnology. Plant Physiol (2001) 126:485-493.

Xiao W, Jang J. F-box proteins in Arabidopsis. Trends Plant Sci (2000) 5:454-457.

Yahalom A, Kim TH, Winter E, Karniol B, von Arnim AG, Chamovitz DA. Arabidopsis eIF3e (INT-6) associates with both eIF3c and the COP9 signalosome subunit CSN7. J Biol Chem (2001) 276:334-340.

Yamamoto YY, Deng X, Matsui M. Cip4, a new COP1 target, is a nucleus-localized positive regulator of Arabidopsis photomorphogenesis. Plant Cell (2001) 13:399-411.

Yamamoto YY, Matsui M, Ang LH, Deng XW. Role of a COP1 interactive protein in mediating light-regulated gene expression in arabidopsis. Plant Cell (1998) 10:1083-1094.

Yanagawa Y, et al. Arabidopsis COP10 forms a complex with DDB1 and DET1 in vivo and enhances the activity of ubiquitin conjugating enzymes. Genes Dev (2004) 18:2172-2181.

Yang HQ, Tang RH, Cashmore AR. The signaling mechanism of Arabidopsis CRY1 involves direct interaction with COP1. Plant Cell (2001) 13:2573-2587.

Yang J, Lin R, Hoecker U, Liu B, Xu L, Wang H. Repression of light signaling by Arabidopsis SPA1 involves post-translational regulation of HFR1 protein accumulation. Plant J (2005) 43:131-141.

Yanovsky MJ, Kay SA. Molecular basis of seasonal time measurement in Arabidopsis. Nature (2002) 419:308-312.

Yasuhara M, et al. Identification of ASK and clock-associated proteins as molecular partners of LKP2 (LOV kelch protein 2) in Arabidopsis. J Exp Bot (2004) 55:2015-2027.

Yeger-Lotem E, et al. Network motifs in integrated cellular networks of transcription-regulation and protein-protein interaction. Proc Natl Acad Sci U S A (2004) 101:5934-5939.

Yeh KC, Lagarias JC. Eukaryotic phytochromes: light-regulated serine/threonine protein kinases with histidine kinase ancestry. Proc Natl Acad Sci U S A (1998) 95:13976-13981.

Yin Y, et al. A crucial role for the putative Arabidopsis topoisomerase VI in plant growth and development. Proc Natl Acad Sci U S A (2002) 99:10191-10196.

Yu JW, et al. COP1 and ELF3 control circadian function and photoperiodic flowering by regulating GI stability. Mol Cell (2008) 32:617-630.

Literature

Zhang C, Clarke PR. Chromatin-independent nuclear envelope assembly induced by Ran GTPase in Xenopus egg extracts. Science (2000) 288:1429-1432.

Zhang C, Clarke PR. Roles of Ran-GTP and Ran-GDP in precursor vesicle recruitment and fusion during nuclear envelope assembly in a human cell-free system. Curr Biol (2001) 11:208-212.

Zhang C, Goldberg MW, Moore WJ, Allen TD, Clarke PR. Concentration of Ran on chromatin induces decondensation, nuclear envelope formation and nuclear pore complex assembly. Eur J Cell Biol (2002) 81:623-633.

Zhang F, Gonzalez A, Zhao M, Payne CT, Lloyd A. A network of redundant bHLH proteins functions in all TTG1-dependent pathways of Arabidopsis. Development (2003) 130:4859-4869.

Zhou Q, Hare PD, Yang SW, Zeidler M, Huang LF, Chua NH. FHL is required for full phytochrome A signaling and shares overlapping functions with FHY1. Plant J (2005) 43:356-370.

Zhu D, et al. Biochemical characterization of Arabidopsis complexes containing CONSTITUTIVELY PHOTOMORPHOGENIC1 and SUPPRESSOR OF PHYA proteins in light control of plant development. Plant Cell (2008) 20:2307-2323.

Zikihara K, Iwata T, Matsuoka D, Kandori H, Todo T, Tokutomi S. Photoreaction cycle of the light, oxygen, and voltage domain in FKF1 determined by low-temperature absorption spectroscopy. Biochemistry (2006) 45:10828-10837.

Zimmermann IM, Heim MA, Weisshaar B, Uhrig JF. Comprehensive identification of Arabidopsis thaliana MYB transcription factors interacting with R/B-like BHLH proteins. Plant J (2004) 40:22-34.

Mein Dank gilt:

Bei meinem Doktorvater Joachim F. Uhrig möchte ich mich für die Möglichkeit, an diesem interessanten Thema zu arbeiten bedanken, danke aber auch für das große Vertrauen und unzählige wissenschaftliche Diskussionen!

Martin Hülskamp danke ich für den bereitgestellten Laborplatz, Rat und Unterstützung und dafür mich einst für Unkraut begeistert zu haben.

Ute Höcker möchte ich für die wertvolle Unterstützung und Diskussionen danken in einem für uns zunächst noch fremden Themenbereich. Dies hat meine Arbeit sehr bereichert, Motivation gespendet und viel Freude bereitet.

Mein ganz besonderer Dank gilt Karin Komsic-Buchmann, Tamara Zietek und Ulrike Temp - drei Engel für Andrea!!! Es ist unbeschreiblich wie Ihr mich in den letzten Tagen aber auch während der gesamten Arbeit unterstützt habt, mir zur Seite standet, dutzende Stunden im Labor, in der Kiwi-Laube, balancierend beim Tomateninfiltrieren, am Schreibtisch oder am Abend nach erledigter Arbeit verbracht habt. Das hat Freude, Kraft und Spaß bereitet! Ein spezieller Dank auch an Darko - dem Paperboy!

Martina Pesch, deren Einsatz bei der Korrektur meiner Diplomarbeit über Weihnachten (!) ich nie vergessen werde und auf die ich mich auch bei dieser Arbeit voll und ganz verlassen konnte - auf sachliche, hilfreiche Tipps, das Auge fürs Detail, viele Büro - Gespräche am Abend und Auflockerungen nach anstrengenden Arbeitstagen bei Diskussionen über gewisse Körbchen - Dank auch Dir, Birger :)

Bastian Welter möchte ich besonders für seine zuverlässige und kompetente Hilfe bei Groß- und Kleinprojekten aller Art danken. Bastian kann alles, macht alles, ist immer hilfsbereit und mit einem offenen Ohr. So macht Arbeit Spaß, Freude im Mikrotiterplatten-Format :)

Der AG Höcker und insbesondere Petra, Kirsten, Aashish und Alex möchte ich für ihre ständig offenen Arme und Ohren, unendlich viel Rat und Tat zu allen lichtbiologischen Fragestellungen, ihre offene Art und unzähligen Diskussionen danken, das hat Freude gemacht!

Dem Lehrstuhl III mit all seinen aktuellen und ehemaligen Mitarbeitern danke ich für ein halbes Jahrzehnt Wegbegleitung. Vor allem die vielen schönen Feiern im alten Gebäude, die WM, 100% Karneval, Hogwarts, das Wandern im Siebengebirge, unzählige mit viel Mühe zubereitete kulinarische Eindrücke und vor allem der Austausch über diverse Nationalitäten hinweg habe mich geprägt und bereichert!

Der Firma phytowelt danke ich für die Unterstützung gerade zu Beginn meiner Arbeit und insbesondere für den Austausch mit Guido Jach.

Viktor Kirik hat den Boden bereitet für diese Arbeit, indem ich bei ihm in meiner Diplomarbeit über MIDGET arbeiten durfte und er mich in den Laboralltag eingeführt hat.

Jürgen Schmidt und Thomas Colby danke ich für die erfolgreiche und kompetente Zusammenarbeit.

Siegfried Werth hat unzählige Bilder mit unfassbarer Auflösung von "meinem Gemüse" erstellt. Unvergessen auch, wie er hunderte von Tomaten vor den Augen hatte :)

Der Gärtnerei und insbesondere Klaus Menrath danke ich für die Spezialpflege meiner Minis.

Nicht zuletzt möchte ich meiner Tante Gina Kühn danken, die immer an mich geglaubt hat und mir immer zur Seite steht.

Meiner Verlobten, Petra Thoms, danke ich für das gemeinsame Durchleben einer langen Reise durch Dissermania von Delhi bis nach Köln und das erfolgreiche Verhindern von Schiffbruch. Danke für alles!

Mein ganz besonderer Dank gilt Ilse Magnus, die immer da war und mir in schweren Zeiten zur Seite stand.

Erklärung

Ich versichere, dass ich die von mir vorgelegte Dissertation selbständig angefertigt, die benutzten Quellen und Hilfsmittel vollständig angegeben und die Stellen der Arbeit − einschließlich Tabellen, Karten und Abbildungen − die anderen Werken im Wortlaut oder dem Sinn nach entnommen sind, in jedem Einzelfall als Entlehnung kenntlich gemacht habe; dass diese Dissertation noch keiner anderen Fakultät oder Universität zur Prüfung vorgelegen hat; dass sie − abgesehen von unten angegebenen Teilpublikationen − noch nicht veröffentlicht worden ist sowie, dass ich eine solche Veröffentlichung vor Abschluss des Promotionsverfahrens nicht vornehmen werde. Die Bestimmungen der Promotionsordnung sind mir bekannt. Die von mir vorgelegte Dissertation ist von Joachim F. Uhrig betreut worden.

Andrea Schrader